Non-perturbative methods and Chiral Perturbation Theory applied to Meson-Meson and Nucleon-Nucleon interactions

Miguel Albaladejo Serrano

Tesis Doctoral

Director: José Antonio Oller Berber

Departamento de Física

Universidad de Murcia

(...) Thus in the thirteenth century the great Franciscan theologian Bonaventure felt obliged to reproach his colleagues of the philosophical faculty at Paris with having learned how to measure the world but having forgotten how to measure themselves.

J. Ratzinger (Benedict XVI), Introduction to Christianity

(...) En el siglo XIII san Buenaventura, gran teólogo franciscano, echaba en cara a sus colegas de la facultad de París que habían aprendido a medir el mundo, pero se habían olvidado de medirse a sí mismos.

J. Ratzinger (Benedicto XVI), Introducción al Cristianismo

Agradecimientos

Quizá sea esta la parte que más difícil me resulte escribir. La razón es bien sencilla: en el resto de la tesis, hablo de algo que me gusta, de física. En esta parte, en cambio, hablo de algo de lo que me cuesta hablar: de mí mismo.

Quisiera empezar agradeciendo a mi familia (padres, hermanos, tíos, *yaya*, padrinos, suegros, cuñados ...) y amigos todo el apoyo que me han prestado siempre, y el haber podido crecer entre ellos y con ellos. Sin el ambiente vivido en mi casa, aprendiendo tanto de mis padres como de mis hermanos a buscar siempre la verdad, nada de esto sería posible. También debo estar agradecido a mis padres por la educación que me han proporcionado, pero, sobre todo, por los dones de la Vida y de la Fe.

A mi esposa, Cristina, y a mis hijas, Belén, Isabel y Cristina, no puedo sino agradecerles la paciencia que han tenido conmigo estos últimos años. Ellas son las principales víctimas de esta tesis. Y, sin embargo, siempre han estado ahí, siendo la alegría de mi corazón. Cris, gracias porque, en realidad, *nunca estás ausente*. A Pablo, gracias por ser *mi hermano*. Y al resto del *sector*, gracias por todos los momentos (buenos y malos) que hemos pasado juntos.

Quiero recordar ahora a Cándido, con quien empecé a trabajar al principio. He aprendido mucho de él, y disfrutado siempre con nuestras conversaciones. También tengo presente a todos los que han sido mis profesores durante la carrera de Física: de algunos aprendí mucho y de otros muchísimo. Y también recuerdo especialmente a Valentín, que fue mi profesor de Física durante COU, y que me hizo interesarme realmente por esta Ciencia.

I would also like to thank to all the people I have worked with in these years: José Manuel Alarcón, Luis Álvarez, Zi-Hui Guo, Luis Roca, Guillermo Ríos, Eulogio Oset. I have discussed with them many things related to this thesis, and I have learned always quite a lot from them. To the latter three, I would also like to acknowledge the pleasure of having worked with them in some papers that are, indeed, contained in this thesis. Finally, I am grateful for discussions I have had with, or simply, encouraging words I have received from, several people: D. Bugg, M. Chanowitz, H. Leutwyler, U. Meißner, J. R. Peláez.

Finalmente, siendo esta mi tesis doctoral, guardo un último lugar para José Antonio Oller, mi director de tesis. Para mí ha sido profesor, director, amigo, *colega*, pero sobre todo maestro. Ha sido crítico y exigente conmigo cuando tenía que serlo (a menudo, de hecho), por lo cual le estoy enormemente agradecido. Su inagotable capacidad de trabajo, su lúcida y aguda visión para los problemas de la física y su pulcritud teórica han sido y serán siempre una inspiración para mí. No sé si alguien llegará a pensar que, con el trabajo contenido en esta tesis, se ha aportado algo de luz a problemas específicos de la física hadrónica actual. Si alguien lo pensare, que sepa que fue por que me subí *a hombros de gigantes.*

Contents

List of Figures

List of Tables

Introduction and Summary

Up to where scientists know, the Universe is made of particles, space, time, and the laws that dictate their interactions. One of these forces is the strong force, from which there emerge, in turn, the forces inside the nuclei of the atoms. The particles that *suffer* these strong interactions are called *hadrons*. Quantum Chromodynamics (QCD) [1–7] is the theory that describes the strong interactions. It is a relativistic, non-abelian, Yang-Mills [8] quantum field theory, in which *quarks* and *gluons* are the fundamental degrees of freedom (the quantum fields of the theory). Quarks are matter particles, and gluons are the particles that carry the strong interactions. It is a beautiful and successful theory, one of the cornerstones of the greatest scientific theory ever: the Standard Model. QCD has proven successful to describe a wealth of physical phenomena.

However, as it stands, that is, with quarks and gluons as dynamical degrees of freedom, it can only be used in the high energy regime, where, due to the (predicted by QCD) *asymptotic freedom*, quarks manifest themselves as weakly interacting point-like particles, and then pertubartive methods can be used, as in as much it is done in Quantum Electrodynamics. For low energy interactions, the complementary behaviour of QCD, the *infrared slavery*, points to the confinement of quarks inside hadrons. However, confinement is an obscure point not well understood in QCD yet, though lattice QCD offers new insights to the problem. Still, in the QCD mass spectrum of hadrons, we find a remarkable fact, the appearence of an isospin triplet of pseudoscalar mesons, the pions, π, whose mass is much smaller than the others. This key feature points to the fact that a well known approximate symmetry of QCD, namely the chiral symmetry, $SU(2)_L \otimes SU(2)_R$, is spontaneously broken [9–14] to $SU(2)_{L+R} \equiv SU(2)_V$, whereas the generators of the broken symmetry would give rise to a massless triplet of particles, the so called Goldstone bosons. As the symmetry is not exact due to the finite quark masses, the pions are not exactly massless, and so they are called *pseudo*-Goldstone bosons. Although we have considered $SU(2)$ giving rise to a triplet of pions, we can extend these considerations the $SU(3)$ symmetry. Then, we include the other lightest pseudoscalar mesons, kaons (K) and eta (η), which, together with the triplet of pions, would form an octet. The hadrons are thus organized into $SU(3)$ multiplets, the so called *Eightfold way* [15]. From the previous considerations, one could attempt to construct an effective quantum field theory in which the dynamical degrees of freedom are not quarks and gluons themselves, but the pions instead. Indeed, this scheme has been put in practice, and a theory has emerged: Chiral Perturbation Theory (ChPT) [16–19]. It is, then, the *effective* theory of QCD at low energies, and it can be treated perturbatively, allowing for a systematic expansion in powers of momenta of the external pseudo-Goldstone bosons and quark masses. In **Chapter 1**, we shall attempt the formal and rigorous construction of ChPT, with the general formalism for the construction

of effective Lagrangians [20, 21], that will be reviewed first, and the knowledge of the chiral symmetry of the strong interactions and its spontaneous breakdown.

* * *

Together with its great successes, ChPT has some evident shortcomings in practical applications. On one hand, it cannot reproduce the conspicuous resonant behaviour found in the hadronic spectrum. Being a perturbative expansion, it cannot generate the pole structure attached to resonances in the scattering amplitudes of hadrons. On the other hand, the predictive power of the theory is progressively lost as one increases the order of the expansions, because of the appearence of the so called low energy constants, that encode information from the underlying theory (QCD) and thus not fixed by the symmetries. These shortcomings imply that non-pertubative schemes are necessary as complementary tools to be used together with the pertubative information that we can extract from ChPT. In the meson–meson or meson–baryon interactions, among these nonperturbative methods, one can cite the Inverse Amplitude Method (IAM) [22–32], the Bethe-Salpeter (BS) approach [33–37] and the N/D method, which was originally devised in Ref. [38] and afterwards used in several works. Later on, it was retaken in connection with the more recent advances of effective field theory (ChPT) and applied to meson–meson or meson–baryon interactions [39–47]. We shall refer to some of these works later on, when introducing the scalar sector and, specially, the σ meson (nowadays denoted by $f_0(500)$ by the Particle Data Group (PDG) [48].) Most of this thesis will be related to the applications of one of this non-pertubative schemes, the N/D method, that we refer as Unitarized Chiral Perturbation Theory (UChPT). Its formalism will be briefly explained in **Chapter 2**. There, a physical fundamental concept, unitarity, is introduced, and its consequences are studied. We also introduce here the concepts of scattering amplitudes and partial waves. We shall study from a general point of view the appearence of resonances attached to poles in the unphysical Riemann sheets of the scattering amplitudes. Convinced of the importance of unitarity, we will review the application of the N/D method to deduce the most general structure of a partial wave amplitude when the so called unphysical cuts are neglected [39]. The N/D method is a unitarization method, that splits the contribution of the unitarity and unphysical cuts in two different functions, D and N, respectively. We shall also explain how to introduce the unphysical cuts in a perturbative way.

In **Part I**, then, we have derived the basic framework of this thesis, that will be applied to a variety of problems in **Part II**. We now comment on the different issues that will be treated in the body of the thesis. We try to give an overview of the experimental and theoretical status of each analyzed topic, motivating thus our study. We give some details of the methods used and an advance of the main results, trying to connect them with earlier works.

* * *

We shall start by studying the scalar sector of the meson–meson interactions in **Chapter 3**. In ChPT, due to its perturbative character, the scalars (with $J^{PC} = 0^{++}$ quantum numbers)

do not appear straightforwardly. The lightest of these scalars (with masses below 1 GeV) are the σ, κ, $f_0(980)$ and $a_0(980)$ mesons. Its connection with the dynamics of the lightest pseudoscalars (the dynamical degrees of freedom in ChPT) and its relation to unitarity or final state interactions was realized along several works. Regarding the $\pi\pi$ interactions specifically, one has first to mention the works of Truong and collaborators [22–27] who first emphasized the important role played by the null isospin (I) S-wave $\pi\pi$ final state interactions, through the IAM technique. Within this formalism, the σ pole was first obtained in Ref. [28], together with the $K^\star$ and ρ resonances in the P-waves. Because of the lack of coupled channels in the IAM at that time, it was not possible to obtain other light scalar resonances as the $f_0(980)$ and $a_0(980)$. Simultaneously, in Ref. [33], within the BS approach, it was obtained the σ pole, together with the $f_0(980)$ and $a_0(980)$. The interplay of some of the authors of the previous works led to the coupled channel extension of the IAM method [29], obtaining then in Refs. [29–31] the whole lightest scalar nonet, together with the lightest vector nonet. In turn, the approach of Ref. [33] was settled on more general grounds in Ref. [39] by means of the N/D method (from which one can also derive the IAM equations). From a theoretical point of view, most of these works stress the role of the unitarity cut and the strong final state interactions among mesons, and also show that crossed cuts can be treated perturbatively when studying the resonant scalar dynamics. Finally, let us quote that the pole positions obtained in Refs. [28], [33] and [30], are, respectively, $440 - i\ 245$, $469 - i\ 194$ and $442 - i\ 227$ MeV. References [33, 39] clearly established that the σ resonance is dynamically generated by the pion strong self-interactions.

Other approaches to the problem of the lightest scalar can be found in Refs. [49–52]. Indeed, Refs. [49, 50], within the MIT bag model, already predicted in the late 1970s a light scalar nonet of four quark broad resonances, with masses (in modern notation for the states) $M_\sigma \sim 650$ MeV, $M_{a_0} = M_{f_0} \sim 1100$ MeV and $M_\kappa \sim 900$ MeV. In Refs. [53–58] the mixing between these resonances was considered. Other successful phenomenological approach to study the lightest scalar resonances is based on meson-exchange models [59–61]. Recently, Refs. [62,63] studied the possibility of the construction of a chiral Lagrangian with an explicit scalar singlet field.

Concerning the heavier scalar resonances, we also study in this thesis the isoscalar-scalar resonances $f_0(1370)$, $f_0(1500)$, $f_0(1710)$ and $f_0(1790)$, listed by the PDG [48]. Crystal Barrel Collaboration (see [64] for a comprehensive review) data at LEAR at CERN improved the knowledge of the 0^{++} spectrum, confirming or discovering the $a_0(1450)$, $f_0(1370)$ and $f_0(1500)$ resonances, whereas the BES Collaboration [65–67] confirmed the spin assignment of the $f_0(1710)$ and found another resonance, $f_0(1790)$. We will discuss further on controversies and results about these states in the body of the thesis, when presenting our own results, and we refer the reader to the reviews of Refs. [64, 68]. Besides the general interest of these states in the determination of the hadron spectrum, they are relevant for another issue of the scalar-isoscalar spectrum, namely, the identification of glueballs. In QED, photons do not carry electric charge, so they do not directly interact among them. In QCD, gluons carry color charge and interact between them, due to the Yang–Mills nature of the theory. It is generally believed that QCD predicts the existence of mesons without valence quarks, the so-called glueballs. Its confirmation in the spectrum of strong interactions is then at the heart of the theory. Interest in the glueballs started since the early days of QCD, and its study was one of the first applications of QCD sum rules [71, 72]. Due to the strong coupling of the vacuum with the 0^{++} channel, the results are not conclusive yet [71–78]. In general, these

works agree with the presence of a glueball around 1.5 GeV, though the existence of an extra glueball around 0.5 GeV is also proposed. A glueball with a mass around $\gtrsim 1.5$ GeV is also predicted in several models [79–83]. In the quenched lattice QCD spectrum [84–89] the mass of the lightest scalar glueball is predicted with a mass $M = 1660 \pm 50$ MeV, close to the $f_0(1500)$ and $f_0(1710)$ resonances, so that these are considered strong candidates to have a large glueball component. Reference [88] obtains that the $f_0(1710)$ is mainly a pure glueball. Reference [89] evaluated in quenched lattice QCD the decays of the latter resonance to two pseudoscalars and calculated a pattern of decays in agreement with some reported data on the $f_0(1710)$ [48]. Studies with dynamical fermions, mixing glueballs and quarkonia, are still at a preliminary stage (see Ref. [90] and references therein, as well as references in Sec. 3.1.) In Ref. [91] (see also Refs. [92–94]) it was found a chiral supression of the couplings of the scalar glueball G_0 to $\bar{q}q$, $\Gamma(G_0 \to s\bar{s}) \gg \Gamma(G_0 \to u\bar{u}+d\bar{d})$, in agreement with the result of Ref. [89] in lattice QCD. This mechanism also implies that the scalar glueball should not mix. However, the situation is not clear yet and different results are obtained in different works [95–100], following the same idea of mixing of the glueball with the nearby $n\bar{n}$ and $s\bar{s}$ states.

To sudy the scalar sector, we calculate the null isospin I S-wave meson-meson partial wave in terms of thirteen coupled channels, $\pi\pi$, $\sigma\sigma$, $K\bar{K}$, $\eta\eta$, $\eta\eta'$, $\eta'\eta'$, $\rho\rho$, $\omega\omega$, $K^*\overline{K}^*$, $\omega\phi$, $\phi\phi$, $a_1\pi$ and $\pi^*\pi$. The $SU(3)$ symmetry is enlarged to $U(3)$ as to include the effects of the η' meson [101–104]. The multipion states are effectively simulated in terms of the two-body resonance states $\sigma\sigma$, $\rho\rho$, $a_1\pi$ and $\pi^*\pi$, although we will conclude that the inclusion of the latter two channels is not relevant. Simultaneously, we also study the S-wave amplitude $K^-\pi^+ \to K^-\pi^+$, involving the $I = 1/2$ and $I = 3/2$, with the coupled channels $K\pi$, $K\eta$ and $K\eta'$, in the line of Refs. [43,44]. The interaction kernels among the different states are obtained from chiral Lagrangians. The chiral symmetry is also gauged, so as to derive those vertices involving vector resonances by minimal coupling. For the σ resonance we take advantage of the fact that this resonance is dynamically generated in UChPT, as previously stressed, in terms of two pion rescattering. This allows us to fix its elementary transition matrix elements with other channels without including any new free parameter. We also consider the exchange of *bare* resonances [105, 106] in the s–channel. We observe that, in order to describe data, we need two octets (with *bare* masses at 1300 MeV and 1900 MeV) and a singlet (with a *bare* mass $M \simeq 900$ MeV.) We are then able to provide fits to a rich set of data involving several phase shifts and inelastic cross sections up total centre mass energy of around $\sqrt{s} \simeq 2$ GeV. We pay special attention to the role of 4π, in particular below the $K\bar{K}$ threshold. We then study the spectroscopy content of our fits and find poles corresponding to the large set of resonances: σ, $f_0(980)$, $f_0(1370)$, $f_0(1500)$, $f_0(1710)$ and $f_0(1790)$ for $I = 0$ and κ, $K_0^*(1430)$ and $K^*(1950)$ for $I = 1/2$. Their pole positions and couplings to the different channels are also given. We shall also see that one pole, mainly corresponding to the $f_0(1370)$, is a pure octet state, as well as his companion in $I = 1/2$, the $K_0^*(1430)$. We identify the $f_0(1710)$ and an important contribution to the $f_0(1500)$ as an unmixed glueball. This is based on an accurate agreement of our results with the aforementioned predictions of lattice QCD [89] and the chiral suppression of the coupling of a scalar glueball to $\bar{q}q$ [91].

* * *

Another interesting problem is the presence of excited pseudoscalars, with quantum number as those of the pseudo–Goldstone bosons, but heavier in mass (lying in a range of 1 GeV and 2 GeV), that we adress in **Chapter 4**. In $I = 1$, one has the $\pi(1300)$ and $\pi(1800)$ resonances, and in $I = 1/2$ the $K(1460)$ and $K(1630)$ resonances. Maybe, the most interesting case here is the $I = 0$ sector, where, according to PDG [48], there are three resonances in a narrow range of masses, namely $\eta(1295)$, $\eta(1405)$ and $\eta(1475)$. A review of the experimental situation can be found in Ref. [107]. One of these resonances would be an extra state if we arrange the nearby pseudoscalars in a nonet. Given the clear signal of the $\eta(1405)$ resonance in gluon–rich processes (*e.g.*, J/Ψ radiative decays), it becomes then a perfect candidate to be the lightest pseudoscalar glueball [108–110]. However, the lattice QCD prediction for the lowest mass pseudoscalar glueball is about 2.4 GeV [84–86], a quite exciting discrepancy. This picture for the classification of these resonances has been criticized in [111], where it is stated that just one of these states exists. It is questioned the mere existence of $\eta(1295)$, and it is argued that the $\eta(1405)$ and $\eta(1475)$ are actually the same state, $\eta(1440)$. Recently, this suggestion has received support in Ref. [112]. Another resonance, called $X(1835)$, has been recently observed, and the analyses suggest $I^G(J^{PC}) = 0^+(0^{-+})$ quantum numbers.

If the scalars are generated through the interactions among the lightest pseudoscalars, it is therefore tempting to think that higher pseudoscalars are generated from the interactions of the lightest pseudoscalars with the lightest scalars, in a beautiful picture resembling the *bootstrap hypothesis* of the *old days*. This also shows a pattern in which spontaneous chiral symmetry breaking manifests in the hadron spectrum. In order to shed some light into the question of the pseudoscalars above 1 GeV, we study the interactions between the $f_0(980)$ and $a_0(980)$ scalar resonances and the lightest pseudoscalar mesons. We first obtain the elementary interaction amplitudes, or interacting kernels, without including any *ad hoc* free parameter. This is achieved by using the previous results on the nature of the lightest scalar resonances as dynamically generated from the rescattering of S-wave two-meson pairs. Afterwards, the interaction kernels are unitarized through UChPT and the final S-wave amplitudes result. We find that these interactions are very rich and generate a large amount of pseudoscalar resonances that could be associated with the $K(1460)$, $\pi(1300)$, $\pi(1800)$, $\eta(1475)$ and $X(1835)$. Then we can say, at least, that an important contribution to these states is of a dynamical origin. We also consider the exotic channels (that is, with quantum numbers that cannot be obtained with $\bar{q}q$ combinations), with $I = 3/2$ and $I = 1$, having the latter positive G-parity. The former could be also resonant in agreement with a previous prediction [113]. Later works [114,115], studying three-pseudoscalar systems by means of the Fadeev equations, also obtain some of the cited resonances, namely, $K(1460)$ and $\pi(1300)$.

* * *

The nature of the σ meson is studied in **Chapter 5**. It is the lightest resonance with the quantum numbers of the vacuum, $J^{PC} = 0^{++}$. The history of the σ meson is a long one. We already commented about the works that, putting together the chiral dynamics of the lightest pseudoscalars (pions, for the case of the σ) and the effects of unitarity, could obtain the σ pole. More recently, Ref. [116], based on the solution of the Roy equations and ChPT at two-loops, obtained the value $445^{+16}_{-8} - i\ 272^{+9}_{-13}$ MeV. The Roy equations implement crossing symmetry

exactly, while the works related to IAM, N/D and BS do it perturbatively. Another recent precise determination [117], based on dispersion relations, yields $484 \pm 17 - i\ 255 \pm 10$ MeV. Let us also mention that all these analyses neglect altogether the inelasticity due to the 4π channel in $\pi\pi$ S-waves, whereas in our study of the scalar sector in Chapter 3 the 4π channel was approached as $\sigma\sigma$ and $\rho\rho$ states. The fact that all these pole positions (the latter ones and those obtained in the works previously mentioned) for the σ lie rather close to each other (particularly one can say that convergence is reached very accurately for the real part) is another indication for the correctness of treating crossed-channel dynamics perturbatively, as done in the framework of the works mentioned above. Whence, we could conclude that our present knowledge on the pole position of the σ resonance is quite precise and, furthermore, we understand the underlying physics at the hadronic level. Experimentally, new interest is triggered on the σ resonance from recent high-statistics results, *e.g.* $J/\Psi \to \omega\pi\pi$, where a conspicuous peak is seen [118]. Indeed, this decay mode was the first clear experimental signal of a σ resonance [119, 120]. Another marked peak around the σ energy region is also observed in several heavy meson decays, *e.g.*, it was observed with high statistical significance in $D \to \pi^+\pi^-\pi^+$ [121].

Besides the pole position and the couplings of this resonance, a natural question is about its nature: $q\bar{q}$, four quark, meson molecule, glueball, etc. A four-quark nature is assigned in [49, 50], since a whole nonet of scalars is predicted, with masses and widths compatible with those of σ, κ, $f_0(980)$ and $a_0(980)$. The four-quark nature of the lightest scalars is also favored in other works, see *e.g.* Ref. [122]. The relative strength of the σ coupling to $K\bar{K}$ compared to $\pi\pi$ is also taken as an important property in order to disentangle between different models for the nature of the σ meson, as stressed in Ref. [123]. This reference points out that the not so much suppressed coupling of the σ to K^+K^- as compared with that to $\pi^+\pi^-$, is a key ingredient to advocate for a gluonium nature of the σ meson. According to Ref. [123], a simple $q\bar{q}$ interpretation of the σ fails to explain the large width of the σ while a four-quark scenario has difficulties to explain its large coupling to K^+K^-. It is then worth emphasizing that the T-matrices obtained in Refs. [33, 39] and similar works (and also in Chapter 3) also predict a ratio for the σ couplings to K^+K^- and $\pi^+\pi^-$ in perfect agreement with the value given by Ref. [123]. However, in this case this stems from the dynamical generation of the σ resonance from the Goldstone boson dynamics associated to the strong scalar isoscalar $\pi\pi$ interaction. QCD sum rules were also applied for the study of the lightest scalar meson, *e.g.* in Refs. [123–127]. It is argued too that the σ resonance is the chiral partner of the pion [128–134] and the way in which the σ pole evolves when approaching the chiral symmetry restoration limit is different according to the nature of this resonance [135].

Considerations based on increasing the QCD number of colors, N_C, were exploited in Refs. [39, 136–139], showing that the σ resonance has a non-standard N_C dependence. This can be done more safely for $N_C \gtrsim 3$, not too large, while statements for $N_C \gg 3$ depend much more on fine details of the approach [138, 140–146]. The N_C evolution of the σ-pole trajectory is clearly at odds with the expectations for a purely $\bar{q}q$ or glueball resonance, but in the lines of what it is expected for a meson-meson or four quark resonance [138, 141–147]. In the large N_C limit it is well known that loops are suppressed so that the $\pi\pi$ rescattering vanishes away and then the σ resonance pole disappears according to Refs. [39, 136–138, 148].

In this Chapter, the nature of the σ or $f_0(500)$ resonance is elucidated further by evaluating

its quadratic scalar radius, $\langle r^2\rangle_s^\sigma$. This allows one to have a quantitative estimate for the size of this resonance. Within our approach, the σ is a dynamically generated state from the pion-pion interactions. This allows us to obtain its scalar form factor from chiral Lagrangians, and from it we calculate its quadratic scalar radius. We obtain that the σ resonance is a compact object with $\langle r^2\rangle_s^\sigma = (0.19 \pm 0.02) + i\, 0.06 \pm 0.02$ fm^2. For comparison, the quadratic scalar radius of the pion is $\langle r^2\rangle_s^\pi = 0.65 \pm 0.05$ fm^2 [149]. However, $\langle r^2\rangle_s^\sigma$ is similar to the measured $K^\pm$ quadratic charge radius [150], $\langle r^2\rangle_V^{K^\pm} = 0.28 \pm 0.07$ fm^2. A four-quark picture seems adequate, rather than a $\pi\pi$ molecule. Our results are connected with other recent works, mentioned above, that support a non standard nature of the σ as well, while fulfilling strong QCD constraints. We shall also study the Feynman–Hellman theorem [151, 152] relating the σ meson mass to that of the pion through the scalar form factor of the former.

We also offer a detailed study of the low-energy S-wave $\pi\pi$ scattering amplitude, using UChPT with the chiral amplitudes calculated in $SU(2)$ at $\mathcal{O}(p^4)$. From the amplitudes, we extract our values for the threshold parameters of S-wave $\pi\pi$ phase shifts, the $\mathcal{O}(p^4)$ chiral perturbation theory low energy constants as well as the σ pole position. Our result for the pole position is $\sqrt{s_\sigma} = 440 \pm 10\ -i\ 238 \pm 10$ MeV, whereas we also have an accurate description of the threshold parameters $a_0^0 = 0.219 \pm 0.005$, $b_0^0 m_\pi^2 = 0.281 \pm 0.006$. From the comparison with other accurate determinations in the literature we obtain average values for the latter quantities $\sqrt{s}_\sigma = 458 \pm 14 - i\, 261 \pm 17$ MeV and $a_0^0 = 0.220 \pm 0.003$, $b_0^0 = 0.279 \pm 0.003\ m_\pi^{-2}$, in good agreement with our own results. We also obtain reliable results for the $SU(2)$ $\mathcal{O}(p^4)$ LECs, namely $\bar{l}_1 = 0.8 \pm 0.9$, $\bar{l}_2 = 4.6 \pm 0.4$, $\bar{l}_3 = 2 \pm 4$ and $\bar{l}_4 = 3.9 \pm 0.5$. These results are compared with other works, both from phenomenological studies and lattice results.

The quark mass dependence of the size of the σ as well as its mass and width is considered too. The latter are compared with lattice QCD results [153] and theoretical calculations obtained within the IAM [154], finding a general agreement. The fact that the mass of this resonance tends to follow the threshold of two pions, as found in lattice QCD, is another clear indication that this resonance is a dynamically generated meson-meson resonance. We find that, for a pion mass large enough ($m_\pi \gtrsim 470$ MeV at NLO and $m_\pi \gtrsim 370$ MeV at LO), the σ meson becomes a $\pi\pi$ bound state. The dependence of $\langle r^2\rangle_s^\sigma$ with the pion mass is also studied. For those pion masses in wich the σ meson is a bound state, we find a larger value for $\langle r^2\rangle_s^\sigma$. In this situation, hence, a molecular picture is more appropriate.

* * *

It has already been remarked the non–perturbative character of the strong interactions. For this reason, Lattice QCD has become a powerful tool to study them, and, in particular, the hadronic spectrum. A recent review on the methods and results (excluding however the glueball question) can be found in Ref. [155]. In Lattice QCD, through the path integral formalism, one studies the interactions of quarks and gluons in a lattice box of finite volume. Whence, one needs to connect the results obtained within this discrete and finite space to the continuum and infinite real space. The standard Lüscher method [156, 157] provides such a link and is the most used one. However, an improvement over this method was recently given in Ref. [158]. The derivation in Ref. [158] is done using the techniques of UChPT. It

assumes a volume independent kernel to be unitarized. Analogously, the Lüscher method shows that volume dependent contributions are exponentially suppressed with L, the size of the box. However, loops in t– and u–crossed channel are volume dependent in finite volume calculations in Quantum Field Theory. Furthermore, also contributions from tadpole loop functions (that contribute directly to the amplitude, but also through m_π and f_π) are volume dependent. What we intend in **Chapter 6** is to investigate these contributions in the case of $\pi\pi$ S-wave interactions, both for the $I = 0$ and $I = 2$ cases. The former, as has already been stated, is relevant for the σ meson case (the $f_0(980)$ also, if the $K\bar{K}$ channel were also considered). The $I = 2$ case is also important, because it is well known that the crossed channel dynamics contributions are important here. We compare three different approaches for $\pi\pi$ scattering: BS, N/D and IAM. The BS approach can be considered as an $\mathcal{O}(p^2)$ version of the N/D method. Since it has just tree-level amplitudes in the kernel (no loop functions), it has no volume dependence. On the contrary, the IAM and the N/D approaches include the $\mathcal{O}(p^4)$ chiral amplitudes, which are explictly volume dependent. We then derive the necessary modifications of the infinite volume versions of these amplitudes and calculate them for the case of a finite box. In essence, these modifications consist in an appropiate substitution of momentum integrals by sums over the allowed momenta in a finite box. We quantify the error made by neglecting the exponentially supressed effects in usual extractions of physical observables from lattice QCD spectra. We conclude that for $\pi\pi$ phase-shifts in the $I = 0$ channel up to 800 MeV this effect is negligible for box sizes bigger than $2.5m_\pi^{-1}$ and of the order of 5% at around $1.5 - 2m_\pi^{-1}$. For $I = 2$ the finite size effects can reach up to 10% for that energy. We also quantify the error made when using the standard Lüscher method to extract physical observables from lattice QCD, which is widely used in the literature but is an approximation to the one used in the present work.

* * *

In the previous chapters we have worked exclusively with meson–meson interactions. In **Chapter 7** we deal with nucleon–nucleon (NN) interactions. This is a basic process, whose understanding is necessary in a large number of problems in physics, ranging from nuclear structure to neutron stars. Recent interesting reviews, from a modern perspective of Effective Field Theory, can be found in Refs. [159–162]. Weinberg proposed [163–165], in the early 1990s, to use ChPT to calculate the NN potential in terms of the explicit degrees of freedom (nucleons and pions). At this point, it is worth emphasizing the irony of going back to Yukawa's view (pion exchanges among nucleons) but with the remarkable difference that nowadays thanks to ChPT one can calculate systematically the NN potential and connect with QCD through the chiral symmetry, its spontaneous and explicit breaking and the values of the chiral counterterms.

Since NN interactions are non–perturbative, the chiral NN potential must be iterated. Weinberg suggested to solve a Lippmann–Schwinger (LS) equation in terms of the former. However, the chiral potential is singular at the origin, thus some kind of regularization is required, typically, a three momentum cut-off Λ. This program was first carried out in Refs. [166–169]. Many works are done within this formalism, and we refer the reader to the above reviews, and also to the Introduction in Chapter 7 for further references.

Despite the great phenomenological success of this approach, several works in the literature [170–176] showed, from different approaches, that the chiral counterterms that appear in the ChPT Lagrangian following the standard power counting are not enough to renormalize the amplitude, that is, to absorb the LS equation cut-off dependence. Some works thus proposed to *promote* some higher orders counterterms to lower ones (one should rather say *demote*.) So doing, Ref. [170] obtained stable results in the limit $\Lambda \to \infty$. However, it should be stressed that this implies a violation of the standard ChPT power counting, but also of the low energy theorems relating the parameters in the effective range expansion [177]. Besides, one should bear in mind that in the limit $\Lambda \to \infty$ a more complicated power counting arises [178, 179]. On the other side of the question are the works in Refs. [177, 180] that, following the lines of Refs. [181, 182], show that the cut-off Λ should not be taken beyond the breakdown scale of the EFT, typically below 1 GeV. We will discuss further on this issue through Chapter Chapter 7, and a more detailed account can also be found in Section 4.5 of Ref. [159].

In our work, we consider NN interactions from Chiral Effective Field Theory. We apply the N/D method to NN partial waves taking as input the one-pion exchange (OPE) discontinuity along the left-hand cut. This discontinuity is amenable to a chiral power counting as discussed in Refs. [162, 183, 184], being OPE its leading order contribution. In the first part of the Chapter, we restrict to uncoupled partial waves. By applying the N/D method, we obtain a linear integral equation for each partial wave. For S– and P–waves (orbital angular momentum $\ell \leqslant 1$) our method can be directly applied. For D– and higher waves ($\ell \geqslant 2$), the integral equations must be solved in the presence of $\ell - 1$ constraints, so as to guarantee the right behavior of the D- and higher partial waves near threshold. This is accomplished by the introduction of Castillejo–Dyson–Dalitz (CDD) poles [185], which is always allowed in the N/D method. Later on, we generalize our formalism to coupled channels, discussing in some detail the case of the deuteron in the ${}^3S_1$–${}^3D_1$ partial waves. Our phase shifts and mixing angle in every wave are compared with those of the Nijmegen group [186], which stem from a partial wave analysis (PWA) of experimental data. We would like to emphasize now that we present here a novel method to study the NN interaction, in which the calculated NN partial waves are based on dispersion relations and chiral Lagrangians and are independent of regulator. At this stage, our calculation is at leading–order and thus not yet competitive with present high–precision calculations. Though, we must stress that this method can be systematically improved order–by–order, and that the basic input is calculated from ChPT. Both features are in harmony with the modern perspective of Effective Field Theories.

* * *

After having treated all these topics in the body of the thesis, we attempt to draw our conclusions in **Chapter 8**, pointing out the main achievements of our work. In order to facilitate the reading of the thesis, we relegate some technical aspects in several appendices given in **Part III**, at the end of the thesis. The references are collected at the very end of this thesis. We include separatedly, as an *author publication list*, those that have appeared due to the work contained in it, namely [A, B, C, D, E, F, i, ii, iii, iv, v]. .

I

Formalism

1

Construction of effective Lagrangians. Chiral Lagrangians.

Contents of this Chapter:

1.1 Introduction

In this Chapter we attempt the formal and rigorous construction of Chiral Perturbation Theory (ChPT). We employ the general formalism to derive effective Lagrangians [20, 21] in Quantum Field Theory and the knowledge of the chiral symmetry of the strong interactions and its spontaneous breakdown.

First, in Sec. 1.2, the Goldstone theorem [9, 10] is deduced. It dictates the appearence of massless particles if a global symmetry of a quantum field theory spontaneously breaks down. In Secs. 1.3 to 1.7 a detailed review of the construction of effective Lagrangians is done. The Lagrangian of QCD and its chiral symmetry is investigated in Sec. 1.8. The implications of the spontaneous symmetry breaking on the hadronic spectrum of the latter is also studied. In Sec. 1.9 we give the basic building blocks to construct chiral Lagrangians together with their transformation properties under Lorentz transformations, chiral symmetry, parity, charge conjugation and Hermiticity. Then, the most general lowest order Lagrangian invariant under the previous symmetry transformations is constructed in Sec. 1.10. In Sec. 1.11, the Lagrangians up to order $\mathcal{O}(p^4)$ are given, whereas in Sec. 1.13 the extension of the formalism to include explicit resonances is reviewed. Finally, in Sec. 1.12, an example of an actual calculation made from the deduced chiral Lagrangians is performed.

1.2 Goldstone theorem

Let A be a generic observable, and consider the continuous global symmetry group $\mathfrak{G}$, that leaves invariant the ground state, $|0\rangle$. Then

$$\mathfrak{g}\,|0\rangle \quad \stackrel{\mathfrak{g}\in\mathfrak{G}}{\longrightarrow} \quad \mathfrak{g}\,|0\rangle \equiv e^{-i\theta_a Q_a}\,|0\rangle \tag{1.1}$$

$$\langle 0\,|A|\,0\rangle \quad \longrightarrow \quad \left\langle 0\left|\mathfrak{g}^{-1}A\mathfrak{g}\right|0\right\rangle \tag{1.2}$$

To first order in the parameters θ_a,

$$\left\langle 0\left|\mathfrak{g}^{-1}A\mathfrak{g}\right|0\right\rangle = \left\langle 0\left|e^{+i\theta_a Q_a}Ae^{-i\theta_a Q_a}\right|0\right\rangle = \langle 0\,|A|\,0\rangle + i\,\langle 0\,|\,[\theta_a Q_a, A]\,|\,0\rangle + \mathcal{O}(\theta^2)\ . \tag{1.3}$$

If each charge Q_a is a Noether charge, then $Q = \theta_a Q_a$ is conserved with $j^\mu = \sum \theta_a j_a^\mu$ the associated current,

$$Q \;=\; \int \mathrm{d}^3x\ j^0(\vec{x},t)\ , \tag{1.4}$$

$$\frac{\partial j^\mu(\vec{x},t)}{\partial x^\mu} \;=\; 0\ . \tag{1.5}$$

Now consider the vacuum expectation value, $\langle\cdots\rangle_{\rm VAC}$, of the conmutator of the operator A with the current (instead of the charge),

$$\begin{aligned}
&\left\langle\left[j^\lambda(y),A(x)\right]\right\rangle_{\rm VAC} = \\
&= \sum_N \left(\left\langle 0\left|j^\lambda(y)\right|N\right\rangle\langle N\left|A(x)\right|0\rangle - \langle 0\left|A(x)\right|N\rangle\left\langle N\left|j^\lambda(y)\right|0\right\rangle\right) \\
&= \sum_N \left(\left\langle 0\left|j^\lambda(0)\right|N\right\rangle\langle N\left|A(0)\right|0\rangle e^{-iP_N(y-x)} - \langle 0\left|A(0)\right|N\rangle\left\langle N\left|j^\lambda(0)\right|0\right\rangle e^{-iP_N(x-y)}\right) \\
&= \frac{i}{(2\pi)^3}\int \mathrm{d}^4p\left(\rho^\lambda(p)e^{-ip(y-x)} - \tilde\rho^\lambda(p)e^{-ip(x-y)}\right) \ , \qquad (1.6)
\end{aligned}$$

where

$$i\,(2\pi)^{-3}\,\rho^\lambda(p) = \sum_N \left\langle 0\left|j^\lambda(0)\right|N\right\rangle\langle N\left|A(0)\right|0\rangle\,\delta(p-p_N) \qquad (1.7a)$$

$$i\,(2\pi)^{-3}\,\tilde\rho^\lambda(p) = \sum_N \langle 0\left|A(0)\right|N\rangle\left\langle N\left|j^\lambda(0)\right|0\right\rangle\,\delta(p-p_N)\ . \qquad (1.7b)$$

Due to Lorentz invariance $\rho(p)$ and $\tilde\rho(p)$ must have the form

$$\rho^\lambda(p) = p^\lambda\rho_n(p^2)\theta(p^0) \qquad (1.8)$$

$$\tilde\rho^\lambda(p) = p^\lambda\tilde\rho_n(p^2)\theta(p^0)\ . \qquad (1.9)$$

When these expressions are inserted into Eq. (1.6), the p^λ can be written as derivatives, so that:

$$\begin{aligned}
&\left\langle\left[j^\lambda(y),A(x)\right]\right\rangle_{\rm VAC} = \\
&= -\frac{1}{(2\pi)^3}\frac{\partial}{\partial y_\lambda}\int \mathrm{d}^4p\left(\rho_n(p^2)\theta(p^0)e^{-ip(y-x)} + \tilde\rho_n(p^2)\theta(p^0)e^{-ip(x-y)}\right) \\
&= -\frac{\partial}{\partial y_\lambda}\int \mathrm{d}\mu^2\left(\rho_n(\mu^2)\Delta_+(y-x;\mu^2) + \tilde\rho_n(\mu^2)\Delta_+(x-y;\mu^2)\right) \ , \qquad (1.10)
\end{aligned}$$

where

$$\Delta_+(z;\mu^2) = \frac{1}{(2\pi)^3}\int \mathrm{d}^4p\theta(p^0)e^{-ipz}\delta(p^2-\mu^2) \qquad (1.11)$$

is the propagator containing the particle contribution, but not the antiparticle one, due to the $\theta(p^0)$ factor. An identity was inserted through

$$\rho_n(p^2) = \int \mathrm{d}\mu^2\delta(p^2-\mu^2)\rho_n(\mu^2)\ ,$$

and analogously for $\tilde\rho(p^2)$. Now, if $y-x$ is spacelike, $(y-x)^2<0$, then the time component is not invariant under a proper Lorentz transformation, so $\Delta_+(z;\mu^2)$ can depend only on z^2 and μ^2, which implies $\Delta_+(y-x;\mu^2) = \Delta_+(x-y;\mu^2)$. In addition, due to microcausality, in this case all conmutators must vanish when evaluated for y and x with $y-x$ spacelike, and then

$$\left\langle\left[j^\lambda(y),A(x)\right]\right\rangle_{\rm VAC} = -\frac{\partial}{\partial y_\lambda}\int \mathrm{d}\mu^2\Delta_+(y-x;\mu^2)\left(\rho_n(\mu^2)+\tilde\rho_n(\mu^2)\right) = 0\ ,$$

and whence

$$\rho_n(\mu^2) = -\tilde{\rho}_n(\mu^2) \quad \forall \mu^2 \tag{1.12}$$

Now, going back to the general case where Δ_+ is not even,

$$\Big\langle \Big[j^\lambda(y), A(x) \Big] \Big\rangle_{\rm VAC} = -\frac{\partial}{\partial y_\lambda} \int \mathrm{d}\mu^2 \rho_n(\mu^2) \Big(\Delta_+(y-x;\mu^2) - \Delta_+(x-y;\mu^2) \Big) \ , \tag{1.13}$$

and, as the current is conserved, Eq. (1.5), then

$$\begin{aligned} & -\frac{\partial}{\partial y^\lambda} \Big\langle \Big[j^\lambda(y), A(x) \Big] \Big\rangle_{\rm VAC} = \\ = \ & -\int \mathrm{d}\mu^2 \rho_n(\mu^2) \, \Box_y \Big(\Delta_+(y-x;\mu^2) - \Delta_+(x-y;\mu^2) \Big) = \\ = \ & +\int \mathrm{d}\mu^2 \mu^2 \rho_n(\mu^2) \Big(\Delta_+(y-x;\mu^2) - \Delta_+(x-y;\mu^2) \Big) = 0 \ , \end{aligned} \tag{1.14}$$

because Δ_+ satisfies

$$\begin{aligned} (\Box_y + \mu^2) \Delta_+(y-x;\mu^2) &= 0 \\ \Box_y \ \Delta_+(y-x;\mu^2) &= \Box_y \ \Delta_+(x-y;\mu^2) \ . \end{aligned}$$

An important conclusion is reached, namely that

$$\mu^2 \rho(\mu^2) = 0 \ , \tag{1.15}$$

but it should not be concluded that $\rho(\mu^2) = 0$, rather, it is shown in what follows that $\rho(\mu^2) \sim \delta(\mu^2)$. We now try to explicitly integrate Eq. (1.13) for $\lambda = 0$:

$$\begin{aligned} \Big\langle \Big[j^0(y), A(x) \Big] \Big\rangle_{\rm VAC} &= \frac{i}{(2\pi)^3} \int \mathrm{d}^4 p \int \mathrm{d}\mu^2 \rho_n(\mu^2) p^0 \theta(p^0) \delta(p^2 - \mu^2) \Big(e^{-ip(y-x)} + e^{+ip(y-x)} \Big) \\ &= \frac{1}{2} \frac{i}{(2\pi)^3} \int \mathrm{d}\mu^2 \rho_n(\mu^2) \int \mathrm{d}^3 \vec{p} \Big(e^{-i\omega(\vec{p}^2)(y^0-x^0)} e^{i\vec{p}(\vec{y}-\vec{x})} + e^{i\omega(\vec{p}^2)(y^0-x^0)} e^{-i\vec{p}(\vec{y}-\vec{x})} \Big) \ , \end{aligned}$$

with $\omega(\vec{p}^2) = \sqrt{\vec{p}^2 + \mu^2}$. In order to go further, since the integration in $\vec{p}$ cannot be easily performed unless one takes $x^0 = y^0$, we integrate instead over $\vec{y}$. On the l.h.s. this will give the conmutator of the charge, whereas the integral in the r.h.s. will simply give a Dirac delta function $\delta^{(3)}(\vec{p})$, so that

$$\langle [Q, A(x)] \rangle_{\rm VAC} = \frac{i}{2} \int \mathrm{d}\mu^2 \rho(\mu^2) \Big(e^{-i\mu(y^0-x^0)} + e^{i\mu(y^0-x^0)} \Big) \ . \tag{1.16a}$$

For the case $x^0 = y^0$, it reduces to:

$$\Big\langle \Big[Q, A(y^0, \vec{x}) \Big] \Big\rangle_{\rm VAC} = i \int \mathrm{d}\mu^2 \rho(\mu^2) \ . \tag{1.16b}$$

To satisfy together Eqs. (1.15) and (1.16), it is necessary then that

$$\rho(\mu^2) = i\delta(\mu^2) \langle [Q, A(x)] \rangle_{\rm VAC} \ . \tag{1.17}$$

In view of this result and comparing with Eq. (1.7), we notice that there must exist a single-particle state with $p_N^2 = 0$, that is, a massless particle. This is the content of the Goldstone

theorem [9, 10]. In words, it states that, for each generator Q that does not anihilate the ground state, there must be a spin-zero massless particle, called Goldstone boson, with the same quantum numbers as Q (because this particle is generated from the vacuum through these operators.)

For example, consider QCD, with $SU(2)_L \otimes SU(2)_R \to SU(2)_V$. As $SU(2)$ has three generators, we find three Goldstone bosons, the isospin triplet of pions, π^+, π^- and π^0. If instead we consider $SU(3)$, then eight generators are present, so the set of Goldstone bosons is enlarged to π^+, π^-, π^0, η_8, K^+, K^-, K^0 and $\bar{K}^0$. Of course, as this symmetry is not exact, the masses are not exactly zero, being this effect more remarkable in $SU(3)$.

1.3 Properties of nonlinear Lagrangians

Throughout the next sections (Secs. 1.3 to 1.7) the formalism for the construction of effective Lagrangians [20, 21] will be reviewed. This will make possible to deduce the most general invariant Lagrangian under chiral symmetry transformations. It is worth mentioning that this formalism is very general and, besides the applications that we study here, it is widely used in other fields of theoretical physics, *i.e.*, in supersymmetry [187].

Let L be the Lagrangian of a specific quantum field theory, in terms of some fields, ϕ,

$$L[\phi] = L_0[\phi] + L_1[\phi] \tag{1.18}$$

being L_0 the free field Lagrangian and L_1 the interaction Lagrangian. The following change of variables is done,

$$\phi = \chi F[\chi] \qquad F[0] = 1 \tag{1.19}$$

so that, to first order in χ, $\phi = \chi + \mathcal{O}(\chi^2)$ and χ creates and anihilates the same particles than ϕ does. In terms of χ, the Lagrangian is

$$L[\chi F[\chi]] = L_0[\chi] + L_2[\chi] \ , \tag{1.20}$$

or, in words, we get the same free Lagrangian, but the interaction Lagrangian is different. However, there is a theorem [188] valid for relativistic quantum field theory with weak restrictions on the form of $F[\chi]$ that states that the on-shell matrix elements of this Lagrangian are the same than those obtained from

$$L'[\phi] = L_0[\phi] + L_2[\phi] \tag{1.21}$$

In all physically relevant cases, L and F are expansions in power of the ϕ fields and their derivatives (this will be the case of QCD and ChPT), and this condition is enough for the theorem to be valid. The very reason of the validity of the theorem lies on the fact that terms of order greater than the first do not contribute on shell because they do not contain one-particle singularities. This theorem holds for the exact solution, but also order-by-order, as we show in the following lines. Consider, for an arbitrary parameter a, the Lagrangian

$$L[\phi; a] = a^{-2} L[a\phi] \ , \tag{1.22}$$

so that the free Lagrangian remains invariant.

For a connected Feynman diagram, if we denote by

P	the power of a,
V	the number of vertices,
N_i	the number of lines flowing into/from vertex i,
E	the number of external legs,
I	the number of internal legs,
L	the number of loops,

then it results that:

$$P = \sum_{i=1}^{V} (N_i - 2) \ .$$

Because of the following identities,

$$\sum_{i}^{V} N_i = E + 2I \ , \tag{1.23}$$

$$L = I - V + 1 \ , \tag{1.24}$$

then

$$P = E - 2 + 2L \ . \tag{1.25}$$

This means that, for a fixed reaction (this is, for the same external particles, fixed E) the power of a increases with the number of loops. The aforementioned theorem is valid for the exact solution, and we are expressing the latter as a power series in a, which has shown to be equivalent to a power series in the number of loops. Introducing a in the field transformation Eq. (1.19),

$$a\phi = a\chi F[a\chi]$$

we get

$$L[\phi; a] = a^{-2} L[a\chi F[a\chi]] \ . \tag{1.26}$$

The same rules as before apply to $a^{-2}L_2[a\chi]$ and then, because of the aforementioned theorem on reparametrization field independence, each coeffcient in the a power expansion of the on-shell S-matrix should be the same. Note that each of these coefficient-amplitude are calculated with the same number of loops.

1.4 Standard form of nonlinear representations

Consider a connected, compact, semisimple Lie group $\mathfrak{G}$ with n parameters, and a continuous subgroup $\mathfrak{H} \subseteq \mathfrak{G}$ whose generators anihilate the vacuum, $\mathfrak{H}\,|0\rangle = 0$, $e^{iV_i\phi_i}\,|0\rangle = |0\rangle$. Let

$$V_i, \quad i = 1, \ldots, n - d \tag{1.27}$$

be the generators of $\mathfrak{H}$ and

$$A_l, \quad l = 1, \ldots, d \tag{1.28}$$

be the remaining generators of the group $\mathfrak{G}$. For the case of Chiral Perturbation Theory, though it will be treated in detail later in Secs. 1.8–1.10, let us determine now the group $\mathfrak{G}$

and the subgroup $\mathfrak{H}$. The massless QCD Lagrangian with N_f flavours has a global invariance under the group $SU_L(N_\mathrm{f}) \otimes SU_R(N_\mathrm{f}) \otimes U_V(1) \otimes U_A(1)$. The $U_V(1)$ is exactly conserved and its generator is the baryon number. The $U_A(1)$ symmetry is broken at the quantum level, giving rise to the so called $U_A(1)$ anomaly. We identify $\mathfrak{G}$ with the group of chiral transformations, $\mathfrak{G} = SU_L(N_\mathrm{f}) \otimes SU_R(N_\mathrm{f})$. Chiral symmetry is spontaneously broken [9–14], and the subgroup that remains unbroken is $\mathfrak{H} = SU_V(N_\mathrm{f}) \equiv SU_{L+R}(N_\mathrm{f})$, that originates the famous eightfold way [15]. The lightest pseudoscalar mesons are the Goldstone bosons generated by the spontaneous symmetry breaking of $\mathfrak{G}$ into $\mathfrak{H}$.

Any element $\mathfrak{g} \in \mathfrak{G}$ has the form $\mathfrak{g} = e^{\bar{\xi}A + \bar{u}V}$, where $\bar{\xi}A$ means $\sum_{i=1}^{d} \bar{\xi}_i \cdot A_i \equiv \bar{\xi}_i A_i$,[1] and analogously for $\bar{u}V$. With a suitable choice of parameters, this element can be uniquely decomposed in a neighborhood of the identity element of $\mathfrak{G}$, denoted by $\mathfrak{e}$, as $\mathfrak{g} = e^{\xi A} e^{uV}$. We now proof this latter statement.

For infinitesimal transformations, this is clear, since

$$\mathfrak{g} = e^{\bar{\xi}A + \bar{u}V} \simeq \mathfrak{e} + \bar{\xi}A + \bar{u}V \simeq e^{\bar{\xi}A} e^{\bar{u}V} \ , \tag{1.29}$$

but we can show that this decomposition is more general than the restricted case of infinitesimal transformations. If $\mathfrak{H}$ is an invariant subgroup, then

$$\begin{aligned} \mathfrak{g} &= e^{\bar{\xi}A + \bar{u}V} = \lim_{N\to\infty} \left(\mathfrak{e} + \frac{\bar{\xi}A}{N} + \frac{\bar{u}V}{N} \right)^N = \\ &= \lim_{N\to\infty} \left(\mathfrak{g}_A \mathfrak{h}_V \right)^N = \lim_{N\to\infty} \left(\mathfrak{g}_A \mathfrak{h}_V \mathfrak{g}_A^{-1} \right) \left(\mathfrak{g}_A^2 \mathfrak{h}_V \mathfrak{g}_A^{-2} \right) \dots \left(\mathfrak{g}_A^N \mathfrak{h}_V \mathfrak{g}_A^{-N} \right) \mathfrak{g}_A^N = \\ &= \mathfrak{h} \lim_{N\to\infty} {\mathfrak{g}_A}^N = \mathfrak{h} e^{\bar{\xi}A} = \mathfrak{h} e^{\bar{\xi}A} \mathfrak{h}^{-1} \mathfrak{h} = e^{\xi A} \mathfrak{h} = e^{\xi A} e^{uV} \end{aligned} \tag{1.30}$$

$\mathfrak{g}_A = e^{\bar{\xi}A/N}$ and $\mathfrak{h}_V = e^{\bar{u}V/N}$ are infinitesimal transformations because $N \to \infty$. Use of the invariance of $\mathfrak{H}$ has been made to put ${\mathfrak{g}_A}^m \mathfrak{h}_V {\mathfrak{g}_A}^{-m} = \mathfrak{h}_V^{(m)}$, where the last superscript means that it is some element of $\mathfrak{H}$, depending of the power of $\mathfrak{g}_A$ in the left-hand side of the equation. As $\mathfrak{H}$ is a subgroup, the product of these $\mathfrak{h}_V^{(m)}$ is again some element $\mathfrak{h} \in \mathfrak{H}$, and we write it as $\mathfrak{h} = e^{uV}$. The orthonormal condition of the generators, $\mathrm{Tr}(V_i A_j) = 0$,[2] has been used to write $\mathfrak{h} e^{\bar{\xi}A} \mathfrak{h}^{-1} = e^{\xi A}$ for some new coordinates ξ. Let us calculate

$$\mathrm{Tr}(V_i \mathfrak{h} A_j \mathfrak{h}^{-1}) = \mathrm{Tr}(\mathfrak{h}^{-1} V_i \mathfrak{h} A_j) = E_{ik} \mathrm{Tr}(V_k A_j) = 0 \ , \tag{1.31}$$

where it was used that $\mathfrak{h}^{-1} V_i \mathfrak{h} = E_{ik} V_k$ because $\mathfrak{H}$ is invariant. The above equation implies that $\mathfrak{h} A_j \mathfrak{h}^{-1}$ contains just A generators, otherwise the trace would be different from zero. Thus,

$$\mathfrak{h} e^{\bar{\xi}A} \mathfrak{h}^{-1} = \sum_n \frac{1}{n!} \mathfrak{h} \bar{\xi}_j A_j \mathfrak{h}^{-1} \ \mathfrak{h} \bar{\xi}_k A_k \mathfrak{h}^{-1} \cdots = \sum_n \frac{1}{n!} \underbrace{C_{jl} \bar{\xi}_j}_{\xi_l} A_l \cdots = \sum_n \frac{1}{n!} (\xi A)^n = e^{\xi A} \ . \tag{1.32}$$

So we have shown, in the case of $\mathfrak{H}$ being an invariant subgroup, that

$$\mathfrak{g} = e^{\bar{\xi}A + \bar{u}V} = e^{\xi A} e^{uV} = e^{uV} e^{\bar{\xi}A} \ , \tag{1.33}$$

[1] In the following, we use the sum convention of Einstein on repeated indices.

[2] This is the one that holds for chiral symmetry.

without restricting to the case of infinitesimal transformations. The last equality follows from one of the intermediate steps of Eq. (1.30). Finally, let us also note that the transformation $\mathfrak{g} = e^{\bar{\xi}A+\bar{u}V} = e^{\xi A}e^{uV}$ induces a transformation of variables $(\bar{\xi}, \bar{u}) \to (\xi, u)$, which has, for the case $\mathfrak{g} = \mathfrak{e}$, a non-zero Jacobian, namely, $J = 1$. Thus, invoking continuity, the transformation has a non-zero Jacobian in a neighborhood of the identity element of $\mathfrak{G}$, so the transformation is valid, which is another proof.

Consider now the element $\mathfrak{g}_0 e^{\xi A}$ with $\mathfrak{g}_0 \in \mathfrak{G}$. As shown, we can write

$$\mathfrak{g}_0 e^{\xi A} = e^{\xi' A} e^{u' V} \text{ where } \xi' \equiv \xi'(\xi, \mathfrak{g}_0) \text{ and } u' \equiv u'(\xi, \mathfrak{g}_0) \tag{1.34}$$

Let also be a unitary and linear representation $\mathfrak{h} : \psi \to D(\mathfrak{h})\psi$, with $\mathfrak{h} \in \mathfrak{H}$. To each element $\mathfrak{g}_0$ we assign a pair of transformations

$$\begin{aligned} \mathfrak{g}_0 : \quad & \xi \to \xi' \\ & \psi \to D\left(e^{u' V}\right)\psi \ . \end{aligned} \tag{1.35}$$

These transformations give a non-linear realization of the group $\mathfrak{G}$. To show this, notice that

$$\begin{aligned} &\mathfrak{g}_0 e^{\xi A} = e^{\xi' A} e^{u' V} \\ &\mathfrak{g}_1 e^{\xi' A} = e^{\xi'' A} e^{u'' V} \\ &\mathfrak{g}_1 \mathfrak{g}_0 e^{\xi A} = \mathfrak{g}_1 e^{\xi' A} e^{u' V} = e^{\xi'' A} e^{u'' V} e^{u' V} = e^{\chi'' A} e^{u''' V} \ , \end{aligned}$$

so that

$$\begin{aligned} \mathfrak{g}_1 \mathfrak{g}_0 : & \xi \to \xi'' \\ & \psi \to D\left(e^{u''' V}\right)\psi = D\left(e^{u'' V} e^{u' V}\right)\psi = D\left(e^{u'' V}\right) D\left(e^{u' V}\right)\psi \ , \end{aligned} \tag{1.36}$$

which is the required composition rule:

$$\xi'' = \xi''(\xi'(\xi, \mathfrak{g}_0), \mathfrak{g}_1) \ , \tag{1.37}$$

$$D(e^{u''' V}) = D(e^{u'' V}) D(e^{u' V}) \ . \tag{1.38}$$

The matrices $D(\mathfrak{H})$ of a representation depend just on the elements of the group: this is the case for the transformation on ξ under $\mathfrak{h} \in \mathfrak{H}$. However, the transformation on ψ depends also on the ξ through u', and thus this transformation is meaningful (and the equality in Eq. (1.36) is true) only if considered together with that on ξ. In what follows, we will suppose that $D(\mathfrak{h})$ is in its completely decomposed form, and we will call Eq. (1.35) our *standard form* for a realization.

Let us see now that, when restricted to the subgroup $\mathfrak{H}$, the realization Eq. (1.35) becomes a linear representation. First, we have:

$$\mathfrak{h} e^{\xi A} = \mathfrak{h} e^{\xi A} \mathfrak{h}^{-1} \mathfrak{h} = e^{\xi' A} \mathfrak{h} \equiv e^{\xi' A} e^{uV} \ , \tag{1.39}$$

and thus $D(e^{uV}) = D(\mathfrak{h})$. As u is obviously independent of ξ, then this transformation is linear. Second, $\xi' = D^{(b)}(\mathfrak{h})\xi$, where $D^{(b)}$ is a linear representation of $\mathfrak{H}$. For example, If we

have $\mathfrak{G} = SU_L(N) \otimes SU_R(N)$ and $\mathfrak{H} = SU_V(N)$, then $D^{(b)}$ is the adjoint representation of $SU(N)$:

$$\xi'_a A_a = \mathfrak{h}\xi_b A_b \mathfrak{h}^{-1} = \xi_b \mathfrak{h} A_b \mathfrak{h}^{-1} = \underbrace{\mathcal{D}(\mathfrak{h})_{ab}\xi_b}_{\xi'_a} A_a \ ,$$

where $\mathcal{D}$ is the adjoint representation, which we call, from now on, $D^{(b)}$, and, as promised,

$$\xi' = \mathcal{D}(\mathfrak{h})\xi \ .$$

There is a special case in which the form of the transformation of ξ can be further simplified, namely, when the group $\mathfrak{G}$ has an automorphism $R : \mathfrak{g} \to R(\mathfrak{g})$ so that

$$\begin{array}{ccc} V_i & \stackrel{R}{\to} & V_i \\ A_l & \stackrel{R}{\to} & -A_l \end{array}$$

Chiral groups are within this case: the parity operator induces an automorphism that changes the sign of the axial generators. Applying the automorphism to

$$e^{u'V} = e^{-\xi' A}\mathfrak{g}_0 e^{\xi A}$$

we get

$$e^{u'V} = e^{\xi' A} R(\mathfrak{g}_0) e^{-\xi A}$$

so that

$$e^{2\xi' A} = \mathfrak{g}_0 e^{2\xi A} R(\mathfrak{g}_0^{-1}) \ . \tag{1.40}$$

For chiral groups, one has $\mathfrak{g} = \mathfrak{g}_L\mathfrak{g}_R$, with $\mathfrak{g}_L = e^{\varphi\lambda_L}$ and $\mathfrak{g}_R = e^{\theta\lambda_R}$. Then $R(\mathfrak{g}) = e^{\varphi\lambda_R}e^{\theta\lambda_L}$, and

$$\begin{array}{rcl} e^{2\xi A} & = & e^{2\xi\lambda_R}e^{-2\xi\lambda_L} \\ e^{2\xi' A} & = & e^{\varphi\lambda_L}e^{\theta\lambda_R}e^{2\xi A}e^{-\varphi\lambda_R}e^{-\theta\lambda_L} \\ & = & e^{\varphi\lambda_L}e^{-2\xi\lambda_L}e^{-\theta\lambda_L}e^{\theta\lambda_R}e^{2\xi\lambda_R}e^{-\varphi\lambda_R} \end{array}$$

thus

$$\begin{array}{rcl} e^{2\xi'\lambda_R} & = & e^{\theta\lambda_R}e^{2\xi\lambda_R}e^{-\varphi\lambda_R} \\ e^{-2\xi'\lambda_L} & = & e^{\varphi\lambda_L}e^{-2\xi\lambda_L}e^{-\theta\lambda_L} \end{array}$$

Both results are consistent, for the generators λ_L and λ_R behave in their respective spaces as Gell–Mann matrices, and so we can obtain the transformation law for $e^{-2\xi\lambda_L}$ from that of $e^{2\xi\lambda_R}$ because

$$e^{-2\xi'\lambda_R} = e^{\varphi\lambda_R}e^{-2\xi\lambda_R}e^{-\theta\lambda_R}$$

which is the same transformation for $e^{-2\xi\lambda_L}$ with the change $L \leftrightarrow R$.

1.5 Classification of all nonlinear realizations

In this section, we give the most general form of a nonlinear realization. It will be shown that all of them can be brought into the *standard form* studied above, by a reparametrization of fields, see Eq. (1.19) in Sec. 1.3.

This problem will be considered from a broader point of view. Let M be a n-dimensional real differentiable manifold. Let $\mathfrak{G}$ be a compact connected semisimple Lie group, used as a transformation over M,

$$\mathfrak{g} : x \to T_{\mathfrak{g}} x \qquad x \in M \ , \ \mathfrak{g} \in \mathfrak{G} \tag{1.41}$$

where x can denote both a point of M and a n-dimensional column vector in some coordinate system. We suppose that $T_{\mathfrak{g}} x$ is an analytic function both on $\mathfrak{g}$ and x. Next we identify the fields of the effective theory to be studied with some particular set of cordinates in M. Thus, the problem of finding all field transformation laws under a group is equivalent to find all possible ways of realizing a group in a differentiable manifold M.

It turns out to be advantageous to consider the problem in this manner, since going from one set of fields to another just means a change in the coordinates of M, which has no geometrical consequences, nor changes on the on-shell S-matrix elements. The *analyticity* hypothesis is necessary due to the *power series expansions* we make in field theory, and also because we want to preserve *locality*. However, the analogy is not complete, since in field theory *general coordinates transformations are not allowed*, as seen in Sec. 1.3; rather, these transformations must preserve the origin, according to Eq. (1.19). This leads us to suppose that there exists a special point in the manifold M, that we call *origin*, and allow just for coordinate systems that share the origin, *i.e.*, systems in which the origin is represented by the same point. There is no need to characterize globally the action of the group on the manifold, but just in a neighborhood of the origin, because fields are ultimately used in a power-series expansion. Also, for the usual properties of connected compact Lie groups, we will pay attention only to a neighborhood of the identity element of $\mathfrak{G}$.

There can be elements of the group $\mathfrak{G}$ that leave invariant the origin of M. These elements form a subgroup $\mathfrak{H}$, $\mathfrak{H} \subseteq \mathfrak{G}$, called the origin stability group. It can consist of a single element, the identity element of $\mathfrak{G}$, and could extend up to the whole group $\mathfrak{G}$. We will suppose that $\mathfrak{H}$ is continuous.

Summarizing, our problem can be stated as follows: given $\mathfrak{G}$ and $\mathfrak{H}$, we want to find the most general way of realizing them over the manifold M, with all the restrictions commented above. This problem, as shown in what follows, is equivalent to that of finding all nonlinear realizations of $\mathfrak{G}$ that become linear when restricted to the subgroup $\mathfrak{H} \subseteq \mathfrak{G}$.

Theorem (Linearization theorem)**.** *Let $\mathfrak{G}$ be a semisimple connected compact Lie group and let $\mathfrak{H} \subseteq \mathfrak{G}$ be the subgroup of all elements that leave invariant the origin so that, in these coordinates,*

$$T_{\mathfrak{h}} 0 = 0 \quad \forall \ \mathfrak{h} \in \mathfrak{H}$$

Then there exists a set of coordinates y in a neighborhood of the origin so that, in these new

coordinates,

$$T_{\mathfrak{h}} y = D(\mathfrak{h}) y \quad \forall\ \mathfrak{h} \in \mathfrak{H}\ , \tag{1.42}$$

being $D(\mathfrak{h})$ *a linear representation of* $\mathfrak{H}$.

Proof. Given that $T_{\mathfrak{g}} x$ is continuous in x and that $T_{\mathfrak{h}} 0 = 0$ it follows that, close to the origin, there must exist a neighborhood which is invariant under the action of the subgroup $\mathfrak{H}$, because the latter is continuous, compact and bounded. Thus, expanding $T_{\mathfrak{h}} x$,

$$T_{\mathfrak{h}} x = D(\mathfrak{h}) x + \mathcal{O}(x^2)\ ,$$

being $D(\mathfrak{h})$ a linear realization of $\mathfrak{H}$. We define now n functions,

$$y = \int_{\mathfrak{H}} \mathrm{d}\mathfrak{h}\ D^{-1}(\mathfrak{h}) T_{\mathfrak{h}} x\ , \tag{1.43}$$

where $\mathrm{d}\mathfrak{h}$ is the invariant measure and the group integral is normalized to $\int_{\mathfrak{H}} \mathrm{d}\mathfrak{h} = 1$. The functions y are analytical in x and, in fact, we have

$$y = x + \mathcal{O}(x^2)\ .$$

Whence the Jacobian determinant $[\partial y / \partial x]$ is one in the origin, and so we can use the y as a new system of coordinates around the origin. Under the action of an element $\mathfrak{h}_0 \in \mathfrak{H}$,

$$\begin{aligned} \mathfrak{h}_0 : y \ \longrightarrow\ & \int_{\mathfrak{H}} \mathrm{d}\mathfrak{h}\ D^{-1}(\mathfrak{h}) T_{\mathfrak{h}} T_{\mathfrak{h}_0} x = \int_{\mathfrak{H}} \mathrm{d}\mathfrak{h}\ D^{-1}(\mathfrak{h}) T_{\mathfrak{h}\mathfrak{h}_0} x = \\ = \ & \int_{\mathfrak{H}} \mathrm{d}(\mathfrak{h}\mathfrak{h}_0)\ D^{-1}(\mathfrak{h}\mathfrak{h}_0\mathfrak{h}_0^{-1}) T_{\mathfrak{h}\mathfrak{h}_0} x = \\ = \ & D(\mathfrak{h}_0) \int_{\mathfrak{H}} \mathrm{d}(\mathfrak{h}\mathfrak{h}_0)\ D^{-1}(\mathfrak{h}\mathfrak{h}_0) T_{\mathfrak{h}\mathfrak{h}_0} x = D(\mathfrak{h}_0) y\ , \end{aligned}$$

and this proves the theorem. □

This theorem is useful as a simple test of linearizability, and also, if the transformation law can be linearized, it provides a formula to obtain the new coordinates.

Let us proceed now to consider our main problem. Our complete set of orthonormal generators is composed by V_i, the generators of $\mathfrak{H}$ and A_l, the rest of the generators of $\mathfrak{G}$. Let us define the differentiable manifold N consisting of all the points of the form $T_{\mathfrak{g}} 0$. We can associate the coordinates ξ_l to the points of N through $e^{\xi A} 0$. As every transformation rule can be written as $\mathfrak{g} = e^{\xi A} e^{uV}$ in a neighborhood of the identity, it is clear then that in some neighborhood of the origin we can write

$$\forall\ x \in N \quad x = \mathfrak{g} 0 = e^{\xi A} e^{uV} 0 = e^{\xi A} 0\ \text{, because } e^{uV} 0 = 0$$

Therefore, in the aforesaid neighborhood there is a unique set of parameters ξ_l for each point of N acting as coordinates for N in that neighborhood. Let us prove this last statement, namely, that $N = \{ e^{\xi A} 0 = e^{\xi A} e^{uV} 0 = \mathfrak{g} 0 \mid \mathfrak{g} \in \mathfrak{G} \}$ admits as a unique system of coordinates

the parameters ξ_a, $a = 1, \ldots, d$. Suppose that there exist two such sets, $(\xi_1)_a$ and $(\xi_2)_a$, $a = 1, \ldots, d$. Then

$$e^{\xi_1 A}0 = e^{\xi_2 A}0 \to e^{-\xi_2 A}e^{\xi_1 A}0 = 0 \to e^{-\xi_2 A}e^{\xi_1 A} = e^{uV} \in \mathfrak{H} \ .$$

Performing a power expansion in the last equality,

$$-(\xi_2)_l A_l + (\xi_1)_l A_l - (\xi_1)_l(\xi_2)_m A_l A_m + \cdots = u_i V_i + \cdots \ ,$$

where the ellipsis indicate higher orders in the power expansion. In order to generate a V we have to go to the $A_l A_m$ product, so the u are $\mathcal{O}(\xi^2)$ and the leading term of the left hand side of the previous equation must be zero, so $\xi_1 = \xi_2$.

The transformation properties of N are now completely determined,

$$\mathfrak{g}(e^{\xi A}0) = e^{\xi' A}e^{u' V}0 = e^{\xi' A}0 \ .$$

Let us now introduce $n - d$ coordinates in a real vector ψ. Then a point of M, in some neighborhood of the origin has coordinates $(\xi, \psi)^*$. The origin 0 is now $(0, 0)^*$. Points of the form $(\xi, 0)^*$ are in N, for:

$$\mathfrak{g}(\xi, 0)^* = \mathfrak{g}e^{\xi A}(0, 0)^* = e^{\xi' A}e^{u' V}(0, 0)^* = e^{\xi' A}(0, 0)^* = (\xi', 0)^* \qquad \xi' \equiv \xi'(\xi, \mathfrak{g}) \ .$$

The representation of $\mathfrak{G}$ is then reducible. From the *linearization theorem* above, it follows that the coordinates $(\xi, \psi)^*$ can be chosen so that $\mathfrak{H}$ acts linearly, since it leaves the origin invariant. With a suitable choice of coordinates ψ, the representation, since $\mathfrak{H}$ is compact, becomes completely irreducible,

$$e^{uV}(\xi, \psi)^* = \left(D^{(b)}(e^{uV})\xi, D(e^{uV})\psi\right)^* \ ,$$

and the ξ transform under the adjoint representation of $\mathfrak{G}$ restricted to $\mathfrak{H}$, $D^{(b)}$, induced by

$$\begin{aligned} e^{\xi' A} &= e^{uV}e^{\xi A}e^{-uV} \\ \xi' &= D^{(b)}(\mathfrak{h})\xi \end{aligned}$$

We introduce new coordinates, that we call *standard coordinates*,

$$(\xi, \psi) = e^{\xi A}(0, \psi)^* \ , \tag{1.44}$$

connecting the subspace of $\xi = 0$ with that of ξ. For $\xi = 0$, we have $(0, \psi) = (0, \psi)^*$, the Jacobian is thus 1 and the transformation is allowed in a neighborhood of the origin. We can work out the transformation of the new coordinates under the action of $\mathfrak{h} \in \mathfrak{H}$:

$$\mathfrak{h}(\xi, \psi) = \mathfrak{h}e^{\xi A}(0, \psi)^* = e^{\xi' A}\mathfrak{h}(0, \psi)^* = e^{\xi' A}(0, D(\mathfrak{h})\psi)^* = (\xi', D(\mathfrak{h})\psi) \ , \tag{1.45}$$

with $\xi' = D^{(b)}(\mathfrak{h})\xi$. Whence, we have proven the following:

Lemma. *Under the subgroup $\mathfrak{H}$ the standard coordinates transform as $(D^{(b)}(\mathfrak{h})\xi, D(\mathfrak{h})\psi)$ with the same linear representation as for the original coordinates.*

With the results gathered in this Section, we already know how a generic element $\mathfrak{g} \in \mathfrak{G}$ acts in the new coordinates. Let us see now that they transform like Eq. (1.35), *i.e.*, like our *standard form*:

$$\begin{aligned} \mathfrak{g}(\xi,\psi) &= \mathfrak{g}e^{\xi A}(0,\psi)^* = e^{\xi' A}e^{u' V}(0,\psi)^* = \\ &= e^{\xi' A}(0, D(e^{u' V})\psi)^* = (\xi', D(e^{u' V})\psi) \ , \end{aligned}$$

where the last step follows from the previous lemma. Therefore, we see that, as promised in the beginning of this Section, the most general nonlinear realization of a group $\mathfrak{G}$ with a subgroup $\mathfrak{H}$ that leaves invariant the origin reduces to the standard form after a suitable change of coordinates in a neighborhood of the origin.

1.6 Covariant derivatives

Through Sec. 1.5 the transformation porperties of the fields were considered, and now the transformations of their derivatives must be studied, since Lagrangian densities, used in quantum field theories, are functions of the fields and their derivatives. In Sec. 1.5 a generic set of coordinates was chosen and brought into an adequate form, called *standard form*. In this Section, essentially the same procedure is followed, but with the derivatives of the fields. Of course, the transformation properties of these derivatives are determined by those of the fields themselves. Thus, the derivatives $\partial_\mu \xi$ and $\partial_\mu \psi$ are introduced as independent coordinates on the manifold M:

$$(\xi, \psi, \partial_\mu \xi, \partial_\mu \psi)^* \ . \tag{1.46}$$

As we saw in Sec. 1.4, under the subgroup $\mathfrak{H}$, ξ and ψ transform linearly (under their respective transformations), and the associated u' are independent of ξ, and then

$$(\xi, \psi, \partial_\mu \xi, \partial_\mu \psi)^* \xrightarrow{\mathfrak{h}} (D^{(b)}(\mathfrak{h})\xi, D(\mathfrak{h})\psi, D^{(b)}(\mathfrak{h})\partial_\mu \xi, D(\mathfrak{h})\partial_\mu \psi)^* \tag{1.47}$$

The derivatives, as said, are not in *standard form*, but as shown, they transform linearly under $\mathfrak{H}$ and they can be brought into *standard form* with a suitable change of coordinates. The new coordinates, transforming in the standard way, are denoted with $D_\mu \xi$, $D_\mu \psi$, and are defined as

$$(\xi, \psi, D_\mu \xi, D_\mu \psi) = e^{\xi A}(0, \psi, \partial_\mu \xi, \partial_\mu \psi)^* \tag{1.48}$$

They are constructed so that they transform under $\mathfrak{G}$ in a *standard form*, analogous to (1.35),

$$(D_\mu \xi)' = D^{(b)}(e^{u' V})(D_\mu \xi) \tag{1.49}$$

$$(D_\mu \psi)' = D(e^{u' V})(D_\mu \psi) \ . \tag{1.50}$$

We consider now the following derivative:

$$\partial_\mu(\xi(x), \psi(x)) = \partial_\mu e^{\xi(x) A}(0, \psi(x))^* \ . \tag{1.51}$$

One has:

$$\partial_\mu e^{\xi(x) A}(0,\psi)^* = e^{\xi(x) A}\left[e^{-\xi(x) A}\partial_\mu e^{\xi(x) A}(0,\psi)^*\right] \ ,$$

and we define:[3]

$$e^{\xi(x)A}\partial_\mu e^{-\xi(x)A} \equiv p_\mu A + v_\mu V \ . \tag{1.52}$$

Inserting this above, we finally get:

$$\begin{aligned} & e^{\xi(x)A}\left[e^{-\xi(x)A}\partial_\mu e^{\xi(x)A}(0,\psi)^*\right] = e^{\xi(x)A}\left(e^{-\xi(x)A}\partial_\mu e^{\xi(x)A}\right)(0,\psi)^* + e^{\xi(x)A}(0,\partial_\mu\psi)^* \\ & = e^{\xi(x)A}\left(p_\mu A + v_\mu V + \partial_\mu\right)(0,\psi)^* \equiv (\xi,\psi,p_\mu,(\partial_\mu + v_\mu T)\psi) \ , \end{aligned} \tag{1.53}$$

where in the last step we have added two extra coordinates, representing the covariant derivatives of $\xi(x)$ and $\psi(x)$, given, respectively, by:

$$D_\mu\xi(x) = p_\mu(x) \ , \tag{1.54}$$

$$D_\mu\psi(x) = (\partial_\mu + v_\mu V)\,\psi(x) \ . \tag{1.55}$$

Let us now explicitly check the transformation rules for $D_\mu\xi$ and $D_\mu\psi$, Eq. (1.49) and Eq. (1.50). Let $\mathfrak{g} \in \mathfrak{G}$ (recall that $\mathfrak{g}$ is not space-time dependent). We have:

$$\begin{aligned} \mathfrak{g}e^{\xi A} &= e^{\xi' A}e^{u'V} \\ \mathfrak{g}\partial_\mu e^{\xi A} &= (\partial_\mu e^{\xi' A})e^{u'V} + e^{\xi' A}(\partial_\mu e^{u'V}) \end{aligned}$$

and thus, eliminating $\mathfrak{g}$,

$$\begin{aligned} \mathfrak{g} &= e^{\xi' A}e^{u'V}e^{-\xi A} \\ e^{\xi' A}e^{u'V}e^{-\xi A}\partial_\mu e^{\xi A} &= (\partial_\mu e^{\xi' A})e^{u'V} + e^{\xi' A}(\partial_\mu e^{u'V}) \\ e^{-\xi' A}\partial_\mu e^{\xi' A} &= e^{u'V}e^{-\xi A}(\partial_\mu e^{\xi A})e^{-u'V} - (\partial_\mu e^{u'V})e^{-u'V} = \\ &= e^{u'V}\underbrace{e^{-\xi A}(\partial_\mu e^{\xi A})}_{(v_\mu V + p_\mu A)}e^{-u'V} + e^{u'V}(\partial_\mu e^{-u'V}) = \\ &= e^{u'V}\left(v_\mu V + p_\mu A\right)e^{-u'V} + e^{u'V}(\partial_\mu e^{-u'V}) \equiv \\ &\equiv v'_\mu V + p'_\mu A \ . \end{aligned}$$

Identifying terms,

$$p'_\mu A = e^{u'V}p_\mu A e^{-u'V} \tag{1.56}$$

$$v'_\mu V = e^{u'V}(v_\mu V)e^{-u'V} - (\partial_\mu e^{u'V})e^{-u'V} \ . \tag{1.57}$$

From the first of these equations, recalling that $D^{(b)}(\mathfrak{h})$ is the representation induced by $\mathfrak{h}e^{\xi A}\mathfrak{h}^{-1} = e^{\xi' A}$, we read that

$$p'_\mu = D^{(b)}(e^{u'V})p_\mu \ . \tag{1.58}$$

We have to work out now the expression of $(D_\mu\psi)'$,

$$\begin{aligned} (D_\mu\psi)' &= \partial_\mu\psi' + v'_\mu V\psi' = \\ &= (\partial_\mu e^{u'V})\psi + e^{u'V}\partial_\mu\psi + (e^{u'V}v_\mu V - \partial_\mu e^{u'V})e^{-u'V}e^{u'V}\psi = \\ &= e^{u'V}(\partial_\mu + v_\mu V)\psi = e^{u'V}D_\mu\psi = D(e^{u'V})D_\mu\psi \ , \end{aligned}$$

so that:

$$(D_\mu\psi)' = D(e^{u'V})D_\mu\psi \ . \tag{1.59}$$

[3]Notice that, for the explicit developments that follow, we should write the matrices representing the generators V_i in some representation with a different symbol, T_i. However, since no confusion will arise, we will make some notation abuse, and will denote them still by V_i.

1.7 Gauge fields

Now we take one further step, considering that the transformations $\mathfrak{g}$ depend of space-time. In this case, $\partial_\mu \xi$ and $\partial_\mu \psi$ do not transform linearly under $\mathfrak{H}$, and thus *gauge fields* must be introduced. We denote them by ρ_{i_μ} and $a_{l\mu}$ associated with generators V_i and A_l, respectively. Their transformation laws are given by:

$$\rho_\mu V + a_\mu A \xrightarrow{\mathfrak{g}} \rho'_\mu V + a'_\mu A = \mathfrak{g}(\rho_\mu V + a_\mu A)\mathfrak{g}^{-1} - f^{-1}(\partial_\mu \mathfrak{g})\mathfrak{g}^{-1} \ , \tag{1.60}$$

being f a universal coupling constant of the gauge fields. Now, the fields a_μ and v_μ are introduced through:

$$e^{-\xi A}\left(\partial_\mu + f(\rho_\mu V + a_\mu A)\right) e^{\xi A} = v_\mu V + p_\mu A \ , \tag{1.61}$$

which is the analogous to Eq. (1.52). In what follows, we take $f = 1$ for clearness and conciseness.

Instead of $\partial_\mu \psi$, we have to consider now $(\partial_\mu + \rho_\mu V)\psi$. This combination transforms linearly under $\mathfrak{H}$, since, for $\mathfrak{g} = \mathfrak{h} \in \mathfrak{H}$,

$$\rho'_\mu V = \mathfrak{h}\rho_\mu V \mathfrak{h}^{-1} - (\partial_\mu \mathfrak{h})\mathfrak{h}^{-1} \ , \tag{1.62}$$

so that:

$$\left(\partial_\mu + \rho'_\mu V\right)\psi' = \mathfrak{h}\left(\partial_\mu + \rho_\mu V\right)\psi \ . \tag{1.63}$$

Next we show the transformation law of Eq. (1.61). As $\mathfrak{g}e^{\xi A} = e^{\xi' A}e^{u' V}$, then $e^{\xi' A} = \mathfrak{g}e^{\xi A}e^{-u' V}$. Inserting this into the *transformed* version of (1.61),

$$\begin{aligned}
v'_\mu V + p'_\mu A &= e^{-\xi' A}\left(\partial_\mu + \rho'_\mu V + a'_\mu A\right) e^{\xi' A} = \\
&= e^{u' V} e^{-\xi A}\mathfrak{g}^{-1}\left(\partial_\mu + \rho'_\mu V + a'_\mu A\right)\mathfrak{g} e^{\xi A} e^{-u' V} = \\
&= e^{u' V} e^{-\xi A}\underbrace{\left(\mathfrak{g}^{-1}\partial_\mu \mathfrak{g} + \mathfrak{g}^{-1}(\rho'_\mu V + a'_\mu A)\mathfrak{g}\right)}_{\rho_\mu V + a_\mu A} e^{\xi A} e^{-u' V} + \\
&+ e^{u' V} e^{-\xi A}(\partial_\mu e^{\xi A})e^{-u' V} + e^{u' V}(\partial_\mu e^{-u' V}) = \\
&= e^{u' V}\underbrace{\left[e^{-\xi A}\left(\partial_\mu + \rho_\mu V + a_\mu A\right) e^{\xi A}\right]}_{p_\mu A + v_\mu V} e^{-u' V} + e^{u' V}\partial_\mu e^{-u' V} = \\
v'_\mu V + p'_\mu A &= e^{u' V}\left(p_\mu A + v_\mu V\right) e^{-u' V} + e^{u' V}\partial_\mu e^{-u' V} \ .
\end{aligned}$$

Whence, identifying terms:

$$p'_\mu A = e^{u' V} p_\mu A e^{-u' V} \tag{1.64}$$

$$v'_\mu V = e^{u' V}(v_\mu V)e^{-u' V} - (\partial_\mu e^{u' V})e^{-u' V} \ . \tag{1.65}$$

Comparing with (1.56) and (1.57), we see that the transformation properties are the same as in the *global* (instead of *local*) case, which drive to the wanted results for the covariant derivatives.

1.8 The chiral symmetry of the QCD Lagrangian

1.8.1 The Lagrangian

Quantum Chromodynamics (QCD) [1–7] is a non-abelian Yang-Mills theory [8] with gauged color $SU(3)$ symmetry. The Lagrangian density of QCD is:

$$\mathcal{L}_{\rm QCD} = \sum_f \bar{q}_f \left(i\not{D} - m_f \right) q_f - \frac{1}{2} {\rm Tr} \mathcal{G}^a_{\mu\nu} \mathcal{G}^{a\mu\nu} \ ; \tag{1.66}$$

Two shorthand are used here: $\not{D} = \gamma^\mu D_\mu$, and $\bar{q} = q^\dagger \gamma^0$, with γ_μ the Dirac matrices. The *flavors* of the quarks are $f = u, d, s, c, b, t$, and each flavor contains three *colors*. The covariant derivative is

$$iD_\mu = i\partial_\mu - g A^a_\mu \frac{\lambda_a}{2} \ , \tag{1.67}$$

where λ_a, $a = 1, \ldots, 8$ are the $SU(3)$ Gell-Mann matrices, acting in the *color space*, and A^a_μ are the octet of color gauge vector bosons, *gluons*. The color field or strength field $\mathcal{G}_{\mu\nu}$ is

$$\mathcal{G}^a_{\mu\nu} = \partial_\mu A^a_\nu - \partial_\nu A^a_\mu - g f_{abc} \left[A^b_\mu, A^c_\nu \right] \ , \tag{1.68}$$

so that the gluons are coupled among themselves with a universal coupling constant g. From now on, we focus on the bilinear part of the QCD Lagrangian in the quark fields, since obviously the strength part has no flavor content. We also use a matrix notation for the quark flavours, as:

$$\begin{aligned} \mathcal{L}_{\rm QCD} &= \bar{q} \left(i\not{D} - M \right) q + \cdots \ , \\ q &= \begin{pmatrix} u \\ d \\ s \end{pmatrix} \end{aligned}$$

with $M = {\rm diag}(m_u, m_d, m_s)$, and we are anticipating here that we will restrict ourselves to the so called light quarks, u, d and s. Heavier quarks are neglected in this effective Lagrangian approach since we will restrict here to energies well below the production threshold of particles involving these quarks.

1.8.2 Chiral symmetry

Chiral symmetry is a symmetry[4] of the Lagrangian in the limit of massless quarks. *Massless* here will be a good aproximation for the u, d quarks ($SU(2)$ symmetry) having current masses $m_u \sim 5$ MeV, $m_d \sim 10$ MeV [48, 189, 190]. These are small compared to a $\Lambda_{\rm QCD} \simeq 0.3$ GeV. For the s quark the situation is not so clear, because its mass is around a factor 1/3 of $\Lambda_{\rm QCD}$.

Let us introduce (helicity) projection operators,

$$P_\pm = \frac{\mathbb{I} \pm \gamma_5}{2} = P_\pm^\dagger \ , \tag{1.69}$$

[4] We define *symmetry* as an operation made over an object that leaves it invariant. In this case, a transformation of the fields of the Lagrangian that leaves the equations of motion invariant.

where $\mathbb{I}$ is the identity operator, and γ_5, the chirality matrix, acting on Dirac space, is defined as $\gamma_5 = i\gamma_0\gamma_1\gamma_2\gamma_3 = \gamma_5^\dagger$, so that γ_5 anticommutes with γ^μ,

$$\{\gamma_5, \gamma^\mu\} = 0 \ . \tag{1.70}$$

The usual properties of Dirac matrices determine those of γ_5, and from these we can show that the operators defined in Eq. (1.69) are indeed projection operators,

$$\begin{aligned} P_\pm^2 &= P_\pm^2 \ , \\ P_+ + P_- &= \mathbb{I} \ , \\ P_\pm P_\mp &= 0 \ . \end{aligned} \tag{1.71}$$

P_+ and P_- project into the positive and negative helicity eigenstates in the massless limit, respectively, and they are also usually denoted by P_R and P_L (right-handed and left-handed). We define right- and left- handed quark fields as

$$\begin{aligned} q_R = P_+ q \qquad \bar{q}_R = \bar{q} P_- \ , \\ q_L = P_- q \qquad \bar{q}_L = \bar{q} P_+ \ , \end{aligned}$$

so that $q = (P_+ + P_-)q = q_R + q_L$ and $\bar{q} = \bar{q}(P_- + P_+) = q_L + q_R$. Whence, the derivative piece of the Lagrangian can be written as

$$\begin{aligned} \bar{q}\gamma_\mu D^\mu q &= \bar{q}\left((P_+ + P_-)\gamma_\mu(P_- + P_+)\right) D^\mu q \\ &= \bar{q}\left(P_-\gamma_\mu P_+ + P_+\gamma_\mu P_- + \underbrace{P_+\gamma_\mu P_+}_{P_+P_-\gamma_\mu = 0} + \underbrace{P_-\gamma_\mu P_-}_{P_-P_+\gamma_\mu = 0} \right) D^\mu q \\ &= \bar{q}_R \not{D} q_R + \bar{q}_L \not{D} q_L \ . \end{aligned}$$

Proceeding in an analogous way, one has for the mass term:

$$-\bar{q} M q = -\bar{q}_R M q_L - \bar{q}_L M q_R \ , \tag{1.72}$$

and chirality is mixed.

If we now set $M = 0$, massless quarks, the flavor independence of the Lagrangian makes it invariant under global $U(3)_L \otimes U(3)_R$ transformations,

$$q_L \ \rightarrow \ \exp\left(i \sum_{a=0}^{8} \theta_a^L \lambda_a \right) q_L \tag{1.73}$$

$$q_R \ \rightarrow \ \exp\left(i \sum_{a=0}^{8} \theta_a^R \lambda_a \right) q_R \tag{1.74}$$

where $\lambda_0 = \sqrt{2/3}\,\mathbb{I}$, as to enlarge the generators of $SU(3)$ to complete the ones of $U(3)$. The associated Noether currents are:

$$L_a^\mu = \bar{q}_L \gamma^\mu \frac{\lambda_a}{2} q_L \qquad R_a^\mu = \bar{q}_R \gamma^\mu \frac{\lambda_a}{2} q_R \qquad a = 1, \ldots, 8 \tag{1.75a}$$

$$L^\mu = \bar{q}_L \gamma^\mu q_L \qquad R^\mu = \bar{q}_R \gamma^\mu q_R \tag{1.75b}$$

and the equations satisfied by these currents are:

$$\partial_\mu L_a^\mu = -i\left(\bar{q}_L \frac{\lambda_a}{2} M q_R - \bar{q}_R M \frac{\lambda_a}{2} q_L\right) \tag{1.76a}$$

$$\partial_\mu L^\mu = -i\left(\bar{q}_L M q_R - \bar{q}_R M q_L\right) \tag{1.76b}$$

$$\partial_\mu R_a^\mu = -i\left(\bar{q}_R \frac{\lambda_a}{2} M q_L - \bar{q}_L M \frac{\lambda_a}{2} q_R\right) \tag{1.76c}$$

$$\partial_\mu R^\mu = -i\left(\bar{q}_R M q_L - \bar{q}_L M q_R\right) \tag{1.76d}$$

which are zero in the case $M = 0$, as advanced, meaning that there would be a conserved charge in that case. The divergence of the currents are proportional to the *current quark mass* parameters. The charge operators are the integrals over full space of the $\mu = 0$ component (in Dirac space) of the currents, the charge densities,

$$Q_a^L(t) = \int \mathrm{d}\vec{x}\; L_a^0(\vec{x},t) = \int \mathrm{d}\vec{x}\; \bar{q}_L(\vec{x},t)\gamma^0 \frac{\lambda_a}{2} q_L(\vec{x},t) \tag{1.77a}$$

$$Q_a^R(t) = \int \mathrm{d}\vec{x}\; R_a^0(\vec{x},t) = \int \mathrm{d}\vec{x}\; \bar{q}_R(\vec{x},t)\gamma^0 \frac{\lambda_a}{2} q_R(\vec{x},t) \tag{1.77b}$$

$$Q^L(t) = \int \mathrm{d}\vec{x}\; L^0(\vec{x},t) = \int \mathrm{d}\vec{x}\; \bar{q}_L(\vec{x},t)\gamma^0 q_L(\vec{x},t) \tag{1.77c}$$

$$Q^R(t) = \int \mathrm{d}\vec{x}\; R^0(\vec{x},t) = \int \mathrm{d}\vec{x}\; \bar{q}_R(\vec{x},t)\gamma^0 q_R(\vec{x},t) \tag{1.77d}$$

Denoting by f_{abc} the structure constants of $SU(3)$ symmetry, such that $\left[\frac{\lambda_a}{2}, \frac{\lambda_b}{2}\right] = i f_{abc} \frac{\lambda_c}{2}$, the algebra of the charges is:

$$\left[Q_a^L, Q_b^L\right] = i f_{abc} Q_c^L \tag{1.78}$$

$$\left[Q_a^R, Q_b^R\right] = i f_{abc} Q_c^R \tag{1.79}$$

$$\left[Q_a^L, Q_b^R\right] = 0 \tag{1.80}$$

The last equation of the algebra reflects the fact that the charges L/R operate on different spaces. The first two are obtained inserting the explicit expressions for $Q_a^{L,R}$ in the commutators, and through the use of the equal time commutation relation of the quark fields and the commutator of the Gell-Mann matrices.

So far, we have developed the algebra of the group $SU(3)_L \otimes SU(3)_R$,[5] which is a subgroup of the $U(3)_L \otimes U(3)_R$. However, the former is not realized (a la Wigner) in Nature, as we will discuss below. Still, we can introduce a linear combination of left and right charges/currents to obtain vector and axial charges/currents,

$$J^{\mu V}_a = R^\mu_a + L^\mu_a \;\rightarrow\; Q^V_a = Q^R_a + Q^L_a \tag{1.81a}$$

$$J^{\mu A}_a = R^\mu_a - L^\mu_a \;\rightarrow\; Q^A_a = Q^R_a - Q^L_a \tag{1.81b}$$

$$J^{\mu V} = R^\mu + L^\mu \;\rightarrow\; Q^V = Q^R + Q^L \tag{1.81c}$$

$$J^{\mu A} = R^\mu - L^\mu \;\rightarrow\; Q^A = Q^R - Q^L \tag{1.81d}$$

[5] In analogous way one could proceed for $SU(2)_L \otimes SU(2)_R$.

$$Q_a^V(t) = \int \mathrm{d}\vec{x}\ \bar{q}\gamma^0\frac{\lambda_a}{2}q(\vec{x},t) \tag{1.82a}$$

$$Q_a^A(t) = \int \mathrm{d}\vec{x}\ \bar{q}\gamma^0\gamma_5\frac{\lambda_a}{2}q(\vec{x},t) \tag{1.82b}$$

$$Q^V(t) = \int \mathrm{d}\vec{x}\ \bar{q}\gamma^0 q(\vec{x},t) \tag{1.82c}$$

$$Q^A(t) = \int \mathrm{d}\vec{x}\ \bar{q}\gamma^0\gamma_5 q(\vec{x},t) \tag{1.82d}$$

$$\left[Q_a^V, Q_b^V\right] = if_{abc}Q_c^V \tag{1.83}$$

$$\left[Q_a^V, Q_b^A\right] = if_{abc}Q_c^A \tag{1.84}$$

$$\left[Q_a^A, Q_b^A\right] = if_{abc}Q_c^V \tag{1.85}$$

$$\partial_\mu J^{\mu V}_a = i\bar{q}\left[M, \frac{\lambda_a}{2}\right]q \tag{1.86}$$

$$\partial_\mu J^{\mu A}_a = i\bar{q}\left\{M, \frac{\lambda_a}{2}\right\}\gamma_5 q \tag{1.87}$$

$$\partial_\mu J^{\mu V} = 0 \tag{1.88}$$

$$\partial_\mu J^{\mu A} = 2i\bar{q}M\gamma_5 q + \frac{3g^2}{32\pi^2}\epsilon^{\mu\nu\rho\sigma}\mathcal{G}^a_{\mu\nu}\mathcal{G}^a_{\rho\sigma} \tag{1.89}$$

We will briefly discuss the singlet vector and axial charges/currents (the last two equations) because we will not further refer to them. The singlet vector current, $J^{\mu V} = \bar{q}\gamma^\mu q$ is conserved ($\partial_\mu J^{\mu V} = 0$) even when quarks are massive. This exact $U(1)_V$ symmetry implies baryon number B conservation, thus leading to the organization of hadrons in *mesons*, $B = 0$, and *baryons*, $B = 1$. The singlet axial current should be conserved from classical symmetry considerations. However, it is not conserved at the quantum level, giving rise to the $U(1)_A$ *anomaly* [191–193],[6] which is indeed responsible for the appearence of the term involving the tensor form in the last line.

From symmetry considerations of the Lagrangian, and thus, of the Hamiltonian, we would expect the hadron spectrum to be composed of degenerate multiplets with quantum numbers following the pattern of $\mathfrak{G} = SU(3)_L \otimes SU(3)_R$. As Q_a^V and Q_a^A are linear combinations of left- and right- handed charges, they commute with the Hamiltonian. They have opposite parities, so one would expect the existence of degenerate multiplets with opposite parities (parity doubling), but this is not seen in Nature. The argument would go as follows. Consider a one-particle state, $|\alpha, +\rangle$ such that it has definite parity (positive, in this case) and mass (energy), *i.e.*, it is an eigenstate of the Hamiltonian and of the parity operator:

$$H|\alpha,+\rangle = M|\alpha,+\rangle$$
$$P|\alpha,+\rangle = +|\alpha,+\rangle\ .$$

[6] In the large N_C (number of colors) limit, this symmetry is restored, since the divergence of the current is proportional to g^2 and this scales as N_C^{-1} [194–196].

Let us consider the state $|\Omega_{\alpha,+}\rangle$, defined as:

$$|\Omega_{\alpha,+}\rangle = Q_a^A |\alpha,+\rangle ,$$

such that it has energy and parity given by

$$\begin{aligned} H|\Omega_{\alpha,+}\rangle &= HQ_a^A|\alpha,+\rangle = Q_a^A H|\alpha,+\rangle = MQ_a^A|\alpha,+\rangle = M|\Omega\rangle \\ P|\Omega_{\alpha,+}\rangle &= PQ_a^A P^{-1}P|\alpha,+\rangle = -Q_a^A|\alpha,+\rangle = -|\Omega_{\alpha,+}\rangle \ , \end{aligned}$$

where we have used the fact that $\left[Q_a^A, H\right] = 0$ and $\left\{Q_a^A, P\right\} = 0$. This follows because Q_a^A is a symmetry of the Hamiltonian, as stated before, and thus commutes with it, and because Q_a^A is an operator with negative parity. Now, $|\Omega_{\alpha,+}\rangle$ can be expanded in terms of negative parity states,[7]

$$\begin{aligned} |\Omega_{\alpha,+}\rangle = Q_a^A|\alpha,+\rangle &= \sum_{\alpha'}|\alpha',+\rangle \underbrace{\left\langle \alpha',+\left|Q_a^A\right|\alpha,+\right\rangle}_{0} + \\ &+ \sum_{\beta'}|\beta',-\rangle\left\langle \beta',-\left|Q_a^A\right|\alpha,+\right\rangle \equiv \sum_{\beta'} C^a_{(\beta',-),(\alpha,+)}|\beta',-\rangle \ , \end{aligned} \tag{1.90}$$

Now, if we *assume* that $Q_a^A|0\rangle = 0$, we have:

$$\begin{aligned} |\Omega_{\alpha,+}\rangle = Q_a^A|\alpha,+\rangle = Q_a^A b^\dagger_{\alpha,+}|0\rangle &= \left[Q_a^A, b^\dagger_{\alpha,+}\right]|0\rangle + \underbrace{b^\dagger_{\alpha,+}Q_a^A|0\rangle}_{0} \\ &= \sum_{\beta'} C^a_{(\beta',-),(\alpha,+)}|\beta',-\rangle \ . \end{aligned} \tag{1.91}$$

where $b^\dagger$ are creation operators. The last step follows from Eq. (1.90). Thus,

$$\left[Q_a^A, b^\dagger_{\alpha,+}\right] = \sum_{\beta'} C^a_{(\beta',-),(\alpha,+)} b^\dagger_{\beta',-} \ . \tag{1.92}$$

The key assumption here was $Q_a^A|0\rangle = 0$. This is called a *Wigner-Weyl* realization of the symmetry. The states $|\beta,-\rangle$ are states degenerate in mass with $|\alpha,+\rangle$ and with opposite parity, leading to a spectrum with parity doubling, as stated before. That is, there are multiplets of $SU(2)_R \otimes SU(2)_L$, in which the states transform one into another under the action of the generators. As stated before, no such multiplets are seen in the spectrum. But if $Q_a^A|0\rangle \neq 0$, which is called a *Nambu-Goldstone* realization of the symmetry, then this argument does not follow. Indeed, if $Q_a^A|0\rangle \neq 0$, then this state is not even defined [197].

Actually, from the experimental point of view, no such parity doubling is observed, see Fig. 1.1, *i.e.*, comparing the sector $J^P = 0^-$ with that of $J^P = 0^+$ we see that they are not degenerate in mass, rather, the latter has resonances heavier than the particles found in the former. Thus, the non-existence of parity doubling in the hadronic spectrum together with

[7] The fact that $\left\langle \alpha',+\left|Q_a^A\right|\alpha,+\right\rangle = 0$ can be shown by inserting the identity through the parity operator in the right way,

$$\left\langle \alpha',+\left|Q_a^A\right|\alpha,+\right\rangle = \left\langle \alpha',+\left|P^{-1}PQ_a^AP^{-1}P\right|\alpha,+\right\rangle = -\left\langle \alpha',+\left|Q_a^A\right|\alpha,+\right\rangle = 0 \ ,$$

and analogously $\left\langle \beta',-\left|Q_a^A\right|\beta,-\right\rangle = 0$.

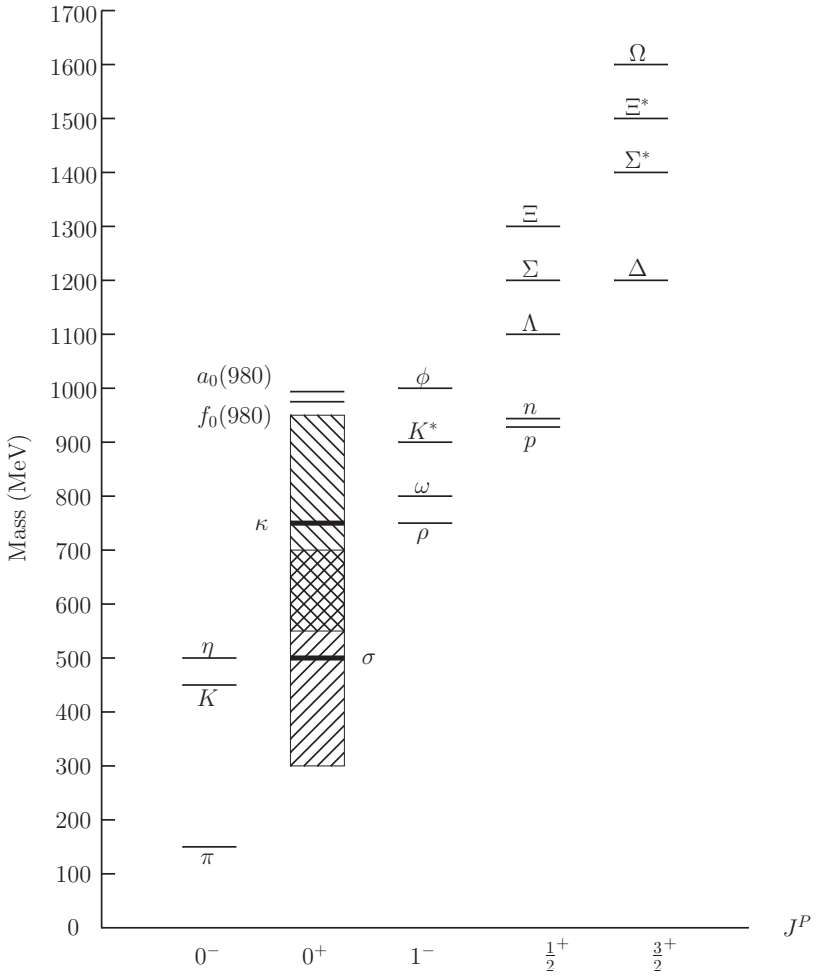

Figure 1.1: Schematic representation of the hadronic spectrum. We show here the hadrons considered in Figures 1.2, 1.3 and 1.4, in order to see how they organize in approximately degenerate multiplets. Considering the multiplets $J^P = 0^-$ and $J^P = 0^+$, it is clear that no parity doubling is observed, as a Wigner-Weyl realization of the symmetry would require.

the fact that it is still organized in multiplets points to $SU(3)_V$ and not $SU(3)_L \otimes SU(3)_R$ as the approximate realization of the symmetry. And even more, we see also from Fig. 1.1 that the $J^P = 0^-$ masses are much smaller than the others,[8] which leads us to think of them as candidates for the Goldstone bosons that come out from the Goldstone theorem, which holds if there are some generators that do not anihilate the vacuum. Thus, the chiral symmetry seems to be spontaneously broken [9–14] down to $SU(3)_V$. Let us also remark here that global vector-like symmetries, as the former, cannot be spontaneously broken, according to Vafa–Witten theorem [198, 199].

On the other side, there is a theorem due to Coleman [200], that can be stated as:

Theorem (Coleman theorem)**.** *Let Q be a generator of a continuous symmetry group $\mathfrak{G}$,*

[8]The fact that the mass of the pion, π, which is an isospin triplet, is much smaller than that of the other pseudoscalars is due to the fact that the $SU(2)$ symmetry, which would generate three pseudoscalar Goldstone boson, is a better approximate symmetry than $SU(3)$, which would generate eight of them.

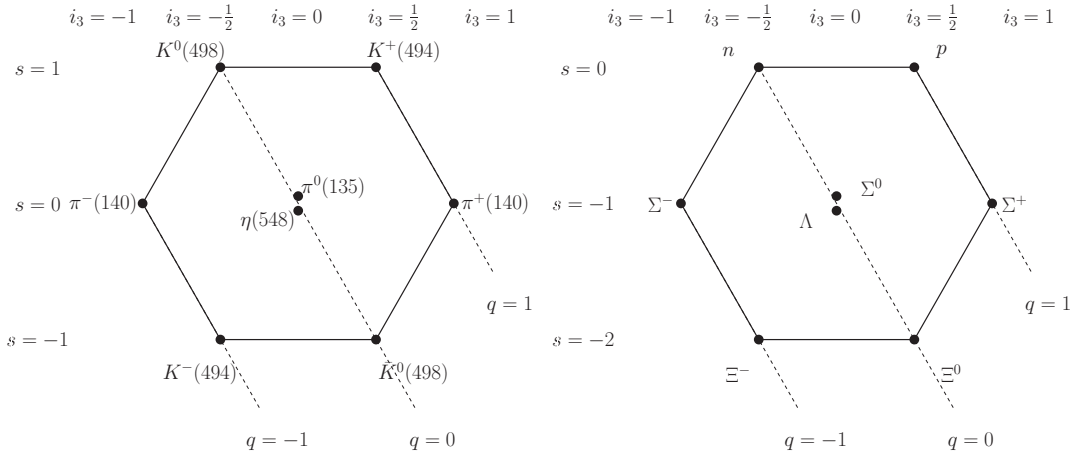

Figure 1.2: The lightest pseudoscalar meson octet, $J^P = 0^-$ and $B = 0$ (left) and the lightest baryon octet, $J^P = \frac{1}{2}^+$ and $B = 1$ (right).

defined through a space integral of the time component of a given current density $J^\mu(x)$, such that it anihilates the vacuum (i.e., the vacuum is invariant under $\mathfrak{G}$.) Then the Hamiltonian of the theory is invariant under the transformations of the field induced by $\mathfrak{G}$, and the current is conserved.

The best summary of the theorem is given by the title of the original article: *The Invariance of the Vacuum is the Invariance of the World*. The symmetry of the ground state thus determines the symmetry of the spectrum. The spectrum thus is telling us the symmetry of the ground state. Whence, we are lead to consider that:

$$Q_a^V |0\rangle = Q^V |0\rangle = 0 , \tag{1.93}$$

$$Q_a^A |0\rangle \neq 0 . \tag{1.94}$$

As stated before, the fact that the ground state is not invariant under the axial transformations naturally leads to the appearence of Goldstone bosons. To each axial generator Q_a^A that does not anihilate the ground state there corresponds a *massless* Goldstone boson whose quantum numbers are the same than those of the corresponding generator. In this case, the Goldstone bosons, denoted by $\phi_a(x)$, are pseudoscalars, and transform one into each other under the subgroup $\mathfrak{H} = SU(3)_V$ as an octet,

$$\left[Q_a^V, \phi_b(x)\right] = i f_{abc} \phi_c(x) , \tag{1.95}$$

corresponding to the adjoint representation of $SU(3)_V$, see Eq. (1.45). Accordingly, the spectrum is organized into approximately degenerate multiplets of $SU(3)_V$. In Figs. 1.2, 1.3 and 1.4 some of these multiplets, transforming under irreducible representations of $SU(3)$, are shown.

We are now in position to link the results of the first part of this chapter with the symmetry group considered so far. The group $\mathfrak{G}$ is $SU(3)_L \otimes SU(3)_R$, and $\mathfrak{H} = SU(3)_V$ is the subgroup that leaves invariant the vacuum or ground state, with $\left[Q_a^V, Q_b^V\right] = i f_{abc} Q_c^V$. This is the

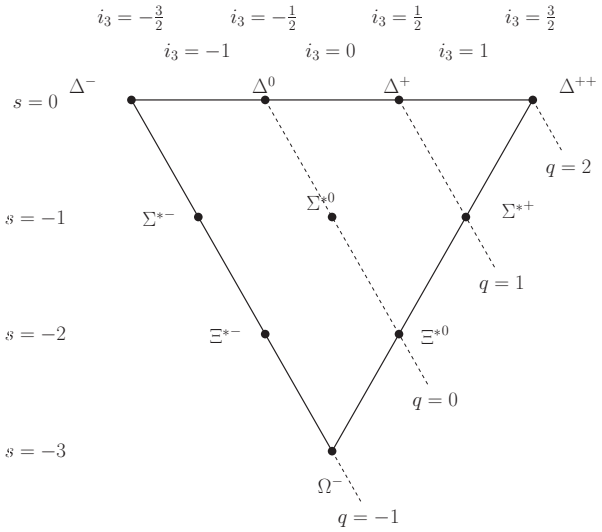

Figure 1.3: The baryon decuplet, $J^P = \frac{3}{2}^+$ and $B = 1$.

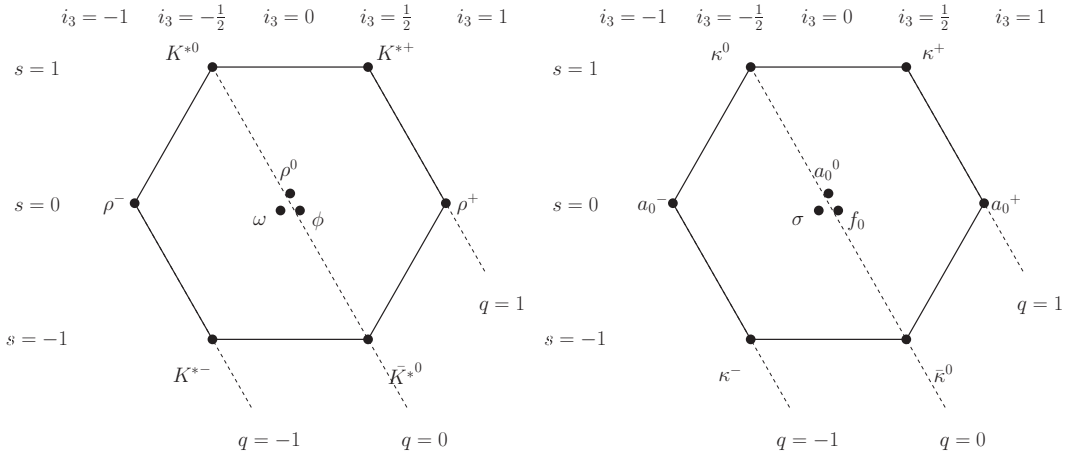

Figure 1.4: The lightest vector meson nonet, $J^P = 1^-$ and $B = 0$ (left) and the lightest scalar meson nonet, $J^P = 0^+$ and $B = 0$ (right) (See [53] and Chapters 3 and 5).

subgroup considered in the general analysis done at the begining of this chapter, so we identify Q_a^V with the generators V_i in the general formalism. The rest of the generators are those that do not anihilate the vacuum, *i.e.*, the vacuum is not invariant under the group elements generated by these generators, Q_a^A, which are thus identified with the A_l considered in the general formalism.

1.8.3 The Lagrangian with external sources

We want to construct the most general Lagrangian, with the following properties:

- It must be invariant under chiral transformations (see Subsection 1.9.1).
- It must be invariant under charge conjugation (1.9.2) and parity (1.9.5).
- It must be Lorentz invariant, *i.e.*, scalar under Lorentz transformations (1.9.4).
- It must be Hermitean (1.9.3).

In order to construct such a Lagrangian, we introduce in our original Lagrangian the couplings of external sources $s(x)$, $p(x)$, $v_\mu(x)$ and $a_\mu(x)$ to quark currents and densities through [18]

$$\mathcal{L}_{\rm ext} = -\bar{q}s(x)q + i\bar{q}\gamma_5 p(x)q + \bar{q}\gamma^\mu v_\mu(x)q + \bar{q}\gamma^\mu\gamma_5 a_\mu(x)q \ . \tag{1.96}$$

We can then introduce the mass term in this Lagrangian as $s(x) = M$, and the electroweak interactions through the substitutions

$$v_\mu = -eQA_\mu - \frac{g}{2\cos\theta_W}\left(Q\cos 2\theta_W - \frac{1}{6}\right)Z_\mu - \frac{g}{2\sqrt{2}}\left(T_+ W_\mu^+ + \text{h.c.}\right) \tag{1.97a}$$

$$a_\mu = \frac{g}{2\cos\theta_W}\left(Q - \frac{1}{6}\right)Z_\mu + \frac{g}{2\sqrt{2}}\left(T_+ W_\mu^+ + \text{h.c.}\right) \tag{1.97b}$$

$$Q = \frac{1}{3}\begin{pmatrix} 2 & 0 & 0 \\ 0 & -1 & 0 \\ 0 & 0 & -1 \end{pmatrix} \tag{1.97c}$$

$$T_+ = \begin{pmatrix} 0 & V_{ud} & V_{us} \\ 0 & 0 & 0 \\ 0 & 0 & 0 \end{pmatrix} \tag{1.97d}$$

Use of this substitution will be made latter in the discussion of the meaning of the constant f_π, the pion decay constant. By now, we must discuss the transformation properties of these external sources under Lorentz, parity, charge conjugation and, in particular, chiral transformations.

1.9 Transformation properties of the building blocks

1.9.1 Chiral transformations

We want to impose gauge invariance under the $SU(3)$ version of the chiral transformations in Eqs. (1.73) and (1.74), which can be written as:

$$q'_R = V_R q_R \qquad q'_L = V_L q_L \ ,$$

where $V_{R,L} \equiv V_{R,L}(x)$. From time to time, we will omit the space-time dependence of the transformations V_R and of the fields. The piece of $\mathcal{L}_{\rm ext}$ containing v_μ and a_μ plus the derivative term of $\mathcal{L}_0$ can be written as:

$$\begin{aligned} \mathcal{L}_{\rm ext+der} &= \bar{q}\gamma^\mu\left(v_\mu + \gamma_5 a_\mu + i\partial_\mu\right)q = \\ &= \bar{q}_R\gamma^\mu\left(v_\mu + \gamma_5 a_\mu + i\partial_\mu\right)q_R + \bar{q}_L\gamma^\mu\left(v_\mu + \gamma_5 a_\mu + i\partial_\mu\right)q_L \end{aligned}$$

Under the transformations, the Lagrangian reads

$$\begin{aligned} \mathcal{L}_{\rm ext+der} &= \bar{q}_R\gamma^\mu V_R^\dagger\left(v'_\mu + \gamma_5 a'_\mu + i\partial_\mu\right)V_R q_R + \bar{q}_L\gamma^\mu V_L^\dagger\left(v'_\mu + \gamma_5 a'_\mu + i\partial_\mu\right)V_L q_L + \\ &+ i\bar{q}_R\gamma^\mu\partial_\mu q_R + i\bar{q}_L\gamma^\mu\partial_\mu q_L \end{aligned}$$

Recalling the properties in Eq. (1.70) and Eq. (1.71), this can be cast as:

$$\mathcal{L}_{\rm ext+der} = \tfrac{1}{2}\bar{q}\gamma^\mu \quad \left[V_R^\dagger\left(v'_\mu + a'_\mu + i\partial_\mu\right)V_R + V_L^\dagger\left(v'_\mu - a'_\mu + i\partial_\mu\right)V_L\right]q +$$

$$+\tfrac{1}{2}\bar{q}\gamma^\mu\gamma_5 \quad \left[V_R^\dagger\left(v'_\mu+a'_\mu+i\partial_\mu\right)V_R - V_L^\dagger\left(v'_\mu-a'_\mu+i\partial_\mu\right)V_L\right]q + \\ +i\bar{q}\gamma^\mu\partial_\mu q \tag{1.98}$$

Identifying terms, so that the Lagrangian becomes invariant, we have:

$$v_\mu = \frac{1}{2}V_R^\dagger\left(v'_\mu+a'_\mu+i\partial_\mu\right)V_R + \frac{1}{2}V_L^\dagger\left(v'_\mu-a'_\mu+i\partial_\mu\right)V_L \tag{1.99}$$

$$a_\mu = \frac{1}{2}V_R^\dagger\left(v'_\mu+a'_\mu+i\partial_\mu\right)V_R - \frac{1}{2}V_L^\dagger\left(v'_\mu-a'_\mu+i\partial_\mu\right)V_L \tag{1.100}$$

It is simpler to work in terms of the right/left fields, defined as:

$$r_\mu \equiv v_\mu + a_\mu = V_R^\dagger r'_\mu V_R + iV_R^\dagger\partial_\mu V_R \ , \tag{1.101}$$

$$l_\mu \equiv v_\mu - a_\mu = V_L^\dagger l'_\mu V_L + iV_L^\dagger\partial_\mu V_L \ , \tag{1.102}$$

and invert these equations to get finally:

Chiral transformations	$r'_\mu(x) = V_R(x)\left(r_\mu(x)+i\partial_\mu\right)V_R(x)^\dagger \ ,$	(1.103a)
	$l'_\mu(x) = V_L(x)\left(l_\mu(x)+i\partial_\mu\right)V_L(x)^\dagger \ .$	(1.103b)

Completely analogous work can be done with $s(x)$, $p(x)$, where it is also convenient to work with the linear combinations

$$\chi = s + ip \tag{1.104}$$

$$\chi^\dagger = s - ip \tag{1.105}$$

and we get:

Chiral transformations	$\chi' = V_R\ \chi\ V_L^\dagger \ ,$	(1.106a)
	$\chi^{\dagger\prime} = V_L\ \chi^\dagger\ V_R^\dagger \ .$	(1.106b)

For the external right/left fields, we can introduce the corresponding field strength tensors,

$$f^R_{\mu\nu} = \partial_\mu r_\nu - \partial_\nu r_\mu - i\left[r_\mu, r_\nu\right] \ , \tag{1.107a}$$

$$f^L_{\mu\nu} = \partial_\mu l_\nu - \partial_\nu l_\mu - i\left[l_\mu, l_\nu\right] \ . \tag{1.107b}$$

Under chiral transformations, Eq. (1.103), these tensors are transformed into

$$\begin{aligned}(f^L_{\mu\nu})' = &\underbrace{\partial_\mu V_L\ l_\nu V_L^\dagger}_{①} + \underbrace{V_L\ \partial_\mu l_\nu\ V_L^\dagger}_{②} + \underbrace{V_L l_\nu\ \partial_\mu V_L^\dagger}_{③} + \underbrace{i\partial_\mu V_L\ \partial_\nu V_L^\dagger}_{④} + i\underbrace{V_L\ \partial_\mu\partial_\nu V_L^\dagger}_{⑤} \\ &- \underbrace{\partial_\nu V_L\ l_\mu V_L^\dagger}_{⑥} - \underbrace{V_L\ \partial_\nu l_\mu\ V_L^\dagger}_{⑦} - \underbrace{V_L l_\mu\ \partial_\nu V_L^\dagger}_{⑧} - \underbrace{i\partial_\nu V_L\ \partial_\mu V_L^\dagger}_{⑨} - \underbrace{iV_L\ \partial_\nu\partial_\mu V_L^\dagger}_{⑩} \\ &- \underbrace{i\left[V_L l_\mu V_L^\dagger, V_L l_\nu V_L^\dagger\right]}_{⑪} + \underbrace{\left[V_L\partial_\mu V_L^\dagger, V_L l_\nu V_L^\dagger\right]}_{⑫} \\ &+ \underbrace{\left[V_L l_\mu V_L^\dagger, V_L\partial_\nu V_L^\dagger\right]}_{⑬} + i\underbrace{\left[V_L\partial_\mu V_L^\dagger, V_L\partial_\nu V_L^\dagger\right]}_{⑭}\end{aligned}$$

Now, as

$$\begin{aligned}\left[V_L\partial_\mu V_L^\dagger, V_L\partial_\nu V_L^\dagger\right] &= -\partial_\mu V_L\partial_\nu V_L^\dagger - \partial_\nu V_L\partial_\mu V_L^\dagger\\ \left[V_L\partial_\mu V_L^\dagger, V_L l_\nu V_L^\dagger\right] &= -\partial_\mu V_L l_\nu V_L^\dagger - V_L l_\nu\partial_\mu V_L^\dagger\\ \left[V_L l_\mu V_L^\dagger, V_L\partial_\nu V_L^\dagger\right] &= V_L l_\mu\partial_\nu V_L^\dagger + \partial_\nu V_L l_\mu V_L^\dagger\end{aligned}$$

then

$$\begin{aligned}④ + ⑨ + ⑭ &= 0\\ ① + ③ + ⑫ &= 0\\ ⑥ + ⑧ + ⑬ &= 0\\ ⑤ + ⑩ &= 0\end{aligned}$$

so we are left with

$$② + ⑦ + ⑪ = V_L\left(\partial_\mu l_\nu - \partial_\nu l_\mu - i\left[l_\mu, l_\nu\right]\right)V_L^\dagger\ .$$

Summarizing,

Chiral transformations	$(f^L_{\mu\nu}(x))' = V_L(x)\left(f^L_{\mu\nu}\right)V_L(x)^\dagger\ ,$	(1.108a)
	$(f^R_{\mu\nu}(x))' = V_R(x)\left(f^R_{\mu\nu}\right)V_R(x)^\dagger\ .$	(1.108b)

We can proceed now with the chiral transformations of the Goldstone bosons, and exploit the results of the first sections. Recall that we had (Eq. (1.34)):

$$\mathfrak{g}e^{\xi A} = e^{\xi' A}e^{u'V} \tag{1.109}$$

and $\mathfrak{g} = V_L V_R$. It is perhaps more comfortable to write this, at least the first time, recalling that $\mathfrak{G}$ is a direct product, so $\mathfrak{g}$ actually means $\mathfrak{g} = V_L \otimes V_R$, and the last equation is, therefore,

$$(V_L\otimes V_R)\left(e^{-\xi\lambda_L}\otimes e^{\xi\lambda_R}\right) = \left(e^{-\xi'\lambda_L}\otimes e^{\xi'\lambda_R}\right)\left(e^{u'\lambda_L}\otimes e^{u'\lambda_R}\right) \tag{1.110}$$

so that, for both sectors,

$$V_R e^{\xi\lambda_R} = e^{\xi'\lambda_R}e^{u'\lambda_R}\ , \tag{1.111a}$$

$$V_L e^{-\xi\lambda_L} = e^{-\xi'\lambda_L}e^{u'\lambda_L}\ . \tag{1.111b}$$

For the automorphism R we had, according to Eq. (1.40),

$$e^{2\xi' A} = \mathfrak{g}e^{2\xi A}R(\mathfrak{g}^{-1})\ , \tag{1.112}$$

and, if $\mathfrak{g} = V_L\otimes V_R$, then $\mathfrak{g}^{-1} = V_L^\dagger\otimes V_R^\dagger$ and $R(\mathfrak{g}^{-1}) = V_R^\dagger\otimes V_L^\dagger$, because the automorphism changes $R\leftrightarrow L$ (corresponding to parity). Thus, the last equation means that

$$e^{-2\xi'\lambda_L}\otimes e^{2\xi'\lambda_R} = (V_L\otimes V_R)\left(e^{-2\xi\lambda_L}\otimes e^{2\xi\lambda_R}\right)\left(V_R^\dagger\otimes V_L^\dagger\right) \tag{1.113}$$

$$e^{2\xi'\lambda_R} = V_R e^{2\xi\lambda_R}V_L^\dagger \tag{1.114a}$$

$$e^{-2\xi'\lambda_L} = V_L e^{-2\xi\lambda_L} V_R^\dagger \tag{1.114b}$$

The matrix $u(x) = e^{\xi\lambda}$ is one of the basic objects. Denote $h = e^{u'\lambda}$, and then Eq. (1.111a) can be cast as

Chiral transformations	$u' = V_R u h^\dagger \to u'^\dagger = h u^\dagger V_R^\dagger$	(1.115a)
	$u'^\dagger = V_L u^\dagger h^\dagger \to u' = h u V_L^\dagger$	(1.115b)

From $u(x)$ we define $U(x) = u(x)u(x)$, and, using the last equations appropiately, it is seen that $U(x)$ transforms as

Chiral transformations	$U'(x) = V_R U(x) V_L^\dagger$	(1.116)

Notice that we could have defined directly $U(x)$ instead of $u(x)$ and read its transformation properties from Eq. (1.114), that are seen to be consistent with Eq. (1.116).

We now proceed to calculate the covariant derivative of $U(x)$, from the results of Sec. 1.6 and Sec. 1.7. Let us rewrite Eq. (1.61) as

$$e^{-\xi A}\left(\partial_\mu - i\tilde{\rho}_\mu V - i\tilde{a}_\mu A\right) e^{\xi A} = -i\tilde{v}_\mu V - i\tilde{p}_\mu A \ , \tag{1.117a}$$

$$e^{\xi A}\left(\partial_\mu - i\tilde{\rho}_\mu V + i\tilde{a}_\mu A\right) e^{-\xi A} = -i\tilde{v}_\mu V + i\tilde{p}_\mu A \ , \tag{1.117b}$$

where we introduced some i factors in the definitions of the fields for convenience, and took advantage of the automorphism of chiral groups (recall that $R \leftrightarrow L$ under a parity transformation) to write the second equation. We have also introduced the fields with a tilde, $\tilde{v}$, $\tilde{\rho}$, $\tilde{a}$ and $\tilde{p}$ to avoid confussion with the external fields originally introduced in the QCD Lagrangian. Indeed, they are the same external fields but rewritten in terms of the generators V^a and A^a for $\tilde{p}_\mu V$ and $\tilde{a}_\mu A$, respectively. From Eq. (1.117), we can obtain

$$\begin{aligned} -2i\tilde{v}_\mu V &= u^\dagger\partial_\mu u + u\partial_\mu u^\dagger - iu^\dagger\left(\tilde{\rho}_\mu V + \tilde{a}_\mu A\right)u - iu\left(\tilde{\rho}_\mu V - \tilde{a}_\mu A\right)u^\dagger && (1.118a)\\ &= \left[u^\dagger, \partial_\mu u\right] - iu^\dagger r_\mu u - iu l_\mu u^\dagger \equiv 2\Gamma_\mu \ , \\ \Gamma_\mu &= \frac{1}{2}\left(\left[u^\dagger, \partial_\mu u\right] - iu^\dagger r_\mu u - iu l_\mu u^\dagger\right) \ , && (1.118b)\\ -2i\tilde{p}_\mu A &= u^\dagger\partial_\mu u + \partial_\mu u u^\dagger - iu^\dagger\left(\tilde{\rho}_\mu V + \tilde{a}_\mu A\right)u + iu\left(\tilde{\rho}_\mu V - \tilde{a}_\mu A\right)u^\dagger = && (1.118c)\\ &= u^\dagger\left(\partial_\mu u\ u + u\partial_\mu u - ir_\mu U + iU l_\mu\right)u^\dagger \equiv u^\dagger D_\mu U u^\dagger \equiv -iu_\mu \ , \\ u_\mu &= iu^\dagger D_\mu U u^\dagger \ , && (1.118d)\\ D_\mu U &\equiv \partial_\mu U - ir_\mu U + iU l_\mu \ . && (1.118e) \end{aligned}$$

$D_\mu U(x)$ is the covariant derivative of the Goldstone fields matrix $U(x)$. Its transformation can be deduced from Eqs. (1.64) and (1.115), because[9]

$$u'^\dagger D_\mu U' u'^\dagger = -2i\tilde{p}'_\mu A = e^{u'V}(-2i\tilde{p}_\mu A)e^{-u'V} \tag{1.119}$$

$$= h u^\dagger D_\mu U u^\dagger h^\dagger = u'^\dagger\left(V_R D_\mu U V_L^\dagger\right)u'^\dagger \tag{1.120}$$

[9]Notice that $D_\mu U'$ is a shorthand for $(D_\mu U)'$.

so that

$$\boxed{\begin{array}{ll}\text{Chiral transformations} & D_\mu U' = V_R D_\mu U V_L^\dagger \ , \\ & u'_\mu = h u_\mu h^\dagger \ .\end{array}} \tag{1.121}$$

$$u'_\mu = h u_\mu h^\dagger \ . \tag{1.122}$$

It is perhaps instructive to explicitly check the last transformation, and how the covariant derivative is such that it compensates for the terms arising from derivatives. Proceeding,

$$\begin{aligned} D_\mu U' &= \partial_\mu U' - i\left(r'_\mu U' - U' l'_\mu\right) = \partial_\mu V_R\ U\ V_L^\dagger + V_R\ \partial_\mu U\ V_L^\dagger + V_R\ U\ \partial_\mu V_L^\dagger - \\ &- i\left(V_R r_\mu V_R^\dagger + i V_R \partial_\mu V_R^\dagger\right)\left(V_R U V_L^\dagger\right) + i\left(V_R U V_L^\dagger\right)\left(V_L l_\mu V_L^\dagger + i V_L \partial_\mu V_L^\dagger\right) = \\ &= \partial_\mu V_R\ U\ V_L^\dagger + V_R\ \partial_\mu U\ V_L^\dagger + V_R\ U\ \partial_\mu V_L^\dagger - i V_R\ r_\mu\ U\ V_L^\dagger + \\ &+ V_R\ \partial_\mu V_R^\dagger\ V_R U V_L^\dagger - i V_R U V_L^\dagger V_L l_\mu V_L^\dagger - V_R U V_L^\dagger V_L^\dagger\ \partial_\mu V_L^\dagger \end{aligned}$$

and, as

$$\begin{aligned} V_R\ \partial_\mu V_R^\dagger\ V_R U V_L^\dagger &= -V_R V_R^\dagger \partial_\mu V_R U V_L^\dagger = -\partial_\mu V_R\ U V_L^\dagger \\ V_R U V_L^\dagger V_L \partial_\mu V_L^\dagger &= V_R U \partial_\mu V_L^\dagger \end{aligned}$$

then

$$D_\mu U' = V_R\left(\partial_\mu U - i r_\mu U + i U l_\mu\right) V_L^\dagger = V_R\left(D_\mu U\right) V_L^\dagger \ , \tag{1.123}$$

as expected.

We have, by now, worked out the transformation properties of all the basic ingredients we can use to achieve our goal of building the most general chiral Lagrangians. However, some additional definitions are customary in the literature, that ease the work. They are:

$$F_{\mu\nu}^L = u f_{\mu\nu}^L u^\dagger \ , \tag{1.124a}$$

$$F_{\mu\nu}^R = u^\dagger f_{\mu\nu}^R u \ , \tag{1.124b}$$

$$\chi_\pm = 2B_0\left(u^\dagger(s+ip)u^\dagger \pm u(s-ip)u\right) = 2B_0\left(u^\dagger \chi u^\dagger \pm u \chi^\dagger u\right) \tag{1.124c}$$

and B_0 is a constant added for later convenience. Their transformation properties are

$$\boxed{\begin{array}{ll}\text{Chiral transformations} & \left(F_{\mu\nu}^L\right)' = h F_{\mu\nu}^L h^\dagger \ , \\ & \left(F_{\mu\nu}^R\right)' = h F_{\mu\nu}^R h^\dagger \ , \\ & \chi'_\pm = h \chi_\pm h^\dagger \ .\end{array}} \tag{1.125}$$

$$\left(F_{\mu\nu}^R\right)' = h F_{\mu\nu}^R h^\dagger \ , \tag{1.126}$$

$$\chi'_\pm = h \chi_\pm h^\dagger \ . \tag{1.127}$$

The matrix $u(x) = e^{\xi\lambda}$ contains the Goldstone bosons fields, $\phi_a(x)$, which are identified with the coordinates ξ, and the matrices $\lambda \to \frac{\lambda_a}{2}$ are the Gell-Mann matrices for $SU(3)$, or $\lambda \to \frac{\sigma_i}{2}$, the Pauli matrices, for $SU(2)$, so that[10]

$$u(x) = e^{i\frac{\Phi(x)}{\sqrt{2}f}} \ , \tag{1.128}$$

$$U(x) = e^{i\frac{\sqrt{2}\Phi(x)}{f}} \ , \tag{1.129}$$

[10]The $\sqrt{2}$ factors in the following definitions can vary through the literature; what must be the same in the parametrization is the whole exponent within the exponential.

where f is a constant[11] to be specified later, and Φ is

$$\sqrt{2}\Phi(x) = \phi_a(x)\lambda^a \ . \tag{1.130}$$

The transformation (1.116), though simple in terms of the $U(x)$ matrix, would be very complicated in terms of the $\phi_a(x)$ fields, *i.e.*, these do not have a simple transformation under a generic element of the group $\mathfrak{G}$. However, when the transformation is restricted to $\mathfrak{H} = SU_V(N)$, $V_R = V_L = V$, it implies

$$U = e^{i\frac{\sqrt{2}\Phi}{f}} \to U' = VUV^\dagger = Ve^{i\frac{\sqrt{2}\Phi}{f}}V^\dagger = e^{iV\frac{\sqrt{2}\Phi}{f}V^\dagger}$$

so

$$\Phi \to V\Phi V^\dagger \ .$$

which means that the $\phi_a(x)$ transform, under $\mathfrak{H}$, as an octet, because, parametrizing $V = e^{i\theta_a\frac{\lambda_a}{2}}$, the last expresion can be expanded to get

$$\phi_c\frac{\lambda_c}{2} \to (\phi_c - \theta_a\phi_b f_{abc})\frac{\lambda_c}{2} \ ,$$

which means that they transform under the adjoint representation, $(T_c)_{ab} = if_{abc}$. Notice that this result is in agreement with Eq. (1.95).

With these considerations, and by restricting the transformation V to be an isospin or an hypercharge rotation, the quantum numbers of the different Goldstone bosons can be given, and we can write $\Phi(x)$ as:

$$\sqrt{2}\Phi(x)\Big|_{SU(2)} = \sum_{i=1}^{3}\phi_i\sigma_i = \begin{pmatrix} \pi^0 & \sqrt{2}\pi^+ \\ \sqrt{2}\pi^- & -\pi^0 \end{pmatrix} \ , \tag{1.131}$$

$$\sqrt{2}\Phi(x)\Big|_{SU(3)} = \sum_{i=1}^{8}\phi_a\lambda_a = \begin{pmatrix} \pi^0 + \frac{1}{\sqrt{3}}\eta & \sqrt{2}\pi^+ & \sqrt{2}K^+ \\ \sqrt{2}\pi^- & -\pi^0 + \frac{1}{\sqrt{3}}\eta & \sqrt{2}K^0 \\ \sqrt{2}K^- & \sqrt{2}\bar{K}^0 & -\frac{2}{\sqrt{3}}\eta \end{pmatrix} \ . \tag{1.132}$$

1.9.2 Charge conjugation

Under charge conjugation $\mathbb{C}$, a term containing quark spinors $\psi(x)$ tansforms as

$$\bar{\psi}(x)M(x)\psi(x) \longrightarrow \mathbb{C}\bar{\psi}(x)M(x)\psi(x)\mathbb{C}^{-1} = \bar{\psi}(x)\mathcal{C}(M'(x))^T\mathcal{C}^{-1}\psi(x) \tag{1.133}$$

where $\mathcal{C} = \gamma^0\gamma^2$ is a matrix acting on Dirac space, $M'(x)$ denotes the transformed $M(x)$ under charge conjugation (because it will often contain fields in addition to Dirac and/or flavor matrices) and A^T denotes the transpose matrix. The matrix $\mathcal{C}$ can be shown to fulfill the following properties:

$$\mathcal{C}\left\{\gamma_5, \gamma_5\gamma^\mu\right\}^T\mathcal{C}^{-1} = \left\{\gamma_5, \gamma_5\gamma^\mu\right\} \ , \tag{1.134}$$

[11] The fields $\phi_a(x)$ have energy dimensions, $[\phi_a] = E$, which can be inferred from the fact that $\partial_\mu\phi_a\partial^\mu\phi_a$ must have dimension E^4. Thus, in order to have a dimensionless argument in the exponential, we must have $\frac{\phi}{f}$ with f a dimensionful constant, $[f] = E$.

$$\mathcal{C}\left\{\gamma^{\mu}\right\}^{T}\mathcal{C}^{-1}=-\left\{\gamma^{\mu}\right\}\ . \tag{1.135}$$

Consider the term $\bar{q}\gamma^{\mu}v_{\mu}q$. It transforms as

$$\bar{q}\gamma^{\mu}v_{\mu}q\to\bar{q}\mathcal{C}\gamma^{\mu T}\mathcal{C}^{-1}{v'_{\mu}}^{T}q=-\bar{q}\gamma^{\mu}{v'_{\mu}}^{T}q=\bar{q}\gamma^{\mu}v_{\mu}q \tag{1.136}$$

where the last equality means that we impose invariance under charge conjugation. Thus, under charge conjugation, v_{μ} transforms as $v'_{\mu}(x)=-v_{\mu}(x)^{T}$. In a similar way, we can also work out the transformation of a_{μ}, s and p, and the results are:

Charge conjugation	$v'_{\mu}(x)=-v_{\mu}(x)^{T}\ ,$	(1.137)
	$a'_{\mu}(x)=a_{\mu}(x)^{T}\ ,$	(1.138)
	$s'(x)=s(x)^{T}\ ,$	(1.139)
	$p'(x)=p(x)^{T}\ .$	(1.140)

From these relations, it is inmediate to obtain

Charge conjugation	$r'_{\mu}(x)=-l_{\mu}^{T}\ ,$	(1.141)
	$l'_{\mu}(x)=-r_{\mu}^{T}\ ,$	(1.142)
	$\chi'(x)=\chi^{T}\ ,$	(1.143)
	$\chi^{\dagger\prime}(x)=\chi^{\dagger T}=\chi^{*}\ .$	(1.144)

The transformation of the field strength tensor is also straigthforward,

$$\left(f_{\mu\nu}^{R}\right)'=\partial_{\mu}r'_{\nu}-\partial_{\nu}r'_{\mu}-i\left[r'_{\mu},r'_{\nu}\right]=-\partial_{\mu}l_{\nu}^{T}+\partial_{\nu}l_{\mu}^{T}-i\underbrace{\left[l_{\mu}^{T},l_{\nu}^{T}\right]}_{-[l_{\mu},l_{\nu}]^{T}}=$$

$$=-\left(\partial_{\mu}l_{\nu}-\partial_{\nu}l_{\mu}-i\left[l_{\mu},l_{\nu}\right]\right)^{T}$$

Thus,

Charge conjugation	$\left(f_{\mu\nu}^{R}\right)'=-\left(f_{\mu\nu}^{L}\right)^{T}$	(1.145)
	$\left(f_{\mu\nu}^{L}\right)'=-\left(f_{\mu\nu}^{R}\right)^{T}$	(1.146)

The charge conjugation properties of the Goldstone bosons can be worked out from those of the axial charges Q_{a}^{A},

$$Q_{a}^{A}(t)=\int\mathrm{d}\vec{x}\ \bar{q}\gamma^{0}\gamma_{5}\frac{\lambda_{a}}{2}q(\vec{x},t) \tag{1.147}$$

Thus we have to calculate

$$\mathcal{C}\gamma^{0}\gamma_{5}\mathcal{C}^{-1}\frac{\lambda_{a}^{T}}{2}=\gamma^{0}\gamma_{5}\frac{\lambda_{a}^{T}}{2} \tag{1.148}$$

which means that $Q_{a}^{A}\to{Q'}_{a}^{A}=(Q_{a}^{A})^{T}$. For completeness, we also give the transformation of left/right and vector charges:

$$Q_{a}^{L}\to{Q'}_{a}^{L}=-(Q_{a}^{R})^{T}\ , \tag{1.149}$$

$$Q_a^R \to Q'^R_a = -(Q_a^L)^T \ , \tag{1.150}$$
$$Q_a^V \to Q'^V_a = -(Q_a^V)^T \ , \tag{1.151}$$
$$Q_a^A \to Q'^A_a = +(Q_a^A)^T \ . \tag{1.152}$$

As commented, the last transformation gives us, in turn, the transformation law for the Goldstone bosons, and thus, $\Phi(x) \to \Phi'(x) = \Phi^T(x)$, which implies

Charge conjugation	$\Phi'(x) = \Phi^T(x)$	(1.153)
	$u'(x) = u(x)^T$	(1.154)
	$U'(x) = U(x)^T$	(1.155)

The covariant derivative, taking into account the transformation of r, l and U, is

$$\begin{aligned}(D_\mu U)' &= \partial_\mu U^T - i r'_\mu U^T + i U^T l'_\mu = \partial_\mu U^T + i l_\mu^T U^T - i U^T r_\mu^T = \\ &= (\partial_\mu U - i r_\mu U + i U l_\mu)^T\end{aligned}$$

so that:

Charge conjugation	$(D_\mu U(x))' = (D_\mu U(x))^T$	(1.156)
	$u'_\mu(x) = u_\mu(x)^T$	(1.157)

The following transformations can also be derived:

Charge conjugation	$\left(F_{\mu\nu}^{R,L}\right)' = -\left(F_{\mu\nu}^{L,R}\right)^T$	(1.158)
	$\chi'_\pm = \chi_\pm^T$	(1.159)

A technical problem with charge conjugation is that, as seen, it gives $A \to A' = (-1)^{c_A} A^T$ (recall that A are matrices in flavor space). Thus, when forming terms for the Lagrangian from the product of two building blocks, A and B, it will transform as $AB \to (AB)' = (-1)^{c_A+c_B} A^T B^T$ instead of $\sim (AB)^T$, which makes it harder to check the invariance under charge conjugation. If we have just the product of two terms, it is not a problem, for $\langle A^T B^T \rangle = \langle AB \rangle$. For products of more than two terms, the trick is to consider commutators and anticommutators, so that

$$[A,B]' = (-1)^{c_A+c_B} [A,B]^T \ , \tag{1.160}$$
$$\{A,B\}' = (-1)^{c_A+c_B+1} \{A,B\}^T \ . \tag{1.161}$$

1.9.3 Hermiticity

If we consider a term in the Lagrangian like $\bar{q}(x)M(x)q(x)$, its hermitian conjugate is

$$(\bar{q}(x)M(x)q(x))^\dagger = \bar{q}(x)\gamma^0 M^\dagger(x)\gamma^0 q(x) \ .$$

Thus, we need some properties of the Dirac matrices, namely:

$$\gamma^0\gamma^{\mu\dagger}\gamma^0 = \gamma^\mu \qquad \gamma^0\gamma_5{}^\dagger\gamma^0 = -\gamma^5 \qquad \gamma^0\gamma_5^\dagger\gamma^{\mu\dagger}\gamma^0 = -\gamma_5\gamma^\mu = \gamma^\mu\gamma_5 \ .$$

In order to ensure hermiticity, the external fields must be hermitean themselves:

$$\boxed{\begin{array}{ll} \text{Hermiticity} & v_\mu^\dagger(x) = v_\mu(x) \\ & a_\mu^\dagger(x) = a_\mu(x) \\ & s^\dagger(x) = s(x) \\ & p^\dagger(x) = p(x) \end{array}} \tag{1.162}$$
(1.163)
(1.164)
(1.165)

and thus

$$\boxed{\begin{array}{ll} \text{Hermiticity} & r_\mu^\dagger(x) = r_\mu(x) \\ & l_\mu^\dagger(x) = l_\mu(x) \end{array}} \tag{1.166a}$$
(1.166b)

χ and $\chi^\dagger$ obviously transform one into each other. The field strength $f_{\mu\nu}^{R,L}$ also transform in a simple way, since $[r_\mu, r_\nu]^\dagger = -[r_\mu, r_\nu]$, and thus

$$\boxed{\text{Hermiticity} \qquad \left(f_{\mu\nu}^{R,L}(x)\right)^\dagger = f_{\mu\nu}^{R,L}(x)} \tag{1.167}$$

The matrix $\Phi(x)$ is hermitian as well, as follows directly from its definition, Eq. (1.130):

$$\boxed{\text{Hermiticity} \qquad \Phi^\dagger(x) = \Phi(x)\ ,} \tag{1.168}$$

Applying this to $U(x)$, it follows that:

$$U^\dagger(x) = e^{-i\frac{\sqrt{2}\Phi^\dagger(x)}{f}} = e^{-i\frac{\sqrt{2}\Phi(x)}{f}} = U^{-1}(x) \tag{1.169}$$

or

$$\boxed{\begin{array}{ll} \text{Hermiticity} & U^\dagger(x) = U^{-1}(x) \\ & u^\dagger(x) = u^{-1}(x) \end{array}} \tag{1.170}$$
(1.171)

The covariant derivative transforms as

$$D_\mu U^\dagger = \partial_\mu U^\dagger + iU^\dagger r_\mu - il_\mu U^\dagger = -U^\dagger \partial_\mu U^\dagger + iU^\dagger r_\mu - il_\mu U^\dagger = \tag{1.172}$$
$$= -U^\dagger \left(\partial_\mu U - ir_\mu U + iUl_\mu\right) U^\dagger \tag{1.173}$$

so that

$$\boxed{\begin{array}{ll} \text{Hermiticity} & D_\mu U(x)^\dagger = -U(x)^\dagger D_\mu U(x) U(x)^\dagger \\ & u_\mu^\dagger(x) = u_\mu(x) \end{array}} \tag{1.174}$$
(1.175)

Finally, with these results, the following transformations are easy to derive:

$$\boxed{\begin{array}{ll} \text{Hermiticity} & \left(F_{\mu\nu}^{R,L}(x)\right)^\dagger = F_{\mu\nu}^{R,L}(x) \\ & \chi_\pm^\dagger(x) = \pm\chi_\pm(x) \end{array}} \tag{1.176}$$
(1.177)

1.9.4 Lorentz transformations

Lorentz as well as parity transformations are somewhat different to the transformations discussed up to now, for they involve change in the space-time coordinates. Consider a Lagrangian density depending on a generic field $\varphi(x)$. Thus, a transformation of the field will be a symmetry if:

$$\mathcal{L}(\varphi'(x'), \partial'_\mu \varphi(x')) = \mathcal{L}(\varphi(x), \partial_\mu \varphi(x)) \ , \tag{1.178}$$

that is, if the Lagrangian written in terms of the transform field φ' at the transformed coordinate x' is the same as the original Lagrangian. Consider a proper, ortochronus, Lorentz transformation Λ in Minkowski space:[12]

$$x'^\mu = \Lambda^\mu{}_\nu x^\nu \ . \tag{1.179}$$

From a general point of view, Lorentz transformations on the fields can be described through a unitary operator $U(\Lambda)$ (acting on the operators, not on the coordinates), giving:

$$U^{-1}(\Lambda)\varphi(x)U(\Lambda) = \varphi'(x) \ , \tag{1.180}$$

whereas:

$$\varphi'(x') = D(\Lambda)\varphi(x) \ , \tag{1.181}$$

being $D(\Lambda)$ a matrix of a representation of the Lorentz group acting on the space of the φ fields indices. Then:

$$\begin{aligned} U^{-1}(\Lambda)\varphi(x)U(\Lambda) &= D(\Lambda)\varphi(\Lambda^{-1}x) && (1.182)\\ &= \varphi'(x) \ . && (1.183) \end{aligned}$$

For a scalar field $\Phi(x)$, we have the simplest transformation possible, $\Phi'(x') = \Phi(x)$, or $\Phi'(x) = \Phi(\Lambda^{-1}x)$ (that is, $D(\Lambda) = 1$). Its decomposition in creation and anhilation operators, $a^\dagger$ and a, respectively, is (up to irrelevant normalization constants):

$$\Phi(x) = \int \mathrm{d}^4k \delta(k^2 - m^2)\theta(k^0)\left(e^{-ikx}a(k) + e^{+ikx}a^\dagger(k)\right) \ . \tag{1.184}$$

Under the transformation Eq. (1.180), one has:

$$\begin{aligned} U^{-1}(\Lambda)\Phi(x)U(\Lambda) &= \int \mathrm{d}^4k \delta(k^2 - m^2)\theta(k^0)\left(e^{-ikx}U^{-1}a(k)U + e^{+ikx}U^{-1}a^\dagger(k)U\right) \\ = \Phi(\Lambda^{-1}x) &= \int \mathrm{d}^4k \delta(k^2 - m^2)\theta(k^0)\left(e^{-ik(\Lambda^{-1}x)}a(k) + e^{+ik(\Lambda^{-1}x)}a^\dagger(k)\right) \\ &\overset{p=\Lambda k}{=} \int \mathrm{d}^4p \delta(p^2 - m^2)\theta(p^0)\left(e^{-ipx}a(\Lambda^{-1}p) + e^{+ipx}a^\dagger(\Lambda^{-1}p)\right) \ , \end{aligned} \tag{1.185}$$

and then:

$$\begin{aligned} U^{-1}(\Lambda)a(k)U(\Lambda) &= a(\Lambda^{-1}k) \ , && (1.186a)\\ U^{-1}(\Lambda)a^\dagger(k)U(\Lambda) &= a^\dagger(\Lambda^{-1}k) \ . && (1.186b) \end{aligned}$$

Acting on a one-particle state $|\Phi(k)\rangle \equiv a^\dagger(k)|0\rangle$, it is found:

$$U^{-1}(\Lambda)|\Phi(k)\rangle = U^{-1}(\Lambda)a^\dagger(k)U(\Lambda)\underbrace{U^{-1}(\Lambda)|0\rangle}_{|0\rangle} = a^\dagger(\Lambda^{-1}k)|0\rangle = \left|\Phi(\Lambda^{-1}k)\right\rangle \ , \tag{1.187}$$

[12] Recall that $\Lambda^\mu{}_\nu \Lambda_\mu{}^\sigma = \delta^\sigma_\nu = g^\sigma_\nu$, and that $\left(\Lambda^{-1}\right)^\mu{}_\nu = \Lambda_\nu{}^\mu$, so $\left(\Lambda^{-1}\right)^\mu{}_\nu \Lambda^\nu{}_\rho = \delta^\mu_\rho$.

or

$$U(\Lambda)\,|\Phi(k)\rangle = |\Phi(\Lambda k)\rangle \ . \tag{1.188}$$

In terms of the operator $U(\Lambda)$, the Lorentz invariance of the Lagrangian, Eq. (1.178), can be recast as:

$$U^{-1}(\Lambda)\mathcal{L}(x)U(\Lambda) = \mathcal{L}(\Lambda^{-1}x) \ . \tag{1.189}$$

Let us move now to the spinor case, to study the Lorentz transformation properties of the fields in the external Lagrangian. The free Dirac Lagrangian density is:

$$\mathcal{L}(\psi(x), \partial_\mu\psi(x)) = \bar{\psi}(x)\,(i\gamma^\mu\partial_\mu - m)\,\psi(x) \ . \tag{1.190}$$

A spinor $\psi(x)$ transforms as:

$$\psi'(x') = S(\Lambda)\psi(x) \ , \tag{1.191}$$

$$\bar{\psi}'(x') = \bar{\psi}(x)\gamma^0 S^\dagger\gamma^0 \ . \tag{1.192}$$

The *transformed* mass term is given by:

$$\bar{\psi}'(x')\psi'(x') = \bar{\psi}(x)\gamma^0 S^\dagger(\Lambda)\gamma^0\psi(x) \equiv \bar{\psi}(x)\psi(x) \tag{1.193}$$

where in the last equality we impose the invariance as in Eq. (1.178). Then the matrices $S(\Lambda)$ must satisfy:

$$\gamma^0 S^\dagger(\Lambda)\gamma^0 = S^{-1}(\Lambda) \ . \tag{1.194}$$

For the derivative term of the Lagrangian, we have:

$$\bar{\psi}'(x')\gamma^\mu\partial'_\mu\psi'(x') = \bar{\psi}(x)S^{-1}(\Lambda)\gamma^\mu\Lambda_\mu{}^\nu\partial_\nu\psi(x) \equiv \bar{\psi}(x)\gamma^\nu\partial_\nu\psi(x) \ . \tag{1.195}$$

Here, the derivative ∂'_μ refers to the transformed coordinates, and thus ∂'_μ transforms as a vector:

$$\partial'_\mu \equiv \frac{\partial}{\partial x'^\mu} = \Lambda_\mu{}^\rho\partial_\rho \ . \tag{1.196}$$

From Eq. (1.195), it is deduced that:

$$S^{-1}(\Lambda)\gamma^\mu\Lambda_\mu{}^\nu S(\Lambda) = \gamma^\nu \ , \tag{1.197}$$

$$S^{-1}(\Lambda)\gamma^\mu S(\Lambda) = \Lambda^\mu{}_\nu\gamma^\nu \ , \tag{1.198}$$

and thus the γ^ν matrices are usually said to transform as vectors. Now, in the Lagrangian with external fields, let us consider the term $\bar{q}(x)\gamma^\mu v_\mu(x)q(x)$, where the quark spinors are denoted by $q(x)$. The transformed Lagrangian is:

$$\bar{q}'(x')\gamma^\mu v'_\mu(x')q'(x') = \bar{q}(x)S^{-1}(\Lambda)\gamma^\mu S(\Lambda)v'_\mu(x')q(x) \equiv \bar{q}(x)\gamma^\mu v_\mu(x)q(x) \tag{1.199}$$

which implies that v_μ must transform as $v'^\mu(\Lambda x) = \Lambda^\mu{}_\nu v^\nu(x)$, or $v'^\mu(x) = \Lambda^\mu{}_\nu v^\nu(\Lambda^{-1}x)$. Proceeding analogously with a_μ, s and p, we get

Lorentz	$v'_\mu(x) = \Lambda_\mu{}^\rho v_\rho(\Lambda^{-1}x)$	(1.200)
	$a'_\mu(x) = \Lambda_\mu{}^\rho a_\rho(\Lambda^{-1}x)$	(1.201)
	$s'(x) = s(\Lambda^{-1}x)$	(1.202)
	$p'(x) = p(\Lambda^{-1}x)$.	(1.203)

Above, we also used that:

$$S^{-1}(\Lambda)\gamma_5 S(\Lambda) = \gamma_5 \ . \tag{1.204}$$

Together with parity (as shown below), this means that $v_\mu(x)$ is a vector, $a_\mu(x)$ is an axial-vector, $s(x)$ is a scalar, and $p(x)$ is a pseudoscalar. As there is no change of sign, we directly get:

Lorentz	$r'_\mu(x) = \Lambda_\mu{}^\rho r_\rho(\Lambda^{-1}x)$	(1.205)
	$l'_\mu(x) = \Lambda_\mu{}^\rho l_\rho(\Lambda^{-1}x)$	(1.206)
	$\chi'(x) = \chi(\Lambda^{-1}x)$	(1.207)
	$\chi'^\dagger(x) = \chi^\dagger(\Lambda^{-1}x)$	(1.208)

The tensors $f^{R,L}_{\mu\nu}(x)$ have a derivative, that also transforms as a vector, thus

Lorentz	$f'^{\,R,L}_{\mu\nu}(x) = \Lambda_\mu{}^\alpha \Lambda_\nu{}^\beta f^{R,L}_{\alpha\beta}(\Lambda^{-1}x)$	(1.209)

As usual, the axial charges will give us the transformation properties of the Goldstone bosons. Thus,

Lorentz	$\Phi'(x) = \Phi(\Lambda^{-1}x)$	(1.210)
	$\phi'_a(x) = \phi_a(\Lambda^{-1}x)$	(1.211)
	$U'(x) = U(\Lambda^{-1}x)$	(1.212)
	$u'(x) = u(\Lambda^{-1}x)$	(1.213)
	$D_\mu U'(x) = \Lambda_\mu{}^\rho D_\rho U(\Lambda^{-1}x)$	(1.214)
	$u'_\mu(x) = \Lambda_\mu{}^\rho u_\rho(\Lambda^{-1}x)$	(1.215)
	$F'^{\,R,L}_{\mu\nu}(x) = \Lambda_\mu{}^\alpha \Lambda_\nu{}^\beta F^{R,L}_{\alpha\beta}(\Lambda^{-1}x)$	(1.216)
	$\chi'_\pm(x) = \chi_\pm(\Lambda^{-1}x)$	(1.217)

The transformation of $D_\mu U$ as a vector is due to the fact that the three terms of $D_\mu U$ contain, respectively, ∂_μ, r_μ, l_μ, all of them transforming as a vector. The same argument applies to u_μ and $F^{R,L}_{\mu\nu}$.

1.9.5 Parity

Let us consider parity transformations,

$$x'^\mu = \mathscr{P}^\mu{}_\nu x^\nu = (x^0, -\vec{x}) \ . \tag{1.218}$$

The following properties of the Dirac matrices will be useful here:

$$\gamma^0\gamma^0 = 1 \qquad \gamma^0\gamma^\mu\gamma^0 = \mathscr{P}^\mu{}_\nu\gamma^\nu \tag{1.219}$$

$$\gamma^0\gamma_5\gamma^0 = -\gamma_5 \qquad \gamma^0\gamma^\mu\gamma_5\gamma^0 = -\mathscr{P}^\mu{}_\nu\gamma^\nu\gamma_5 \tag{1.220}$$

Under parity transformations, a spinor of intrinsic parity $\eta_S = \pm 1$ transforms as:

$$\psi'(\mathscr{P}x) = \eta_S\gamma^0\psi(x) \ , \tag{1.221a}$$

$$\bar{\psi}'(\mathscr{P}x) = \eta_S\bar{\psi}(x)\gamma^0 \ , \tag{1.221b}$$

or

$$\psi'(x) = \eta_S \gamma^0 \psi(\mathscr{P}x) \ , \tag{1.222a}$$
$$\bar{\psi}'(x) = \eta_S \bar{\psi}(\mathscr{P}x)\gamma^0 \ , \tag{1.222b}$$

since $\mathscr{P}^2 x = x$. In terms of a unitary operator, we have:

$$U_p \psi(x) U_p^{-1} = \psi'(x) = \eta_S \gamma^0 \psi(\mathscr{P}x) \ . \tag{1.223}$$

The different terms in the Lagrangian with external sources transform as:

$$\bar{q}(x)M(x)q(x) \to \bar{q'}(\mathscr{P}x)M'(\mathscr{P}x)\gamma^0 q'(\mathscr{P}x) = \bar{q}(x)\gamma^0 M'(\mathscr{P}x)\gamma^0 q(x) \equiv \bar{q}(x)M(x)q(x) \ . \tag{1.224}$$

In general, there will be field and Dirac matrices in $M(x)$. The transformation on $M(x)$ is thus:

$$M'(x) = \gamma^0 M(\mathscr{P}x)\gamma^0 \ . \tag{1.225}$$

Let us consider the term $\bar{q}\gamma^\mu\gamma_5 a_\mu q$. We must have:

$$\gamma^\mu\gamma_5 a'_\mu(x) = \gamma^0\gamma^\mu\gamma_5\gamma^0 a_\mu(\mathscr{P}x) = -\mathscr{P}^\mu{}_\nu \gamma^\nu \gamma_5 a_\mu(\mathscr{P}x) \ , \tag{1.226}$$

so that a_μ transforms as $a'_\mu(x) = -\mathscr{P}_\mu{}^\nu a_\nu(\mathscr{P}x)$. For the rest of the external source, the transformations are

Parity	$s'(x) = s(\mathscr{P}x)$	(1.227)
	$p'(x) = -p(\mathscr{P}x)$	(1.228)
	$v'_\mu(x) = \mathscr{P}_\mu{}^\nu v_\nu(\mathscr{P}x)$	(1.229)
	$a'_\mu(x) = -\mathscr{P}_\mu{}^\nu a_\nu(\mathscr{P}x)$	(1.230)

The change of sign in a_μ and not in v_μ (in charge conjugation it was the opposite) induces a change $r \leftrightarrow l$, and, in the same way ocurs with χ,

Parity	$r'_\mu(x) = \mathscr{P}_\mu{}^\nu l_\nu(\mathscr{P}x)$	(1.231)
	$l'_\mu(x) = \mathscr{P}_\mu{}^\nu r_\nu(\mathscr{P}x)$	(1.232)
	$\chi'(x) = \chi^\dagger(\mathscr{P}x)$	(1.233)
	$\chi'^\dagger(x) = \chi(\mathscr{P}x)$	(1.234)

In $f^{R,L}_{\mu\nu}$ we have two indices: the derivative changes under parity as v_μ, and, again, there is a change $r \leftrightarrow l$, which results in

Parity	$f'_{\mu\nu}{}^{L,R}(x) = \mathscr{P}_\mu{}^\alpha \mathscr{P}_\nu{}^\beta f^{R,L}_{\alpha\beta}(\mathscr{P}x)$	(1.235)

The parity transformations of the Goldstone bosons are derived from those of the charges Q^A_a, which implies a change of sign because

$$\gamma^0 \left(\gamma^0\gamma_5\right)\gamma^0 = -\gamma_0\gamma_5 \ , \tag{1.236}$$

whence, and as $U(x) = \exp i\frac{\sqrt{2}\Phi(x)}{f}$,

$$\boxed{\text{Parity}} \quad \begin{aligned} \Phi'(x) &= -\Phi(\mathscr{P}x) && (1.237)\\ \phi_a'(x) &= -\phi_a(\mathscr{P}x) && (1.238)\\ U'(x) &= U^{-1}(\mathscr{P}x) = U^\dagger(\mathscr{P}x) && (1.239)\\ u'(x) &= u^{-1}(\mathscr{P}x) = u^\dagger(\mathscr{P}x) && (1.240) \end{aligned}$$

where we have used Eq. (1.170). For the covariant derivative, ∂, r and l give a common factor $\mathscr{P}_\mu{}^\nu$, so that:

$$\begin{aligned} D_\mu U'(x) &= \mathscr{P}_\mu{}^\nu \left(\frac{\partial}{\partial(\mathscr{P}x)^\nu} U^\dagger(\mathscr{P}x) - i l_\nu(\mathscr{P}x) U^\dagger(\mathscr{P}x) + i U^\dagger(\mathscr{P}x) r_\nu(\mathscr{P}x) \right) \\ &= \mathscr{P}_\mu{}^\nu (D_\nu U(\mathscr{P}x))^\dagger \end{aligned} \tag{1.241}$$

and we have used Eq. (1.166). Thus we can write:

$$\boxed{\text{Parity}} \quad \begin{aligned} D_\mu U(x)' &= \mathscr{P}_\mu{}^\nu D_\nu U^\dagger(\mathscr{P}x) && (1.242)\\ u_\mu(x)' &= -\mathscr{P}_\mu{}^\nu u_\nu^\dagger(\mathscr{P}x) && (1.243) \end{aligned}$$

At last, for the fields defined in Eqs. (1.124), we can also derive the following transformations:

$$\boxed{\text{Parity}} \quad \begin{aligned} F_{\mu\nu}^{R,L}(x)' &= \mathscr{P}_\mu{}^\alpha \mathscr{P}_\nu{}^\beta F_{\alpha\beta}^{L,R}(\mathscr{P}x) && (1.244)\\ \chi_\pm(x)' &= \pm\chi_\pm(\mathscr{P}x) && (1.245) \end{aligned}$$

1.9.6 Cayley–Hamilton theorem

The Cayley–Hamilton theorem is a useful tool to reduce the number of independent terms in the Lagrangian. For our purposes, it can be stated as follows.

Theorem (Cayley–Hamilton)**.** *Let A be an square $n \times n$ matrix, and let $p(\lambda)$ be its characteristic polynomial,*

$$p(\lambda) = \det(A - \lambda \mathbb{I}_n)$$

where $\mathbb{I}_n$ is the $n \times n$ identity matrix. Then,

$$p(A) = 0\ . \tag{1.246}$$

Notice that some abuse of notation has been made in the theorem, for $p(\lambda)$ refers to a polynomial in complex or real variable λ, thus being $p(\lambda)$ itself a real or complex number, and $p(A)$ refers to the formal replacement of λ by A, thus $p(A)$ is itself a matrix (the zero matrix, in this case). We apply it for the two cases we could be interested, $n = 2$ or $n = 3$.

$n = 2$ The polynomial can be written as

$$p(\lambda) = \lambda^2 - \langle A\rangle\lambda + \det A$$

with $\langle A\rangle = \mathrm{Tr}A$ the trace of the matrix A. Thus,

$$p(A) = A^2 - \langle A\rangle A + \det A\ \mathbb{I}_2 = 0$$

which allows to write $\det A$ in terms of traces of A and powers of it.

$n = 3$ We can write

$$p(\lambda) = \lambda^3 - \langle A\rangle\lambda^2 + \frac{1}{2}\left(\langle A\rangle^2 - \langle A^2\rangle\right)\lambda - \det A$$

and thus

$$p(A) = A^3 - \langle A\rangle A^2 + \frac{1}{2}\left(\langle A\rangle^2 - \langle A^2\rangle\right)A - \det A\ \mathbb{I}_3\ .$$

Then, for both cases, we can write the determinant of the matrix in term of the traces, and this will diminish the number of independent term in our Lagrangians (where, in fact, no determinants will be present). One can also obtain relations between traces of monomials involving different number of terms by multiplying $p(A)$ by A^n, $n \geqslant 1$.

1.10 Chiral power counting and effective Lagrangian at $\mathcal{O}(p^2)$

1.10.1 Lowest order Lagrangian and Goldstone boson masses

If we set the quark masses to zero, $M = 0$, as well as the external field, $v_\mu = a_\mu = p = s = 0$, every Lagrangian we could build would contain derivatives. Besides an unimportant term $UU^\dagger = \mathbb{I}$, the *lowest order* Lagrangian we can construct is

$$\mathcal{L}_{\text{eff}} \sim \langle \partial_\mu U \partial^\mu U^\dagger\rangle \tag{1.247}$$

where $\langle\cdots\rangle$ denotes the trace in flavour space. Let us assign to U the zeroth order, $U \sim \mathcal{O}(p^0)$. We count the derivatives as $\mathcal{O}(p)$, since they tipically introduce an external momentum p. This means that the previous Lagrangian $\mathcal{L}_{\text{eff}}$ is $\mathcal{O}(p^2)$. From the definition of $D_\mu U$, which involves r_μ and l_μ in the same foot that ∂_μ, it seems to be convenient to count r_μ, l_μ as $\mathcal{O}(p)$, and thus, $D_\mu U$, $u_\mu \sim \mathcal{O}(p)$. The χ building blocks will have inside the term $s(x) = M + \cdots$, and one could think that $s(x) \sim \mathcal{O}(p)$. However, the term that involves χ would be $\langle U^\dagger\chi + \chi^\dagger U\rangle$, which, upon expansion, will give the standard mass terms of Klein–Gordon fields, $\mathcal{L} \sim m^2\varphi^2$, so the correct chiral order of χ is $\chi \sim \mathcal{O}(p^2)$. Another argument not to assign $\chi \sim \mathcal{O}(p)$ is that, in that case, the leading order Lagrangian would be $\mathcal{L} \sim \langle\chi\rangle$, thus no kinetic term of the pseudoscalar Goldstone bosons would be present, because it enters through the term $\langle\partial_\mu U\partial^\mu U^\dagger\rangle$. The assignments of the chiral order of the building blocks are summarized in Table 1.1.

Given two matrices A and B transforming as $A \to V_R A V_L^\dagger$ and $B \to V_R B V_L^\dagger$, we can construct an invariant term as $AB^\dagger \to V_R A V_L^\dagger V_L B^\dagger V_R^\dagger = V_R A B^\dagger V_R^\dagger$, which, due to the cyclical

$\mathcal{O}(p^0)$	$\mathcal{O}(p)$	$\mathcal{O}(p^2)$
U	u_μ,$D_\mu U$	$f^{R,L}_{\mu\nu}$
	r_μ, l_μ	χ, $\chi_\pm$

Table 1.1: Chiral order of the building blocks.

property of the trace, $\langle V_R A B^\dagger V_R^\dagger\rangle = \langle V_R^\dagger V_R A B^\dagger\rangle = \langle A B^\dagger\rangle$, *i.e.*, it is invariant under chiral transformations. If, instead, we have two matrices C and D transforming as $C \to hCh^\dagger$ and $D \to hDh^\dagger$, then, $\langle CD\rangle \to \langle hCh^\dagger hDh^\dagger\rangle = \langle CD\rangle$, which is automatically invariant.

The effective Lagrangian $\mathcal{L}_{\text{eff}}$ will have an expansion in *chiral powers* as

$$\mathcal{L}_{\text{eff}} = \sum_d \mathcal{L}^{(d)} \tag{1.248}$$

As we have seen, the lowest possible order is $\mathcal{O}(p^2)$. Given the transformation properties of the building blocks we have discussed so far, the most general Lagrangian is

$$\mathcal{L}^{(2)} = a\langle D_\mu U D^\mu U^\dagger\rangle + b\langle\chi_+\rangle \tag{1.249}$$

Up to now, we have been solely guided by the light of symmetry arguments, but the values of the constants will never be given by symmetry considerations.

The term $\langle\partial_\mu U\partial^\mu U^\dagger\rangle$ gives the kinetic term. Expanding U in powers of Φ, we are left with

$$\begin{aligned} a\langle\partial_\mu U\partial^\mu U^\dagger\rangle &= \frac{2a}{f^2}\langle\partial_\mu\Phi\partial^\mu\Phi\rangle = \\ &= \frac{4a}{f^2}\left(\partial_\mu\pi^0\partial^\mu\pi^0 + \partial_\mu\eta\partial^\mu\eta + 2\partial_\mu\pi^+\partial_\mu\pi^- + \partial_\mu K^+\partial_\mu K^- + \partial_\mu K^0\partial_\mu\bar{K}^0\right) , \end{aligned}$$

which gives the proper normalization of a kinetic term for $a = \frac{f^2}{4}$. For the mass term, take $s = M$ and $p = 0$ to get

$$\begin{aligned} b\langle\chi_+\rangle =& b\ 2B_0\langle\left(U + U^\dagger\right) M\rangle = -\frac{2b}{f^2}2B_0\langle\Phi^2 M\rangle = \\ =& -\frac{4b}{f^2}2B_0\left(\hat{m}\ {\pi^0}^2 + 2\hat{m}\ \pi^+\pi^- + \frac{1}{3}\left(\hat{m} + 2m_s\right)\eta^2 + \right. \\ &\left. + \left(\hat{m} + m_s\right)K^+K^- + \left(\hat{m} + m_s\right)K^0\bar{K^0}\right) , \end{aligned}$$

where we have taken $M = \text{diag}(m_u, m_d, m_s)$ and $m_u = m_d = \hat{m}$, which means exact isospin symmetry. The mass term for π^0 is thus

$$-\frac{4b}{f^2}\ 2B_0\ m = -m_\pi^2$$

The constant b can thus be absorbed into B_0 with the definition $b = \frac{f^2}{4}$, and thus

$$m_\pi^2 = 2B_0\ \hat{m}\ , \tag{1.250a}$$

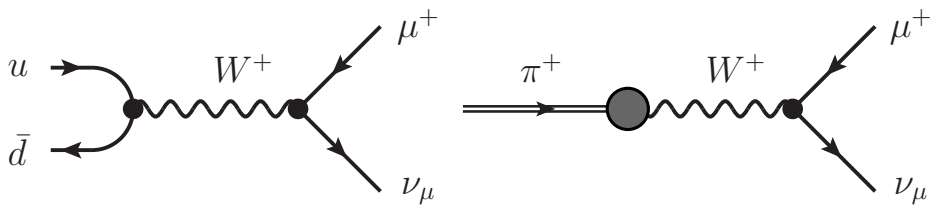

Figure 1.5: Feynman diagrams for the pion weak decay constant, f_π..

$$m_K^2 = 2B_0\left(\frac{\hat{m}+m_s}{2}\right) , \tag{1.250b}$$

$$m_\eta^2 = 2B_0\left(\frac{\hat{m}+2m_s}{3}\right) . \tag{1.250c}$$

The most general effective Lagrangian at $\mathcal{O}(p^2)$ is thus [16–19]:

$$\mathcal{L}^{(2)} = \frac{f^2}{4}\langle D_\mu U D^\mu U^\dagger\rangle + \frac{f^2}{4}\langle\chi_+\rangle \tag{1.251}$$

which depends upon two constants, f and B_0, which is hidden in the definition of χ_+. Even without the (experimental) knowledge of these constants, we have achieved predictive power, because, from relations Eq. (1.250), we have

$$3m_\eta^2 + m_\pi^2 = 4m_K^2 \tag{1.252}$$

which is the well-known Gell–Mann-Okubo mass formula, which is satisfied within 10 %.

1.10.2 The weak decay constant of the pion at $\mathcal{O}(p^2)$

To obtain an experimental value for f, we calculate, from our Lagrangian, the lifetime τ of the pion. The charged pion π^+ decays mainly to $\mu^+\nu_\mu$ through an intermediate W^+, see the left diagram of Fig. 1.5 for a very schematic plot, with a branching fraction of $\Gamma_i/\Gamma \simeq 0.99$. The hadronic term of the amplitude, corresponding to the vertex $\pi^+ \to W^+$, represented in the right diagram of Fig. 1.5 by a blob, is given by the Lagrangian term contained in $\langle D_\mu U D^\mu U^\dagger\rangle$, with the substitutions of Eq. (1.97),

$$v_\mu = -a_\mu = -\frac{g}{2\sqrt{2}}\left(T_+ W_\mu^+ + \text{h.c.}\right)$$

which results in the Lagrangian

$$\begin{aligned}\mathcal{L}_{W\phi} &= -\frac{gf}{2}\left(W_\mu^+\langle T_+\partial^\mu\Phi\rangle + W_\mu^-\langle T_+^\dagger\partial^\mu\Phi\rangle\right) = \\ &= -\frac{gf}{2}\left(V_{ud}W_\mu^+\partial^\mu\pi^- + V_{ud}^* W_\mu^-\partial^\mu\pi^+\right)\end{aligned}$$

The leptonic vertex is taken from the standard electroweak Lagrangian, and the whole amplitude is

$$\mathcal{M} = -G_F V_{ud} f\,\bar{u}(\nu_\mu)\not{p}(1-\gamma_5)v(\mu^+)$$

where $G_F = \frac{\sqrt{2}g^2}{8M_W^2}$ is the Fermi constant. Finally, the decay rate is

$$\frac{1}{\tau} = \frac{G_F^2 |V_{ud}|^2}{4\pi} f^2 m_\pi m_\mu^2 \left(1 - \frac{m_\mu^2}{m_\pi^2}\right)^2$$

with the values $\tau \approx 2.6 \cdot 10^{-8}$ s, $G_F \approx 1.17 \cdot 10^{-11}$ MeV^{-2}, $m_\pi \approx 140$ MeV, $m_\mu \approx 106$ MeV and $|V_{ud}| \approx 0.97$, we get the value $f \approx 93$ MeV. The meaning of this constant, which from now on we call the pion weak decay constant, and denote with f_π, is thus clear: it gives the strength of the weak decay of the charged pion (whence its name).

1.11 Chiral Lagrangians for $SU(2)$ and $SU(3)$ at $\mathcal{O}(p^4)$

In this Section, we give the NLO Lagrangians, considering first the $SU(3)$ case and later discussing the $SU(2)$ ones.

1.11.1 $SU(3)$ and standard power counting formula

With the techniques described so far, that lead us to the $\mathcal{O}(p^2)$ Lagrangian in Eq. (1.249), one can construct the most general Lagrangian up to $\mathcal{O}(p^4)$, that is, a Lagrangian which includes all the terms with $\mathcal{O}(p^4)$ power counting and invariant under the symmetry of the theory. For $SU(3)$, this reads

$$\begin{aligned}
\mathcal{L}^{(4)}_{SU(3)} = & L_1 \langle D_\mu U^\dagger D^\mu U\rangle^2 + L_2 \langle D_\mu U^\dagger D_\nu U\rangle \langle D^\mu U^\dagger D^\nu U\rangle \\
& + L_3 \langle D_\mu U^\dagger D^\mu U D_\nu U^\dagger D^\nu U\rangle + L_4 \langle D_\mu U^\dagger D^\mu U\rangle \langle \chi^\dagger U + \chi U^\dagger\rangle \\
& + L_5 \langle D_\mu U^\dagger D^\mu U (\chi^\dagger U + U^\dagger \chi)\rangle + L_6 \langle \chi^\dagger U + \chi U^\dagger\rangle^2 + L_7 \langle \chi^\dagger U - \chi U^\dagger\rangle^2 \\
& + L_8 \langle \chi^\dagger U \chi^\dagger U + \chi U^\dagger \chi U^\dagger\rangle - i L_9 \langle f_R^{\mu\nu} D_\mu U D_\nu U^\dagger + f_L^{\mu\nu} D_\mu U^\dagger D_\nu U\rangle \\
& + L_{10} \langle U^\dagger f_R^{\mu\nu} U f_{L\mu\nu}\rangle + H_1 \langle f_{R\mu\nu} f_R^{\mu\nu} + f_{L\mu\nu} f_L^{\mu\nu}\rangle + H_2 \langle \chi^\dagger \chi\rangle
\end{aligned} \tag{1.253}$$

The L_i attached to each term of the Lagrangian are the so called *low energy constants*, which we will discuss later on, in the context of the $SU(2)$ Lagrangians. To reduce the number of independent constants and thus have more predictive power, one should reduce the number of independent terms of the Lagrangian to the minimum. This can be done through the use of trace identities, like the ones shown in Subsec. 1.9.6, and the use of the classical equation of motion of pions, derived from Eq. (1.249). If this is not done, one would have a correlation between the different low energy constants attached to each term of the Lagrangian.

The chiral expansion is performed over a typical hadronic mass scale $\Lambda_\chi \simeq 1$ GeV, which roughly corresponds to the more massive states in the spectrum in Fig. 1.1, that are integrated out, like the ρ, ω, etc.[13] In this way, comparing the $\mathcal{O}(p^4)$ and $\mathcal{O}(p^2)$ Lagrangian, one has

$$L_i \sim \frac{f_\pi^2/4}{\Lambda_\chi^2} \sim 10^{-3} \ . \tag{1.254}$$

[13]The lightest scalar resonances, σ, κ, $f_0(980)$ and $a_0(980)$, require extra qualification that will be fully discussed along this thesis.

Also, from the unitary corrections, one can deduce [201]:

$$\Lambda_\chi \simeq 4\pi f_\pi \simeq 1 \text{ GeV} . \tag{1.255}$$

The standard chiral power counting of a connected diagram, p^D (where p is a generic small momentum compared to $\Lambda_\chi \simeq 1$ GeV), obeys the equation [18, 221]

$$D = 2 + \sum_d N_d (d-2) + 2L . \tag{1.256}$$

In this equation, d is the chiral dimension of a vertex, N_d the number of vertices with dimension d and L is the number of loops. Each derivative increases the counting by one unit and the lightest quark masses add two units to D. The $\mathcal{O}(p^2)$ or *leading order* (LO) calculations have $D = 2$ with no loops ($L = 0$) and involve only $d = 2$ vertices. For the $\mathcal{O}(p^4)$ ones, or *next-to-leading order* (NLO), $D = 4$, and one has diagrams with $L = 1$ that involve only $d = 2$ vertices. There are also diagrams with $L = 0$ with only one $d = 4$ vertex, with the rest of vertices having $d = 2$.

1.11.2 *SU*(2) Lagrangian in *O*(4) notation

The original Lagrangians for $SU(2)$ given by Gasser and Leutwyler [18] were written in terms of invariant scalar products of $O(4)$ vectors, instead of traces from $SU(2)$, since these two groups are isomorphic. In that notation, the $SU(2)$ chiral Lagrangians at $\mathcal{O}(p^2)$, $\mathcal{L}_2$, and $\mathcal{O}(p^4)$, $\mathcal{L}_4$, are:

$$\mathcal{L}^{(2)}_{SU(2),\text{GL}} = \frac{f^2}{2} \nabla_\mu U_A \nabla^\mu U_A + 2 f^2 (\chi_A U_A) \tag{1.257a}$$

$$\begin{aligned} \mathcal{L}^{(4)}_{SU(2),\text{GL}} = {} & l_1 \left(\nabla^\mu U_A \nabla_\mu U_A\right)^2 + l_2 \left(\nabla^\mu U_A \nabla^\nu U_A\right) \left(\nabla_\mu U_B \nabla_\nu U_B\right) + l_3 \left(\chi_A U_A\right)^2 \\ & + l_4 \left(\nabla^\mu \chi_A \nabla_\mu U_A\right) + l_5 \left(U_A F_{\mu\nu,AB} F^{\mu\nu}_{BC} U_C\right) + l_6 \left(\nabla^\mu U_A F_{\mu\nu,AB} \nabla^\nu U_B\right) \\ & + l_7 \left(\tilde{\chi}_A U_A\right)^2 + h_1 \left(\chi_A \chi_A\right) + h_2 \left(F_{\mu\nu,AB} F^{\mu\nu}_{BA}\right) + h_3 \left(\tilde{\chi}_A \tilde{\chi}_A\right) , \end{aligned} \tag{1.257b}$$

Above, uppercase subscripts denote the components of the $O(4)$ vectors, $A = 0, 1, 2, 3$, whereas, in the following, lowercase ones denote the last three components, $i = 1, 2, 3$. The pion fields are included through the $O(4)$ real vector field with components $U_A(x)$ of unit length, $U_A U_A = 1$, as:

$$\vec{U}(x) \equiv (U_1, U_2, U_3) = \frac{\vec{\pi}(x)}{f} = \frac{1}{f} (\pi_1, \pi_2, \pi_3) \tag{1.258}$$

$$U^0(x) = \sqrt{1 - \vec{U}(x)^2} = 1 - \frac{1}{2}\vec{U}^2 - \frac{1}{8}\vec{U}^4 - \cdots \tag{1.259}$$

The relation between the charged and Cartesian pion fields is given by:

$$\pi^\pm = \frac{\pi_1 \mp i\pi_2}{\sqrt{2}} \quad , \quad \pi^0 = \pi^3 . \tag{1.260}$$

The vectors $\chi_i(x)$, $\tilde{\chi}_i(x)$, are proportional to the scalar and pseudoscalar sources,

$$\chi_0 = 2Bs^0(x) , \tag{1.261}$$

$$\chi_i = 2Bp^i(x) \ , \tag{1.262}$$
$$\tilde{\chi}_0 = 2Bp^0(x) \ , \tag{1.263}$$
$$\tilde{\chi}_i = -2Bs^i(x) \ . \tag{1.264}$$

The explicit chiral symmetry breaking due to the finite u and d quark masses enters through the χ_0 term, by putting $\chi_0 = 2B(s^0(x) + \hat{m})$. Here, $2B\hat{m} = m^2$ is the pion mass at leading chiral order. That is, in our notation m represents the pion mass at LO, *i.e.*, the parameter that appears directly from the Lagrangian, while m_π refers to the physical pion mass. We consider exact isospin symmetry, so that $\hat{m}$ is the algebraic mean of the u and d quark masses. The fields $s^0(x)$ and $p^i(x)$ refer to the scalar and pseudoscalar c-number external sources, in order. The parameter B is related to the value of the quark condensate in the chiral limit $\langle \bar{q}^i q^j \rangle = -\delta^{ij} f^2 B$ [18]. In this notation, the covariant derivative ∇_μ is defined by:

$$\nabla_\mu U_0 = \partial_\mu U_0 + a_{\mu,i} U_i \tag{1.265}$$
$$\nabla_\mu U_i = \partial_\mu U_i - a_{\mu,i} U_0 + \sum_{j,k=1}^{3} \epsilon^{ijk} v_{\mu,j} U_k \quad (i = 1,2,3) \tag{1.266}$$

Finally, the tensor $F_{\mu\nu,AB}$ is defined by:

$$(\nabla_\mu \nabla_\nu - \nabla_\nu \nabla_\mu) U_A = F_{\mu\nu,AB} U_B \tag{1.267}$$

It is customary to employ the finite and scale independent constants $\bar{l}_i$ defined by

$$\begin{aligned}
l_i &= l_i^r + \gamma_i \frac{R}{32\pi^2} \ , \\
l_i^r(\mu) &= \frac{\gamma_i}{32\pi^2} \left(\bar{l}_i + \log \frac{m^2}{\mu^2} \right) \ , \\
h_i &= h_i^r + \delta_i \frac{R}{32\pi^2} \ , \\
h_i^r(\mu) &= \frac{\delta_i}{32\pi^2} \left(\bar{h}_i + \log \frac{m^2}{\mu^2} \right) \ , \\
R &= \mu^{n-4} \left(\frac{2}{n-4} - (\log 4\pi + \Gamma'(1) + 1) \right) \ .
\end{aligned} \tag{1.268}$$

Above, $n \to 4$ is the dimension of the Minkowski space, and the quantity R is infinite. It is cancelled with the infinities that originate from loops, through the loop functions calculated in dimensional regularization, as seen in Appendix B for the case of $\pi\pi$ scattering in the presence of a scalar source, studied in Chapter 5, or in Sec. 1.12, where the scalar pion form factor is worked out as an example. The dependence on the renormalization scale μ is also reabsorbed by the constants l_i. The $\bar{l}_i$ are, up to a numerical factor, the renormalized coupling constants l_i^r at the scale $\mu = m \simeq m_\pi$. In the chiral limit the $\bar{l}_i$ are not defined as they are then divergent quantities. We have also defined analogously the $\bar{h}_i$ low energy constants. The needed γ_i, δ_i coefficients are [18]:

$$\gamma_1 = \frac{1}{3} \ , \quad \gamma_2 = \frac{2}{3} \ , \quad \gamma_3 = -\frac{1}{2} \ , \quad \gamma_4 = 2 \ , \quad \gamma_5 = -\frac{1}{6} \ , \quad \gamma_6 = -\frac{1}{3} \ , \quad \gamma_7 = 0 \ . \tag{1.269}$$

$$\delta_1 = 2 \ , \quad \delta_2 = \frac{1}{12}, \quad \delta_3 = 0 \ . \tag{1.270}$$

1.11.3 $SU(2)$ Lagrangian in matrix notation

The Lagrangian written before can be put in the general matrix notation that has been worked out up to now (as in the case of $SU(3)$). For that purpose, the U matrix is written in terms of the components U_A as [203]:

$$U(x) = U_0(x) + i\vec{\tau}\vec{U}(x) \ , \tag{1.271}$$

and then, the Lagrangians can be written as:

$$\mathcal{L}^{(2)}_{SU(2)} = \frac{f^2}{4}\langle D_\mu U D^\mu U^\dagger\rangle + \frac{f^2}{4}\langle \chi_+\rangle \ , \tag{1.272a}$$

$$\begin{aligned}\mathcal{L}^{(4)}_{SU(2)} = {} & \frac{l_1}{4}\langle D_\mu U D^\mu U^\dagger\rangle^2 + \frac{l_2}{4}\langle D_\mu U D_\nu U^\dagger\rangle\langle D^\mu U D^\nu U^\dagger\rangle \\ & + \frac{l_3}{16}\langle \chi U^\dagger + U\chi^\dagger\rangle^2 + \frac{l_4}{4}\langle D_\mu U D^\mu \chi^\dagger + D_\mu \chi D^\mu U^\dagger\rangle \\ & + \frac{l_5}{2}\langle 2 f^R_{\mu\nu} U f^{\mu\nu} U^\dagger - f^L_{\mu\nu} f^{\mu\nu}_L - f^R_{\mu\nu} f^{\mu\nu}_R\rangle + i\frac{l_6}{2}\langle f^R_{\mu\nu} D^\mu U D^\nu U^\dagger + f^L_{\mu\nu} D^\mu U^\dagger D^\nu U\rangle \\ & - \frac{l_7}{16}\langle \chi U^\dagger - U\chi^\dagger\rangle^2 + \frac{h_1+h_3}{4}\langle \chi\chi^\dagger\rangle - 2h_2\langle f^L_{\mu\nu} f^{\mu\nu}_L + f^R_{\mu\nu} f^{\mu\nu}_R\rangle \\ & \frac{h_1-h_3}{16}\left(\langle \chi U^\dagger + U\chi^\dagger\rangle^2 + \langle \chi U^\dagger - U\chi^\dagger\rangle^2 - 2\langle \chi U^\dagger \chi U^\dagger + U\chi^\dagger U\chi^\dagger\rangle^2\right) \ ,\end{aligned} \tag{1.272b}$$

and we have rewritten the leading order Lagrangian for reference easiness.

We finally note that for $SU(2)$, alongside with the so called exponential parametrization,

$$U(x) = \exp\left(i\frac{\sqrt{2}\Phi}{f}\right) \ , \tag{1.273}$$

where Φ is given by Eq. (1.131), there is also another frequently used one,

$$U(x) = \frac{\sigma(x) + i\vec{\tau}\vec{\pi}}{f} \quad \sigma(x) = \sqrt{f^2 - \vec{\pi}^2(x)} \ , \tag{1.274}$$

related indeed to Eq. (1.271). All parametrizations must give the same results for on-shell amplitudes or observables in general, but the relation of the parametrization in Eq. (1.274) (for the Lagrangians in Eq. (1.272)) to that of Subsec. 1.11.2 is that both give the same results also off the mass shell.

1.12 Self-energy, form factor and quadratic scalar radius of the pion

In this Section, an explicit calculation from $SU(2)$ ChPT is worked out, namely, the pion scalar form factor and, from it, the pion quadratic scalar radius. In this way, through an explicit example, we put in practice the previous theoretical formalism. As a by-product, it also gives us an introduction to the renormalization procedure, the cancellation of divergences, and all that. Finally, as we will have the opportunity to compute an observable quantity, that can be compared with the experiments, we can have a first idea on the accuracy of ChPT.

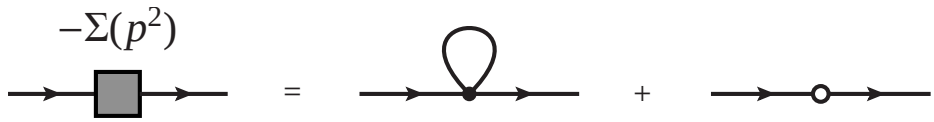

Figure 1.6: Diagrams for the one-loop calculation of the pion self-energy. Full circles represent $\mathcal{O}(p^2)$ vertices, while the empty ones correspond to the $\mathcal{O}(p^4)$ vertices.

1.12.1 Pion self-energy and $\mathcal{O}(p^4)$ pion mass. Renormalization

The calculation of the pion self-energy, $-i\Sigma(p^2)$, is necessary in order to take into account the renormalization of the wave function of the initial and final pions. It also defines the *physical* mass, m_π, in terms of the *bare* mass, m. The diagrams that contribute to the pion self-energy at $\mathcal{O}(p^4)$ are depicted in Fig. 1.6. We use the $O(4)$ form of the Lagrangian, with the parametrization given in Eq. (1.259). There is a one-loop contribution from the $\mathcal{O}(p^2)$ Lagrangian, as well as a tree level contribution from the counterterms of the $\mathcal{O}(p^4)$ Lagrangian. One has:

$$\Sigma(p^2) = \frac{3m^2 A_0(m^2)}{2f^2} + \frac{2m^4 l_3}{f^2} - \frac{p^2 A_0(m^2)}{f^2} \ . \tag{1.275}$$

Notice that $\Sigma(p^2)$ is linear in its argument. The one-point function $A_0(m^2)$ is given in Eq. (B.2), Appendix B, together with the different n-point loop function used in this and other chapters.

The pion *bare* propagator,[14] $\Delta_0(p^2)$, is given by:

$$i\Delta_0(p^2) = \frac{i}{p^2 - m^2 + i0^+} \ , \tag{1.276}$$

where $m^2 = 2Bm$, the pion mass at $\mathcal{O}(p^2)$. The summation of the Dyson series, as seen in Fig. 1.7, results in the appearence of the self-energy in the *renormalized* or *dressed* propagator, $\Delta_R(p^2)$,

$$i\Delta_R(p^2) = i\Delta_0(p^2) + i\Delta_0(-i\Sigma)i\Delta_0 + \cdots = i\Delta_0(1 - i\Sigma\ i\Delta_R) \tag{1.277}$$

so that:

$$i\Delta_R(p^2) = \frac{i\Delta_0(p^2)}{1 + i\Delta_0(p^2)\ i\Sigma(p^2)} = \frac{i}{\Delta_0^{-1}(p^2) - \Sigma(p^2)} = \frac{i}{p^2 - m^2 - \Sigma(p^2)} \ . \tag{1.278}$$

If we make a Taylor series in $\Sigma(p^2)$ around $p^2 = m_\pi^2$, we have:

$$\Sigma(p^2) = \Sigma(m_\pi^2) + (p^2 - m_\pi^2)\Sigma'(m_\pi^2) + \cdots \ , \tag{1.279}$$

and then we can write:

$$\Delta_R^{-1}(p^2) = p^2 - m^2 - \Sigma(p^2) = (p^2 - m_\pi^2)(1 - \Sigma'(m_\pi^2)) + (m_\pi^2 - m^2 - \Sigma(m_\pi^2)) \ . \tag{1.280}$$

We impose now the condition that the dressed propagator has a pole for $p^2 = m_\pi^2$, the mass of the pion at $\mathcal{O}(p^4)$. Recall that, at $\mathcal{O}(p^2)$, we have $m_\pi^2 = m^2$. Then the mass of the pion at $\mathcal{O}(p^4)$ is given by the equation:

$$m_\pi^2 - m^2 - \Sigma(m_\pi^2) = 0 \ , \tag{1.281}$$

[14] From now on, we ommit here the $i0^+$ in the propagators, since it is not relevant for our discussion.

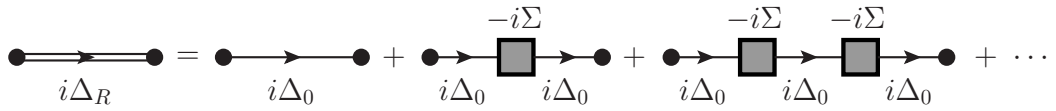

Figure 1.7: Dyson series for the propagator: the dressed propagator consists of the sum of all possible insertions of self-energies in the bare propagator.

and the dressed propagator at $\mathcal{O}(p^4)$ is written as:

$$i\Delta_R(p^2) = \frac{i}{(p^2 - m_\pi^2)(1 - \Sigma')} \simeq \frac{i(1 + \Sigma')}{p^2 - m_\pi^2} \equiv \frac{iZ}{p^2 - m_\pi^2} \ , \tag{1.282}$$

where the constant Z is the so called wave-function renormalization constant:

$$Z = 1 + \delta Z = 1 + \Sigma'(m_\pi^2). \tag{1.283}$$

The bare propagator is defined in term of the bare field Φ_0 as:

$$i\Delta_0(p^2) = \int \mathrm{d}^4x e^{-ipx} \left\langle 0 \left| T[\Phi_0(x)\Phi_0(0)] \right| 0 \right\rangle \ , \tag{1.284}$$

whereas the dressed propagator reads:

$$i\Delta_R(p^2) = \int \mathrm{d}^4x e^{-ipx} \left\langle 0 \left| T[\Phi_R(x)\Phi_R(0)] \right| 0 \right\rangle \ , \tag{1.285}$$

which means that the renormalized field is defined in terms of the bare one as $\Phi_R = Z^{1/2}\Phi_0$. Whence, in order to have a proper normalization in our amplitudes, when these have n external legs, we have to multiply them by $(Z^{1/2})^n \simeq 1 + \frac{n}{2}\delta Z$. This procedure is called *wave function renormalization*, since by means of this procedure the fields, *i.e.*, the wave functions, are renormalized.

Now we can calculate m_π^2 taking into account Eq. (1.281) and Eq. (1.275). We can write:

$$\Sigma(m_\pi^2) = \frac{4m^4 l_3 + m_\pi^2 A_0(m^2)}{2f^2} \ , \tag{1.286}$$

and, as stated in Sec. 1.11, the l_i are defined such that the divergences of the loops (in this case, A_0) are cancelled. Thus,

$$4m^4 l_3 + m_\pi^2 A_0(m^2) = -\frac{m_\pi^4}{16\pi^2}\bar{l}_3 \ , \tag{1.287}$$

which is indeed finite, and we have taken into account that $m^2 - m_\pi^2 = \mathcal{O}(p^4)$, as Eq. (1.281) shows. This is an important result: the mass at $\mathcal{O}(p^4)$ remains finite, and also independent of the renormalization scale μ, and it is:

$$m_\pi^2 = m^2 \left(1 - \frac{m^2}{32\pi^2 f^2}\bar{l}_3\right) + \mathcal{O}(p^6) \ , \tag{1.288}$$

Notice also that, as one would expect, the masses of the Goldstone bosons go to zero when the masses of the quarks go to zero (because $m^2 \propto \hat{m}$).

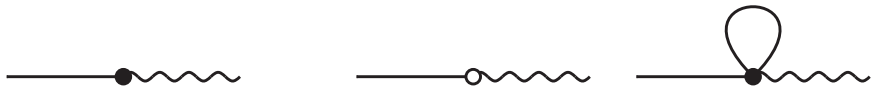

Figure 1.8: Diagrams for the coupling of a pion (solid lines) to the axial current (wiggly lines), needed to calculate f_π at $\mathcal{O}(p^4)$. Full and empty vertex are $\mathcal{O}(p^2)$ and $\mathcal{O}(p^4)$, respectively. The leftmost diagram, which is $\mathcal{O}(p^2)$, was included in Fig. 1.5, whereas the other two are the $\mathcal{O}(p^4)$ contributions.

In the same way that we have calculated the physical pion mass, we calculate the physical weak decay constant of the pion, f_π, by repeating the calculation in Subsec. 1.10.2 at $\mathcal{O}(p^4)$, with the basic diagrams of Fig. 1.8. One finds that:

$$f_\pi = f\left(1 + \frac{m^2}{16\pi^2 f^2}\,\bar{l}_4\right) + \mathcal{O}(p^4)\ . \tag{1.289}$$

1.12.2 Pion form factor and quadratic scalar radius

The diagrams that contribute the to pion form factor at $\mathcal{O}(p^4)$ are depicted in Fig. 1.9. There are contributions from the $\mathcal{O}(p^4)$ Lagrangian and also from the $\mathcal{O}(p^2)$ to one loop. As we shall see below, the latter have infinities that can be derived with some renormalization method (dimensional regularization here), and the former are defined in such a way that they cancel these divergences (hence the name of *counterterms*). The different amplitudes, from left to right and top to bottom in Fig. 1.9, read:

$$iT_0 = -2Bi\ , \tag{1.290a}$$

$$iT_1 = -2Bi\frac{l_4 q^2 + 4l_3 m^2}{f^2}\ , \tag{1.290b}$$

$$iT_2 = -\frac{5Bi}{f^2}A_0(m^2)\ , \tag{1.290c}$$

$$iT_3 = \frac{2Bi}{f^2}\left(A_0(m^2) + \left(q^2 - \frac{m^2}{2}\right)B_0(q^2, m^2)\right)\ , \tag{1.290d}$$

where the loop functions A_0 and B_0, as commented, are given in Appendix B. The infinite and scale dependent terms arise from these loop functions and from the l_i, see Eq. (1.268), namely:

$$\begin{aligned} A_0^\infty &= +\frac{m^2}{16\pi^2}\tilde{R}\ , & B_0^\infty &= +\frac{1}{16\pi^2}\tilde{R}\ , \\ l_3^\infty &= -\frac{1}{64\pi^2}\tilde{R}\ , & l_4^\infty &= +\frac{1}{16\pi^2}\tilde{R}\ , \end{aligned} \tag{1.291}$$

where $\tilde{R} = R + \ln(m^2/\mu^2)$, and R is given in Eq. (1.268), and the infinite terms add up to:

$$iT^\infty = i\sum_{i=0}^{3} T_i^\infty = -2Bi\frac{m^2}{16\pi^2 f^2}\tilde{R}\ . \tag{1.292}$$

The whole amplitude is then:

$$iT_S = i(T_0 + T^\infty + T_{\text{finite}})\ . \tag{1.293}$$

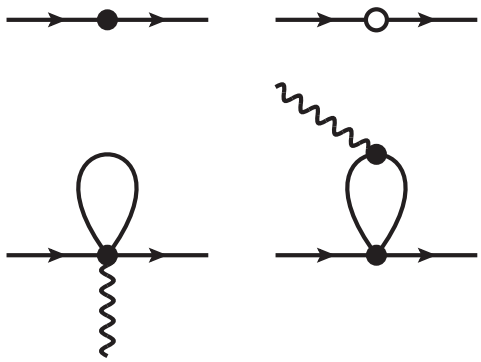

Figure 1.9: Diagrams needed for the scalar form factor of the pion at $\mathcal{O}(p^4)$. The wiggly lines represent here an scalar source, whereas the solid ones denote the pion. Full vertices represent $\mathcal{O}(p^2)$ vertices, while the white ones are $\mathcal{O}(p^4)$.

We will consider later $T_{\rm finite}$, the finite part of the $\mathcal{O}(p^4)$ contribution to the amplitude. Now, as seen in Subsec. 1.12.1, we have to multiply the amplitude by a factor $(Z^{(1/2)})^2 = Z = 1+\delta Z$, with Z given in Eq. (1.283), and then:

$$iT_S Z = i(T_0\delta Z + T^\infty + T_0 + T_{\rm finite}) + \mathcal{O}(p^6)\ . \tag{1.294}$$

Terms like $T^\infty\delta Z$ and $T_{\rm finite}\delta Z$ are neglected because this is an $\mathcal{O}(p^4)$ calculation, and they are $\mathcal{O}(p^6)$ (δZ is $\mathcal{O}(p^2)$ and T^∞ and $T_{\rm finite}$ are $\mathcal{O}(p^4)$). The important point to stress is that, now,

$$T_0\delta Z + T^\infty = 0\ , \tag{1.295}$$

that is, the divergences cancel exactly. The final, finite result is:

$$T_{\rm final} = T_0 + T_{\rm finite} = T_0 - \frac{2B}{16\pi^2 f^2}\left(\bar{l}_4 q^2 - \bar{l}_3 m^2 - \left(q^2 - \frac{m^2}{2}\right)\bar{B}_0(q^2, m^2)\right) \tag{1.296}$$

with $\bar{B}_0$ the finite and scale independent piece of B_0 (*cf.* Appendix B).

Actually, the form factor is defined as $F_\pi(q^2) = -\hat{m}T_{\rm final} = 2B\hat{m}(\cdots) = m^2(\cdots)$. Expanding m^2 in terms of m_π^2 up to $\mathcal{O}(p^4)$, and for low q^2, one has:

$$F_\pi(q^2) = m_\pi^2\left(1 - \frac{m_\pi^2}{32\pi^2 f_\pi^2}\left(\bar{l}_3 - 1\right) + \frac{q^2}{16\pi^2 f_\pi^2}\left(\bar{l}_4 - \frac{13}{12}\right)\right)$$

From this expansion, the quadratic scalar radius of the pion is defined as:

$$F_\pi(q^2) = F_\pi(0)\left(1 + \frac{1}{F_\pi(0)}\frac{\partial F_\pi(q^2)}{\partial q^2}\bigg|_{q^2=0} + \cdots\right) = F_\pi(0)\left(1 + \frac{1}{6}\langle r_\pi^2\rangle q^2 + \cdots\right)\ ,$$

so that it results:

$$\langle r_\pi^2\rangle = \frac{3}{8\pi^2 f_\pi^2}\left(\bar{l}_4 - \frac{13}{12}\right) \tag{1.297}$$

Just as an estimate, taking $\bar{l}_3 = 2.9 \pm 2.4$ and $\bar{l}_4 = 4.6 \pm 0.9$ [18], we get $\langle r_\pi^2\rangle \simeq 0.6$ fm^2. For more details on the issue of the quadratic scalar radius, see Ref. [149] and references therein.

1.13 Including explicit resonances in the Chiral Lagrangians

So far, the interactions of the lightest hadrons have been derived as an Effective Field Theory, resulting in a Quantum Field Theory given by the Lagrangians of the previous sections. In Refs. [105, 106] an extension of this formalism is performed, allowing for the inclusion of hadron states other than the lightest pseudoscalar mesons. At lowest order, these explicit resonances include scalar (S_1, $J^{PC} = 0^{++}$) and pseudoscalar (P_1, 0^{-+}) singlets, scalar (S_8, 0^{++}), pseudoscalar (S_8, 0^{-+}), axial (A, 1^{++}) and vector (V, 1^{--}) octects. The kinetic part of the Lagrangians is given by:

$$\mathcal{L}_{\rm kin}(R=V,A) = -\frac{1}{2}\langle \nabla^\lambda R_{\lambda\mu}\nabla_\nu R^{\nu\mu} - \frac{1}{2}M_R^2 R_{\mu\nu}R^{\mu\nu}\rangle \tag{1.298a}$$

$$\mathcal{L}_{\rm kin}(R=S,P) = \frac{1}{2}\langle \nabla^\mu R\nabla_\mu R - M_R^2 R^2\rangle + \frac{1}{2}\partial^\mu R_1 \partial_\mu R_1 - \frac{1}{2}M_{R_1}^2 R_1^2 \tag{1.298b}$$

where R corresponds to octets of resonances, and R_1 to the singlets. The covariant derivative defined by $\nabla_\mu R$ is given by:

$$\nabla_\mu R = \partial_\mu R + [\Gamma_\mu, R] \tag{1.298c}$$

$$\Gamma_\mu = \frac{1}{2}\left(u^\dagger\left(\partial_\mu - ir_\mu\right)u + u\left(\partial_\mu - il_\mu\right)u^\dagger\right) \ . \tag{1.298d}$$

The latter has already been introduced in Eq. (1.118b), but we include it here for reference easiness. Since R is an octet, the action of the covariant derivative corresponds to the adjoint representation. This is why it appears inside the commutator symbol.

The interaction Lagrangians are given by:

$$\mathcal{L}_{1^{--}} = \frac{F_V}{2\sqrt{2}}\langle V_{\mu\nu} f_+^{\mu\nu}\rangle + i\frac{G_V}{\sqrt{2}}\langle V_{\mu\nu}u^\mu u^\nu\rangle \ , \tag{1.298e}$$

$$\mathcal{L}_{1^{++}} = \frac{F_A}{2\sqrt{2}}\langle A_{\mu\nu} f_-^{\mu\nu}\rangle \ , \tag{1.298f}$$

$$\mathcal{L}_{0^{++}} = c_d\langle S_8 u_\mu u^\mu\rangle + c_m\langle S_8\chi_+\rangle \ , \tag{1.298g}$$

$$\mathcal{L}_{0^{++}} = \tilde{c}_d S_1\langle u_\mu u^\mu\rangle + \tilde{c}_m S_1\langle\chi_+\rangle \ , \tag{1.298h}$$

$$\mathcal{L}_{0^{-+}} = id_m\langle P_8\chi_-\rangle \ , \tag{1.298i}$$

$$\mathcal{L}_{0^{-+}} = i\tilde{d}_m P_1\langle\chi_-\rangle \ . \tag{1.298j}$$

In the above Lagrangians, we have introduced one new notation,

$$f_\pm^{\mu\nu} = F_L^{\mu\nu} \pm F_R^{\mu\nu} \ , \tag{1.299}$$

where the $F_{L,R}^{\mu\nu}$ are defined in Eq. (1.124). The different octets are given by:[15]

$$S_8 = \begin{pmatrix} \frac{a_0}{\sqrt{2}} + \frac{f_8}{\sqrt{6}} & a_0^+ & K_0^{*+} \\ a_0^- & -\frac{a_0}{\sqrt{2}} + \frac{f_8}{\sqrt{6}} & K_0^{*0} \\ K_0^{*-} & \overline{K}_0^{*0} & -\frac{2}{\sqrt{6}}f_8 \end{pmatrix} \ , \tag{1.300a}$$

[15]Note that, in P_8 and P_1, the fields π, K and η refer to particles different from those in the lightest pseudoscalar nonet, but with the same quantum numbers.

$$P_8 = \begin{pmatrix} \frac{\pi^0}{\sqrt{2}} + \frac{\eta}{\sqrt{6}} & \pi^+ & K^+ \\ \pi^- & -\frac{\pi^0}{\sqrt{2}} + \frac{\eta}{\sqrt{6}} & K^0 \\ K^- & \bar{K}^0 & -\frac{2}{\sqrt{6}}\eta \end{pmatrix} , \tag{1.300b}$$

$$V_{\mu\nu} = \begin{pmatrix} \frac{\rho^0}{\sqrt{2}} + \frac{\omega_8}{\sqrt{6}} & \rho^+ & K^{*+} \\ \rho^- & -\frac{\rho^0}{\sqrt{2}} + \frac{\omega_8}{\sqrt{6}} & K^{*0} \\ K^{*-} & \overline{K}^{*0} & -\frac{2}{\sqrt{6}}\omega_8 \end{pmatrix}_{\mu\nu} , \tag{1.300c}$$

$$A_{\mu\nu} = \begin{pmatrix} \frac{a_1^0}{\sqrt{2}} + \frac{f_1}{\sqrt{6}} & a_1^+ & K_1^+ \\ a_1^- & -\frac{a_1^0}{\sqrt{2}} + \frac{f_1}{\sqrt{6}} & K_1^0 \\ K_1^- & \overline{K_1}^0 & -\frac{2}{\sqrt{6}} f_1 \end{pmatrix}_{\mu\nu} . \tag{1.300d}$$

Above, the vector ($V_{\mu\nu}$) and axial–vector fields ($A_{\mu\nu}$) have been introduced as antisymmetric tensor fields. Denoting both type of fields with $W_{\mu\nu}$, they are normalized such that, for a state $|W, p\rangle$ with momentum p and polarization vector $\epsilon(p)$, one has:

$$\langle 0 \left| W_{\mu\nu} \right| W, p \rangle = \frac{i}{M_W} \left(p_\mu \epsilon_\nu(p) - p_\nu \epsilon_\mu(p) \right) , \tag{1.301}$$

and the propagator is given by:

$$\langle 0 \left| T \left\{ W_{\mu\nu} W_{\rho\sigma} \right\} \right| 0 \rangle = \frac{i\, M_W^{-2}}{p^2 - M_W^2 + i\epsilon} \Big(g_{\mu\rho} g_{\nu\sigma} (p^2 - M_W^2) - g_{\mu\rho} p_\nu p_\sigma + g_{\mu\sigma} p_\nu p_\rho - (\mu \leftrightarrow \nu) \Big) . \tag{1.302}$$

For a formulation in terms of vector fields instead of tensor ones or a discussion on the differences, see Refs. [106, 204–206].

In subsequent chapters, we will use the Lagrangians for the scalar and pseudoscalar nonets. However, when dealing with the vector and axial fields in Chapter 3, we will introduce another formalism, in which they are considered as Yang-Mills fields, through minimal coupling, identifying the classical external gauge fields r^μ and l^μ with the proper combinations of axial and vector fields.

2

Unitarity, resonances and Riemann sheets. Unitarized Chiral Perturbation Theory

Contents of this Chapter:

2.1 Introduction

Unitarity is one of the cornerstones of quantum mechanics. In plain words, it is the statement that the probability is conserved. It is difficult to overestimate its importance. Its fundamental implications will be treated in Sec. 2.2, in the context of S-matrix theory. An introduction to the formalism of partial waves is delivered to Sec. 2.3.

One of the most striking features of the strong interactions is the conspicuous apearence of

peaks, dips and valleys when the results of experiments on cross sections are plotted versus the energy of the particles involved. These peaks (sometimes dips) are evidence of intermediate states or particles, called resonances, whose presence makes the reaction more likely, hence increasing the cross section (or producing other effects in other observables). The difference with elementary particles is just a matter of life time: resonances are much more short-lived. Of course, the concept of isolated resonance is an ideal one. In most cases, what is seen in the experiments is the superposition of several efects, as the presence of other resonances, thresholds, and so on. An introduction to the appearence of resonances and bound states in the context of one-dimensional Quantum Mechanics is found in Sec. 2.4. A general approach to the appearence of resonances in the amplitudes will be given in Sec. 2.5.

When the amplitude for a given process is known mathematically for the physical region in terms of a certain variable (usually, the center of mass energy squared, s), one can analitically continue the amplitude to the complex plane of that variable. In this picture, the resonances correspond to simple poles in the complex plane for that variable, being the pole position related to the mass and width parameters of the resonance associated to. As the resonances appear as simple poles in the so called unphysical Riemann sheet, in Sec. 2.6 we will treat the topic of the Riemann sheets in detail.

Most of the content of this thesis is related, to a greater or lesser extent, to Unitarized Chiral Perturbation Theory (UChPT), which is a non-perturbative scheme to be used together with the perturbative results of Chiral Pertubation Theory. The master equation of UChPT and its foundations will be studied in Sec. 2.7. Finally, a real example of the application of UChPT as well as the other general results of this Chapter can be found in Sec. 2.8, namely, the two-meson scattering in the channel $I^G(J^{PC}) = 1^-(0^{++})$ and the appearence of the $a_0(1450)$ resonance.

2.2 *S*-matrix and unitarity

When dealing with S-matrix theory, we have to assume that the states are asymptotically free. Given a system in an initial state $|\beta\rangle$, the probability amplitude of finding the system in the final state $|\alpha\rangle$ is given by the S-matrix element $\langle\alpha\,|S|\,\beta\rangle$. For simplicity, let us assume that the set of states $\{|n\rangle\}$ forms a complete and orthonormal set of states,

$$\langle m|\,n\rangle = \delta_{m,n} \tag{2.1}$$

$$\sum_m |m\rangle\,\langle m| = \mathbb{I} \tag{2.2}$$

i.e., they form a basis that allows one to express any state $|\phi\rangle$ as a linear combination of them, $|\phi\rangle = \sum_n a_n\,|n\rangle$, the coefficients satisfying $\sum_n |a_m|^2 = 1$. Unitarity is the statement that, given an initial state $|\phi\rangle$, the probability that when, measured, it ends in some of the basis state $|m\rangle$, is one. That is,

$$\sum_m |\langle m\,|S|\,\phi\rangle|^2 = 1 = \sum_m \left\langle \phi \left| S^\dagger \right| m \right\rangle \langle m\,|S|\,\phi\rangle =$$

$$= \left\langle \phi \left| S^\dagger S \right| \phi \right\rangle = \sum_{m,m'} a^*_{m'} a_m \left\langle m' \left| S^\dagger S \right| m \right\rangle$$

As this must hold for any choice of the coefficients a_m, we must conclude that

$$\left\langle m' \left| S^\dagger S \right| m \right\rangle = \delta_{m,m'} \qquad S^\dagger S = \mathbb{I} \qquad S S^\dagger = \mathbb{I} \tag{2.3}$$

where the last equality can be proved analogously.

Let $|p\rangle$ be the state of a spinless meson with four momentum p such that $p^2 = m^2 = p^{0\,2} - \vec{p}^2$. The normalization of these states is given by

$$\langle p' | \, p \rangle = (2\pi)^3 2p^0 \delta(\vec{p} - \vec{p}') \tag{2.4}$$

and orthonormality can be expressed through

$$\int \left(|p'\rangle \, \frac{\mathrm{d}^3 \vec{p}'}{2p'_0 (2\pi)^3} \, \langle p'| \right) |p\rangle = |p\rangle \tag{2.5}$$

Of course, these relations can be generalized to multiparticle states using the direct products of monoparticle states.

Now, let us consider a two-particle scattering process $|i\rangle \to |f\rangle$,

$$a(p_1) \; b(p_2) \to c(p_3) \; d(p_4) \tag{2.6}$$

We can split the S-matrix as

$$S = \mathbb{I} + iT \tag{2.7}$$

explicitly separating the situation when the particles are widely separated in space and thus not interacting at all. Due to energy conservation and translation invariance (the center of mass motion does not affect the scattering amplitude) we can write:

$$\langle f \, | S | \, i \rangle = (2\pi)^4 \delta^{(4)} \left(\mathscr{P}_f - \mathscr{P}_i \right) \langle \alpha \, | S_{\mathscr{P}} | \, \beta \rangle \tag{2.8}$$

The states $|\beta\rangle$ and $|\alpha\rangle$ represent the same states than $|i\rangle$ and $|f\rangle$ once the center of mass motion is removed, and then, the operator $S_{\mathscr{P}}$ connects states with the same total four momenta. Analogously, we can split the T-matrix, and define

$$S_{\mathscr{P}} = \mathbb{I} + iT_{\mathscr{P}} \tag{2.9}$$

The unitarity condition of the S-matrix translates into the T-matrix as

$$T - T^\dagger = iTT^\dagger \tag{2.10a}$$

$$T_{\mathscr{P}} - T^\dagger_{\mathscr{P}} = iT_{\mathscr{P}} T^\dagger_{\mathscr{P}} \tag{2.10b}$$

and, by inserting a resolution of the identity operator in terms of the set of intermediate states on the right-hand side of Eq. (2.10), we can write the latter equation as:

$$\langle \alpha \, | T_{\mathscr{P}} | \, \beta \rangle - \left\langle \alpha \left| T^\dagger_{\mathscr{P}} \right| \beta \right\rangle = i \sum_a \int \mathrm{d}\mathcal{Q}_a \left\langle \alpha \left| T_{\mathscr{P}} \right| a \right\rangle \left\langle a \left| T^\dagger_{\mathscr{P}} \right| \beta \right\rangle \tag{2.11}$$

where the element of phase space is:

$$\mathrm{d}\mathcal{Q}_a = \int \prod_{i=1}^{n_a} \mathrm{d}^3 \vec{p}_i (2\pi)^4 \delta(\mathscr{P} - \sum_{i=1}^{n_a} p_i) \; , \tag{2.12}$$

being n_a the number of particles in the state a. For the two-particle case, the phase space is given in terms of the center-of-mass variables,

$$\mathrm{d}\mathcal{Q}_a = \frac{\mathrm{d}\Omega}{4\sqrt{s}}\frac{|\vec{p}|}{4\pi^2} \ . \tag{2.13}$$

Above, s the Mandelstam variable that represents the total center of mass energy squared, and $|\vec{p}|$ is the center of mass momentum.

2.3 Partial waves

In general, for a given two-spinless-particle scattering process like Eq. (2.6), it can be described by the Mandelstam variable s and two polar angles, θ and ϕ. However, rotational invariance ensures that the matrix elements are independent of the azimut ϕ. As a result, we can always choose the coordinate axis with the z-axis pointing in the direction of the initial three-momentum (the direction of the center of mass). We take profit of this fact to expand the $T_{\mathscr{P}}(s,\theta)$ matrix elements[1] in terms of Legendre polynomials[2] $P_L(\cos\theta)$ as

$$T_{\mathscr{P}}(s,\theta) = \sum_{L=0}^{\infty}(2L+1)P_L(\cos\theta)T_L(s) \ , \tag{2.14}$$

$$T_L(s) = \frac{1}{2}\int_{-1}^{1}\mathrm{d}\cos\theta \ P_L(\cos\theta)T_{\mathscr{P}}(s,\theta) \ , \tag{2.15}$$

with $\cos\theta = \hat{p}\cdot\hat{p}'$. The amplitude $T_L(s)$, called *partial wave amplitude* with angular momentum L, depends now just on the variable s.

By inserting the partial wave expansion into the unitarity condition Eq. (2.11), the l.h.s. side becomes:

$$\langle\alpha\,|T_{\mathscr{P}}|\,\beta\rangle - \left\langle\alpha\left|T^{\dagger}_{\mathscr{P}}\right|\beta\right\rangle = 2i\sum_{L}P_L(\cos\theta)\mathrm{Im}T_L^{(\alpha\beta)}(s) \ , \tag{2.16}$$

and the amplitudes on the r.h.s. give rise to:

$$\left\langle\alpha\left|T_{\mathscr{P}}\right|a\right\rangle\left\langle a\left|T^{\dagger}_{\mathscr{P}}\right|\beta\right\rangle = \sum_{L,L'}T_L^{(\alpha a)}(s)T_L^{(\beta a)^*}(s)(2L+1)(2L'+1)P_{L'}(\cos\theta')P_L(\cos\theta'') \ . \tag{2.17}$$

Taking into account Eq. (2.13) with $\mathrm{d}\Omega = \mathrm{d}\cos\theta'\mathrm{d}\phi'$, and also the addition theorem for the spherical harmonics [207, Sec. (3.7)]:

$$P_L(\cos\theta'') = \frac{4\pi}{2L+1}\sum_{M}Y^*_{LM}(\theta,0)Y_{LM}(\theta',\phi') \ , \tag{2.18}$$

[1] We do not distinguish here between the operator and the matrix elements since no ambiguity can arise in what follows.

[2] Their normalization is given by:

$$\frac{1}{2}\int_{-1}^{1}\mathrm{d}\cos\theta \ P_L(\cos\theta)P_{L'}(\cos\theta) = \frac{\delta_{L,L'}}{2L+1} \ .$$

we have:

$$\int_0^{2\pi} \mathrm{d}\phi' P_L(\cos\theta'') = \frac{4\pi}{2L+1} \sum_M \int_0^{2\pi} \mathrm{d}\phi' Y^*_{LM}(\theta,0) Y_{LM}(\theta',\phi') = 2\pi P_L(\cos\theta) P_L(\cos\theta') \ . \quad (2.19)$$

Then, the $\cos\theta'$ integral, given the Legendre polynomials normalization, can be performed straightforwardly, and the final result is:

$$i \sum_a \int \mathrm{d}\mathcal{Q}_a \left\langle \alpha \left| T_{\mathscr{P}} \right| a \right\rangle \left\langle a \left| T^\dagger_{\mathscr{P}} \right| \beta \right\rangle = \frac{i\,|\vec{p}_a|}{4\pi\sqrt{s}} \sum_L (2L+1) P_L(\cos\theta) T_L^{(\alpha a)}(s) T_L^{(\beta a)^*}(s) \ . \quad (2.20)$$

We end with the important result:

$$\mathrm{Im} T_L^{(\alpha\beta)}(s) = \sum_a \frac{|\vec{p}_a|}{8\pi\sqrt{s}} T_L^{(a\alpha)}(s) T_L^{(\beta a)^*}(s) \theta(s - s^a_{\mathrm{th}}) \ , \quad (2.21)$$

where s^a_{th} the s-value for the threshold of the state a. We can write the last equation (which is a sum over open intermediate states) as a product of matrices, as

$$\mathrm{Im} T_L = T_L \ \rho \ T_L^\dagger \quad (2.22a)$$

where ρ is a diagonal matrix:

$$\rho_{ij} = \frac{|\vec{p}_i|}{8\pi\sqrt{s}} \delta_{ij}. \quad (2.22b)$$

This equation can be written also as:

$$\mathrm{Im} T_L^{-1} = -\rho \ . \quad (2.22c)$$

Let us consider an *elastic* reaction, which means that the process is $ab \to ab$ with no possible intermediate states other than the ab state itself. Then the matrices are one dimensional, and $T_L^{-1} = \nu - i\rho$ so that $T_L = (\nu + i\rho)/(\nu^2 + \rho^2)$, with $\rho = |\vec{p}\,|/(8\pi\sqrt{s})$, so that, writting $\nu = \sqrt{\nu^2+\rho^2}\cos\delta_L$, $\rho = \sqrt{\nu^2+\rho^2}\sin\delta_L$, we have

$$T_L = \frac{8\pi\sqrt{s}}{|\vec{p}|} e^{i\delta_L} \sin\delta_L \ . \quad (2.23)$$

The phase δ_L, which depends on s, is called the *phase shift*.[3] We define the S_L matrix element for the elastic process as

$$S_L = 1 + 2i\rho T_L = 1 + i\frac{|\vec{p}|}{4\pi\sqrt{s}} T_L = e^{2i\delta_L} \quad (2.24)$$

and, of course, $|S_L|^2 = 1$.

The generalization to the inelastic case, when n coupled channels are involved, defines the S-matrix with angular momentum L, S_L, as:

$$S_L = \mathbb{I} + 2i\rho^{1/2} T_L \rho^{1/2} \ , \quad (2.25)$$

[3] From a wave function point of view, the only effect of elastic scattering on the asymptotic wave function is the modification of the outgoing part of it by this factor $e^{2i\delta_L}$: the scattering *shifts* the phase.

Due to Eq. (2.22a), S_L satisfies:

$$S_L S_L^\dagger = S_L^\dagger S_L = \mathbb{I} \ . \tag{2.26}$$

Unitarity imposes then that $|S_L^{ii}| \leq 1$, because, for $n \geq 2$ channels,

$$(S_L S_L^\dagger)_{mm} = 1 = \left|S_L^{1m}\right|^2 + \left|S_L^{2m}\right|^2 + \cdots + |S_L^{nm}|^2 = |S_L^{mm}|^2 + \sum_{i\neq m}^{n} \left|S_L^{im}\right|^2 \ .$$

For a two-particle scattering, the S-matrix can be parametrized in term of three real parameters as

$$S_L = \begin{pmatrix} \eta e^{2i\delta_1} & i\sqrt{1-\eta^2}e^{i(\delta_1+\delta_2)} \\ i\sqrt{1-\eta^2}e^{i(\delta_1+\delta_2)} & \eta e^{2i\delta_2} \end{pmatrix} \ . \tag{2.27}$$

For the nucleon-nucleon scattering, to be studied in detail in Chapter 7, one usually writes $\eta = \cos\epsilon$, and ϵ is called the mixing angle.

2.4 Resonances: a first approach from Quantum Mechanics

In this section, a first approach to the general features of resonances is given from the point of view of elementary, non-relativistic Quantum Mechanics. For that purpose, we consider an example from one-dimensional quantum mechanics, which is rather simple, yet illuminating. Let us consider the *scattering* of two particles in one dimension, interacting through a central potential. The Hamiltonian of the system is given by:

$$\hat{H}_{\rm sys}(\vec{r}_1, \vec{r}_2) = -\frac{\hbar^2}{2m_1}\vec{\nabla}_1^2 - \frac{\hbar^2}{2m_2}\vec{\nabla}_2^2 + V(|\vec{r}_1 - \vec{r}_2|) \ . \tag{2.28}$$

Now, we separate the relative motion, $\vec{r}$, from that of the center of mass (CM), $\vec{R}$,

$$\begin{aligned} \vec{r} &= \vec{r}_1 - \vec{r}_2 \ , \\ \vec{R} &= \frac{m_1\vec{r}_1 + m_2\vec{r}_2}{m_1+m_2} \ , \\ M &= m_1 + m_2 \quad \text{(total mass)} \ , \\ \mu &= m_1 m_2/(m_1+m_2) \quad \text{(reduced mass)} \ . \end{aligned} \tag{2.29}$$

The inverse of the first two equations are:

$$\begin{aligned} \vec{r}_1 &= \vec{R} + \frac{m_2}{m_1+m_2}\vec{r} \ , \\ \vec{r}_2 &= \vec{R} - \frac{m_1}{m_1+m_2}\vec{r} \ . \end{aligned} \tag{2.30}$$

The relations between the gradients are:

$$\begin{aligned} \vec{\nabla}_1 &= +\vec{\nabla}_r + \frac{m_1}{m_1+m_2}\vec{\nabla}_R \ , \\ \vec{\nabla}_2 &= -\vec{\nabla}_r + \frac{m_2}{m_1+m_2}\vec{\nabla}_R \ , \end{aligned} \tag{2.31}$$

in an obvious notation. Hence,

$$-\frac{\hbar^2}{2m_1}\vec{\nabla}_1^2-\frac{\hbar^2}{2m_2}\vec{\nabla}_2^2=-\frac{\hbar^2}{2M}\vec{\nabla}_R^2-\frac{\hbar^2}{2\mu}\vec{\nabla}_r^2 \tag{2.32}$$

Whence, we can write the wave function as $\Psi(\vec{r}_1,\vec{r}_2)=\psi_{\rm CM}(\vec{R})\psi(\vec{r})$, and the Schrödinger equation can be separated:

$$\begin{aligned}\hat{H}_{\rm CM}\ \psi_{\rm CM}(\vec{R})&=E_{\rm CM}\ \psi_{\rm CM}(\vec{R})\ ,\\ \hat{H}\psi(\vec{r})&=E\psi(\vec{r})\ ,\end{aligned} \tag{2.33}$$

being

$$\begin{aligned}\hat{H}_{\rm CM}&=-\frac{\hbar^2}{2M}\vec{\nabla}_R^2\ ,\\ \hat{H}&=-\frac{\hbar^2}{2\mu}\vec{\nabla}_r^2+V(|\vec{r}|)\ .\end{aligned} \tag{2.34}$$

In words, we have reduced the movement of the system to that of the CM, behaving as a free particle (because there is no potential in its Hamiltonian) of mass M, and that of the relative movement, which is that of a particle of mass μ interacting through the potential V. Notice that the center of mass momentum, $\vec{P}$, and the relative one, $\vec{p}$, are given by

$$\begin{aligned}\vec{P}&=-i\hbar\vec{\nabla}_R=-i\hbar\left(\vec{\nabla}_1+\vec{\nabla}_2\right)=\vec{p}_1+\vec{p}_2\ ,\\ \vec{p}&=-i\hbar\vec{\nabla}_r=-i\hbar\left(\frac{m_2}{m_1+m_2}\vec{\nabla}_1-\frac{m_1}{m_1+m_2}\vec{\nabla}_2\right)=\frac{m_2}{m_1+m_2}\vec{p}_1-\frac{m_1}{m_1+m_2}\vec{p}_2\ .\end{aligned} \tag{2.35}$$

Now we study the particular case of two identical masses, $m_1=m_2=m$, so that $M=2m$, $\mu=M/2$, and the relative three-momentum is $\vec{p}=(\vec{p}_1-\vec{p}_2)/2$. The relation to relativistic kinematics, which is the usual one in this thesis, goes as follows. The four-momenta of the two particles in their CM of mass frame is:

$$p_1=\left(\frac{\sqrt{s}}{2},+\vec{p}\right)\qquad p_2=\left(\frac{\sqrt{s}}{2},-\vec{p}\right)\ . \tag{2.36}$$

Thus, $\vec{p}_1-\vec{p}_2=2\vec{p}$. This momentum is related to the energy E as $E=-\frac{\vec{p}^2}{2\mu}$, so that

$$\frac{\sqrt{s}}{2}=\sqrt{\vec{p}^2+m^2}\simeq m+\frac{\vec{p}^2}{2m}=m+\frac{1}{2m}2\mu E=m+\frac{1}{2}E\ , \tag{2.37}$$

or

$$\sqrt{s}=2m+E\ , \tag{2.38}$$

that is, the above threshold condition $\sqrt{s}\geqslant 2m$ translates into $E\geqslant 0$.

We now turn our attention to the specific potential given in Fig. 2.1, specified by:

$$V(x)\begin{cases}0 & \text{for} \quad |x|>a+b\ ,\\ V_1>0 & \text{for} \quad a<|x|<a+b\ ,\\ V_0<0 & \text{for} \quad |x|<a\ .\end{cases} \tag{2.39}$$

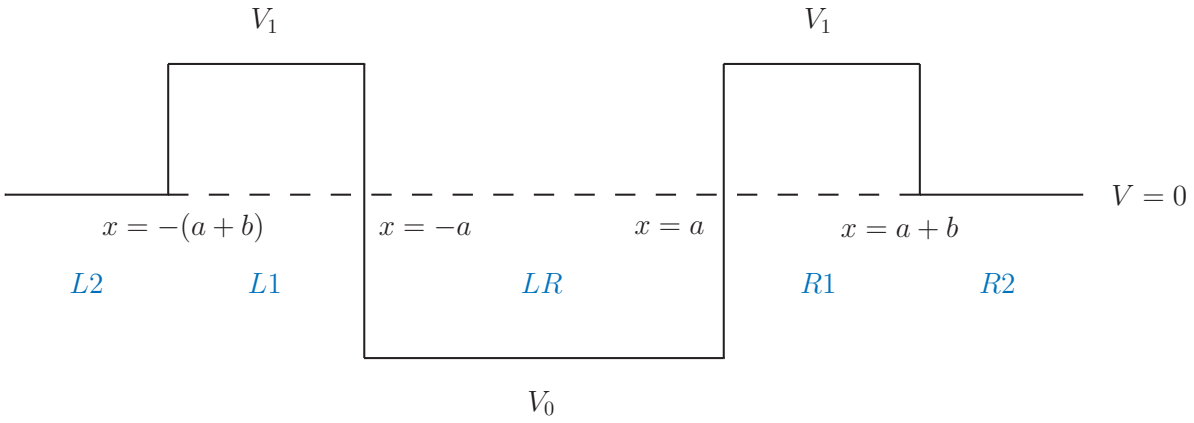

Figure 2.1: The potential for the study of scattering, resonances and bound states.

The most general form of the wave function can be written as:

$$\begin{aligned} \psi_{L2}(x) &= I_{L2}e^{ikx} + O_{L2}e^{-ikx} \ , \qquad \psi_{R2}(x) = I_{R2}e^{ikx} + O_{R2}e^{-ikx} \ , \\ \psi_{L1}(x) &= I_{L1}e^{ik_2x} + O_{L1}e^{-ik_2x} \ , \qquad \psi_{R1}(x) = I_{R1}e^{ik_2x} + O_{R1}e^{-ik_2x} \ , \\ \psi_{LR}(x) &= I_{LR}e^{ik_1x} + O_{LR}e^{-ik_1x} \ , \end{aligned} \tag{2.40}$$

with k, k_1 and k_2 given by the Schrödinger equation,

$$\begin{aligned} k &= \sqrt{2\mu E} \ , \\ k_1 &= \sqrt{2\mu(E - V_0)} \ , \\ k_2 &= \sqrt{2\mu(E - V_1)} \ . \end{aligned} \tag{2.41}$$

We must obtain the coefficients of the exponentials in the wave function by imposing continuity of the wave function and the first derivative in $x = \pm a$ and $x = \pm(a+b)$. The problem is easier to solve by considering solutions with well-defined parity, since the potential is symmetric under $x \to -x$. Define functions $\psi^{\pm}(x) = \psi(x) \pm \psi(-x)$, so that

$$\begin{aligned} \psi(+x) &= \frac{\psi^+(x) + \psi^-(x)}{2} \ , \\ \psi(-x) &= \frac{\psi^+(x) - \psi^-(x)}{2} \ , \end{aligned} \tag{2.42}$$

and with $\psi^{\pm}(x) = \pm\psi^{\pm}(x)$. We just need to consider the zones LR, $R1$ and $R2$,

$$\begin{aligned} \psi^{\pm}_{LR}(x) &= A_{\pm}\left(e^{ik_1x} \pm e^{-ik_1x}\right) \ , \\ \psi^{\pm}_{R1}(x) &= B_{\pm}e^{ik_2x} + C_{\pm}e^{-ik_2x} \ , \\ \psi^{\pm}_{R2}(x) &= D_{\pm}e^{ikx} + P_{\pm}e^{-ikx} \ . \end{aligned} \tag{2.43}$$

The relation among the two set of coefficients is given by:

$$I_{R1} = \frac{B_+ + B_-}{2} \qquad O_{R1} = \frac{C_+ + C_-}{2} \qquad I_{R2} = \frac{D_+ + D_-}{2} \qquad O_{R2} = \frac{P_+ + P_-}{2}$$

$$O_{L1} = \frac{B_+ - B_-}{2} \qquad I_{L1} = \frac{C_+ - C_-}{2} \qquad O_{L2} = \frac{D_+ - D_-}{2} \qquad I_{L2} = \frac{P_+ - P_-}{2}$$
$$I_{LR} = \frac{A_+ + A_-}{2} \qquad O_{LR} = \frac{A_+ - A_-}{2} \tag{2.44}$$

The solution of the continuity conditions can be written in terms of $A_\pm$ as

$$\begin{aligned} 2k_2 B_\pm e^{+ik_2 a} &= A_\pm \left(e^{ik_1 a}(k_2 + k_1) \pm e^{-ik_1 a}(k_2 - k_1) \right) \\ 2k_2 C_\pm e^{-ik_2 a} &= A_\pm \left(e^{ik_1 a}(k_2 - k_1) \pm e^{-ik_1 a}(k_2 + k_1) \right) \\ 4kk_2 D_\pm e^{+ik(a+b)} &= A_\pm G_\pm(E) \\ 4kk_2 P_\pm e^{-ik(a+b)} &= A_\pm F_\pm(E) \end{aligned} \tag{2.45}$$

where the functions $G_\pm$ and $F\pm$, that play an important role in the following, are given by:

$$\begin{aligned} G_\pm(E) = {} & e^{+ik_2 b} e^{+ik_1 a}(k + k_2)(k_2 + k_1) \pm e^{+ik_2 b} e^{-ik_1 a}(k + k_2)(k_2 - k_1) \\ & + e^{-ik_2 b} e^{+ik_1 a}(k - k_2)(k_2 - k_1) \pm e^{-ik_2 b} e^{-ik_1 a}(k - k_2)(k_2 + k_1) \end{aligned} \tag{2.46a}$$

$$\begin{aligned} F_\pm(E) = {} & e^{+ik_2 b} e^{+ik_1 a}(k - k_2)(k_2 + k_1) \pm e^{+ik_2 b} e^{-ik_1 a}(k - k_2)(k_2 - k_1) \\ & + e^{-ik_2 b} e^{+ik_1 a}(k + k_2)(k_2 - k_1) \pm e^{-ik_2 b} e^{-ik_1 a}(k + k_2)(k_2 + k_1) \end{aligned} \tag{2.46b}$$

We will take, for the numerical examples in what follows, $V_0 = -800$ MeV, $V_1 = +400$ MeV, $a = 3$ fm and $b = 3$ fm, and a mass $m_1 = m_2 = m = 140$ MeV, similar to that of the pion.

2.4.1 Bound states: $V_0 < E < 0$

Let us consider first the case $V_0 < E < 0$, which gives a *discrete* spectrum of *bound states*, lying in the *physical* Riemann sheet of the momentum k, characterized by Im$k > 0$. By putting $k = i\kappa$, we see that, in order to end with normalizable wave-functions, solutions of the type $e^{-ikx} = e^{\kappa x}$ must be avoided for $x > a + b$, and those $e^{+ikx} = e^{-\kappa x}$ for $x < -(a + b)$. Thus, we must set $I_{L2} = O_{R2} = 0$, that is, $P_+ = P_- = 0$, which can be done simultaneously only if $F_+ = A_- = 0$ or $F_- = A_+ = 0$.[4] The first condition leads to *even* wave functions, since $A_- = 0$ implies $B_- = C_- = D_- = 0$. Analogously, the condition $F_- = A_+ = 0$ leads to *odd* wave functions. From their definitions, we see that the function F_+ is purely real and F_- is purely imaginary for $V_0 < E < 0$. This means that the conditions $F_+ = 0$ *or* $F_- = 0$ select *eigenvalues* for the energy E with $V_0 < E < 0$, corresponding to *bound states* with well-defined parity. The energy eigenvalues for the bound states of our numerical calculation are given in Table 2.1, according to their parity. We also show the value $\sqrt{\langle x^2 \rangle}$, which is smaller for the ground state than for the others. This can be understood easily in terms of the wave functions, because the ground state has an even wave function without nodes, that is more peaked around zero. In general terms, odd wave functions, since they are zero for $x = 0$, are spread all over the potential well.

2.4.2 Scattering and resonances: $E > 0$

The scattering problem consists in the study for $E > 0$ of this potential when there is an incoming wave, for instance, from the left, $x = -\infty$, and no incoming wave from the right. In

[4] Notice that, according to their definitions, it is not possible to simultaneously have $F_+ = F_- = 0$. On the other hand, if $A_+ = A_- = 0$, the wave-function vanishes altogether.

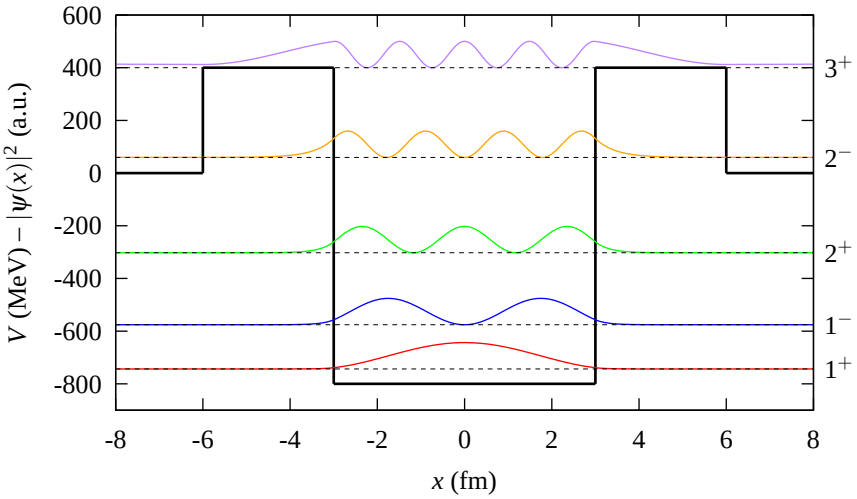

Figure 2.2: The modulus squared of the wave function, $|\psi(x)|^2$, plotted for the different states in Table 2.1.

terms of the coefficients, it means $O_{R2} = 0$, that is $P_+ = -P_-$, so that $I_{L2} = (P_+ - P_-)/2 = P_+$. Thus, $A_+F_+(E) = -A_-F_-(E)$. It is important here to study the transmission and reflection coefficients, which are the ratios:

$$T = \frac{I_{R2}}{I_{L2}} \qquad R = \frac{O_{L2}}{I_{L2}} \ . \tag{2.47}$$

In terms of the functions $G_\pm$ and $F_\pm$,

$$T = \frac{e^{-2ik(a+b)}}{2}\left(\frac{G_+(E)}{F_+(E)} - \frac{G_-(E)}{F_-(E)}\right) \ , \tag{2.48a}$$

$$R = \frac{e^{-2ik(a+b)}}{2}\left(\frac{G_+(E)}{F_+(E)} + \frac{G_-(E)}{F_-(E)}\right) \ . \tag{2.48b}$$

These satisfy the important relation $|T|^2 + |R|^2 = 1$, that is, the particle is transmited or reflected. This fact is related to unitarity. When plotted against the energy E, as in Fig. 2.3 (solid blue line), the transmission coefficient shows an structure of peaks, that corresponds to *resonances*. These have the form:

$$|T|^2 \simeq \frac{(\Gamma/2)^2}{(E - E_0)^2 + (\Gamma/2)^2} \ , \tag{2.49}$$

which is called a Breit-Wigner amplitude. In Fig. 2.3 it is also plotted (dashed red line) an incoherent sum of two such amplitudes corresponding to the resonances 2^+ and 3^- shown in Table 2.1. These structures correspond to poles of T in the second Riemann sheet in the E-complex plane at positions $E = E_0 - i\Gamma/2$, and Γ is called the *width* of the resonance. It is worth noticing that the condition for the poles to appear is then $F_+(E) = 0$ or $F_-(E) = 0$, just as in the case of the bound state problem, giving rise to a coherent global picture of the problem of resonances and bound states, that is, the problem of the *spectrum* of the theory.

In Fig. 2.2 the wave functions for the resonances are also plotted. However, since the widths of both states 2^+ and 3^- are small, there is a fact that cannot be fully appreciated there. In the region $R2$, the wave function is proportional to e^{+ikx}, both for the case of a

State (n^P)	E (MeV)	Γ (MeV)	$\sqrt{\langle x^2 \rangle}$ (fm)
1^+	-743.5		1.3
1^-	-575.6		1.9
2^+	-302.4		2.0
2^-	59.4	0.4	
3^+	442.7	28.9	

Table 2.1: Bound states and resonances parameters for the potential studied, $V_0 = -800$ MeV, $V_1 = +400$ MeV, $a = 3$ fm and $b = 3$ fm.

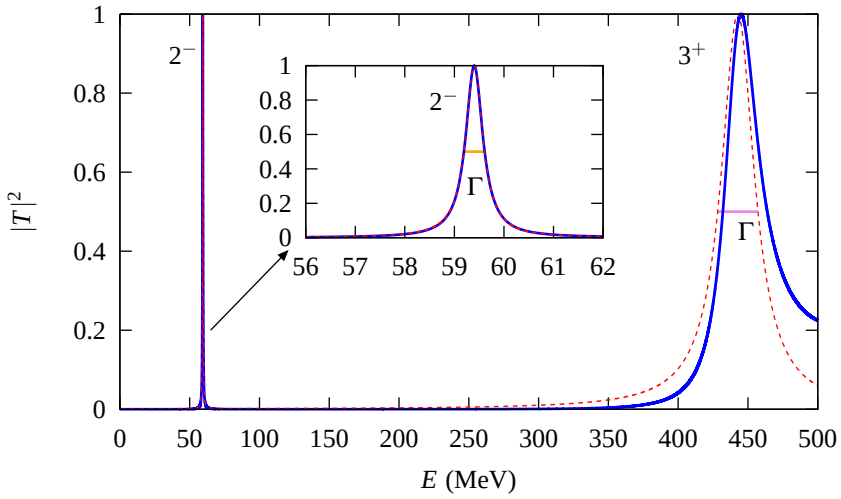

Figure 2.3: Modulus squared of the transmission coefficient, $|T|^2$. Resonant structures are around energies $E = 60$ MeV and $E = 440$ MeV. The solid blue line represents the exact value, Eq. (2.48), whereas the red dashed line is the incoherent sum of two Breit-Wigner amplitudes, Eq. (2.49), with the parameters of Table 2.1. The first structure is reproduced with high accuracy, whereas for the second one the agreement is worse because of interference with higher resonances not shown here.

bound state and a resonance. For the latter, however, since $k = k_r - ik_i$ with $k_i > 0$, the wave function is $e^{ik_r x} e^{k_i x}$. The first term gives an oscillating wave functions, with modulus $|e^{ik_r x}| = 1$, but the second term grows exponentially for $x \to +\infty$. A similar reasoning applies in the case $x \to -\infty$. Thus, the wave function diverges and cannot be normalized, and mean values of observables, such as $\langle x^2 \rangle$, cannot be calculated. This is a serious problem largely studied in the literature. Some approaches to calculate normalizable wave functions have been developed [208–216].

2.5 Resonances

We first discuss resonances in the elastic amplitude case, and then generalize the discussion to inelastic transitions.

2.5.1 Elastic case

In Sec. 2.1 it was stated that resonances appear as simple poles in the so called unphysical Riemann sheets of the amplitude. We have also seen that this is the case in Quantum Mechanics in Sec. 2.4. In this Section we concentrate in the former point (the appearence of poles), whereas the question of the Riemann sheet is delivered in Sec. 2.6. For this purpose, suppose that the amplitude[5] of an elastic channel has a pole at the position $s_0 = s_R - i\gamma$,

$$T(s) = -\frac{g^2}{s - s_0} = -\frac{g^2}{s - s_R + i\gamma} \ . \tag{2.50}$$

The minus sign is an arbitrary convention. We suppose that γ is small enough (that is, the resonance is narrow) for the following developments. For physical (real) $s \simeq s_R$, one has

$$|T(s)|^2 \simeq \frac{1}{4} \frac{|g|^4 / s_R}{\left(\sqrt{s} - M\right)^2 + \frac{\Gamma^2}{4}} \tag{2.51}$$

where $M = \sqrt{s_R}$ is the *mass* of the resonance, $\Gamma = \gamma/M$ is its *width*, and the *coupling* of the resonance to the channel is $|g|$. The previous equation is known as the Breit-Wigner resonance formula. It is clear that the amplitude squared has a maximum at $s = M^2$, and, since the cross section is proportional to the former, it will have also a maximum when the center of mass energy ($E = \sqrt{s}$) reaches the resonance mass M. In addition,

$$\left|T\left((M \pm \Gamma/2)^2\right)\right|^2 = \frac{1}{2}\left|T\left(M^2\right)\right|^2 \ , \tag{2.52}$$

which can be used to estimate the width of a resonance, as it is done in Chapter 4, where pseudoscalar resonances are studied.

Due to unitarity, some restrictions arise for the coupling g. For simplicity, let us consider the case of the elastic scattering $aa \to aa$. Then

$$|p(s)| = \sqrt{\frac{s}{4} - M_a^2} \ , \tag{2.53}$$

where M_a is the mass of the a particle. Writing $g^2 = |g^2|\, e^{i\phi}$, one has:

$$-\frac{|g^2|}{T(s)} = (s - s_R)\cos\phi + \gamma \sin\phi + i\left(\gamma\cos\phi - (s - s_R)\sin\phi\right) \ , \tag{2.54}$$

Close to the resonance mass, $s \simeq s_R = M^2$, we have

$$8\pi\rho(s) = \frac{|p(s_R)|}{M} + \frac{M_a^2(s - M^2)}{2M^3\,|p(s_R)|} + \mathcal{O}((s - M^2)^2) \ . \tag{2.55}$$

Imposing Im $T^{-1}(s) = -\rho$, Eq. (2.22c), we get:

$$\begin{aligned} \gamma\frac{\cos\phi}{|g^2|} &= \frac{1}{8\pi}\frac{|p(s_R)|}{M} \ , \\ \frac{\sin\phi}{|g^2|} &= -\frac{1}{8\pi}\frac{M_a^2}{2M^3\,|p(s_R)|} \ . \end{aligned} \tag{2.56}$$

[5] We disregard here the index in T_L for clearness.

These relations can be cast as

$$\tan\phi = -\frac{\Gamma}{2M}\frac{1}{|p(s_R)/M_a|^2} \tag{2.57a}$$

$$\left|g^2\right| = 8\pi\frac{\Gamma M^2}{|p(s_R)|}\frac{1}{\sqrt{1+\tan^2\phi}} \tag{2.57b}$$

If we take the condition $\Gamma \ll M$ further, these equations reduce to $\tan\phi = 0$, and g^2 is real and positive (because $\cos\phi > 0$), so that

$$g^2 = 8\pi\frac{\Gamma M^2}{|p(s_R)|} \tag{2.57c}$$

Now, coming back to $T^{-1}(s)$, its real part will go through zero *near* the resonance mass, namely at $s = s_c$,

$$s_c = M^2 - \gamma\tan\phi = M^2\left(1 - \frac{\Gamma}{M}\tan\phi\right) , \tag{2.58}$$

and taking again the condition $\Gamma \ll M$ further, then $s_c = M^2$. If Re $T^{-1}(s)$ goes (quickly) trhough zero, then the phase shift goes through an odd multiple of $\pi/2$, $\delta(s_R) = (2n+1)\pi/2$.

Thus, a resonance manifests in the amplitude as a simple pole, and in what refers to the observables, if it is narrow enough, it will make the amplitude squared (and thus the cross section) have a maximum and the phase shift go through (an odd multiple of) $\pi/2$.

2.5.2 Inelastic case

We will now generalize this discussion to the multichannel case.[6] If the amplitude has a pole at $s = M^2 - i\Gamma M$, then we can write $s - M^2 - i\Gamma M = (E - M + i\Gamma/2)(E + M - i\Gamma/2)$, neglecting the term with Γ^2. Thus, a pole for $\sqrt{s} = E$, $E = M - i\Gamma/2$, arises. Then we can write the S-matrix as

$$S(E) = \mathscr{S}_0 + \frac{1}{E - M + i\Gamma/2}\mathscr{R} \tag{2.59}$$

where $\mathscr{S}_0$ is the *background* matrix and $\mathscr{R}$ is the matrix of *residues*. In the discussion of the elastic case we did not consider the background (that is, we set it to $\mathscr{S}_0 = \mathbb{I}$). We set $\mathscr{R}$ as a constant[7] (in the elastic case, we considered its energy dependence) close to the resonance $E \simeq E_R$. Unitarity implies that:

$$SS^\dagger = \mathbb{I} = \mathscr{S}_0\mathscr{S}_0^\dagger + \frac{1}{(E-M)^2 + \frac{\Gamma^2}{4}}\left((E - E_R)\left(\mathscr{R}\mathscr{S}_0^\dagger + \mathscr{S}_0\mathscr{R}^\dagger\right) - i\frac{\Gamma}{2}\left(\mathscr{R}\mathscr{S}_0^\dagger - \mathscr{S}_0\mathscr{R}^\dagger\right) + \mathscr{R}\mathscr{R}^\dagger\right)$$

and thus, the background must be unitary, $\mathscr{S}_0\mathscr{S}_0^\dagger = \mathbb{I}$, and, in addition, we have the following conditions[8] on $\mathscr{R}$:

$$\mathscr{R}\mathscr{S}_0^\dagger + \mathscr{S}_0\mathscr{R}^\dagger = 0 , \tag{2.60a}$$

[6] I will follow the lines of Weinberg, Ref. [217], p. 161-165, but see also [218].

[7] We are thus assuming that the width is small and that the resonance is far away from threshold.

[8] Note the erratum in Eq. (3.8.6) in Ref. [217].

$$\mathscr{R}\mathscr{R}^\dagger - i\frac{\Gamma}{2}\left(\mathscr{R}\mathscr{S}_0^\dagger - \mathscr{S}_0\mathscr{R}^\dagger\right) = 0 \ . \tag{2.60b}$$

By setting $\mathscr{R} = -i\Gamma\mathscr{A}\mathscr{S}_0$, these equations are simply:

$$\mathscr{A} = \mathscr{A}^\dagger \ , \tag{2.60c}$$
$$\mathscr{A}^2 = \mathscr{A} \ , \tag{2.60d}$$

which allows to write

$$S = \left(\mathbb{I} - i\frac{\Gamma}{E - M + i\frac{\Gamma}{2}}\mathscr{A}\right)\mathscr{S}_0 \ . \tag{2.61}$$

The deep meaning of the Eqs. (2.60) is that, given a resonance, only the absolute value of the coupling makes sense, since its phase is fixed by unitarity and the background, if present.

For the elastic case without background, Eqs. (2.60) reduce to the conditions Eqs. (2.57). In this case, $\mathscr{S}_0 = 1$, and thus $\mathscr{R} = -i\Gamma$. By comparing with T, we have $\mathscr{R} = -i\,|p|\,g^2/(8\pi M^2)$, and then the condition Eq. (2.57c) is reached, and also g^2 is found to be real and positive.

The condition for the matrix $\mathscr{A}$ implies that it can be written as [218]:

$$\mathscr{A}_{ij} = u_i u_j^* \quad \text{with} \quad \sum_i |u_i|^2 = 1 \ , \tag{2.62}$$

Considering the term between brackets in Eq. (2.61), which is the resonant S-matrix, S_R, it follows that:

$$S_{R,ij} = \delta_{ij} - i\frac{\Gamma}{E - M + i\frac{\Gamma}{2}}u_i {u_j}^* \ . \tag{2.63}$$

From the condition Eq. (2.62) we see that $|u_i|^2 \leq 1$. We call the *partial width* to the product

$$\Gamma_i = \Gamma\,|u_i|^2 \ . \tag{2.64}$$

By construction, $\sum_i \Gamma_i = \Gamma$. By comparing with the definition

$$T_{ii} = -\frac{g_{ii}^2}{s - s_0} \simeq -\frac{g_{ii}^2/(2M)}{E - M + i\frac{\Gamma}{2}} \ , \tag{2.65}$$

we reach the condition

$$\Gamma_i = \frac{g_{ii}^2\,|p_i(s_R)|}{8\pi M^2} \ , \tag{2.66}$$

which is like Eq. (2.57c), but for the coupled channel case.

The couplings g_{ij}, related to the residues of the pole in the amplitude in the unphysical Riemann sheet, can be obtained, for $s \simeq s_0$, by:

$$T_{ij}(s) = -\frac{g_i g_j}{s - s_0} + \text{regular terms} \ . \tag{2.67a}$$

Numerically, it is usually better to obtain them through the Cauchy theorem:

$$g_i g_j = -\frac{1}{2\pi i}\oint_{\Gamma_{s_0}} T_{ij}(s')\mathrm{d}s' = -\frac{\lambda}{2\pi}\int_0^{2\pi} e^{i\theta}T_{ij}(s_0 + \lambda e^{i\theta})\mathrm{d}\theta \ , \tag{2.67b}$$

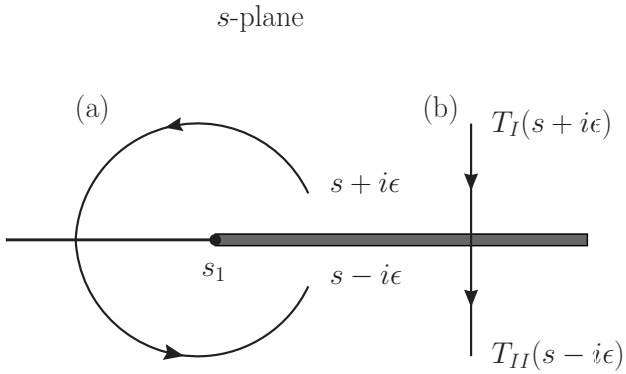

Figure 2.4: Complex s-plane, where the unitarity branch cut is shown, starting at threshold, $s = s_1$, and extending to infinity.

with $\lambda \to 0$, and being Γ_{s_0} a counterclock closed path around enclosing s_0 (but no other poles).

Finally, we would like to end here with some remarks. The cases considered so far in this Section are somewhat ideal, and the situation to disentangle the different resonances in a given channel as well as their partial widths can be very involved. An example of this is the scalar sector, to be studied in Chapter 3. Usually, resonances appear close to thresholds, and then their shape can be rather distorted, due to the *Flatté effect* [219], first noticed in the scalar sector for the case of the $a_0(980)$ resonance. Also, if the background is sizeable, the width of the amplitude needs not to be the same width Γ deduced from the pole, nor the phase go through $\pi/2$. Needless to say, if the width of the resonance is very large, this simple picture does not embrace sufficiently the complexity of physical scattering in the energy region under consideration.

2.6 Unitarity cut and Riemann sheets

The appearence of the unphysical Riemann sheets of an amplitude in two-body scattering reactions is due to the presence of branch points sitting in the thresholds of the different channels. Let us consider, for definiteness, an elastic amplitude, so that there is just one threshold, s_1. Due to the usual $\pm i\epsilon$ prescriptions in Quantum Field Theory, such an amplitude is defined for $s \to s + i\epsilon$. If we analytically continue the amplitude in the variable s, to the upper half-plane, that is, for finite ϵ, $s + i\epsilon \to s + i\gamma$, we are moving through the so called *physical sheet*. The amplitude in the physical sheet is analytic except for the so called *unitarity* or *right hand cut*,[9] and thus, the lower half plane of the complex variable s can be reached by moving from $s + i\epsilon$ to $s - i\epsilon$ below threshold. This is the movement (a) in Fig. 2.4.

However, if we cross the unitarity cut, moving *continuously* to the lower half plane, as indicated in Fig. 2.4 by (b), we reach the *unphysical sheet*. As it is connected continuously

[9]The presence of the *crossed cuts*, that arise from crossing symmetry has no influence on the following discussion, so we will not refer to it.

with the physical sheet in the real axis above threshold, $s > s_1$, it must be that:

$$T_I(s + i\epsilon) = T_{II}(s - i\epsilon) \ , \tag{2.68a}$$

where $T_I(s)$ indicates the amplitude in the physical sheet and $T_{II}(s)$ the amplitude in the unphysical or second Riemann sheet. Then, once $T_{II}(s)$ is defined, it can be analytically continued to any region of the complex s-plane. Taking into account the Schwarz reflection principle, $T_I(s^*) = T_I(s)^*$, the previous equation can be rewritten as:

$$T_{II}(s - i\epsilon) = T_I(s - i\epsilon) - 2i\text{Im}\ T_I(s - i\epsilon) \ , \tag{2.68b}$$

or, in a maybe more useful form,

$$T_{II}^{-1}(s - i\epsilon) = T_I^{-1}(s - i\epsilon) - 2i\text{Im}\ T_I^{-1}(s - i\epsilon) = T_I^{-1}(s - i\epsilon) + 2i\rho \ . \tag{2.68c}$$

The last equation applies for a partial wave amplitude, satisfying Eqs. (2.22), in the elastic case, or as a matrix equation for the coupled channel case.

Given that an amplitude satisfies unitarity, Eqs. (2.22), then it cannot have poles on the physical sheet on the real axis above threshold. From Eq. (2.22), it can be seen that a cancellation $\infty = \text{constant} \times \infty^2$, should occur, which is not possible. Alternatively, thinking in terms of an elastic channel, the representation Eq. (2.23) for the amplitude $T_L(s)$ shows that it must be finite in the physical region, so it cannot have a pole. Notice also that, since above threshold and on the real axis the physical and the unphysical Riemann sheets of the amplitude coincide, no pole can appear there neither in the unphysical Riemann sheet. Below the lowest threshold it is possible to have a pole in the physical Riemann sheet, however, and this is the case of a *bound state*. An example is the deuteron, a neutron–proton bound state in the ${}^3S_1 - {}^3D_1$ waves, which will be considered in Chapter 7. But note also that nothing prevents a pole appearing on the real axis, below threshold, but on the unphysical Riemann sheet: these are *anti-bound* or *virtual* states. We saw, in our simple problem of Quantum Mechanics in Sec. 2.4, that *bound states* appear as real eigenvalues of the Hamiltonian for energy values below threshold, as stated above. However, *resonances* appeared in the *second* or *unphysical* Riemann sheet of the amplitude. This is because the eigenvalues of the Hamiltonian must be real, but resonances correspond to complex eigenvalues. Whence, we can summarize the appearence of poles as follows:

- On the real axis, below threshold, we can have poles in the physical Riemann sheet (bound states) or in the unphysical Riemann sheet (antibound states).
- On the real axis, but above threshold, we cannot have poles (neither in the physical nor the unphysical Riemann sheet), because of unitarity.
- On the complex plane, there can be poles in the unphysical Riemann sheet (resonances), but not in the physical Riemann sheet (because the Hamiltonian eigenvalues must be real).

2.7 Unitarized Chiral Perturbation Theory

We have seen in Chapter 1 that the spontaneous chiral symmetry breaking imposes strong constraints in the interactions of the lightest scalar pseudoscalars. These interactions can

thus be derived in the framework of an effective field theory: Chiral Perturbation Theory (ChPT). Beyond its great success [220–223], we can point out some shortcomings in the range of applicability of the theory. As seen in Chapter 1, it contains *free* parameters, not fixed by the symmetries. The number of these parameters increases with the order of the studied Lagrangians. At $\mathcal{O}(p^2)$, beyond the masses of the lightest pseudoscalars, there is the weak decay constant of the pion, f_π, but, at $\mathcal{O}(p^4)$, several low energy constants appear, and, at $\mathcal{O}(p^6)$, this number increases up to about one hundred, so that its predictive power is lost to a large extent with the chiral order. In addition, being a perturbative expansion, it does not incorporate full unitarity, which is seen to be an important ingredient in strong interactions. By including more and more orders (that include loop diagrams), unitarity is perturbatively satisfied because of its nonlinear dependence on the scattering amplitude, Eq. (2.10a). For the same reason, the perturbative character of the theory makes it impossible to reproduce resonances, that are associated with poles in the amplitudes, and that appear at masses already below 1 GeV. From the pointed drawbacks of the theory, it is clear that non-perturbative schemes are, not just desiderable, but necessary in order to study hadron physics comprising its full richness.

We will follow here the procedure of Ref. [39], where the most general structure of an arbitrary partial wave when the unphysical cuts are neglected is given. It is then the zeroth order approach to a partial wave when the unphysical cuts are treated perturbatively. The amplitudes so obtained are then matched to the lowest order of ChPT and its extension to include explicit resonances. A similar formalism, connected to the one presented here, is obtained in Ref. [33], where it is related to the Bethe–Salpeter equation.

Besides the unitary or right hand cut, starting at threshold (denoted here with $s_{\rm th}$), a partial wave $T(s)$ has the so-called unphysical or crossed cuts, due to crossed channel dynamics. For example, in nucleon-nucleon scattering, to be studied in Chapter 7, the left-hand cut in the low energy extent is due to multipion exchange diagrams. Then, the cut starts at $s = s_{\rm left} = -m_\pi^2/4$, and extends to $s = -\infty$. For simplicity, from now on, we refer to the set of different possible unphysical cuts as left-hand cut. Thus, for $s < s_{\rm left}$, the left-hand cut is given by:

$$T(s + i\epsilon) - T(s - i\epsilon) = 2i\text{Im}\ T_{\rm left}(s) \tag{2.69}$$

The standard way to simultaneously solve Eqs. (2.22) and (2.69) is the N/D method [38] (Cf. also [224, Ch. 8]). For simplicity, let us consider the elastic case first. This method rests on the separation of the unitary cut and the unphysical cuts, due to crossed channel dynamics, by writting

$$T(s) = \frac{N(s)}{D(s)} \tag{2.70}$$

where the function $N(s)$ carries the left-hand cut and $D(s)$ bears the right hand cut. The explicit threshold behaviour of an l partial wave, $T(s) \propto (\vec{p}^2)^l \equiv \nu^l$, can be taken into account by defining $T'(s) = T(s)/\nu^l$, and then

$$T'(s) = \frac{N'(s)}{D'(s)} \tag{2.71}$$

It is clear then that:

$$\text{Im } D'(s) = \begin{cases} \text{Im } (T'(s))^{-1} = -\rho(s)N'(s)\nu^l & , \quad s > s_{\text{th}} \\ 0 & , \quad s < s_{\text{th}} \end{cases} \tag{2.72a}$$

$$\text{Im } N'(s) = \begin{cases} \text{Im } T'_{\text{left}}(s)D'(s) & , \quad s < s_{\text{left}} \\ 0 & , \quad s > s_{\text{left}} \end{cases} \tag{2.72b}$$

As $T'(s)$ is determined by the ratio of $N'(s)$ and $D'(s)$, we can multiply both by any arbitrary real analytic function without changing $T'(s)$ nor the conditions Eqs. (2.72). If $N'(s)$ had poles, we could apply this procedure to remove them, and so we consider in the following that $N'(s)$ is free of them.

An $n+1$-subtracted dispersion relation for $N'(s)$ can be written down then as:

$$N'(s) = \frac{(s-s_0)^{n+1}}{\pi} \int_{-\infty}^{s_{\text{left}}} \mathrm{d}s' \frac{\text{Im } T'_{\text{left}}(s')D'(s')}{(s'-s_0)^{n+1}(s'-s)} + \sum_{m=0}^{n} \tilde{a}_m s^m \ , \tag{2.73}$$

and the $n+1$ subtractions are such that:

$$\lim_{s\to\infty} \frac{N'(s)}{s^{n+1}} = 0 \ . \tag{2.74}$$

If we neglect the left-hand cut, then $N'(s)$ is just a polynomial, and, as remarked before, we can divide both $N'(s)$ and $D'(s)$ by this polynomial, setting thus $N'(s) = 1$ and obtaining a dispersion relation for $D'(s)$ that reads:

$$D'(s) = -\frac{(s-s_0)^{l+1}}{\pi} \int_{s_{\text{th}}}^{\infty} \mathrm{d}s' \frac{\nu^l \rho(s')}{(s'-s)(s'-s_0)^{l+1}} + \sum_{m=0}^{l} a_m s^m + \sum_{i=1}^{M_L} \frac{R_i}{s-s_i} \tag{2.75}$$

The last term accounts for the possible presence of Castillejo-Dalitz-Dyson (CDD) poles [185], and, among other effects, it absorbs the zeroes of the polynomial used to set $N'(s) = 1$. The CDD poles will appear again in Chapter 7, when dealing with nucleon-nucleon scattering.

In order to proceed further, we will make some considerations about the $N_C \to \infty$ limit, with N_C being the numbers of colours in QCD.[10] We split the subtraction constant into two pieces,

$$a_m = a_m^L + a_m^{SL}(s_0) \ , \tag{2.76}$$

where the superscripts L and SL refer to leading and subleading order in the large N_C limit, respectively. As the meson-meson amplitudes scale as N_C^{-1} [194,196], $D'(s)$ and a_m^L run as N_C. The integral in Eq. (2.75) is zeroth order in this counting. Its dependence on the subtraction point s_0 is reabsorbed in $a_m^{SL}(s_0)$, which is of the same order in N_C. Thus, in the limit $N_C \to \infty$, $D'(s)$ simplifies to:

$$D'^{\infty}(s) = \sum_{m=0}^{L} a_m^L s^m + \sum_{i}^{M_L^\infty} \frac{R_i^\infty}{s-s_i} \ , \tag{2.77}$$

[10] As a funny anecdote, I remember that M. Scadron, in the SCADRON70 Workshop, at the occasion of his 70th birthday, listening to a talk where the $N_C \to \infty$ limit was copiously considered, said to the speaker: "You can talk about the large N_C limit, but $N_C = 3$ is its actual value!".

where the sum of poles now picks up just the relevant CDD poles in this limit, and R_i^∞ is also the leading part of R_i. In the previous equation, the left and right pieces represent contact and pole terms, respectively, that is, tree level amplitudes. The contact terms can be matched with the standard lowest order ChPT amplitudes, and the pole terms, with the explicit interchange of resonances in the s-channel (t- and u- interchanges are neglected, consistently with the assumption that the left-hand cut is neglected). By denoting these contributions as T_2 and T_R, respectively, one is lead to write:

$$T^\infty(s) \equiv T_2(s) + T_R(s) = \nu^l (D'^\infty(s))^{-1} \tag{2.78}$$

Finally, by defining the function $g_l(s)$ as

$$g_l(s)\nu^l = \sum_{m=0}^{L} a_m^{SL}(s_0) s^m - \frac{(s-s_0)^{l+1}}{\pi} \int_{s_{\rm th}}^{\infty} \mathrm{d}s' \frac{\nu(s)^l \rho(s')}{(s'-s)(s'-s_0)^{l+1}} \ , \tag{2.79}$$

the final amplitude can be written as

$$T(s) = \Big((T^\infty(s))^{-1} + g_l(s) \Big)^{-1} \ . \tag{2.80}$$

In the previous equation, T^∞ corresponds to the tree level amplitudes before unitarization is accomplished, and then the latter is done through the $g_l(s)$ function.

This formalism can be generalized to the case of coupled channels straightforwardly. The matrix $T(s)$ will be given by the inverse of $(T^\infty)^{-1} + G$, where the matrix T^∞ will have as matrix elements the amplitudes of the different channels as given by ChPT plus the interchange of resonances, and $G_l(s)$ will be a diagonal matrix whose elements will be the $g_l(s)$ functions with the integrand $\rho(s')$ particularized for each of the channels.

We can make and additional generalization, allowing also to include crossed channel contributions in a perturbative manner [41,225], and keeping the matrix formulation for coupled channels. For that purpose, we expand Eq. (2.70) (writting K instead of T^∞, since it also includes now subleading contributions in the N_C expansion),

$$\begin{aligned} T &= \Big(K^{-1} + G \Big)^{-1} = \Big((K_2 + K_4 + K_6 + \cdots)^{-1} + G \Big)^{-1} \\ &= K_2 + K_4 - K_2\, G\, K_2 + K_6 - K_4\, G\, K_2 - K_2\, G\, K_4 + K_2\, G\, K_2\, G\, K_2 + \cdots \\ &= T_2 + T_4 + T_6 + \cdots \ , \end{aligned} \tag{2.81}$$

where in the last step we indicate that this expansion must be matched with the ChPT perturbative calculation, and the chiral orders are indicated by the subscripts. The former set of matrix equation can be solved (starting from the lowest order) to get:

$$K_2 = T_2 \ , \tag{2.82a}$$
$$K_4 = T_4 + T_2\, G\, T_2 \ , \tag{2.82b}$$
$$K_6 = T_6 + T_4\, G\, T_2 + T_2\, G\, T_4 + T_2\, G\, T_2\, G\, T_2 \ , \tag{2.82c}$$
$$K_8 = T_8 + \cdots \ . \tag{2.82d}$$

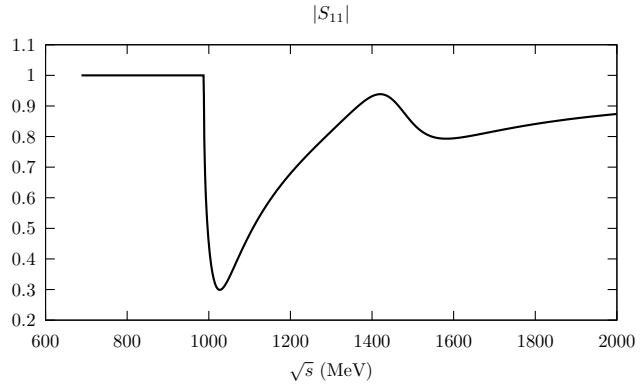

Figure 2.5: Absolute value of the matrix element S_{11}, corresponding to $\pi\eta$ with $I^G(J^{PC}) = 1^-(0^{++})$.

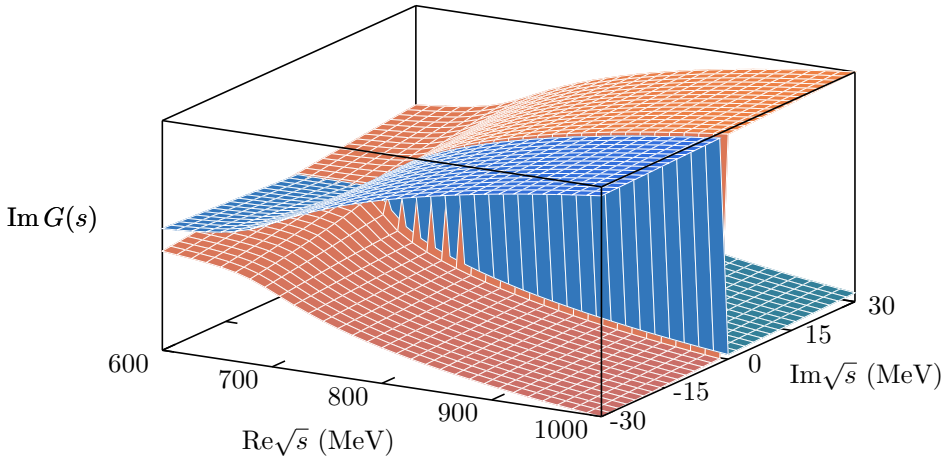

Figure 2.6: The two Riemann sheets of the function $G(s)$ for the case of $\pi\eta$ scattering. The threshold is located at $\sqrt{s_1} \approx 690$ MeV. The blue surface is the physical Riemann sheet, whereas the red one is the unphysical Riemann sheet.

2.8 A detailed example: two-meson scattering in the $I^G(J^{PC}) = 1^-(0^{++})$ channel

In this section we offer a detailed example in which all the subjects treated so far in this Chapter can be seen at work. We will study the three-coupled channel with quantum numbers $1^-(0^{++})$, given by the two-meson channels $\pi\eta$, $K\bar{K}$ and $\pi\eta'$. We make use of the amplitudes, formalism and fit to the data presented in Chapter 4 and in Appendix D, so that we do not extend on these details. In this channel, the $a_0(980)$ resonance appears, but we will not focus on it, but rather on the $a_0(1450)$ resonance, higher in mass, and not affected by the presence of the nearby threshold of $K\bar{K}$, which makes the discussion of the $a_0(980)$ more involved.[11] It should be remarked that we do not pursue here an accurate description of this resonance, but just to present a realistic calculation which, at the same time, will allow us to put in practice some of the concepts and ideas seen so far in this Chapter.

In Fig. 2.5 we show the absolute value of the matrix element S_{11}. Up to the opening of

[11] For more details on this issue, see the introductory sections in Chapters 3 and 5.

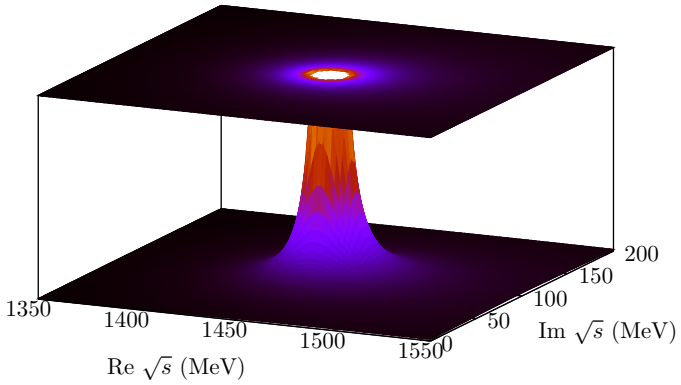

Figure 2.7: The amplitude $|T_{33}|^2$ is shown in the Riemann sheet where the pole appears. The z axis range is arbitrarily cut, so the effects of the pole can be seen. A contour plot is shown at the top where the location of the pole can be seen.

Channel	Coupling $\lvert g_{ii}\rvert$ (GeV)	Partial width Γ_i (MeV)
$\pi\eta$	1.26	18
$K\bar{K}$	2.46	61
$\pi\eta'$	3.53	92

Table 2.2: Couplings and partial widths of the $a_0(1450)$ resonance.

the $K\bar{K}$ threshold, at $\sqrt{s} \approx 1$ GeV, the channel $\pi\eta$ is elastic, thus satisfying $|S_{11}| = 1$. Above threshold, other channels open up and thus $|S_{11}| \leqslant 1$. The dip at above 1 GeV is characteristic of the $a_0(980)$.

We have seen that the poles to which resonances are associated are located in the unphysical Riemann sheet. Now we describe how to change from the physical to the unphysical Riemann sheet in the context of UChPT. As we have seen in the previous Section, we can write a partial wave amplitude as:

$$T^{-1}(s) = V^{-1}(s) + G(s) \ , \tag{2.83}$$

where $V(s)$ contains the dynamical information of the theory and is real on the real axis, and $G(s)$ is the matrix that contains the one-loop two-meson propagators, whose imaginary part is

$$\text{Im } G(s) = -\rho(s) \ , \tag{2.84}$$

thus satisfying unitarity, Eqs. (2.22). We consider, for definiteness, the elastic case. The $G(s)$ function is given in Eq. (4.12). As we have seen in Eq. (2.68c), the change of the Riemann sheet of an amplitude concerns basically the piece in the last equation. Then,

$$G_{II}(s - i\epsilon) = G_I(s - i\epsilon) + 2i\rho(s) \ , \tag{2.85}$$

where, recall, $\rho(s) = \sqrt{\vec{p}^2}/(8\pi\sqrt{s})$. A technical detail is that, in the previous equations, one must take $\sqrt{\vec{p}^2}$ such that Im $\sqrt{\vec{p}^2} > 0$. In Fig. 2.6 we see an example of the two Riemann sheets, for the case of $\pi\eta$ scattering, being the threshold at $\sqrt{s_1} \approx 690$ MeV. We plot there

the imaginary part of $G(s)$. We see the unitarity cut, opening at threshold, and that one can move to the lower half plane without changing the Riemann sheet, by moving around threshold from below. It is also seen the condition Eq. (2.68a) over the real axis for $s > s_1$.

As there are three channels, we have 2^3 posible Riemann sheets of the amplitudes. As we have seen, the physical Riemann sheet has no poles. Usually the Riemann sheets that must be inspected when searching for poles are those that are conected continuously with the physical one, such as the example in Fig. 2.6. If we are looking for the $a_0(1450)$, well above the highest threshold, $\sqrt{s_{\pi\eta'}} \approx 1100$ MeV, we must change to their respective Riemann sheets all of the $G(s)$ functions associated with each channel. The pole, shown in Fig. 2.7, is found at $\sqrt{s_0} = 1454 - i94$ MeV. Thus, from $\mathrm{Im}\sqrt{s_0}$, we deduce $\Gamma = 188$ MeV. This compares well with the PDG [48], that quotes $M = 1474 \pm 19$ MeV and $\Gamma = 265 \pm 13$ MeV. One should take into account that we miss multiparticle states and that our calculated width should indeed be smaller than the total one quoted in the PDG [48].

The couplings of the poles to the channels, obtained with Eq. (2.67), are given in Table 2.2, together with their respective partial widths, as given by Eq. (2.66). From the partial widths, calculated as in Eq. (2.66), we see that $\sum_i \Gamma_i = 171$ MeV, quite close to $\Gamma = 188$ MeV deduced from the pole. The slight disagreement is due to the finite and not so small width, $\Gamma/M \simeq 0.13$. Whence, there arise differences when formulas valid for $\Gamma \ll M$ are used.

II

Results

3

The Scalar Sector and the Scalar Glueball

Contents of this Chapter:

3.1 Introduction

One of the main features of strong interactions at low energy is the spontaneous breaking of the chiral symmetry, which implies the existence of Goldstone bosons, to be identified in $SU(2)$ with the triplet of pions (which acquire mass due to the small, but finite, light quark masses), and in $SU(3)$ with the octet of the lightest pseudoscalars, $J^{PC} = 0^{-+}$, π, K and η. In the limit of chiral symmetry restoration there should be scalars, 0^{++}, degenerate in mass with the pseudoscalars. As a result, one can also say that the appearance of 0^{++} mesons in QCD is a benchmark characteristic of any theory of strong interactions and, furthermore, the difference in mass between the pions and the σ is an order parameter of spontaneous chiral symmetry breaking.[1]

An explicit realization of these considerations is the linear sigma model [226–232]. However, we have seen in Chapter 1 that the Effective Field Theory that takes into account the consequences of the spontaneous breaking of chiral symmetry at low energy QCD, with sufficient generality [233, 234], is Chiral Perturbation Theory (ChPT) [17–19], a non-linear sigma model. In ChPT, however, due to its perturbative nature, the presence of the scalars is not readily connected with the appearance and dynamics of the lightest multiplet of pseudoscalars. The tight relationship between the lightest pseudoscalars and scalars in ChPT was recovered when resuming an infinite string of diagrams (related with unitarity) through the Inverse Amplitude Method (IAM) [26,28–30,32], Bethe-Salpeter [33] and N/D frameworks [39]. From these analyses it was clear, as expected on general grounds and given the smallness of the left-hand cut contributions in the resonance S-wave meson-meson amplitudes below $\sqrt{s} \simeq 1$ GeV [39], that chiral symmetry, in terms of resummed ChPT, requires the presence of light scalars in the spectrum of the strong interaction realm. These resonances correspond to the σ or $f_0(500)$, κ, $f_0(980)$ and $a_0(980)$, which not by accident, due to their referred relation with the lightest pseudoscalars, are also the lightest among the scalars. In Refs. [53–58] the mixing between these resonances was considered. Other successful phenomenological approach to study the lightest scalar resonances is based on meson-exchange models [59–61].

Crystal Barrel data at LEAR improved significantly the knowledge of the 0^{++} spectrum above 1 GeV with the discovery or confirmation of the $a_0(1450)$, $f_0(1370)$ and $f_0(1500)$ [64]. BES Collaboration fixed the spin of the $f_0(1710)$ [65] and found a new resonance, $f_0(1790)$ [66, 67]. There is some recent controversy on the existence of the broad $f_0(1370)$ [68] and another state reported is the $f_0(2020)$ [69]. For more references on these states see *e.g.* [48,70]. All these resonances are specially relevant for another issue of great interest in the $I = 0$, 0^{++} spectroscopy, which is the identification of glueballs. Since QCD is a non-abelian Yang-Mills theory, the gluons interact among themselves, a major difference with QED, where photons do not couple each other. Whence, it is generally believed that QCD predicts the existence of mesons without valence quarks (or with valence gluons, see a discussion in Ref. [82].) In a pure Yang-Mills theory the identification of these states would be straightforward. In the real world, however, they can be mixed with other non-glueball states of the Fock space. Interest in the glueballs dates back to the early days of QCD [1, 6, 7] and was one of the first issues of application of QCD sum rules [71, 72]. This application however is not without difficulties due to the strong coupling of the vacuum with the 0^{++} channel and the results

[1] In the study of Ref. [134] the σ was determined as the chiral partner of the π.

are not conclusive yet [71–76]. In recent papers the role of instanton contributions has been stressed [77,78]. Both papers agree with the presence of a glueball around 1.5 GeV but obtain different conclusions about the existence of a lighter glueball around 0.5 GeV, depending on how the instantons are treated. A glueball with a mass around $\gtrsim$ 1.5 GeV is also predicted in several models [79–83].

The glueball spectrum in quenched lattice QCD is already established [84–87] and predicts that the mass of the lightest 0^{++} glueball is 1660 ± 50 MeV (plus a 10% error in fixing the physical scale due to the quench approximation). The main issue with these calculations is that dynamical fermions are not included (infinitely heavy quarks) and hence the comparison with experimental phenomenology is not straightforward. Since the seminal calculation by the IBM group [88], a typical scenario for the identification of the lightest glueball consists of mixing the latter with the $n\bar{n}$ and $s\bar{s}$ states closest in energy. The output resonances are always the $f_0(1370)$, $f_0(1500)$ and $f_0(1710)$. Ref. [88] obtains that the $f_0(1710)$ is mainly a pure glueball. Ref. [89] evaluated in quenched lattice QCD the decays of the latter resonance to two pseudoscalars and calculated a pattern of decays in agreement with some reported data on the $f_0(1710)$ [48].

This scheme has recently been confirmed in Ref. [91] (see also Refs. [92–94]) which finds a chiral suppression in the way $\Gamma(G_0 \to s\bar{s})/\Gamma(G_0 \to u\bar{u} + d\bar{d}) \gg 1$, with G_0 the glueball. However, the situation is not clear yet and different results are obtained in different works [95–100], following the same idea of mixing of the glueball with the nearby $n\bar{n}$ and $s\bar{s}$ states. On the other hand, the presence of the nearby $f_0(1790)$ [66,67] has not been taken into account in all these studies and this could make some difference.

The mixing between quarkonia and glueballs sets up for the calculations of unquenched lattice QCD with two flavours of dynamical fermions in Refs. [235–238]. The most recent computations are Refs. [90, 239–241]. These studies find a low scalar singlet at energies that follow the trend of the two pion threshold simulated in the lattice. On the other hand, they also find a singlet resonance with a mass in the range of quenched results for the lightest glueball.

In our study, published in Ref. [A], we consider the coupled channel 0^{++} scattering between the two body $I = 0$ states made from the members of the lightest 0^{-+} and 1^{-+} multiplets from $\pi\pi$ threshold up to 2 GeV. Thus, we consider the scattering between the $\pi\pi$, $K\overline{K}$, $\eta\eta$, $\eta\eta'$, $\eta'\eta'$, $\rho\rho$, $\omega\omega$, $\omega\phi$, $\phi\phi$ and $K^*\overline{K^*}$ channels. In addition, we take into account the $\sigma\sigma$ channel. The $\sigma\sigma$ and $\rho\rho$ states play an important role to mimic the S-wave $I = 0$ 4π channel. This multipion channel plays a crucial role for energies somewhat above 1.2 GeV, see *e.g.* Ref. [64]. However, the multipion channels do not give rise to any sign of specific branch cut near 0.56 GeV for the 4π state nor around 0.84 GeV for the 6π one. This indicates, as signaled in Ref. [242], that the production of four or six pions occurs mainly via intermmediate two resonance states like $\sigma\sigma$, $\rho\rho$ and $\omega\omega$. There are experimental evidences [243, 244] that the 2π in 4π clusters around the masses of σ and ρ. We shall also explore the significance of the contribution from the $a_1(1260)\pi$ and $\pi(1300)\pi$ channels, although since the $a_1(1260)$ decays mainly to $\rho\pi$ and $\sigma\pi$ [48], as probably for the $\pi(1300)$, we expect that they are taken into account by the $\sigma\sigma$ and $\rho\rho$ channels already included. This will turn to be the case, as discussed below. We also study simultaneously the I =1/2 and I =3/2 S-wave amplitudes following the scheme

of Ref. [43, 44], so that we have more data to constraint our free parameters. Finally, let us mention that we include in our amplitudes the contributions of s–channel exchange of octets and singlets of scalar resonances, as discussed in Sec. 1.13. We consider many phase shifts, elastic and inelastic cross sections that are fitted simultaneously.

To obtain the interaction kernel among the channels we employ chiral Lagrangians at $\mathcal{O}(p^2)$ (see Chapter 1), but with the $SU(3)$ symmetry enlarged to $U(3)$ so as to include the η' meson. No free parameters are present in the elementary kernels. This is due to the fact that the we employ ChPT and the couplings involving vector resonances are obtained by minimal coupling gauging chiral symmetry. To evaluate the $\sigma\sigma$ couplings we make use of UChPT (Chapter 2), where the σ resonance appears as dynamically generated from the self interactions between the pions in the scalar isoscalar pair of pions composing the resonance [33,39]. The interaction kernels are then unitarized to resum unitarity and the analyticity requirements of the RHC, following the scheme of UChPT [33, 39, 41, 225].

Other hadronic studies in a similar energy region as ours interested in the S-wave $I = 0$ scattering are [68, 245–249]. Refs. [245–247] follow an scheme based on coupled channels, as we also do here. But while these references only considers 3 or 4 channels we have included many more, namely 13 coupled channels. Let us also mention that our interaction kernels are calculated from chiral Lagrangians that establish constraints on the type of interaction vertices allowed, while those of Refs. [245–247] are quite *ad hoc*. Refs. [68, 248, 249] follow a different strategy, based on overlapping resonances employing the method of Dalitz-Tuan [250] based on multiplying diagonally one-resonance S-matrices. The couplings of those resonances are typically fitted and do not come either from any general Lagrangian. In addition these references have a large number of free parametres, typically around 40, many more than the 13 ones we use here. In our study no form factors are included either, instead, we include a subtraction constant for each channel, though some relations between the values of these constants for different channels can be also established.

We pay special attention to the spectroscopical content of our fits, related to the poles in the unphysical Riemann sheets of our solutions. In this way, we connect on the conflictive aspects previously referred concerning the 0^{++} resonances. Many schemes have been implemented so far that usually emphasize one aspect or the other of the 0^{++} dynamics [49–52, 116, 136, 137, 251–271].

This Chapter is organized as follows. Sec. 3.2 developes the formalism employed to calculate the interaction kernels, paying special to the way used to include the vector-vector (Subsec. 3.2.2) and the $\sigma\sigma$ (Subsec. 3.2.3) channels. In Sec. 3.3 these interaction kernels are gathered to construct the unitary partial waves. In Sec. 3.4 we obtain the fits to the scattering data. The relevant poles of our solutions and their connection with physical states are discussed in Sec. 3.5, and more support to our spectroscopy is given in Sec. 3.6. One of the main results of this work, the identification of the scalar glueball, is treated in Sec. 3.7. Our summary and the conclusions are delivered in Sec. 3.8.

3.2 Coupling the different channels

In order to obtain the coupling between the different channels we employ $U(3)$ ChPT at the lowest order including explict scalar resonances. Note that for $I = 0$ one needs to consider the channels $\eta\eta$, $\eta\eta'$ and $\eta'\eta'$ so as to study energies up to $s^{1/2} \lesssim 2$ GeV, and hence $U(3)$ symmetry is invoked. We follow here a similar scheme to that already employed in Refs. [43, 44], where the $K\eta$ and $K\eta'$ were included so as to describe data up to similar energies. As commented above, for the $I = 1/2$ and $I = 3/2$ S-wave we take the same formulae of Refs. [43, 44], but now describing simultaneously the $I = 0$ S-waves.

3.2.1 Lagrangians

We need first to consider the extended version of $SU(3)$ ChPT [19] to the $U(3)$ case. In the large N_C limit, the singlet η_1 field becomes the ninth Goldstone boson field and can then be incorporated with an extended $U(3)_L \otimes U(3)_R$ chiral Lagrangian [101–104]. A consistent counting that combines the chiral expansion in powers of momenta, quark masses and $1/N_C$ can be built, such that $m_q \sim 1/N_C \sim \mathcal{O}(p^2)$ [272]. At the lowest order the extension to $U(3)$ is straightforward. We can employ the same Lagrangians for $SU(3)$ ChPT [19] (given in Sec. 1.10) and with resonances [105, 106] (see Sec. 1.13) but with $U(x)$ being then the 3×3 matrix:

$$
\begin{aligned}
U(x) &= \exp\left(i\frac{\sqrt{2}\Phi}{f}\right) \\
\Phi &= \sum_{i=1}^{8}\phi_i\frac{\lambda_i}{\sqrt{2}} + \frac{1}{\sqrt{3}}\eta_1\mathbb{I} \equiv \sum_{i=0}^{8}\phi_i\lambda_i \\
&= \begin{pmatrix} \frac{\pi^0}{\sqrt{2}} + \frac{1}{\sqrt{6}}\eta_8 + \frac{1}{\sqrt{3}}\eta_1 & \pi^+ & K^+ \\ \pi^- & -\frac{\pi^0}{\sqrt{2}} + \frac{1}{\sqrt{6}}\eta_8 + \frac{1}{\sqrt{3}}\eta_1 & K^0 \\ K^- & \overline{K}^0 & -\frac{2}{\sqrt{6}}\eta_8 + \frac{1}{\sqrt{3}}\eta_1 \end{pmatrix} ,
\end{aligned}
\tag{3.1}
$$

where f is the pseudoscalar weak decay couplings in the $SU(3)$ chiral limit. We also have $\phi_0 = \eta_1$ and $\lambda_0 = \sqrt{2/3}\,\mathbb{I}$. The corresponding Lagrangians are those given in Eq. (1.10) plus the η_1 mass term:

$$
\mathcal{L}_2 = \frac{f^2}{4}\left\{\langle D_\mu U^\dagger D^\mu U\rangle + \langle \chi^\dagger U + \chi U^\dagger\rangle\right\} - \frac{1}{2}M_1^2\eta_1^2 \ . \tag{3.2}
$$

Here, the covariant derivative is

$$
D_\mu U = \partial_\mu U - ir_\mu U + iUl_\mu \ , \tag{3.3}
$$

with r_μ and l_μ the right and left external vector fields, respectively, introduced for gauging the $U(3)_L \otimes U(3)_R$ chiral group, as seen in Secs. 1.6–1.7, and also Subsec. 1.9.1. The M_1 is a term originating from the $U(1)_A$ anomaly, which is large though formally of $\mathcal{O}(1/N_C)$. It is responsible of the large mass of the η_1, see *e.g.* [273]. The quark masses are included in $\chi = 2B_0\mathcal{M}$ with $\mathcal{M} = \mathrm{diag}(m_u, m_d, m_s)$, the matrix of the light quark masses. The diagonalization of the mass term is achieved via the pseudoscalar mixing

$$
\begin{pmatrix} \eta' \\ \eta \end{pmatrix} = \begin{pmatrix} \cos\theta & \sin\theta \\ -\sin\theta & \cos\theta \end{pmatrix}\begin{pmatrix} \eta_1 \\ \eta_8 \end{pmatrix} \ .
$$

For the numerical analysis that follows we take $\sin\theta = -1/3 \simeq -20^\circ$.

The other Lagrangians that we employ are the ones corresponding to the $J^{PC} = 0^{++}$ octet and singlet of scalar resonances, from the chiral invariant resonance Lagrangians of Refs. [105, 106]. They were already introduced in Chapter 1, Sec. 1.13, but we include them here for easiness of reference for the following discussions:

$$\begin{aligned} \mathcal{L}_{S_8} &= c_d\langle S_8 u_\mu u^\mu\rangle + c_m\langle S_8\chi_+\rangle \ , \\ \mathcal{L}_{S_1} &= \widetilde{c}_d S_1\langle u_\mu u^\mu\rangle + \widetilde{c}_m S_1\langle\chi_+\rangle \ , \\ \chi_+ &= u^\dagger\chi u^\dagger + u\chi^\dagger u \ . \end{aligned} \tag{3.4}$$

Recall that S_1 denotes a singlet and S_8, whose form is given in Eq. (1.300a), an octet. In the large N_C limit one expects, because of the $U(3)$ symmetry, that the S_1 and S_8 fields would join in the $3\otimes 3$ matrix $S_8 + S_1/\sqrt{3}$, analogously to Eq. (3.1). Then, a relation between the singlet and octet couplings would arise, namely $c_d = \widetilde{c}_d/\sqrt{3}$ and $c_m = \widetilde{c}_m/\sqrt{3}$. In addition, the mass of the S_1 and that of the octet S_8 would be the same [105, 106]. Nevertheless, in the following we do not use these relations. In fact, the previous study in the meson-meson $I = 0$ S-wave [39], the formalism of which we extend here (so that we include more channels, simulating multipion states, and move to higher energies), indicates that this relation between the couplings of singlets and octets can suffer of large deviations. We also point here that similar values to those of c_d and c_m of Ref. [39], were also obtained in Ref. [43, 44] in a detailed study of the I =1/2 and 3/2 meson-meson S-wave up to 2 GeV. In that reference the previously mentioned $U(3)$ relations among the couplings and masses of scalar octets and singlets were used. Notice, however, that the I =1/2 and 3/2 S-waves are not directly sensitive to the scalar singlets, as I =0 S-wave does, but only through to the bulk properties coming from crossed channel exchanges. The same Lagrangians of Eq. (3.4) can be used repeatedly when including more than one octet or singlet of scalar resonances. In this case, as it will occur here, one must distinguish between the couplings and masses of the scalars according to the multiplet that they belong to.

Our two body I =0 states are:

$$|\pi\pi\rangle_0 = -\frac{1}{\sqrt{6}}\Big(|\pi^0(\mathbf{p})\pi^0(-\mathbf{p})\rangle + |\pi^+(\mathbf{p})\pi^-(-\mathbf{p})\rangle + |\pi^-(\mathbf{p})\pi^+(-\mathbf{p})\rangle\Big) \tag{3.5a}$$

$$|\sigma\sigma\rangle_0 = \frac{1}{\sqrt{2}}|\sigma(\mathbf{p})\sigma(-\mathbf{p})\rangle \ , \tag{3.5b}$$

$$|K\overline{K}\rangle_0 = -\frac{1}{\sqrt{2}}\Big(|K^+(\mathbf{p})K^-(-\mathbf{p})\rangle + |K^0(\mathbf{p})\overline{K}^0(-\mathbf{p})\rangle\Big) \ , \tag{3.5c}$$

$$|\eta\eta\rangle_0 = \frac{1}{\sqrt{2}}|\eta(\mathbf{p})\eta(-\mathbf{p})\rangle \ , \tag{3.5d}$$

$$|\eta\eta'\rangle_0 = \frac{1}{\sqrt{2}}|\eta(\mathbf{p})\eta'(-\mathbf{p})\rangle \ , \tag{3.5e}$$

$$|\eta'\eta'\rangle_0 = \frac{1}{\sqrt{2}}|\eta'(\mathbf{p})\eta'(-\mathbf{p})\rangle \ , \tag{3.5f}$$

$$|\rho\rho\rangle_0 = -\frac{1}{\sqrt{6}}\Big(|\rho^0(\mathbf{p})\rho^0(-\mathbf{p})\rangle + |\rho^+(\mathbf{p})\rho^-(-\mathbf{p})\rangle + |\rho^-(\mathbf{p})\rho^+(-\mathbf{p})\rangle\Big) \ , \tag{3.5g}$$

$$|\omega\omega\rangle_0 = \frac{1}{\sqrt{2}}|\omega(\mathbf{p})\omega(-\mathbf{p})\rangle \ , \tag{3.5h}$$

$$|K^*\overline{K^*}\rangle_0 = -\frac{1}{\sqrt{2}}\left(|K^{*+}(\mathbf{p})K^{*-}(-\mathbf{p})\rangle + |K^{*0}(\mathbf{p})\overline{K}^{*0}(-\mathbf{p})\rangle\right) \ , \tag{3.5i}$$

$$|\omega\phi\rangle_0 = |\omega(\mathbf{p})\phi(-\mathbf{p})\rangle \ , \tag{3.5j}$$

$$|\phi\phi\rangle_0 = |\phi(\mathbf{p})\phi(-\mathbf{p})\rangle \ , \tag{3.5k}$$

$$|\pi(1300)\pi\rangle_0 = -\frac{1}{\sqrt{3}}\left(|\pi(1300)^0(\mathbf{p})\pi^0(-\mathbf{p})\rangle + |\pi(1300)^+(\mathbf{p})\pi^-(-\mathbf{p})\rangle + |\pi(1300)^-(\mathbf{p})\pi^+(-\mathbf{p})\rangle\right) \ , \tag{3.5l}$$

$$|a_1\pi\rangle_0 = -\frac{1}{\sqrt{3}}\left(|a_1{}^0(\mathbf{p})\pi^0(-\mathbf{p})\rangle + |a_1{}^+(\mathbf{p})\pi^-(-\mathbf{p})\rangle + |a_1{}^-(\mathbf{p})\pi^+(-\mathbf{p})\rangle\right) \ . \tag{3.5m}$$

Note the extra factors $1/\sqrt{2}$ in the definition of the states $|\pi\pi\rangle_0$, $|\sigma\sigma\rangle_0$, $|\eta\eta\rangle_0$, $|\eta\eta'\rangle_0$, $|\eta'\eta'\rangle_0$, $|\rho\rho\rangle_0$ and $|\omega\omega\rangle_0$. These are symmetry factors introduced because these states are invariant under the exchange $\mathbf{p} \leftrightarrow -\mathbf{p}$. In this way, they can be treated on the same foot as the rest of states, like *e.g.* the $|K\overline{K}\rangle_0$ one. For the I =1/2 states one has:

$$\begin{aligned} |K\pi\rangle_{1/2} &= \frac{1}{\sqrt{3}}\left(|K^+\pi^0\rangle + \sqrt{2}|K^0\pi^+\rangle\right) \ , \\ |K\eta\rangle_{1/2} &= |K^+\eta\rangle \ , \\ |K\eta'\rangle_{1/2} &= |K^+\eta'\rangle \ . \end{aligned} \tag{3.6}$$

3.2.2 Two-vector resonance states

We take the two-vector resonance states $\rho\rho$, $\omega\omega$, $K^*\bar{K}^*$, $\omega\phi$ and $\phi\phi$. We note that the threshold for such states is around 1500 MeV for the $\rho\rho$ and $\omega\omega$, 1800 MeV for the $K^*\bar{K}^*$ and $\omega\phi$ and 2000 MeV for $\phi\phi$. These thresholds coincide with regions where resonance states are expected as shown by experiment [48]. There are also phenomenological studies [243, 244] that indicate that the 4π state is accounted for as $\sigma\sigma$ and $\rho\rho$ two body clusters, however signals as $\pi(1300)\pi$ and $a_1\pi$ are also reported [48]. These latter states are also included here, as explained in Subsec. 3.2.4. Similar studies and other theoretical ones [274] indicate that the $\omega\omega$ contributes very little to this partial wave. We shall see that we agree on that.

In order to include these two-vector resonance states we make use of the Lagrangians in Eqs. (3.2) and (3.4), identifying the external classical gauge fields r_μ and l_μ with the proper combinations of vector and axial-vector fields. In this way the couplings of the vector and axial-vector are obtained through minimal coupling. This is a generalization of the way that vector mesons are introduced in vector meson dominance attending the isospin, hypercharge and baryon number currents [275, 276] (see also [277].) The couplings of the vector and axial-vector are calculated within the Extended Nambu-Jona-Laisinio model in Ref. [278], where these resonances appear, except for a mass term, in the same way as through minimal coupling at the level of the constituent chiral-quark Lagrangian.[2] In this section we are only interested in the vector ones and then we have:

$$r_\mu = g\, v_\mu \ , \ l_\mu = g\, v_\mu \ , \tag{3.7}$$

[2]We thank the late J. Prades for a useful discussion on this issue.

with g a universal proportionality constant and

$$v_\mu = \begin{pmatrix} \frac{\rho^0}{\sqrt{2}} + \frac{1}{\sqrt{6}}\omega_8 + \frac{1}{\sqrt{3}}\omega_1 & \rho^+ & K^{*+} \\ \rho^- & -\frac{\rho^0}{\sqrt{2}} + \frac{1}{\sqrt{6}}\omega_8 + \frac{1}{\sqrt{3}}\omega_1 & K^{*0} \\ K^{*-} & \overline{K}^{*0} & -\frac{2}{\sqrt{6}}\omega_8 + \frac{1}{\sqrt{3}}\omega_1 \end{pmatrix} . \tag{3.8}$$

The coupling g in Eq. (3.7) is determined from the width $\rho \to \pi\pi$, with the result $g = 4.3$. Making use of ideal mixing, one has $\phi = -\sqrt{\frac{2}{3}}\omega_8 + \frac{1}{\sqrt{3}}\omega_1$ and $\omega = \frac{1}{\sqrt{3}}\omega_8 + \sqrt{\frac{2}{3}}\omega_1$. As a result, one can obtain from Eq. (3.8) and the Lagrangians Eq. (3.2) and Eq. (3.4) the different amplitudes involving the two-vector resonances. In this way, the Lagrangians for the transition of two-vector to two and four pseudoscalar are given by:

$$\begin{aligned} \mathcal{L}_{VV\Phi^2} &= g^2\langle v_\mu v^\mu \Phi^2 - v_\mu \Phi v^\mu \Phi\rangle \ , \\ \mathcal{L}_{VV\Phi^4} &= -\frac{g^2}{6f^2}\langle v_\mu v^\mu \Phi^4 - 4 v_\mu \Phi^3 v^\mu \Phi + 3 v_\mu \Phi^2 v^\mu \Phi^2\rangle \ . \end{aligned} \tag{3.9}$$

There is no transition at this order from the Lagrangians in Eq. (3.4) of the scalar resonances to VV. Note that the previous Lagrangians in Eq. (3.9) do not involve derivatives on the pseudoscalar fields, as generally required by chiral symmetry. However, one should take into account that the VV channel is only relevant for energies around and above its threshold (always larger than 1.5 GeV) so that the two pseudoscalars are very energetic and away from the soft chiral limit. In this way, the energy dependence that would be implied by the momenta of the pseudoscalar due to derivatives is soft in the coupling of the VV with PP (P referring to any pseudoscalar) and for practical purposes, Eq. (3.9) is a good approximation. This is certainly not the case at low energies where the pseudo-Goldstone nature of the pseudoscalar implies derivative couplings and this is essential to be kept.

For the projection of the VV system in $I = 0$ with $J = 0$ it is appropriate in our case to work in the basis where the mono-particle state is defined in terms of the three-momentum and the spin in its rest frame. In this way [217, 224], the total momentum $\vec{J}$ of a two-vector resonance state is given by the sum of the orbital angular momentum $\vec{L}$ plus the total spin $\vec{S}$ in the centre of mass frame, like in non-relativistic quantum mechanics. It is a fact of the Lagrangian in Eq. (3.9) that the resulting amplitudes are directly in S-wave. They are proportional to $\epsilon_\mu(\vec{p},\lambda_1)\epsilon^\mu(-\vec{p},\lambda_2)$, with $\vec{p}$ parallel to the z-axis (initial state), and $\epsilon^\mu(\vec{p},\lambda)$ is the polarization vector of V with λ the three component of the spin at rest. The projection in $S = 0$ is straightforward. The only point is to write the polarization vector $\epsilon^\mu(\vec{p},\lambda)$ for $\vec{p} = \pm|\vec{p}|\hat{z}$ in terms of the four-vectors in the rest frame, $\epsilon_3^\mu = (0,0,0,1)$, $\epsilon_+^\mu = -(0,1,i,0)/\sqrt{2}$, $\epsilon_-^\mu = (0,1,-i,0)/\sqrt{2}$, with well defined third component of spin 0, 1 and -1, respectively. The polarization vectors with finite three-momentum $\pm p\hat{z}$ are obtained by performing a boost in the $\mp\hat{z}$ direction, respectively, with velocity $v = p/p^0$ and $p^0 = \sqrt{M_V^2 + \vec{p}^2}$. The resulting vectors are given by $\epsilon_3^\mu(\pm|\vec{p}|\vec{z},0) = (\pm v,0,0,1)/\sqrt{1-v^2}$, $\epsilon_+^\mu(\pm|\vec{p}|\vec{z},+1) = (0,1,-i,0)/\sqrt{2}$, $\epsilon_-^\mu(\pm|\vec{p}|\vec{z},-1) = (0,1,+i,0)/\sqrt{2}$. Thus, the $S = 0$ combination $\sum_{\lambda_1}\langle 1\lambda_1\, 1-\lambda_1|00\,11\rangle\epsilon^\mu(p,\lambda_1)\epsilon_\mu(p,-\lambda_1)$ gives rise to the factor $(3+2|\vec{p}|^2/M_V^2)/\sqrt{3}$. The $I = 0$ projection is straightforward taking into account the isospin states given in Eq. (3.5).

3.2.3 Two-σ states

In this Subsection we discuss the calculation of the elementary amplitudes from the Lagrangians of Eqs. (3.2) and (3.4) involving the $\sigma\sigma$ state. The key point is to realize that, according to the results of UChPT [33,39], the σ resonance is made up from the interactions between two pions in $I=0$ and S-wave. This will allow us to obtain the couplings involving the σ meson without introducing any new free parameters. In order to obtain two-σ resonances, one needs four pions grouped in two $I=0$ S-wave $\pi\pi$ states. Let us denote by s_1 and s_2 the total CM energy squared of every of the two $I=0$ $\pi\pi$ states. The desired transition amplitude is then obtained taking the limit $s_1,\, s_2 \to s_\sigma$, with s_σ the σ pole position in the sheet with the reversed sign for the pion CM three-momentum (second Riemann sheet). This can be straightforwardly generalized to any number of σ mesons, *e.g.*, for the transition amplitude $\sigma\sigma \to \sigma\sigma$ one needs eight pions grouped in 4 sets of $\pi\pi$ in $I=0$ and S-wave. For $\pi\pi \to \sigma\sigma$ six pions are involved grouped in three sets and so on. Then, several s_i (with i running from 1 up to the number of σ's that scatter) are needed, and the limit $s_i \to s_\sigma$ must be finally taken.

For illustration let us show how to proceed for the calculation of $|K\bar{K}\rangle_0 \to (\sigma\sigma)_0$. First, from the Lagrangians of Eqs. (3.2) and (3.4) one calculates the amplitude $|K\bar{K}\rangle_0 \to |\pi\pi\rangle_0|\pi\pi\rangle_0$, which is given by the sum $T^{(2)}_{(K\bar{K})_0\to(\pi\pi)_0(\pi\pi)_0} + T^{(R)}_{(K\bar{K})_0\to(\pi\pi)_0(\pi\pi)_0}$ with:

$$\begin{aligned} T^{(2)}_{(K\bar{K})_0\to(\pi\pi)_0(\pi\pi)_0} &= \frac{\sqrt{2}}{36f^4}\left(5(s_1+s_2)-10m_\pi^2\right)\,, \\ T^{(R)}_{(K\bar{K})_0\to(\pi\pi)_0(\pi\pi)_0} &= \sum_{S_8}\frac{\alpha_{(K\bar{K})_0}\alpha_{(\pi\pi)_0(\pi\pi)_0}}{M_{S_8}^2-s}+\sum_{S_1}\frac{\beta_{(K\bar{K})_0}\beta_{(\pi\pi)_0(\pi\pi)_0}}{M_{S_1}^2-s}\,. \end{aligned} \tag{3.10}$$

The superscript 2 means that the amplitude is calculated at lowest order in ChPT and the superscript R indicates that this amplitude is due to the exchange of explicit scalar resonances. The sums in S_8 and S_1 extend over the octets and singlets of scalar resonances, respectively. The couplings α_i and β_i are given in Appendix A.

Now, every $I=0$ S-wave $\pi\pi$ state, because of its rescattering, gives rise to a σ pole. Note that in Eqs. (3.10) the $I=0$ $\pi\pi$ pairs are already in S-wave and the angular projection is not necessary. This also happens for the rest of transition amplitudes involving the $\sigma\sigma$ state. The rescattering between the pions in a $\pi\pi$ pair is taken into account by multiplying Eqs. (3.10) by $1/D(s_1)D(s_2)$ with

$$D(s) = 1 + t_2\; G(s)\;, \tag{3.11}$$

where $t_2 = (s-m_\pi^2/2)/f_\pi^2$, the $I=0$ S-wave $\pi\pi$ amplitude at lowest in ChPT and $G(s) = (\alpha + \log\frac{m_\pi^2}{\mu^2} - \sigma(s)\log\frac{\sigma(s)-1}{\sigma(s)+1})/(4\pi)^2$, $\sigma = \sqrt{1-4m_\pi^2/s}$ and s is the total CM energy squared. The subtraction constant α is fixed such that $t_2/D(s)$ describes properly the $I=0$ S-wave $\pi\pi$ phase shifts in the elastic region [39], $\alpha \simeq -0.7$ for $\mu = M_\rho$, with $M_\rho = 770$ MeV (the ρ mass.) The value of α depends on that of the renormalization scale μ, being the results independent of the value taken for the latter. We follow Ref. [279] to treat the rescattering between two pions in $I=0$ and S-wave, similarly also as in Refs. [34, 40, 46, 280, 281]. From Ref. [39] a general partial wave in the elastic case can be written as,

$$T = [I + N(s)\cdot G(s)]^{-1}\cdot N(s)\;. \tag{3.12}$$

The interaction kernel N is fixed by matching the previous general expression with the chiral series order by order. For instance at leading order, $N(s) = t_2(s)$. Eq. (3.12) implies that once the two pions in $I = 0$ and S-wave are produced from the primary vertex N, the rescattering between them takes place according to the factor $1/D(s)$ and Eq. (3.12) arises. In the same way here, the dressing of Eq. (3.10) by the $I = 0$ S-wave $\pi\pi$ rescattering in every $I = 0$ S-wave $\pi\pi$ subset implies then

$$T_{(K\bar{K})_0\to(\pi\pi)_0(\pi\pi)_0} = T^{(2+R)}_{(K\bar{K})_0\to(\pi\pi)_0(\pi\pi)_0}\frac{1}{D(s_1)D(s_2)} \ . \tag{3.13}$$

In the previous equation the superscript $2+R$ indicates that $T^{(2+R)}_{(K\bar{K})_0\to(\pi\pi)_0(\pi\pi)_0}$ is given by the sum of $T^{(2)}$ and $T^{(R)}$ in Eq. (3.10)).

The σ pole is contained in each of the factors $1/D(s_i)$ in the unphysical Riemann sheet on which

$$G(s) \equiv G_{II}(s) = \frac{1}{(4\pi)^2}\left\{\alpha + \log\frac{m_\pi^2}{\mu^2} - \sigma(s)\left(\log\frac{\sigma(s)-1}{\sigma(s)+1} + 2i\pi\right)\right\} \ , \ \mathrm{Im}(s) > 0 \ , \tag{3.14}$$

and the complex conjugate of this expression for $\mathrm{Im}(s) < 0$. In the subsequent the subscript II means that the corresponding function is evaluated on the second $\pi\pi$ Riemann sheet. In this way, when taking the limit s_1, $s_2 \to s_\sigma$ in Eq. (3.13) one has,

$$\lim_{s_1,\, s_2\to s_\sigma} T_{(K\bar{K})_0\to(\pi\pi)_0(\pi\pi)_0} = N_{(K\bar{K})_0\to\sigma\sigma}\frac{g^2_{\sigma(\pi\pi)_0}}{(s_1-s_\sigma)(s_2-s_\sigma)} \ , \ i = 1, 2 \ . \tag{3.15}$$

where $g_{\sigma(\pi\pi)_0}$ is the σ coupling to an $I = 0$ S-wave $\pi\pi$ state and $N_{(K\bar{K})_0\to\sigma\sigma}$ is the transition amplitude we are interested in. From this equation we can write,

$$N_{(K\bar{K})_0\to\sigma\sigma} = \lim_{s_1,\, s_2\to s_\sigma}\frac{(s_1-s_\sigma)(s_2-s_\sigma)}{D_{II}(s_1)D_{II}(s_2)g^2_{\sigma(\pi\pi)_0}}T^{(2+R)}_{(K\bar{K})_0\to(\pi\pi)_0(\pi\pi)_0}. \tag{3.16}$$

Note that the limiting factor $\lim_{s_i\to s_\sigma}(s_i - s_\sigma)/(D_{II}(s)g_{\sigma(\pi\pi)_0})$ always appears related with every of the $\pi\pi$ $I = 0$ S-wave pairs and hence is worth calculating it once for ever. This can be easily done by a Laurent expansion of $D_{II}(s)$ around s_σ, as in Ref. [279],

$$\lim_{s_1\to s_\sigma}\frac{s_1-s_\sigma}{g_{\sigma(\pi\pi)_0}D_{\rm II}(s_1)} = \lim_{s_1\to s_\sigma}\frac{1}{g_{\sigma(\pi\pi)_0}t_2(s_1)}\frac{t_2(s_1)}{D_{\rm II}(s_1)}(s_1-s_\sigma) = -\frac{g_{\sigma(\pi\pi)_0}}{t_2(s_\sigma)} \ . \tag{3.17}$$

Above, we made use of the following Laurent series of the full amplitude:

$$\frac{t_2(s_1)}{D_{II}(s_1)} = \frac{t_2(s_1)}{1+t_2(s_1)G_{II}(s_1)} \simeq -\frac{g^2_{\sigma(\pi\pi)_0}}{s_1-s_\sigma} + \text{regular terms} \ . \tag{3.18}$$

Now, the coupling $g^2_{\sigma(\pi\pi)_0}$ can be retrieved from the derivative of the inverse of the elastic amplitude,

$$\frac{1}{g^2_{\sigma(\pi\pi)_0}} = -\frac{d}{ds_1}\left(t_2(s_1)^{-1} + G_{II}(s_1)\right) = \frac{1}{{t_2}^2(s_1)f^2} - \left.\frac{dG_{II}(s_1)}{ds_1}\right|_{s_\sigma} \ , \tag{3.19}$$

so that:

$$\frac{g^2_{\sigma(\pi\pi)_0}}{t_2(s_\sigma)^2} = f^2 \frac{1}{1 - \frac{dG_{II}(s_1)}{ds_1}\Big|_{s_\sigma} t_2{}^2(s_\sigma) f^2} \simeq f_\pi^2 \simeq 9 \times 10^{-3}\ \text{GeV}^2\ . \tag{3.20}$$

This factor f^2 is cancelled by the corresponding ones that appear when calculating multipion tree level amplitudes as each pion field enters together with a $1/f$ factor. For explicit numerical values,[3]

$$\frac{g_{\sigma(\pi\pi)_0}}{t_2(s_\sigma)} = f \frac{1}{\left(1 - \frac{dG_{II}(s_1)}{ds_1}\Big|_{s_\sigma} t_2{}^2(s_\sigma) f^2\right)^{1/2}} = 98 - i\,16\ \text{MeV} \simeq f\ , \tag{3.21}$$

for $s_\sigma^{1/2} = (0.46 - i\,0.24)$ GeV. Note that the previous value is mainly a positive real number. For our computation evaluations we employ finally the value 97.1 MeV, that corresponds to the modulus of $|g_{\sigma(\pi\pi)_0}/t_2(s_\sigma)|$ with the values of Ref. [279]. As a result, from Eqs. (3.16), (3.17) and (3.20), we obtain:

$$N_{(K\bar{K})_0\to(\sigma\sigma)_0} = \frac{1}{\sqrt{2}}\, T^{(2+R)}_{(K\bar{K})\to(\pi\pi)_0(\pi\pi)_0} \left(-\frac{g_{\sigma(\pi\pi)_0}}{t_2(s_\sigma)}\right)^2 \simeq \frac{f^2}{\sqrt{2}}\, T^{(2+R)}_{(K\bar{K})\to(\pi\pi)_0(\pi\pi)_0}\ . \tag{3.22}$$

The factor $1/\sqrt{2}$ included above is a symmetry factor already introduced in the definition of the $I = 0$ $|\sigma\sigma\rangle_0$ state in Eq. (3.5). In calculating the previous expression the variables s_i, in virtue of the limit in Eq. (3.15), are placed at $s_i = s_\sigma$. However, in doing this the elementary amplitude $N_{(K\bar{K})_0\to(\sigma\sigma)_0}$ develops an imaginary part, because s_σ is complex (in Ref. [279] s_σ is given by $s_\sigma = (0.47 - i0.22)^2$ GeV^2.) This is due to the finite width of the σ resonance to two pions. The finite width of a resonance can also be interpreted as giving rise to a mass distribution for the latter. We take this point of view and vary the mass for the σ resonance in $N_{(\sigma\sigma)_0\to\ell}$, as discussed below in Sec. 3.3.

3.2.4 The $\pi(1300)\pi$ channel

We first discuss the evaluation of the elastic transition $\pi(1300)\pi \to \pi(1300)\pi$. We make use of the Weinberg-Tomozawa term for an octet of pseudoscalar resonances (see Sec. 1.13):

$$\mathcal{L}_{kin} = \frac{1}{2}\langle D^\mu \Pi D_\mu \Pi\rangle = \langle \partial^\mu \Pi[\Gamma_\mu, \Pi]\rangle + \dots \tag{3.23}$$

with Π an octet of pseudoscalar resonances including the $\pi(1300)$. The covariant derivative $D_\mu\Pi$ is given by,

$$\begin{aligned} D_\mu \Pi &= \partial_\mu \Pi + [\Gamma_\mu, \Pi]\ , \\ \Gamma_\mu &= \frac{1}{2}\left\{u^\dagger(\partial_\mu - i r_\mu)u + u(\partial_\mu - i l_\mu)u^\dagger\right\}\ . \end{aligned} \tag{3.24}$$

From the Lagrangian in Eq. (3.23) one straightforwardly calculates

$$N_{12,12} = \frac{1}{2sf^2}\left[2s(s - m_\pi^2 - M_{\pi^*}^2) + s^2 - (M_{\pi^*}^2 - m_\pi^2)^2\right]\ , \tag{3.25}$$

[3]Note that the sign given when taking the square root of this quantity is not relevant, since this factor always appears squared, as can be seen in Eq. (3.22) below.

with $M_\pi^* = M_{\pi(1300)} \simeq 1300$ MeV [48].

For the evaluation of the rest of interacting kernels involving one $\pi(1300)\pi$ state, either as final or initial channel, we make use of the interaction Lagrangian from Ref. [105, 106], as presented in Sec. 1.13, involving an octet of pseudoscalar resonances Π,

$$\mathcal{L}_{int} = id_m\langle\Pi\chi_-\rangle = -\frac{d_m}{3\sqrt{8}f^3}\langle\Big(\Phi^3\chi + \chi\Phi^3 + 3\Phi^2\chi\Phi + 3\Phi\chi\Phi^2\Big)\,\Pi\rangle \tag{3.26}$$

with $\chi_- = u^\dagger\chi u^\dagger - u\chi^\dagger u$. From this Lagrangian the transitions $\pi(1300)\pi \leftrightarrow VV'$ are zero, with VV' corresponding to any vector-vector state. The other non-vanishing elementary transition amplitudes involving the $\pi(1300)\pi$ channel are displayed in Appendix A. The coupling constant d_m, when this channel is included, is taken from the literature [105].

3.2.5 The $a_1(1260)\pi$ channel

For the introduction of the axial-vector field $a_1(1260)$, the external fields r_μ and l_μ appearing in the Lagrangian of Eq. (3.2) are identified with λa_μ and $-\lambda a_\mu$, respectively, where λ is a constant and a_μ is an octet of axial-vector resonances with $J^{PC} = 1^{++}$.[4] The constant λ is evaluated from the decay width $a_1^+ \to \gamma\pi^+$ with the value of 640 ± 246 KeV [48]. For this transition one employs Eq. (3.2) keeping one pseudoscalar field and one photon, together with the axial-vector field. The photon enters through the vector field $eA_\mu = r_\mu = l_\mu$ [221]. The resulting Lagrangian is

$$\mathcal{L}(a_1 \to \gamma\pi) = -\sqrt{2}ef_\pi a_1^\mu(1260)^+\pi^- \ , \tag{3.27}$$

and the calculated width is given by

$$\Gamma(a_1 \to \gamma\pi) = \frac{\alpha f_\pi^2\lambda^2}{M_{a_1}^3} \ , \tag{3.28}$$

with $M_{a_1} \simeq 1260$ MeV the mass of the a_1 axial-vector resonance [48]. From this equation one gets $\lambda = 5.8 \pm 1.2$.

Other amplitudes that can be derived from the Lagrangian of Eq. (3.2) involving the $a_1\pi$ state are $a_1\pi \leftrightarrow a_1\pi$ and $a_1\pi \leftrightarrow PQ$, with $P, Q \in \{\pi, K, \eta, \eta'\}$. The appropriate vertices are, respectively,

$$\begin{aligned}
\mathcal{L}_{a_1\pi\to a_\pi\pi} &= \lambda^2\langle a_\mu\Phi a^\mu\Phi - a_\mu a^\mu\Phi^2\rangle \ , \\
\mathcal{L}_{a_1\pi\to PQ} &= \frac{\sqrt{2}\lambda}{3f}\langle a_\mu\Big[\Phi^2\partial^\mu\Phi + \partial^\mu\Phi\,\Phi^2 - 2\Phi\partial^\mu\Phi\,\Phi\Big]\rangle \ .
\end{aligned} \tag{3.29}$$

The transition amplitude $a_1\pi \to \sigma\sigma$ requires the Lagrangian of Eq. (3.2) with 5 pseudoscalar fields,

$$\mathcal{L}_{a_1\pi\to\sigma\sigma} = \frac{\sqrt{2}}{30f^3}\langle a_\mu\Big(4\Phi\partial^\mu\Phi\,\Phi^3 + 4\Phi^3\partial^\mu\Phi\,\Phi - 6\Phi^2\partial^\mu\Phi\,\Phi^2 - \partial^\mu\Phi\,\Phi^4 - \Phi^4\partial^\mu\Phi\Big)\rangle \ . \tag{3.30}$$

[4] The charge conjugation transformation properties of this axial-vector field can be worked out from the requirement that QCD is invariant under this transformation with $a_\mu \propto \bar{q}\gamma^\mu\gamma_5 q$, in standard notation.

By incorporating the axial-vector fields in the Lagrangians involving the scalar resonance multiplets S_8 and S_1, Eqs. (3.4), one can also evaluate the couplings of these resonances with the $a_1\pi$ state. The resulting Lagrangians are:

$$\begin{aligned}\mathcal{L}_{S_8\to a_1\pi} &= -c_d\frac{2\sqrt{2}}{f}\langle a_\mu\partial^\mu\Phi+\partial^\mu\Phi\, a_\mu\rangle\ ,\\ \mathcal{L}_{S_1\to a_1\pi} &= -\widetilde{c}_d\frac{4\sqrt{2}}{f}S_1\langle a_\mu\partial^\mu\Phi\rangle\ .\end{aligned}\tag{3.31}$$

Total angular momentum and parity conservation require the state $a_1\pi$ to be in a P-wave for the relative orbital angular momentum. The appropriate projected state for our porpuses is given by:

$$|a_1\pi;J=0,\ell=1\rangle=\frac{1}{\sqrt{4\pi}}\sum_m\int d\hat{\mathbf{p}}Y_1^m(\hat{\mathbf{p}})(m\sigma 0|110)\,|a_1\pi;\vec{p}\,\sigma\rangle\ ,\tag{3.32}$$

with the notation for the Clebsch-Gordan coefficients $(m_1m_2m_3|j_1j_2j_3)$, for the composition of spins $\mathbf{j}_1+\mathbf{j}_2=\mathbf{j}_3$. In the previous equation σ is the third component of spin of the a_1 resonance in its rest frame.

Since the axial-vector state $|a_1;\mathbf{p}_1,\sigma\rangle$ can be both in the final or initial state we give the general expression for the polarization vector $\epsilon(\mathbf{p}_1,\sigma)$ for arbitrary $\mathbf{p}$ and σ,

$$\epsilon(\mathbf{p},0)=\begin{pmatrix}\gamma p\cos\theta/p^0\\ (\gamma-1)\cos\theta\,\sin\theta\,\cos\phi\\ (\gamma-1)\cos\theta\,\sin\theta\,\sin\phi\\ 1+(\gamma-1)\cos^2\theta\end{pmatrix}\ ,$$

$$\epsilon(\mathbf{p},+1)=\frac{-1}{\sqrt{2}}\begin{pmatrix}\gamma p\sin\theta e^{i\phi}/p^0\\ 1+e^{i\phi}(\gamma-1)\sin^2\theta\,\cos\phi\\ i+e^{i\phi}(\gamma-1)\sin^2\theta\,\sin\phi\\ e^{i\phi}(\gamma-1)\sin\theta\,\cos\theta\end{pmatrix}$$

and $\epsilon(\mathbf{p},-1)=-\epsilon(\mathbf{p},+1)^*$. In the previous equation $p^0=\sqrt{\mathbf{p}^2+M_{a_1}^2}$ and $\gamma=1/\sqrt{1-\mathbf{p}^2/p_0^2}$.

A technical point worth being mentioned is related to the time reversal invariance properties associated with the Lagrangians $\mathcal{L}_{a_1\pi\to PQ}$, $\mathcal{L}_{S_8\to a_1\pi}$ and $\mathcal{L}_{S_1\to a_1\pi}$. The issue is that the amplitudes calculated from these Lagrangians, and also the projected partial waves, contain explicitly a $\pm i$ factor whose sign depends on whether we take the $a_1\pi$ as initial or final state. This i factor originates because the presence of just one derivative acting on the meson fields. A general result is that partial waves are symmetric under this exchange because time reversal invariance. However, the way a state transforms under time reversal is affected by an arbitrary phase and it turns that depending on this phase the partial waves are or are not symmetric under the exchange of the inital $\leftrightarrow$ final states. As we make use later of this symmetry when working out the coupled channel partial wave amplitudes, we have chosen the phase of the $a_1(x)$ field so as the partial wave amplitudes are symmetric under such exchange. For that we

use the fields,

$$\begin{aligned} a_1^0(x) &= +i\int \frac{d^3p}{(2\pi)^2 2p^0}\left[c(\mathbf{p},\sigma)\epsilon(\mathbf{p},\sigma)e^{-ipx} - c^\dagger(\mathbf{p},\sigma)\epsilon(\mathbf{p},\sigma)^* e^{ipx}\right] , \\ a_1^+(x) &= -i\int \frac{d^3p}{(2\pi)^3 2p^0}\left[a(\mathbf{p},\sigma)e(\mathbf{p},\sigma)e^{-ipx} + b^\dagger(\mathbf{p},\sigma)\epsilon(\mathbf{p},\sigma)^* e^{ipx}\right] , \\ a_1^-(x) &= a_1^+(x)^\dagger . \end{aligned} \tag{3.33}$$

Note the multiplying factors $\pm i$ in front and our notation is such that $[a(\mathbf{p},\sigma), a^\dagger(\mathbf{p}',\sigma')] = (2\pi)^3 2p^0 \delta_{\sigma\sigma'}\delta(\mathbf{p}-\mathbf{p}')$. This phase selection also respects the isospin convention followed in the construction of the states in Eq. (3.5). This fixes the $+i$ sign in front of the $a_1^0(x)$ field with respect to the $-i$ in front of the $a_1^+(x)$ field.

Due to the P-wave nature of the relative orbital angular momentum in the $|a_1\pi\rangle$ state each amplitude involving the $a_1\pi$ system is proportional to $|\mathbf{p}|^n$, with $\mathbf{p}$ the three-momentum of the $a_1\pi$ state and $n = 1$ or 2 depending of whether the amplitude under consideration involves one or two $a_1\pi$ states, respectively. This makes that such elementary amplitudes grow as $\left(M_{a_1}^2/\sqrt{s}\right)^n$ for $s \ll M_{a_1}^2$. Notice that such values of s are not physical at all for the $a_1\pi$ state because they are much smaller than the threshold for such channel. In order to avoid such behaviour we multiply the resulting elementary amplitudes by a decreasing function $\exp\left(-|\mathbf{p}|^2/\Lambda^2|\right)$, with $\Lambda \simeq 1$ GeV. The final results depend only marginally on the precise value for Λ. Indeed, as we discuss later, the $a_1\pi$ channel has very small effects on the physical final results.

3.3 Full amplitudes

We use here the general method of Ref. [39], exposed in Sec. 2.7 to obtain unitarized partial waves by resumming the RHC [29, 30, 39, 41, 225]. The key point is the general expression, now in coupled channels,

$$T = [I + N(s)g(s)]^{-1} N(s) , \tag{3.34}$$

where $N(s)$ is a $n \times n$ matrix (with n the number of channels) whose matrix elements are the elementary amplitudes obtained from the previous sections. They can be found in Appendix A. The function $g(s)$ is a diagonal $n \times n$ matrix whose matrix elements correspond to the unitarity bubbles, Fig.3.1. The latter are given by the once subtracted dispersion relation as explained in Sec. 2.7,

$$g_i(s) = g_i(s_0) - \frac{s-s_0}{\pi}\int_{s_{th;i}}^\infty ds' \frac{q_i(s')/(8\pi\sqrt{s'})}{(s'-s_0)(s'-s-i\epsilon)} , \tag{3.35}$$

with s_0 the subtraction point, which is convenient to take on the real axis below threshold ($s_{th;i}$). On the other hand, q_i is the CM three-momentum for channel i. For completeness, we give here the $g_i(s)$ function for the cases of equal and an equal masses of the intermediate particles. If we denote by M_1 and M_2 the masses of the particles 1 and 2 in a channel, the following explicit expressions for $g_i(s)$ result:

$$\begin{aligned} M_1 &= M_2 = M \\ g_i(s) &= \frac{1}{(4\pi)^2}\left(\alpha_i + \log\frac{M^2}{\mu^2} - \sigma(s)\log\frac{\sigma(s)-1}{\sigma(s)+1}\right) , \ \sigma(s) = \sqrt{1-4M^2/s} , \end{aligned} \tag{3.36}$$

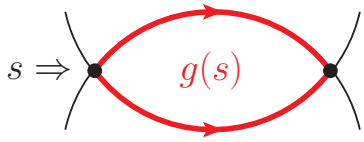

Figure 3.1: The function $g(s)$ as a loop in terms of Feynman diagrams.

$$\begin{aligned} M_1 &\neq M_2 \\ g_i(s) &= \frac{1}{(4\pi)^2}\left(\alpha_i + \log\frac{M_1^2}{\mu^2} + \frac{M_2^2 - M_1^2 + s}{2s}\log\frac{M_2^2}{M_1^2} - \frac{q(s)}{\sqrt{s}}\log\frac{M_1^2 + M_2^2 - s + 2q_i\sqrt{s}}{M_1^2 + M_2^2 - s - 2q_i\sqrt{s}}\right) . \end{aligned}$$

The logarithm is taken such that $\log(-1) = i\pi$ and α_i is the subtraction constant for channel i. Notice that the function $g_i(s)$ for two pions was already used in Subsec. 3.2.3 when the function $1/D(s)$ was introduced.

Equation (3.34) is expanded in powers of Ng (numbers of unitarity loops), in order to fix the matrix $N(s)$,

$$T = N - NgN + \ldots \tag{3.37}$$

This expansion is matched with the elementary amplitudes calculated in Sec. 3.2 from the Lagrangians of Eqs. (3.2) and (3.4) which do not involve loops. As a result N_{ij} is directly identified with the S-wave amplitudes given in Appendix A.

It is interesting to remark here that our unitarization scheme is not equivalent to the Inverse Amplitude Method [29, 30] (IAM). The differences arise because in the IAM one performs an extra chiral expansion of $N^{-1} = N_2^{-1} - N_2^{-1}N_4N_2^{-1} + \ldots$, the subscript indicates the chiral order. This further expansion is here avoided. Notice that this assumption does not always hold even at low energies, as it is the case close to the Adler zeroes. In this case, N_2 vanishes around the Adler zero and hence $|N_4|$ is not longer smaller than $|N_2|$. However, in our approach we do not assume that $|N_4(s)| \ll |N_2(s)|$ for all values of s at low energies but only at the level of the chiral expansion, similarly as in ChPT.[5] We perform the previous expansion at low energies, in order to match with the resonance ChPT results. The problem of the IAM in conjunction with the Adler zeroes was discussed in detail in Refs. [282, 283].

In applying Eq. (3.34) to the $I = 0$ S-wave one has to face the problem of the mass distribution of the σ resonance because of its large width. Let us take first the Lehmann representation for a propagator $P(s)$:

$$P(s) = \frac{-1}{\pi}\int_{s_{th}}^{+\infty} ds' \frac{\mathrm{Im}P(s')}{s - s' + i\epsilon} . \tag{3.38}$$

The so called spectral function $\mathrm{Im}P(s)$ is *a priori* unknown but as a first approach we take it to be:

$$\mathrm{Im}P(s') = \mathrm{Im}\left\{\frac{1}{s' - m_\sigma^2 + im_\sigma\Gamma_\sigma(s')}\right\} , \tag{3.39}$$

with $\Gamma_\sigma(s') = \Gamma_\sigma\ (1 - 4m_\pi^2/s')^{1/2}/(1 - 4m_\pi^2/m_\sigma^2)^{1/2}$, since the width must tend to zero as the phase space of the two pions. On the other hand, m_σ and Γ_σ are, respectively, the real and

[5] For example, it could occur that $N_2(s) = 0$ but not $N_4(s)$. The point is that the latter must be sufficiently small to be qualified as $\mathcal{O}(p^4)$.

minus twice the imaginary part of $s_\sigma^{1/2}$. The latter was given above, although one can also take m_σ and Γ_σ from other references. We furthermore normalize Eq. (3.39) so as to always have

$$\int_{s_{th}}^{+\infty} ds' \, \mathrm{Im}P(s') = 1 \ . \tag{3.40}$$

Eq. (3.38) is specially suited for our purposes as it gives the propagator for the σ resonance as a superposition in s' of a standard one with mass square equal to s'. In this way, from Eq. (3.36), we can express the $g(s)_4$ function as,

$$g(s)_4 = \int_{s_{th}}^{+\infty} ds_1' \int_{s_{th}}^{+\infty} ds_2' \, \mathrm{Im}P(s_1')\mathrm{Im}P(s_2') g(s; s_1', s_2')_4 \ , \tag{3.41}$$

where s_1' and s_2' as arguments in $g(s; s_1', s_2')_4$ refer to the squared masses M_1^2 and M_2^2 with which this function is evaluated according to Eq. (3.36). That is, the channel $\sigma\sigma$ can be considered as a continuum set of channels with different masses squared s_1' and s_2', and a mass distribution governed by $\mathrm{Im}P(s_1')\mathrm{Im}P(s_2')$.

Because of this continuum of channels embedded in $\sigma\sigma$, Eq. (3.34) is indeed an integral equation. In order to solve it we discretize the mass distribution so that it is transformed in an algebraic one that can be easily solved. We check then that for a sufficiently large number of partitions the results are stable if further increased this number. In this way, the $g(s)$ matrix has diagonal matrix elements,

$$g(s)_i \ , \ i \neq 4 \ , \tag{3.42}$$

$$g(s; s_1', s_2')_4 \, \mathrm{Im}P(s_1')\mathrm{Im}P(s_2')\Delta_1\Delta_2 \ , \tag{3.43}$$

Here, Δ_1 and Δ_2 are the steps in s_1' and s_2', respectively, that result from the discretization, and s_1' and s_2' must be identified with M_1^2 and M_2^2 in Eq. (3.36). Similarly, the interaction kernels $N_{4,i} = N_{i,4}$ depend on s_1' and s_2' and $N_{4,4}$ as well on s_3' and s_4', see Appendix A. These variables run when multiplying $N(s)$ with $g(s)$. There is here a technicality due to the fact that these interaction kernels increase power with s_i' (at most quadratically) and this causes troubles in the convergence of the sum over s_i'. As a result we shall fix s_i' in $N_{4,i} = N_{i,4}$ and $N_{4,4}$ to a given value. We have then checked that the results do not depend on this precise value as long as the mass taken satisfies $\sqrt{s_i'} \lesssim 500$ MeV. This also implies that Eq. (3.34) becomes finally an algebraic one with $g(s)_4$ calculated as in Eq. (3.41) whithout folding with the kernels N_{4i} because now they are calculated with fixed values for the s_i'.

3.4 Results

3.4.1 Experimental data

In order to fix our free parameters we then fit a large amount of scattering data from the $\pi\pi$ threshold up to $\sqrt{s} \lesssim 2$ GeV. Above this energy further channels are expected to be relevant, *e.g.* $f_0(980)f_0(980)$, $a_0(980)a_0(980)$, etc, so that this extension to higher energies is left as future work. We now list the different data used:

- $I = 0$ S-wave $\pi\pi$ elastic phase shifts, $\delta_0^0(s)$. The low energy data come from K_{e4} decays [284, 285] which are very precise but only span energies below the kaon mass.

For $0.45 \leqslant \sqrt{s} \leqslant 0.63$ GeV. we take the data considered in Ref. [39], which is an average between data of Refs. [286–290]. Above 0.63 GeV, the data taken are from Ref. [290] alone since its analysis takes additionally into account the polarization of the proton target. In Ref. [291] it was found that only the the so called "down-flat" solution of Ref. [290] should be considered, while the "up-flat" solution can be rejected because it is not compatible with $\pi\pi$ Roy equations. The upper energy limit of these data is $\sqrt{s} \leqslant 1.6$ GeV. Ref. [286] gives data up to higher energies, but we do not agree with the steady increase of the data for energies above 1.4 GeV and this is why they have not been included in the fit. Instead, our results generate a rapid upwards motion at around $1.4 - 1.5$ GeV, similarly as in Ref. [290]. This behaviour was already found Ref. [274], which can be considered as an indication of the scalar resonances $f_0(1370)$ and $f_0(1500)$. These data and our results are shown in the upper part of Fig. 3.2.

- $I = 0$ S-wave elastic parameter $\eta = |S_{11}|$. We employ the data of Refs. [289] and [290]. Given the large errors, both data sets are compatible. These data, as well as our results, are shown in the bottom part of Fig. 3.2.

- $I = 0$ S-wave $\pi\pi \to K\bar{K}$ phase shifts. Here we consider the data from Refs. [292, 293]. Ref. [292] provides data up to $\sqrt{s} \simeq 2.4$ GeV while Ref. [293] up to $\sqrt{s} \simeq 1.6$ GeV. As shown in Fig. 3.3 the errors for the latter data are rather small and give a higher value for the phase of the peak at ~ 1.5 GeV.

- $I = 0$ S-wave $\pi\pi \to K\bar{K}$ $|S_{12}|$, the data are from the sames references as the previous data, Refs. [292, 293]. The data of Etkin *et al.* [292] are not normalized so that a global constant is allowed to float when fitting them. The central value of this constant given by our fits has been used to plot these data in Fig. 3.3.

- $I = 0$ S-wave $\pi\pi \to \eta\eta$ $|S_{13}|^2$. The data are not normalized and correspond to the S-wave contribution separated out in Ref. [294]. A normalization constant is then included as a free parameter.

- $I = 0$ S-wave $\pi\pi \to \eta\eta'$ $|S_{15}|^2$. The data are from Ref. [295] and as in the $\pi\pi \to \eta\eta$ case they are not normalized, so that a normalization constant is also included. The data for $\eta\eta$ and $\eta\eta'$ data are shown in Fig. 3.4.

- $K^-\pi^+$ scattering from Ref. [296], both the modulus of the amplitude, A_0, and the phase, ϕ_0, are given and fitted. This scattering can be written in terms of the $I = 1/2$ and $3/2$ amplitudes as in Ref. [43, 44]. In Fig. 3.5 we show the solution[6] A of Ref. [296]. In Ref. [43,44] it was shown that the solutions B and D of Ref. [296] are not physical because they violate unitarity. The solutions A and C are indeed very similar for $\sqrt{s} \geqslant 1.85$ GeV, and this is why only the solution A of Ref. [296] is shown. We also recall that for these data we are using the same approach as in Ref. [43, 44], but now we simultaneously fit the $I = 0$ S-wave previous data.

- We also fit the values of Ref. [297] $a_0^0 = 0.220 \pm 0.005$ and $M_\pi^2 b_0^0 = 0.276 \pm 0.006$ for the threshold parameters (see Chapter 5, Eq. (5.9) for their definition and a more accurate determination and a discussion of these parameters.) Our results for these parameters are $a_0^0 = 0.216$ and $M_\pi^2 b_0^0 = 0.277$, in good agreement with the cited values.

[6] There is a four-fold ambiguity for energies above 1.85 GeV in Ref. [296].

	M (MeV)	c_d or $\tilde{c}_d$ (MeV)	c_m or $\tilde{c}_m$ (MeV)
$S_8^{(1)}$	$\mathbf{1290 \pm 5}$	$\mathbf{25.8 \pm 0.5}$	$\mathbf{25.8 \pm 1.1}$
$S_8^{(2)}$	$\mathbf{1905 \pm 13}$	20.3 ± 1.4	-13.9 ± 2.0
$S_1^{(1)}$	894 ± 13	14.4 ± 0.3	46.6 ± 1.1

Table 3.1: Parameters of the bare resonances included. We show in boldface the parameters that have been fixed to previous works, as explained in the text.

3.4.2 Free parameters

We have performed two type of fits, with and without including the $\pi(1300)\pi$ and $a_1(1260)\pi$ channels. As commented in Sec. 3.1, the contribution to the observables of these channels is found to be marginal, so we show our fit results without them.

Apart from normalization constants of the data (which cannot be considered as free parameters of our approach), we have the free parameters of the bare resonances and the subtraction constants of the loop functions. The former are shown in Table 3.1. With our fits, we deduce that two octets and one singlet of scalar resonances are needed. The mass and couplings of the first octet are fixed to the values of Refs. [43, 44], as well as the mass of the second octet. The mass of the singlet is difficult to fix, because of its correlation to the couplings, that is, similar results can be obtained with lower values of the mass altogether with higher values of the couplings, specially for the coupling $\tilde{c}_m$.

Regarding the subtraction constants, since the $SU(3)$ breaking is softer in the vector sector, and in order to reduce further the number of free parameters, we take one common subtraction constant for every VV channel (recall that these comprise $\rho\rho$, $K^*\bar{K}^*$, $\omega\omega$, $\omega\phi$ and $\phi\phi$). Once fixed, if we let them free, small variations are found. The subtraction constants are found to be natural sized, which indicates that we are not generating poles in artificial ways. The values of the subtraction constants are as follows: $a_{\pi\pi} = -1.36 \pm 0.05$, $a_{K\bar{K}} = -0.47 \pm 0.04$, $a_{\eta\eta} = -0.96 \pm 0.06$, $a_{\sigma\sigma} = 1.54 \pm 0.08$, $a_{\eta\eta'} = 0.86 \pm 0.09$, $a_{\rho\rho} = -2.31 \pm 0.04$ and $a_{\eta'\eta'} = 6.0 \pm 0.3$.

In total, we have 12 free parameters (15, when including $a_1\pi$ and $\pi(1300)\pi$ channels), for about 370 data points, for different observables, which come from different and independent experiments, so that we perform a global description of the experimental results, which allows in turn a global description of the spectroscopy. We want to stress that we employ standard chiral Lagrangians to calculate the interaction kernels avoiding *ad hoc* parameterizations as in other studies, which do not incorporate so many coupled channels as we do, see *e.g.* [248, 249, 274]. Refs. [248, 249] employ around 40 parameters, a number larger than we do here. Refs. [245–247, 274] use also 13-14 free parameters (as we do) but only consider 3 coupled channels at most.

3.4.3 Results for the observables

All the experimental data can be deduced from the S-matrix. With our normalization, its matrix elements are given by:

$$S_{i,j} = \delta_{ij} + 2i\sqrt{\rho_i}\, T^{(I)}_{i,j} \sqrt{\rho_j} \ , \tag{3.44}$$

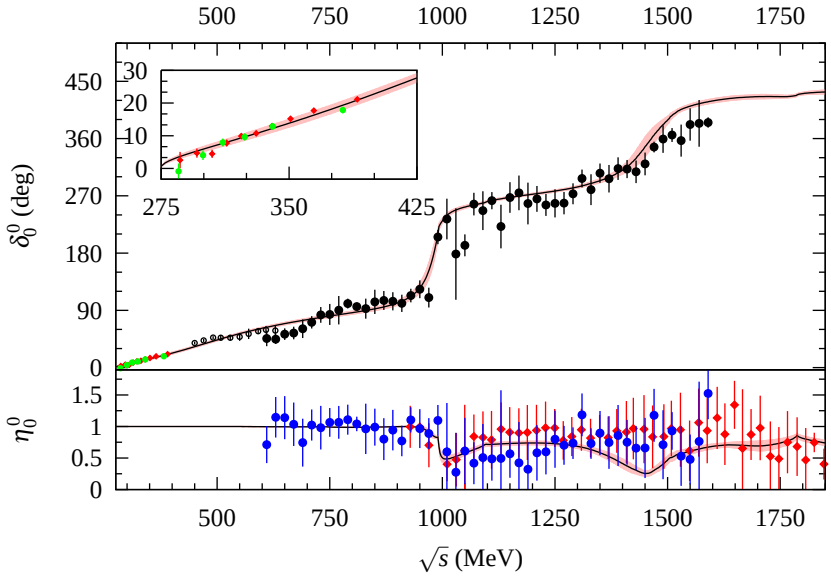

Figure 3.2: Fit to $\pi\pi \to \pi\pi$ experimental data. In the upper panel, we show the phase shift. In the region 0.45 GeV $\leqslant \sqrt{s} \leqslant$ 0.63 GeV, they are the average employed in Ref. [39], and for $\sqrt{s} \geqslant 0.63$ GeV, they are taken directly from Ref. [290]. The data of the low energy region, $\sqrt{s} \leqslant 0.45$ GeV, enlarged in the inset, are from Refs. [284, 285]. In the bottom panel, we show the elasticity parameter η_0^0. Blue circles are from Ref. [290] and green diamonds, from Ref. [289].

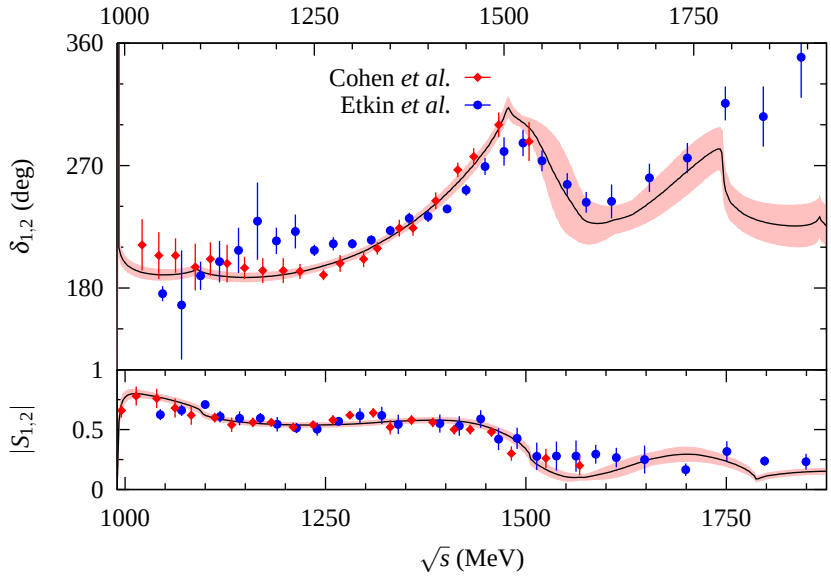

Figure 3.3: Fit to $\pi\pi \to K\bar{K}$ experimental data. Blue circles are from Ref. [292] and red diamonds from Ref. [293].

where $\rho_i(s) = q_i(s)/8\pi\sqrt{s}$ and $q_i(s)$ is the CM three-momentum for channel i.

Our results for the observables are shown throughout Figs. 3.2–3.5. The width of the band around the curves takes into account two standard deviations from the χ^2 resulting from the central fit, denoted by χ_1^2. Monte-Carlo samples for the values of the free parameters (including those that have been fixed), have been generated allowing a large variation in the values of the parameters derived from the central fit. For each sample a χ^2 is calculated and

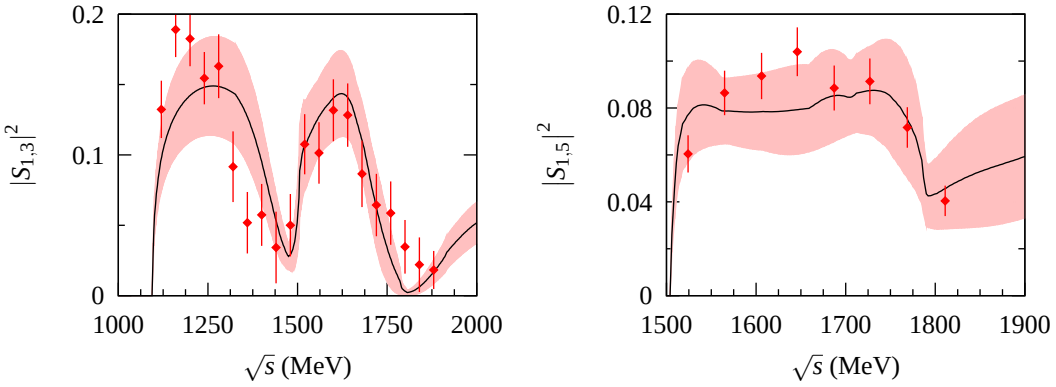

Figure 3.4: Fit to $\pi\pi \to \eta\eta$ (left) [294] and $\eta\eta'$ (right) [295] experimental data.

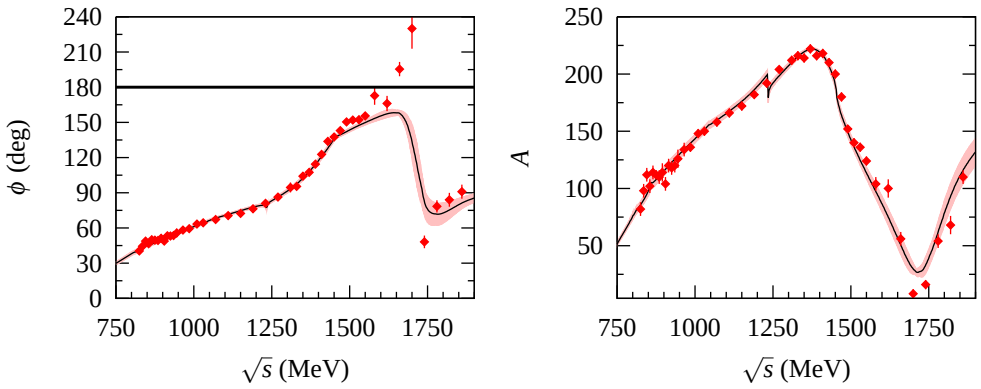

Figure 3.5: Fit to $K^-\pi^+$ experimental data from Ref. [296], both phase (left) and amplitude (right).

only those χ^2 that satisfy

$$n_\sigma \geqslant \Delta\chi^2/(2\chi_1^2)^{1/2} \ , \tag{3.45}$$

are kept. Here n_σ is the number of standard deviations, that we take equal to two. This equation is derived from simple statistical considerations in appendix A of Ref. [292]. We find a good overall agreement with data.

Regarding the $\pi\pi \to \pi\pi$ scattering data, we want to stress that we are able to accurately reproduce the precise data from K_{e4} decays without destroying the agreement with higher energies, as can be seen in Fig. 3.2. One observes a rapid increase of the phases around $1.4 - 1.6$ GeV in contrast with the steady increase of Ref. [286]. This increase is related with the marked peak in the $\pi\pi \to K\bar{K}$ phase shifts at $\sqrt{s} \simeq 1.5$ GeV, which is also connected with the appeareance in our amplitudes of the $f_0(1370)$ and $f_0(1500)$ resonances.

For the $\pi\pi \to K\bar{K}$ $I = 0$ S-wave phase shifts, shown in the upper panel of Fig. 3.3, our curve follows better the data from Ref. [293]. These data show an even more marked peak in the 1.5 GeV region than the [292] ones, as found in our results. Our curve also reproduces closely $|S_{1,2}|$, as shown in the bottom panel of Fig. 3.3. It is also interesting to observe the good agrement with the $\pi\pi \to \eta\eta$ and $\eta\eta'$ shown in the two panels of Fig. 3.4, even if they contribute with a necessarily low weight in χ^2 (this makes the error band much wider than in other observables.)

PDG			This work		
Resonance	M (MeV)	Γ (MeV)	$I=0$ Poles (MeV)	M (MeV)	Γ (MeV)
$\sigma \equiv f_0(500)$			$456 \pm 6 - i\ 241 \pm 7$		
$f_0(980)$	980 ± 10	$40 - 100$	$983 \pm 4 - i\ 25 \pm 4$	983 ± 4	50 ± 8
$f_0(1370)$	$1200 - 1500$	$200 - 500$	$f_0^L\ 1466 \pm 15 - i\ 158 \pm 12$	1370 ± 30	316 ± 24
$f_0(1500)$	1505 ± 6	109 ± 7	$f_0^R\ 1602 \pm 15 - i\ 44 \pm 15$	1502 ± 15	105 ± 30
$f_0(1710)$	1724 ± 7	137 ± 8	$1690 \pm 20 - i\ 110 \pm 20$	1700 ± 20	160 ± 40
$f_0(1790)$	1790^{+40}_{-30}	270^{+30}_{-60}	$1810 \pm 15 - i\ 190 \pm 20$	1810 ± 30	380 ± 40

PDG			This work
Resonance	M (MeV)	Γ (MeV)	$I=1/2$ Poles (MeV)
$\kappa \equiv K_0^*(800)$	–	–	$708 \pm 6 - i\ 313 \pm 10$
$K_0^*(1430)$	1414 ± 6	290 ± 21	$1435 \pm 6 - i\ 142 \pm 8$
$K_0^*(1950)$	–	–	$1750 \pm 20 - i\ 150 \pm 20$

Table 3.2: Pole content of our amplitudes, as compared with the PDG. Top: $I=0$ poles. Bottom: $I=1/2$ poles.

Regarding the $K^-\pi^+$ data, we also observe for the phase $\phi_0(s)$ that our curve lies below the rapid increase at 1.7 GeV. We recall here the discussion on this issue in Refs. [43,44], where it was shown that unitarity requires that $\phi_0 < 180^o$. Once those points with $\phi_0(s) > 180^o$ are eliminated, the agreement is good.

3.5 Spectroscopy

Let us now focus on the spectroscopy that we can obtain from our amplitudes. We find poles corresponding to the σ, $f_0(980)$, $f_0(1370)$, $f_0(1500)$, $f_0(1710)$ and $f_0(1790)$ for $I=0$ and for $I=1/2$ we have the poles of the κ, $K_0^*(1430)$ and $K_0^*(1950)$. The pole positions are collected in Table 3.2. However, the resonance spectrum cannot be understood by just quoting the pole positions, and some further explanations will be given in this Section.

The poles appear in different Riemann-sheets of the many 2^n Riemann sheets existing for an n coupled channel problem. Here $n=11$ or 13 depending of whether the $a_1(1260)\pi$ and $\pi(1300)\pi$ states are included or not, respectively. Along the real $s-$axis on the physical sheet, there is always a non-physical Riemann sheet that matches with the physical one. Then one has to study the poles in this non-physical Riemann sheet as they contribute to the behaviour of the physical amplitudes between the opening of the previous and next Riemann sheets. Each different sheet is characterized by the sign in front of the definition of the three-momentum of chanenl i,

$$q_i = \frac{\sqrt{(s-(M_1+M_2)^2)(s-(M_1-M_2)^2)}}{2\sqrt{s}}\ , \tag{3.46}$$

with M_1 and M_2 the masses of the two particles composing the channel i. In this way either

$f_0(1370)$ $(I=0)$			$K_0^*(1430)$ $(I=1/2)$		
Coupling	bare	final	Coupling	bare	final
$g_{\pi^+\pi^-}$	3.9	3.59 ± 0.16	$g_{K\pi}$	5.0	4.8
$g_{K^0\bar{K}^0}$	2.3	2.23 ± 0.18	$g_{K\eta}$	0.7	0.9
$g_{\eta\eta}$	1.4	1.70 ± 0.30	$g_{K\eta'}$	3.4	3.8
$g_{\eta\eta'}$	3.7	4.00 ± 0.30			
$g_{\eta'\eta'}$	3.8	3.70 ± 0.40			

Table 3.3: The couplings (in GeV) of the $f_0(1370)$ and $K_0^*(1430)$ resonances to different channels, and the couplings of the bare octet, $S_8^{(1)}$. Their similarities show that the former are mainly an octet, not mixed with nearby resonances.

$\mathrm{Im}(q_i) \geqslant 0$ or $\mathrm{Im}(q_i) \leqslant 0$. The physical sheet is that with the positive sign for all the channels. For a given value of s along the real axis the non-physical Riemmann connected continuously with the physical one is that sheet with $\mathrm{Im}(q_i) \leqslant 0$ for all the channels i whose threshold, $s_{th,i}$, is $s_{th,i} \leqslant s$. For $\sigma\sigma$, $\rho\rho$, $a_1\pi$ and $\pi(1300)\pi$ states, whose composite particles are one or both resonances with a significant width and have a non definite threshold, the sign of q_i is changed for those values of $\sqrt{s_1'} + \sqrt{s_2'} < \mathrm{Re}\sqrt{s}$, see Eq. (3.41) for the meaning of s_1' and s_2'. In this way the continuous extrapolation to the physical sheet is guaranteed.

Our description of the scalar isoscalar resonances below 1 GeV, the σ and the $f_0(980)$ for $I = 0$ and the κ for $I = 1/2$, is in good agreement with previous works on the subject (see references in Sec. 3.1), so we may focus on the more complicated region 1 GeV $\leqslant \sqrt{s} \leqslant 2$ GeV. Four resonances with $I = 0$ are found there: $f_0(1370)$, $f_0(1500)$, $f_0(1710)$ and $f_0(1790)$, that we discuss in the following. After the description of these resonances, we discuss altogether those in the $I = 1/2$ sector.

3.5.1 $f_0(1370)$

A pole is found at $\sqrt{s} = 1466 \pm 15 - i(158 \pm 12)$ MeV, which we denote by f_0^L. This pole can be seen in Fig. 3.6 in the $\sigma\sigma \to \sigma\sigma$ amplitude. Though the mass deduced from the pole is found to be closer to 1.5 GeV, in most of the amplitudes the peak is located at 1.37 GeV, which is closer to its nominal mass. However, the value favored by the high statistics study of the Belle Collaboration on $\gamma\gamma \to \pi^0\pi^0$ is 1.47 GeV, close to the mass deduced from the pole. It should be noted that the PDG value has a large uncertainty, $M = 1200 - 1500$ MeV. Regarding its width, we deduce $\Gamma = 316 \pm 24$ MeV, also inside the PDG values, $\Gamma = 200 - 500$ MeV. It is found to have a large width to $\pi\pi$, $\Gamma(4\pi)/\Gamma(2\pi) = 0.30 \pm 0.12$, in agreement with the interval $0.10 - 0.25$ of Ref. [68]. In Table 3.3, we show the couplings of the $f_0(1370)$ and compare them with those of the bare octet we have introduced, $S_8^{(1)}$ (recall that it has $M_8^{(1)} = 1.29$ GeV, and $c_d^{(1)} = c_m^{(1)} = 26$ MeV), showing that they are indeed very similar. The same can be said of the $K_0^*(1430)$ in the $I = \frac{1}{2}$ channel. From the similarities of the couplings of these poles with respect to the bare ones we deduce that the first scalar octet is a pure one, not mixed with the nearby resonances.

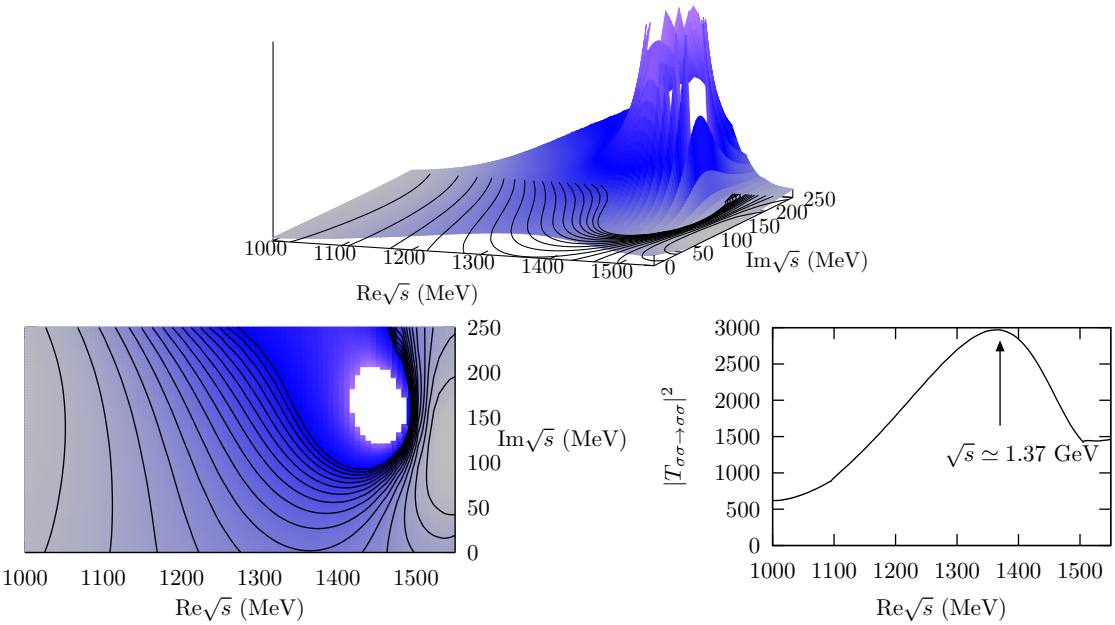

Figure 3.6: We show the $f_0^L \sim f_0(1370)$ pole effects in the $\sigma\sigma$ elastic amplitude. In the upper plot, it is shown the pole in the complex s plane (actually, we use $\sqrt{s}$). In the bottom left, a contour plot of the previous one is shown, where it can be well appreciated that the gradient of the amplitude is not parallel to the imaginary axis, giving rise to a shift in the peak of the amplitude, as can be seen in the bottom right picture. The amplitude is finally peaked at 1.37 GeV.

3.5.2 $f_0(1500)$

We find a pole located at $1602 \pm 15 - i(44 \pm 15)$ MeV, denoted by f_0^R, lying on the Riemann sheet that connects with the physical one up to the $\eta\eta'$ threshold, $\sqrt{s} \simeq 1.5$ GeV. Thus, it is located 100 MeV above the maximum energy at which the two Riemann sheets are connected, but, however, its influence on the physical amplitudes is large, as can be seen in Fig. 3.7. The mass peak of the $f_0(1500)$ is thus at 1.5 GeV due to the $\eta\eta'$ threshold. This is a similar effect to the one relating $a_0(980)$ and $K\bar{K}$ threshold, see Ref. [39]. In addition, we have the nearby f_0^L pole. The width is $\Gamma = 1.2 \times 88$ MeV $= 105 \pm 36$ MeV, because a Breit-Wigner at $\sqrt{s} = 1.6 - i0.04$ GeV is cut by $\eta\eta'$ threshold. Summarizing, this is a complicated energy region, where no simple approaches nor analysis without proper coupled channels mechanisms should be employed. We have found three interfering effects giving raise to $f_0(1500)$, namely (i) the f_0^R pole at $\sqrt{s} = 1.6 - i0.04$ GeV; (ii) the $f_0^L \sim f_0(1370)$ pole, at $1.47 - i0.16$ GeV; and (iii) the nearby thresholds $\eta\eta'$ and $\omega\omega$.

3.5.3 $f_0(1710)$

This resonance is given by a pole located at $\sqrt{s} = 1690 \pm 20 - i110 \pm 20$ MeV on a Riemann sheet continuosly connected with the physical one at the real s axis. In Fig. 3.8 this pole is shown in the $\eta'\eta'$ elastic amplitude. It can be seen there that the mass peak is slightly shifted to $\sqrt{s} \simeq 1.7$ GeV. The effective width on this amplitude is $\Gamma = 160$ MeV, closer to the value quoted by the PDG, $\Gamma = 137 \pm 8$ MeV, than that deduced directly from the imaginary part of the pole position, that would be $\Gamma = 220 \pm 40$ MeV (yet not far to the PDG value.) However,

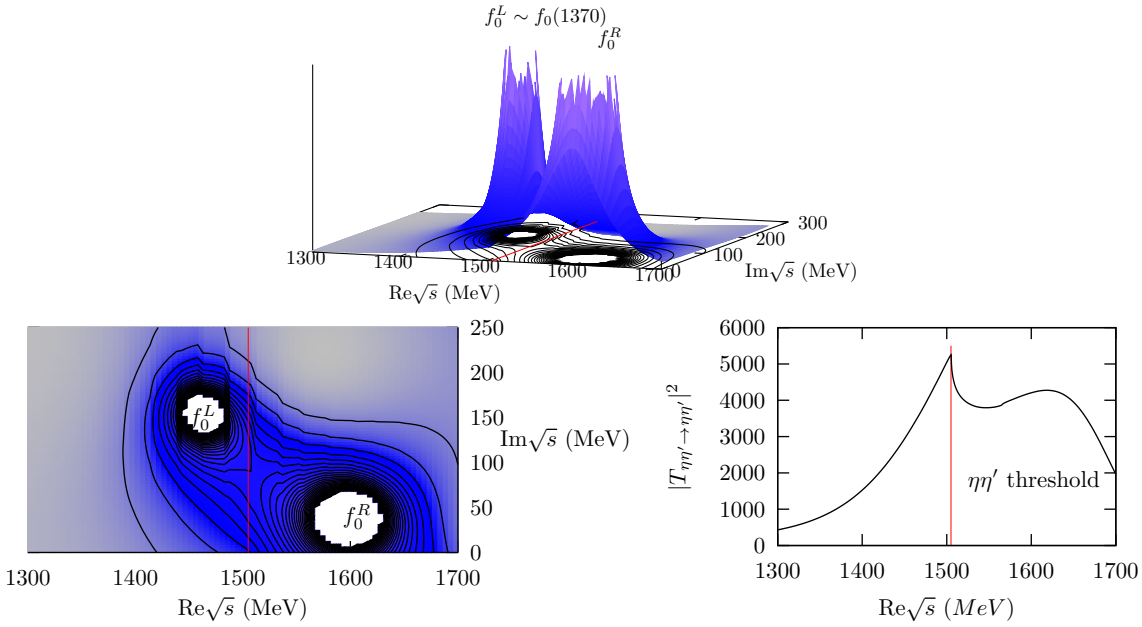

Figure 3.7: We show the three interfering effects giving rise to the $f_0(1500)$ resonance. The main one is the f_0^R pole. The $f_0^L \sim f_0(1370)$ also contributes. The $\eta\eta'$ threshold is also shown with a red line.

the effective width can depend on the process. In Table 3.4 we show some of the branching ratios calculated from the residues and compare them with the PDG values, finding a very good agreement.

An striking feature we find in our approach is that the $f_0(1500)$ and $f_0(1710)$ resonances are tightly connected. The $f_0(1500)$ originates mainly from the f_0^R pole, but, if we continuosly change from the Riemman sheet in which it is located to the one where the $f_0(1710)$ pole is located, we see that the former continuosly moves to the latter. They are the same underlying pole reflected in different Riemann sheets, and the origin of this pole is not the higher octet we have introduced. However, the final pole position of f_0^R and $f_0(1710)$ and the effects they produce are different enough to consider them as different resonances. The identification of the $f_0(1710)$ resonance as mainly the lightest scalar glueball is treated in Sec. 3.7.

BR	This work	PDG
$\frac{\Gamma(K\bar{K})}{\Gamma_{\text{total}}}$	0.36 ± 0.12	$0.38^{+0.09}_{-0.19}$
$\frac{\Gamma(\eta\eta)}{\Gamma_{\text{total}}}$	0.22 ± 0.12	$0.18^{+0.03}_{-0.13}$
$\frac{\Gamma(\pi\pi)}{\Gamma(K\bar{K})}$	0.32 ± 0.14	$0.41^{+0.11}_{-0.17}$
$\frac{\Gamma(\eta\eta)}{\Gamma(K\bar{K})}$	0.64 ± 0.38	0.48 ± 0.15

Table 3.4: Branching ratios of the $f_0(1710)$

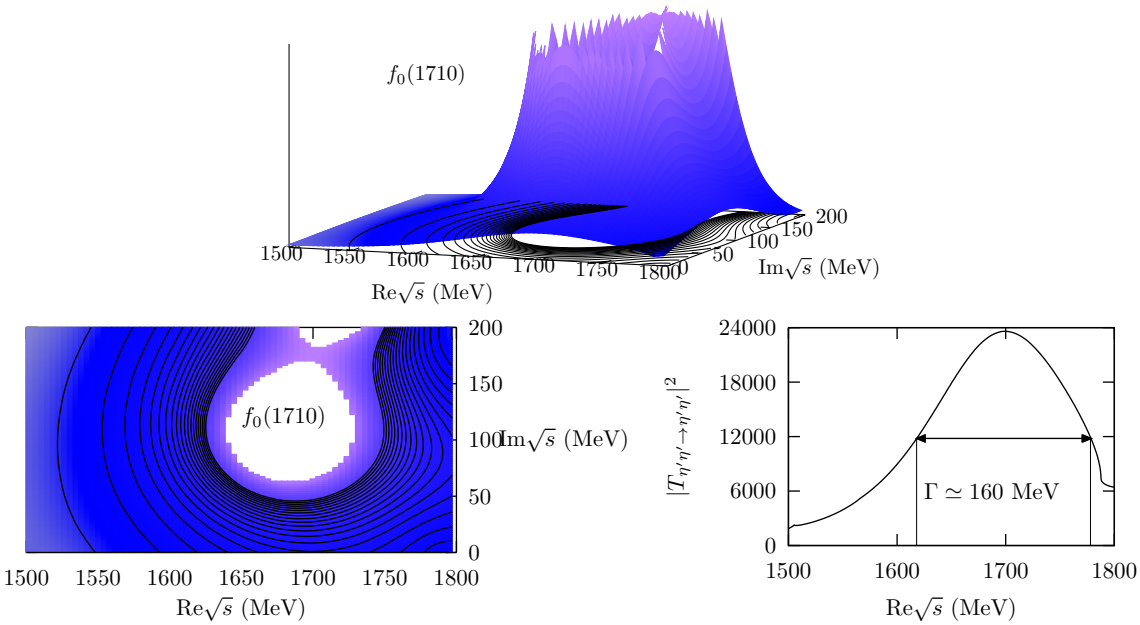

Figure 3.8: The $f_0(1710)$ pole in the $\eta'\eta' \to \eta'\eta'$ amplitude is shown. In the picture of the pole in the complex plane, the shift of the mass peak towards higher energies is shown. Over the real axis, the resonance appears narrower than what can be expected from the pole position.

3.5.4 $f_0(1790)$

It originates from a pole located at $\sqrt{s} = 1810 - i(190 \pm 20)$ MeV, but shows weak signals on the real axis. It couples weakly to $K\bar{K}$, a major difference with respect to $f_0(1710)$, as also observed by BESII. It is the partner of the pole at $\sqrt{s} = 1.75 - i0.15$ GeV in $I = 1/2$, and they originate from the dressing of the higher bare octet we have introduced, $S_8^{(2)}$, with $M = 1.9$ GeV and couplings given by $c_d = 20$ MeV and $c_m = -14$ MeV.

3.5.5 $I = 1/2$

Concerning the $I = 1/2$ S-wave amplitudes we obtain the same resonances as in Refs. [43,44] with pole positions for the κ, $K_0^*(1430)$ and $K_0^*(1950)$ given in Table 3.2. We recall here the discussion in Subsec. 3.5.1 leading to deduce that $f_0(1370)$ and $K_0^*(1430)$ are pure octets. Note that now all these resonances in $I = 1/2$ have been obtained consistently witht the spectroscopy content of the $I = 0$ S-wave.

3.6 WA102 and CBC data

In order to find further support to our approach and, specially, to our spectroscopy, we fit the data from the WA102 Collaboration on $pp \to pp\pi^+\pi^-$, K^+K^- [298] and $\eta\eta$ at 450 GeV/c [299] and those of the Crystal Barrel Collaboration (CBC) on $p\bar{p} \to \pi^0\eta\eta$ [300] and $p\bar{p} \to \pi^0\eta\eta'$ [301]. These data are also very convenient theoretically as the two mesons produced interact negligibly with the two protons because the latter are very energetic [302]. To fit the data we

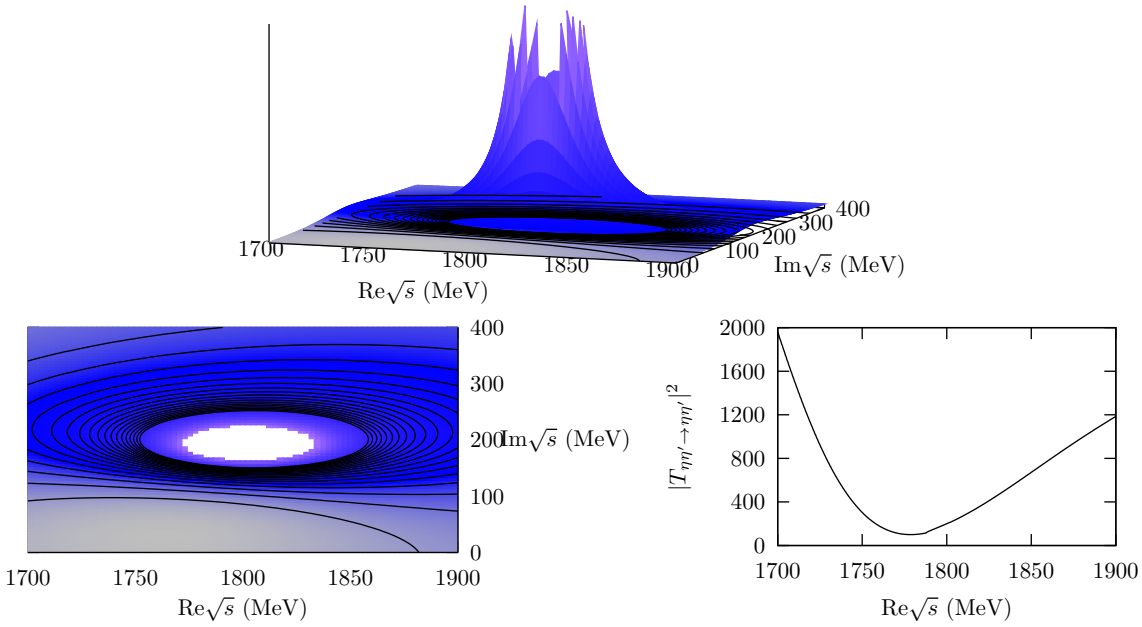

Figure 3.9: The $f_0(1790)$ pole is shown in the $\eta\eta' \to \eta\eta'$ amplitude, where it appears as a dip in the real axis.

employ a coherent sum of Breit-Wigner functions and a non-resonant term, similarly as done by the WA102 Collab. [298]:

$$A(\sqrt{s})_i = NR(\sqrt{s})_i + \sum_{j\in A} \frac{a_j e^{i\theta_j} g_{j;i}}{M_j^2 - s - i\, M_j \Gamma_j} \qquad \sqrt{s} \leqslant m_\eta + m'_\eta \tag{3.47a}$$

$$A(\sqrt{s})_i = NR(\sqrt{s})_i + r_i + \sum_{j\in B} \frac{a_j e^{i\theta_j} g_{j;i}}{M_j^2 - s - i\, M_j \Gamma_j} \qquad \sqrt{s} \geqslant m_\eta + m'_\eta \tag{3.47b}$$

$$NR(\sqrt{s})_i = \alpha(\sqrt{s} - m_k - m_\ell)^\beta e^{-\gamma\sqrt{s} - \delta s} \tag{3.47c}$$

The subset of resonances A and B are given by

$$A = \left\{\sigma, f_0(980), f_0^L, f_0^R\right\}$$
$$B = \{\sigma, f_0(980), f_0(1710), f_0(1790)\}$$

The parameters a_j and θ_j are the modulus and the phase of the production vertex of the j_{th} resonance, M_j, Γ_j and $g_{j;i}$ are, respectively, the mass, width and the coupling to channel i of the same resonance. The mass M_j is determined from the pole position and the coupling $g_{j;i}$ is given by the residue of the partial waves at the pole position. On the other hand, Γ_j in Eq. (3.47) is the largest between its value from the pole position and the one calculated by summing the partial decay widths $\Gamma_{j;i} = \theta(\sqrt{s} - m_k - m_\ell)\lambda_i |g_{j;i}|^2 q_i/(8\pi M_j^2)$, with $\lambda_i = 1/2$ for identical particles. In addition, $m_k + m_l$ is the threshold for the channel i and α, β, γ, δ are real parameters. The form of the non-resonant term is taken from the WA102 Collaboration [298]. The constant r_i is fixed so that the amplitude $A(\sqrt{s})_i$ is continuous at $\omega_{\eta\eta'} \equiv m_\eta + m'_\eta$. Equation (3.47) incorporates important new facts compared to the analyses of the WA102 Collaboration. First, the pole positions and couplings for the different resonances are those

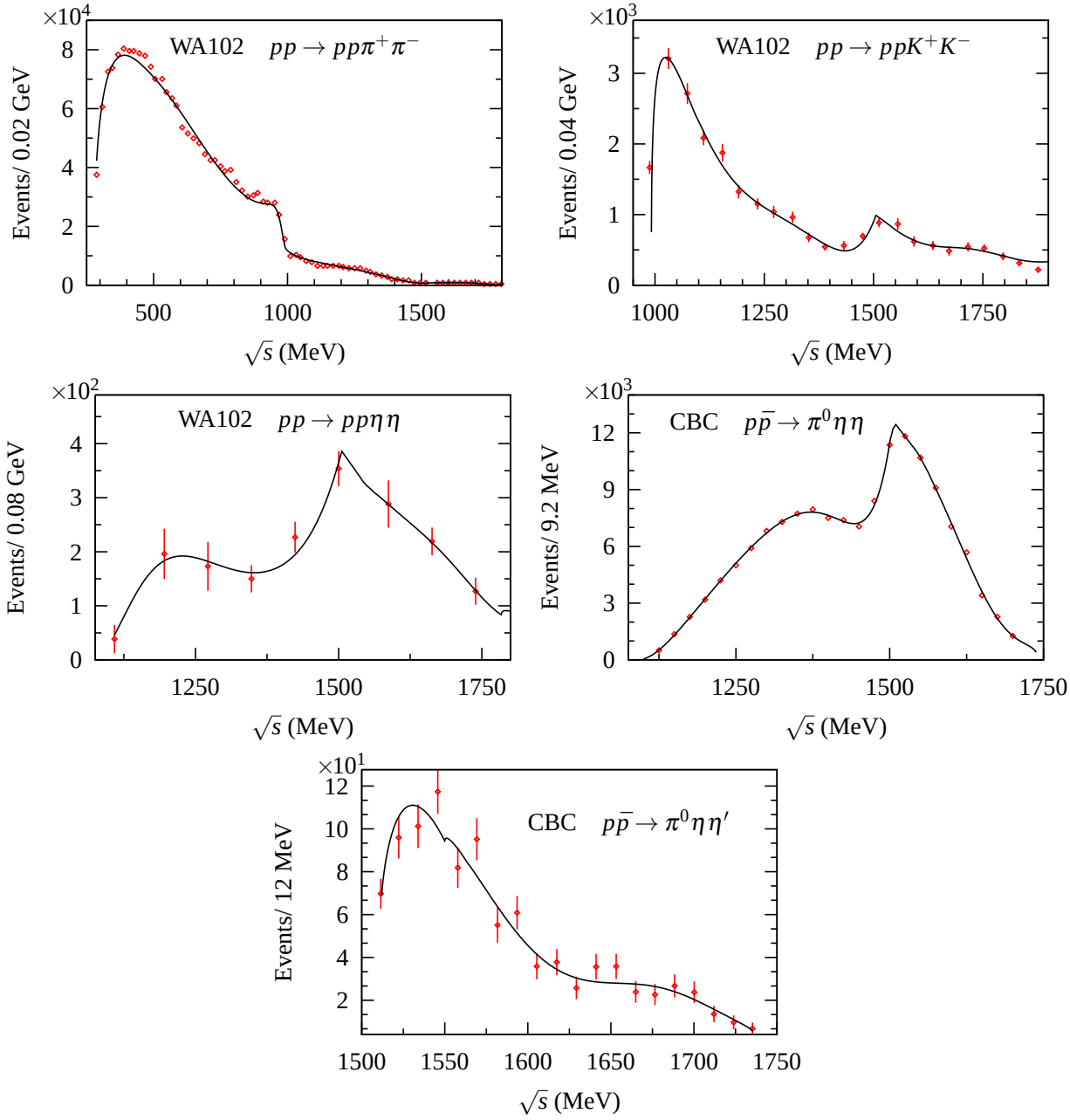

Figure 3.10: Fits to the data of WA102 and CBC Collaborations data. Prominent peaks associated with the resonances described in this work are clearly seen.

already determined from our study of the scattering data. Second, the a_j and θ_j parameters are the same for all the WA102 reactions considered. On the other hand, Eq. (3.47) is a toy model which shows in simple terms how the change of sheet at the $\eta\eta'$ threshold takes place with the corresponding change in the poles involved. Above $w_{\eta\eta'}$ the σ and $f_0(980)$ give tiny contributions. Our fitted curves correspond to the solid lines in Fig. 3.10, where they are compared to the data. Prominent peaks associated with the $f_0(980)$, $f_0(1710)$ and $f_0(1500)$ are observed. We also show our good reproduction of the CBC data for the $\eta\eta$ and $\eta\eta'$ mass projections from $p\bar{p}$ annihilation into $\pi^0\eta\eta$ and $\pi^0\eta\eta'$. We also use Eq. (3.47) but without the non-resonant term, $NR(\sqrt{s})$.

3.7 Identification of the scalar glueball

QCD, the theory of strong interactions, is a non-abelian Yang Mills theory so that gluons carry colour charge and interact between them. It is generally believed that QCD predicts the existence of mesons without valence quarks, the so called glueballs. Its confirmation in the spectrum of strong interactions is then at the heart of the theory. In quenched lattice QCD the lightest glueball has the quantum numbers $J^{PC} = 0^{++}$, with a mass of (1.66 ± 0.05) GeV [85–87]. The closest 0^{++} scalar resonances to this energy range that are listed in the PDG [48] are the $f_0(1500)$ and $f_0(1710)$. Some references favour the former as the lightest scalar glueball [100], while others do so for the latter [89, 91].

Let us now take a look at the couplings of the $f_0(1710)$ resonance, given in Table 3.5. This pattern suggests an enhancement in $s\bar{s}$ production. Indeed, in the following we show that it corresponds to the chiral supression mechanism of the coupling of a scalar glueball to $\bar{q}q$, explained in Ref. [91] (see also Refs. [92–94]). According to this mechanism, this coupling is proportional to the quark mass, thus implying a strong suppression in the production of $\bar{n}n$ relative to that of $\bar{s}s$. This mechanism is not in disagreement with the by now scarce results in lattice QCD, as shown in Fig. 3.11.

Let us denote

$$\eta_s = s\bar{s} \qquad \eta_n = \frac{u\bar{u} + d\bar{d}}{\sqrt{2}} \ , \tag{3.48}$$

so that:

$$\eta_1 = \frac{u\bar{u} + d\bar{d} + s\bar{s}}{\sqrt{3}} = \frac{\sqrt{2}\eta_n + \eta_s}{\sqrt{3}} \tag{3.49}$$

$$\eta_8 = \frac{u\bar{u} + d\bar{d} - 2s\bar{s}}{\sqrt{6}} = \frac{\eta_n - \sqrt{2}\eta_s}{\sqrt{3}} \tag{3.50}$$

With a pseudoscalar mixing angle given by $\sin\beta = -\frac{1}{3}$ for η and η', we have

$$\eta = -\eta_s \frac{1}{\sqrt{3}} + \eta_n \sqrt{\frac{2}{3}}$$
$$\eta' = \eta_s \sqrt{\frac{2}{3}} + \eta_n \frac{1}{\sqrt{3}}$$

By denoting the production of $\eta_s\eta_s$, $\eta_s\eta_n$ and $\eta_n\eta_n$ by g_{ss}, g_{sn} and g_{nn}, respectively, we can write:

$$g_{\eta'\eta'} = \frac{2}{3}g_{ss} + \frac{1}{3}g_{nn} + \frac{2\sqrt{2}}{3}g_{ns}$$
$$g_{\eta\eta'} = -\frac{\sqrt{2}}{3}g_{ss} + \frac{\sqrt{2}}{3}g_{nn} + \frac{1}{3}g_{ns}$$
$$g_{\eta\eta} = \frac{1}{3}g_{ss} + \frac{2}{3}g_{nn} - \frac{2\sqrt{2}}{3}g_{ns}$$

With these equations, we can solve for g_{ss}, g_{ns} and g_{nn}, and the results, for f_0^R and $f_0(1710)$ are shown in Table 3.6. The chiral supression mechanism implies then that $|g_{ss}| \gg |g_{nn}|$. Then

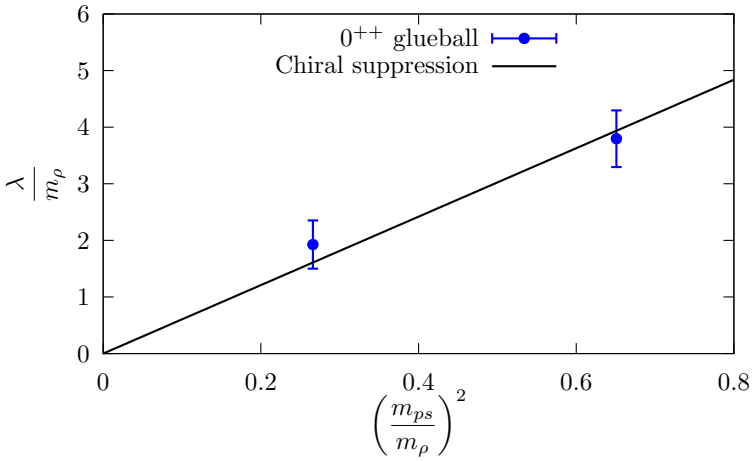

Figure 3.11: Coupling of the scalar glueball to pseudoscalar pairs. The points correspond to the quenched lattice calculations [89], whereas the line correspond to a coupling proportional to pseudoscalar masses squared (that is, proportional to quark masses), as predicted by the chiral supression mechanism [91].

the OZI rule together with this fact supress the coupling $|g_{ns}|$. Taking *e.g.* the couplings of f_0^R one obtains $g_{ss} = 11.5 \pm 0.5$, $g_{ns} = -0.2$ and $g_{nn} = -1.4$ GeV, and the strong suppression is clear.

$\lvert g\rvert$ (GeV)	$f_0(1370)$	f_0^R	$f_0(1710)$
$\lvert g_{\pi^+\pi^-}\rvert$	3.59 ± 0.16	1.30 ± 0.22	1.21 ± 0.16
$\lvert g_{K^0\bar{K}^0}\rvert$	2.23 ± 0.18	2.06 ± 0.17	2.0 ± 0.3
$\lvert g_{\eta\eta}\rvert$	1.7 ± 0.3	3.78 ± 0.26	3.3 ± 0.8
$\lvert g_{\eta\eta'}\rvert$	4.0 ± 0.3	4.99 ± 0.24	5.1 ± 0.8
$\lvert g_{\eta'\eta'}\rvert$	3.7 ± 0.4	8.3 ± 0.6	11.7 ± 1.6

Table 3.5: Couplings of the $f_0(1370)$, f_0^R and $f_0(1710)$ resonances to the different pseudoscalar-pseudoscalar channels.

Coupling (GeV)	f_0^R	$f_0(1710)$
g_{ss}	11.5 ± 0.5	13.0 ± 1.0
g_{ns}	-0.2	2.1
g_{nn}	-1.4	1.2
$g_{ss}/6$	1.9 ± 0.1	2.1 ± 0.2

Table 3.6: Couplings of f_0^R and $f_0(1710)$ in terms of η_s and η_n.

We now consider the $K\bar{K}$ coupling. A K^0 in terms of valence quarks corresponds to $\sum_{i=1}^{3} \bar{s}_i u^i/\sqrt{3}$, summing over the colour indices, and analogously for the $\bar{K}^0$. The production of a colour singlet $\bar{s}s$ from the $K^0\bar{K}^0$ requires then the combination $\bar{s}_i s^j = \delta_i^j \bar{s}s/3 + (\bar{s}_i s^j - \delta_i^j \bar{s}s/3)$, and similarly for $\bar{u}_j u^i$. As the production occurs from the colour singlet $\bar{s}s$ source, only the configuration $\bar{s}s\,\bar{u}u$ contributes, picking up a suppression factor of 1/3. In addition, the coupling g_{ss} has an extra factor 2 compared to that of a $\bar{s}s\,\bar{u}u$, because the former contains two $\bar{s}s$. One then expects for the coupling to $K^0\bar{K}^0$ an absolute value $g_{ss}/6$, $|g_{K^0\bar{K}^0}| \simeq 2$ GeV, as can be seen in Table 3.5.

Another resonance with a known enhanced coupling to $\bar{s}s$ is the $f_0(980)$. However, the sizes of its couplings to $\eta\eta$, $\eta\eta'$ and $\eta'\eta'$ follow the opposite order to the $f_0(1710)$ and f_0^R cases and all of them are much smaller than the coupling to $K\bar{K}$.

It should be stressed that the chiral supression mechanism also implies that the glueball should remain unmixed. This accurately fits with our previous result that both the f_0^R and $f_0(1710)$ do not mix with the nearby f_0^L. In addition, the masses of the f_0^R and $f_0(1710)$ poles are in excellent agreement with the quenched latticed QCD result [85–87].

One final remark is in order here. It should be noted that our work proceeds *completely independent* of the chiral suppression mechanism of Chanowitz [91], that is, no hypothesis about it is done to construct our amplitudes. Finally, when comparing our spectroscopy and the pattern of the couplings and mixing, this mechanism naturally fits in our results.

3.8 Summary and conclusions

In this Chapter, we have studied the scalar sector (0^{++}) of meson–meson interactions, with a special focus on the isoscalar ($I = 0$) channels, within the framework of UChPT. Our amplitudes are calculated from chiral Lagrangians, and then unitarized through the N/D method. In the isoscalar channel, we have included almost all the relevant channels up to a CM energy about $\sqrt{s} \simeq 2$ GeV. The pseudoscalar-pseudoscalar interactions include the η' meson, through the extension of the $SU(3)$ symmetry to $U(3)$.

The 4π channels are effectively included by considering the $\sigma\sigma$ and $\rho\rho$ channels. We have followed a novel method to work out the amplitudes involving the σ meson, without including any *ad hoc* parametrization, but directly from chiral Lagrangians. This can be done by taking into account the nature of this resonance, which is a dynamically generated one in the $\pi\pi$ scalar-isoscalar scattering. Whence we can determine its coupling, which appears in the amplitudes, without introducing any free parameter. The desired amplitudes are obtained by considering the σ-pole limit, $s \to s_\sigma$, in the amplitudes involving $\pi\pi$ channels. The $\rho\rho$ interactions (more generally, the vector-vector interactions), on the other hand, are introduced through minimal coupling, identifying the external classical gauge fields in the chiral Lagrangians with the appropriate vector and axial fields. In this way, up to a global coupling, determined from the decay width of the ρ, these channels are introduced in a free-parameter way. We have also considered the $a_1\pi$ and $\pi^\star\pi$ channels, but these barely contribute to the amplitudes. We have also considered for our amplitudes the s–channel interchange of scalar resonances, determined from resonance chiral Lagrangians. The couplings and bare masses are fitted then to experiment.

Our relatively small number of free parameters are fitted to a wide variety of meson-meson scattering data (370 data points), consisting mostly of phase-shifts and amplitude intensities. Our fits indicate the need of two octets at $M \simeq 1290$ MeV and $M \simeq 1900$ MeV and one singlet at $M \simeq 900$ MeV in the scalar-isoscalar sector. Once our amplitudes are determined, we pay special attention to the spectroscopic content of them. The scalar-isoscalar resonances listed in the PDG up to $\sqrt{s} \simeq 2$ GeV are reproduced. We find the σ, $f_0(980)$ and κ pole positions in agreement with previous works. Regarding the $f_0(1370)$, it originates from a pole, f_0^L, located

at $\sqrt{s} \simeq 1470 - i160$ MeV. However, the amplitudes are peaked mostly at $\sqrt{s} = 1370$ MeV, close to its nominal mass. We find that its couplings to pseudoscalar-pseudoscalar pairs are very similar to those of a bare octet. Whence we conclude that it is a pure octet, which does not mix with the nearby resonances. Similar conclusions can be drawn for the $K_0^*(1430)$ resonance in $I = 1/2$. In our approach, the $f_0(1500)$ resonance appears as an interfering effect of the nearby $\eta\eta'$ and $\omega\omega$ thresholds and the poles f_0^L and f_0^R, the latter located at $\sqrt{s} \simeq 1505 - i110$ MeV. Though further study would be desiderable, what can be deduced from our analysis is that no simple approach (as *e.g.* simple sums of Breit–Wigner amplitudes, and so on) can be used in this complicated energy region. We also find a pole that can be identified with the $f_0(1790)$, with a weak coupling to $K\bar{K}$, as pointed out by the experiments. We discuss about the $f_0(1710)$ at the end of this Section.

As further support to our spectroscopic study, we fit the data of the WA102 Collab. on $pp \to ppPQ$ ($PQ = \pi^+\pi^-,\ K^+K^-$ or $\eta\eta$) and those of the CBC Collab. on $p\bar{p} \to PQ$ ($PQ = \eta\eta,\ \eta\eta'$). This is done *a posteriori*, that is, we use the spectroscopic content of our previous fits in the fits of these latter amplitudes, and we find an excellent agreement.

The $f_0(1710)$ is associated to the pole located at $\sqrt{s} = 1690 - i110$ MeV. It is striking that, by continuosly changing from the Riemann sheet in which it is located to the one in which the f_0^R is present, we move continuosly from one to another pole. That is to say, both poles correspond to the same resonance but reflected on different sheets. From the pattern of its couplings to pseudoscalar–pseudoscalar channels, we realize that it perfectly fits into the chiral supression mechanism of Ref. [91] (deduced from QCD) for the glueball decay into these channels. Besides, its mass is very close to the ones predicted by lattice QCD simulations. Strikingly, we can conclude then that the $f_0(1710)$ can be identified with the lightest scalar glueball. The latter should also reflect through the f_0^R pole in the behaviour of the physical $f_0(1500)$ resonance. This could explain why some studies [100] also indicate this resonance as a candidate for the lightest scalar glueball.

4

Dynamical generation of pseudoscalar resonances

Contents of this Chapter:

4.1 Introduction: Pseudoscalar resonances above 1 GeV

As shown in Chapter 1, due to the spontaneous chiral symmetry breaking of strong interactions [11–14] strong constraints among the interactions between the lightest pseudoscalars arise, which are most efficiently derived in the framework of ChPT [16–19]. For the isospin (I) $I = 0, 1$ and $1/2$ channels, the scattering of the pseudoscalars in S-wave is strong enough to generate dynamically the lightest scalar resonances, namely, the $f_0(980)$, $a_0(980)$, κ and σ, as shown in Refs. [27, 29, 30, 33, 39]. Indeed, in Chapter 3, it was studied the spectroscopy of the scalar resonances (including the above cited) up to $\sqrt{s} = 2$ GeV. Still one can make use of the tightly constrained interactions among the lightest pseudoscalars in order to work out approximately the scattering between the latter mesons and scalar resonances, as we show below. We concentrate here on the much narrower resonances $f_0(980)$ and $a_0(980)$ and consider their interactions with the pseudoscalars π, K, η and η'. If these interactions are strong enough new pseudoscalar resonances with $J^{PC} = 0^{-+}$ would come up. This is the case and the resulting pseudoscalar resonances have a mass larger than 1 GeV (this energy

limit is close to the masses of the $f_0(980)$ or $a_0(980)$), typically following the relevant scalar–pseudoscalar thresholds.

The problem of the excited pseudoscalars above 1 GeV is interesting by itself. These resonances are not typically well-known [48]. In $I = 1/2$ one has the $K(1460)$ and $K(1630)$ resonances. The $I = 1$ resonances $\pi(1300)$, $\pi(1800)$ are somewhat better known [48]. They are broad resonances with a large uncertainty in the width of the former, which is reported to range between 200-600 MeV in the PDG [48]. Some controversy exists for interpreting the decay channels of the $\pi(1800)$ within a quarkonium picture [111, 303]. It was suggested in [303] that, together with the second radial excitation of the pion, there would be a hybrid resonance somewhat higher in mass [303–305]. The recent works in Refs. [114, 115], studying three-pseudoscalar systems by means of the Fadeev equations, obtained conclusions similar to the ones reported below. The $\pi(1300)$ resonance is obtained in $\pi K\bar{K}$ when the $K\bar{K}$ system gets reorganized as $f_0(980)$, while the $K(1460)$ is obtained in the $KK\bar{K}$ system.

Special mention deserves the $I = 0$ channel where the $\eta(1295)$, $\eta(1405)$, $\eta(1475)$ have been object of an intense theoretical and experimental study. For an exhaustive review on the experiments performed on these resonances and the nearby 1^{++} axial-vector resonance $f_1(1420)$ see Ref. [107]. Experimentally it has been established that, while the $\eta(1405)$ decays mainly to $a_0\pi$, the $\eta(1475)$ does so to $K^*\bar{K} + c.c$ [48, 107]. In this way, the study of the $\eta\pi\pi$ system is certainly the most adequate one for isolating the $\eta(1405)$ resonance because both the $f_1(1420)$ and $\eta(1475)$ have a suppressed partial decay width to this channel [48]. References [48, 107] favor the interpretation of considering the $\eta(1295)$ and $\eta(1475)$ as ideally mixed states (because the $\eta(1295)$ and the $\pi(1300)$ are close in mass) of the same nonet of pseudoscalar resonances with the other members being the $\pi(1300)$ and $K(1460)$. All these resonances would be the first radial excitation of the lightest pseudoscalars [303]. The $\eta(1405)$ would then be an extra state in this classification whose clear signal in gluon-rich process, like $p\bar{p}$ [306–309] or J/Ψ radiative decays [310, 311], and its absence in $\gamma\gamma$ collision [312], would favor its interpretation as a glueball in QCD [108–110].

However, this interpretation opens in turn a serious problem because present results from lattice QCD predict the lowest mass for the pseudoscalar glueball at around 2.4 GeV [84–86]. Given the success of the lattice QCD prediction for the lightest scalar glueball, with a mass at around 1.7 GeV [A, 91, 93], this discrepancy for the pseudoscalar channel would be quite exciting. QCD sum rules [76] give a mass for the lightest pseudoscalar gluonium of 2.05 ± 0.19 GeV and an upper bound of 2.34 ± 0.42 GeV. However, the $\eta(1405)$ would fit as a 0^{-+} glueball if the latter is a closed gluonic fluxtube [313]. On the other hand, it has also been pointed out that the mass and properties of the $\eta(1405)$ are consistent with predictions for a gluino-gluino bound state [110,314,315]. The previous whole picture for classifying the lightest pseudoscalar resonances has been challenged in Ref. [111]. The authors question the existence of the $\eta(1295)$ and argue that, due to a node in the $^3P_0$ wave function of the $\eta(1475)$ [316], only one isoscalar pseudoscalar resonance in the 1.4-1.5 GeV region exists. This node shifts the resonant peak position depending on the channel, $a_0\pi$ or $K^*\bar{K} + c.c.$ In turn, Ref. [112] establishes a new mechanism, based on a $K^\star K\bar{K}$ triangle loop, that could explain the shift in the resonance peak position for the $\eta(1405/1475)$ in terms of only one resonance in this energy region.

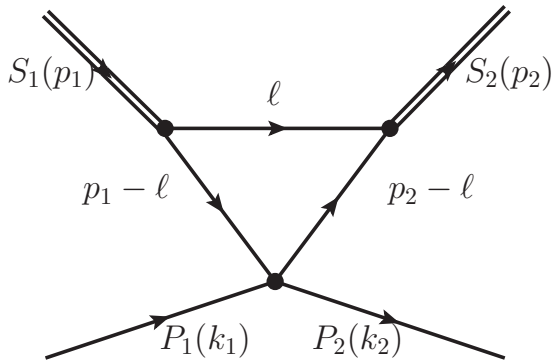

Figure 4.1: Triangle loop for calculating the interacting kernel for $S_1(p_1)P_1(k_1) \to S_2(p_2)P_2(k_2)$, where the four-momentum for each particle is given between brackets. $S_{1,2}$ represents the initial, final scalar resonances and similarly for $P_{1,2}$ regarding the pseudoscalar mesons.

It has been also recently observed by the BES Collaboration the resonance $X(1835)$ with quantum numbers favored as a pseudoscalar 0^{-+} resonance both in $J/\Psi \to \gamma p\bar{p}$ [317] and in $J/\Psi \to \gamma\pi^+\pi^-\eta'$ [318]. For the former decay Ref. [319–321] offers an alternative explanation in terms of the $p\bar{p}$ final state interactions.

We consider in this Chapter the S-wave interactions between the scalar resonances $f_0(980)$ and $a_0(980)$ with the pseudoscalar mesons π, K, η and η'. The approach followed is an extended version of that of Refs. [322, 323] applied to study the S-wave interactions of the $\phi(1020)$ with the $f_0(980)$ and $a_0(980)$ resonances, respectively. We show that the interactions derived generate resonances dynamically that can be associated with many of the previous pseudoscalar resonances listed above, namely, with the $K(1460)$, $\pi(1300)$, $\pi(1800)$, $\eta(1475)$ and $X(1835)$. In this way, new contributions to the physical resonant signals result from this novel mechanism not explored so far. In addition, we also study other exotic channels and find that the $I = 3/2$ a_0K channel could also be resonant. The developments in this Chapter were published in Ref. [B].

After this introduction we present the formalism and derive the S-wave scattering amplitudes for scalar-pseudoscalar interactions in Sec. 4.2. The results are presented and discussed in Sec. 4.3. Conclusions are given in Sec. 4.4.

4.2 Formalism. Setting the model

Our approach is based on the triangle diagram shown in Fig. 4.1 where an incident scalar resonance S_1 decays into a virtual $K\bar{K}$ pair. The filled dot in the vertex on the bottom of the diagram corresponds to the interaction of the incident (anti)kaon in the loop with the pseudoscalar P_1 giving rise to the pseudoscalar P_2 and the same (anti)kaon. The out-going scalar resonance is denoted by S_2. The basic point is that this diagram is enhanced because the masses of both the $f_0(980)$ and $a_0(980)$ resonances are very close to the $K\bar{K}$ threshold. In this way, for scattering near the threshold of the reaction, one of the kaon lines in the bottom of the diagram is almost on-shell. Indeed, at threshold and in the limit for the mass of the scalar

equal to twice the kaon mass this diagram becomes infinite. This fact is discussed in detail in Ref. [322] where it was already applied for studying successfully the $\phi(1020)f_0(980)$ scattering and the associated 1^{--} $Y(2175)$ resonance. The BABAR [324, 325] and BELLE [326] data on $e^+e^- \to \phi(1020)f_0(980)$ were reproduced accurately, where a strong peak for the latter resonance arises. An important conclusion of Ref. [322] is that the $Y(2175)$ can be qualified as being a resonance dynamically generated due to the interactions between the $\phi(1020)$ and the $f_0(980)$ resonances, see also Ref. [327]. This work was extended to $I = 1$ in [323] for studying the $\phi(1020)a_0(980)$ S-wave. There it was remarked the interest of measuring the cross sections $e^+e^- \to \phi(1020)\pi^0\eta$ because it is quite likely that an isovector companion of the $Y(2175)$ appears. In our present study, as well as in Refs. [322, 323], one takes advantage of the fact that both the $f_0(980)$ and $a_0(980)$ resonances are dynamically generated by the meson-meson self-interactions [33,39,53]. This conclusion is also shared with other approaches like Refs. [52, 251, 328]. In this way, we can calculate the couplings of the scalar resonances considered to two pseudoscalars, including their relative phase. The coupling of the $f_0(980)$ and $a_0(980)$ resonances to a $K\bar{K}$ pair in $I = 0$ and 1, respectively, is denoted by g_{f_0} and g_{a_0}. These states $|K\bar{K}\rangle_{I=0}$ and $|K\bar{K}\rangle_{I=1}$ are given by

$$|K\bar{K}\rangle_{I=0} = -\frac{1}{\sqrt{2}}|K^+K^- + K^0\bar{K}^0\rangle \ ,$$
$$|K\bar{K}\rangle_{I=1} = -\frac{1}{\sqrt{2}}|K^+K^- - K^0\bar{K}^0\rangle \ . \tag{4.1}$$

In this way, the $f_0(980)$ couples to $K^+K^-(K^0\bar{K}^0)$ as $-\frac{1}{\sqrt{2}}(-\frac{1}{\sqrt{2}})g_{f_0}$ while the $a_0(980)$ couples as $-\frac{1}{\sqrt{2}}(\frac{1}{\sqrt{2}})g_{a_0}$.

Let us indicate by P the total four-momentum $P = p_1 + k_1 = p_2 + k_2$ in Fig. 4.1. This diagram is given by $g_1 g_2 L_K$, with g_1 and g_2 the coupling of the initial and final scalar resonance to a $K\bar{K}$ pair, respectively, and L_K is given by

$$L_K = i\int \frac{d^4\ell}{(2\pi)^4}\frac{T((P-\ell)^2)}{(\ell^2 - m_K^2 + i\varepsilon)((p_1-\ell)^2 - m_K^2 + i\varepsilon)((p_2-\ell)^2 - m_K^2 + i\varepsilon)} \ . \tag{4.2}$$

In this equation $T((P-\ell)^2)$ represents the interaction amplitude between the kaons with the external pseudoscalars. Here, we employ the meson-meson unitarized scattering amplitudes obtained in Ref. [39] but now enlarged (as in Chapter 3) so that states with the pseudoscalar η' are included in the calculation of $T((P-\ell)^2)$. In Appendix D, we show these amplitudes and how they are obtained from different fits. These amplitudes contain the poles corresponding to the scalar resonances σ, κ, $f_0(980)$, $a_0(980)$ and other poles in the region around 1.4 GeV [39]. Their pole positions and relevant couplings are shown in the aforesaid Appendix, in Tables D.2 and D.3, respectively.

In order to proceed further we have to know the dependence of $T((P-\ell)^2)$ on its argument that includes the integration variable ℓ. This can be done by writing the dispersion relation satisfied by $T(q^2)$ which is of the form:[1]

$$T(q^2) = T(s_A) + \sum_i \frac{q^2 - s_A}{q^2 - s_i}\frac{\mathrm{Res}_i}{s_i - s_A} + \frac{q^2 - s_A}{\pi}\int_{s_{th}}^{\infty} ds' \frac{\mathrm{Im}T(s')}{(s' - q^2)(s' - s_A)} \ . \tag{4.3}$$

[1]The $T(q^2)$ amplitude is on-shell because off-shell contributions would cancel propagators [33] in the loop represented in Fig. 4.1 and the enhancements discussed above no longer take place. This is why we neglect such off-shell contributions in $T(q^2)$.

One subtraction at s_A has been taken because $T(q^2)$ is bound by a constant for $q^2 \to \infty$, with $T(s_A)$ the subtraction constant. Typically there are also present poles deep in the q^2-complex plane located at s_i whose residues are Res_i. These poles appear on the first Riemann sheet and are an artifact of the parameterization employed [39,190]. For q^2 along the physical region they just give rise to soft extra contributions that could be mimicked by a polynomial of low degree in q^2. Inserting Eq. (4.3) into Eq. (4.2), with $(P-\ell)^2 = q^2$, one can write for L_K

$$\begin{aligned} L_K = &\left(T(s_A) + \sum \frac{\mathrm{Res}_i}{s_i - s_A} \right) C_3 + \sum_i C_4(s_i) \mathrm{Res}_i \\ &- \frac{1}{\pi} \int_{s_{th}}^{\infty} ds' \mathrm{Im} T(s') \left[\frac{C_3}{s' - s_A} + C_4(s') \right] . \end{aligned} \tag{4.4}$$

Here we have introduced the three- and four-point Green functions C_3 and $C_4(M_4^2)$ defined by

$$\begin{aligned} C_3 &= i \int \frac{d^4\ell}{(2\pi)^4} \frac{1}{(\ell^2 - m_K^2 + i\varepsilon)((p_1-\ell)^2 - m_K^2 + i\varepsilon)((p_2-\ell)^2 - m_K^2 + i\varepsilon)} , \\ C_4(M_4^2) &= i \int \frac{d^4\ell}{(2\pi)^4} \frac{1}{(\ell^2 - m_K^2 + i\varepsilon)((p_1-\ell)^2 - m_K^2 + i\varepsilon)((p_2-\ell)^2 - m_K^2 + i\varepsilon)} \\ &\times \frac{1}{((P-\ell)^2 - M_4^2 + i\epsilon)} . \end{aligned} \tag{4.5}$$

Notice that M_4^2 can be real positive (when $M_4^2 = s'$ in the dispersion relation), but it could also be negative or even complex when $M_4^2 = s_i$ from the poles. One has still to perform the angular projection for C_3 and $C_4(M_4^2)$. Once this is done, Eq. (4.4) can still be used but with C_3 and $C_4(M_4^2)$ projected in S-wave, as we take for granted in the following. These functions and their S-wave projection are discussed in Appendix E. For $S_1(p_1)P_1(k_1) \to S_2(p_2)P_2(k_2)$ we have the usual Mandelstam variables $s = (p_1+k_1)^2 = (p_2+k_2)^2$, $t = (p_1-p_2)^2 = (k_1-k_2)^2$ and $u = (p_1-k_2)^2 = (p_2-k_1)^2 = M_{S_1}^2 + M_{S_2}^2 + M_{P_1}^2 + M_{P_2}^2 - s - t$, with the masses of the particles indicated by M with the subscript distinguishing between them. The dependence on the relative angle θ enters in t as $t = (p_1^0 - k_1^0)^2 - (\mathbf{p} - \mathbf{p}')^2 = (p_1^0 - k_1^0)^2 - \mathbf{p}^2 - \mathbf{p}'^2 + 2|\mathbf{p}||\mathbf{p}'|\cos\theta$ with $\mathbf{p}$ and $\mathbf{p}'$ the CM three-momentum of the initial and final particles, respectively.

Our basic equation for evaluating the interaction kernels is Eq. (4.4). One has only to specify the pseudoscalars actually involved in the amplitude $T(q^2)$ according to the specific reaction under consideration. We now list all the channels involved for the different quantum numbers and indicate the actual pseudoscalar-pseudoscalar amplitudes required as the argument of L_K:

- $I = 0$, $G = +1$

$$\begin{aligned} T_L(a_0\pi \to a_0\pi) &= \frac{2g_{a_0}^2}{3} L_K[4\, T^{I=3/2}_{\pi K \to \pi K} - T^{I=1/2}_{\pi K \to \pi K}] , \\ T_L(a_0\pi \to f_0\eta) &= 2 g_{f_0} g_{a_0} L_K[T^{I=1/2}_{\eta K \to \pi K}] , \\ T_L(f_0\eta \to f_0\eta) &= 2 g_{f_0}^2 L_K[T^{I=1/2}_{\eta K \to \eta K}] , \\ T_L(a_0\pi \to f_0\eta') &= 2 g_{f_0} g_{a_0} L_K[T^{I=1/2}_{\eta' K \to \pi K}] , \\ T_L(f_0\eta \to f_0\eta') &= 2 g_{f_0}^2 L_K[T^{I=1/2}_{\eta K \to \eta' K}] , \end{aligned}$$

$$T_L(f_0\eta' \to f_0\eta') = 2g_{f_0}^2 L_K[T^{I=1/2}_{\eta' K\to\eta' K}] \ . \tag{4.6}$$

- $I = 1/2$

$$\begin{aligned}
T_L(f_0K \to f_0K) &= \frac{g_{f_0}^2}{2} L_K[3\, T^{I=1}_{K\bar{K}\to K\bar{K}} + T^{I=0}_{K\bar{K}\to K\bar{K}}] \ , \\
T_L(f_0K \to a_0K) &= \frac{\sqrt{3} g_{f_0} g_{a_0}}{2} L_K[T^{I=1}_{K\bar{K}\to K\bar{K}} - T^{I=0}_{K\bar{K}\to K\bar{K}}] \ , \\
T_L(a_0K \to a_0K) &= \frac{g_{a_0}^2}{2} L_K[3\, T^{I=0}_{K\bar{K}\to K\bar{K}} + T^{I=1}_{K\bar{K}\to K\bar{K}}] \ .
\end{aligned} \tag{4.7}$$

- $I = 1$, $G = -1$

$$\begin{aligned}
T_L(f_0\pi \to f_0\pi) &= \frac{2g_{f_0}^2}{3} L_K[2\, T^{I=3/2}_{\pi K\to\pi K} + T^{I=1/2}_{\pi K\to\pi K}] \ , \\
T_L(f_0\pi \to a_0\eta) &= \frac{2g_{f_0} g_{a_0}}{\sqrt{3}} L_K[T^{1/2}_{\pi K\to\eta K}] \ , \\
T_L(a_0\eta \to a_0\eta) &= 2g_{a_0}^2 L_K[T^{I=1/2}_{\eta K\to\eta K}] \ , \\
T_L(f_0\pi \to a_0\eta') &= \frac{2g_{f_0} g_{a_0}}{\sqrt{3}} L_K[T^{I=1/2}_{\pi K\to\eta' K}] \ , \\
T_L(a_0\eta \to a_0\eta') &= 2g_{a_0}^2 L_K[T^{I=1/2}_{\eta K\to\eta' K}] \ , \\
T_L(a_0\eta' \to a_0\eta') &= 2g_{a_0}^2 L_K[T^{I=1/2}_{\eta' K\to\eta' K}] \ .
\end{aligned} \tag{4.8}$$

- $I = 1$, $G = +1$

$$T_L(a_0\pi \to a_0\pi) = \frac{2g_{a_0}^2}{3} L_K[4T^{I=1/2}_{\pi K\to\pi K} - T^{I=3/2}_{\pi K\to\pi K}] \ . \tag{4.9}$$

- $I = 3/2$

$$T_L(a_0K \to a_0K) = 2g_{a_0}^2 L_K[T^{I=1}_{K\bar{K}\to K\bar{K}}] \ . \tag{4.10}$$

In the previous equations the different scalar-pseudoscalar states are pure isospin ones corresponding to the isospin I indicated for each item. This also applies to the pseudoscalar-pseudoscalar states, with I as indicated in the superscript of T. The symbol G refers to G-parity. On the other hand the $I = 3/2$ πK amplitude, being much smaller than the $I = 1/2$ one, has negligible effects, although it has been kept in the previous expressions.

For each set of quantum numbers specified by the isospin I and G-parity G (if the latter is not defined this label should be omitted) we join in a symmetric matrix $\mathcal{T}_{IG}$ the different $T_L(i \to j)$ calculated above. Then, in order to resum the unitarity loops, as indicated in Fig. 4.2, and obtain the final S-wave scalar-pseudoscalar T-matrix, T_{IG}, we make use of the equation

$$T_{IG} = [I + \mathcal{T}_{IG} \cdot g_{IG}(s)]^{-1} \cdot \mathcal{T}_{IG} \ . \tag{4.11}$$

The general derivation of this equation, based on the N/D method [38], was given in Chapter 2. See Refs. [39, 41] and Ref. [33], where it is connected with the Bethe-Salpeter equation. In

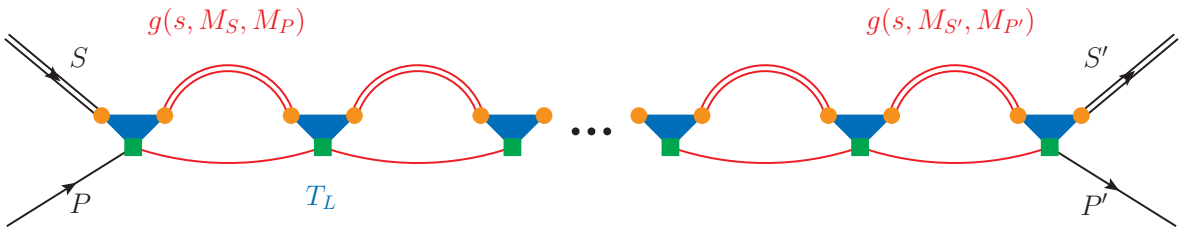

Figure 4.2: Iteration of the interaction kernels (blue triangles) by inserting scalar-pseudoscalar intermediate states (red lines). Double lines denote the scalars, whereas the single ones represent the pseudoscalars. The orange circles represent thus the $S \to K\bar{K}$ coupling, and the green squares are the unitarized pseudoscalar-pseudoscalar amplitudes.

Eq. (4.11) $g_{IG}(s)$ is a diagonal matrix whose elements are the scalar unitarity loop function with a scalar-pseudoscalar intermediate state. For the calculation of $g_{IG}(s)_i$, corresponding to the i_{th} state with the quantum numbers IG and made up by the scalar resonance S_i and the pseudoscalar P_i, we make use of a once subtracted dispersion relation [39]. The result is

$$\begin{aligned} g_{IG}(s)_i = \frac{1}{(4\pi)^2}\Bigg\{ a_1 + \log\frac{M_{S_i}^2}{\mu^2} - \frac{M_{P_i}^2 - M_{S_i}^2 + s}{2s}\log\frac{M_{S_i}^2}{M_{P_i}^2} \\ + \frac{|\mathbf{p}|}{\sqrt{s}}\Bigg[\log(s - \Delta + 2\sqrt{s}|\mathbf{p}|) + \log(s + \Delta + 2\sqrt{s}|\mathbf{p}|) \\ - \log(-s + \Delta + 2\sqrt{s}|\mathbf{p}|) - \log(-s - \Delta + 2\sqrt{s}|\mathbf{p}|)\Bigg]\Bigg\} \end{aligned} \tag{4.12}$$

with $|\mathbf{p}|$ the three-momentum of the channel S_iP_i for a given s and $\Delta = M_{P_i}^2 - M_{S_i}^2$. The subtraction a_1 is restricted to have natural values so that the unitarity scale [322] $4\pi f_\pi/\sqrt{|a_1|}$ becomes not too small (*e.g.* below the ρ-mass) so that $|a_1| \lesssim 3$. In addition, we require the sign of a_1 to be negative so that resonances could be generated when the interaction kernel is positive (attractive).

As already indicated in Ref. [323] to ensure a continuous limit to zero $a_0(980)$ width, one has to evaluate $\mathcal{T}_{IG}$ at the $a_0(980)$ pole position with positive imaginary part so that $p_{1,2}^2 \to \mathrm{Re}\,[M_{a_0}]^2 + i\epsilon$, in agreement with Eq. (4.2). Instead, in $g_{IG}(s)_{a_0P}$, with P one of the lightest pseudoscalars, M_{a_0} should appear with a negative imaginary part to guarantee that, in the zero-width limit, the sign of the imaginary part is the same as dictated by the $-i\epsilon$ prescription for masses squared of the intermediate states. Such analytical extrapolations in the masses of external particles are discussed in Refs. [329–331]. The same applies of course to the case of the $f_0(980)$ resonance.

4.3 Results

In this section we show the results that follow by applying Eq. (4.11) to the different channels characterized by the quantum numbers IG, as given in the list from Eq. (4.6) to Eq. (4.10). As discussed after Eq. (4.12) we consider values for the subtraction constant such that they

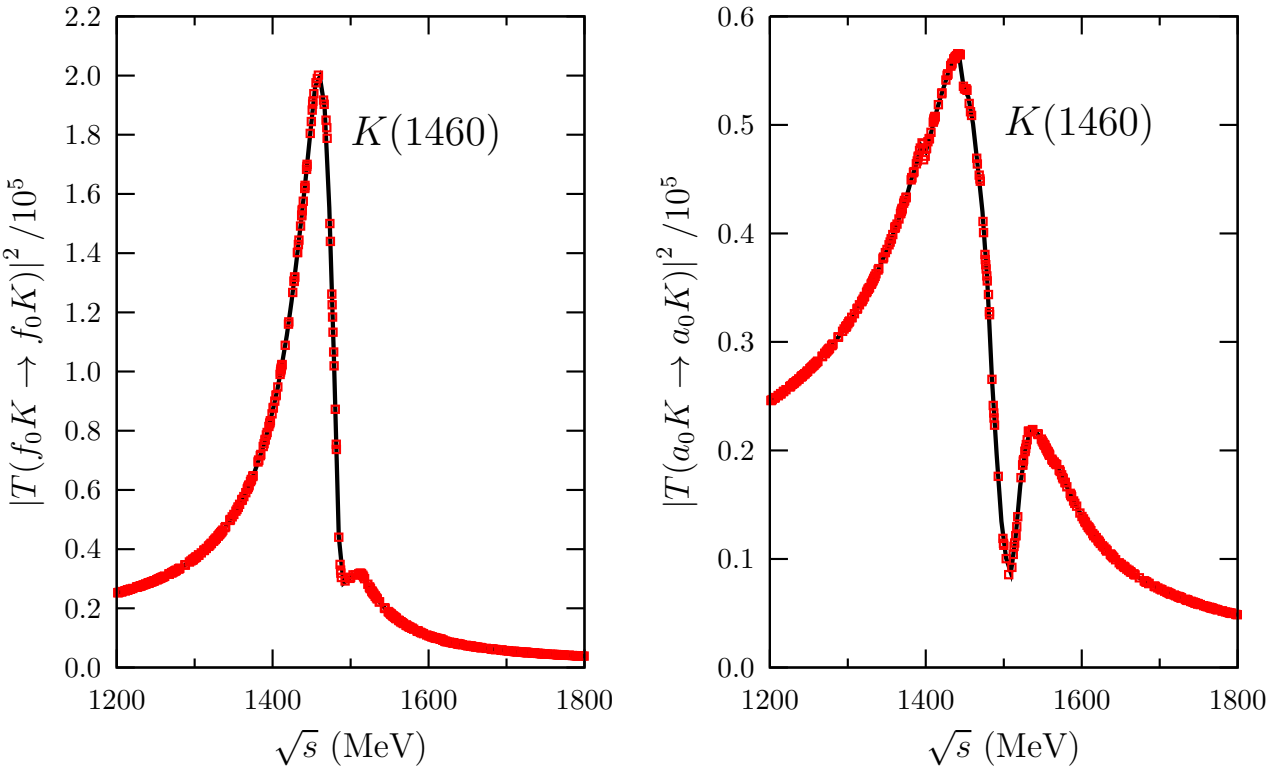

Figure 4.3: Modulus squared of the $f_0K \to f_0K$ (left) and $a_0K \to a_0K$ (right) S-wave amplitudes for $a_1 = -0.5$. The points correspond to the energies where the amplitudes have been actually calculated.

are negative and not very large in modulus ($|a_1| \lesssim 3$). In this way, the resonances generated might be qualified as dynamically generated due to the iteration of the unitarity loops. We present the results for each of the channels with definite IG separately.

4.3.1 $I = 1/2$

First we show the results for the $I = 1/2$ sector that couples together the channels $f_0(980)K$ and $a_0(980)K$. We show the modulus squared of the $f_0K \to f_0K$ and $a_0K \to a_0K$ S-wave amplitudes in the left and right panel of Fig. 4.3, respectively. We obtain a clear resonant peak with its maximum at 1460 MeV for a_1 around -0.5, that corresponds to the nominal mass of the $K(1460)$ resonance [48]. The results are not very sensitive to the actual value of a_1 but the position of the peak displaces to lower values for decreasing a_1 and the width somewhat increases. The visual width of the peak is around 100 MeV, although it appears wider in $a_0K \to a_0K$ scattering. In Refs. [332, 333] a larger width of around 250 MeV is referred. One has to take into account that the channel $K^*(892)\pi$ is not included and it seems to couple strongly with the $K(1460)$ resonance [48]. It is also clear from the figure that the peak is asymmetric due to the opening of the f_0K and a_0K thresholds involved. Taking into account the relative sizes of the peaks in the left and right panels of Fig. 4.3 one infers that the $K(1460)$ couples more strongly to f_0K than to a_0K, with the ratio of couplings as $|g_{f_0K}/g_{a_0K}| \simeq (\frac{20.2}{5.7})^{1/4} \simeq 1.4$.

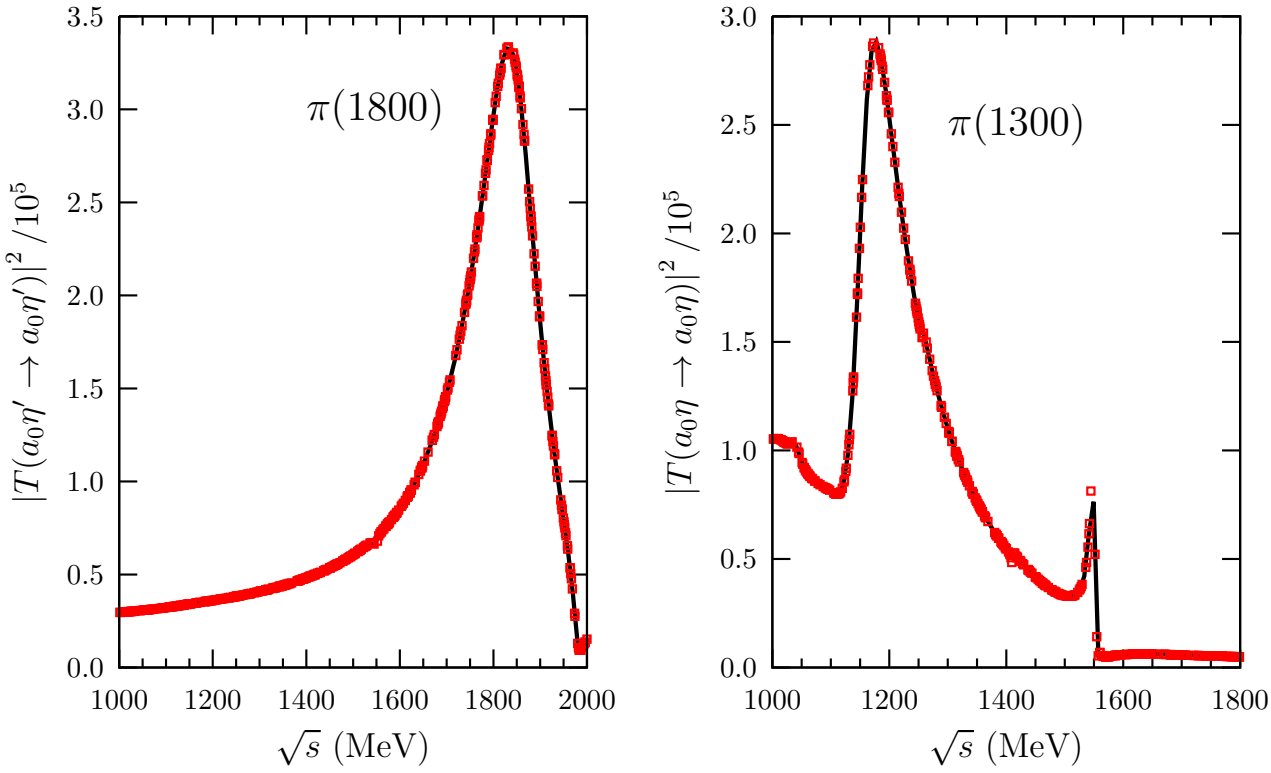

Figure 4.4: Modulus squared of the $a_0\eta' \to a_0\eta'$ (left) and $a_0\eta \to a_0\eta$ (right) S-wave amplitudes. For the former $a_1 = -1.3$ and for the latter $a_1 = -2.0$, see the text for details. The notation is as in Fig. 4.3.

4.3.2 $I = 1$

We now consider the $I = 1$ case. As commented in the introduction two broad resonances are referred in the PDG, the $\pi(1300)$ and $\pi(1800)$. In our amplitudes we find quite independently of the value of a_1 that the $a_0(980)\eta'$ channel is almost elastic. This is due to the fact that the interaction kernels $\mathcal{T}(a_0\eta' \to a_0\eta)$ and $\mathcal{T}(a_0\eta' \to f_0\pi)$ are much smaller than the rest of kernels, typically by an order of magnitude. This happens because the kernels are dominated by the threshold region. However, the threshold for $a_0(980)\eta'$ is much heavier than the thresholds for the other two channels. In this way, for the inelastic processes involving the $a_0\eta'$ channel, even at threshold for one of the channels, there is always a large three-momentum for the other channel and the kernel is suppressed. Of course, this does not apply for the $a_0\eta'$ elastic case where the kernel has a standard size and produces around 1.8 GeV a strong resonant signal that could be associated with the $\pi(1800)$ resonance. To reproduce the mass value given in the PDG [48] for this resonance, 1816 ± 14 MeV one takes a_1 for $a_0\eta'$ around -1.3. The visual width of the peak is around 200 MeV, close to the width quoted in the PDG [48] of 208 ± 12 MeV. The other two channels couple quite strongly between each other and typically give rise to an enhancement between 1.2–1.4 GeV when varying a_1 equal for each of them, which could be associated with the $\pi(1300)$. However, for $|a_1|$ between 1 and 1.8 a too strong signal in the $a_0\eta$ threshold originates. For $|a_1|$ below 1 the resonant peak in the $|T(a_0\eta \to a_0\eta)|^2$ lies around 1.4–1.5 GeV, somewhat too high for the $\pi(1300)$ resonance [48]. This is why we show in Fig. 4.4 the modulus squared of $a_0\eta \to a_0\eta$ for $a_1 = -2$ where a peak close to 1.2 GeV is seen with a width of around 200 MeV. One can also see the strong effect

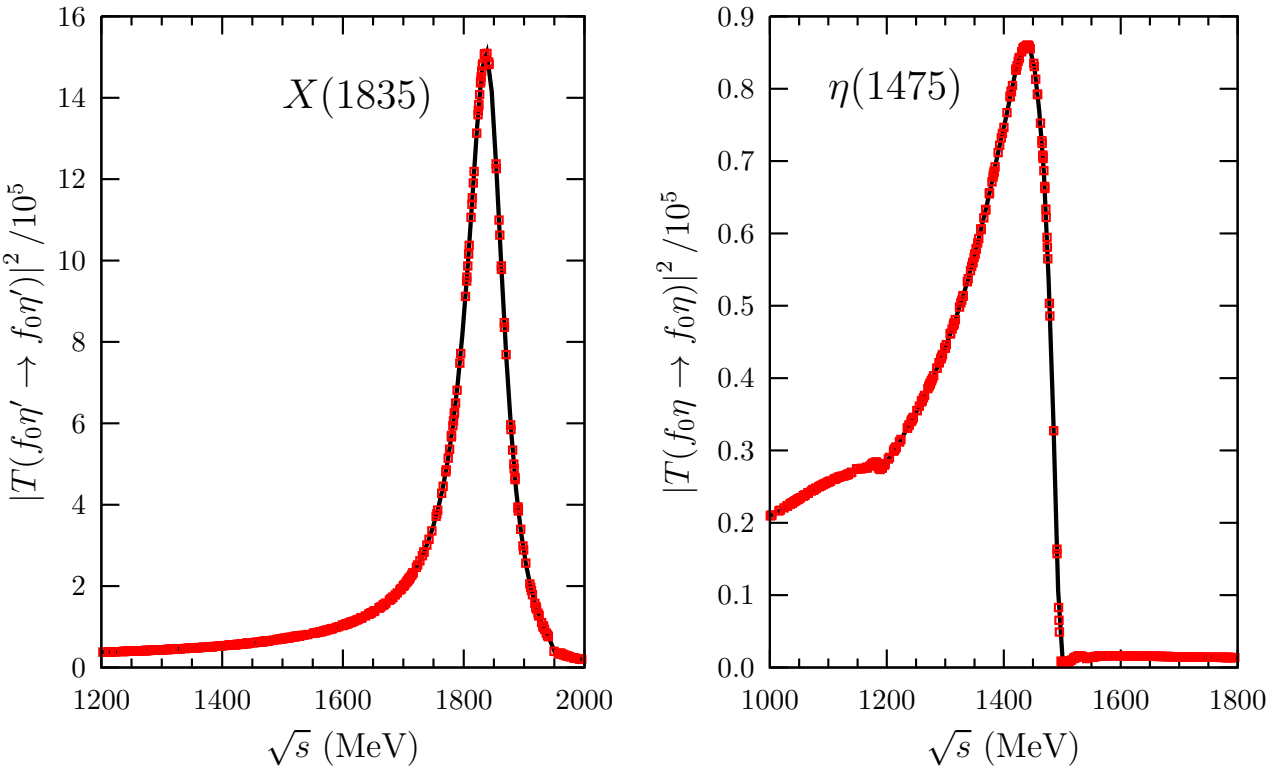

Figure 4.5: Modulus squared of the $f_0\eta' \to f_0\eta'$ (left) and $f_0\eta \to f_0\eta$ (right) S-wave amplitudes. For the former $a_1 = -1.25$ and for the latter $a_1 = -0.8$, see the text for details. The notation is as in Fig. 4.3.

of the $a_0\eta$ threshold at around 1.52 GeV. Its size is rather sensitive to the actual vale of $|a_1|$ when this lies between 1 and 1.8. There is the interesting fact, which is independent of the value of a_1, that there is no signal for $\pi(1800)$ in the $a_0\eta$ system nor signal of the peak at 1.2 GeV in the $a_0\eta'$. We have also checked that this is also the case for the $f_0\pi$ state, that is, it does not couple with the $\pi(1800)$. This is another reflection of the fact that the $a_0\eta'$ tends to decouple from the other states.

4.3.3 $I = 0$

We move next to the $I = 0$ system where the $f_0\eta$, $a_0\pi$ and $f_0\eta'$ couple. Here occurs similarly to $I = 1$, so that the much higher $f_0\eta'$ channel mostly decouples from the other two channels. We then proceed similarly and distinguish between the subtraction constant a_1 attached to $a_0\eta'$ and to the other two channels $a_0\pi$ and $f_0\eta$. For a_1 around -1.2 one obtains a resonance of the $f_0\eta'$ channel at a mass of 1835 MeV, in agreement with that quoted in the PDG for the $X(1835)$, $1833.7 \pm 6.1 \pm 2.7$ MeV. This is shown in the left panel of Fig. 4.5 where the modulus squared of the $f_0(980)\eta' \to f_0(980)\eta'$ S-wave amplitude is shown. The width of the peak at half its maximum value is around 70 MeV, in good agreement with the width given in the PDG for the $X(1835)$ of $67.7 \pm 20.3 \pm 7.7$ MeV. We consider next the other two coupled channels, $a_0(980)\pi$ and $f_0(980)\eta$. We obtain a clear resonant signal with mass around 1.45 GeV for $|a_1| \lesssim 1$. This is shown in the right panel of Fig. 4.5, where the modulus squared of the $f_0(980)\eta \to f_0(980)\eta$ is given for $a_1 = -0.8$. It is not possible to increase

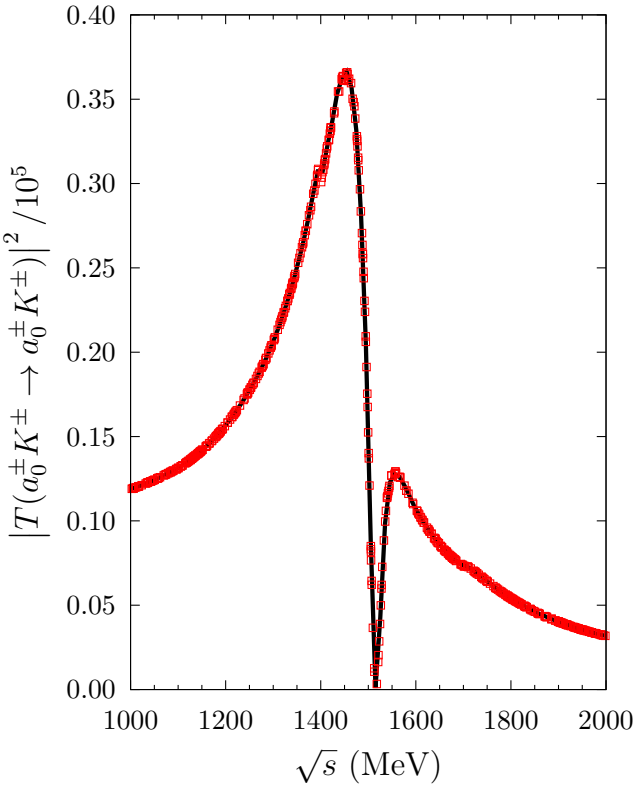

Figure 4.6: Modulus squared of the exotic $I = 3/2$ $a_0K \to a_0K$ S-wave amplitude with $a_1 = -0.5$. The notation is as in Fig. 4.3.

further the mass of this peak by varying a_1. An important fact of this resonance is that it does not couple to the $a_0\pi$ channel. For example, the analogous curve for the modulus squared of the $a_0(980)\pi \to a_0(980)\pi$ S-wave in the 1.4 GeV region is absolutely flat (by considering the inelastic process $f_0(980)\eta \to a_0(980)\pi$ we estimate a coupling to the latter channel more than 14 times smaller than to $f_0(980)\eta$.) Because the $\eta(1405)$ resonance couples mostly to $a_0(980)\pi$ [48] we then conclude that the generated resonant signal around 1.45 GeV should correspond to the $\eta(1475)$. Its form is rather asymmetric due to the opening of the $f_0(980)\eta$ threshold, with a width at half the maximum of its peak of around 150 MeV. The width quoted in the PDG [48] is 85 ± 9 MeV. It is also known that the $\eta(1475)$ couples strongly to $K^*(892)\bar{K}+c.c$, a channel not included in our study. The threshold for this channel, at around 1.39 GeV at the decreasing slop of our present signal, should certainly modify its shape. For higher values of $|a_1|$ the peak tends to become too light in mass compared with the $\eta(1475)$. For the $a_0(980)\pi \to a_0(980)\pi$ reaction one also appreciates a strong $a_0(980)\pi$ threshold effect at around 1.16 GeV. No resonance around the mass of the $\eta(1295)$ is observed.

4.3.4 Exotic channels

Regarding the exotic channel with $I = 3/2$ we find an interesting result. Our amplitude gives rise to a clear resonant structure at around 1.4 GeV for $|a_1| \lesssim 1.5$. We show the modulus squared of $T(a_0^\pm K^\pm \to a_0^\pm K^\pm)$, because the $a_0^\pm K^\pm$ states are purely $I = 3/2$, for $a_1 = -0.5$ (the same value used before in Fig. 4.3 studying the $I = 1/2$ case) in Fig. 4.6. One also observes that the shape of the resonance peak is asymmetric with a clear impact of the a_0K threshold. Our results for $|a_1| \lesssim 1$ tends to confirm the predictions of Longacre [113] that

Resonance	$I^{(G)}$	Width (MeV)	Properties
$K(1460)$	$I=\frac{1}{2}$	$\Gamma \gtrsim 100$	$\lvert g_{f_0K}/g_{a_0K}\rvert \simeq 1.4$
$\pi(1800)$	$I^G=1^-$	$\Gamma \simeq 200$	$a_0\eta'$ elastic
$\pi(1300)$	$I^G=1^-$	$\Gamma \gtrsim 200$	$a_0\pi$, $f_0\eta$ coupled channels
$X(1835)$	$I^G=0^+$	$\Gamma \simeq 70$	$f_0\eta'$ elastic
$\eta(1475)$	$I^G=0^+$	$\Gamma \simeq 150$	$f_0\eta$ elastic
Exotic	$I=\frac{3}{2}$	$\Gamma \simeq 200$	a_0K threshold

Table 4.1: Resonances resulting from our study. For more details see the discussions of the results in the text.

studied the $K\bar{K}\pi$ and $K\bar{K}K$ system and concluded that the exotic $I=3/2$ $J^P=0^-$ $K\bar{K}K$ system was resonant around its threshold due to the successive interactions between a K, $\bar{K}$ and a π. For $|a_1| \gtrsim 1$ we find that the resonance shape in $|T(a_0^\pm K^\pm \to a_0^\pm K^\pm)|^2$ progressively distorts becoming lighter and flatter. Let us notice also that the a_0K system was not isolated in the two experiments quoted in the PDG where the $I=1/2$ $K(1460)$ was observed [332,333].

The other exotic channel with $I=1$ and $G=+1$ involves the isovector $a_0\pi$ state. Whether a resonance behavior stems at around 1.4 GeV depends on the actual value of a_1. For $|a_1| \lesssim 1$ the enhancement near 1.4 GeV is much weaker and is overcome by the cusp effect at the $a_0\pi$ threshold. For larger values of $|a_1|$ the resonant signal is much more prominent. No such resonance has been found experimentally, *e.g.* in peripheral hadron production [334], so that $|a_1| \lesssim 1$ should be finally taken.

In Table 4.1 we collect all the resonances found in our study for the different quantum numbers discussed.

4.4 Summary and conclusions

In summary, we have presented a study of the S-wave interactions between the scalar resonances $f_0(980)$ and $a_0(980)$ with the lightest pseudoscalars (π, K, η and η') in the region between 1 and 2 GeV. The different channels studied comprise those alike the η, K and π, and the exotic ones with isospin 3/2 and 1, the latter having positive G-parity. First, interaction kernels have been derived by considering the interactions of the external pseudoscalars involved in the reaction with those making the scalar resonance. We take advantage here of previous studies that establish the $f_0(980)$ and $a_0(980)$ as dynamically generated from the interactions of two pseudoscalars, so that no free parameters are introduced in their calculation. Afterwards, the final S-wave amplitudes are determined by employing techniques borrowed from Unitary Chiral Perturbation Theory. Interestingly, we have obtained resonant peaks that for the non-exotic channels could be associated with the pseudoscalar resonances $K(1460)$, $\pi(1300)$, $\pi(1800)$, $\eta(1475)$ and $X(1835)$, following the notation of the PDG [48]. The resonances that come out from this study can be qualified as dynamically generated from the interactions between the scalar resonances and the pseudoscalar mesons. This establishes that an important contribution to the physical signal of the resonances just mentioned has a

dynamical origin. The exotic $I = 3/2$ channel could also exhibit a resonant structure around the a_0K threshold, in agreement with the behavior predicted by Longacre [113] twenty years ago. However, larger values for the subtraction constant $|a_1|$ tends to destroy this resonant behavior. No signal of the intriguing $\eta(1405)$ resonance is obtained.

This approach should be pursued further by including simultaneously to the interaction between the scalar resonances and the pseudoscalar mesons, considered here, those arising from the lightest vector resonances with the same pseudoscalars in P-wave. In this way, both pseudoscalar and axial resonances will be studied together.

5

On the size and the nature of the σ meson

Contents of this Chapter:

5.1 Introduction. History of the σ meson

The lightest resonance in QCD with the quantum numbers of the vacuum, $J^{PC} = 0^{++}$, is the σ or $f_0(500)$ resonance [48]. Its connection with chiral symmetry has been stressed since the sixties in the linear sigma model [227], while its tight relation with the non-linear sigma model was realized in the nineties. In this respect there have been several papers that clearly connect this resonance with chiral dynamics of the two-pion system. One has first to mention the works of Truong and collaborators [22–24, 26] who first emphasized the important role played by the null isospin (I) S-wave $\pi\pi$ final state interactions in several processes giving

rise to a strong numerical impact on the estimations based on current algebra technique or ChPT [18, 19, 220, 221, 223]. A notoriously improved comparison with experiment was then obtained, *e.g.* for K_{ℓ_4} decays [23], $\eta \to 3\pi$ [22], scalar and pion vector form factors [24] and $\pi\pi$ scattering [26]. These works stress the role of the right-hand or unitarity cut and make use of a method to resum unitarity based on the expansion of the inverse of a form factor or scattering amplitude. This is the so called Inverse Amplitude Method (IAM), that in the end is analogous to a Paddè method of resummation. Within this technique the σ pole was first obtained in Ref. [28], together with the K^* and ρ resonances in the P-waves. However, due to the lack of coupled channels, no further light scalar resonances were generated, in particular the $f_0(980)$ and $a_0(980)$. Independently, the σ resonance pole was also obtained simultaneously in Ref. [33], together with the $I = 0$ $f_0(980)$ and $a_0(980)$ resonances. The associated amplitudes were determined by solving the Bethe-Salpeter equation taking as potential the lowest order ChPT Lagrangian. Only one free parameter (a natural sized cut-off) was involved. Later on, when the IAM was extended to coupled channels [29], it was possible to obtain in Refs. [29–31] the σ, $f_0(980)$, $a_0(980)$ and κ resonances altogether, that is, the whole nonet of the lightest scalar resonances [39, 49, 51, 53, 54, 335], together with the nonet of the lightest vector resonances.

The approach of Ref. [33], based on solving a Bethe-Salpeter equation, was put on more general grounds in Ref. [39] by applying the N/D method [38], as exposed in Sec. 2.7 in Chapter 2. In this way, it is possible to include higher orders in the chiral counting [41, 225] as well as explicit resonant fields [105] and crossed-channel dynamics, if required. Later works based on this scheme are Refs. [A, ii, B, 43]. With this approach [39] one builds a unitarized meson-meson scattering amplitude by solving the N/D equations in an algebraic way so that an approximate solution is obtained by treating perturbatively the crossed cuts. As a result, the ChPT expansion is reproduced order by order, while the unitarity cut is resummed [41]. In this respect, one should stress that the crossed cuts can be treated perturbatively for the isoscalar $\pi\pi$ S-wave. Its size was estimated to be smaller than 10% in Ref. [39] along the physical region for energies up to around 1 GeV. Indeed, different approaches with various degrees of sophistication provide very similar values for the σ pole resonance parameters, mass and width. Either by employing just the leading order (LO) ChPT [33] (without left-hand cut at all), next-to-leading order (NLO) [28] or next-to-next-to-leading order (N^{2}LO) [283]. In these two later references the left-hand cut is included as calculated by ChPT at one and two-loop orders, respectively. The fact that the results are very similar clearly indicates that the left-hand cut is indeed a perturbation. The σ pole positions in $\sqrt{s}$, with s the total center of mass energy squared, obtained in these works are: $\sqrt{s_\sigma} = 469 - i\ 194$ MeV [33], $440 - i\ 245$ MeV [28] and $445 - i\ 235$ MeV [283]. In the following we identify the mass and half width of the σ resonance from the pole position as $M_\sigma - i\,\Gamma_\sigma/2 \equiv \sqrt{s_\sigma}$.

More recently, Ref. [116], based on the solution of the Roy equations [336] and ChPT at two-loops [297,337], obtained the value $445^{+16}_{-8} - i\ 272^{+9}_{-13}$ MeV. The Roy equations implement crossing symmetry exactly, while the previous references [28, 33, 39, 283] do it perturbatively. The fact that all these pole positions for the σ lie rather close to each other (particularly one can say that convergence is reached very accurately for the real part) is another indication for the correctness of treating crossed-channel dynamics perturbatively, as done in the framework of Refs. [39, 162] (see also [E, F, 144].) Indeed, to our mind, both schemes are complementary because the Roy equations need for their implementation of the knowledge of large amount

of data in several partial waves up to high energies, which is affected by systematics errors in experiments (many of them old ones) and also in theory (*e.g.* high energy extrapolations), not always well under control. Let us also mention that all these analyses neglect altogether the inelasticity due to the 4π channel in $\pi\pi$ S-waves so that, up to the opening of the $K\bar{K}$ threshold at around 1 GeV, no inelasticity is assumed. The 4π channel was approached in Ref. [A] as $\sigma\sigma$ and $\rho\rho$ states (with their couplings to all the channels predicted from chiral dynamics) and found the σ pole at $456\pm6-i\,241\pm7$ MeV.[1] This pole position is quite close to those in the previous references and compatible with the result $484\pm17-i\,255\pm10$ MeV from Ref. [117]. Thus, since the pole positions of Refs. [A, 28, 33, 116, 117, 283] lie so close to each other we could conclude that our present knowledge on the pole position of the σ resonance is quite precise and, furthermore, we understand the underlying physics at the hadronic level.

Between earlier approaches to the previous discussed results based on ChPT concerning the lightest scalars, we have Refs. [49, 50] within the MIT bag model that already in the late seventies predicted a complete nonet of four-quark 0^{++} resonances (comprising the σ, $f_0(980)$, $a_0(980)$ and κ), with $M_\sigma = 660\pm100$ MeV and $\Gamma_\sigma = 640\pm140$ MeV. The four-quark nature of the lightest scalars is also favored in Refs. [122, 338–341] attending to scattering and production data, including two-photon fusion, J/Ψ and ϕ decays, and in Refs. [139, 267]. The important role played by two-meson unitarity for understanding the scalar sector for $\sqrt{s}\lesssim 1$ GeV was also stressed in Ref. [51] (a similar approach was later followed in Ref. [259]), employing a unitarized chiral quark model, and in Ref. [52], within the Jülich meson-exchange models. Considerations based on increasing the QCD number of colors, N_C, were exploited in Refs. [39, 136–139], showing that the σ resonance has a non-standard N_C dependence. This can be done more safely for $N_C \gtrsim 3$, not too large, while statements for $N_C \gg 3$ depend much more on fine details of the approach [138, 140–146]. QCD sum rules were also applied for the study of the lightest scalar meson, *e.g.* in Refs. [123–127]. It is argued too that the σ resonance is the chiral partner of the pion [128–134] and the way in which the σ pole evolves when approaching the chiral symmetry restoration limit is different according to the nature of this resonance [135].

From an experimental point of view new interest is triggered on the σ resonance from recent high-statistics results, *e.g.* $J/\Psi\to\omega\pi\pi$ where a conspicuous peak is seen [118]. Indeed, this decay mode was the first clear experimental signal of a σ resonance [119, 120]. Another marked peak around the σ energy region is also observed in several heavy meson decays. *E.g.* it was observed with high statistical significance in $D\to\pi^+\pi^-\pi^+$ [121]. Both types of decays present a strong peak in the σ mass energy region because the absence of the Adler zero in the pion scalar form factor, as explained in Refs. [279, 342].[2] However, for the low-energy scalar and isoscalar $\pi\pi$ scattering the presence of an Adler zero at $s\simeq m_\pi^2/2$ requires of a strong nonresonant background to cancel the pole contribution from the σ resonance, as discussed in Ref. [279]. The role of this large nonresonant background, taking into account the Adler zero constraint, was already stressed in Ref. [257] in order to understand S-wave $I=0$ $\pi\pi$ scattering. These results triggered other studies on the σ and κ resonances, *e.g.*, Refs. [54, 253, 335, 344–347]. Another field of increasing activity, both experimental [348–351]

[1] In addition this reference was able to reproduce simultaneously all the isoscalar S-wave resonances quoted in the PDG [48] from $\pi\pi$ threshold up to 2 GeV. A coherent picture of the scalar sector dynamics and spectroscopy then arose, including the identification of the lightest scalar glueball.

[2] One can explain consistently both types of decays in terms of the pion scalar form factors [279, 280, 343].

and theoretical, concerns the fusion of two photons into a pair of pions and from there to extract the width of the σ to $\gamma\gamma$ [34,352–359]. This is also expected to shed light on the nature of the σ meson [353, 354], once nonresonant background effects are properly considered. At this point, Refs. [353, 354] relies on the fact that nonresonant terms in the S-matrix mainly affect the phases of residues but not their modulus for sufficiently narrow resonances [217], which is arguable for the σ case [352, 360].

The relative strength of the σ coupling to $K\bar{K}$ compared to $\pi\pi$ is also taken as an important property in order to disentangle between different models for the nature of the σ meson ($q\bar{q}$, four-quarks, glueball or $\pi\pi$-molecule), as stressed in Ref. [123]. This reference points out that the not so much suppressed coupling of the σ to K^+K^- ($g_{\sigma K^+K^-}$), as compared with that to $\pi^+\pi^-$ ($g_{\sigma\pi^+\pi^-}$), $|g_{\sigma K^+K^-}|/|g_{\sigma\pi^+\pi^-}| = 0.37 \pm 0.06$ [123], is a key ingredient to advocate for a gluonium nature of the σ meson. According to Ref. [123], a simple $q\bar{q}$ interpretation of the σ fails to explain the large width of the σ while a four-quark scenario has difficulties to explain its large coupling to K^+K^-. It is then worth emphasizing that the T-matrices obtained in Refs. [A, 33, 39] also predict a ratio for the σ couplings to K^+K^- and $\pi^+\pi^-$ in perfect agreement with the value above of Refs. [123, 124, 361]. Explicitly, we have $|g_{\sigma K^+K^-}|/|g_{\sigma\pi^+\pi^-}| = 0.36 \pm 0.04$ from the average collected in Ref. [53]. However, in our case this stems from the dynamical generation of the σ resonance from the Goldstone boson dynamics associated to the strong scalar isoscalar $\pi\pi$ interaction. We also stress that this approach has been confronted with a large amount of data from different reactions, both scattering and production experiments, in most of the reactions already quoted in this introduction. However, the extensive phenomenological studies of Refs. [339–341, 362] obtained much smaller values for the previous ratio of couplings.

In this Chapter we report on our work in Ref. [C]. One of the main aims here is to show that the often identification of dynamically generated resonances from the interactions of two mesons (pions in our case) as meson-meson molecules is misleading. As we show here, depending on the meson mass, one can have situations where the size of a dynamically generated meson-meson resonance is certainly too small to be qualified as a two-meson molecule. Indeed, its size could be as small as that of one of the mesons involved in their formation. The fact that the σ is such a tight compact object clearly hints that the two pions pack so much that it is not meaningful anymore to keep their identities separately. At this stage, a four quark compact resonance seems a more appropriate picture. This is also supported by the N_C evolution of the σ-pole trajectory which is clearly at odds with the expectations for a purely $\bar{q}q$ or glueball resonance, but in the lines of what it is expected for a meson-meson or four quark resonance [138, 141–147]. However, by increasing the pion mass the σ resonance pole tends to follow the two pion threshold, and when it is close to the latter its size increases, becoming a spread object. This is a clear indication for the molecular character of the σ for large enough pion masses, $m_\pi \gtrsim 400$ MeV. In addition, let us also emphasize that our work is the first calculation of the size of the σ resonance. This is a novel way to study its nature in the literature.

The rest of the Chapter is organized as follows. In Sec. 5.2 we shall comment on the Lagrangians to be used in the calculations. Next we dedicate Sec. 5.3 to evaluate $\pi\pi$ scattering at one-loop order in Unitary ChPT. A wide set of data is fitted, including some recent lattice QCD determinations as a function of m_π. We pay special attention to the threshold parameters

and the σ pole position. For these quantities we also compare with previous phenomenological determinations and the lattice QCD results on the dependence of the σ pole mass as a function of the pion mass. We dedicate Sec. 5.4 to the calculation of the scalar form factor of the σ resonance. First pion scattering in the presence of a scalar source is discussed. The scalar form factor of the σ is calculated from the double σ pole present in the amplitude for the previous process, once $\pi\pi$ initial and final state interactions are taken into account. As a result, we can determine the quadratic scalar radius of the σ and then have some information on the size of this resonance. We stress that this radius is pretty small, around 0.5 fm, indicating that the σ is a compact object. We also discuss the relation between the value of the σ scalar form factor at the origin and the dependence of the σ pole with the pion mass, related by the Feynman-Hellmann theorem. Both issues, the quadratic scalar radius of the σ and the Feynman-Hellman theorem, are addressed in Sec. 5.5. Conclusions are given in Sec. 5.6. Related to the calculations in this Chapter, we dedicate Appendix B to the loop functions used throughout the amplitudes calculated, which are in turn given in Appendix C for pion scattering in the presence of a scalar source.

5.2 $SU(2)$ Chiral Lagrangians

We follow the standard ChPT counting, Eq. (1.256) and the processes under consideration, the scattering of pions with and without the presence of a c-number external scalar source, are calculated both at LO and NLO. The LO calculation has $D = 2$ with no loops ($L = 0$) and involves only $d = 2$ vertices. At NLO, $D = 4$, one has diagrams with $L = 1$ that involve only $d = 2$ vertices. There are also diagrams with $L = 0$ with only one $d = 4$ vertex, with the rest of vertices having $d = 2$. Up to NLO, $\mathcal{O}(p^4)$, one has to consider the $SU(2)$ chiral Lagrangians at $\mathcal{O}(p^2)$, $\mathcal{L}_2$, and $\mathcal{O}(p^4)$, $\mathcal{L}_4$, that we take from Ref. [18], as in Eq. (1.257). The covariant derivative ∇_μ reduces in the problem that we are studying to the standard derivative, $\nabla_\mu \to \partial_\mu$, since we do not consider here external vector nor axial-vector currents. We stress that, in the following, the pion propagators employed are $i\Delta_R(p^2)$, Eq. (1.282), in terms of the physical pion mass. This will make simpler the calculation of some diagrams for the process $\pi\pi s \to \pi\pi$. Let us also mention that the amplitudes calculated are given in terms of the physical mass and weak decay constant of the pion. The latter is given by Eq. (1.289).

5.3 $\pi\pi$ scattering and the σ meson

5.3.1 The $\pi\pi \to \pi\pi$ amplitude

The chiral Lagrangians exposed in Sec. 5.2 comprise four low energy constants (LECs), $\bar{l}_i$, at $\mathcal{O}(p^4)$. Additionally, our resummation procedure, explained below, includes a subtraction constant through the two-meson unitarity one-loop function. Before considering the $\pi\pi s \to \pi\pi$ amplitude, we must fix these free parameters. This is accomplished by comparing our results for the scalar $\pi\pi \to \pi\pi$ phase shifts with $I = 0,\ 2$ with experiment, and also other observables with lattice QCD determinations.

We denote by $\chi_n(s,t)$ the $I = 0$ $\pi\pi$ scattering amplitudes calculated from Fig. 5.1 in ChPT

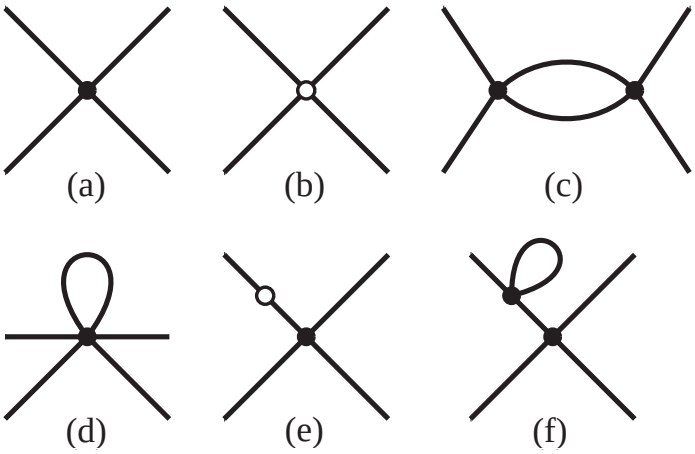

Figure 5.1: Feynman diagrams for $\pi\pi$ scattering up to NLO. Full circles represent $\mathcal{O}(p^2)$ vertices, while the empty ones correspond to the $\mathcal{O}(p^4)$ vertices.

at $\mathcal{O}(p^n)$, with $n = 2$ or 4. Their projection in S-wave are indicated by $\xi_n(s)$. Diagram a) is the LO contribution, while the rest of diagrams are the NLO ones. The last two diagrams, namely, e) and f) contribute to the wave-function renormalization of the pion external legs. We introduce the usual Mandelstam variables s, t and u. The variable s corresponds to the total energy squared of the two pions in their center of mass frame (CM), while the other two are defined as:

$$\begin{aligned} t &= -2\mathbf{p}^2(1-\cos\theta) \\ u &= -2\mathbf{p}^2(1+\cos\theta) \\ s+t+u &= 4m_\pi^2 \\ \mathbf{p}^2 &= \frac{s}{4} - m_\pi^2 \end{aligned} \tag{5.1}$$

Here, $\mathbf{p}^2$ is the three-momentum squared of the pions in their CM and θ is the scattering angle in the same reference frame. The amplitudes $\xi_n(s)$ are then given by,

$$\xi_n(s) = \frac{1}{4}\int_{-1}^{-1} \mathrm{d}\cos\theta\ \chi_n(s,t)\ . \tag{5.2}$$

In the previous equation an extra factor of $1/2$ has been included, in correspondence with the so called unitarity normalization [33]. The $I = 0$ $\pi\pi$ state is symmetric under the exchange of the two pions so that the unitarity normalization avoids having to take into account the presence of the factor $1/2$ whenever it appears as an intermediate state. In this way, the same formulas as for distinguishable particles can be employed. In what follows, we employ the unitarity normalization in all the isoscalar $\pi\pi$ matrix elements unless the opposite is stated.

Let us indicate by $T(s)$ the scalar-isoscalar unitarized $\pi\pi$ partial-wave amplitude. Following the unitarization method of Refs. [39,41], the right-hand cut or unitarity cut is resummed by the master formula:

$$T(s) = \frac{V(s)}{1+V(s)G(s)}\ . \tag{5.3}$$

As shown in Chapter 2, this formula is deduced by solving algebraically the N/D method [38, 39], treating perturbatively the crossed cuts, whereas the unitarity cut is resummed exactly.

Here, $G(s)$ is the scalar two-point function,

$$G(s) = \frac{1}{16\pi^2}\left(a + \log\frac{m_\pi^2}{\mu^2} - \sigma(s)\log\frac{\sigma(s)-1}{\sigma(s)+1}\right) , \tag{5.4}$$

with chiral order p^0. In the previous equation $\sigma(s) = \sqrt{1-4m_\pi^2/(s+i\epsilon)}$. The interaction kernel $V(s)$ has a chiral expansion, $V(s) = V_2(s)+V_4(s)+\cdots$, with the chiral order determined by the subscript. The different chiral orders of $V(s)$ are calculated by matching $T(s)$ with its perturbative expansion calculated in ChPT. In this way up to $\mathcal{O}(p^4)$,

$$\begin{aligned} T(s) &= \frac{V(s)}{1+V(s)G(s)} \\ &= \xi_2(s) + \xi_4(s) + \dots \\ &= V_2(s) + V_4(s) - V_2^2(s)G(s) + \dots , \end{aligned} \tag{5.5}$$

where the ellipsis indicate $\mathcal{O}(p^6)$ and higher orders in the expansion. It results then:

$$\begin{aligned} V_2(s) &= \xi_2(s) , \\ V_4(s) &= \xi_4(s) + \xi_2(s)^2 G(s) . \end{aligned} \tag{5.6}$$

The finite piece of the unitarity term in Fig. 5.1 (that is, the term of $\xi_4(s)$ that contains the unitarity cut and is proportional to the unitarity two-point one-loop function) is given by:

$$\xi_4^U(s) = -\xi_2^2(s)\bar{B}_0(s) . \tag{5.7}$$

Here, $\bar{B}_0(s)$ is the two-meson loop in dimensional regularization, without the $R+\log(m^2/\mu^2)$ piece (that cancels out with the other infinite and scale dependent terms, see Eqs. (B.5) and (B.6) in Appendix B.) In this way, the kernel $V(s) = V_2(s) + V_4(s)$ has no unitarity cut because:

$$\xi_4^U(s) + \xi_2^2(s)G(s) = -\xi_2^2(s)(\bar{B}_0(s) - G(s)) , \tag{5.8}$$

and the cut cancels in the r.h.s. of the previous equation. The full unitarity cut arises from the denominator $1+V(s)G(s)$ in Eq. (5.3).

In this Section we have dealt with the $I = 0$ unitarized amplitudes but, needless to say, the same formalism applies to the $I = 2$ ones, by just changing the kernel $V(s)$. We additionally note here that the same subtraction constant is used for both channels, as required by isospin symmetry [47].

5.3.2 Fits and the σ meson

At LO, there is just one free parameter corresponding to the subtraction constant in $G(s)$. At NLO, there are, in addition, four LECs, $\bar{l}_i$, $i = 1, 2, 3, 4$. For $I = 0$, the phase shifts that we fit contain the very precise data of K_{e4} decays below $\sqrt{s} = 400$ MeV [285, 363–366]. These data are corrected for isospin breaking effects, as explained in Ref. [367]. Above that energy, the data of Ref. [368] and the average of different experiments [287–290, 369, 370], as used *e.g.* in Ref. [39], are taken into account. For $I = 2$, the data come from Refs. [371, 372].

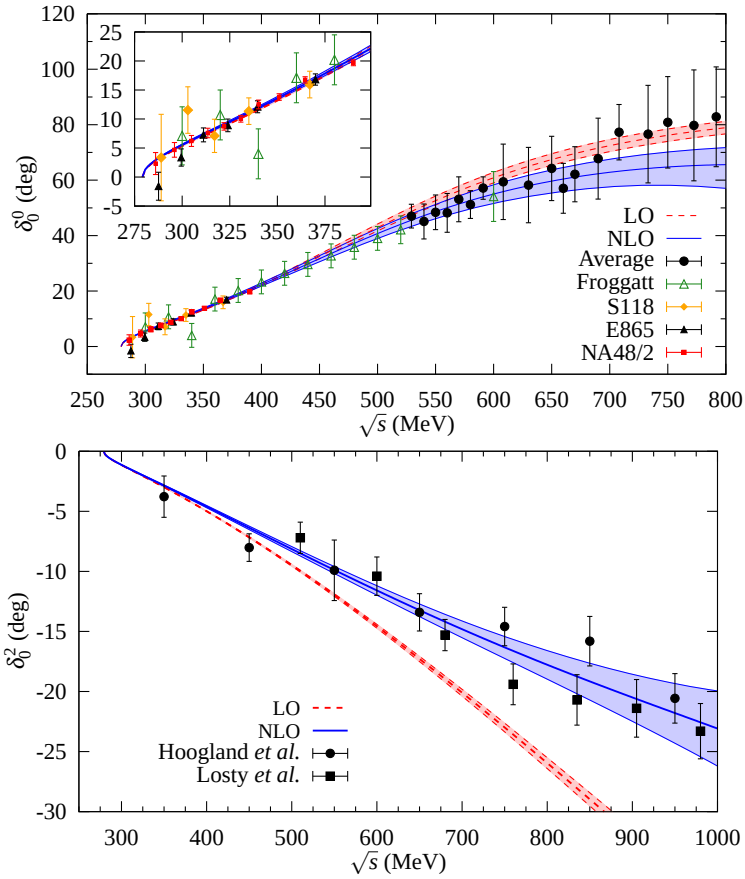

Figure 5.2: Comparison of our scalar $\pi\pi$ phase shifts to experimental data for $I = 0$ (top panel) and $I = 2$ (bottom panel). The (red) dashed line shows our fit for the LO case ($V(s) \equiv V_2(s)$), whereas the (blue) solid one shows the NLO fit ($V(s) = V_2(s) + V_4(s)$). The bands represent our uncertainties. The inset in the top panel shows in more detail the low energy K_{e4} decays data. The data for $I = 0$ are from the K_{e4} decay data of Refs. [285, 363–366] (with isospin breaking effects taken into account as in [367]) and other data from Refs. [287–290, 368–370]. For $I = 2$ the phase shifts are from Refs. [371, 372].

Table 5.1: Summary of our LO and NLO fits. In the last column the χ^2 per degree of freedom is given.

Fit	a	$\bar{l}_1$	$\bar{l}_2$	$\bar{l}_3$	$\bar{l}_4$	$\frac{\chi^2}{\text{d.o.f.}}$
LO	-1.36 ± 0.12	-	-	-	-	1.6
NLO	-1.2 ± 0.4	0.8 ± 0.9	4.6 ± 0.4	2 ± 4	3.9 ± 0.5	0.7

The fits extended to a maximum energy $\sqrt{s_{\text{max}}} = 0.8$ GeV at LO, both for $I = 0$ and $I = 2$, whereas at NLO we extend this range up to $\sqrt{s_{\text{max}}} = 1$ GeV for $I = 2$. This is not done for $I = 0$ because of the related presence of the $K\bar{K}$ threshold and the $f_0(980)$ resonance. The phase shifts are denoted by δ_0^I, with $I = 0,\ 2$. For our NLO fits we also fit recent lattice QCD results as functions of the pion mass for f_π [373, 374] and the isotensor scalar scattering length, a_0^2 [374, 375].[3] For the latter there are also the results of Ref. [376], that we show also

[3] We consider the spread of these lattice QCD results as a source of systematic error for our fits. The final errors included in the fit are depicted by the dashed error bars in Fig. 5.3.

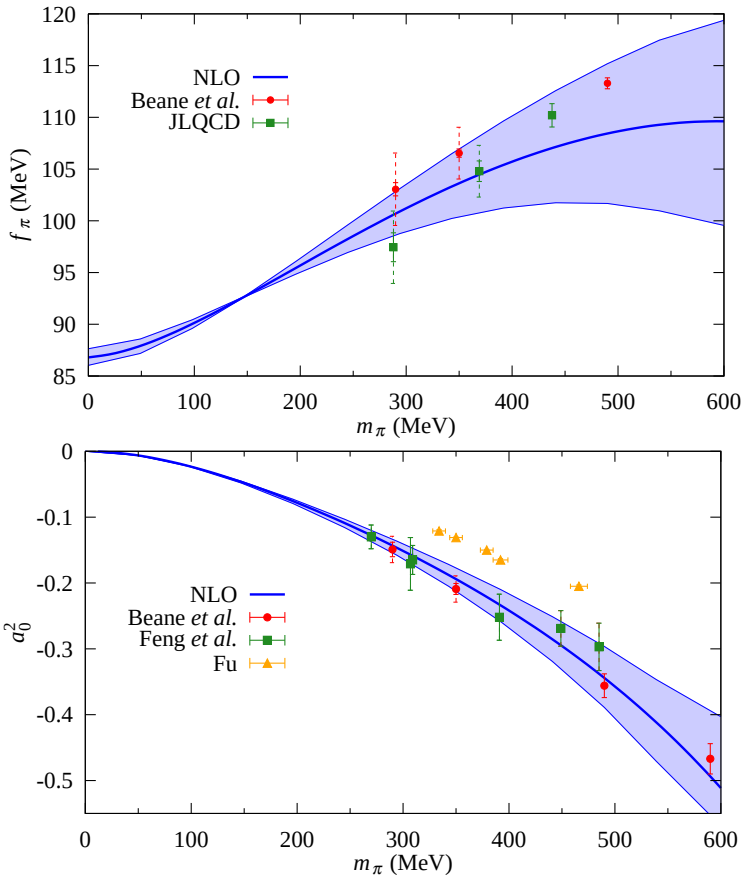

Figure 5.3: Dependence of f_π (top panel) and a_0^2 (bottom panel) with m_π as compared with lattice QCD data. The (blue) solid line is given by our NLO fit, whereas the band represents our estimated error. The data are from Refs. [373–375]. For a_0^2 we also show the data of Ref. [376], although we do not include them in our fits.

in Fig. 5.3, though they are not included in our fits. The dependence of f_π with the pion mass is calculated at NLO in ChPT, Eq. (1.289). The scattering length a_0^2 is defined through the threshold expansion in powers of $\mathbf{p}^2$ of our full results:

$$\frac{\mathrm{Re}T_0^I}{16\pi} = a_0^I + b_0^I \mathbf{p}^2 + \mathcal{O}(|\mathbf{p}|^4) \ , \tag{5.9}$$

that we extrapolate in terms of the pion mass squared.

The resulting values for the fitted parameters are given in Table 5.1. At LO the subtraction constant for the $G(s)$ function is $a = -1.36 \pm 0.12$. Four LECs appear additionally to the subtraction constant as free parameters at NLO. In order to avoid large correlation among them, the subtraction constant at NLO is constrained to remain near its value at LO. This is done by adding a new term to the χ^2 taking into account the difference between the values of a at LO and NLO, but enlarging its error at LO from 0.12 to 0.2, so that its contribution to the resulting χ^2 is tiny but enough to remove the large correlations that would appear otherwise among the LECs and the subtraction constant. The parameters of both fits (LO and NLO) are shown in Table 5.1, and the corresponding phase shifts are plotted in Fig. 5.2 with their respective errors. The left panel is for $I = 0$ and the right one for $I = 2$. The (red) dashed lines arise from our fit at LO ($V(s) \equiv V_2(s)$), whereas the (blue) solid ones show the NLO

Ref.		$\bar{l}_1$	$\bar{l}_2$	$\bar{l}_3$	$\bar{l}_4$
[18]	GL	-2.3 ± 3.7	6.0 ± 1.3	2.9 ± 2.4	4.6 ± 0.9
[337]	CGL	-0.4 ± 0.6	4.31 ± 0.11	-	4.4 ± 0.2
[377]	ABT	0.4 ± 2.4	4.9 ± 1.0	$2.5^{+1.9}_{-2.4}$	4.20 ± 0.18
[378]	PP	-0.3 ± 1.1	4.5 ± 0.5	-	-
[379]	GKMS	0.37 ± 1.96	4.17 ± 0.47	-	-
[380]	BCT	-	-	-	4.4 ± 0.3
[149]	OR	-	-	-	4.5 ± 0.3
[381]	DFGS	-	-	-15 ± 16	4.2 ± 1.0
[366]	NA48/2	-	-	2.6 ± 3.2	-
[382]	RBC-UKQCD	-	-	2.57 ± 0.18	3.83 ± 0.9
[383]	PACS-CS	-	-	3.14 ± 0.23	4.04 ± 0.19
[384]	ETM	-	-	$3.70 \pm 0.07 \pm 0.26$	$4.67 \pm 0.03 \pm 0.1$
[385, 386]	JLQCD/TWQCD	-	-	$3.38 \pm 0.40 \pm 0.24^{+0.31}_{-0}$	$4.09 \pm 0.50 \pm 0.52$
[387]	MILC	-	-	$2.85 \pm 0.81^{+0.37}_{-0.92}$	$3.98 \pm 0.32^{+0.51}_{-0.28}$
This work		0.8 ± 0.9	4.6 ± 0.4	2 ± 4	3.9 ± 0.5

Table 5.2: Comparison of different phenomenological and lattice QCD determinations of the LECs $\bar{l}_i$, $i = 1, 2, 3, 4$. Together with every reference, for an easier comparison the initials of the authors or those of the collaboration are given.

fit ($V(s) = V_2(s) + V_4(s)$). In the inset of the upper panel the agreement of our results with the lower energy data from K_{e4} decay can be appreciated. We must stress that the difference between LO and NLO manifests mostly in the $I = 2$ channel phase shifts, as can be seen in Fig. 5.2. In this channel, the left-hand cut is more important, but our amplitudes only incorporates the latter in a perturbative way, so that at NLO it is well reproduced, but it is absent at LO. In Fig. 5.3 our results for f_π (left panel) and a_0^2 (right panel) are shown, and compared with the aforementioned lattice QCD results.

In Table 5.2 we collect some phenomenological [18, 149, 337, 377–381] and lattice QCD [382–387] determinations of the LECs. For the latter the last values of each collaboration are taken, and, in addition, the direct $SU(2)$ fit results are selected if values for $SU(2)$ and $SU(3)$ fits are offered. We have also included the range obtained for $\bar{l}_3$ from the data of the NA48/2 Collaboration [366]. These determinations are compared graphically in Fig. 5.4, where for every LEC the different results are compatible within errors. The lattice QCD results concerning $\bar{l}_{1,2}$ are scarce. The JLQCD and TWQCD Collaborations [385] recently reported $\bar{l}_1 - \bar{l}_2 = -2.9 \pm 0.9 \pm 1.3$, whereas, from our fit, we obtain $\bar{l}_1 - \bar{l}_2 = -3.8 \pm 1.3$. For the phenomenological determinations in Table 5.2, since $\bar{l}_{1,2}$ agree well between each other, also the aforementioned difference between these LECs does. We finally note that from our fit we obtain at NLO ChPT that $f = 86.8 \pm 0.8$ MeV, so that $f_\pi/f = 1.065 \pm 0.010$, compatible with the estimate of lattice QCD results given in Ref. [388], $f_\pi/f = 1.073 \pm 0.015$.

Our function $G(s)$ stems from the calculation of a once-subtracted dispersion relation (see *e.g.* Ref. [39].) If, instead, it is calculated approximately by employing a three-momentum

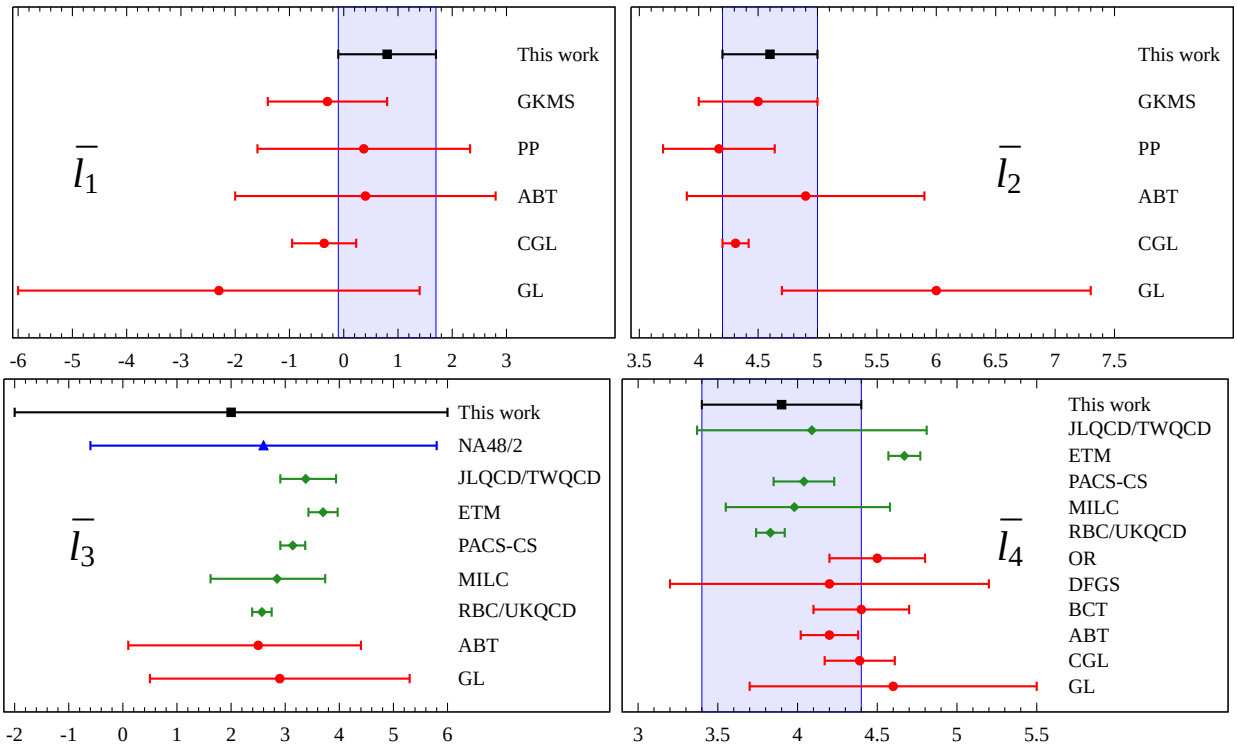

Figure 5.4: Comparison of the different lattice QCD and phenomenological determinations of the LECs collected in Table 5.2. The (green) diamonds are lattice QCD determinations, and (red) circles are the phenomenological ones. The range obtained for $\bar{l}_3$ by the NA48/2 Collaboration is represented by a (blue) triangle. The (black) squares are our results. For an easier comparison, we have included a shaded area that represents our results (except for $\bar{l}_3$.)

cut-off Λ, one has the following relation between the subtraction constant and Λ [30, 41]:

$$a(\mu) = -1 + \log \frac{e\mu^2}{4\Lambda^2} + \mathcal{O}\left(\frac{m_\pi^2}{\Lambda^2}\right) \ . \tag{5.10}$$

Our values for the fitted subtraction constant gives a cut-off $\Lambda \simeq 750$ MeV $\simeq M_\rho$, which is quite a natural value. We will make use of these considerations based on Eq. (5.10) later on, when dealing with the m_π dependence of the σ pole position.

Fit	$\sqrt{s_\sigma}$ (MeV)	a_0^0	$b_0^0 m_\pi^2$
LO	$465 \pm 2 - i\ 231 \pm 7$	0.209 ± 0.002	0.278 ± 0.005
NLO	$440 \pm 10 - i\ 238 \pm 10$	0.219 ± 0.005	0.281 ± 0.006

Table 5.3: σ pole position and threshold parameters for the isoscalar scalar partial-wave amplitude.

The σ pole appears in the second or unphysical Riemann sheet of the amplitude. This sheet is reached by changing the function $G(s)$ in the following manner [33]. For s real and above threshold we have

$$G_{\rm II}(s + i\epsilon) = G_{\rm I}(s + i\epsilon) - \Delta G(s) \ , \tag{5.11}$$

where the subscript denotes the physical (I) or the unphysical (II) Riemann sheet. In the

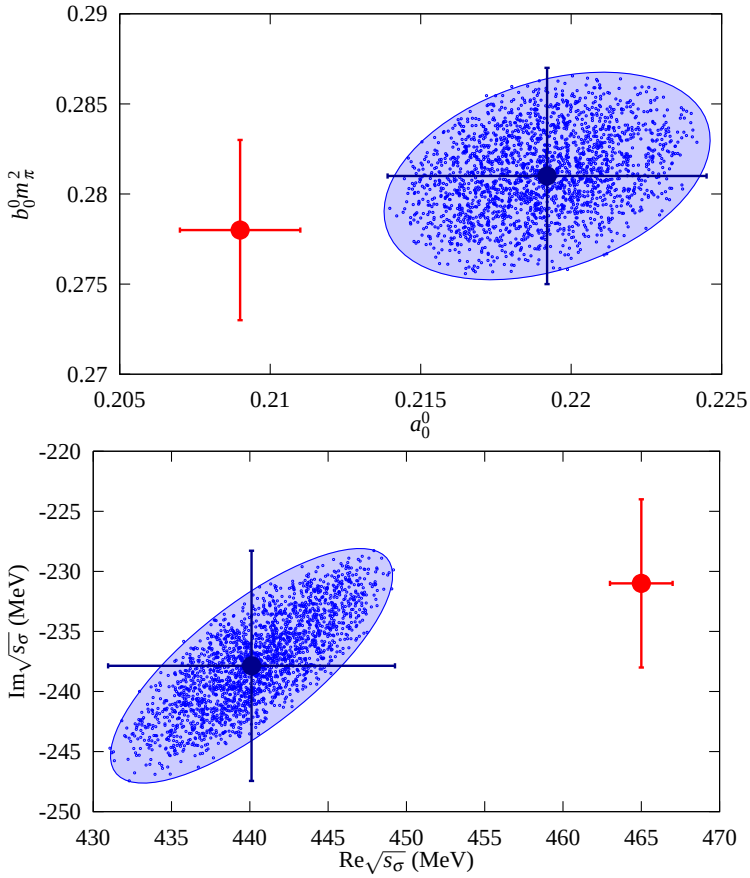

Figure 5.5: Montecarlo-like error analysis for the σ mass ($M_\sigma \equiv \mathrm{Re}\sqrt{s_\sigma}$) and half-width ($\Gamma_\sigma/2 \equiv -\mathrm{Im}\sqrt{s_\sigma}$) and threshold parameters a_0^0 and b_0^0. The (blue) error ellipses correspond to the NLO fit while the single (red) point with errors is for the LO result.

previous equation, $\Delta G(s)$ is the discontinuity along the unitarity cut,

$$\Delta G(s) = G_{\rm I}(s+i\epsilon) - G_{\rm I}(s-i\epsilon) = -i\frac{p(s)}{8\pi\sqrt{s}} \ , \tag{5.12}$$

with $p(s) = \sqrt{\mathbf{p}^2} = \sqrt{s/4 - m_\pi^2}$, the CM pion three-momentum, such that $\mathrm{Im}\, p(s) > 0$. In order to explore the unphysical Riemann sheet, one then makes the analytical extrapolation in the cut complex s plane of Eq. (5.11).

In the second sheet the σ resonance is a pole in the $I = 0$ S-wave $\pi\pi$ amplitude,

$$T_{\rm II}(s \simeq s_\sigma) = -\frac{g_\sigma^2}{s - s_\sigma} + \cdots \ , \tag{5.13}$$

being g_σ the coupling to the $\pi\pi$ channel and the ellipsis indicate the rest of terms in the Laurent series around s_σ (with $\mathrm{Im}s_\sigma < 0$.) The pole position s_σ is given in Table 5.3, together with the resulting values for the threshold parameters of the scalar-isoscalar partial wave. The σ pole position is used to define its mass and width, $M_\sigma - i\,\Gamma_\sigma/2 \equiv \sqrt{s_\sigma}$.

The error analysis for any quantities calculated here (*e.g.* the fitted values for the LECs, σ pole position, etc) is performed by randomly varying our parameters around their fitted

Ref.	M_σ (MeV)	$\Gamma_\sigma/2$ (MeV)	a_0^0	$b_0^0 m_\pi^2$
[389]	470 ± 50	285 ± 25	-	-
[116]	441^{+16}_{-8}	272^{+9}_{-13}	-	-
[117]	484 ± 17	255 ± 10	0.233 ± 0.013	0.285 ± 0.012
[A]	456 ± 12	241 ± 14	-	-
[390]	$463 \pm 6^{+31}_{-17}$	$254 \pm 6^{+33}_{-34}$	0.218 ± 0.014	0.276 ± 0.013
[123]	452 ± 12	260 ± 15	-	-
[391]	457^{+14}_{-13}	279^{+11}_{-7}	-	-
[366]	-	-	0.222 ± 0.014	-
[297]	-	-	0.220 ± 0.005	0.276 ± 0.006
This work	440 ± 10	238 ± 10	0.219 ± 0.005	0.281 ± 0.006
Average	453 ± 5	258 ± 5	0.220 ± 0.003	0.279 ± 0.003
Mean	458 ± 14	261 ± 17	0.223 ± 0.007	0.280 ± 0.004

Table 5.4: Values of M_σ, $\Gamma_\sigma/2$, a_0^0 and b_0^0 extracted from the literature. The value of Ref. [366] corresponds to the latest experiment on K_{e4} decays (with the errors added in quadrature for an easier comparison.)

values and accepting those values for the parameters which have a $\chi^2 < \chi^2_{\rm min} + \Delta\chi^2$. Here $\chi^2_{\rm min}$ is the best value for the χ^2. For the LO case, since there is just one free parameter, we give our two-sigma confidence interval (otherwise the errors would be too small), given by $\Delta\chi^2 = 4$. At NLO the one-sigma confidence interval corresponds to $\Delta\chi^2 = 5.9$. The resulting error ellipses are shown in Fig. 5.5 for the threshold parameters, upper panel, and for the σ mass and width, lower panel. Notice that since there is only one free parameter at LO then a curve results instead of an error ellipse as in NLO. This is why at LO we have just shown the resulting value with its errors.

5.3.3 The σ meson. Comparison with other determinations

We compare now our results for the σ mass and width as well as for the threshold parameters with other determinations from Refs. [A,116,117,123,389–391]. References [116,117] are recent sophisticated determinations of the pion pole position claiming to be very precise. In Ref. [A] (see Chapter 3) based on chiral Lagrangians and the implementation of the N/D method, a detailed study of meson-meson scattering in the scalar sector up to around $\sqrt{s} = 2$ GeV was performed. All the relevant channels were taken into account, even the 4π channel through the $\sigma\sigma$ and $\rho\rho$ channels whose interactions kernels were predicted making use of chiral symmetry and vector meson dominance. A good description of the data considered was achieved, which allowed a full description of the resonances experimentally seen up to that energy.[4]

The relevant quantities contained in those references are collected in Table 5.4, and compared in Figs. 5.6 and 5.7 with our LO and NLO determinations. If all these determinations can be considered as different *measures* of the same physical quantity, then they should be

[4]In Table 5.4 we double the errors of our previous determination [A], so as they have a similar size as those from other calculations. In this way the weighted average is not so much biassed from just one determination.

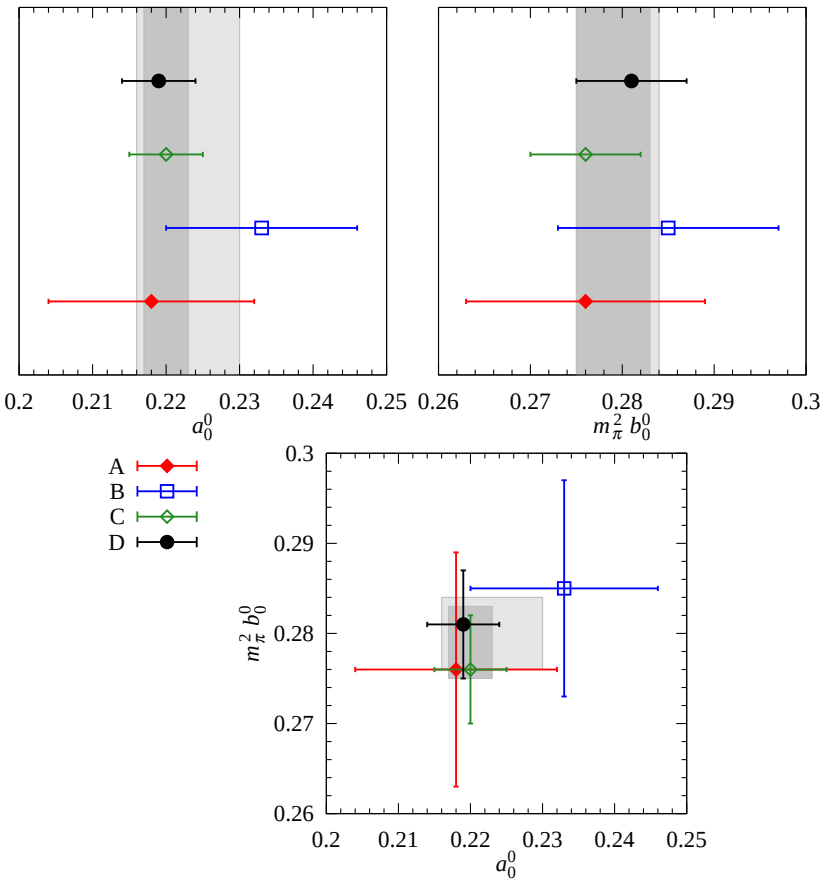

Figure 5.6: In this figure we show the values for the threshold parameters a_0^0 and b_0^0 from different papers in the literature, as indicated in the plots. In the first two panels, from left to right, the (dark gray) inner strip corresponds to the interval covered by the weighted average whereas the (light gray) outer strip is for the mean value, both given in Table 5.4. In the last panel, the rectangles correspond to the aforementioned intervals in the a_0^0–$b_0^0 m_\pi^2$ plane. The references are: A [390], B [117], C [297] and D refers to the NLO determination of this work.

compatible. A good check of their mutual compatibility is to determine whether they are compatible within errors with their weighted average.[5] These values are calculated and given in Table 5.4.

The ideal situation is that for the threshold parameters a_0 and b_0, as can be seen by simple inspection of Fig. 5.6, or directly from the values in Table 5.4. All values agree within errors with their weighted average:

$$\begin{aligned} a_0^0 &= 0.220 \pm 0.003 \ , \\ b_0^0 m_\pi^2 &= 0.279 \pm 0.003 \ . \end{aligned} \tag{5.14}$$

The latest NA48/2 Collaboration result [366] is $a_0^0 = 0.2220 \pm 0.0128_{\rm stat} \pm 0.0050_{\rm syst} \pm 0.0037_{\rm th}$, in good agreement with Eq. (5.14). For completeness we also report our result at NLO for the $I = 2$ isoscalar scattering length:

$$a_0^2 = -0.0424 \pm 0.0012 \ . \tag{5.15}$$

[5] For a given set of N independent measures x_i with their errors σ_i, the (weighted) average is given by $\bar{x} = \left(\sum_{i=1}^N x_i/\sigma_i^2\right) / \left(\sum_{i=1}^N 1/\sigma_i^2\right)$ and the standard deviation σ by $1/\sigma^2 = \sum_{i=1}^N 1/\sigma_i^2$.

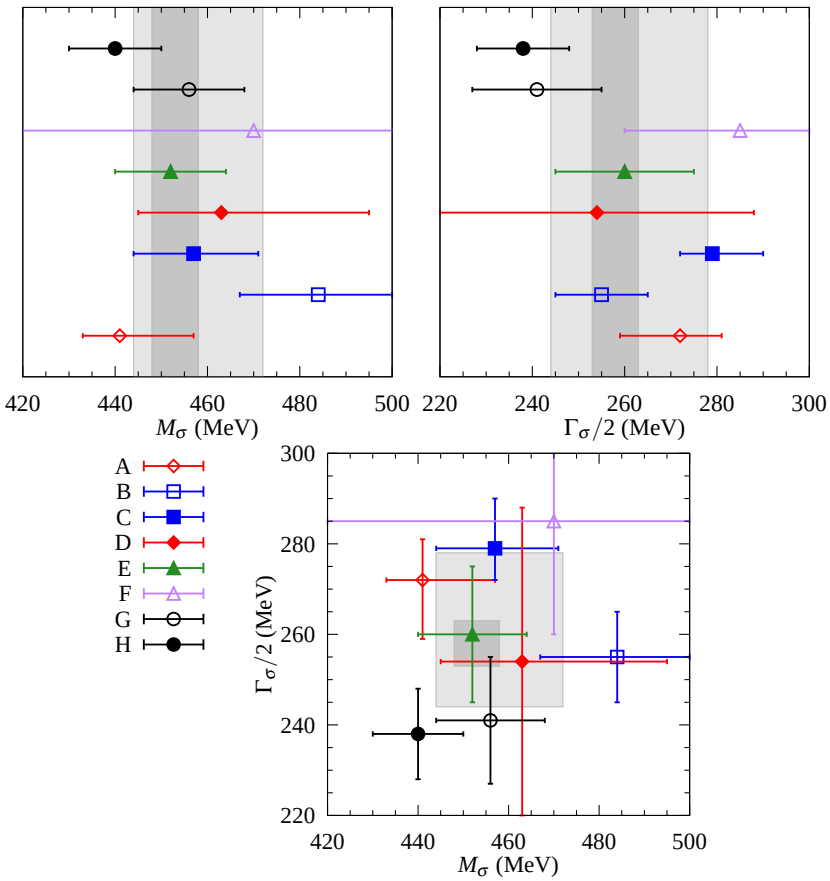

Figure 5.7: In this figure we show the values for the mass and width of the σ resonance from different papers in the literature, as indicated in the plots. In the first two panels, from left to right, the (dark gray) inner strip corresponds to the interval covered by the weighted average whereas the (light gray) outer strip is for the mean value, both given in Table 5.4. In the last panel, the rectangles correspond to the aforementioned intervals in the M_σ–$\Gamma_\sigma/2$ plane. The references are: A [116], B [117], C [391], D [390], E [123], F [389], G [A], and H refers to the NLO determination of this work.

The last value from K_{e4} decays of the NA48/2 Collaboration [366] is $a_0^2 = -0.0432 \pm 0.0086_{\rm stat} \pm 0.0034_{\rm syst} \pm 0.0028_{\rm th}$, whereas the precise determination of Ref. [297] gives $a_0^2 = -0.0444 \pm 0.0010$. At this point, it is worth stressing that our unitarized amplitudes with the kernels calculated at NLO allow a good reproduction of the low energy behavior (K_{e4} data and scattering lengths) while keeping the agreement with the higher energy data.

The case of the σ mass and width is not so mild. In Fig. 5.7 one can see that the agreement within errors of the different values with the weighted average starts at the level of $(2-3)\sigma$. At this stage it is then preferable to take the mean of the different measures instead of the weighted average. In this way we have:

$$\begin{aligned} M_\sigma &= 458 \pm 14 \text{ MeV} , \\ \Gamma_\sigma/2 &= 261 \pm 17 \text{ MeV} . \end{aligned} \tag{5.16}$$

The resulting error is around 3 times bigger than that for the weighted average over the different values considered. The different determinations agree within errors with the above

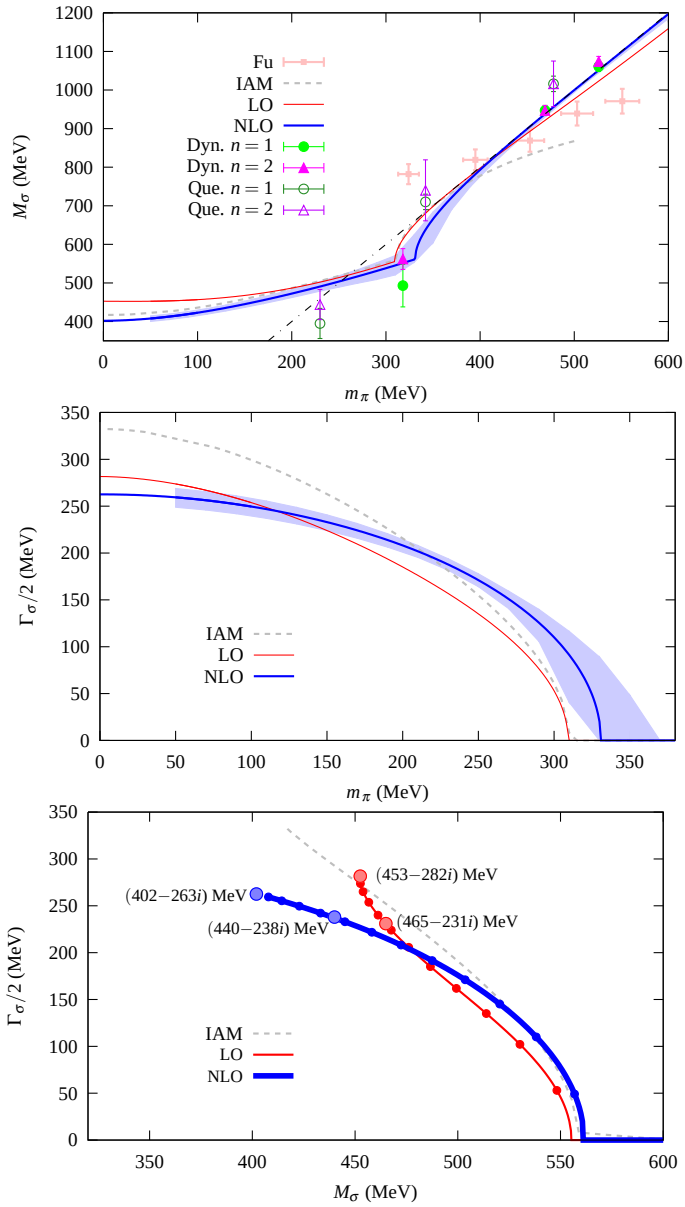

Figure 5.8: From top to bottom. First (second) panel: Mass (half width) of the σ as a function of m_π. In the last panel we show the half-width as a function of the mass of the σ while varying m_π. In the figures the (red) thinner and (blue) thicker solid lines correspond to the LO and NLO results, respectively. In the upper panel the (black) thin dot-dashed line represents the two-pion threshold, $2m_\pi$. The larger circles in the last panel highlight the chiral limit and physical case results, whereas the smaller circles represent 25 MeV steps in m_π, starting at $m_\pi = 50$ MeV. The dashed, gray lines are the results of Ref. [154]. The squares in the first panel correspond to the lattice QCD results of Ref. [392], while the rest of points are taken from Ref. [153].

result, Eq. (5.16). It can be concluded that our present knowledge on the pole position of the σ meson is quite precise, with the uncertainty of the order of few tens of MeV, lying in a range much narrower than the values nowadays reported in the PDG.

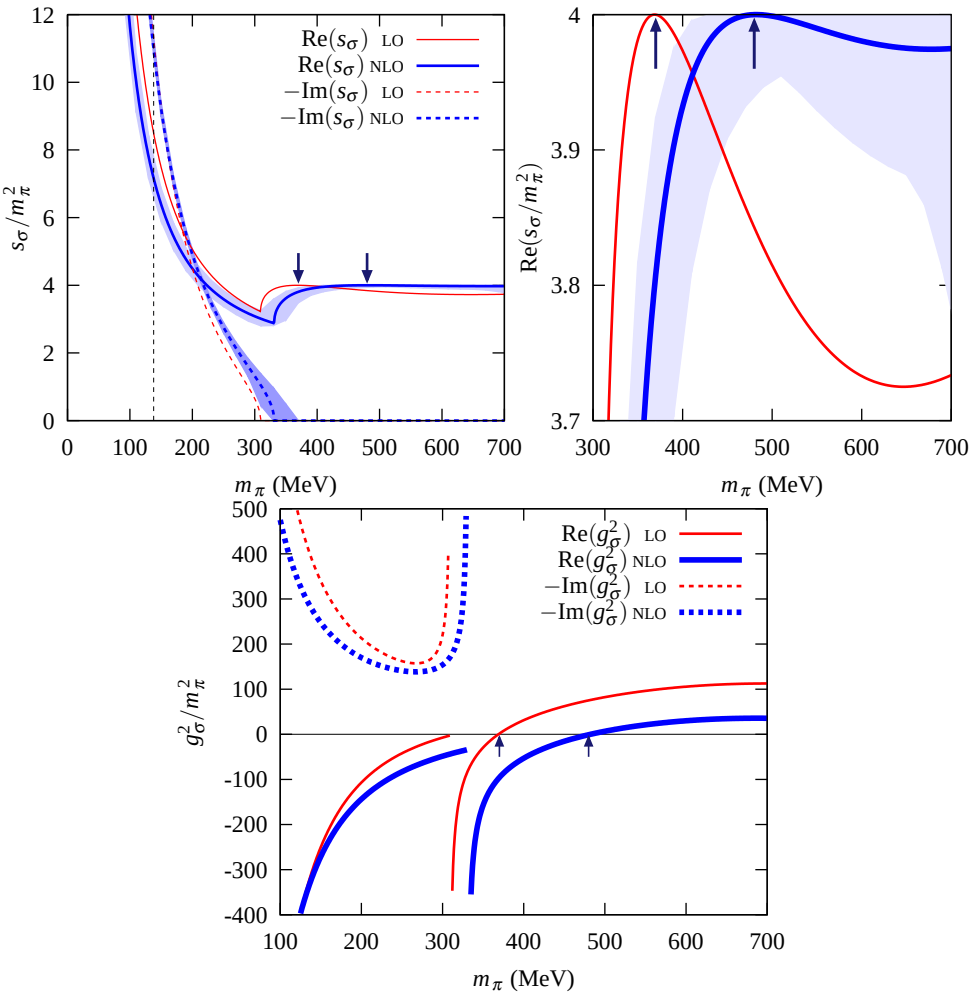

Figure 5.9: From left to right. In the first two panel we show s_σ in units of the pion mass squared as a function of m_π. The second panel shows in more detail the region for $m_\pi \geqslant 300$ MeV. In the last panel g_σ^2 is depicted in the same units. In the figure the (red) thinner solid lines are for the LO results, and the (blue) thicker solid ones correspond to NLO. The solid lines correspond to the real part of the quantity shown, whereas the dashed ones represent its imaginary part. We indicate with arrows the points at which $s_\sigma = 4m_\pi^2$ at LO and NLO.

5.3.4 Dependence with m_π of the σ meson mass and width

We can now study the evolution of the σ meson properties when the physical pion mass m_π varies (*e.g.* by changing the current quark masses in QCD.) This is an interesting problem by itself. It is also related to the form factor of the σ meson, $F_\sigma(s)$, since $\mathrm{d}s_\sigma/\mathrm{d}m_\pi^2$ and $F_\sigma(0)$ are proportional by the Feynman-Hellman theorem, as discussed below. At LO, the only changes produced by varying m_π^2 are those occurring inside the kernel $V_2(s)$ and the loop function $G(s)$. At NLO, f_π varies with m_π^2 because of Eq. (1.289), and also the LECs because it follows from Eq. (1.268) that:

$$\bar{l}_i\left(m_\pi^2\right) = \bar{l}_i\left(m_{\pi,\,\mathrm{phys}}^2\right) - \log\frac{m_\pi^2}{m_{\pi,\,\mathrm{phys}}^2}\ . \tag{5.17}$$

We can consider the subtraction constant a in the function $G(s)$ as independent of m_π in view of Eq. (5.10). With the above considerations one searches the σ pole position in the s-complex plane, s_σ, for different values of m_π, just as in the physical pion mass case. The coupling g_σ^2

is also obtained by means of the Cauchy theorem.

Before discussing this evolution, it is useful to make some analytical derivations. Let us consider the unitarized $\pi\pi$ amplitude, Eq. (5.3), as a function of both the Mandelstam variable s and the pion mass squared, $T(s, m_\pi^2)$. In the second Riemann sheet it reads:

$$T(s, m_\pi^2) = \frac{V(s, m_\pi^2)}{1 + V(s, m_\pi^2) G_{II}(s, m_\pi^2)} \ . \tag{5.18}$$

This function has a Laurent series around s_σ expressed in Eq. (5.13). Taking the derivative of $T(s, m_\pi^2)$ with respect to m_π^2 in both sides of Eq. (5.13), and attending to the double-pole terms, one obtains:

$$\dot{s}_\sigma(m_\pi^2) = -\frac{g_\sigma^2(m_\pi^2)}{V(s_\sigma, m_\pi^2)^2} \left(\dot{V}(s_\sigma, m_\pi^2) - V(s_\sigma, m_\pi^2)^2 \dot{G}_{II}(s_\sigma, m_\pi^2) \right) \ , \tag{5.19}$$

where the dot denotes derivative with respect to m_π^2. In the previous equation we have taken into account that Eq. (5.18) requires that $G_{II}(s_\sigma) = -1/V(s_\sigma)$ at the pole position s_σ.

Analogously, since $g_\sigma(m_\pi^2)^2$ is minus the residue of the pole of the amplitude in the s variable, one gets:

$$g_\sigma^2(m_\pi^2) = \frac{V(s_\sigma, m_\pi^2)^2}{V'(s_\sigma, m_\pi^2) - V(s_\sigma, m_\pi^2)^2 G'_{II}(s_\sigma, m_\pi^2)} \ , \tag{5.20}$$

where the prime denotes a derivative with respect to the s variable. One should replace $G_{II}(s_\sigma, m_\pi^2)$ by $G(s_\sigma, m_\pi^2)$ (the function in the physical Riemann sheet) in Eqs. (5.19) and (5.20) for the case when the σ pole becomes a bound state. From Eqs. (5.19) and (5.20), given the knowledge of s_σ and g_σ^2 in the physical case, the evolution of the pion pole and the coupling with m_π^2 could be studied directly. We have checked that the numerical results are the same as those obtained by looking for the pole in the complex plane for different pion masses, as explained above.

The main features of the evolution of the σ meson with m_π can be grasped by the inspection of Figs. 5.8 and 5.9. In Fig. 5.8 we show $\sqrt{s_\sigma}$ as a function of m_π, so that, M_σ is shown is the upper plane, $\Gamma_\sigma/2$ in the middle one and the plane M_σ–$\Gamma_\sigma/2$ in the panel on the bottom. The (red) thinner solid lines originate from the LO calculation, $V = V_2$, and the (blue) thicker solid ones from the NLO results, $V = V_2 + V_4$, Eq. (5.6). For the physical situation ($m_\pi \simeq 140$ MeV), we have the case just described, that is, the σ meson is seen as a pole in the unphysical Riemann sheet. As we increase m_π, the imaginary part of $\sqrt{s_\sigma}$ decreases, becoming zero at $m_\pi \simeq 310$ MeV for LO and at $m_\pi \simeq 330$ MeV for NLO.[6]

In Fig. 5.9 we show s_σ in units of the pion mass squared in the first and second panels from left to right. In the latter the scale of the ordinate axis changes and is restricted to

[6]At this point another pole (not shown in the figures) starts to appear below the σ one. This is due to the appearance of two real solutions for the equation $1 + V(s)G(s) = 0$, since the imaginary part of s_σ is zero in this region. There is no need to consider further this pole since, irrespectively of whether it lies in the same Riemann sheet than the higher pole, the effects of the latter overwhelmingly dominate over those of the former. For smaller m_π, since the solutions are not real, the σ corresponds to two complex conjugated values.

values slightly slower than $4m_\pi^2$, so that one can appreciate the evolution of the real part of s_σ and distinguish it from the line $s_\sigma = 4\,m_\pi^2$ (which is difficult to realize from the first panel for $m_\pi \geqslant 300$ MeV.) In the last panel we show g_σ^2 in the same units for varying m_π. For all the panels the solid (dashed) lines are for the real (imaginary) part, and the thicker (thinner) lines correspond to NLO (LO) results. Notice that both for LO and NLO, g_σ^2 diverges at the point where s_σ becomes purely real. Approaching this point from lower values of m_π, Im g_σ^2 diverges, whereas, approaching it from higher values of m_π then Re g_σ^2 is the one that diverges. This can be understood from the behavior of the derivative of s_σ, that is not defined precisely at this point, and in view of Eq. (5.19), where it is seen that $\dot{s}_\sigma \propto g_\sigma^2$.

For even larger values of m_π ($m_\pi \simeq 370$ MeV at LO and $m_\pi \simeq 480$ MeV at NLO), s_σ osculates the 2π threshold, while standing below it, and changes from the unphysical Riemann sheet to the physical one, becoming a bound state. Since $s_\sigma \simeq 4m_\pi^2$ close to this point, the binding energy is small, and so is the coupling, becoming exactly zero when $s_\sigma = 4m_\pi^2$. These points are indicated with arrows in Fig. 5.9. This behavior can be shown analytically. From Eq. (5.20), one deduces that for $s_\sigma \simeq 4m_\pi^2$,

$$g_\sigma^2 = -\eta\; 64\pi m_\pi \sqrt{|s_\sigma - 4m_\pi^2|}\;, \tag{5.21}$$

with $\eta = +1$ for the unphysical Riemann sheet (at the left of this point) and $\eta = -1$ for the physical Riemann sheet (at the right.) Therefore, $g_\sigma^2 = 0$ for $s_\sigma = 4m_\pi^2$, as indicated by the arrows in the rightmost panel of Fig. 5.9. However, it is worth noticing that from Eq. (5.21) it follows that $g_\sigma^2/\sqrt{|s_\sigma/4 - m_\pi^2|} \equiv g_\sigma^2/|\mathbf{p}_\sigma|$ is finite. On the other hand, the fact that the pole changes from one Riemann sheet to the other in a continuous way can be understood in terms of Eqs. (5.11) and (5.12). The difference between the $G(s)$ function calculated in the two Riemann sheets is given by a piece proportional to $\sigma(s_\sigma) = \sqrt{1 - 4m_\pi^2/s_\sigma}$ that vanishes for $s_\sigma = 4m_\pi^2$. At this point, where the σ is a zero bound state, one also has an infinite value for the scattering length.

The mere existence of this *critical* point can be examined analytically. For $s = 4m_\pi^2$, the function $G(s)$ can be written as:

$$G(s = 4m_\pi^2) = \frac{a + \log \frac{m_\pi^2}{\mu^2}}{16\pi^2} \equiv \frac{\log \frac{m_\pi^2}{\mu_a^2}}{16\pi^2}\;, \tag{5.22}$$

with $\mu_a^2 = e^{-a}\mu^2$ a new scale. If we concentrate on the simpler case of LO, $V(4m_\pi^2) = 7m_\pi^2/2f_\pi^2$, the equation for finding a pole at $s = 4m_\pi^2$, $V^{-1} + G = 0$, can be cast as $f(x) = 0$, with

$$f(x) = 1 + \alpha x \log x\;, \tag{5.23}$$

where

$$x = m_\pi^2/\mu_a^2 \tag{5.24}$$

and

$$\alpha = 7\mu_a^2/(32\pi^2 f_\pi^2) \geqslant 0\;. \tag{5.25}$$

Since $\alpha \geqslant 0$ a zero of the $f(x)$ function is only possible for $0 \leqslant x \leqslant 1$. Actually two zeros of this function exists if the value of the function at its minimum $x_0 = e^{-1}$ is negative (see

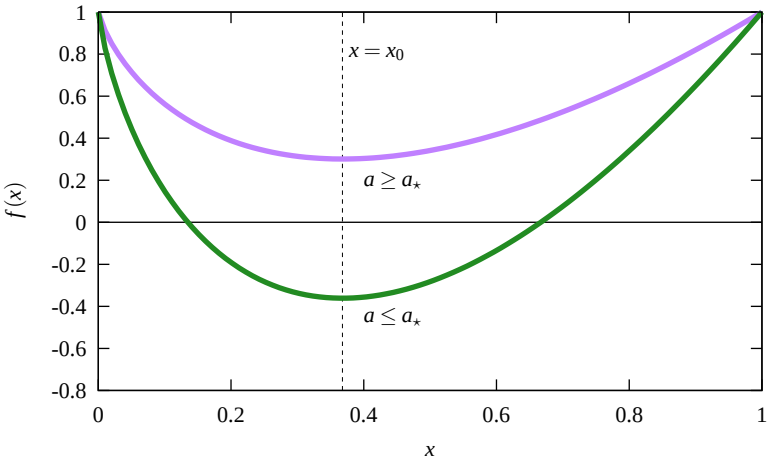

Figure 5.10: Representation of the function $f(x)$, Eq. (5.23), for two values of a, $a > a_\star$ (upper line) and $a < a_\star$ (bottom line). The variable x is defined in Eq. (5.24).

Fig. 5.10.) This condition in terms of the variable a requires that the latter is smaller than the critical value $a_\star$,

$$a_\star = -1 + \log \frac{7\mu^2}{32\pi^2 f_\pi^2} \ . \tag{5.26}$$

If this is the case there is a zero for $0 < x < x_0$ and another one for $x_0 < x < 1$. For our value of the renormalization scale, $\mu = 770$ MeV, $a_\star \simeq -0.6$, so that the fitted value $a \simeq -1.4$ given in Table 5.1 is much smaller than $a_\star$. We also have that our value for x_0 corresponds to $m_\pi \simeq 900$ MeV, then a pole with $s_\sigma = 4m_\pi^2$ exists for $0 < m_\pi < 900$ MeV. The solution of Eq. (5.23) for the value of a fitted gives that this pole is located at $m_\pi \simeq 370$ MeV, as stated above and indicated by the left most arrow in the panels of Fig. 5.9.

For the NLO case, the situation becomes somewhat more involved, and the function $f(x)$ is now:

$$f(x) = 1 + \alpha(x) x \log x \Big(1 + \alpha(x)\beta(x) x \Big) \ , \tag{5.27}$$

where $\alpha(x)$ is defined as in Eq. (5.25), but at NLO one has to take into account its implicit dependence on $x \propto m_\pi^2$ through f_π. On the other hand, $\beta(x)$ is defined as

$$\begin{aligned} \beta(x) &= \frac{40}{147} L - \frac{2}{7} \log x \ , \\ L &= \bar{l}_1^p + 2\bar{l}_2^p - \frac{3}{8}\bar{l}_3^p + \frac{21}{10}\bar{l}_4^p + \frac{21}{8} + \frac{189}{40} \log x_p \ , \end{aligned} \tag{5.28}$$

where $\bar{l}_i^p \equiv \bar{l}_i(m^2_{\pi,\mathrm{phys}})$ corresponds to the LECs calculated at the physical pion mass and

$$x_p = m^2_{\pi,\mathrm{phys}}/\mu_a^2 \ . \tag{5.29}$$

For the values collected in Table 5.1 we find that $s_\sigma = 4m_\pi^2$ for $m_\pi \simeq 480$ MeV. Nevertheless, this value is quite sensitive to the LECs, and it should be taken merely as indicative (for some values of the LECs not far from the fitted ones the change from virtual to bound state does not occur at all.) This sensitivity is illustrated by the error band in Figs. 5.8 and 5.9.

In Fig. 5.8 our results on the pion mass dependence of the σ pole position, partially presented in Ref. [v], are compared with other works. The (gray) dashed line, denoted by IAM, gives the results of Ref. [154] in the framework of the IAM. The points shown come from the lattice QCD studies of Refs. [153,392]. Interestingly, we find a remarkably good agreement with the curve from the IAM results [154] for $m_\pi \lesssim 400$ MeV. As stated by the authors, the point where $s_\sigma = 4m_\pi^2$, and thus the σ meson becomes a bound state, is $m_\pi \simeq 460$ MeV when they employed the NLO ChPT amplitudes [393], whereas $m_\pi \simeq 290$–350 MeV when the N^{2}LO ChPT amplitudes were used. We show in Fig. 5.8 the curves of Ref. [154] corresponding to this latter case.

A lattice QCD search of light scalar tetraquarks with $J^{PC} = 0^{++}$ (we focus here on the $I = 0$ results) is performed in Ref. [153]. Along with the lowest $\pi(\mathbf{p})\pi(-\mathbf{p})$ scattering state, an additional lighter state is found. For the dynamical simulations of Ref. [153] the former state is denoted in Fig. 5.8 with $n = 1$ (green filled circles) and the latter one with $n = 2$ (pink filled triangles). For the quenched simulations we use the (green) empty circles and the (purple) empty triangles, in the same order as before.[7] The points with $n = 1$ and 2 overlap at each pion mass, and the quantitative agreement with our curves is satisfactory. However, both our curves and the lattice QCD results of Ref. [153] do not agree with most of the points of the lattice QCD calculation of Ref. [392] and, in addition, the tendency of the points is qualitatively different to that for our results and those of Ref. [153].

For larger values of m_π we obtain values for the σ meson mass, both at LO and NLO, that remain below but always close to the $\pi\pi$ threshold, in agreement with the lattice QCD results of Ref. [153]. Note that this is not the case for the IAM calculation of Ref. [154] for $m_\pi \gtrsim 400$ MeV. The fact that the σ meson follows so closely the threshold for higher values of m_π, both according to our calculation and to the lattice QCD calculation of Ref. [153], clearly indicates that for such masses it is dynamically generated from the $\pi\pi$ interactions. We elaborate further on the nature of the σ resonance below. However, one should keep in mind that the σ meson becomes an anti-bound or virtual state between those pion masses in which it has zero width and has not crossed to the physical Riemann sheet yet. In the bound state case, an additional state appears in the energy levels spectrum in the box, whereas an anti-bound state does not. In order to discern the latter situation one should look at other computable quantities, such as the sign of the $I = 0$ S-wave $\pi\pi$ scattering length.

It is also interesting to study the chiral limit, $m_\pi \to 0$. As can be seen in Fig. 5.9, $s_\sigma/m_\pi^2 \to \infty$, because s_σ remains finite in this limit. Indeed, the values calculated for s_σ near the chiral limit behave as (for $m_\pi \leqslant 150$ MeV),

$$s_\sigma(m_\pi^2) = s_{\sigma,\chi} + a\, m_\pi^2 + b\, m_\pi^2 \log \frac{m_\pi^2}{M_{\pi,\mathrm{phys}}^2} \,, \tag{5.30}$$

with the values of the σ pole position in the chiral limit given by $\sqrt{s_{\sigma,\chi}} = 453 - i\,282$ MeV (LO) and $\sqrt{s_{\sigma,\chi}} = 402 - i\,263$ MeV (NLO), see Fig. 5.8.

[7] However, we must also point out that the lattice QCD simulations are performed for each pion mass at a single volume and lattice spacing, so the continuum and infinite volume values of the σ meson mass in the bound state case may differ from those values.

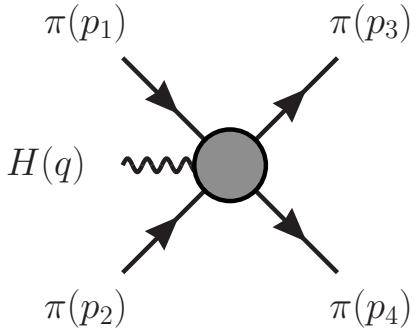

Figure 5.11: Kinematics of the $\pi\pi$ scattering process in the presence of a scalar source, $\pi(p_1)\pi(p_2)H(q) \to \pi(p_3)\pi(p_4)$. Pions correspond to the solid lines and the scalar source to the wavy one. The gray blob indicates the interactions involved.

5.4 The scalar form factor of the σ meson

We turn now our attention to the calculation of the scalar form factor of the σ meson, that is, the interaction of the σ resonance with a scalar source (denoted in the following by H.) As an intermediate step we calculate first the scattering of two pions in the presence of a scalar source, from which we extract the scalar form factor of the σ. This can be done because the σ originates as a pole in the interaction of a scalar isoscalar pair of pions, as discussed in Sec. 5.3. We start by considering in Subsec. 5.4.1 the kinematics of the $\pi\pi H \to \pi\pi$ reaction, which is somewhat more complicated than the standard kinematics of a two-body reaction. In Subsec. 5.4.2, we discuss the one-loop calculation of the amplitude $\pi\pi H \to \pi\pi$ from the chiral Lagrangians of Sec. 5.2. In terms of this amplitude one can derive the scalar form factor of the σ meson, as performed in Subsec. 5.4.3. This is accomplished by taking into account pion rescattering, similarly as done above for $\pi\pi$ scattering, with some modifications that are carefully examined.

5.4.1 Kinematics

We are interested in pion-pion scattering with a scalar source, $\pi(p_1)+\pi(p_2)+H(q) \to \pi(p_3)+\pi(p_4)$, Fig. 5.11. The overall center-of-mass frame, CM, is the same as the rest frame of the final pions, while that corresponding to the initial ones is denoted by CMB. Due to the presence of the scalar source CMB does not coincide with CM. In the CM one has

$$\begin{aligned} p_3 &= \left(\frac{\sqrt{s}}{2}, +\mathbf{p}\right), \\ p_4 &= \left(\frac{\sqrt{s}}{2}, -\mathbf{p}\right), \\ \mathbf{p}^2 &= \frac{s}{4} - m_\pi^2 \ , \end{aligned} \tag{5.31}$$

and

$$\begin{aligned} \mathbf{p}_1 + \mathbf{p}_2 &= -\mathbf{q} \\ p_1^0 + p_2^0 &= \sqrt{s} - q^0 \\ q &\equiv (q^0, \mathbf{q}) \ . \end{aligned} \tag{5.32}$$

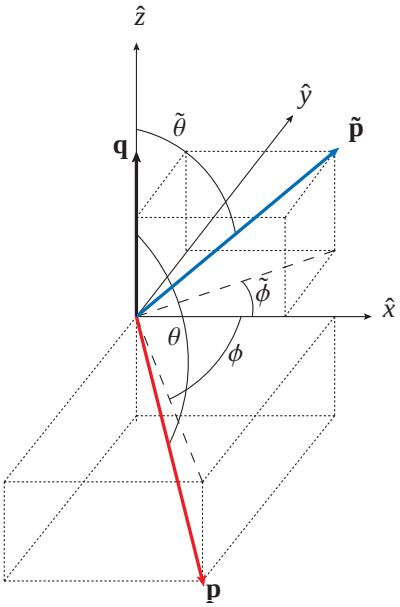

Figure 5.12: The unit three-momenta in terms of the polar and azimuthal angles.

We denote by s and s' the invariant masses squared for the final and initial pions, in order. At the end of the calculation, the limit $s,\ s' \to s_\sigma$ is taken. It follows that

$$(p_1+p_2)^2 = s' = \left(\sqrt{s}-q^0\right)^2 - \mathbf{q}^{\,2} = s + q^2 - 2q^0\sqrt{s}\ , \tag{5.33}$$

and then,

$$\begin{aligned} q^0 &= \frac{s-s'+q^2}{2\sqrt{s}}\ , \\ \mathbf{q}^2 &= \frac{(s+s'-q^2)^2}{4s} - s'\ . \end{aligned} \tag{5.34}$$

Analogously, one has in CMB:

$$\begin{aligned} p_1 &= \left(\frac{\sqrt{s'}}{2}, +\tilde{\mathbf{p}}\right)\ , \\ p_2 &= \left(\frac{\sqrt{s'}}{2}, -\tilde{\mathbf{p}}\right)\ , \\ \tilde{\mathbf{p}}^2 &= \frac{s'}{4} - m_\pi^2\ , \\ \tilde{q}^0 &= \frac{s-s'-q^2}{2\sqrt{s'}}\ , \\ \tilde{\mathbf{q}}^2 &= \frac{(s+s'-q^2)^2}{4s'} - s\ . \end{aligned} \tag{5.35}$$

In the following quantities with a tilde are expressed in CMB. Notice that $\tilde{\mathbf{p}}$ is the three-momentum of the first pion in CMB, while $\mathbf{p}$ refers to the three-momentum of the third pion in CM.

The final (initial) two-pion states are projected into S-wave in CM (CMB) because the σ resonance is defined as a pole in the second Riemann sheet of the $\pi\pi$ isoscalar S-wave in CM (CMB). The unit three-momenta (indicated with a hat) are given in terms of the polar and azimuthal angles (see Fig. 5.12) as:

$$\begin{aligned} \hat{\mathbf{p}} &= (\sin\theta\cos\phi, \sin\theta\sin\phi, \cos\theta) \ , \\ \hat{\tilde{\mathbf{p}}} &= \left(\sin\tilde{\theta}\cos\tilde{\phi}, \sin\tilde{\theta}\sin\tilde{\phi}, \cos\tilde{\theta}\right) \ , \\ \hat{\mathbf{q}} &= (0,0,1) \ , \end{aligned} \tag{5.36}$$

where we have chosen the z-axis to be the direction pointed by $\hat{\mathbf{q}}$. We now work out the Lorentz transformation from CMB to CM:

$$\begin{aligned} (p_1+p_2)_{CMB} &= \left(\sqrt{s'}, \vec{0}\right) \ , \\ (p_1+p_2)_{CM} &= \left(\sqrt{s}-q^0, -\mathbf{q}\right) = (\frac{s+s'-q^2}{2\sqrt{s}}, -\mathbf{q}\,) \ . \end{aligned} \tag{5.37}$$

The transformation reads:

$$\begin{aligned} \frac{s+s'-q^2}{2\sqrt{s}} &= \gamma\sqrt{s'} \ , \\ -\mathbf{q} &= -\gamma\sqrt{s'}\mathbf{v} \ . \end{aligned} \tag{5.38}$$

It follows then that $\gamma = 1/\sqrt{1-\mathbf{v}^2}$ and $\mathbf{v}$ are

$$\gamma = \frac{s+s'-q^2}{2\sqrt{s}\sqrt{s'}} \ , \tag{5.39}$$

$$\mathbf{v} = \frac{\mathbf{q}}{\gamma\sqrt{s'}} = \frac{2\sqrt{s}}{s+s'-q^2}\mathbf{q} \ . \tag{5.40}$$

We further define the four-momenta Σ and Δ given by

$$\begin{aligned} \Sigma &\equiv (p_1+p_2) \ , \\ \Delta &\equiv (p_1-p_2) \ . \end{aligned} \tag{5.41}$$

In the CM

$$\Sigma = \left(\sqrt{s}-q^0, -\mathbf{q}\right) \ . \tag{5.42}$$

The momentum transfer Δ has a simple expression in CMB where it is given by $\Delta = (0, 2\tilde{\mathbf{p}})$. We then perform its Lorentz transformation to CM, with the result

$$\begin{aligned} \Delta^0 &= -2\frac{\mathbf{q}\cdot\tilde{\mathbf{p}}}{\sqrt{s'}} \ , \\ \mathbf{\Delta} &= 2\tilde{\mathbf{p}} + 2\,(\gamma-1)\,|\tilde{\mathbf{p}}|\,(\hat{\mathbf{p}}\cdot\hat{\mathbf{q}})\,\hat{\mathbf{q}} \ . \end{aligned} \tag{5.43}$$

The problem has six independent Lorentz invariant kinematical variables.[8] We define, in analogy with two body scattering, the following six alike Mandelstam variables,

$$s = (p_3+p_4)^2 \ ,$$

[8] One the five four-momenta involved in the reaction is fixed by energy-momentum conservation. From the other four ones we can construct 6 independent scalar products. Notice that $p_1^2 = p_2^2 = p_3^2 = m_\pi^2$ and that q^2 can be derived from Eq. (5.45) in terms of other Lorentz invariants.

$$\begin{aligned} s' &= (p_1+p_2)^2 \ , \\ t &= (p_1-p_3)^2 \ , \\ t' &= (p_2-p_4)^2 \ , \\ u &= (p_1-p_4)^2 \ , \\ u' &= (p_2-p_3)^2 \ . \end{aligned} \tag{5.44}$$

These variables fulfill the relationship

$$s+t+u+s'+t'+u' = q^2+8m_\pi^2 \ , \tag{5.45}$$

which is the analogous one to $s+t+u=4m_\pi^2$ valid for two-pion scattering, Eq. (5.1). Though q^2 and the variables in Eq. (5.44) are not independent because of Eq. (5.45), it is convenient to write the different amplitudes $\pi\pi H \to \pi\pi$ in terms of all of them, given the symmetries present in the calculation.

In virtue of the previously worked Lorentz transformation, Eq. (5.40), we have the four-momenta properly defined in CM in terms of the key variables s, s', q^2 and the polar and azimuthal angles in the two-pion center of mass frames (the Lorentz invariants only depend on the difference between the azimuthal angles, see Eq. (5.47) below.) It is convenient to express $p_1=(\Sigma+\Delta)/2$ and $p_2=(\Sigma-\Delta)/2$, with Σ and Δ given in CM by Eqs. (5.42) and (5.43). In terms of this set of variables, the Lorentz invariants of Eq. (5.44) are given by

$$\begin{aligned} t &= 2m_\pi^2 - 2\,(\alpha+A+B+C) \ , \\ t' &= 2m_\pi^2 - 2\,(\alpha-A-B+C) \ , \\ u &= 2m_\pi^2 - 2\,(\alpha+A-B-C) \ , \\ u' &= 2m_\pi^2 - 2\,(\alpha-A+B-C) \ , \end{aligned} \tag{5.46}$$

where

$$\begin{aligned} \alpha &= \frac{1}{2}\Sigma^0\cdot p_{3,4}^0 = \frac{1}{8}(s+s'-q^2) \ , \\ A &= \frac{1}{2}\Delta^0\cdot p_{3,4}^0 = -\frac{1}{2}\,|\mathbf{q}\,|\,|\tilde{\mathbf{p}}|\,\frac{\sqrt{s}}{\sqrt{s'}}\cos\tilde{\theta} \ , \\ B &= -\frac{1}{2}\vec{\Sigma}\cdot\mathbf{p} = +\frac{1}{2}\,|\mathbf{q}\,|\,|\mathbf{p}|\cos\theta \ , \\ C &= -\frac{1}{2}\vec{\Delta}\cdot\mathbf{p} = -|\mathbf{p}||\tilde{\mathbf{p}}|\left(\hat{\mathbf{p}}\cdot\hat{\tilde{\mathbf{p}}} + \frac{(\sqrt{s}-\sqrt{s'})^2-q^2}{2\sqrt{s}\sqrt{s'}}\cos\theta\cos\tilde{\theta}\right) \ . \end{aligned} \tag{5.47}$$

In the previous equation the five kinematical variables, s, s', q^2, $\cos\theta$, $\cos\tilde{\theta}$ are used together with the scalar product

$$\hat{\mathbf{p}}\cdot\hat{\tilde{\mathbf{p}}} = \sin\theta\,\sin\tilde{\theta}\cos(\phi-\tilde{\phi}) + \cos\theta\,\cos\tilde{\theta} \ . \tag{5.48}$$

In terms of the variables in Eq. (5.44) one can express the inverses of several pion propagators that appear in many Feynman diagrams that contain the scalar source attached to an external pion leg, *cf.* diagram (a.2) of Fig. 5.13. It results:

$$D_1 = (q+p_1)^2 - m_\pi^2 = s\ + t' + u' - 4m_\pi^2 \ ,$$

$$
\begin{aligned}
D_2 &= (q+p_2)^2 - m_\pi^2 = s\ + t\ + u\ - 4m_\pi^2\ , \\
D_3 &= (q-p_3)^2 - m_\pi^2 = s' + t' + u\ - 4m_\pi^2\ , \\
D_4 &= (q-p_4)^2 - m_\pi^2 = s' + t\ + u' - 4m_\pi^2\ .
\end{aligned}
\tag{5.49}
$$

Because of Eqs. (5.47), the angular dependence of these inverse propagators is rather simple: D_1 and D_2 depend just on $\cos\tilde{\theta}$, while D_3 and D_4 do on $\cos\theta$. The propagating pion can become on-shell for certain angles, giving rise to a pole in the propagators. These poles, when the S-wave angular projections are performed, result in logarithmic divergences. In particular, there is always a pole for $q^2 \to 0$. We treat this issue later on.

5.4.2 The $\pi\pi\, H \to \pi\pi$ scattering amplitude

To determine the Feynman diagrams required for the $\pi\pi$ scattering in the presence of a scalar source up to $\mathcal{O}(p^4)$ in ChPT it is useful to have in mind first those diagrams of plain $\pi\pi$ scattering in Sec. 5.3, Fig. 5.1. Now, one external scalar source has to be added in all the possible ways to those diagrams. As deduced from the Lagrangians $\mathcal{L}_2$ and $\mathcal{L}_4$, Eqs. (1.257), the scalar source can couple to any even number of pions. In Fig. 5.13 we show the diagrams that must be calculated at the one-loop level, where the external scalar source is indicated by a wiggly line. The LO diagrams correspond to (a.1) and (a.2).[9] Diagrams (a.2), (e.1) and (f.1) can be handled together because their sum corresponds to taking the full pion propagator in between the external source and the four-pion vertex, Eqs. (1.282), (1.283) and (1.288). In addition, all the diagrams on the bottom line of Fig. 5.13, namely, ($\tilde{\text{e}}$.1)–($\tilde{\text{f}}$.3), correspond to the wave function renormalization of the LO ones. Both issues are derived to NLO from the pion self-energy diagrams, Fig. 1.6, Eq. (1.288). Once the the renormalization of the pion propagator and the the wave function renormalization are taken into account, as well as the rest of diagrams diagrams in Fig. 5.13, one has the basic topologies shown in Fig. 5.14.

Compared with $\pi\pi$ scattering the presence of the c-number external scalar source H complicates considerably the simple expressions for the former [18]. The calculation for each of the diagrams in Fig. 5.14 is given in Appendix C. Specifically, we calculate the processes $\pi^0(p_1)\pi^0(p_2)H(q) \to \pi^0(p_3)\pi^0(p_4)$ and $\pi^0(p_1)\pi^0(p_2)H(q) \to \pi^+(p_3)\pi^-(p_4)$, with the former denoted by T_{nn} and the latter by T_{nc}. These two processes are considered in order to isolate the pion pairs with definite isospin (I) by taking the appropriate linear combinations. The standard decomposition of the $\pi^0\pi^0$ and $\pi^+\pi^-$ states in two-pion isospin definite states, $|\pi\pi(I I_3)\rangle$, being I_3 the third-component of isospin, is

$$
\begin{aligned}
|\pi^0\pi^0\rangle &= \sqrt{\frac{2}{3}}|\pi\pi(20)\rangle - \sqrt{\frac{1}{3}}|\pi\pi(00)\rangle\ , \\
|\pi^+\pi^-\rangle &= -\sqrt{\frac{1}{6}}|\pi\pi(20)\rangle - \sqrt{\frac{1}{2}}|\pi\pi(10)\rangle - \sqrt{\frac{1}{3}}|\pi\pi(00)\rangle\ ,
\end{aligned}
$$

where we have taken into account that $|\pi^+\rangle = -|\pi; I = 1\, I_3 = -1\rangle$, as follows from the definition of the π^+ field, Eq. (1.260). Because of isospin conservation (the scalar source $H(q)$

[9] Of course, the scalar source can be attached to any of the pion legs but for conciseness we draw explicitly the attachment to only one. This should be understood in the following.

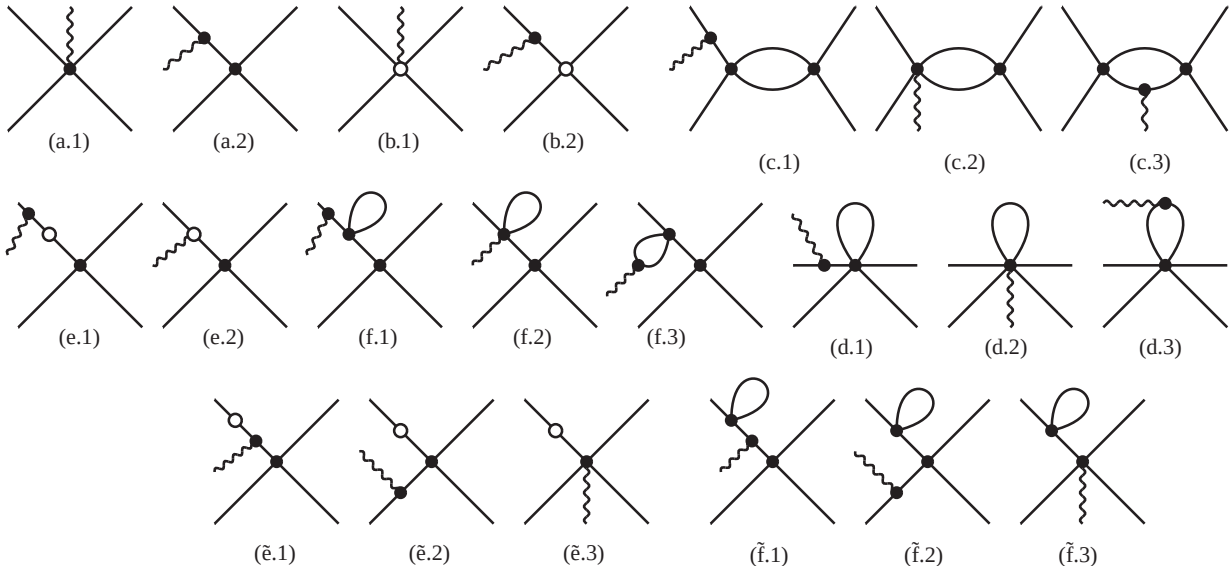

Figure 5.13: Feynman diagrams for the $\pi\pi$ scattering amplitude in the presence of a scalar source, $\pi\pi\, H \to \pi\pi$, at one-loop order in ChPT.

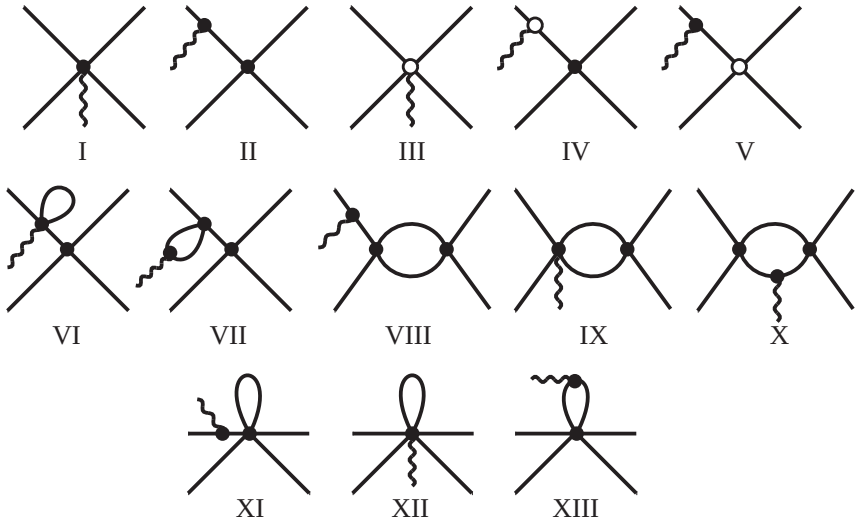

Figure 5.14: Final set of Feynman diagrams for the $\pi\pi$ scattering in the presence of a scalar source, $\pi\pi\, H \to \pi\pi$, at $\mathcal{O}(p^4)$ in ChPT omitting the pion propagator dressing and wave function renormalization of the leading order diagrams in Fig. 5.13.

is isoscalar), the Wigner-Eckart theorem implies

$$\begin{aligned}\langle\pi^0\pi^0|\mathcal{S}|\pi^0\pi^0\, s\rangle &= +\frac{2}{3}\langle\pi\pi(20)|\mathcal{S}|\pi\pi(20)H\rangle \\ &\quad +\frac{1}{3}\langle\pi\pi(00)|\mathcal{S}|\pi\pi(00)H\rangle\ , \\ \langle\pi^+\pi^-|\mathcal{S}|\pi^0\pi^0\, s\rangle &= -\frac{1}{3}\langle\pi\pi(20)|\mathcal{S}|\pi\pi(20)H\rangle \\ &\quad +\frac{1}{3}\langle\pi\pi(00)|\mathcal{S}|\pi\pi(00)H\rangle\ ,\end{aligned} \tag{5.50}$$

with $\mathcal{S}$ the S-matrix. From this equation we can isolate the purely $I = 0$ matrix element,

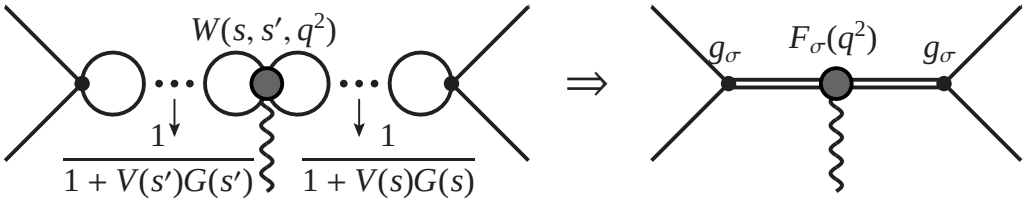

Figure 5.15: External scalar source coupled to a double σ pole in the $\pi\pi\, H \to \pi\pi$ process. The σ pole is originated by the resummation of pion re-scattering, as indicated in the left diagram by the iteration of the unitarity two-point function.

$\mathcal{A}(s, s', q^2, \theta, \tilde{\theta}, \phi, \tilde{\phi})$, corresponding to

$$\mathcal{A}(s, s', q^2, \theta, \tilde{\theta}, \phi, \tilde{\phi}) \equiv \langle \pi\pi(00)|\mathcal{S}|\pi\pi(00)H\rangle \ . \tag{5.51}$$

From Eq. (5.50), we have:

$$\begin{aligned}\mathcal{A}(s, s', q^2, \theta, \tilde{\theta}, \phi, \tilde{\phi}) &= \langle \pi^0\pi^0|\mathcal{S}|\pi^0\pi^0\, s\rangle + 2\langle \pi^+\pi^-|\mathcal{S}|\pi^0\pi^0\, s\rangle \\ &= T_{nn} + 2T_{nc} \ .\end{aligned} \tag{5.52}$$

We are interested in this matrix element because the σ is isoscalar.

The σ is an S-wave resonance so that it is also required the S-wave angular projection of the initial and final isoscalar pion pairs. This is straightforward for the final pions because the CM coincides with its own rest frame, with the result:

$$|\pi\pi; 00\rangle_{34} \equiv \frac{1}{4\pi}\int d\hat{\mathbf{p}}\, |\pi(p_3)\pi(p_4)(00)\rangle \ . \tag{5.53}$$

Regarding the initial pair of pions, its state is defined in CMB analogously as in the previous expression. One has still to perform the Lorentz boost to the CM frame so that

$$|\pi\pi; 00\rangle_{12} \equiv U(\mathbf{v})\frac{1}{4\pi}\int d\hat{\tilde{\mathbf{p}}}\, |\pi(\frac{\sqrt{s'}}{2}, \tilde{\mathbf{p}})\pi(\frac{\sqrt{s'}}{2}, -\tilde{\mathbf{p}})(00)\rangle \ , \tag{5.54}$$

where $U(\mathbf{v})$ is the Lorentz boost operator from CMB to CM, with the velocity $\mathbf{v}$ given in Eq. (5.40). When acting on the pion states (which have zero spin) the only effect is the transformation of the four-momenta from CMB to CM. Then, we can also write Eq. (5.54) as

$$|\pi\pi; 00\rangle_{12} = \frac{1}{4\pi}\int d\hat{\tilde{\mathbf{p}}}\, |\pi(p_1(\tilde{\mathbf{p}}))\pi(p_2(\tilde{\mathbf{p}}))(00)\rangle \ , \tag{5.55}$$

where p_1 and p_2 are written in terms of the four-momenta in CMB. From Eq. (5.41), $p_1 = (\Sigma + \Delta)/2$, $p_2 = (\Sigma - \Delta)/2$ with Σ and Δ given in Eqs. (5.42) and (5.43), in order, as a function of the CMB kinematical variables.

Employing the states projected in S-wave, Eqs. (5.53) and (5.55), we are then ready to calculate the required matrix element in ChPT, $\varphi(s, s', q^2)$:

$$\varphi(s, s', q^2) \equiv \frac{1}{32\pi^2}\int \mathrm{d}^2\Omega\ \mathcal{A}(s, s', q^2, \theta, \tilde{\theta}, \phi, \tilde{\phi}) \ . \tag{5.56}$$

Note that the extra factor 1/2 in Eq. (5.56) arises because of the unitary normalization, as explained after Eq. (5.2). In the last equation, the double solid angle integration is

$$\int \mathrm{d}^2\Omega = \int_{-1}^{1} \mathrm{d}\cos\theta \int_{-1}^{1} \mathrm{d}\cos\tilde{\theta} \int_0^{2\pi} \mathrm{d}\phi \int_0^{2\pi} \mathrm{d}\tilde{\phi} \ . \tag{5.57}$$

One linear combination of azimuthal angles, ϕ and $\tilde{\phi}$, is a spare variable, and then one integration in Eq. (5.57) is trivial. This is so because they appear just through the expression $\cos(\phi - \tilde{\phi})$, as explained above, Eq. (5.47). In fact, for any periodic angular function, $f(\gamma) = f(\gamma + 2\pi)$, one has:

$$\int_0^{2\pi} \mathrm{d}\phi \int_0^{2\pi} \mathrm{d}\tilde{\phi} \ f(\phi - \tilde{\phi}) = 2\pi \int_0^{2\pi} \mathrm{d}\gamma \ f(\gamma) \ . \tag{5.58}$$

5.4.3 Scalar form factor

Once the perturbative amplitude for the process $\pi\pi\, H \to \pi\pi$ is calculated, we proceed by taking into account pion rescattering, similarly as was done for $\pi\pi \to \pi\pi$, see Eqs. (5.3)-(5.6). The resulting amplitude is denoted by $T_S(s, s', q^2)$, and following the same unitarization method as in Sec. 5.3 from Refs. [39, 41], it can be written as:

$$T_S(s, s', q^2) = \frac{W(s, s', q^2)}{(1 + V(s)G(s))\,(1 + V(s')G(s'))} \ . \tag{5.59}$$

This is the analog to Eq. (5.3) but now for the process $\pi\pi\, H \to \pi\pi$, with the new kernel $W(s, s', q^2)$ instead of $V(s)$ in Eq. (5.3). It is important to stress the presence of two factors $1 + VG$ in the denominator of Eq. (5.59). This is so because in $\pi\pi\, H \to \pi\pi$ the presence of the scalar source $H(q)$ makes necessary to resum the unitarity loops corresponding to both final and initial state interactions.

The kernel $W(s, s', q^2)$ is obtained in a chiral expansion by matching Eq. (5.59) order by order with its perturbative calculation. The chiral expansion of the kernel is

$$W = W_2 + W_4 + \mathcal{O}(p^6) \ , \tag{5.60}$$

where we omit the dependence on the arguments s, s' and q^2 for easy reading. The subscripts in Eq. (5.60) refer to the chiral order. Then, the amplitude Eq.(5.59) is expanded, as it was done in Eq. (5.5), so that one has:

$$\begin{aligned} T_S(s, s', q^2) =& W_2 + W_4 \\ & - W_2 V_2(s) G(s) - W_2 V_2(s') G(s') + \mathcal{O}(p^6) \\ =& \varphi_2 + \varphi_4 + \mathcal{O}(p^6) \ , \end{aligned} \tag{5.61}$$

where $\varphi_n(s, s', q^2)$ is the $\mathcal{O}(p^n)$ contribution to $\varphi(s, s', q^2)$ defined in Eq. (5.56). The kernels $W_n(s, s', q^2)$ are determined by matching the above expressions order by order, so that:

$$\begin{aligned} W_2(s, s', q^2) &= \varphi_2(s, s', q^2) \\ W_4(s, s', q^2) &= \varphi_4(s, s', q^2) + \varphi_2\, \xi_2(s) G(s) + \varphi_2\, \xi_2(s') G(s') \ , \end{aligned} \tag{5.62}$$

where it was used that $V_2(s) = \xi_2(s)$, Eq. (5.6).

The form factor of the σ meson, $F_\sigma(q^2)$, can now be extracted from $T_S(s, s', q^2)$, employing $W = W_2 + W_4$ in Eq. (5.59). For that one has to isolate the double σ pole present in $T_S(s, s', q^2)$, as drawn on the right-hand side of Fig. 5.15. The double σ-pole contribution can be written as:[10]

$$\frac{F_\sigma(q^2)\ g_\sigma^2}{(s - s_\sigma)(s' - s_\sigma)} = \lim_{s,s' \to s_\sigma} \frac{W(s, s', q^2)}{(1 + V(s)G(s))\,(1 + V(s')G(s'))} \tag{5.63}$$

Expanding the r.h.s. of the above equation around $s, s' \to s_\sigma$, and equating the double-pole term, the result is:

$$F_\sigma(q^2) = \frac{g_\sigma^2}{V(s_\sigma)^2} W(s_\sigma, s_\sigma, q^2)\ . \tag{5.64}$$

In determining the kernels $W_n(s, s', q^2)$, we have followed the master guidelines of pure $\pi\pi$ scattering procedure to take into account the rescattering of the pions given in Sec. 5.3.1. However, some modifications are needed in our case because of the presence of the pion propagators in the external pion legs attached to a scalar source, see Fig. 5.14. Let us focus, for clearness, in the LO amplitudes $\varphi_2(s, s', q^2)$, corresponding to the diagrams I and II in Fig. 5.14 (the amplitudes are given in Appendix C). Before the angular projection in Eq. (5.56), one has

$$\mathcal{A}_2(s, s', q^2, \theta, \tilde{\theta}, \phi, \tilde{\phi}) = -\frac{2B}{f_\pi^2}\left(1 - 2\sum_{i=1}^{4} \frac{s_i - m_\pi^2/2}{D_i}\right)\ , \tag{5.65}$$

where the subscript in $\mathcal{A}$ refers to the chiral order, $s_{1,2} = s'$ and $s_{3,4} = s$, and the D_i are the inverse of the pion propagators given in Eq. (5.49). These contributions proportional to the propagators stem from the piece of diagram II in which the on-shell part of the 4π vertex is retained, so that the pion propagator is not cancelled out by an off-shell part from the 4π vertex (*cf.* Ref. [33]). Considering, for conciseness, the case $s = s'$ (the one interesting for the σ scalar form factor for which $s = s' = s_\sigma$), these propagators can be written as:

$$\frac{1}{D_1} = \frac{1}{\frac{q^2}{2} - 2|\mathbf{p}||\mathbf{q}|\cos\tilde{\theta}}\ , \tag{5.66}$$

and similarly for the other D_i. It should be noted that for certain values of q^2 and s, these propagators can have a pole in the variable $\cos\tilde{\theta}$. In particular, for $q^2 \to 0$ this is always the case. Upon angular integration, this contribution gives rise to an imaginary part that diverges as $1/\sqrt{|q^2|}$ for $q^2 \to 0^-$. As shown below, this limit is the one that matters in order to calculate the quadratic scalar radius of the σ, but this divergence would lead to an undetermined value for it. This fact is not acceptable and indicates a deficiency in the procedure followed up to now.

Let us clarify this important technical point and the way it can be solved. The term of the amplitude $\mathcal{A}_2(s, s', q^2, \theta, \tilde{\theta}, \phi, \tilde{\phi})$ in Eq. (5.65) that is proportional to the pion propagators,

[10] Because of invariance under temporal inversion the amplitudes for $\pi\pi \to \sigma$ and $\sigma \to \pi\pi$ are equal.

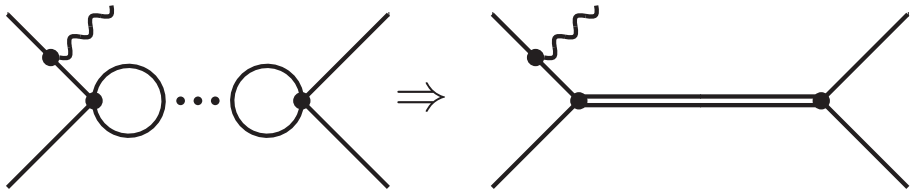

Figure 5.16: String of unitary diagrams to be resummed when the scalar source is attached to an external leg. On the right, the resulting single σ pole contribution is depicted.

that we denote by $\mathcal{A}_{2,\text{prop}}$,[11] can be written as:

$$\mathcal{A}_{2,\text{prop}} = \xi_2(s) \sum_{i=1}^{4} \frac{4B}{D_i} \ , \tag{5.67}$$

where we have taken into account that $\xi_2(s) = (s - m_\pi^2/2)/f_\pi^2$. Once $\mathcal{A}_{2,\text{prop}}$ is projected in the S-waves for the initial and final pion pairs, Eq. (5.56), we end with the contribution $W_{2,\text{prop}}$ to the kernel $W(s,s,q^2)$ in Eq. (5.59). Keeping in this resummation only terms up to one-loop, and hence proportional to $G(s)$, one obtains $T_{S2,\text{prop}}$ given by

$$T_{S2,\text{prop}} = -2\xi_2(s)G(s)W_{2,\text{prop}}(s,s,q^2) \ , \tag{5.68}$$

where the expansion

$$\frac{1}{(1+\xi_2(s)G(s))^2} = \sum_{n=0}^{\infty} (-1)^n (n+1) \left(\xi_2(s)G(s)\right)^n \ , \tag{5.69}$$

is employed.[12]

However, the result of the one loop calculation in ChPT of the diagram VIII, once properly projected in isospin and S-waves as discussed above, gives half of the amplitude in Eq. (5.68). Whence Eq. (5.59) is double counting this kind of terms at the one-loop level. Analogously, it can be seen in the n-loop terms of the resummation that the contribution of the kernel proportional to $W_{2,\text{prop}}$ is counted $n+1$ times, Eq. (5.69). This is so because we are missing the proper combinatoric factors as an on-shell factorization scheme for unitarizing is employed. Thus, instead of resumming these terms with $1/(1+VG)^2$, they should be resummed with just $1/(1+VG)$ in order to give the proper diagram counting. Notice that in this case they do not contribute to the double-pole term needed for $F_\sigma(q^2)$, as can be seen from Eqs. (5.63) and Eq. (5.64). This is also shown schematically in Fig. 5.16. Had we considered an integral equation for the resummation procedure instead, this kind of contributions would be integrated giving terms proportional to the three-point function $C_0(s,s',q^2)$, in which the scalar source interacts with intermediate pions, like the terms appearing in the diagram X of Fig. 5.14. This is not a shortcoming of our approach, because this kind of diagrams are properly included when the kernel $W(s,s',q^2)$ is calculated at higher orders in the chiral counting, as can be seen in Fig. 5.14. *E.g.* at the one-loop level calculation of $W(s,s',q^2)$ one has the diagram X of Fig. 5.14, that arises from iterating once the pion-propagator contributions at tree level.

[11] Recall that we are interested in the $s = s'$ case.

[12] Recall that $V(s)$ in Eq. (5.59) is $\xi_2(s)$ because we are unitarizing a one-loop ChPT calculation for $\pi\pi\, H \to \pi\pi$.

From the previous discussion we remove the terms of the amplitudes with the external scalar source coupled to initial or final asymptotic pion legs from the kernel $W(s,s',q^2)$ in Eq. (5.59), as they do not contribute to the scalar form factor of the σ. The latter requires the coupling of the external scalar source to intermediate pions and vertices. Now the question arises of how to remove properly the terms arising from the Feynman diagrams with the scalar source attached to a pion propagator in an external pion leg. We cannot simply drop these diagrams because the pion propagator between the source coupling and a pure pionic vertex in an external pion leg may be cancelled by off-shell terms from the $\pi\pi$ interaction vertex [33]. Indeed, such contributions are required in order to have results independent of pion field redefinitions that mix diagrams with different number of pion propagators. Rather, a procedure based on the full on-shell amplitude calculated in ChPT up to some order, which is independent of the former redefinitions, must be given.

Let us consider the general case, and write these contributions as:

$$\frac{f(x,y)}{x-x_0}\,, \tag{5.70}$$

where $x=\cos\tilde{\theta}$ and $x_0=q^2/(4|\mathbf{p}||\mathbf{q}|)$.[13] Here we have collected in y the rest of the variables. In order to subtract the pure pole contribution in Eq. (5.70) we subtract from the numerator above the residue of the pole,

$$\frac{f(x,y)-f(x_0,y)}{x-x_0}\,. \tag{5.71}$$

In the LO case, in view of Eq. (5.65), this amounts to removing the whole term proportional to the propagator, since it just depends on s (or s') and not on $\tilde{\theta}$ (or θ), that is, $\partial f(x,y)/\partial x=0$. This subtraction procedure is independent of pion field redefinition because in $f(x_0,y)$ all the pion lines are put on-shell so it cannot contain any off-shell remainder that could be counterbalanced by other off-shell parts coming from other vertices, and giving rise to possible pion field redefinition dependences.

With this procedure we are then ready to calculate $F_\sigma(q^2)$. For that we define the new amplitude $\mathcal{B}(s,s',q^2,\theta,\tilde{\theta},\phi,\tilde{\phi})$ obtained from the original $\mathcal{A}(s,s',q^2,\theta,\tilde{\theta},\phi,\tilde{\phi})$, Eq. (5.52), by removing the contributions with the scalar source attached to an external pion leg, following the procedure in Eq. (5.71). In terms of the former we calculate its angular projection as in Eq. (5.56), obtaining the new amplitude $\Phi(s,s',q^2)$:

$$\Phi(s,s',q^2)=\frac{1}{32\pi^2}\int \mathrm{d}^2\Omega\;\mathcal{B}(s,s',q^2,\theta,\tilde{\theta},\phi,\tilde{\phi})\;. \tag{5.72}$$

Then, the final expression for the interaction kernel, that we now denote by $\mathcal{W}(s,s',q^2)$, is (*cf.* Eq. (5.62))

$$\begin{aligned}\mathcal{W}&=\mathcal{W}_2+\mathcal{W}_4\;,\\ \mathcal{W}_2&=\Phi_2\;,\\ \mathcal{W}_4&=\Phi_4+\Phi_2\,\xi_2(s)G(s)+\Phi_2\,\xi_2(s')G(s')\;,\end{aligned} \tag{5.73}$$

[13] We are considering again the case in which the scalar source is attached to $\pi(p_1)$, since the argument for the the other cases is analogous.

with the subscripts indicating the chiral order as usual.

The scalar form factor of the σ is finally given by

$$F_\sigma(q^2) = \frac{g_\sigma^2}{V(s_\sigma)^2}\mathcal{W}(s_\sigma, s_\sigma, q^2) \ . \tag{5.74}$$

For definiteness let us explicitly give the expressions at LO and NLO for $F_\sigma(q^2)$ from the previous equation:

$$\begin{aligned} F_\sigma^{\rm LO}(q^2) &= \frac{(g_\sigma^{\rm LO})^2}{V_2(s_\sigma)^2}\mathcal{W}_2(s_\sigma, s_\sigma, q^2) \ , \\ F_\sigma^{\rm NLO}(q^2) &= \frac{(g_\sigma^{\rm NLO})^2}{\left(V_2(s_\sigma)+V_4(s_\sigma)\right)^2} \\ &\quad \times \Big(\mathcal{W}_2(s_\sigma, s_\sigma, q^2) + \mathcal{W}_4(s_\sigma, s_\sigma, q^2)\Big) \ . \end{aligned} \tag{5.75}$$

With

$$\begin{aligned} \left(g_\sigma^{\rm LO}\right)^2 &= \lim_{s\to s_\sigma^{\rm LO}}(s_\sigma^{\rm LO}-s)\frac{V_2(s)}{1+V_2(s)G(s)} \ , \\ \left(g_\sigma^{\rm NLO}\right)^2 &= \lim_{s\to s_\sigma^{\rm NLO}}(s_\sigma^{\rm NLO}-s)\frac{V_2(s)+V_4(s)}{1+\left(V_2(s)+V_4(s)\right)G(s)} \ , \end{aligned} \tag{5.76}$$

where $s_\sigma^{\rm LO}$ and $s_\sigma^{\rm NLO}$ are the σ pole positions at LO and NLO, respectively, given in Table 5.3, and for V_2 and V_4 see Eq. (5.6).

One technical detail is in order. The σ resonance is a pole in the second Riemann sheet of $\pi\pi$ scattering for the physical pion mass. As we have seen in Sec. 5.3.4 when increasing the pion mass above some value the σ meson becomes a bound state and moves into the first Riemann sheet (the corresponding pion mass value is indicated by the arrows in Fig. 5.6). Then, Eq. (5.74) has to be understood in the same Riemann sheet as the σ pole happens. This requires the evaluation of $\mathcal{W}(s, s', q^2)$ in Eq. (5.73) either in the first or second Riemann, according to the value taken for the pion mass.[14]

We now discuss the analytical continuation of the loop function $C_0(s, s, q^2)$ to the second Riemann sheet (we take from the beginning in the present discussion that $s' = s$), where it is denoted by $C_{0;II}(s, s, q^2)$. The function $C_0(s, s', q^2)$ corresponds to the three-point one-loop function of diagram X in Fig. 5.14 and its calculation is discussed in Appendix B. In order to proceed with the analytical continuation we first evaluate the difference

$$\Delta C(s, q^2) = C_0(s + i\epsilon, s + i\epsilon, q^2) - C_0(s - i\epsilon, s - i\epsilon, q^2) \tag{5.77}$$

for s and q^2 real and $q^2 < 4m_\pi^2$.[15] The second Riemann sheet in $\pi\pi$ scattering is reached by crossing the real s-axis above threshold, $s > 4m_\pi^2$, and so we have to consider Eq. (5.77) for

[14] This qualification is only relevant for $\mathcal{W}_4(s, s, q^2)$.

[15] For $q^2 > 4m_\pi^2$ the opening of the 2π production process introduces additional complications that we skip now since we are mostly interested to values of q^2 around zero, used below to calculate the quadratic scalar radius of the σ resonance. The whole region $q^2 < 4m_\pi^2$ is of interest and considered by us as well.

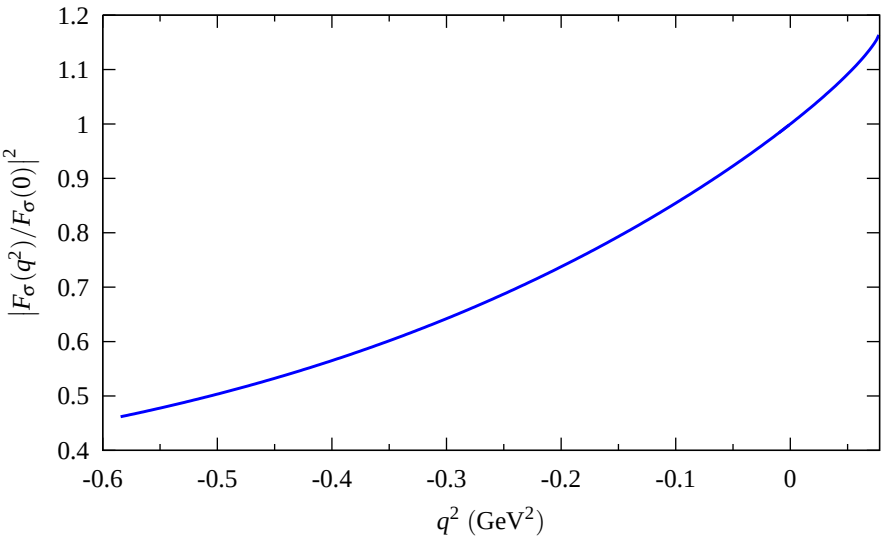

Figure 5.17: The normalized scalar form factor of the σ meson calculated at NLO for the physical case with $\sqrt{s_\sigma}$ given in Table 5.3. The range in q^2 extends from $q^2 \simeq -0.6$ GeV$^2 \simeq -30m_\pi^2$ up to $q^2 \simeq 0.08$ GeV$^2 \simeq 4m_\pi^2$.

the same values of s. It turns out that a cut in s extends for $s > 2m_\pi^2 + m_\pi\sqrt{4m_\pi^2 - q^2} \equiv s_{\rm rc}$ for which $\Delta C(s,q^2)$ is non-zero (the same expression for the cut also occurs for $s < 2m_\pi^2 - m_\pi\sqrt{4m_\pi^2 - q^2}$). When $q^2 \to 0^+$ (this limits gives the same value for the quadratic scalar radius as $q^2 \to 0^-$) to cross the real axis for $s > 4m_\pi^2$ implies to consider $\Delta C(s,q^2)$ given by the mentioned cut for C_0, $s > s_{\rm rc}$, corresponding to $\Delta_b C_0$ in Eq. (B.17). Once this discontinuity is evaluated we continue it analytically in s and q^2 and subtract it to $C_0(s,s,q^2)$ (calculated in the first Riemann sheet), as done above to determine $G_{II}(s)$, Eq. (5.11). It results,

$$C_{0;II}(s,q^2) = C_0(s,q^2) - \Delta C(s,q^2)\ . \tag{5.78}$$

Notice that for calculating $\mathcal{W}_4$, Eq. (5.73), it is not necessary to use $G_{II}(s)$ when the σ pole remains in the second Riemann sheet. This is due to the fact that Φ_4 contains the two-point one-loop function $B_0(s)$, evaluated in Appendix B, so that the discontinuity when crossing the unitarity cut above threshold cancels mutually between these two functions.

We show in Fig. 5.17 the modulus squared of $F_\sigma(q^2)$ normalized to $F_\sigma(0)$ for $q^2 < 4m_\pi^2$ calculated at NLO with the physical value of m_π. We observe a monotonous increasing function with q^2. The LO result is just a constant because Φ_2 is so and is not shown in the figure (it would be just 1.)

5.5 Quadratic scalar radius of the σ meson and the Feynman–Hellman theorem

The quadratic scalar radius of the σ resonance, $\langle r^2\rangle_s^\sigma$, is related to the scalar form factor of the σ by a Taylor expansion around $q^2 = 0$,

$$F_\sigma(q^2) = F_\sigma(0) + \left.\frac{\partial F_\sigma(q^2)}{\partial q^2}\right|_{q^2=0} q^2 + \cdots$$

$$= F_\sigma(0)\left(1+\frac{q^2}{6}\langle r^2\rangle_s^\sigma+\cdots\right)\ , \tag{5.79}$$

where the ellipsis indicate higher powers of q^2 in the Taylor expansion. In this way,

$$\langle r^2\rangle_s^\sigma = \frac{6}{F_\sigma(0)}\left.\frac{\partial F_\sigma(q^2)}{\partial q^2}\right|_{q^2=0}\ . \tag{5.80}$$

Notice that, since the form factor reduces to a constant (independent of q^2) at LO, we find that $\langle r^2\rangle_s^\sigma = 0$ for this case, similarly as the case for the quadratic scalar radius of the pion [18] within standard ChPT. Whence, the quadratic scalar radius must be calculated at least at NLO. Before discussing the results for the physical pion mass case, we study the dependence of $\langle r^2\rangle_s^\sigma$ with the pion mass. We show the square root of the quadratic scalar radius of the σ, $\sqrt{\langle r^2\rangle_s^\sigma}$, in the upper panel of Fig. 5.18 as a function of m_π, with its real part given by the (blue) solid line and its imaginary part by the (red) dashed line. It diverges in the chiral limit ($m_\pi = 0$) and where the σ pole coincides with the two-pion threshold (indicated by the rightmost arrow in Fig. 5.9.) The latter point corresponds to a zero energy bound state and as such it must have infinite size, as dictated by elementary quantum mechanics. On the other hand, in the chiral limit $\langle r^2\rangle_s^\sigma$ also diverges as $\log m_\pi$, similarly as the quadratic scalar or vector radius of the pion [18], because the infinite size of the pion cloud around the bosons. It is relevant to note that the imaginary part of this quantity, despite the σ meson has a width larger than 200 MeV for pion masses up to around 300 MeV, as shown in Fig. 5.8, is much smaller than its real part, which makes its interpretation easier. In the lower panel of the same figure we depict the real (blue solid line) and imaginary (red dashed line) parts of the quadratic scalar radius of the σ, $\langle r^2\rangle_s^\sigma$. It is notorious that in most of this range of pion mass values the square root of $\langle r^2\rangle_s^\sigma$ is around 0.5 fm quite independently of the width of the σ meson.

For the physical pion mass we find the values

$$\begin{aligned}\langle r^2\rangle_s^\sigma &= (0.19\pm 0.02) - i\,(0.06\pm 0.02)\ \text{fm}^2,\\ \sqrt{\langle r^2\rangle_s^\sigma} &= (0.44\pm 0.03) - i\,(0.07\pm 0.03)\ \text{fm}\ ,\end{aligned} \tag{5.81}$$

with the errors calculated as explained in Sec. 5.3. This value is almost the same as the corresponding quadratic scalar radius for $K\pi$, $\langle r^2\rangle_s^{K\pi} = 0.1806 \pm 0.0049$ fm^2 [189], for which the scalar resonance κ (or $K_0^*(800)$), tightly related to the σ resonance by $SU(3)$ symmetry [39, 49, 51, 53, 54], plays a leading role [43, 44]. For comparison, the quadratic scalar radius of the pion is $\langle r^2\rangle_s^\pi = 0.65 \pm 0.05$ fm^2 [149].[16] It is notorious that the value determined for the scalar radius of the σ resonance is smaller than that for the pion. It is even smaller than the measured quadratic electromagnetic pion radius, $\langle r^2\rangle_V^{\pi^\pm} = 0.439 \pm 0.008$ fm^2 [394]. However, $\langle r^2\rangle_s^\sigma$ is similar to the measured $K^\pm$ quadratic charge radius [150], $\langle r^2\rangle_V^{K^\pm} = 0.28 \pm 0.07$ fm^2. Scalar glueballs are expected to have even smaller sizes, 0.1–0.2 fm [395, 396].

The value obtained for $\langle r^2\rangle_s^\sigma$ in Eq. (5.81) implies that the two scalar isoscalar pions generating the σ resonance are so tightly packed that the σ resonance becomes a compact state.

[16] A recent lattice QCD determination [385] gives $\langle r^2\rangle_s^\pi = 0.617 \pm 0.079 \pm 0.066$ fm^2, or, adding the errors in quadrature, $\langle r^2\rangle_s^\pi = 0.6 \pm 0.1$ fm^2, in good agreement with the value given in Ref. [149].

Whether the two pairs of color singlet valence quarks $\bar{q}q$ in the two-pion state recombine giving rise to combinations of other possible QCD states as *e.g.* $q^2\bar{q}^2$ [49,50,54,58,126,267,397–405], glueball, etc is beyond the scope of our study based on hadronic degrees of freedom. In this respect the large N_C evolution of the σ pole position [39, 136–139, 148] is enlightening and clearly indicates that the σ resonance is not dominantly a glueball or a $\bar{q}q$ resonance. In Refs. [138, 148] it was found that this large N_C behavior is compatible with the fact that this resonance owes its origin to $\pi\pi$ interactions becoming a $\pi\pi$ resonance. This large N_C behavior is also compatible with a $(q\bar{q})^2$ state that fades away as two $q\bar{q}$ mesons as expected in the large N_C limit [147]. This picture on the dynamical generation from $\pi\pi$ interactions of the σ meson is also supported by the nontrivial simultaneous fulfillment [148] of semi-local duality [148, 406] and scalar, pseudoscalar spectral function sum rules [148], both for $N_C = 3$ and varying N_C.

On the other hand, for larger values of m_π, the σ meson closely follows the 2π threshold, as demonstrated in the previous section, and its size is then large. Thus, in this range of pion masses, the σ meson progressively becomes a two-pion molecule and its nature is then much more clear and simple (for $m_\pi \gtrsim 400$ MeV it follows from Fig. 5.18 that $\sqrt{\langle r^2\rangle_S^\sigma} > 1.5$ fm).[17] This can also be related to the behavior of the quantity $g^2 dG/ds$ evaluated at $s = s_\sigma$ (and G evaluated in the Riemann sheet in which the pole appears). This quantity is close to one for a composite meson [215, 216, 411–414]. We have checked that for the large values of m_π in which the σ meson is a bound state, we have $g^2 dG/ds \gtrsim 0.8$, which points to a molecular nature. For values of the pion mass close to the physical one, we have instead $g^2 dG/ds \simeq 0$.

Another interesting point is to consider the relation between $F_\sigma(0)$ and the derivative of the σ pole with respect to the quark mass. According to the Feynman-Hellmann theorem [151, 152], one has the relation:

$$\frac{ds_\sigma}{dm^2} = -\frac{F_\sigma(0)}{2B} \ . \tag{5.82}$$

Notice that $F_\sigma(0)$ is proportional to B and precisely their ratio is not ambiguous. On the other hand, ds_σ/dm_π^2 is given in Eq. (5.19). Then we can write:

$$\begin{aligned}\frac{ds_\sigma}{dm^2} =& -\frac{g_\sigma^2(m_\pi^2)}{V(s_\sigma, m_\pi^2)^2}\left(\dot{V}(s_\sigma, m_\pi^2) - V(s_\sigma, m_\pi^2)^2 \dot{G}_{II}(s_\sigma, m_\pi^2)\right) \\ &\times \frac{dm_\pi^2}{dm^2} \ .\end{aligned} \tag{5.83}$$

The dependence of m_π^2 on m^2 is worked out up to $\mathcal{O}(m_\pi^4)$ in Eq. (1.288) from where one obtains:

$$\frac{dm_\pi^2}{dm^2} = 1 - \frac{m_\pi^2}{16\pi^2 f_\pi^2}\left(\bar{l}_3 - \frac{1}{2}\right) + \mathcal{O}(m_\pi^4) \ . \tag{5.84}$$

We show our results for $-F_\sigma(0)/2B$ at NLO and compare them with ds_σ/dm^2 in Fig. 5.19, so as to check Eq. (5.82). In the upper two panels we show the real part and in the bottom one the

[17] A similar value was obtained for the size of the $\Lambda(1405)$ resonance in Ref. [407], which is also a resonance that qualifies as dynamically generated form the meson-baryon interactions [35, 41, 47, 408, 409]. In Ref. [410] the matter or scalar form factor for this resonance was studied.

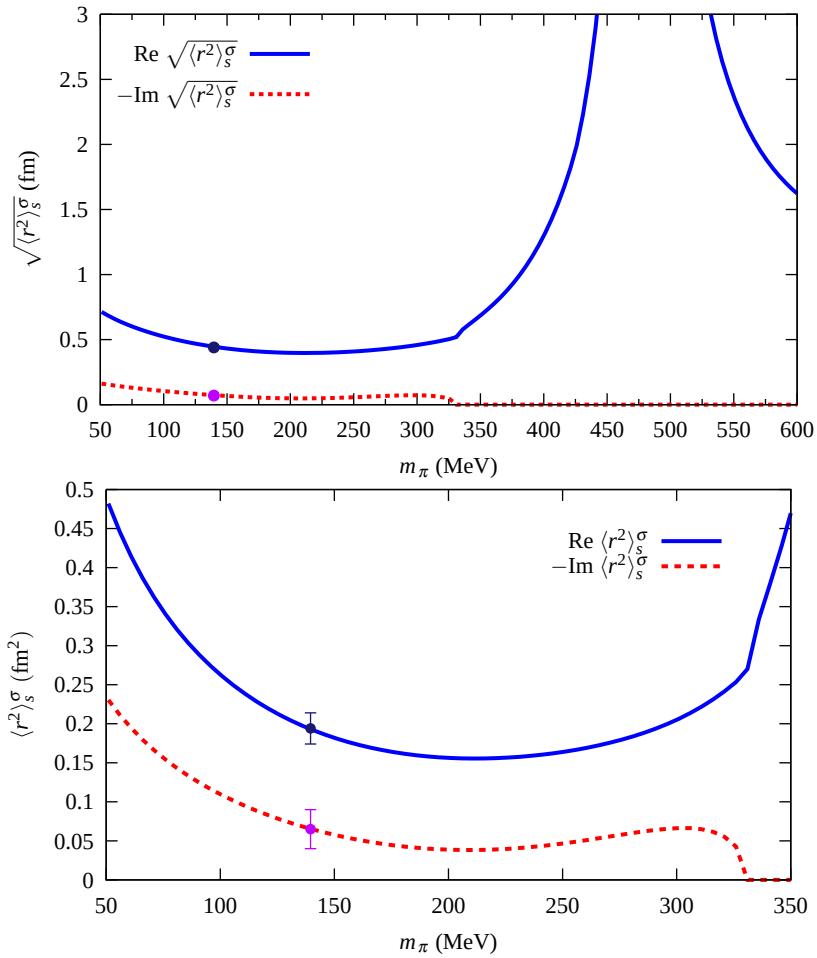

Figure 5.18: Top: the square root of the quadratic scalar radius of the σ as a function of m_π is shown for $0 < m_\pi < 600$ MeV. Bottom: the quadratic scalar radius is represented in the range $0 < m_\pi < 350$ MeV. In both panels, the (blue) solid lines represent the real part of each quantity, whereas the (red) dashed line is the imaginary part. The points over the curves represent our results for the physical case with their statistical errors, Eq. (5.81). Due to the scale used they cannot be appreciated in the upper panel.

imaginary part. The agreement is certainly remarkable for $m_\pi \lesssim 300$ MeV, at the level of just a few percents of difference. This range of pion masses is highlighted in the second and third panels, from top to bottom. Let us note that in Eq. (5.82) we are comparing two quantities that are obtained from the chiral expansion of two different interacting kernels. The expansion is not performed on the full amplitudes and this is why there is not a perfect agreement, as it is the case in the standard perturbative calculations of ChPT [18, 19]. In our case the factor $V(s_\sigma, m_\pi^2)^2$ multiplying $\dot{G}_{II}(s_\sigma, m_\pi^2)$ in the right-hand side of Eq. (5.83) is equal to $(V_2 + V_4)^2$, while Φ_4 from Eq. (5.72) only contains V_2^2, because it is a ChPT one-loop calculation at $\mathcal{O}(p^4)$.[18] Thus, the differences correspond to higher order terms in the calculation of $F_\sigma(0)$, beyond the $\mathcal{O}(p^4)$ or NLO calculation of the kernel $\mathcal{W}(s, s', q^2)$, Eq. (5.73), performed in the present work.

Another point also worth mentioning is the fact that the left-hand side of Eq. (5.83) does

[18]Notice that the derivative with respect to m_π^2 of the function $G(s, m_\pi^2)$ is proportional to $C_0(s, s, m_\pi^2)$.

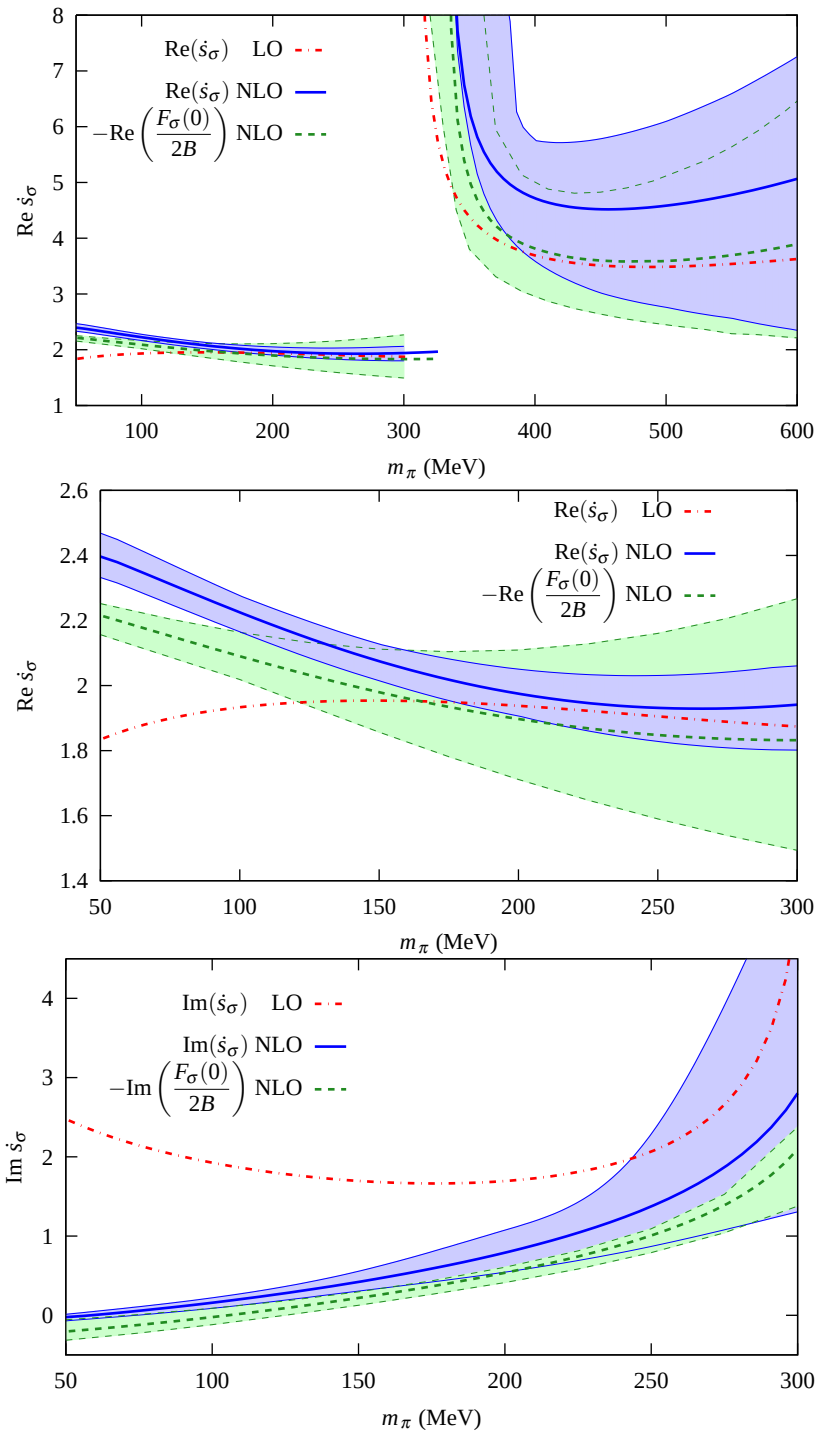

Figure 5.19: Feynman-Hellmann theorem: comparison between ds_σ/dm^2 and $-F_\sigma(0)/2B$, Eq. (5.83), as a function of the pion mass. The (blue) thick solid lines correspond to ds_σ/dm^2 at NLO, Eq. (5.19), whereas the (red) dot-dashed lines are evaluated at LO, where $ds_\sigma/dm^2 = ds_\sigma/dm_\pi^2$. The (green) dashed lines are $-F_\sigma(0)/2B$. From top to bottom, in the first panel the real part of the quantities are represented in the range m_π, $50 < m_\pi < 600$ MeV. In the second panel, the same is shown for $50 < m_\pi < 300$ MeV. The bottom panel shows their imaginary part.

not involve any contribution with pion propagators in the external legs but the derivative acts on the vertices and intermediate pion propagators in loop functions. This is also the case in $F_\sigma(0)$ once the pion propagators in the external legs are removed as explained in Sec. 5.4.3.

5.6 Summary and conclusions

In this Chapter we have discussed the nature of the σ resonance (nowadays also called $f_0(500)$ in the PDG [48]) by evaluating its quadratic scalar radius, $\langle r^2\rangle_s^\sigma$. This allows one to have a quantitative idea of the size of this resonance.

There are many studies since the nineties based on supplementing Chiral Perturbation Theory with non-perturbative S-matrix methods, that clearly indicate a dynamical origin for the σ resonance due to the isoscalar scalar $\pi\pi$ strong self interactions [22–24, 26, 28, 29, 33]. More recent studies based on the dependence with N_C of the σ pole [39, 136–138, 144] also corroborate that this resonance cannot be qualified as a purely $\bar{q}q$ or glueball, with the pole trajectories compatible with the expectations for a meson-meson dynamically generated object or a four-quark state. In the large N_C limit it is well known that loops are suppressed so that the $\pi\pi$ rescattering vanishes away and then the σ resonance pole disappears according to Refs. [39, 138, 148]. These results have been strongly supported recently [148] by the simultaneous fulfillment of semi-local duality [148, 406] and scalar, pseudoscalar spectral sum rules [148], both for $N_C = 3$ and varying N_C.

The next question is whether the two pions are loosely distributed, so that the σ meson might be qualified as molecular or, on the contrary, they overlap each other giving rise to a compact object of a size comparable or even smaller than that of its constituents. A proper way to answer this question is to determine quantitatively the size of the σ resonance. For that we calculate in this work the quadratic scalar radius of this resonance obtaining the value $\langle r^2\rangle_s^\sigma = (0.19 \pm 0.02) - i\,(0.06 \pm 0.02)$ fm^2. Despite the σ has a large width the resulting value for the quadratic scalar radius is almost a real quantity, which makes easier its physical interpretation. This value is very close to the $K\pi$ quadratic scalar radius, $\langle r^2\rangle_s^{K\pi} = 0.1806 \pm 0.0049$ fm^2 [189], similar to the measured $K^\pm$ quadratic charge radius [150], $\langle r^2\rangle_V^{K^\pm} = 0.28 \pm 0.07$ fm^2, and smaller than the quadratic scalar radius of the pion, $\langle r^2\rangle_s^\pi = 0.65 \pm 0.05$ fm^2 [149]. This means that the σ is certainly a compact object. The square root of its quadratic scalar radius is $\sqrt{\langle r^2\rangle_s^\sigma} = (0.44 \pm 0.03) - i\,(0.07 \pm 0.03)$ fm.

We have further tested our result for the size of the σ by considering the dependence of $\langle r^2\rangle_s^\sigma$ on the pion mass. As m_π rises the σ meson mass follows the 2π threshold. This fact has been recently observed in the lattice QCD calculation of Ref. [153], and was pointed out much earlier in Refs. [39, 53] as well as in the more recent work [154]. In such situation, with a small binding energy, the expected size of the σ resonance should be definitely larger than that of a hadron. We obtain a quadratic scalar radius that increases rapidly as soon as the width of the σ meson tends to vanish, which for our present NLO fit occurs for pion masses above $\simeq 330$ MeV. In this way, already for pion masses around 370 MeV, $\sqrt{\langle r^2\rangle_s^\sigma}$ is larger than 1 fm and diverges for $m_\pi \simeq 470$ MeV, precisely the value at which the σ resonance becomes a zero binding energy bound state. In this case, a molecular or $\pi\pi$ bound state image is appropriate

for the σ meson. For even higher pion masses, the binding energy is still small which gives rise to large sizes for the σ. Nevertheless, we observe a steady (albeit weak) tendency to increase the binding energy for higher pion masses so that its size tends to dismiss progressively, but for the mass range explored in this work it is always $\gtrsim 1.5$ fm. The clear tendency of the σ resonance to follow the two-pion threshold is a manifest indication for this resonance being a meson-meson dynamically generated one. For smaller pion masses between 50 and 300 MeV the square root of the quadratic scalar radius of the σ meson is rather stable with a value around 0.5 fm, independently of its width.

The value of the scalar form factor of the σ resonance at $q^2 = 0$, $F_\sigma(0)$, is related via the Feynman-Hellmann theorem with the derivative of the σ pole position with respect to the pion mass. Within uncertainties, we have checked the fulfillment of such relation.

We have studied $\pi\pi$ scattering in NLO $SU(2)$ Unitary Chiral Perturbation Theory as well. We obtain a good reproduction of $\pi\pi$ phase shifts for $I = 0$ and $I = 2$, and also for lattice QCD results of the $I = 2$ scattering length a_0^2 and f_π. We have offered a detailed comparison between different precise determinations in the literature, including our present calculation, of the σ meson mass and width, and of the threshold parameters a_0^0, b_0^0. The resulting average values are $a_0^0 = 0.220 \pm 0.003$ and $b_0^0 m_\pi^2 = 0.279 \pm 0.003$. For the σ meson pole parameters we take the mean of the different values with the result $M_\sigma = 458 \pm 14$ MeV and $\Gamma_\sigma/2 = 261 \pm 17$ MeV. Our own determinations obtained here at NLO in Unitary ChPT are $a_0^0 = 0.219 \pm 0.005$, $b_0^0 m_\pi^2 = 0.281 \pm 0.006$, $M_\sigma = 440 \pm 10$ MeV and $\Gamma_\sigma/2 = 238 \pm 10$ MeV.

6

Finite volume treatment of $\pi\pi$ scattering and limits to phase shifts extraction from lattice QCD

Contents of this Chapter:

6.1 Introduction

One of the aims in present lattice QCD calculations is the determination of the hadron spectrum and many efforts are devoted to this task [153, 239, 415–437]. A recent review on the different methods used and results can be seen in [155]. Since one evaluates the spectrum for particles in a finite box, one must use a link from this spectrum to the physical one in infinite space. Sometimes, when it rarely happens, an energy level in a finite box rather independent of the volume is taken as a proof that this is the energy of a state in the infinite volume space. In other works the "avoided level crossing", with lines of spectrum that get close to each other and then separate, is usually taken as a signal of a resonance, but this criterion has been shown insufficient for resonances with a large width [158, 438, 439]. A more accurate method consists on the use of Lüscher's approach, but this works for resonances with only one decay channel. The method allows to reproduce the phase-shifts for the particles of this

decay channel starting from the discrete energy levels in the box [156, 157]. This method has been recently simplified and improved in [158] by keeping the full relativistic two-body propagator (Lüscher's approach makes approximations on the real part, *cf.* Eqs. (6.30) and (6.31) below). The work of [158] also extends the method to two or more coupled channels. The extension to coupled channels has also been worked out in [440–442]. The work of [158] presents an independent method, which is rather practical, and has been tested and proved to work in realistic cases of likely lattice results. The method has been extended in [443] to obtain finite volume results from the Jülich model for the meson-baryon interaction and in [444] to study the interaction of the DK and ηD_s system where the $D_{s0}^*(2317)$ resonance is dynamically generated from the interaction of these particles. The case of the κ resonance in the $K\pi$ channel is also addressed in [445] following the approach of Ref. [158]. It has also been extended to the case of interaction of unstable particles in [446], to the study of the DN interaction [447], the $\pi\pi$ interaction in the ρ channel [448] and to find strategies to determine the two $\Lambda(1405)$ states from lattice results [449].

In Ref. [158] the problem of getting phase-shifts and resonances from lattice QCD results ("inverse problem") using two coupled channels was addressed. Special attention was given to the evaluation of errors and the precision needed on the lattice QCD calculations to obtain phase-shifts and resonance properties with a desired accuracy. The derivation of the basic formula of [158] is done using the method of the chiral unitary approach [42] to obtain the scattering matrix from a potential. This method uses a dispersion relation for the inverse of the amplitude, taking the imaginary part of T^{-1} in the physical region and using unitarity in coupled channels [39, 41]. The method does not integrate explicitly over the left-hand cut (LHC) singularity. Nevertheless, the latter might lead to interesting problems in finite volume calculations because in field theory, loops in the $t-$ or $u-$channel that contribute to crossed cuts, are volume dependent. There is no problem to incorporate these extra terms into the chiral unitary approach by putting them properly in the interaction kernel of the Bethe Salpeter equation or N/D method [39, 138], or using the Inverse Amplitude Method (IAM) [23, 25–28, 30]. However, the method of [158] to analyze lattice spectrum and obtain phase-shifts explicitly relies upon having a kernel in the Bethe Salpeter equation which is volume independent. The same handicap occurs in the use of the standard Lüscher approach, where contributions from possible volume dependence in the potential are shown to be "exponentially suppressed" in the box volume. Yet, there is no way, unless one knows precisely the source of the volume dependent terms, to estimate these effects and determine for which volumes the "exponentially suppressed" corrections have become smaller than a desired quantity. This is however an important information in realistic calculations. The purpose of the work in this Chapter is to address this problem in a practical case, the scattering of pions in S-wave. For that we determine the strength of these volume dependent terms as a function of the size of the box and the impact of these effects in the determination of the phase-shifts in the infinite volume case.

The problem of $\pi\pi$ interaction in the lattice using the Lüscher approach has been studied for the case of $I = 2$, where one has no coupled channels and is technically easier for lattice calculations [374, 450, 451]. Along these lines in [452] a pioneer work is done of the problem that we address here performing a perturbative calculation at threshold for the case of $I = 2$. Our approach is technically different, non perturbative, can be used for scattering energies and to evaluate phase shifts and is done for $I = 0$ and $I = 2$.

We report here the results obtained in our paper, Ref. [D]. The contents of this Chapter are as follows. After this introduction, we summarize in Sec. 6.2 the three models used to evaluate $\pi\pi$ scattering in the infinite and finite volume case. We then follow by studying the dependence on the lattice size of the box L of the resulting phase shifts in Sec. 6.3. Conclusions are collected in Sec. 6.4.

6.2 The $\pi\pi$ scattering in the finite box

In this section we explain the three models that we are going to consider in the present work to evaluate the $\pi\pi$ scattering within the chiral unitary approach: lowest order Bethe-Salpeter (BS), N/D and IAM. The latter two provide contributions to the LHC of the scattering amplitude while the BS does not. After summarizing the models for the infinite volume, we explain for each of them how to evaluate the scattering in a box of finite size L. We study the scalar channel up to total energies of about 800 MeV for both the $I = 0$ and $I = 2$ cases. The former is relevant for the lattice QCD studies of σ (or $f_0(500)$ [48]) meson resonance, while for the latter the LHC is more relevant (see below). Up to those energies the $K\bar{K}$ and $\eta\eta$ channels in the $I = 0$ case are negligible, hence, we deal here only with the $\pi\pi$ channel. The 4π channel, although open at lower energies around 555 MeV, is also neglected. Their effects were included in Chapter 3 (see Ref. [A]) and the resulting inelasticity was negligible up to energies above 900 MeV. This extra intermediate state gives rise to L dependence that is not exponentially suppressed but, since phenomenologically is negligible in the energy range considered here, we do not expect any significant effects from this side. This channel was also neglected in the previous study of $\pi\pi$ scattering at threshold in finite volume [452] and its calculation is beyond our present aim. The 4π channel gives rise to a three-loop or $\mathcal{O}(p^6)$ contribution to the interaction kernel in ChPT, while here we restrict ourselves to the one-loop or $\mathcal{O}(p^4)$ calculation of the interaction kernel. Indeed, any other volume dependence effect not considered by us in our present research is at least part of a two-loop calculation of the interaction kernel in ChPT.

6.2.1 Lowest order Bethe-Salpeter approach

In the chiral unitary approach the scattering matrix can be given by the Bethe-Salpeter equation in its factorized form [33]

$$T = [1 - VG]^{-1}V = [V^{-1} - G]^{-1} \, , \tag{6.1}$$

where V is the $\pi\pi$ potential, $V = -\frac{1}{f_\pi^2}(s - \frac{m^2}{2})$ for $I = 0$ and $V = \frac{1}{2f_\pi^2}(s - 2m^2)$ for $I = 2$, which are obtained from the lowest order chiral Lagrangians [18], with m the pion mass and $f_\pi = 92.4$ MeV. In Eq. (6.1) G is the loop function of two meson propagators, which is defined as

$$G = i \int \frac{d^4p}{(2\pi)^4} \frac{1}{(P-p)^2 - m^2 + i\epsilon} \frac{1}{p^2 - m^2 + i\epsilon} \, , \tag{6.2}$$

with P the four-momentum of the global meson-meson system. This function has already appeared in several of the preceeding chapters. Nonetheless, since it will be often refer-

enced in the following, we include it here again. Note that Eq. (6.1) only has right-hand cut (RHC), unlike the other two approaches discussed in the next subsections. We must note that, throughout this Chapter, the amplitude has a different normalization convention with respect to the one of the preceeding chapters. In particular, the amplitude here has an additional minus sign, which, in turn, makes the chiral amplitudes to have the same additional minus sign.

The loop function in Eq. (6.2) can be regularized either with dimensional regularization or with a three-momentum cutoff. The connection between both methods was shown in Refs. [30, 41]. In dimensional regularization[1] the integral of Eq. (6.2), G^D, is evaluated and gives for the $\pi\pi$ system [41, 453]:

$$G^D(E) = \frac{1}{(4\pi)^2}\left\{a(\mu) + \log\frac{m^2}{\mu^2} + \sigma\log\frac{\sigma+1}{\sigma-1}\right\}, \tag{6.3}$$

where $\sigma = \sqrt{1-\frac{4m^2}{s}}$, $s = E^2$, with E the energy of the system in the center of mass frame, μ is a renormalization scale and $a(\mu)$ is a subtraction constant (note that only the combination $a(\mu) - \log\mu^2$ is the relevant degree of freedom, that is, there is only one independent parameter).

The loop function G can also be regularized with a three momentum cutoff $p_{\max}$ and, after the p^0 integration is performed [33], it results

$$\begin{aligned} G(s) &= \int_{|\vec{p}|<p_{\max}} \frac{d^3\vec{p}}{(2\pi)^3}\frac{1}{\omega(\vec{p})}\frac{1}{s-4\omega(\vec{p})^2+i\epsilon}\,, \\ \omega(\vec{p}) &= \sqrt{m^2+\vec{p}^{\,2}}\,. \end{aligned} \tag{6.4}$$

Let us now address the modifications in order to evaluate the $\pi\pi$ scattering in a finite box following the procedure explained in Ref. [158]. The main difference with respect to the infinite volume case is that instead of integrating over the energy states of the continuum with $\vec{p}$ being a continuous variable as in Eq. (6.4), one must sum over the discrete momenta allowed in a finite box of side L with periodic boundary conditions. We then have to replace G by $\widetilde{G}$, where

$$\begin{aligned} \widetilde{G} &= \frac{1}{L^3}\sum_{\vec{p}}^{|\vec{p}|<p_{\max}}\frac{1}{\omega(\vec{p})}\,\frac{1}{s-4\omega(\vec{p})^2}\,, \\ \vec{p} &= \frac{2\pi}{L}\,\vec{n}\,, \quad \vec{n}\in\mathbb{Z}^3 \end{aligned} \tag{6.5}$$

[1] In our context we refer to the G function given in Eq. (6.3) as calculated in "dimensional regularization". Of course, with the latter procedure the result is infinite. The infinite is removed by the subtraction constant $a(\mu)$. A more accurate formulation can be given in terms of dispersion relations, see Sec. 2.7 and references therein.

For the sake of comparison with the other models considered in the present work, where dimensional regularization is always done, we use the procedure of [444] in order to write the finite volume loop function $\widetilde{G}$ in terms of the infinite volume one G^D evaluated in dimensional regularization:

$$\widetilde{G}^D = G^D + \lim_{p_{\max}\to\infty}\left[\frac{1}{L^3}\sum_{\vec{p}_i}^{p_{\max}} I(\vec{p}_i,s) - \int_{p<p_{\max}} \frac{d^3\vec{p}}{(2\pi)^3} I(\vec{p},s)\right] , \tag{6.6}$$

where $I(\vec{p},s)$ is the integrand of Eq. (6.4),

$$I(\vec{p},s) = \frac{1}{\omega(\vec{p})}\ \frac{1}{s-4\omega(\vec{p})^2} . \tag{6.7}$$

Note that $\widetilde{G}^D$ of Eq. (6.6) depends on the subtraction constant a instead of the three-momentum cutoff $p_{\max}$. The dependence on the latter cancels in the difference between the two terms in the square brackets of Eq. (6.6).

In the box the scattering matrix reads

$$\widetilde{T} = \frac{1}{V^{-1}-\widetilde{G}^D} . \tag{6.8}$$

The eigenenergies of the box correspond to energies that produce poles in the $\widetilde{T}$ matrix, which corresponds to the condition $\widetilde{G}^D(E) = V^{-1}(E)$. Therefore for those values of the energies, the T matrix for infinite volume can be obtained by

$$T(E) = \left(V^{-1}(E) - G^D(E)\right)^{-1} = \left(\widetilde{G}^D(E) - G^D(E)\right)^{-1} . \tag{6.9}$$

The amplitude is related to the phase-shifts by

$$T(E) = -\frac{8\pi E}{p}\frac{1}{\cot\delta - i} , \tag{6.10}$$

where $p = \frac{E}{2}\sqrt{1-\frac{4m^2}{s}}$ is the CM momentum.

Eq. (6.9) is nothing but Lüscher formula [156, 157] except that, as shown in Ref. [158], Eq. (6.9) keeps all the terms of the relativistic two-body propagator, while Lüscher's approach neglects terms in Re $I(p)$ which are exponentially suppressed in the physical region, but can become sizable below threshold, or in other cases when small volumes are used or large energies are involved.

We would like to make the following observation here. Let us consider Eq. (6.9) in the cutoff regularization procedure. We would obtain

$$T(E) = (\widetilde{G} - G)^{-1} \tag{6.11}$$

with G and $\widetilde{G}$ given by Eqs. (6.4) and (6.5) respectively. In the application to Quantum Mechanics of Lüscher formalism, the cutoff would be playing the effect of a finite range.

However, one should note that the difference $\widetilde{G} - G$ has a finite limit when the cutoff goes to infinity and this is what the Lüscher formalism assumes. Note that the difference of the part of the sum and integral from $p_{\rm max}$ to infinity goes rapidly to zero as $p_{\rm max}$ increases, leading to terms exponentially suppressed in L. So, to make the limit of $p_{\rm max}$ infinite in Eq. (6.11) is within the usual assumptions in the derivation of Lüscher formula and makes the results cutoff independent. Then Eq. (6.11) in the limit of $p_{\rm max} \to \infty$ is exactly Lüscher formula, up to the relativistic corrections that we have mentioned. On the other hand, in lattice QCD calculations the information on $p_{\rm max}$ does not exist since the cutoff is implicitly infinite and divergences of the theory are reabsorbed in some physical observable. In this sense a rederivation of the improved Lüscher formula, Eq. (6.9), without invoking cutoffs is advisable and this is done in [444] (Eqs. (11) to (17) of that paper), with the dimensional regularized G functions. This is what we have used in Eq. (6.6) and throughout this Chapter.

6.2.2 Chiral amplitude at $\mathcal{O}(p^4)$ in a finite volume

Both in the IAM and the N/D methods (explained below) the dependence with the finite size of the box enters through the chiral amplitude $A_4(s,t,u)$, which is used to calculate the partial waves at $\mathcal{O}(p^4)$, denoted by T_4. The Feynman diagrams involved in its calculation were shown in Fig. 5.1, in Chapter 5 (since in the first part of Chapter 5 we dealt with $\pi\pi$ scattering at NLO). This amplitude receives contributions from loop diagrams, whose momentum integrals should be replaced by discrete sums over the allowed momenta in the finite box. In particular, these contribution come from s–, t– and u–channel loop diagrams, and also from tadpole diagrams. Note also that, as in Chapter 5, we write the amplitudes in terms of the physical pion mass m_π and decay constant f_π, so that the NLO contributions (tadpole loop-functions in the finite box) to them are included as $\mathcal{O}(p^4)$ terms in the amplitude T_4. The $O(p^4)$ $\pi\pi$ scattering amplitude $A_4(s,t,u)$ can be generically written, both for $I=0$ and $I=2$, in terms of only two one–loop functions G and H:

$$A_4(s,t,u) = P_L + P_H H(m^2) + P_{G,s} G(s) + P_{G,t} G(t) + P_{G,u} G(u) \ , \tag{6.12}$$

where P_X are polynomials of the Mandelstam variables. In particular, the LECs appear only in P_L. In the above equation, H and $G(P^2)$ are the one– and two– point one loop functions[2] respectively:

$$G(P^2) = \int \frac{d^3\vec{q}}{(2\pi)^3} \frac{\omega_{\vec{q}} + \omega_{\vec{P}-\vec{q}}}{2\omega_{\vec{q}}\omega_{\vec{P}-\vec{q}}} \frac{1}{(P^0 - \omega_{\vec{q}} - \omega_{\vec{P}-\vec{q}})(P^0 + \omega_{\vec{q}} + \omega_{\vec{P}-\vec{q}})}, \tag{6.13}$$

$$H = \int \frac{d^3\vec{q}}{(2\pi)^3} \frac{1}{2\omega_{\vec{q}}} \ , \tag{6.14}$$

and P is the four–momentum entering the loop so that $G(s)$, $G(t)$ and $G(u)$ in Eq. (6.12) arise from the s–, t– and u–channel loops (6.13) with $P^2 = s$, t and u respectively. In dimensional regularization and after the divergences and scale dependencies are absorbed in the LECs [18], the loop functions then read

$$G^R(P^2) = \frac{1}{16\pi^2}\left(-1 + \sigma(P^2)\log\frac{1+\sigma(P^2)}{1-\sigma(P^2)}\right) \ , \tag{6.15}$$

[2]Recall that these functions were used in Chapter 5, with the notation A_0 and B_0. The notation in this Chapter for these functions is the one used in the original paper, [D].

with $\sigma(P^2) = \sqrt{1-4m_\pi^2/P^2}$. On the other hand, because of the regularization approach followed, we have $H^R = 0$. The partial waves T_4 are then obtained by projecting the $I = 0$ or $I = 2$ amplitude A_4 on angular momentum J.

The chiral amplitude in finite volume is calculated replacing $T_4(s)$ with $\widetilde{T}_4(s)$, which is the S-wave projection of the $I = 0$ or $I = 2$ $\pi\pi$ scattering amplitude in finite volume $\widetilde{A}_4(s,t,u)$. The latter is obtained from Eq. (6.12), but replacing the loop functions in Eqs. (6.13) and (6.14) with their finite volume counterparts, $\widetilde{G}^R$ and $\widetilde{H}^R$. Following again the procedure in [444] (see also the discussion at the end of subsection 6.2.1), we obtain the finite volume loop functions from the infinite volume ones as

$$\widetilde{G}^R(P) = G^R(P^2) + \lim_{q_{\max}\to\infty}\left[\frac{1}{L^3}\sum_{\vec{q}_i}^{q_{\max}} I(\vec{q}_i,P) - \int\limits_{q<q_{\max}} \frac{d^3\vec{q}}{(2\pi)^3} I(\vec{q},P)\right], \tag{6.16}$$

$$\widetilde{H}^R = H^R + \lim_{q_{\max}\to\infty}\left[\frac{1}{L^3}\sum_{q_i}^{q_{\max}} \frac{1}{2\omega_{\vec{q}}} - \int\limits_{q<q_{\max}} \frac{d^3\vec{q}}{(2\pi)^3}\frac{1}{2\omega_{\vec{q}}}\right], \tag{6.17}$$

where $I(\vec{q},P)$ is the integrand of Eq. (6.13),

$$I(\vec{q},P) = \frac{\omega_{\vec{q}}+\omega_{\vec{P}-\vec{q}}}{2\omega_{\vec{q}}\omega_{\vec{P}-\vec{q}}}\frac{1}{(P^0-\omega_{\vec{q}}-\omega_{\vec{P}-\vec{q}})(P^0+\omega_{\vec{q}}+\omega_{\vec{P}-\vec{q}})}. \tag{6.18}$$

Note that the box breaks Lorentz symmetry and fixes the reference frame to the center of mass frame of the initial pions. For this reason we have used P as the argument of $\widetilde{G}^R$ in Eq. (6.16) instead of P^2.

In the case of the s–channel loop, where $\vec{P} = 0$ so that $(P^0)^2 = P^2 = s$, we obtain $\widetilde{G}^R(P)$ as in Eqs. (6.6) and (6.7), but with G^D replaced by G^R. Note that $\widetilde{G}^R(P)$ in this case only depends on $P^2 = s$. For the t–channel loop, where $P^0 = 0$ so that $P^2 = -\vec{P}^2 = t$, the integrand $I(\vec{q},P)$ reduces to

$$I(\vec{q},P) = -\frac{1}{2\omega_{\vec{q}}\omega_{\vec{P}-\vec{q}}(\omega_{\vec{q}}+\omega_{\vec{P}-\vec{q}})}, \tag{6.19}$$

but now, contrary to the s–channel case, $G(P)$ not only depends on $P^2 = t$, but also on $\vec{P}$ and its relative orientation respect to the cubic lattice of allowed momenta in the box, $\{\vec{q}_i\}$. In the end this translates into a dependence on the scattering angle θ, already present in $t = -2(s/4-m_\pi^2)(1-\cos\theta)$, but also on the azimuthal angle ϕ, and this also happens with the u–channel case. Thus, when projecting into S-wave, $T(s) = \frac{1}{2}\int d(\cos\theta)A(s,\cos\theta)$, we should now also integrate on ϕ, $T(s) = \frac{1}{4\pi}\int d\phi\int d(\cos\theta)A(s,\cos\theta,\phi)$. Finally, $\widetilde{H}^R$ can be evaluated using the Poisson resummation formula (see *e.g.* [452]) and taking into account that $H^R = 0$ we obtain

$$\widetilde{H}^R = \frac{m_\pi}{4\pi^2 L}\sum_{0\neq\vec{n}\in\mathbb{Z}^3}\frac{1}{|\vec{n}|}K_1(|\vec{n}|m_\pi L), \tag{6.20}$$

where K_1 is the Bessel function.

The s–channel loops, though treated in different ways by the IAM and N/D methods, are responsible for the right unitarity cut, and contain the most important L dependence

of the amplitude. This L dependence coming from the unitarity cut is the one used by the Lüscher/chiral unitary approach method to obtain the phase-shift from the energy levels in a finite volume. However, the t– and u–channel loops (which give rise to the LHC when projecting into partial waves) and the tadpoles, give an extra dependence on L (polarization corrections in the terminology of Ref. [157]) that is neglected in the Lüscher/chiral unitary approach method since it is exponentially suppressed.

6.2.3 The IAM approach

We consider now the elastic IAM [24–28], which we briefly review in this section and describe how to extend it to consider scattering in a finite box.

The elastic IAM makes use of elastic unitarity and Chiral Perturbation Theory (ChPT) [18] to evaluate a dispersion relation for the inverse of the $\pi\pi$ scattering partial wave of definite isospin I and angular momentum J, T^{IJ} (in the following we drop the superscript IJ to simplify notation). The advantage of using the inverse of a partial wave stems from the fact that its imaginary part is fixed by unitarity,

$$\text{Im } T = -\frac{\sigma}{16\pi}|T|^2 \quad \Rightarrow \quad \text{Im } T^{-1} = \frac{\sigma}{16\pi} \ . \tag{6.21}$$

Thus, the RHC integral can be evaluated exactly in the elastic regime and the obtained partial wave satisfies unitarity exactly. The partial wave amplitudes calculated in ChPT cannot satisfy unitarity exactly since they are obtained in a perturbative expansion $T = T_2 + T_4 + \mathcal{O}(p^6)$, where $T_2 = \mathcal{O}(p^2)$ and $T_4 = \mathcal{O}(p^4)$ are the Leading Order and Next–to–Leading Order contributions in the chiral expansion of T, respectively. However, unitarity is satisfied in a perturbative way,

$$\text{Im } T_2 = 0, \quad \text{Im } T_4 = -\frac{\sigma}{16\pi}T_2^2, \quad \cdots \ . \tag{6.22}$$

These equations allow us to evaluate the dispersion relation and obtain a compact form for the partial wave as we show below.

We write then a dispersion relation for an auxiliary function $F \equiv T_2^2/T$, whose analytic structure consists on a RHC (RC) from $4m_\pi^2$ to ∞, a LHC from $-\infty$ to 0, and possible poles coming from zeros of T,

$$F(s) = F(0) + F'(0)s + \tfrac{1}{2}F''(0)s^2 + \frac{s^3}{\pi}\int_{RC} ds' \frac{\text{Im } F(s')}{s'^3(s'-s)} + LC(F) + PC \ , \tag{6.23}$$

where we have performed three subtractions to ensure convergence. In the above equation $LC(F)$ stands for the integral over the left-hand cut, and PC stands for possible poles contributions, which are present in the scalar waves due to the Adler zeros. Using Eqs. (6.21) and (6.22) we can evaluate *exactly* in the RHC integral Im $F = -$Im T_4, and obtain for the RHC $RC(F) = -RC(T_4)$. The subtraction constants can be evaluated with ChPT since they only involve amplitudes or their derivatives evaluated at $s = 0$, $F(0) \simeq T_2(0) - T_4(0)$, $F'(0) \simeq T_2'(0) - T_4'(0)$, $F''(0) \simeq -T_4''(0)$. The LHC can be considered to be dominated by its low energy part, since we have three subtractions, and it is also dumped by an extra $1/(s'-s)$ when considering physical values of s. Then, we evaluate it using ChPT to obtain

$LC(F) \simeq -LC(T_4)$. The pole contribution is formally $\mathcal{O}(p^6)$ and we neglect it (this causes some technical problems in the subthreshold region around the Adler zeros which can be easily solved, but they do not affect the description of scattering or resonances, for details see [282]). Taking into account all the above considerations we arrive at

$$\begin{aligned}\frac{T_2^2(s)}{T(s)} &\simeq T_2(0) + T_2'(0)s - T_4(0) - T_4'(0)s - \tfrac{1}{2}T_4''(0)s^2 \\ &\quad - RC(T_4) - LC(T_4) = T_2(s) - T_4(s) \ ,\end{aligned} \tag{6.24}$$

where in the last step we have taken into account that $T_2(s)$ is just a first order polynomial in s so that $T_2(s) = T_2(0) + T_2'(0)s$, and that the remaining piece in the middle member of Eq. (6.24) is a dispersion relation for $-T_4(s)$. Then one obtains the simple IAM formula,

$$T^{IAM} = \frac{T_2^2}{T_2 - T_4} \ . \tag{6.25}$$

This formula can be systematically extended to higher orders by evaluating the subtraction constants and the LHC in the dispersion relation to higher orders. Note that the full one–loop ChPT calculation is used, so the IAM partial waves depend on the chiral Low Energy Constants (LECs), that absorb the loop divergences through their renormalization and depend on a renormalization scale μ. Of course, this μ dependence is canceled out in physical observables. In the case of $\pi\pi$ scattering there appear four LECs, denoted $l_i^r(\mu)$, $i = 1...4$. These LECs are not fixed from symmetry considerations and their value has to be determined from experiment. For the IAM calculations here we take the values used in [393]: $10^3 l_1^r = -3.7 \pm 0.2$, $10^3 l_2^r = 5.0 \pm 0.4$, $10^3 l_3^r = 0.8 \pm 3.8$, $10^3 l_4^r = 6.2 \pm 5.7$, at $\mu = 770$ MeV, which give a good description of phase-shift data.

Now, the energy levels in the box are obtained from the poles in the scattering partial wave, Eq. (6.25), or equivalently, the zeros of $T_2(s) - \widetilde{T}_4(s)$. From these energy levels at several values of L one can re-obtain the phase-shifts for the infinite volume with the Lüscher/chiral unitary approach method, and compare them with the exact infinite volume result to quantify the effect of neglecting the L dependence coming from the crossed channel loops and tadpoles.

6.2.4 The *N/D* method

The case presented in Subsec. 6.2.1 can be put in the more general framework of the N/D method. This was already explained in Sec. 2.7, and it was applied later in different chapters. In particular, the case of $\pi\pi$ scattering at NLO was treated in detail in Sec. 5.3. We recall the main results therein, with the proper sign and notation of this Chapter (recall the different normalization of the amplitude in this Chapter). We have:

$$\begin{aligned}V_2(s) &= T_2(s) \ , \\ V_4(s) &= T_4(s) - T_2(s)^2 G^D(s) \ .\end{aligned} \tag{6.26}$$

Since it will be useful some lines below, we also recall here that there is no RHC in the chiral amplitude V_4, because, as seen in Eq. (5.8),

$$T_4^U(s) - T_2(s)^2 G^D(s) = T_2(s)^2 (G^R(s) - G^D(s)) \ , \tag{6.27}$$

where we have adopted the sign conventions of this Chapter.

For the free parameters ($\bar{l}_i = 1, \ldots, 4$ and a subtraction constant a) we take the values of the fit in Chapter 5, Sec. 5.3, collected in Table 5.1.

In order to study the finite volume scattering, the same replacements as in the IAM and BS methods must be done. In particular, in the kernel $V(s) \to \widetilde{V}(s)$ no change is needed in $V_2(s)$, whereas $V_4(s)$ is changed to $\widetilde{V}_4(s)$,

$$\widetilde{V}_4(s) = \widetilde{T}_4(s) - T_2(s)^2 \widetilde{G}^D(s) \ . \tag{6.28}$$

Notice that, in view of Eq. (6.27), there is no finite volume effect in the s-channel contributions to the kernel $\widetilde{V}(s)$. The volume dependence enters then in the kernel through the t- and u-channel loop functions and tadpoles evaluated as discussed in Sec. 6.2.3. The s–channel volume dependence enters then at the denominator of the amplitude:

$$\widetilde{T}(s) = \frac{\widetilde{V}(s)}{1 - \widetilde{V}(s)\widetilde{G}^D(s)} \tag{6.29}$$

through the function $\widetilde{G}^D(s)$ in its version of Eq. (6.6), which gives the most important contribution to the aforementioned dependence, as in the case of the IAM method. The change in the values of the subtraction constant a with L is not considered because this is accounted for by employing $\widetilde{G}^D(s)$, Eq. (6.6).

6.3 Results

As already explained, the main aim of the present work is to quantify the effect of the dependence of the different potentials considered on the size of the box, L. Hence, we are going to compare the L dependence of the N/D and the IAM methods with that of the BS, which kernel does not depend on L. We discuss first the results for the $I = 0$ case and later those of the $I = 2$ case.

First we show in Fig. 6.1 (left panel) the results for the $\pi\pi$ phase-shifts in S-wave and $I = 0$ for the three different models in infinite volume. Note that in the present work we are not interested in a detailed description of scattering data, but on the effects of ignoring the exponentially suppressed dependence on the box size when using Lüscher's or the chiral unitary approach to obtain the scattering phase-shifts from the energy levels in finite volume. The IAM and N/D results (solid and dashed lines, respectively) are the fits explained in the previous section and the BS (dot-dashed line) is fitted in this work to the experimental data [284–286,289,290,364] shown in the figure up to 800 MeV. The IAM and N/D approaches are essentially equivalent at low energies but differ slightly as the energy increases. Thus the difference between the IAM and N/D phase shifts is mainly due to the different set of data used in the fit and it also gives an idea of the theoretical uncertainty. The BS approach produces a curve in between the other two, closer to the N/D at low energies and to the IAM at higher energies. In any case, the different models are compatible within the experimental uncertainties. Let us note that what matters for the discussions in the present work is not

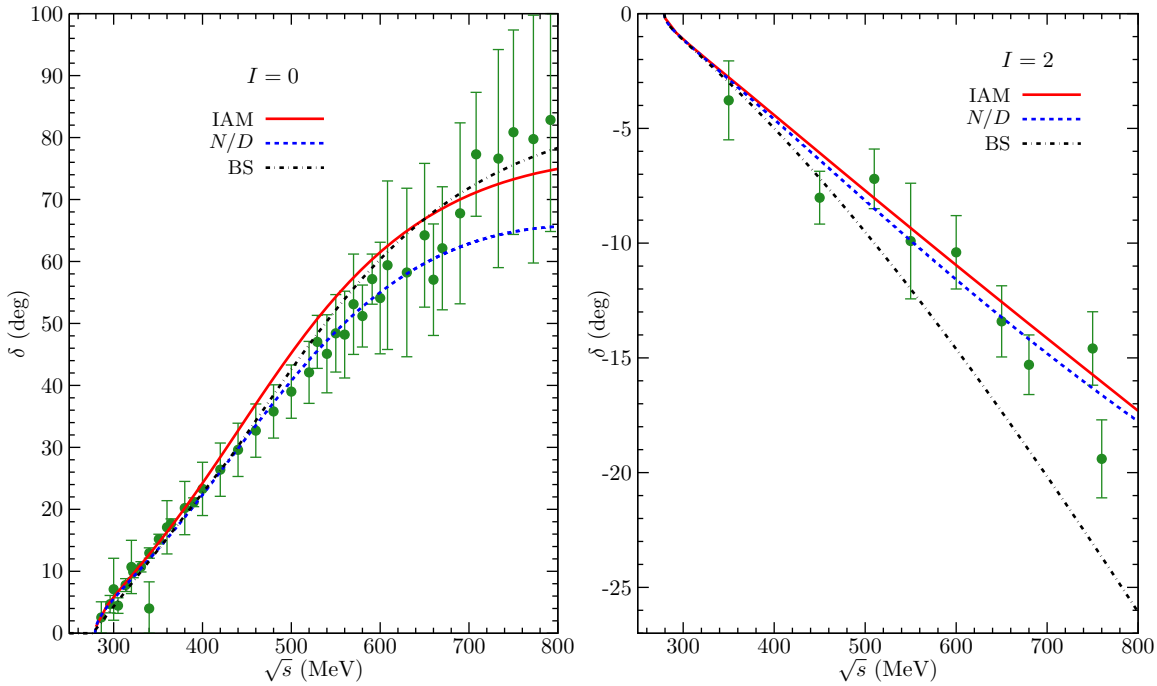

Figure 6.1: S-wave, $\pi\pi \to \pi\pi$ phase-shifts for the three different models considered: solid, dashed and dot-dashed lines correspond to IAM, N/D and BS, respectively. Left: $I = 0$ case. The experimental data are from Refs. [284–286, 289, 290, 364]. Right: $I = 2$ case. The experimental data are from Refs. [371, 372].

the actual values of the phase-shifts at infinite volume but the relative change when going to the finite box.

In Fig. 6.2 (left panel) we show the energy levels for different values of the cubic box size, L, for the different models which have been obtained from the poles of the scattering amplitudes in the finite box as explained in the previous section. The dotted lines represent the free $\pi\pi$ energies in the box, while the other lines correspond to IAM, N/D and BS as in Fig. 6.1.

The differences are very small for the largest values of L shown in the plot but are more important for smaller L, specially between the N/D and IAM methods. The BS approach produces a curve in between the other two, closer to the N/D. The IAM and BS are more similar for larger values of energies as can also be seen in the phase shifts, Fig. 6.1. As an example of small L, we note that for $L = 1.7 m_\pi^{-1}$ the difference between N/D and IAM is about 30 MeV.

An actual lattice calculation would provide some points over analogous trajectories in the E vs. L plots. The "inverse problem" is the problem of getting the actual scattering amplitudes (and hence by-product magnitudes like phase-shifts) in the infinite space from data produced by lattice QCD consisting of points in plots of E vs. L over the energy levels in the box. For points in these levels the amplitude in the infinite volume can be extracted from the generalization of the Lüscher formula, as explained in the previous sections, see Eq. (6.9).

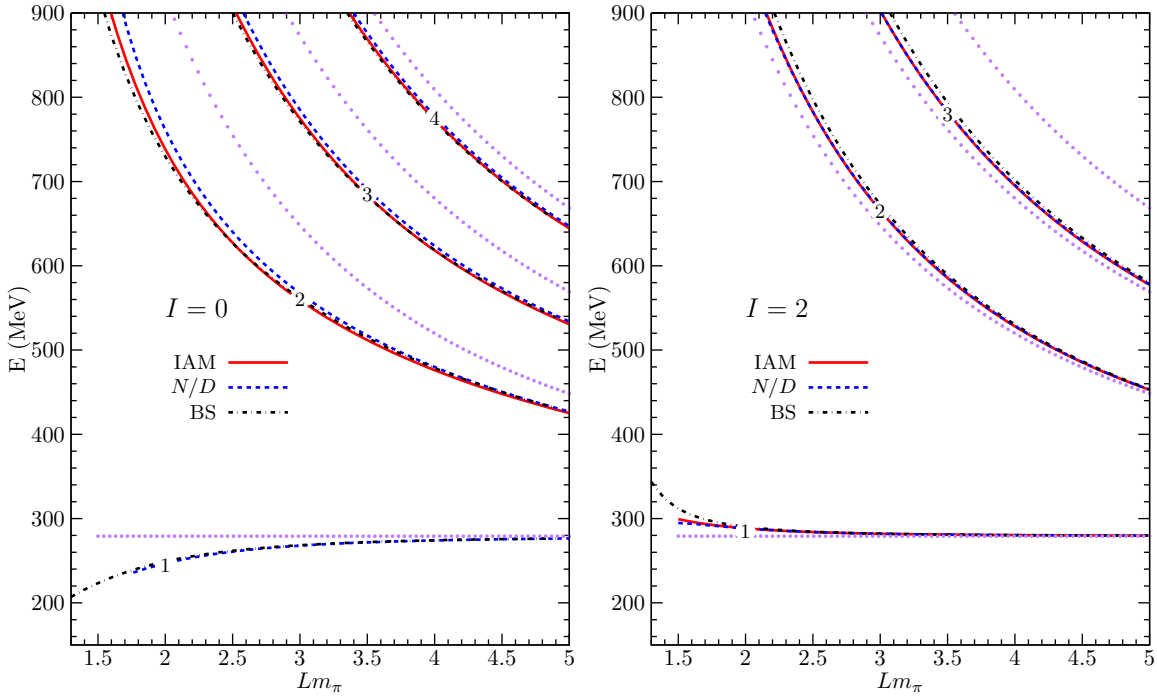

Figure 6.2: The first energy levels as a function of the cubic box size L for the three different models considered. The dotted lines indicate the free $\pi\pi$ energies in the box. The rest of the lines correspond to IAM, N/D and BS as in Fig. 6.1. Left: $I = 0$ case. Right: $I = 2$ case.

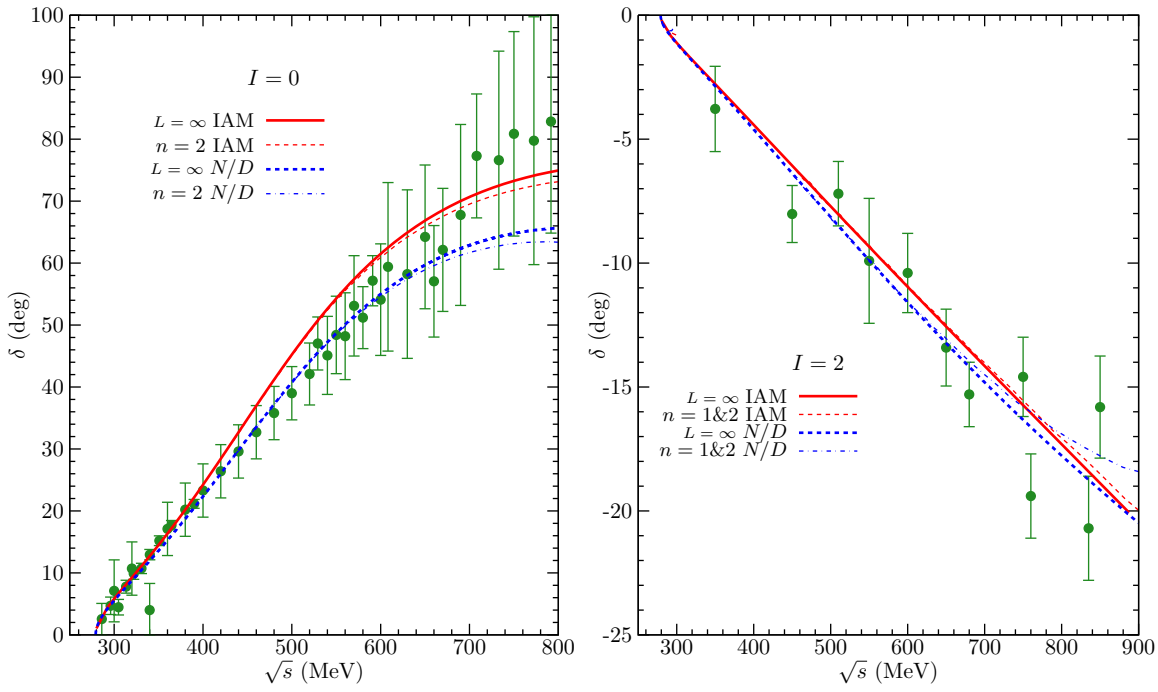

Figure 6.3: Solution of the inverse problem for the IAM and N/D methods. The BS result is the same as in the infinite volume case and thus we do not show it in the figure. Left: $I = 0$. Right: $I = 2$. We show the results obtained only from level 2 ($I = 0$) or levels 1 and 2 ($I = 2$) of Fig. 6.2 since the results with levels above these ones almost overlap with the infinite volume line. For the meaning of each line consult the inset in the figure.

In Fig. 6.3 (left panel) we show the phase-shifts obtained for the different methods implementing the "inverse problem" analysis (or "reconstructed" results) with Eq. (6.9) and from the E vs. L plot. For the BS model the results are independent of the level used for a given E, since the potential does not depend on L, and they are equal to the infinite volume result. Therefore we do not show the BS result since it is the same as in Fig. 6.1. For the IAM and N/D methods the results depend on the level chosen for a given E since the potentials depend on L as explained in the previous sections. Actually, for levels above the second one of Fig. 6.2 the results are almost equal to the infinite volume results and hence we do not show them in the figure since they would almost overlap with the infinite volume line. This is because, as seen in Fig. 6.2, for the higher energies these levels imply large values of L. Indeed, for energies below 800 MeV this implies values of L higher than about $3m_\pi^{-1}$. For the results obtained with level 2, the phase-shifts differ in about 5% of the result in the infinite volume at the higher energies considered. For $E \sim 800$ MeV this implies L values slightly smaller than $2m_\pi^{-1}$, as can be seen in Fig. 6.2. It is worth noting that the effect of the dependence on L of the models with LHC go in the same direction and are of similar size in spite of the different models used. This gives us confidence that the actual L dependence of the LHC cut is properly considered and the real effect of any realistic model would be of the order obtained in the present work. An analysis with Eq. (6.9) applied to actual lattice results of E versus L levels would neglect the possible L dependence of the potential and hence the errors from the L dependence of the LHC would be of the order of the differences shown in the figure. Note also that the L dependence of the results are smaller than the initial difference between the N/D and IAM themselves and also lower than the experimental uncertainties. Therefore, an actual lattice calculation should care about this L dependence only if it aims at getting errors smaller than the effect obtained in the present work.

Let us now discuss the results for $I = 2$. In the right panels of Figs. 6.1, 6.2 and 6.3 we show for the $I = 2$ case the same results that were shown in the left panels for $I = 0$. In Fig. 6.1 we see that the IAM and N/D methods provide very similar results and compatible with the experimental data while the BS approach gets worse phase-shifts. This is because in the IAM and N/D the LHC is included perturbatively order by order, unlike the BS model, and in this channel the LHC cut is more relevant. In Fig. 6.2 (right panel) we show the energy levels in the box for this channel.

Now both IAM and N/D provide similar results. In Fig. 6.3 (right panel) we show the solution of the inverse problem for the phase-shifts. We see that the N/D method provides a higher L dependence for large values of the energies, unlike IAM. At 800 MeV the difference is about 10% for the N/D and 2% for the IAM. The difference in the phase-shifts between the two approaches is large in spite of the energy levels being very similar. This is because the energy levels are very close to the free case, unlike the $I = 0$ case, and then the $\widetilde{G}$ function is very steep. This makes that small variations in E provide large variations in $\widetilde{G}$.

In usual inverse problem analysis from actual lattice results, it is common to use the Lüscher formula [156, 157] which, as explained in section 6.2.1, is an approximation to that used in the present work, Eq. (6.9). Therefore it is worth studying what is the error made in the reconstructed phase-shifts if one uses the Lüscher equation instead of the exact one. In Ref. [158] it was shown that the Lüscher method can be reproduced if in Eq. (6.7) one

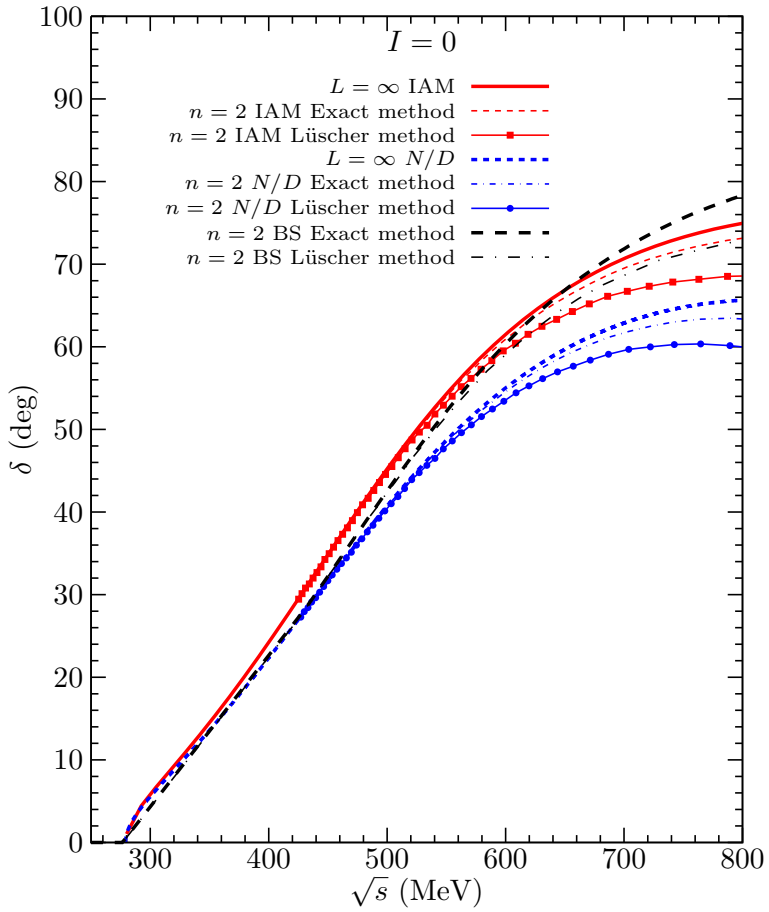

Figure 6.4: Difference between the exact inverse method formula, Eq. (6.9), and the approximated Lüscher formula. The approach corresponding to each line is given in the inset in the figure.

substitutes

$$I(p,s) = \frac{1}{\omega(\vec{p})}\,\frac{1}{s - 4\omega(\vec{p})^2}. \tag{6.30}$$

by

$$I(p,s) = \frac{1}{2\sqrt{s}}\,\frac{1}{p_{\mathrm{ON}}^2 - \vec{p}^{\,2}}. \tag{6.31}$$

where $p_{\mathrm{ON}} = \frac{E}{2}\sqrt{1 - \frac{4m^2}{s}}$.

In Fig. 6.4 we show the effect in the $I = 0$ phase-shifts of using the pure Lüscher method, Eq. (6.31), instead of the exact one, Eq. (6.30). (For the $I = 2$ case the effect is small and thus we do not show any plot.) The difference is significant only for phase-shifts extracted from level 2 of the left panel of Fig. 6.2 since the difference is only relevant for small values of L. Therefore we only plot results extracted from level 2. The difference between the exact method and the Lüscher one is similar for all the three different models for the potential. The size of the difference is similar to the one from the L dependence of the potential discussed above, and goes in the same direction, so that the effect is magnified.

6.4 Summary and conclusions

In this Chapter we have faced the problem of the presence of the LHC of the $\pi\pi$ amplitude for the evaluation of phase-shifts from lattice QCD results using Lüscher's approach. The nonperturbative approach, the study for energies different than threshold and the study of the $I = 0$ $\pi\pi$ system are done in the present work for the first time in the literature. The $t-$ and $u-$channel terms can be taken into account in a field theoretical approach by means of the IAM, or NLO N/D methods, leading to good reproductions of the scattering data. Results from lattice QCD should contain all the dynamics and, as a consequence, should account for these effects too. However, the method to go from the discrete energy level in a box from lattice simulations to the phase shifts for scattering in the infinite volume case requires the use of Lüscher's approach, or its improved version of [158], both of which rely upon the existence of a volume independent potential. Yet, the terms contributing to the LHC, containing loops in the $t-$ and $u-$channels, are explicitly volume dependent. In this work we have investigated the errors induced by making use of [156] or [158] in the reproduction of phase-shifts from the energy spectrum of lattice calculations in the finite box by evaluating the volume dependence of the $\pi\pi$ scattering amplitude in one-loop ChPT. The latter is then implemented in non-perturbative methods to extract the final partial wave amplitudes. We have found that in the case of $\pi\pi$ scattering in S-wave, both for $I = 0$ and $I = 2$, the effect of the L dependence in the potential is smaller than the typical errors from the experimental phase-shifts or the differences between the three models that we have used, the IAM, N/D NLO and BS LO. This is good news for lattice calculations since one of the warnings not to go to small values of L was the possible L dependence of the potential which in some cases, like in the present one, we know that exists. We found that it is quite safe to ignore this dependence for $L > 2.5 m_\pi^{-1}$, and even with values of L around $1.5 - 2 m_\pi^{-1}$ the errors induced are of the order of 5%.

On the other hand we have quantified the error made by using the pure Lüscher formula instead of the exact one, Eq. (6.9). The difference in the phase-shifts between this approximation and that of Eq. (6.9) has a similar size as the difference between the latter and the infinite volume case, and goes in the same direction, so that the effect is magnified.

All these findings, together with the use of the approach of Ref. [158] that also eliminates L depended terms (exponentially suppressed) from the Lüscher's approach, can encourage the performance of lattice calculations with smaller size boxes with the consequent economy in the computing time.

7

Nucleon-Nucleon Interactions from Dispersion Relations

Contents of this Chapter:

7.1 Introduction

The Nucleon-Nucleon (NN) interaction is a basic process whose understanding is necessary for the study of nuclear structure, nuclear reactions, nuclear matter, neutron stars, etc [159–162, 183, 184]. Since the early nineties [163–165] the low energy Effective Field Theory of QCD, Chiral Perturbation Theory (ChPT) [18, 19], has been applied to NN scattering in a large number of studies, see *e.g.* [163–169, 454–465]. Further references can be found in the above reviews. A sophisticated stage has been reached where the NN potential is calculated in ChPT up to N^{3}LO [458, 462].

However, as the NN interaction is nonperturbative, the chiral NN potential must be

iterated. It was proposed by Weinberg in his seminal papers [163, 164] to solve a Lippmann-Schwinger equation in terms of the calculated chiral NN potential, which can be improved order by order. Since the chiral potential is singular at the origin a regularization method, typically a three-momentum cut-off Λ [166,167,458–460,462], should be introduced for solving the Lippmann-Schwinger equation.

Despite the great phenomenological success achieved by the NN chiral potentials in describing NN scattering data [458,462], it was shown in the literature [170–176] that the chiral counterterms introduced in the NN potential following naive dimensional analyses are not enough to renormalize the resulting NN scattering amplitude. In Ref. [170] one counterterm is promoted from higher to lower orders in the partial waves ${}^3P_0$, ${}^3P_2$ and ${}^3D_2$. As a consequence, stable results are achieved, independent of cut-off in the limit $\Lambda \to \infty$, when the LO one-pion exchange (OPE) potential is employed. Similar conclusions are drawn in Ref. [470]. However, this promotion implies a violation of the standard ChPT counting and of the low energy theorems relating the parameters in the effective range expansion. The works in Refs. [177, 180], following the ideas of Refs. [181, 182], stress that the cut-off Λ should not be taken beyond the breakdown scale of the EFT, typically around 1 GeV. If no higher-order counterterms are introduced when the cut-off is taken to infinity the mixing between the S and D waves in the ${}^3S_1$–${}^3D_1$ system vanishes and one has a strong cut-off dependence of the tensor force from the non-local OPE potential so that it vanishes for $\Lambda \to \infty$ [466]. One should be aware that when $\Lambda \to \infty$ a more involved counting emerges [171, 178, 179, 466–468]. The extension of these ideas to higher orders in the chiral potential is not straightforward and cannot avoid cut-off dependence up to now [469,470]. On the other hand, the application of Weinberg's scheme has given rise to a great phenomenological success in the reproduction of NN phase shifts if the cut-off is fine-tuned in a region around 600 MeV, not beyond the breakdown scale of the effective field theory (EFT) (see *e.g.* [456–460, 462–464]). Of course, the cut-off dependence is not removed then.

Partial wave amplitudes with larger orbital angular momentum ℓ, $\ell \geqslant 3$, can be calculated in Born approximation with sufficient accuracy [178, 179, 454, 467, 468]. Then, they do not pose a problem for renormalization, making use of standard perturbative renormalization. It is also argued in the same Ref. [170] that higher orders terms in the chiral NN potential could be treated perturbatively. Ref. [170] was extended along these lines to subleading two-pion exchange (TPE) in Ref. [469]. The promotion of higher orders to lower ones due to nonperturbative renormalizability is studied in detail in Ref. [178, 179, 467, 468] by making use of the regularization group equations (see also Refs. [171–173] for a coordinate space renormalization by imposing appropriate boundary conditions).

In this Chapter, we report on our papers [E, F]. We shall employ the N/D method [38] for studying NN interactions, for both uncoupled and coupled[1] partial waves. The N/D method was exposed for the case of meson-meson partial waves in Sec. 2.7. We just recall here that it is based in the splitting of the left-hand cut (LHC) and the right-hand cut (RHC) in two different functions, N and D, respectively. A linear integral equation then results for

[1]Some words regarding our terminology are in order. NN spin-triplet ($S = 1$) partial waves can mix (except for the ${}^3P_0$, see Appendix F.) Then, we call them *coupled* or *uncoupled*, depending on the case. The term *inelastic*, as opposed to *elastic*, refers in NN interactions terminology to processes in which other particles are produced, *e.g.*, $NN \to NN\pi$ (which is the lowest threshold inelastic process).

determining the NN partial waves. The input is given by the discontinuity of the partial wave along the LHC due to multi-pion exchanges, the lightest one being just OPE. The well known behavior of a partial wave near threshold, that vanishes like $|\mathbf{p}|^{2\ell}$, with $|\mathbf{p}|$ the center of mass (CM) three-momentum and ℓ the orbital angular momentum, is not automatically fulfilled for $\ell \geqslant 2$ in the N/D method [329, 471, 472]. As first shown in Ref. [E], one can accomplish the right threshold behavior solving the N/D method in the presence of $\ell - 1$ constraints. These are satisfied by introducing $\ell - 1$ Castillejo-Dalitz-Dyson (CDD) poles [185], as we discuss below.

In the past Refs. [473–477] applied the N/D method to study quantitatively NN scattering. Ref. [473] was restricted to the S-waves and took only OPE as input along the LHC. Refs. [474,475] included other heavier mesons as source for the discontinuity along the LHC in line with the meson theory of nuclear forces, so popular at those days. A more modern work, Ref. [476], modeled the LHC discontinuity by OPE and one or two ad-hoc poles. We stress that we present here a novel way to introduce the N/D method in harmony with the modern perspective of EFT. In this way, we show that one can calculate systematically within ChPT, according to the standard chiral counting, the discontinuity along the LHC that is the basic input for the N/D method. This allows one to systematically improve the results order by order, which is not the case by applying previous schemes [477]. In addition, the threshold behavior of partial waves with orbital angular momentum ($\ell \geqslant 2$) is satisfied within our approach by including CDD poles, as we show below. However, in the previous works [474, 475] the correct threshold behavior was achieved in an ad-hoc way by including a fictitious pole below threshold, with the subsequent dependence of the results on its location that was fitted to data. Furthermore, in our results we always respect unitarity (for both the coupled and the uncoupled waves cases), which was not the case in Refs. [473–476].

After this Introduction we discuss the N/D method for calculating the NN uncoupled partial waves in Sec. 7.2. Special attention is paid to derive the constraints needed to meet the threshold behavior for a partial wave with $\ell \geqslant 2$ and how to fulfill them. The results for the uncoupled partial waves are discussed in Sec. 7.3. We present the generalization of the method to the case of coupled channels in Sec. 7.4, where the corresponding three linear integral equations needed for each set of coupled partial waves are derived. The results obtained with this formalism are given in Sec. 7.5. We consider in some detail the important case of the ${}^3S_1$–${}^3D_1$ waves, Subsecs. 7.5.1–7.5.2, whereas the higher coupled partial waves are treated in Subsec. 7.5.3. Conclusions are given in Sec. 7.6. The OPE amplitudes used in this Chapter are contained in Appendix F. Appendix G contains the technical way used to solve numerically the integral equations. In Appendix H the cancellation of a potential divergence in a function involved in our equations is treated.

7.2 The N/D method for NN uncoupled partial waves

7.2.1 NN partial waves cuts

We consider the nucleon-nucleon (NN) scattering

$$N(\mathbf{p}_1;\sigma_1\alpha_1)N(\mathbf{p}_2;\sigma_2\alpha_2) \to N(\mathbf{p}_1';\sigma_1'\alpha_1')N(\mathbf{p}_2';\sigma_2'\alpha_2')$$

whose scattering amplitude in the center-of-mass frame (CM) is indicated by

$$\langle \mathbf{p}', \sigma_1'\alpha_1'\sigma_2'\alpha_2'|T_d||\mathbf{p}|\hat{\mathbf{z}}, \sigma_1\alpha_1\sigma_2\alpha_2\rangle \ .$$

Here the initial momentum $\mathbf{p} = |\mathbf{p}|\hat{\mathbf{z}}$ is along the z-axis and the final one corresponds to $\mathbf{p}'$. Its decomposition in partial waves is discussed in detail in Appendix A of Ref. [162], to which we refer for further details. We denote a NN partial wave by $T_{JIS}(\ell', \ell; |\mathbf{p}|^2)$ being ℓ' the final orbital angular momentum and ℓ the initial one, while J, S and I stand for the total angular momentum, spin and isospin of the reaction, respectively:

$$T_{JIS}(\ell', \ell; |\mathbf{p}|^2) = \frac{Y_\ell^0(\hat{\mathbf{z}})}{2J+1} \sum (\sigma_1'\sigma_2's_3'|s_1s_2S)(\sigma_1\sigma_2s_3|s_1s_2S)(0s_3s_3|\ell SJ)(m's_3's_3|\ell' SJ)$$
$$\times (\alpha_1'\alpha_2'i_3|\tau_1\tau_2I)(\alpha_1\alpha_2i_3|\tau_1\tau_2I) \int d\hat{\mathbf{p}}' \, \langle \mathbf{p}', \sigma_1'\alpha_1'\sigma_2'\alpha_2'|T_d||\mathbf{p}|\hat{\mathbf{z}}, \sigma_1\alpha_1\sigma_2\alpha_2\rangle Y_{\ell'}^{m'}(\mathbf{p}')^* \ . \qquad (7.1)$$

In this equation, the Clebsch-Gordan coefficients for the couplings of two angular momentum j_1, j_2 to j_3 is indicated by $(m_1m_2m_3|j_1j_2j_3)$, with m_1, m_2 and m_3 the corresponding third components.

A NN partial wave amplitude has two cuts [224], RHC for $0 < \mathbf{p}^2 < \infty$, due to unitarity, and the LHC for $-\infty < \mathbf{p}^2 < L$ with $L = -m_\pi^2/4$, due the crossed channel dynamics. Both cuts are depicted in Fig. 7.1. The upper limit for the latter is given by the OPE, as the pion is the lightest particle that can be exchanged in the t- and u-channels. Because of unitarity, a partial wave amplitude satisfies in the CM frame above the elastic threshold and below the pion production one, the relation

$$\mathrm{Im}T_{JIS}(\ell', \ell; |\mathbf{p}|^2)^{-1} = -\frac{m|\mathbf{p}|}{4\pi}\delta_{\ell'\ell} \ , \qquad (7.2)$$

with m the mass of the nucleon. In our normalization, the S-matrix is given by:

$$S_{JIS} = \mathbb{I} + i\frac{m|\mathbf{p}|}{2\pi}T_{JIS} \ .$$

As shown in Ref. [162] one can calculate perturbatively in ChPT $\mathrm{Im}T_{JIS}$ along the LHC, since this imaginary part is due to multi-pion exchanges. The infrared enhancements associated with the RHC, see Fig. 7.2, are absent in the discontinuity along the LHC because, according to Cutkosky's theorem [478, 479], it implies to put on-shell pionic lines. Within loops the pion poles are picked up making that the energy along nucleon propagators now is of $\mathcal{O}(p)$, instead of a nucleon kinetic energy. In this way, the order of the diagram rises compared to that of the reducible parts and it becomes a perturbation. At leading order (LO), according to the counting developed in Refs. [162, 183] (that for two nucleon irreducible diagrams coincides with the standard chiral counting [163–165]), the only contribution to $\mathrm{Im}T_{J\ell S}$ along the LHC is OPE.

7.2.2 *S*- and *P*-waves ($\ell = 0, 1$)

In the following we take the uncoupled channel case for which $\ell' = \ell = J$ (except for the ${}^3P_0$.) An scheme of the different waves that are coupled or not in NN scattering can be found

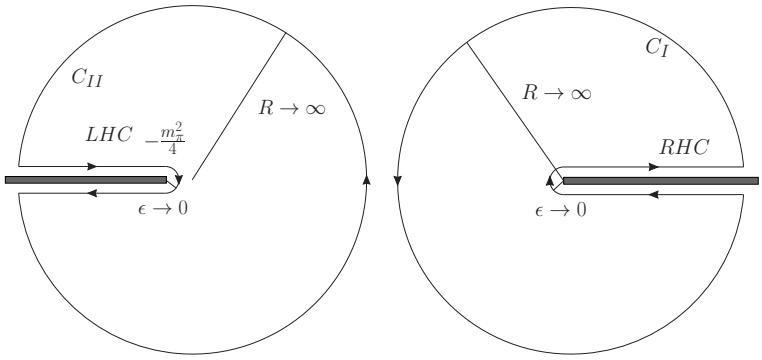

Figure 7.1: The thick lines correspond to the RHC and LHC, from top to bottom. In the same figure the integration contours C_I and C_{II} for evaluating $D_{J\ell S}(A)$ and $N_{J\ell S}(A)$, respectively, are shown. One has to take the limit $\epsilon \to 0^+$.

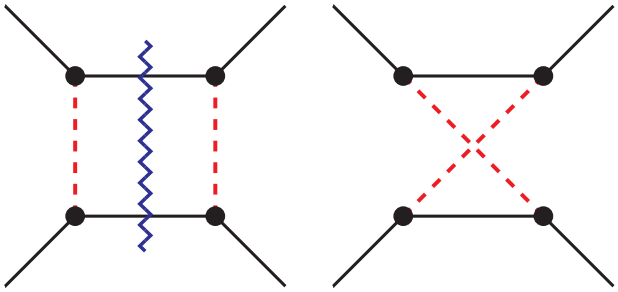

Figure 7.2: RHC enhancements. Left: reducible diagram. No pion lines are put on-shell. The intermediate states are NN, so that typical energies go like $\frac{1}{q} \times \frac{m_N}{q} \gg \frac{1}{q}$, and this gives an enhancement of this diagram on the RHC. Right: irreducible diagram. Pionic lines are put on-shell. The intermediate states are $NN\pi$, so that typical energies are $\simeq \frac{1}{q}$, thus no enhancement is present.

in Appendix F. The N/D method [38], as explained in Subsec. 2.7, rests on the separation between the RHC and LHC. In this way, a partial wave $T_{J\ell S}(A)$ is written as:[2]

$$T_{J\ell S}(A) = \frac{N_{J\ell S}(A)}{D_{J\ell S}(A)} \ . \tag{7.3}$$

The function $N_{J\ell S}(A)$ has only LHC while $D_{J\ell S}(A)$ has only RHC. Taking into account elastic unitarity, Eq. (7.2), one can write:

$$\mathrm{Im}D_{J\ell S}(A) = -N_{J\ell S}(A)\frac{m\sqrt{A}}{4\pi} \quad , \quad A > 0 \ . \tag{7.4}$$

Along the LHC, from Eq. (7.3), one also has:

$$\mathrm{Im}N_{J\ell S}(A) = D_{J\ell S}\,(A)\ \mathrm{Im}T_{J\ell S}(A) \quad , \quad A < -m_\pi^2/4 \ . \tag{7.5}$$

We first write down a dispersion relation (DR) for $D_{J\ell S}(A)$ and $N_{J\ell S}(A)$ taking as integration contours C_I and C_{II} in Fig. 7.1, respectively. The integration along the circle at infinity

[2]We replace the subscript I by ℓ when denoting a partial wave. The former can be deduced from ℓ and S, because of the rule $\ell + S + I =$ odd and $I = 0$ or 1.

vanishes, if necessary, by taking the sufficient number of subtractions. For the case of a once-subtracted DR the following expressions result:

$$D_{J\ell S}(A) = 1 - \frac{A-D}{\pi}\int_0^{+\infty} \mathrm{d}q^2 \frac{\rho(q^2) N_{J\ell S}(q^2)}{(q^2-A)(q^2-D)} \ , \tag{7.6}$$

$$N_{J\ell S}(A) = N_{J\ell S}(D) + \frac{A-D}{\pi}\int_{-\infty}^{L} \mathrm{d}k^2 \frac{\Delta_{J\ell S}(k^2) D_{J\ell S}(k^2)}{(k^2-A)(k^2-D)} \ . \tag{7.7}$$

Here we have indicated by $\rho(A)$ the non-relativistic phase space, for $A > 0$:

$$\rho(A) = m\sqrt{A}/4\pi \ , \tag{7.8}$$

and, for $A < L = -m_\pi^2/4$, whe have defined:

$$\Delta_{J\ell S}(A) = \mathrm{Im} T_{J\ell S}(A) \ . \tag{7.9}$$

For physical scattering, $A \to A + i\epsilon$. The subtraction constant in $D_{J\ell S}(A)$ has been fixed to 1 because, according to Eq. (7.3), only the ratio between $N_{J\ell S}(A)$ and $D_{J\ell S}(A)$ matters for determining $T_{J\ell S}(A)$. In this way one has the freedom to fix the value of $D_{J\ell S}(A)$ at one point. The key difference with Sec. 2.7 is that here we do not neglect the LHC and we do not set $N(A) = 1$.

Asymptotically, for $\mathbf{p}^2 \to -\infty$, OPE tends to constant, so that, according to the Sugawara and Kanazawa theorem [329, 480] one subtraction is necessary for the DR of $N_{J\ell S}(A)$, even though $\Delta_{J\ell S}(A) \to 1/A$ in the case of OPE. On general grounds, a partial wave amplitude is bound by a constant because of unitarity for $A \to +\infty$ and the same theorem then requires that at least one subtraction is necessary.

An integral equation for $D_{J\ell S}(A)$ results by including the DR for $N_{J\ell S}(A)$, Eq. (7.7), into that of $D_{J\ell S}(A)$, Eq. (7.6):

$$\begin{aligned} D_{J\ell S}(A) = 1 &- N_{J\ell S}(D)\frac{A-D}{\pi}\int_0^{+\infty} \mathrm{d}q^2 \frac{\rho(q^2)}{(q^2-A)(q^2-D)} \\ &- \frac{A-D}{\pi^2}\int_0^{+\infty} \mathrm{d}q^2 \frac{\rho(q^2)}{q^2-A}\int_{-\infty}^{L} \mathrm{d}k^2 \frac{\Delta_{J\ell S}(k^2) D_{J\ell S}(k^2)}{(k^2-q^2-i\epsilon)(k^2-D)} \ . \end{aligned} \tag{7.10}$$

We now introduce the function $g(A, C)$ defined as:

$$g(A,C) = \frac{1}{\pi}\int_0^{+\infty} \mathrm{d}q^2 \frac{\rho(q^2)}{(q^2-A)(q^2-C)} \ , \tag{7.11}$$

In terms of this function, Eq. (7.10) can be written as:

$$D_{J\ell S}(A) = 1 - (A-D) N_{J\ell S}(D) g(A,D) + \frac{A-D}{\pi}\int_{-\infty}^{L} \mathrm{d}k^2 \frac{\Delta_{J\ell S}(k^2) D_{J\ell S}(k^2)}{k^2-D} g(A,k^2) \ . \tag{7.12}$$

This is a linear integral equation for $D_{J\ell S}(A)$. Its linearity is an important fact because it allows one to take more subtractions and still being amenable for an iterative solution. We take as a convenient subtraction point $D = 0$. In the case of the S-waves, this relates the subtraction constant, $N_{J\ell S}(0)$, to the corresponding scattering length, a_s, through:

$$N_{J\ell S}(0) = -\frac{4\pi a_s}{m} \tag{7.13}$$

The only uncoupled S-wave is the ${}^1S_0$, and the scattering length for this wave is $a_s = -23.758 \pm 0.04$ fm. Finally, we can write an integral equation for the $D_{J\ell S}$ function for an S-wave as:

$$D_{J\ell S}(A) = 1 - AN_{J\ell S}(0)g(A,0) + \frac{A}{\pi}\int_{-\infty}^{L} \mathrm{d}k^2 \frac{\Delta_{J\ell S}(k^2) D_{J\ell S}(k^2)}{k^2} g(A,k^2) \tag{7.14}$$

This is an integral equation for $D_{J\ell S}(A)$ with A on the LHC, and it can be solved with the method exposed in Appendix G. Once $D_{J\ell S}(A)$ is solved from Eq. (7.14) one can then calculate $N_{J\ell S}(A)$ by inserting the former into Eq. (7.7), with $D = 0$, which now reads:

$$N_{J\ell S}(A) = N_{J\ell S}(0) + \frac{A}{\pi}\int_{-\infty}^{L} \mathrm{d}k^2 \frac{\Delta_{J\ell S}(k^2) D_{J\ell S}(k^2)}{k^2(k^2 - A)} \ . \tag{7.15}$$

For a P-wave, the same equations hold with $N_{J\ell S}(0) = 0$ because a P-wave amplitude vanishes at threshold as $|\mathbf{p}|^2$, and $D_{J\ell S}(0) = 1$.

7.2.3 Higher waves ($\ell \geqslant 2$)

Eqs. (7.14) and (7.15) can be readily applied to S- and P-wave scattering. However, these equations do not guarantee that the resulting partial wave amplitude has the correct behavior as A^ℓ for $A \to 0$, with $\ell \geqslant 2$, because of the full implementation of rescattering in Eq. (7.12). At LO $\Delta_{J\ell S} \equiv \Delta^{1\pi}_{J\ell S}$ gives rise to OPE through the dispersive integral:

$$T^{1\pi}_{J\ell S}(A) = T^{1\pi}_{J\ell S}(0) + \frac{A}{\pi}\int_{-\infty}^{L} \mathrm{d}k^2 \frac{\Delta^{1\pi}_{J\ell S}(k^2)}{k^2(k^2 - A)} \ , \tag{7.16}$$

with $T^{1\pi}_{J\ell S}(0)$ a subtraction constant. As discussed above, since the OPE amplitude [162] tends to constant for $A \to \infty$, the Sugawara and Kanazawa theorem requires that one subtraction is needed. The fact that for $\ell > 0$ a partial wave vanishes as A^ℓ for $A \to 0$ makes that $T^{1\pi}_{J\ell S}(0) = 0$ when $\ell > 0$. This behavior also implies that $\Delta^{1\pi}_{J\ell S}$ must fulfill the set of $\ell - 1$ sum-rules (constraints):

$$\int_{-\infty}^{L} \mathrm{d}k^2 \frac{\Delta^{1\pi}_{J\ell S}(k^2)}{k^{2\lambda}} = 0 \ , \tag{7.17}$$

with $\lambda = 2, 3, \ldots, \ell$ and $\ell \geqslant 2$. These constraints are obtained straightforwardly by performing the power expansion of Eq. (7.16) and imposing that $T_{J\ell S}(A) \to A^\ell$ for $A \to 0$.

Let us now consider again Eq. (7.7). As $D_{J\ell S}(A) \to 1$ for $A \to 0$ then $T_{J\ell S}(A) \to N_{J\ell S}(A)$ in this limit. The expression for $N_{J\ell S}(A)$, Eq. (7.7), is similar to Eq. (7.16). Indeed, they would be the same equation if $D_{J\ell S}(A)$ were replaced by 1 in Eq. (7.7) (and with $\Delta_{J\ell S}(k^2)$ evaluated at LO). As a result, $N_{J\ell S}(A)$, determined by implementing Eq. (7.12) into Eq. (7.7), does not vanish as A^ℓ for $A \to 0$, because of the departure from 1 of $D_{J\ell S}(A)$.

It is then convenient to proceed in such a way that the right behavior of $T_{J\ell S}(A)$ around threshold is incorporated explicitly. For that purpose we consider the N/D equation for $T_{J\ell S}(A)/A^\ell$, instead of that for $T_{J\ell S}(A)$, Eq. (7.3). For that purpose, we consider the N/D

equation for $T_{J\ell S}(A)/A^\ell$ instead of $T_{J\ell S}(A)$. The quotient $T_{J\ell S}(A)/A^\ell$ has no pole at $A=0$ because $T_{J\ell S}(A)\to A^\ell$ when $A\to 0$. Notice also that because of unitarity $T_{J\ell S}(A)/A^\ell\to 0$ for $A\to+\infty$ so that, according to the Sugawara and Kanazawa theorem [329,480], no subtraction are needed for the DR of $N_{J\ell S}(A)$ for $\ell>0$. EFT results do not always share the right high energy behavior so that subtractions will be certainly necessary for a higher order calculation of $\Delta_{J\ell S}(A)$. At LO this is not the case because $\Delta^{1\pi}_{J\ell S}\to 1/A$ for $A\to\infty$. We then have ($\ell>0$):

$$T_{J\ell S}(A)=A^\ell\frac{N_{J\ell S}(A)}{D_{J\ell S}(A)}\ , \tag{7.18}$$

$$N_{J\ell S}(A)=\frac{1}{\pi}\int_{-\infty}^{L}\!\!\mathrm{d}k^2\frac{\Delta_{J\ell S}(k^2)D_{J\ell S}(k^2)}{k^{2\ell}(k^2-A)}\ , \tag{7.19}$$

$$\begin{aligned}D_{J\ell S}(A)&=1-\frac{A}{\pi}\int_0^{\infty}\!\!\mathrm{d}q^2\frac{\rho(q^2)q^{2(\ell-1)}N_{J\ell S}(q^2)}{q^2-A}\\&=1+\frac{A}{\pi^2}\int_{-\infty}^{L}\!\!\mathrm{d}k^2\frac{\Delta_{J\ell S}(k^2)D_{J\ell S}(k^2)}{k^{2\ell}}\int_0^{\infty}\!\!\mathrm{d}q^2\frac{\rho(q^2)q^{2(\ell-1)}}{(q^2-A)(q^2-k^2)}\ ,\end{aligned} \tag{7.20}$$

where the subtraction has been taken at threshold.

The previous equation for $D_{J\ell S}(A)$ is not satisfactory for $\ell\geqslant 2$ because the last integration on the r.h.s. of Eq. (7.20) is divergent. In this way, by applying the N/D method to $T_{J\ell S}(A)/A^\ell$ we have changed the problem of the bad behavior of $T_{J\ell S}(A)$ around threshold into a high energy problem in the form of divergent integrals. To end up with a convergent DR for $D_{J\ell S}(A)$ in Eq. (7.20) it is necessary that $N_{J\ell S}(A)$ vanishes at least as:

$$N_{J\ell S}(A)\to 1/A^\ell\ \ \text{for}\ \ A\to\infty\ . \tag{7.21}$$

However, $N_{J\ell S}(A)$ from the DR in Eq. (7.19) vanishes only as $1/A$, independently of ℓ. The set of constraints needed to satisfy the asymoptic behavior in Eq. (7.21) can be deduced by performing in Eq. (7.19) a high energy expansion of $N_{J\ell S}(A)$ in powers of $1/A$. It results in:

$$\int_{-\infty}^{L}\!\!\mathrm{d}k^2\frac{\Delta_{J\ell S}(k^2)D_{J\ell S}(k^2)}{k^{2\lambda}}=0\ , \tag{7.22}$$

with $\lambda=2,3,\ldots,\ell$ and $\ell\geqslant 2$. These sum rules generalize the ones fulfilled by $\Delta^{1\pi}_{J\ell S}(A)$ in Eq. (7.17).[3]

The usefulness of the $\ell-1$ restrictions in Eq. (7.22) can be well appreciated by rewriting $N_{J\ell S}(A)$ in Eq. (7.19) as:

$$N_{J\ell S}(A)=-\frac{1}{\pi}\sum_{m=0}^{\ell-2}\frac{1}{A^{m+1}}\int_{-\infty}^{L}\!\!\mathrm{d}k^2\frac{\Delta_{J\ell S}(k^2)D_{J\ell S}(k^2)}{k^{2(\ell-m)}}+\frac{1}{\pi A^{\ell-1}}\int_{-\infty}^{L}\!\!\mathrm{d}k^2\frac{\Delta_{J\ell S}(k^2)D_{J\ell S}(k^2)}{k^2(k^2-A)}\ . \tag{7.23}$$

The last term on the r.h.s. of the previous equation vanishes explicitly as $1/A^\ell$ for $A\to\infty$, while the terms in the sum on m of the r.h.s. are zero once the constraints of Eq. (7.22) are fulfilled. In this way, inserting this expression for $N_{J\ell S}(A)$ in Eq. (7.20), one has:

$$D_{J\ell S}(A)=1+\frac{A}{\pi}\int_{-\infty}^{L}\!\!\mathrm{d}k^2\,\frac{\Delta_{J\ell S}(k^2)D_{J\ell S}(k^2)}{k^2}\,g(A,k^2)\ , \tag{7.24}$$

[3]Eq. (7.21) is a consequence of Eq. (7.18) because for $A\to+\infty$, due to unitarity, the ratio $T_{J\ell S}(A)/A^\ell$ tends to $1/A^{\ell+1/2}$ while $D_{J\ell S}(A)\to A^{1/2}$ (when only one subtraction is taken.)

and a convergent DR integral equation for $D_{J\ell S}(A)$ results.

It should be stressed that Eqs. (7.18), (7.19), and (7.24) lead to the same equations as for the case of a P-wave amplitude, $\ell = 1$, cf. Eqs. (7.3), (7.14) and (7.15).[4] In the case of a P-wave, no constraints are needed because the right behavior near threshold is obtained straightforwardly. On the other hand, Eq. (7.24) can be readily applied to S-wave by just adding the term proportional to $N_{J\ell S}(0)$ present in Eq. (7.14). One subtraction should be taken in Eq. (7.19) in order to transform it as Eq. (7.15) for $\ell = 0$.

Now, let us address the way to solve the N/D method, Eqs. (7.18), (7.19) and (7.24), in the presence of the constraints Eq. (7.22). It is well known [224, 329] that the function $D_{J\ell S}(A)$ in the N/D method is determined modulo the addition of Castillejo-Dalitz-Dyson (CDD) poles [185]. These are associated to specific dynamical features of the interaction that arise independently of the LHC discontinuity, $\Delta_{J\ell S}(A)$, and unitarity. Typically, the addition of CDD poles corresponds to the existence of pre-existing resonances or to Adler zeros [33,38,41,43,44]. Both features are indeed absent in the low-energy NN scattering [186]. We exploit this ambiguity in the $D_{J\ell S}(A)$ function and include $\ell - 1$ CDDs at *infinity* so as to satisfy Eq. (7.22):

$$D_{J\ell S} = 1 + \frac{A}{\pi}\int_{-\infty}^{L} \mathrm{d}k^2 \frac{\Delta_{J\ell S}(k^2) D_{J\ell S}(k^2)}{k^2} g(A, k^2) + \sum_{i=1}^{\ell-1} \frac{A}{B_i}\frac{\gamma_i}{A - B_i} \ . \tag{7.25}$$

The last term in the r.h.s. corresponds to adding $\ell - 1$ CDDs. The factor A/B_i in front of every CDD arises because the function $D_{J\ell S}(A)$ is normalized to 1 for $A = 0$ and it has the residue γ_i at $A = B_i$. The sum of the CDDs gives rise to a rational fraction $Q_{\ell-1}/P_{\ell-1}$, where the subscript in Q and P indicate the degree of the polynomial in A. Since the only relevant fact at low energies is the ratio γ_i/B_i^2 we take at the end the limit $B_i \to \infty$ with γ_i/B_i^2 not vanishing. The $\ell - 1$ CDD poles are gathered at the same point B and we write:

$$\sum_{i=1}^{\ell-1} \frac{A}{B_i}\frac{\gamma_i}{A - B_i} \to \frac{A\sum_{n=0}^{\ell-2} c_n A^n}{(A - B)^{\ell-1}} \ . \tag{7.26}$$

The coefficients c_i are finally determined by requiring that the set of $\ell - 1$ constraints in Eq. (7.22) are satisfied (this is done in Appendix G). The calculation is performed in terms of finite but large B, and one has to check that the results are stable by taking B arbitrarily large. At the level of low-energy NN scattering we have modified $D_{J\ell S}(A)$ by adding a polynomial of degree $\ell - 1$ with fixed coefficients.

We end with the following expressions

$$T_{J\ell S}(A) = A^\ell \frac{N_{J\ell S}(A)}{D_{J\ell S}(A)} \ , \tag{7.27}$$

$$N_{J\ell S}(A) = \frac{1}{\pi}\int_{-\infty}^{L} \mathrm{d}k^2 \frac{\Delta_{J\ell S}(k^2) D_{J\ell S}(k^2)}{k^{2\ell}(k^2 - A)} \ , \tag{7.28}$$

$$D_{J\ell S}(A) = 1 + \frac{A}{\pi}\int_{-\infty}^{L} \mathrm{d}k^2 \frac{\Delta_{J\ell S}(k^2) D_{J\ell S}(k^2)}{k^2} g(A, k^2) + \frac{A\sum_{n=0}^{\ell-2} c_n A^n}{(A - B)^{\ell-1}} \ , \tag{7.29}$$

[4] It is equivalent to have the explicit factor A in $T_{J\ell S}$, Eq. (7.18), or included in the definition of $N_{J\ell S}$, Eq. (7.15).

and the constraints

$$\int_{-\infty}^{L} \mathrm{d}k^2 \frac{\Delta_{J\ell S}(k^2) D_{J\ell S}(k^2)}{k^{2\lambda}} = 0 \ , \ \lambda = 2, 3, \ldots, \ell \ , \ \ell \geqslant 2 \ . \tag{7.30}$$

The previous formalism is also meaningful for the case in which $\Delta_{J\ell S}(A) \to C$, with C a constant, as $A \to \infty$. We do not discuss in this work its extension to the case when $\Delta_{J\ell S}(A)$ diverges for $A \to \infty$ as we are interested now only in LO NN scattering. This generalization of our formalism, left as a future work, will be discussed when considering higher orders in the chiral expansion of $\Delta_{J\ell S}(A)$, which include the important TPE contributions [481, 482].

Summarizing the results of this Section, we have presented a general approach based on the N/D method to construct NN scattering partial waves amplitudes. For $\ell = 0, 1$ one employs Eqs. (7.14) and (7.15), being the amplitude $T_{J\ell S}$ given by Eq. (7.3). For $\ell \geqslant 2$, one has Eqs. (7.27)-(7.29), that must be solved in the presence of the constraints given in Eq. (7.30). In Appendix G the solution of this integral equation subject to the constraints is studied.

7.3 Results for uncoupled partial waves

In this Section we present our results for the phase shifts, δ, of the uncoupled partial waves with $\ell \leqslant 5$ obtained by applying the N/D method as explained in Sec. 7.2. We compare them with the Nijmegen partial wave analysis (PWA) [186]. Our results, shown in Figs. 7.3–7.5, are represented with a black line, and the Nijmegen data with a red one, unless otherwise is stated. We show the results up to $|\mathbf{p}| = 300$ MeV. Notice that at $|\mathbf{p}| \simeq 360$ MeV the pion production threshold opens and three-momenta are no longer small, $|\mathbf{p}| \simeq \sqrt{m m_\pi} \gg m_\pi$.

In Fig. 7.3 we show the lowest elastic waves, namely, $^1S_0$, $^1P_1$, $^3P_1$ and $^3P_0$, whose amplitudes do not contain CDD poles because $\ell < 2$. The agreement in $^1P_1$ and $^3P_1$ is quite satisfactory. For the $^1S_0$ it is known that a higher order chiral counterterm is needed to reproduce the large effective range and thus improve the agreement with the data [170]. In the case of the $^3P_0$ wave, large corrections stem from TPE. Since this is a LO calculation, none of these corrections is included. But we want to stress an important point. In this Chapter what we present is a novel method to study the NN interactions. A regulator independent (thus cut-off independent), unitary description of the NN interaction with the right analytical properties, is reached. The inclusion of just OPE, that is, the LO in the calculation, is, of course, just a first step. The agreement with the data can be improved by including higher orders in the LHC.

For the $^1S_0$ and $^3P_0$ waves we have also tried with a *relativistic* calculation of the function $g(A, k^2)$ Eq. (7.11), since these are the waves for which the discrepancies with the data are larger. In this approach, the $\rho(q^2)$ function is replaced in the S-matrix and in the integrals where it is involved by its relativistic counterpart:

$$\rho(q^2) = \frac{\sqrt{q^2} m}{4\pi} \to \rho(q^2) = \frac{\sqrt{q^2} m}{4\pi} \frac{m}{\sqrt{q^2 + m^2}} \ .$$

The results with this relativistic phase-space improvement are represented by the dashed (black) lines in Fig. 7.3. Though the corrections are in the right direction, the discrepancies

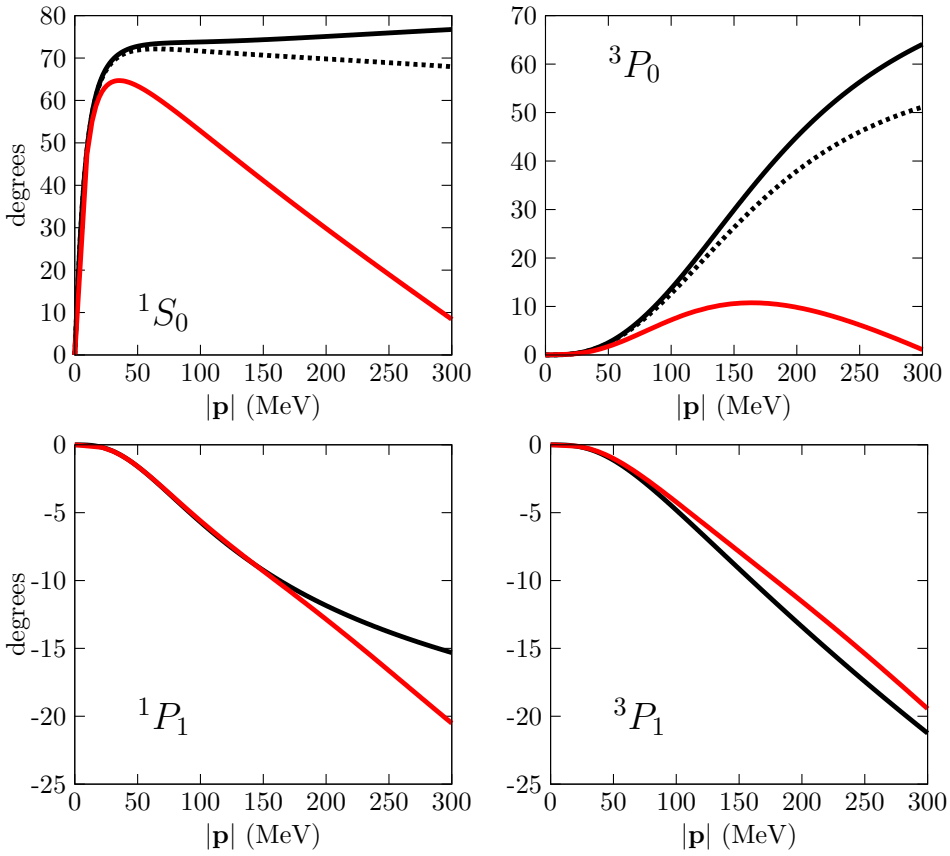

Figure 7.3: Comparison of the $^1S_0$, $^3P_0$, $^1P_1$ and $^3P_1$ waves phase shifts with the Nijmegen PWA. The solid black line represents the results of this work, while the red one represents the Nijmegen PWA [186]. For the $^1S_0$ and $^3P_0$, the dashed black line corresponds to the relativistic version of this work, see the text for details.

are still large. As expected, relativistic corrections are small in the energy range shown, though noticeable for the $^3P_0$ partial wave for $|\mathbf{p}| \gtrsim 200$ MeV.

For higher waves one needs to include $\ell - 1$ CDD poles in order to fulfill the constraints in Eq. (7.30), and guarantee that partial waves have the right behavior at threshold vanishing as $|\mathbf{p}|^{2\ell}$. Our results are shown in Figs. 7.4 and 7.5, and good agreement is found, except for the $^1D_2$ wave. Our curves are quite similar compared with the LO results of Ref. [170]. This reference offers an approach with cut-off independent results with the NN potential (V_{NN}) given by OPE. The largest discrepancy concerns to the $^3P_0$ partial wave where in Ref. [170] a counterterm is promoted from higher orders so as to achieve cut-off stable results for $\Lambda \to \infty$ due to the attractive $1/r^3$ tensor force in OPE. As a result, their agreement with data is much improved. The main difference between our approach and that of Ref. [170] concerns the treatment of the LHC. Namely, for the $^3P_0$ wave the iteration of the NN potential is responsible for the need of this extra counterterm. The first iteration $V_{NN}GV_{NN}$ (with G the unitary two-nucleon reducible loop function) is a new source of LHC discontinuity [483] containing contributions from TPE and iterated OPE. The real part stemming from the former is divergent. Within our approach the sources of LHC discontinuity from $V_{NN}GV_{NN}$ are NLO according with the standard chiral counting. At that order new subtractions are required (as discussed in Subsec. 7.5.2.) which will mimic the role of the extra counterterm taken in

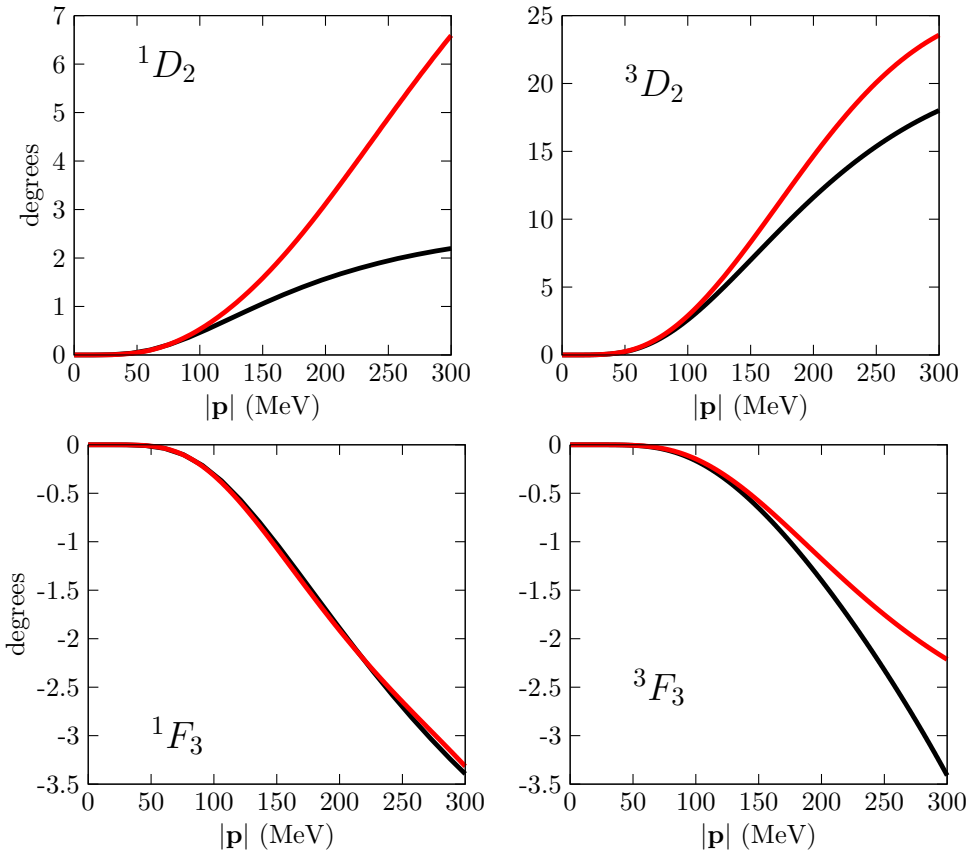

Figure 7.4: Comparison of the $^1D_2$, $^3D_2$, $^1F_3$ and $^3F_3$ waves phase shifts (black solid line) to the Nijmegen PWA (red solid line).

Ref. [170]. While our method is based on the calculation of $\Delta_{J\ell S}(A)$ perturbatively along the LHC, the application of a Lippmann-Schwinger equation with the chiral NN potentials is based on the perturbative calculation of the latter [163–165]. In both cases the diagrams required for the calculation of $\Delta_{J\ell S}$ and V_{NN} are two-nucleon irreducible, in the sense that no intermediate two-nucleon state arises, which justifies its perturbative treatment [162–165,183]. In both cases as well the RHC is exactly resummed, as required because of the enhanced two-nucleon reducible diagrams. This resummation is performed in terms of the interaction kernel, $\Delta_{J\ell S}$ or V_{NN}, depending on the approach. The N/D method respects the LHC discontinuity so that $\Delta_{J\ell S}$ is the same as in the final partial wave amplitude. For a Lippmann-Schwinger equation this is not the case as new sources of imaginary parts along the LHC result from the iteration of V_{NN} [483]. It is also worth stressing that our approach based on the N/D method is a dispersive one offering results that by construction are cut-off independent, while this is still an issue in the application of the Lippmann-Schwinger (or Schrödinger) equation to NN scattering with V_{NN} calculated from ChPT [170,177,180,469].

For the $^1S_0$ and $^1D_2$ partial waves, for which we do not have good agreement at LO with data [186], our results are indeed very similar to those of Ref. [170], too. In the case of the $^1P_1$ partial wave our phase shifts run closer to data at low energies than those of Ref. [170].

In order to show the independence of our results with the value of B, the position of the CDD poles, once this value is large enough, we show in Fig. 7.5 for the $^3G_4$ partial wave

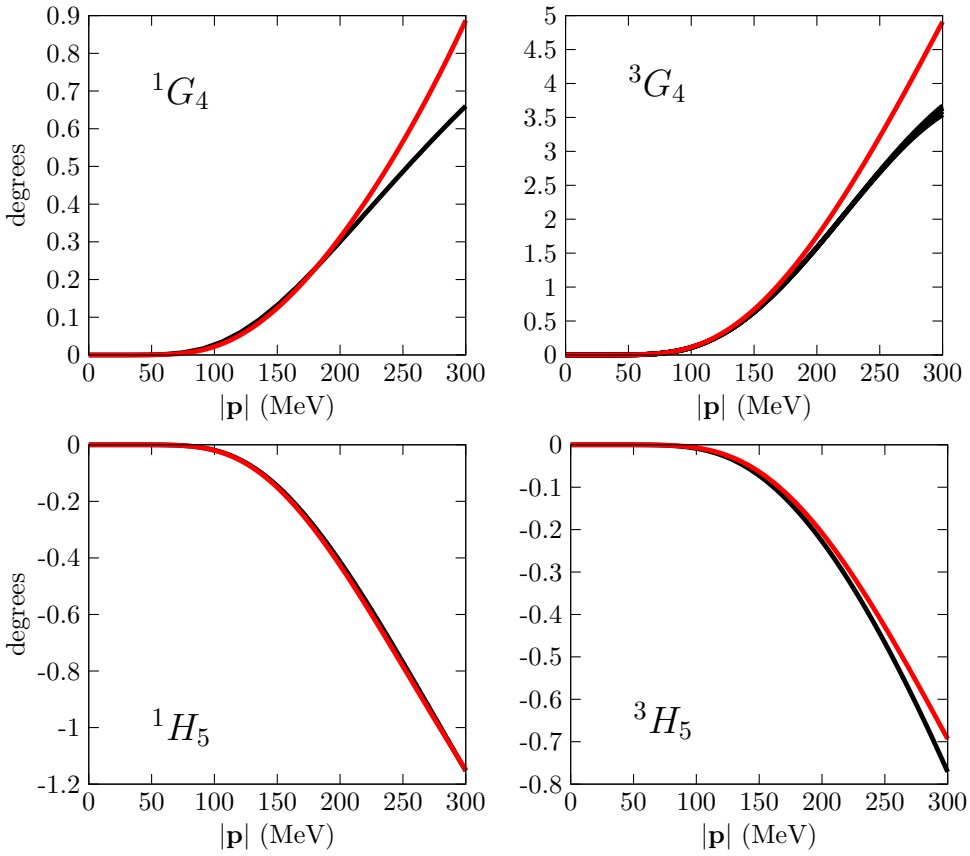

Figure 7.5: Comparison of the $^1G_4$, $^3G_4$, $^1H_5$ and $^3H_5$ waves phase shifts (black solid line) to the Nijmegen PWA (red solid line). The lines in $^1H_5$ are almost overlapping.

different lines corresponding to $B = 10^n m_\pi^2$ for $n = 2, 3, 4, 5$, and 6. A narrow band is obtained despite the large variation in the values of B considered.

7.4 The N/D method for NN coupled partial waves

In this Section, the generalization of the method of Sec. 7.2 for the uncoupled partial waves to the case of coupled channels is developed. For the spin triplet NN partial waves with total angular momentum J one has the mixing of the orbital angular momenta $\ell = J-1$ and $\ell' = J+1$ (except for the $^3P_0$ partial wave.) Each set of coupled partial waves is determined by the quantum numbers S, J, ℓ and ℓ', where S is the total spin. In the following for simplifying the notation we omit them and indicate the different partial waves by T_{ij}, with $i = 1$ corresponding to $\ell = J-1$ and $i = 2$ to $\ell' = J+1$, a convention that we adopt from now on. As a result, a two coupled channel T-matrix results. In our normalization, the resulting S-matrix reads

$$S(A) = \mathbb{I} + i2\rho(A)T(A) = \\ = \begin{pmatrix} \cos 2\epsilon\ e^{2i\delta_1} & i\sin 2\epsilon\ e^{i(\delta_1+\delta_2)} \\ i\sin 2\epsilon\ e^{i(\delta_1+\delta_2)} & \cos 2\epsilon\ e^{2i\delta_2} \end{pmatrix}, \tag{7.31}$$

such that δ_1 refers to the phase shifts for the channel with $\ell = J-1$ and δ_2 to that with $\ell' = J+1$. The non-relativistic phase space is given by $\rho(A)$, defined in Eq. (7.8). Along the RHC, the unitarity of the S-matrix, $SS^\dagger = S^\dagger S = \mathbb{I}$, can be written in terms of the (symmetric) T-matrix as $\mathrm{Im}T^{-1}(A) = -\rho(A)\,\mathbb{I}$. In the following, the imaginary parts above threshold of the inverse of the T-matrix elements, denoted by $t_{ij}(A)$, play an important role,

$$\mathrm{Im}\frac{1}{t_{ij}(A)} \equiv -\nu_{ij}(A)\ , A > 0\ . \tag{7.32}$$

Employing the relationship between the T- and S-matrices, Eq. (7.31), we can express the different ν_{ij} in terms of phase shifts and the mixing angle along the physical region above threshold. In this way, one can write the diagonal partial waves as $t_{ii} = (e^{2i\delta_i}\cos 2\epsilon - 1)/2i\rho$, while for the mixing amplitude $t_{12} = e^{i(\delta_1+\delta_2)}\sin 2\epsilon/2\rho$. From these expressions it is straightforward to obtain for $A > 0$:

$$\nu_{11}(A) = \rho(A)\left[1 - \frac{\frac{1}{2}\sin^2 2\epsilon}{1-\cos 2\epsilon\cos 2\delta_1}\right]^{-1}\ , \tag{7.33}$$

$$\nu_{22}(A) = \rho(A)\left[1 - \frac{\frac{1}{2}\sin^2 2\epsilon}{1-\cos 2\epsilon\cos 2\delta_2}\right]^{-1}\ , \tag{7.34}$$

$$\nu_{12}(A) = 2\rho(A)\frac{\sin(\delta_1+\delta_2)}{\sin 2\epsilon}\ . \tag{7.35}$$

Although not explicitly indicated, it should be understood that the phase shifts and the mixing angle depend on A. Eq. (7.32) generalizes that of an uncoupled partial wave, Eq. (7.2), employed in Sec. 7.2. Indeed, if we set $\epsilon = 0$ in $\nu_{11}(A)$ and $\nu_{22}(A)$, the uncoupled case is recovered. Note also that $\nu_{ii}(A)/\rho(A) \geqslant 1$.

We apply the N/D method to solve our equations for the T-matrix. As has been previously shown, in the N/D method a partial wave t_{ij} is written as the quotient of a numerator function $N_{ij}(A)$ and a denominator one $D_{ij}(A)$. The function N_{ij} only has a LHC while the function D_{ij} has only a RHC. In Refs. [484, 485], a straightforward generalization of the one-channel N/D method of Chew and Mandelstam [38] was given by writing $T = N\cdot D^{-1}$ in matrix notation. This T-matrix would be symmetric, as it is required by temporal inversion, only under the assumption that $D^T(T^T - T)D$ vanishes for $A \to \infty$ [485], where the superscript T indicates the transpose of the corresponding matrix. However, this is not the case for the chiral potentials, even at LO, *e.g.*, in the ${}^3S_1$–${}^3D_1$ coupled partial waves. This condition is then too restrictive for its application to chiral EFT where different numbers of subtractions are taken in the different partial waves involved, whose number also varies according with the chiral order considered in the calculation of the imaginary part of the NN partial wave amplitude along the LHC. Whence, our generalization to the coupled partial waves case must follow other guidelines.

In what follows, we generalize the procedure of Sec. 7.2 to the coupled case. Instead of making use of a matrix notation as in Refs. [484, 485], we write down three N/D equations, one for each of the three independent partial waves t_{ij}, as in Ref. [477],

$$t_{ij}(A) = A^{\ell_{ij}}\frac{N_{ij}(A)}{D_{ij}(A)}\ . \tag{7.36}$$

The factor $A^{\ell_{ij}}$ guarantees the proper threshold behavior with $\ell_{11} = \ell$, $\ell_{22} = \ell' = \ell + 2$ and $\ell_{12} = (\ell + \ell')/2 = \ell + 1$. As stated above the splitting of the $t_{ij}(A)$ function is such that N_{ij} bears the LHC and D_{ij} the RHC, and then:

$$\mathrm{Im}D_{ij}(A) = -N_{ij}(A)A^{\ell_{ij}}\nu_{ij}(A) \ , \ A > 0 \ , \tag{7.37}$$

$$\mathrm{Im}N_{ij}(A) = D_{ij}(A)\Delta_{ij}(A)/A^{\ell_{ij}} \ , \ A < L \ , \tag{7.38}$$

with $\mathrm{Im}t_{ij} \equiv \Delta_{ij}$ along the LHC. The imaginary parts of D_{ij} and N_{ij} are zero elsewhere along the A-real axis.[5] As argued in Ref. [162] and in Sec. 7.2, Δ_{ij} can be calculated perturbatively in ChPT along the LHC, since it originates from multi-pion exchanges putting on-shell pion propagators. The intermediate states require then at least one pion so that we apply ChPT always to irreducible N-nucleon diagrams, responsible for the discontinuity along the LHC.

Two DRs can be written for the functions D_{ij} and N_{ij}, employing the contours C_I and C_{II} in Fig. 7.1, respectively. The integration along the circle at infinity vanishes, if necessary, by taking sufficient number of subtractions. At LO in the chiral counting [162, 183], the only contribution to Δ_{ij} along the LHC is OPE. Asymptotically, for $\mathbf{p}^2 \to -\infty$, OPE tends to constant, so that, according to the Sugawara and Kanazawa theorem [329,480] one subtraction is necessary for the DR of $N_{ij}(A)$ in S-wave, even though $\Delta_{ij}(A) \to 1/A$ in the case of OPE. On general grounds, a partial wave amplitude is bounded because of unitarity by constant$/\sqrt{A}$ for $A \to +\infty$ so that $t_{ij}D_{ij}(A)/A^{\ell_{ij}}$ tends to constant for S-wave and zero for any other partial wave.[6] As a result the same theorem then requires that at least one subtraction is necessary for the S-waves:

$$D_{ij}(A) = 1 - \frac{A}{\pi}\int_0^{+\infty} \mathrm{d}q^2 \frac{\nu_{ij}(q^2)N_{ij}(q^2)q^{2\ell_{ij}}}{q^2(q^2 - A)} \ , \tag{7.39}$$

$$N_{ij}(A) = N_0 + \frac{A}{\pi}\int_{-\infty}^{L} \mathrm{d}k^2 \frac{\Delta_{ij}(k^2)D_{ij}(k^2)}{k^2(k^2 - A)} \ , \ \ell_{ij} = 0 \ , \tag{7.40}$$

$$N_{ij}(A) = \frac{1}{\pi}\int_{-\infty}^{L} \mathrm{d}k^2 \frac{\Delta_{ij}(k^2)D_{ij}(k^2)}{k^{2\ell_{ij}}(k^2 - A)} \ , \ \ell_{ij} \neq 0 \ . \tag{7.41}$$

The subtraction point is taken at threshold. One subtraction is taken for the $D_{ij}(A)$ function which is fixed to 1, as in the uncoupled case. For $\ell_{ij} = 0$, S-wave, one subtraction is taken in $N_{ij}(A)$, as just discussed. In this Section, dedicated to the NN coupled partial waves, this is the case only for the ${}^3S_1$ channel. The subtraction constant N_0 is the amplitude at threshold, $T_{11}(0) = N_0$, and then it can be fixed in terms of the ${}^3S_1$ scattering length, a_t:

$$N_0 = -\frac{4\pi a_t}{m} \ , \tag{7.42}$$

with the value $a_t = 5.424 \pm 0.004$ fm. The former equation is then just like Eq. (7.13), but for the ${}^3S_1$ case. Below in Sec. 7.5.1 we also fix N_0 in terms of the experimental deuteron binding energy.

An integral equation for the function $D_{ij}(A)$ would result by inserting Eq. (7.40) or Eq. (7.41) into Eq. (7.39). However, as argued in detail in Sec. 7.2, divergent integrals appear

[5] Because the Schwartz reflection principle is satisfied by t_{ij}, D_{ij} and N_{ij} the discontinuity across the RHC or LHC is given by $2i$ the imaginary part of the function, just as in the uncoupled case.

[6] Here we are taking that D_{ij} diverges as $\sqrt{A}$ for $A \to \infty$ as in the uncoupled case. This is consistent with the results obtained explicitly in this work.

for $\ell \geqslant 2$ unless a set of $\ell - 1$ constraints are satisfied by $D_{ij}(A)$. The generalization of the sum rules of Sec. 7.2 to the coupled channel case is:

$$\int_{-\infty}^{L} \mathrm{d}k^2 \frac{\Delta_{ij}(k^2) D_{ij}(k^2)}{k^{2\lambda}} = 0 \ , \quad \lambda = 2, 3, \ldots, \ell_{ij} \geqslant 2 \tag{7.43}$$

Expanding the denominator inside the integral of Eq. (7.41), $N_{ij}(A)$ can be written as:

$$N_{ij}(A) = \frac{1}{\pi A^{\ell_{ij}-1}} \int_{-\infty}^{L} \mathrm{d}k^2 \frac{\Delta_{ij}(k^2) D_{ij}(k^2)}{k^2(k^2 - A)} - \frac{1}{\pi} \sum_{m=0}^{\ell_{ij}-2} \frac{1}{A^{m+1}} \int_{-\infty}^{L} \mathrm{d}k^2 \frac{\Delta_{ij}(k^2) D_{ij}(k^2)}{k^{2(\ell_{ij}-m)}} \tag{7.44}$$

and the terms within the sum vanish if the constraints of Eq. (7.43) are fulfilled. This guarantees that $N_{ij}(A)$ vanishes as $1/A^{\ell_{ij}}$ which ensures the convergence of the resulting integral equation for $D_{ij}(A)$.

Let us take first $\ell_{ij} \neq 0$. By inserting the non vanishing piece of N_{ij} into Eq. (7.39), once the constraints Eq. (7.43) are satisfied, we find the following integral equation for $D_{ij}(A)$:

$$D_{ij}(A) = 1 + \frac{A}{\pi} \int_{-\infty}^{L} \mathrm{d}k^2 \frac{\Delta_{ij}(k^2) D_{ij}(k^2)}{k^2} g_{ij}(A, k^2) \ , \tag{7.45}$$

$$g_{ij}(A, k^2) = \frac{1}{\pi} \int_{0}^{+\infty} \mathrm{d}q^2 \frac{\nu_{ij}(q^2)}{(q^2 - A)(q^2 - k^2)} \ . \tag{7.46}$$

The functions $g_{ij}(A, k^2)$ are the generalization of $g(A, k^2)$ given in Sec. 7.2 for the uncoupled case. An important technical detail is discussed in Appendix H. We show there how the constraints in Eq. (7.43) guarantee that the functions $g_{ij}(A, k^2)$ are finite curing a potential divergence for $ij = 22$ in the $q^2 \to 0$ limit. This divergence was noticed in Ref. [477] but no procedure was given there to remove it.

The N/D method in the presence of the constraints Eq. (7.43) was solved in the uncoupled channel case by means of the insertion of CDD poles. This idea is generalized to the case of coupled channels, and the following equations are then obtained:

$$N_{ij}(A) = \frac{1}{\pi} \int_{-\infty}^{L} \mathrm{d}k^2 \frac{\Delta_{ij}(k^2) D_{ij}(k^2)}{k^{2\ell_{ij}}(k^2 - A)} \ , \tag{7.47}$$

$$D_{ij}(A) = 1 + \frac{A}{\pi} \int_{-\infty}^{L} \mathrm{d}k^2 \frac{\Delta_{ij}(k^2) D_{ij}(k^2)}{k^2} g_{ij}(A, k^2) + \frac{A \sum_{n=0}^{\ell_{ij}-2} c_n A^n}{(A - B)^{\ell_{ij}-1}} \ . \tag{7.48}$$

The coefficients c_i, specific for each wave although not explicitly indicated, are determined in such a way that the constraints in Eq. (7.43) are satisfied, as in the uncoupled case.

Notice that for the P-waves ($\ell_{ij} = 1$) (we have in our present study the mixing partial wave in the ${}^3S_1$–${}^3D_1$ system and the ${}^3P_2$ in ${}^3P_2$–${}^3F_2$ scattering), no constraints are needed, so that the sum over the CDD poles is dropped and the same formalism applies. This is also clear because for this case Eq. (7.41) vanishes as $1/A$ so that there is no room for restrictions.

Let us take now the case $\ell_{ij} = 0$, that only occurs for the ${}^3S_1$ wave. Since a subtraction is needed in N_{11}, Eq. (7.40), one should change Eq. (7.48) in two ways as there is no sum over CDD poles and one has to include an extra term associated with the subtraction in $N_{ij}(A)$ for

this case. It is straightforward to obtain by inserting Eq. (7.40) into Eq. (7.39) the appropriate integral equation for $D_{11}(A)$ for the $^3S_1$ partial wave:

$$D_{11}(A) = 1 - AN_0 g_{11}(A,0) + \frac{A}{\pi}\int_{-\infty}^{L} \mathrm{d}k^2 \frac{\Delta_{11}(k^2) D_{11}(k^2)}{k^2} g_{11}(A,k^2) \ , \tag{7.49}$$

with $g_{11}(A,k^2)$ given by Eq. (7.46). Notice also that from Eq. (7.40) it is clear that $N_{ij}(A)$ tends to constant for $\ell_{ij} = 0$ and $A \to \infty$, so that there is no need for constraints. This is why no sum over CDD poles is present in the previous equation.

To obtain the final amplitudes, the $D_{ij}(A)$ functions are obtained along the LHC ($A < -m_\pi^2/4$) by solving the integral equations in Eq. (7.48) or Eq. (7.49). Next, the functions $D_{ij}(A)$ are obtained along the RHC ($A > 0$) from the same equations because the integrand is known. To obtain the functions $N_{ij}(A)$, since the constraints in Eq. (7.43) are obeyed, one can use for $\ell_{ij} \neq 0$ either Eq. (7.47) or the first term on the right hand side of Eq. (7.44) (but the former is more suitable numerically, since it converges faster.) For the $^3S_1$ wave, one should use Eq. (7.40). The partial waves $t_{ij}(A)$ are obtained by employing the resulting $D_{ij}(A)$ and $N_{ij}(A)$ functions in Eq. (7.36).

Summarizing, up to now, we have repeated the steps followed in the construction of the partial waves in the uncoupled channel case. The main difference with respect to the uncoupled case treated in Sec. 7.2 is that now one has to solve simultaneously three N/D equations for ij=11, 12 and 22 with the functions $g_{ij}(A,k^2)$ linked between each other. They depend on the phase shifts δ_1 and δ_2 and on the mixing angle ϵ, defined in Eq. (7.31), which are also the final output of our approach. Thus, we employ an iterative procedure (similar to Ref. [477]) as follows. Given an input for δ_1, δ_2 and ϵ, one solves the three integral equations for $D_{ij}(A)$ along the LHC, and then the amplitudes for the RHC can be calculated. The phase shifts δ_1 and δ_2 are reobtained from the phase of the S-matrix elements S_{11} and S_{22}, while $\sin 2\epsilon = 2\rho A^{\ell_{12}} N_{12}/|D_{12}|$. In this way a new input set of ν_{ij} functions, Eqs. (7.33)-(7.35), is obtained. These are used again in the integral equations, and the iterative procedure is finished when convergence is found (typically, the difference between one iteration in the three independent D_{ij} functions along the LHC is required to be less than one per mil.) As the initial input one can use the results given by UChPT [162], or some put-by-hand phase shifts and mixing angle, and we find no dependence of our final unitary results with the input employed.

It can be shown straightforwardly that unitarity is fulfilled in our coupled channel equations, solved in the way just explained, if $|S_{11}(A)|^2 = |S_{22}(A)|^2 = \cos^2 2\epsilon$ for $A > 0$. From the fact that $\mathrm{Im}t_{12} = \nu_{12}|t_{12}|^2$, as follows from Eq. (7.32), and $\sin 2\epsilon = 2\rho|t_{12}|$ (the latter equality is valid only when convergence is reached), it follows that the phase of t_{12} is $\delta_1 + \delta_2$, as required by unitarity, Eq. (7.31). By construction the phase shifts are equal to one-half the phase of the S-matrix diagonal elements when convergence is achieved.

7.5 Results for coupled partial waves

We now present the reproduction of the phase shifts and mixing angles for the NN coupled partial waves with $J \leqslant 3$ comparing with the data from the Nijmegen PWA [186]. We pay

special attention to the ${}^3S_1$–${}^3D_1$ system and the deuteron, which is treated in Subsec. 7.5.1. An extension of our formalism for this wave to include more subtractions in the DR is presented in Subsec. 7.5.2, which allows a better description of the phase shifts and the properties of the deuteron. Higher partial waves are treated in Subsec. 7.5.3.

7.5.1 ${}^3S_1$–${}^3D_1$ coupled waves

Now we discuss our results for the ${}^3S_1$–${}^3D_1$ coupled waves. Previous papers applying the N/D method to adjust NN scattering are Refs. [473–476]. We already commented about Ref. [473, 476]. The other two works by Wong and Scotti, Refs. [474, 475], include together with OPE other heavier mesons, η, ρ, ω, and the ϕ is also included in Ref. [475]. Then, these works follow the basic ideas of meson theory of nuclear forces, that were also used for the construction of NN potentials (See Ref. [486] and references therein for a historical perspective). There are some approximations in Refs. [473–475] that we avoid in our work. *E.g.* only elastic unitarity is used in Refs. [473, 474] neglecting the mixing between coupled partial waves. Ref. [475] considers the mixing only for the ${}^3S_1$–${}^3D_1$ coupled partial waves. In addition, in order to satisfy the threshold behavior for partial waves with $\ell \geqslant 2$, so that they vanish as A^ℓ, Refs. [474,475] make use of a rather ad-hoc formula. This method was criticized in Ref. [487] because it includes an unphysical pole for every partial wave at a CM squared energy s_1, somewhat below $4m^2$ (the threshold for NN scattering). In addition, Refs. [474,475] also have a cut-off dependence in the way the vector resonance exchanges are damping to avoid their divergences at infinity. Though the results of Refs. [473–475] are interesting and obtain typically a good reproduction of data at the phenomenological level, we offer here a novel way of employing the N/D method in the light of EFT. We then present the method ready to be used in a systematic way by improving order by order the discontinuity of the partial wave amplitudes along the LHC since it involves only NN irreducible diagrams, as discussed above [162]. We satisfy exact unitarity for all the partial waves as well. It is also important to stress that the N/D method for coupled channels is now presented in a way ready to be used at any chiral order, without being constrained to satisfy the too demanding Bjorken-Nauenberg condition [485] in order to end with symmetric partial waves. We accomplish the right threshold behavior for $\ell \geqslant 2$ by adding CDD poles at infinity, which is always legitimate in the N/D method if there are good reasons for including them (which have been offered before, see Sec. 7.2, [E].) Thus, we do not need to modify the right analytical properties of partial waves by including a fictitious pole in s_1 which is then fine tuned to data, as done in Refs. [474, 475].

The deuteron (d) is a neutron-proton (np) bound state with total angular momentum $J = 1$ and spin $S = 1$ (and isospin zero.) As such, it is seen as a pole below threshold ($|\mathbf{p}|^2 < 0$), in the physical Riemann sheet in the ${}^3S_1$–${}^3D_1$ coupled partial waves. The binding energy of the deuteron, E_d (defined positive), is given by

$$E_d = -\frac{k_d^2}{m} \ , \tag{7.50}$$

where k_d^2 is the three-momentum squared at which the pole is located, so that it is negative. Specifically, in our approach it appears as a zero in the functions $D_{ij}(A)$. From the amplitudes calculated in Sec. 7.4 we find the deuteron at the position $k_d^2 = -0.08 m_\pi^2$ in the ${}^3S_1$ amplitude, corresponding to $E_d \simeq 1.7$ MeV. The experimental value is $E_d \simeq 2.2$ MeV. Recall that

the subtraction constant N_0 appearing in the ${}^3S_1$ partial wave is determined by fixing the ${}^3S_1$ scattering length to its experimental value, Eq. (7.42). There is still a remnant input dependence for the ${}^3S_1$–${}^3D_1$ coupled partial waves in our unitary solutions that we fix by requiring that the deuteron pole position is the same in the ${}^3S_1$ and in the mixing partial wave. Independently of the input we do not find any pole in the ${}^3D_1$ partial wave. Indeed, if we disregard the coupling between ${}^3S_1$ and ${}^3D_1$ and use the method of Sec. 7.2 (Ref. [E]) for uncoupled waves, the pole appears in the same position in ${}^3S_1$ and, again, it does not appear in ${}^3D_1$. However, the pole should be located at the same energy in every channel, but this is not the case because we are not using a matrix formalism but solving independently the three linked N/D equations. Notice also that the deuteron is found mainly in a ${}^3S_1$ state, and thus the coupling to ${}^3D_1$ is very weak.

In order to cure this deficiency and having the right pole structure guaranteeing the presence of the deuteron pole in ${}^3D_1$, we write down a twice subtracted DR for the ${}^3D_1$ partial wave, such that the function $D_{22}(A)$ has a zero at a given k_d^2. The DR reads:

$$D_{ij}(A) = 1 - \frac{A}{k_d^2} - \frac{A(A-k_d^2)}{\pi}\int_0^{+\infty} \mathrm{d}q^2 \, \frac{\nu_{ij}(q^2) N_{ij}(q^2) q^{2\ell_{ij}}}{q^2(q^2-A)(q^2-k_d^2)} \, , \tag{7.51}$$

written in a way that is valid for both the ${}^3D_1$ partial wave ($ij = 22$) and for the mixing partial wave ($ij = 12$), although we do not use it for the latter. By inserting the expression for $N_{ij}(A)$, Eq. (7.41), into the previous equation, we end up with the following integral equation:

$$D_{ij}(A) = 1 - \frac{A}{k_d^2} + \frac{A(A-k_d^2)}{\pi}\int_{-\infty}^{L} \mathrm{d}k^2 \, \frac{\Delta_{ij}(k^2) D_{ij}(k^2)}{k^{2\ell_{ij}}} g_{ij}^{(d)}(A,k^2) \, , \tag{7.52}$$

where $g_{ij}^{(d)}(A,k^2)$ is a generalization of the functions $g_{ij}(A,k^2)$ of Eq. (7.46),

$$g_{ij}^{(d)}(A,k^2) = \frac{1}{\pi}\int_0^{+\infty} \mathrm{d}q^2 \, \frac{\nu_{ij}(q^2) q^{2(\ell_{ij}-1)}}{(q^2-A)(q^2-k^2)(q^2-k_d^2)} \, . \tag{7.53}$$

For the ${}^3S_1$–${}^3D_1$ waves, we have $\ell = 0$ and $\ell' = 2$, so that $\ell_{12} = 1$ and $\ell_{22} = 2$, and the previous integrals are convergent because of the extra subtraction taken. Recall that, in the formalism first presented in Sec. 7.4, one must take into account a constraint for the $D_{22}(A)$ partial wave in order to end with a convergent integral equation. Note that from Eqs. (7.52) and (7.53) the high-energy behavior of the functions D_{ij} changes, now diverging as $A^{3/2}$, instead of $A^{1/2}$ as in Sec. 7.4, stressed before for the uncoupled case. As a result the criterion of imposing that $N_{ij} \to 1/A^{\ell_{ij}}$ for $A \to \infty$, the one used in the uncoupled case to deduce the need of constraints, does not hold now because of the extra subtraction.[7] The price to pay for having included a second subtraction is the need for an input value for k_d^2, which has to be provided. It is then more natural for the ${}^3S_1$–${}^3D_1$ system to fix the binding energy of the deuteron to its experimental value than the scattering length, as we do below.

As stated in Sec. 7.4, an iterative procedure is followed in order to obtain our final results for the phase shifts and the mixing angle from the three N/D equations coupled. For every

[7] From Eq. (7.41) it follows immediately that $N_{22} \to 1/A$ which is the behavior required for $N_{22} = T_{22}D_{22}/A^2$, taking into account the high-energy behavior of $D_{22}(A)$ just discussed.

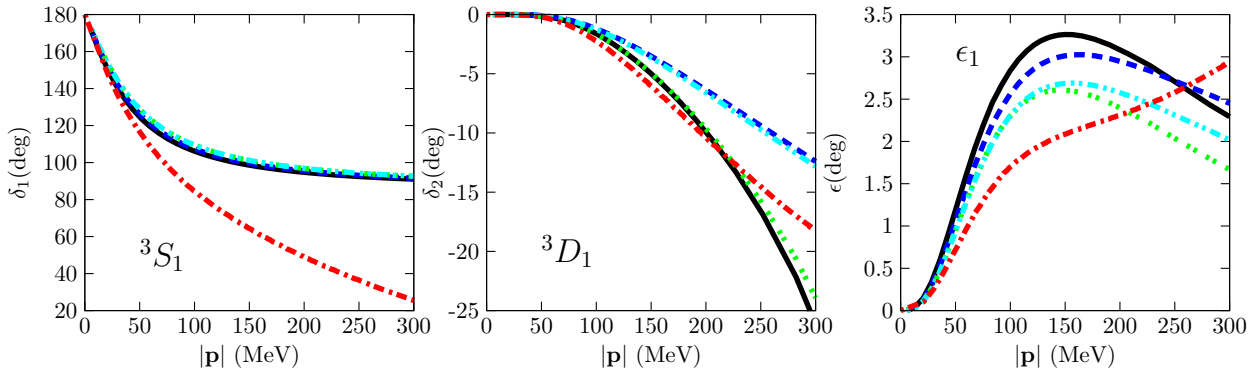

Figure 7.6: Comparison of our results for the $^3S_1$ and $^3D_1$ phase shifts and the mixing angle ϵ_1 to the Nijmegen PWA [186], shown by the dot-dashed (red) lines. The solid (black) lines correspond to fixing the $^3S_1$ scattering length to experiment, while the dashed (blue) lines in addition fix the deuteron pole position in $^3D_1$ at the same value as that in $^3S_1$. On the other hand, the double dotted (green) lines stem by fixing the deuteron pole position in the $^3S_1$ partial wave at its experimental value. The dash-double-dotted (cyan) lines correspond to having additionally fixed the deuteron pole in the $^3D_1$ partial wave at the same point as in $^3S_1$.

iteration along that procedure, one obtains from the $^3S_1$ wave amplitude the deuteron pole position, k_d^2. This is the value used as an input for the function $D_{22}(A)$ at every step. In this way it is not fitted as a free parameter in order to fix the deuteron binding energy, but it comes out in a natural way from $^3S_1$ and the coupled channel mechanism. The results that we obtain with this approach are shown in Fig. 7.6 by the dashed (blue) lines, while those obtained when there is no deuteron pole in $^3D_1$, using Eq. (7.48) instead of Eq. (7.52) with $\ell_{ij} = 2$, correspond to the solid (black) lines. The results are compared with the Nijmegen PWA [186] given by the dash-dotted (red) lines. For the $^3S_1$ phase shifts both lines are very similar. The differences are larger for the $^3D_1$ phase shifts, which are then quite sensitive to reproducing correctly the deuteron pole also in the $^3D_1$ partial wave. Indeed, the result without imposing the deuteron in this partial wave is very similar to that obtained from perturbative OPE [454]. Differences are rather small for the mixing angle ϵ_1. As the main contribution to the deuteron comes from $^3S_1$, its position remains almost unchanged compared with the uncoupled case, with a value obtained for the binding $E_d \simeq 1.7$ MeV, once the experimental scattering length is fixed. This corresponds to an effective range $r \simeq 0.46$ fm, which is much smaller than the experimental value $r = 1.749$ fm, the difference being around a 70%. This fact is already well documented in the literature [488]. Indeed, Ref. [473] shows that when the N/D method is used with only OPE as the source of the imaginary part along the LHC one needs to fit two experimental inputs for every NN S-wave in order to reproduce the scattering length and effective range. For $^3S_1$ the scattering length and the deuteron binding energy are taken (we take the same input in Sec. 7.5.2 below), while for $^1S_0$ two well measured phase shifts at different energies are employed. This result from Ref. [473], and our own ones presented below in Sec. 7.5.2, makes us confident that a NLO study in ChPT with the N/D method will be phenomenologically successful because a new counterterm enters at this order multiplying an energy dependent monomial. The authors of Ref. [473] make the approximation of considering only elastic unitarity for $^3S_1$, neglecting its coupling with $^3D_1$, while our treatment is exact.

It is also interesting to fix the subtraction constant N_0 in terms of the deuteron binding energy and then compare with our previous results when the scattering length was fixed.

Imposing $D_{11}(k_d^2) = 0$ from Eq. (7.49) and solving for N_0 one has

$$N_0 = \frac{1 + \frac{k_d^2}{\pi}\int_{-\infty}^{L} dk^2 \Delta_{11}(k^2) d_{11}(k^2) g_{11}(k^2, k_d^2)/k^2}{k_d^2 \left(g_{11}(k_d^2, 0) + \mathcal{G}(k_d^2)\right)} \ , \tag{7.54}$$

where we have first split

$$D_{11}(A) = d_{11}(A) - k^2 N_0 g_{11}(A, 0) \ , \tag{7.55}$$

from where the function $d_{11}(A)$ is defined. We have also introduced in Eq. (7.54) the function $\mathcal{G}(A)$ given by

$$\mathcal{G}(A) = \frac{1}{\pi}\int_{-\infty}^{L} dk^2 \Delta_{11}(k^2) g_{11}(k^2, 0) g_{11}(A, k^2) \ . \tag{7.56}$$

The integral equation for $d_{11}(A)$ can be obtained from that in Eq. (7.49) taking into account Eq. (7.55) and replacing N_0 by its expression Eq. (7.54). It results

$$\begin{aligned} d_{11}(A) = 1 + \frac{A}{\pi}\int_{-\infty}^{L} dk^2 \frac{\Delta_{11}(k^2) d_{11}(k^2)}{k^2} \Bigg\{ & g_{11}(A, k^2) \\ & - \frac{g_{11}(k^2, k_d^2)\mathcal{G}(A)}{g_{11}(k_d^2, 0) + \mathcal{G}(k_d^2)} \Bigg\} - \frac{A}{k_d^2} \frac{\mathcal{G}(A)}{g_{11}(k_d^2, 0) + \mathcal{G}(k_d^2)} \ . \end{aligned} \tag{7.57}$$

As in the previous case we fix the dependence on the input by requiring that the deuteron pole in the mixing wave is located at the same position as in the ${}^3S_1$ wave, at the k_d^2 corresponding to the binding energy $E_d = 2.2$ MeV. Regarding the ${}^3D_1$ partial wave no pole position is found unless one imposes it in the $D_{22}(A)$ function, making use of Eq. (7.52), having then the right pole structure. Once the deuteron pole is imposed the value that we obtain for the ${}^3S_1$ scattering length is 4.6 fm and for the effective range 0.41 fm. The latter is indeed very similar to the values obtained before when the scattering length was taken as input. The resulting scattering length is around a 15% lower than its experimental value. We show in Fig. 7.6 by the dash-double-dotted (cyan) lines the results obtained when the deuteron pole is imposed in the ${}^3S_1$ and ${}^3D_1$ partial waves, while the double-dotted (green) line is for the case when the deuteron pole position is imposed only in the former. The results are rather similar to the case when the scattering length was fixed. The most sensitive observable is the mixing angle ϵ_1 where the largest difference happens in the peak, somewhat less than 1 degree.

It is worth comparing our results with the pionless effective field theory. In this case pions are integrated out as heavy degrees of freedom. We can reach this limit by taking $g_A \to 0$ in our results, which implies $\Delta_{ij} = 0$. Only the term proportional to N_0 survives in Eq. (7.49) and $N_{11}(A) = N_0$ from Eq. (7.40). We can determine N_0 by fixing the experimental scattering length, Eq. (7.42), or by reproducing the deuteron binding energy $N_0 = -4\pi/\sqrt{m^3 E_d}$. The former case is given by the solid (black) line and the latter by the double-dotted (green) one in Fig. 7.7. For comparison we also show the lines corresponding to our full results, obtained by fixing the scattering length and the deuteron binding energy to their experimental values. The former case corresponds to the dashed (blue) line and the latter to the dash-double-dotted (cyan) line, as already shown in Fig. 7.6. One observes that the inclusion of pions significantly improves the phase shifts and make also the results more stable independently of whether the scattering length or the deuteron pole are adjusted.

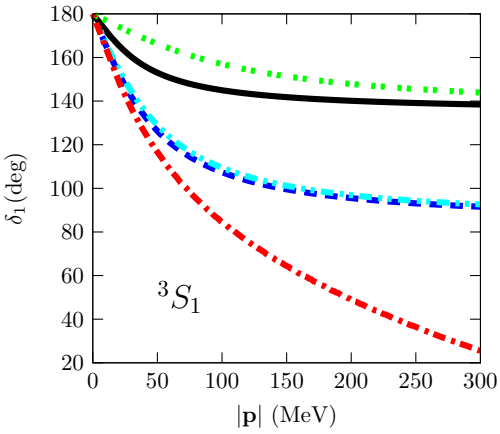

Figure 7.7: Comparison between the results obtained for the theory without pions and our full results at LO. The Nijmegen PWA [186] corresponds to the dot-dashed (red) lines. When the $^3S_1$ scattering length is fixed one has the dashed (blue) line for the pionfull case and the solid (black) line for the pionless one. When the deuteron binding energy is fixed the dash-double-dotted (cyan) line for the pionfull theory and the double-dotted (green) line for the pionless case result.

7.5.2 One extra subtraction

Now we impose that the $^3S_1$ partial wave reproduces at the same time both the experimental values for the $^3S_1$ scattering length, a_t, and the deuteron binding energy, E_d. Similar restrictions were already imposed in Refs. [473, 476]. To accomplish it we introduce one extra subtraction constant in the $D_{11}(A)$ function by taking one more subtraction in the dispersion relation. In this way we enhance the role played by the low energy region because the extra subtraction gives more weight to the low energy part of the integrand in the dispersion relation, so that it vanishes faster as $A \to \infty$. The new dispersion relations for $N_{11}(A)$ and $D_{11}(A)$ read:

$$\begin{aligned} N_{11}(A) &= N_0 + \frac{A}{\pi}\int_{-\infty}^{L} dk^2 \frac{\Delta_{11}(k^2) D_{11}(k^2)}{k^2(k^2-A)} \ , \\ D_{11}(A) &= 1 - \frac{A}{k_d^2} - \frac{A(A-k_d^2)}{\pi} N_0 \int_0^{\infty} dk^2 \frac{\nu_{11}(k^2)}{(k^2-A)(k^2-k_d^2)k^2} \\ &\quad + \frac{A(A-k_d^2)}{\pi}\int_{-\infty}^{L} dk^2 \frac{\Delta_{11}(k^2) D_{11}(k^2)}{k^2} g_{11}^{(d)}(A,k^2) \ , \end{aligned} \tag{7.58}$$

with

$$g_{11}^{(d)}(A,k^2) = \frac{1}{\pi}\int_0^{\infty} dq^2 \frac{\nu_{11}(q^2)}{(q^2-k^2)(q^2-A)(q^2-k_d^2)} \ . \tag{7.59}$$

By construction $D_{11}(k_d^2) = 0$ in Eq. (7.58), which guarantees the presence of the deuteron in its experimental position. Having the right value for the $^3S_1$ scattering length fixes the constant N_0 to Eq. (7.42). The extra subtraction taken in D_{11}, Eq. (7.58), will be also necessary when considering the NLO ChPT contribution to the discontinuity across the LHC because then the resulting $\Delta_{ij}(A)$ diverges as A for $A \to \infty$.

The deuteron pole is also imposed in the $^3D_1$ partial wave by employing Eq. (7.52) so that the right pole structure is accomplished. The input is fixed such that the resulting deuteron

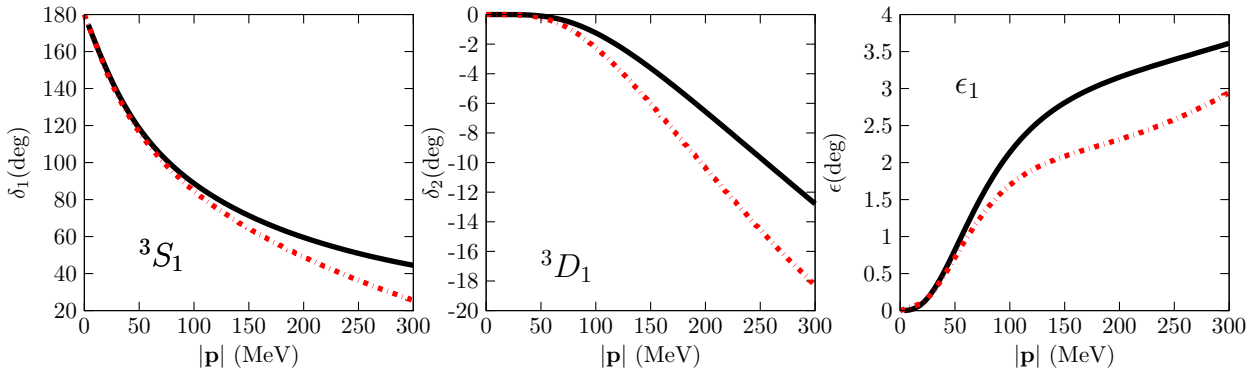

Figure 7.8: From left to right we plot our results, solid (black) curves, for the $^3S_1$ and $^3D_1$ phase shifts and the mixing angle ϵ_1, when the experimental $^3S_1$ scattering length and deuteron binding energy are imposed. The Nijmegen PWA [186] data are shown by the dot-dashed (red) lines.

pole position in the mixing partial wave $^3S_1$-$^3D_1$ is located in the same position as for the other two coupled partial waves, as already discussed above.

In Fig. 7.8 we show from left to right the $^3S_1$ and $^3D_1$ phase shifts and the mixing angle ϵ_1 resulting from Eq. (7.58), in that order. A clear improvement as compared with Fig. 7.6 is observed, so that now the resulting curve run closer to the Nijmegen PWA [186] for the $^3S_1$ phase shifts. An improvement also happens for the mixing angle ϵ_1 which now overlaps better with the Nijmegen results for three-momentum up to around 100 MeV and later the trend of the curve tends to follow that of the Nijmegen PWA. Let us also stress that the failure to reproduce ϵ_1 in the Kaplan-Savage-Wise scheme [174, 175] was the main reason to conclude that its perturbative treatment of pion exchange was not appropriate [489]. In contrast, our LO reproduction of ϵ_1 in Fig. (7.6) is already quite close to the Nijmegen results [186] and improves when considering the extra subtraction, as shown in Fig. 7.8. This is a clear indication that ϵ_1 will be also properly reproduced at NLO in the calculation of $\Delta_{ij}(A)$.

Next we evaluate the three independent deuteron parameters that can be calculated from NN scattering [490]. The first quantity is the binding energy of the deuteron that is fixed to its experimental value as input. The second quantity that we consider is the asymptotic D/S ratio η. For that we make use of the Blatt and Beidenharn parameterization [491] and diagonalize the $^3S_1$–$^3D_1$ S-matrix, S_1, by an orthogonal real matrix $\mathcal{O}$,

$$S_1 = \mathcal{O}\, S_{1;\mathrm{diag}}\, \mathcal{O}^{-1} \ , \qquad \mathcal{O} = \begin{pmatrix} \cos\epsilon_1 & -\sin\epsilon_1 \\ \sin\epsilon_1 & \cos\epsilon_1 \end{pmatrix} \ ,$$
$$S_{1;\mathrm{diag}} \equiv \begin{pmatrix} S_0 & 0 \\ 0 & S_2 \end{pmatrix} \ . \tag{7.60}$$

In terms of ϵ_1 one can write for the asymptotic D/S ratio η as [490, 492]

$$\eta = -\tan\epsilon_1 \ . \tag{7.61}$$

The third quantity that we calculate is i times the residue of the eigenvalue S_0 at the deuteron

pole position $\alpha \equiv \sqrt{-k_d^2}$,

$$S_0 = \frac{N_p^2}{\alpha + i|\mathbf{p}|} + \text{regular terms} \ . \tag{7.62}$$

We should remark that since we do not employ NN potential to study NN scattering we cannot compute the wave function of the deuteron and in terms of it evaluate straightforwardly (in the simplest approximation) other quantities like *e.g.* the deuteron electric quadrupole moment Q or the mean-square deuteron radius $\langle r^2 \rangle^{1/2}$. This does not mean that we cannot obtain such observable quantities from our T-matrix but simply that we should consider other processes beyond pure NN scattering. For instance, in order to calculate the mean-square deuteron radius $\langle r^2 \rangle$ we should proceed like done in Chapter 5 to calculate the same quantity but for the $f_0(500)$ or σ resonance, where $\pi\pi$ scattering in the presence of a scalar source was calculated. Similarly, we should study here NN scattering in the presence of a scalar source giving rise to the matter form factor of the deuteron. This is beyond the present study and requires an independent study by itself.

The resulting values that we obtain are:

$$\eta = 0.028 \ , \quad N_p^2 = 0.74 \ \text{fm}^{-1}. \tag{7.63}$$

Our results compare well with the experimental determinations $\eta = 0.0271(4)$ [493, 494] and $\eta = 0.0263(13)$ [495]. They also are close to those evaluated in Nijmegen PWA 1993 [186]:

$$\eta = 0.02543(7) \ , \quad N_p^2 = 0.7830(7) \ \text{fm}^{-1} \ . \tag{7.64}$$

Thus, once we reproduce simultaneously the NN scattering length and the ${}^3S_1$ scattering length, the deuteron properties that can be extracted from scattering compare well with the values determined in partial wave analyses or experiment. We obtain the following value for the effective range r:

$$r = 1.56(3) \ \text{fm} \ , \tag{7.65}$$

where the error is just statistical by fitting the low-energy phase shifts generated by our own amplitudes. This number is quite close to the Nijmegen PWA 1993 [186] result, $r = 1.753(2)$ fm.

In Ref. [496] the OPE potential from ChPT is employed in a LS equation solved by making use of an interesting method based on identifying the input with the T-matrix deep in the LHC, writing in terms of it the potential. Their results for η and r are very similar to ours in Eqs. (7.64) and (7.65), obtaining the intervals of values $\eta = 0.0281$–0.0293 and $r = 1.36$–1.58 fm. Their results for the elastic ${}^3S_1$ phase shifts are also quite similar to ours, though for ${}^3D_1$ they are closer to Nijmegen points [186]. Regarding the mixing angle ϵ_1, Ref. [496] obtains that for a large renormalization scale μ the resulting curves depart from Nijmegen data [186] by an absolute amount similar to ours for $|\mathbf{p}| \gtrsim 100$ MeV (our results lie above while theirs lie below). One should keep in mind that we have taken the scattering length and the binding energy as input for our calculations, while Ref. [496] only adjusts the scattering length.

It is well known since the sixties that for the ${}^3S_1$–${}^3D_1$ coupled partial waves solving a LS equation in terms of the OPE potential gives a significantly better phenomenology than solving

the N/D method taking for $\Delta_{ij}(A)$ the discontinuity along the LHC induced by OPE [487]. However, it is worth keeping in mind that [496], as well as [170], obtain phase shifts for $^1S_0$ which are very similar to ours in Sec. 7.3. It is known that the $^1S_0$ phase shift data of Nijmegen [186] are reproduced quite closely [458] once TPE contributions and NLO LECs in the four-nucleon Lagrangian are included. In our novel theory, that calculates the NN partial waves from ChPT by employing the N/D method, there is no reason to expect that the phase shifts should be reproduced at LO worse in the $^1S_0$ partial wave than in the $^3S_1$–$^3D_1$ coupled waves (which results strictly correspond to Fig. 7.6 in terms of only one needed subtraction). In this respect, it is rewarding that by considering NLO contributions to the NN potential in the standard Weinberg approach [458] one can obtain good results for $^1S_0$. This should be also expected for the $^3S_1$–$^3D_1$ case within our approach. Indeed, we have already seen that by including one extra subtraction the reproduction of phase shifts (particularly for the $^3S_1$) and mixing angle clearly improves. When considering two-pion exchange at NLO some extra counterterms are needed because $\Delta_{ij}(A)$ diverges as A for $A \to -\infty$ along the LHC.

Solving a LS equation with OPE for the $^3S_1$–$^3D_1$ system is much more successful phenomenologically than for the $^1S_0$ case. One should be aware that this is something that is checked *a posteriori* and is not rooted in the chiral counting (in which our approach, as well as the calculation of the potential in ChPT, is based). From our point of view the ladder resummation in the LS for the $^3S_1$–$^3D_1$ case is providing higher orders terms to $\Delta_{ij}(A)$ in the right direction. However, this improvement should come out when applying the N/D method to (*just* a few) higher orders, because along the LHC $\Delta_{ij}(A)$ is perturbative and amenable to a chiral expansion as discussed. For $^1S_0$ the higher orders in $\Delta(A)$ provided by the LS equation are not the important source of dynamics and one has really to consider the full machinery in order to incorporate at higher orders TPE with the associated chiral counterterms. It is our aim to develop in the time being a NLO (NNLO) study of NN scattering with our approach based on the N/D method and the ChPT calculation of $\Delta(A)$ in order to definitively settle this important issue. We would like to stress once more that at this stage our study is mostly exploratory and not competitive with the nowadays sophisticated potentials [186] or calculated at higher orders from ChPT [458, 462].

The set of works [171,497–499] gives rise to a remarkable description of deuteron properties employing the NN potential given by OPE in a LS equation, *e.g.* Ref. [171] achieves for many observables a $2-3\%$ of deviation with respect to the experimental values. But this is not the only aim of an EFT. That is, one does not expect such a high degree of convergence by taking only the LO ChPT NN potential. This is more a matter of phenomenological success and not rooted in the chiral EFT. For baryon ChPT the expansion scale is not so great, $\Lambda \simeq 12\pi^2 f_\pi^2/g_A^2 m \simeq 500$ MeV [162, 500], and such a great precision is then difficult to understand from the ChPT expansion. We want to emphasize this point (consider *e.g.* the not so great achievement for the $^1S_0$ case) and develop a formalism where contributions to a given process can be obtained order by order systematically in the chiral EFT expansion of $\Delta(A)$.

7.5.3 Higher partial waves

Finally, we present the results for the spin triplet waves with total angular momentum $J = 2$ and 3, obtained with the formalism derived in Sec. 7.4. They are shown by the solid (black)

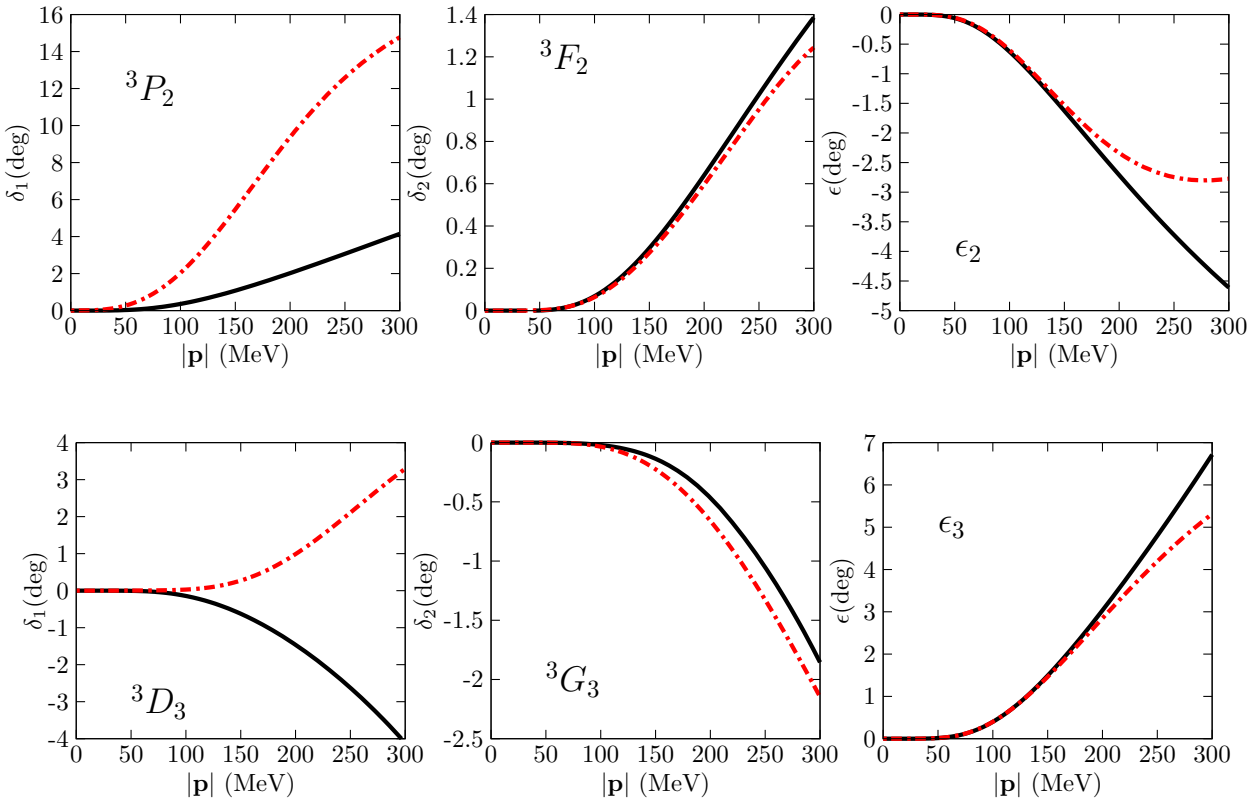

Figure 7.9: Comparison of our results for the $^3P_2$, $^3F_2$, $^3D_3$ and $^3G_3$ phase shifts and the mixing angles ϵ_2 and ϵ_3, shown by the solid (black) lines, to the Nijmegen PWA [186], represented by the dot-dashed (red) lines.

lines in Fig. 7.9, where they are compared with the Nijmegen PWA [186] (dash-dotted (red) lines).

We see already a good agreement with data for $^3F_2$ and $^3G_3$ as well as for the mixing angles ϵ_2 and ϵ_3. The lower partial waves $^3P_2$ and $^3D_3$ are not well reproduced with only OPE yet. This fact for the $^3D_3$ partial wave was already observed in Ref. [454], where OPE was treated perturbatively. In this reference $^3D_3$ is also obtained with opposite sign to data. The same behavior is observed in Ref. [489] at NLO (but not at NNLO). In Ref. [170], with one counterterm promoted to LO for the $^3P_2$ wave, the situation is similar. The $^3P_2$ and $^3D_3$ phase shifts are not well reproduced at LO, while the others compare well with data. We expect to restore the agreement with experiment at higher orders in the application of our method to $^3P_2$ and $^3D_3$.

7.6 Summary and conclusions

We have applied the N/D method to NN scattering from ChPT. In this method the two cuts present in a NN partial wave, the RHC and LHC, are separated in two functions, $D_{J\ell S}(A)$ and $N_{J\ell S}(A)$, with A the center-of-mass three-momentum squared. While $D_{J\ell S}(A)$ has only RHC, the function $N_{J\ell S}(A)$ has only LHC. The NN partial waves, $T_{J\ell S} = N_{J\ell S}/D_{J\ell S}$ ($\ell = 0,\ 1$) and $A^\ell N_{J\ell S}/D_{J\ell S}$ ($\ell \geqslant 2$), are determined in terms of their discontinuity along the LHC cut

due to multi-pion exchanges, $\Delta_{J\ell S}(A)$. At leading order, considered in this work, only OPE contributes. For D- and higher partial waves, with orbital angular momentum $\ell \geqslant 2$, one has to impose the proper behavior of a partial wave at around threshold, such that it vanishes as A^ℓ for $A \to 0$. This gives rise to $\ell - 1$ constraints, for $\ell \geqslant 2$, in the form of sum rules involving the functions $\Delta_{J\ell S}$ and $D_{J\ell S}$, that must be fulfilled when solving the N/D method. Since the function $D_{J\ell S}(A)$ is determined modulo the addition of CDD poles (that corresponds to zeros of the NN partial waves along the real axis) we have then added $\ell - 1$ of such poles at infinity in $D_{J\ell S}$ for $\ell \geqslant 2$. By sending such poles to infinity we do not include any zero of any NN partial wave at finite energies. In addition, the residues of these poles in $D_{J\ell S}$ are fixed once the sum rules are satisfied, so that no new parameters are included. At low energies the CDD poles behaves like adding a polynomial of degree $\ell - 2$ to $D_{J\ell S}$. This method is presented in a novel way, adequate to improve the results order–by–order, both for the uncoupled and the coupled channel case. This should be accomplished by taking higher orders in the chiral expansion of the calculation of the discontinuity of the partial wave amplitudes along the LHC, $\Delta_{ij}(k^2)$.

The resulting NN partial waves do not contain any regulator. A subtraction constant is required for the ${}^1S_0$ partial-wave (and for the ${}^3S_1$ partial-wave, once the formalism is generalized to coupled partial waves) that is fixed by reproducing the experimental scattering length. Our results are very close to those of Nogga, Timmermans and van Kolck [170] that provide cut-off independent NN partial waves with OPE as potential. The only noticeable difference concerns the ${}^3P_0$ partial wave for which Ref. [170] promoted a higher-order counterterm to leading order so as to achieve cut-off stable results. In our approach there is no special treatment to the ${}^3P_0$ partial wave compared to others and our results are a prediction for the ${}^3P_0$ phase shifts at leading order. For the ${}^1P_1$ partial wave our phase shifts run closer to data than those of [170].

Later, we have extended our method to the case of uncoupled partial waves. This extension is accomplished by providing three N/D equations for each set of partial waves coupled. The solution is obtained in an iterative and self-consistent way. The correct solution satisfies coupled channel unitarity, and also the right threshold behavior, by fulfilling sum rules that are a generalization of those of the uncoupled case.

We have studied the ${}^3S_1$–${}^3D_1$ coupled waves either by fixing the resulting subtraction constant to the experimental value of the scattering length or the deuteron binding energy. We find that the ${}^3D_1$ phase shifts are the most sensitive to this choice. As expected, in all the cases the triplet S-wave effective range comes out much smaller than experiment. We have also considered the pionless case and compared with our full results that include OPE. It is then seen that the results clearly improve for the latter case. For the waves with orbital angular momentum $\ell \geqslant 1$ at LO there is no subtraction constant and the results are parameter free. The resulting phase shifts and mixing angles agree well with the Nijmegen partial wave analysis results, except for the ${}^3P_2$ and ${}^3D_3$ partial waves.

Certainly, including OPE as the only source of discontinuity along the LHC is phenomenologically just a first step and a NLO calculation should be undergone to establish the capability of the method to reproduce properly NN scattering data. However, one should stress at this point that our approach based on the N/D method offers a way to calculate NN scattering

independently of any explicit cut-off, because only convergent integrals appear, while keeping the chiral power counting. The dispersive integrals are convergent by taking the appropriate number of subtractions with the related subtraction constants fixed to experimental data. This method allows one to perform calculations systematically, order by order in ChPT.

8

Conclusions

In the following lines, we give a succinct summary of the main achievements within this work, both regarding theoretical methods and practical results.

In **Chapter 3** we studied the scalar sector, focusing mainly on the isoscalar part. We used the N/D method and Chiral Lagrangians for such purpose. A useful method was developed there to treat scattering amplitudes involving states that contain scalar mesons (the σ meson in this case, but it can be easily generalized to other cases) that are dynamically generated from the interactions among the lightest pseudoscalars. With this method, one can calculate such kind of amplitudes directly from Chiral Lagrangians, without introducing any free parameter, and without using *ad hoc* parameterizations. Moreover, we could also include amplitudes involving vector fields by considering the latter as gauge fields of the chiral symmetry. From the point of view of the results, our study is quite global because all the relevant channels, to which the resonances can decay as reported in the PDG [48], up to the maximum energy considered ($\sqrt{s} \simeq 2$ GeV), were included. In this way, we have extended several former (and pioneer) works that studied the scalar sector, also based on the joint implementation of chiral symmetry and unitarity constraints (see Ref. [42] for an early review). We were able to provide a global description of many scattering observables, as well as of the hadronic spectrum in the considered sector. Besides the lightest scalars, we can describe all the resonances listed by the PDG in the isoscalar–scalar sector: $f_0(1370)$, $f_0(1500)$, $f_0(1710)$ and $f_0(1790)$. With these resonances, once their pole positions and residues are known by our study of scattering data, we find also agreement with data of the CBC and WA102 Collaborations in which these channels can be observed. This point is non–trivial, since our description of these data proceeds *a posteriori*, from the resonances we find in our amplitudes without fitting them to these data. The $f_0(1370)$ resonance turns out to be an almost pure octet, hence not mixed with the resonances close in energy. The same can be said about the $K_0(1430)$ in $I = 1/2$. We must stress that, from our study, we can undoubtedly state that this energy region requires a careful study including all the relevant coupled channels, a point frequently underestimated. The main result of our study of the scalar sector regards the $f_0(1710)$ resonance. We can identify it as the lightest scalar glueball, by the comparison of the couplings of this resonance with those predicted by the chiral suppression of the couplings of a glueball to $\bar{q}q$, as predicted by QCD [91], also supported by lattice QCD calculations. In addition, the mass that we find

for it is close to that predicted by quenched lattice QCD [84–89]. This work had some impact in our community. Some of the branching ratios we find for the $f_0(1710)$ are indeed cited by the PDG, and Ref. [A] (in which this Chapter is based) is cited in the PDG *"Note on scalar mesons"* as a support for the scenario in which the $f_0(1710)$ is identified with the glueball.

In **Chapter 4** we studied the interactions between the lighter and narrower scalar resonances ($f_0(980)$ and $a_0(980)$) and the lightest pseudoscalars, in order to explore the possible dyanmical generation of heavier pseudoscalar resonances. We take advantage of the fact that these scalars are dynamically generated in the interactions of pseudoscalars, so that we can calculate the desired amplitudes directly from the Chiral Lagrangians, similarly as done for the σ in the previous chapter. We find that these interactions are very rich, and strong enough to generate pseudoscalar resonances as $K(1460)$, $\pi(1300)$, $\pi(1800)$, $\eta(1475)$ and $X(1835)$, the former with η–quantum numbers, also. There is an open controversy about the possible existence of three η states in a narrow window of mass: $\eta(1295)$, $\eta(1405)$ and $\eta(1475)$. There are suggestions that the latter two could be the same state $\eta(1440)$. We do not find any signal for the $\eta(1295)$, and find just one resonant state that we tentatively identify with the $\eta(1475)$ because of its coupling pattern. This work, which has found some relevance in the community and published in Ref. [B], has already supposed some advance in this issue. We could shed some further light by including other channels (with vectors) in our approach.

The nature of the σ meson is discussed in detail in **Chapter 5** by calculating its quadratic scalar radius, $\langle r^2\rangle_s^\sigma$, so as to have an estimate of its size. We find this size to be small, roughly $\sqrt{\langle r^2\rangle_s^\sigma} = 0.45$ fm, similar to the $K^\pm$ quadratic charge radius, $\langle r^2\rangle_V^{K^\pm} = 0.28 \pm 0.07$ fm^2, and smaller than the quadratic scalar radius of the pion, $\sqrt{\langle r^2\rangle_s^\pi} = 0.81$ fm. This leads us to conclude that the σ meson is a rather compact object, in which the two pions (from which it is dynamically generated) are strongly overlapping. Thus, a four–quark picture seems more appropriate than a $\pi\pi$ molecule. These results are in agreement with other works that rule out the possible $\bar{q}q$ or glueball nature of the σ, but leave open the question of wether it is a pionic molecule or a four–quark object. This is the main result of our work. We have also studied in detail the $\pi\pi$ scattering amplitudes in $SU(2)$ UChPT, by fitting the LECs appearing in the Lagrangian to different data and lattice results. We have obtained values compatible with other phenomenological as well as lattice results. Our values are $\bar{l}_1 = 0.8\pm0.9$, $\bar{l}_2 = 4.6\pm0.4$, $\bar{l}_3 = 2\pm4$ and $\bar{l}_4 = 3.9\pm0.5$. We also find a sensible result for the σ pole position, $\sqrt{s}_\sigma = M_\sigma - i\Gamma_\sigma/2$, with $M_\sigma = 440 \pm 10$ MeV and $\Gamma_\sigma/2 = 238 \pm 10$ MeV. A comparison with other determinations of the σ pole by other groups is offered, finding a general agreement between a large number of different works. Our average values from this comparison are $M_\sigma = 458 \pm 14$ MeV and $\Gamma_\sigma/2 = 261 \pm 17$ MeV. In this respect, it is good news that the PDG has changed the name of the σ meson ($f_0(600)$ is now named $f_0(500)$) but, most importantly, has considerably reduced the uncertainties quoted on its mass and width. This reflects the fact that, due to the work of a large number of people working in the field, our knowledge of the σ pole position is quite precise, lying in a range of tens of MeV and, furthermore, we understand the underlying hadronic physics.

The quark mass dependence of the size of the σ as well as its mass and width is considered as well. The latter ones are compared with lattice QCD results [153] and theoretical calculations obtained within the IAM [154], in remarkable agreement. The fact that the mass of this resonance tends to follow the threshold of two pions is another clear indication that this

resonance is a dynamically generated meson-meson resonance. We find that, for a pion mass large enough ($m_\pi \gtrsim 450$ MeV), the σ meson becomes a spread $\pi\pi$ bound state. Studying the dependence of $\langle r^2\rangle_s^\sigma$ with the pion mass is also useful to understand its physical meaning. For those pion masses in wich the σ meson is a bound state, we find a larger value for $\langle r^2\rangle_s^\sigma$. This value, indeed, becomes infinite when the σ is a zero binding energy bound state, which agrees with what is expected on Quantum Mechanics grounds. In these situations, hence, a molecular picture is more appropriate. Finally, we have studied the dependence of the σ form factor $F_\sigma(q^2)$ (from which $\langle r^2\rangle_s^\sigma$ is extracted) for zero–momentum transfer, q^2. This is related to the dependence of the σ meson pole with m_π through the Feynman–Hellmann theorem, and a good agreement is found. To our mind, this also supports our treatment of the σ. All these studies were published in Ref. [C].

In **Chapter 6** we investigate the $\pi\pi$ interactions in a finite volume, for the cases of isospin $I = 0$ and $I = 2$. This is an important task, that should be useful for the advances of lattice QCD calculations, which has become a powerful and widespread tool to study the strong interactions and, in particular, the hadronic spectrum. In Lattice QCD, through the path integral formalism, one studies the interactions of quarks and gluons in a lattice box of finite volume. But one needs to link the results thereof obtained to the real world interactions, which take place in a continuum and infinite space. In our work, we have studied the corrections that are due to the finite volume in these interactions, by implementing these corrections (that arise due to the crossed loops and tadpoles in a field theoretical approach) into the formalism of Ref. [158], which is an improvement of the Lüscher method [156, 157]. The former is based in UChPT, and assumes a calculated kernel which is volume independent. The latter also neglects finite volume corrections, since these are exponentially supressed. Yet, there is no way, unless one knows precisely the source of the volume dependent terms, to estimate these effects and determine for which volumes the "exponentially suppressed" corrections have become smaller than a desired quantity. This is however an important information in realistic calculations. Our calculation, thus, estimates the size of these supressed contributions. We conclude that for $\pi\pi$ phase-shifts in the $I = 0$ channel up to 800 MeV this effect is negligible for box sizes bigger than $2.5m_\pi^{-1}$ and of the order of 5% at around $1.5 - 2m_\pi^{-1}$. For $I = 2$ the finite size effects can reach up to 10% for that energy. We also quantify the error made when using the standard Lüscher method to extract physical observables from lattice QCD, which is widely used in the literature but is an approximation of the one used in the present work. We must stress that the nonperturbative approach, the study for energies different than threshold and the study of the $I = 0$ $\pi\pi$ system are done in the present work for the first time in the literature. All these findings, published in Ref. [D], are of relevance in the lattice QCD community because, together with the use of the approach of Ref. [158] that also eliminates L depended terms (exponentially suppressed) from the Lüscher's approach, it can encourage the performance of lattice calculations with smaller size boxes with the consequent economy in the computing time.

The topic of **Chapter 7** is the study of NN interactions. This is a crucial process both for applications in nuclear physics and for a deeper understanding of the strong interactions. This problem is usually studied following the Weinberg proposal [163–165] of solving a Lippmann–Schwinger equation in terms of the calculated chiral NN potential in ChPT (which consists of contact terms and irreducible multi–pion exchange diagrams.) Many advances have been done in the last two decades in this issue. There is, however, some controversy about a

possible *inconsistency* in the Weinberg scheme of solving the Lippmann-Schwinger equation from the ChPT calculated potential. Our method is based in solving the N/D method, taking as the input for the N/D equation the discontinuity due to multi–pion exchanges along the left-hand cut. This discontinuity is adequate for a chiral power counting as discussed in Refs. [162, 183, 184]. Whence, this is an interesting method, because in this way we can avoid the aforementioned consistency problems of the Weinberg scheme. Without entering in the fine details of the approach, we must state that it can be applied to uncoupled as well as coupled channel partial waves. For partial waves with orbital angular momentum $\ell \geqslant 2$, in order to satisfy the right threshold behavior, our method requires the presence of some constraints in the functions of the N/D method. These constraints are satisfied by means of CDD poles. We obtain a general agreement for the phase shifts and mixing angles of the partial waves that we calculate, which are compared with the Nijmegen partial wave analysis [186]. When discussing the ${}^3S_1$–${}^3D_1$ case, we made some extension of the dispersion relations involved in the N/D method. This also lead us to be confident regarding future improvements of our method, when calculating the left-hand cut discontinuity in higher orders. Let us remark that our method is a novel one, and that, at present, it has been worked out just at leading order, where the discontinuity along the left-hand cut is given by just one-pion exchange. Hence its predictions are not as precise as those of other methods that offer higher order calculations. We must stress, though, that this method can be improved order by order, by considering higher order pion exchanges in the calculation of the left-hand cut discontinuity, and also that it is based in Chiral Lagrangians, in harmony with the modern persepectives of Effective Field Theories. Our work in this Chapter is given in Refs. [E, F].

III

Appendices

A

Elementary amplitudes for the scalar sector

In the following, in order to make notation simpler, we enumerate the channels as follows: (1)($\pi\pi$), (2)($K\bar{K}$), (3)($\eta\eta$), (4)($\sigma\sigma$), (5)($\eta\eta'$), (6)($\rho\rho$), (7)($\omega\omega$), (8)($\eta'\eta'$), (9)($K^*\overline{K^*}$), (10)($\omega\phi$), (11)($\phi\phi$), (12)($\pi^*\pi$) and (13)($a_1\pi$).

From the Lagrangians of Eqs. (3.2) and (3.4) one can calculate the interaction kernels $N_{i,j} = N_{j,i}$, which are symmetric due to time reversal invariance.[1] In the following equations, we give the matrix elements $N_{i,j}$ with the understanding that those not shown are zero. On the other hand, the octet and singlet scalar resonance couplings, α_i and β_i, respectively, are given below, and the vanishing couplings are not shown. For the $I = 1/2$ and $3/2$ S-waves, involving the $K\pi$, $K\eta$ and $K\eta'$ channels, we take directly the formulae from Refs. [43, 44], where they can be found.

$$N_{1,1} = \frac{s - m_\pi^2/2}{f^2} + \sum_{S_8} \frac{\alpha_1^2}{M_{S_8}^2 - s} + \sum_{S_1} \frac{\beta_1^2}{M_{S_1}^2 - s} \,, \tag{A.1}$$

$$N_{1,2} = \frac{\sqrt{3}s}{4f^2} + \sum_{S_8} \frac{\alpha_1\alpha_2}{M_{S_8}^2 - s} + \sum_{S_1} \frac{\beta_1\beta_2}{M_{S_1}^2 - s} \,, \tag{A.2}$$

$$N_{1,3} = -\frac{m_\pi^2}{\sqrt{3}f^2} + \sum_{S_8} \frac{\alpha_1\alpha_3}{M_{S_8}^2 - s} + \sum_{S_1} \frac{\beta_1\beta_3}{M_{S_1}^2 - s} \,, \tag{A.3}$$

$$N_{1,4} = \left\{ \frac{-75m_\pi^2 + 20(s + s_1 + s_2)}{18\sqrt{3}f^4} + \sum_{S_8} \frac{\alpha_1\alpha_4}{M_{S_8}^2 - s} + \sum_{S_1} \frac{\beta_1\beta_4}{M_{S_1}^2 - s} \right\} \left(\frac{\alpha_0}{g_{\sigma(\pi\pi)_0}} \right)^2 \,, \tag{A.4}$$

$$N_{1,5} = -\frac{m_\pi^2}{\sqrt{3}f^2} + \sum_{S_8} \frac{\alpha_1\alpha_5}{M_{S_8}^2 - s} + \sum_{S_1} \frac{\beta_1\beta_5}{M_{S_1}^2 - s} \,, \tag{A.5}$$

[1] For the $a_1\pi$ state one has to choose conveniently the phase of the state so that this result holds for those transition amplitudes involving this channel.

$$N_{1,6} = \frac{4g^2}{\sqrt{3}}\left(3 + \frac{s/2 - 2M_\rho^2}{M_\rho^2}\right) , \tag{A.6}$$

$$N_{1,8} = -\frac{m_\pi^2}{2\sqrt{3}f^2} + \sum_{S_8}\frac{\alpha_1\alpha_8}{M_{S_8}^2 - s} + \sum_{S_1}\frac{\beta_1\beta_8}{M_{S_1}^2 - s} , \tag{A.7}$$

$$N_{1,9} = g^2\left(3 + \frac{s/2 - 2M_{K^*}^2}{M_{K^*}^2}\right) , \tag{A.8}$$

$$N_{1,12} = -\frac{10d_m}{3f^3}m_\pi^2 , \tag{A.9}$$

$$N_{1,13} = -\frac{4G}{f}\frac{p_{a_1}\sqrt{s}}{M_{a_1}} + \sum_{S_8}\frac{\alpha_1\alpha_{13}}{M_{S_8}^2 - s} + \sum_{S_1}\frac{\beta_1\beta_{13}}{M_{S_1}^2 - s} , \tag{A.10}$$

$$N_{2,2} = \frac{3s}{4f^2} + \sum_{S_8}\frac{\alpha_2^2}{M_{S_8}^2 - s} + \sum_{S_1}\frac{\beta_2^2}{M_{S_1}^2 - s} , \tag{A.11}$$

$$N_{2,3} = -\frac{2(3s - 2m_\eta^2 - m_K^2)}{9f^2} + \sum_{S_8}\frac{\alpha_2\alpha_3}{M_{S_8}^2 - s} + \sum_{S_1}\frac{\beta_2\beta_3}{M_{S_1}^2 - s} , \tag{A.12}$$

$$N_{2,4} = \left\{\frac{5(s_1 + s_2) - 10m_\pi^2)}{36f^4} + \sum_{S_8}\frac{\alpha_2\alpha_4}{M_{S_8}^2 - s} + \sum_{S_1}\frac{\beta_2\beta_4}{M_{S_1}^2 - s}\right\}\left(\frac{\alpha_0}{g_{\sigma(\pi\pi)_0}}\right)^2 , \tag{A.13}$$

$$N_{2,5} = \frac{3s - m_\eta^2 - m_{\eta'}^2 - 3m_\pi^2 + 2m_K^2}{9f^2} + \sum_{S_8}\frac{\alpha_2\alpha_5}{M_{S_8}^2 - s} + \sum_{S_1}\frac{\beta_2\beta_5}{M_{S_1}^2 - s} , \tag{A.14}$$

$$N_{2,6} = g^2\left(3 + \frac{s/2 - 2M_\rho^2}{M_\rho^2}\right) , \tag{A.15}$$

$$N_{2,7} = -\sqrt{\frac{2}{3}}g^2\left(3 + \frac{s/2 - 2M_\omega^2}{M_\omega^2}\right) , \tag{A.16}$$

$$N_{2,8} = -\frac{32m_K^2 + 3s - 2m_{\eta'}^2 - 6m_\pi^2}{36f^2} + \sum_{S_8}\frac{\alpha_2\alpha_8}{M_{S_8}^2 - s} + \sum_{S_1}\frac{\beta_2\beta_8}{M_{S_1}^2 - s} , \tag{A.17}$$

$$N_{2,9} = \frac{4g^2}{\sqrt{3}}\left(3 + \frac{s/2 - 2M_{K^*}^2}{M_{K^*}^2}\right) , \tag{A.18}$$

$$N_{2,10} = \frac{2g^2}{\sqrt{3}}\left(2 + \frac{s - M_\phi^2 - M_\omega^2}{2M_\phi M_\omega}\right) , \tag{A.19}$$

$$N_{2,11} = -\frac{2g^2}{\sqrt{3}}\left(3 + \frac{s/2 - 2M_\phi^2}{M_\phi^2}\right) , \tag{A.20}$$

$$N_{2,12} = -\frac{d_m}{\sqrt{3}f^3}(3m_K^2 + m_\pi^2) , \tag{A.21}$$

$$N_{2,13} = -\frac{\sqrt{3}G}{f}\frac{p_{a_1}\sqrt{s}}{M_{a_1}} + \sum_{S_8}\frac{\alpha_2\alpha_{13}}{M_{S_8}^2 - s} + \sum_{S_1}\frac{\beta_2\beta_{13}}{M_{S_1}^2 - s} , \tag{A.22}$$

$$N_{3,3} = \frac{2m_K^2 + m_\pi^2}{9f^2} + \sum_{S_8}\frac{\alpha_3^2}{M_{S_8}^2 - s} + \sum_{S_1}\frac{\beta_3^2}{M_{S_1}^2 - s} , \tag{A.23}$$

$$N_{3,4} = \left\{-\frac{5m_\pi^2}{18f^4} + \sum_{S_8}\frac{\alpha_3\alpha_4}{M_{S_8}^2 - s} + \sum_{S_1}\frac{\beta_3\beta_4}{M_{S_1}^2 - s}\right\}\left(\frac{\alpha_0}{g_{\sigma(\pi\pi)_0}}\right)^2 , \tag{A.24}$$

$$N_{3,5} = -\frac{4(m_K^2 - m_\pi^2)}{9f^2} + \sum_{S_8}\frac{\alpha_3\alpha_5}{M_{S_8}^2 - s} + \sum_{S_1}\frac{\beta_3\beta_5}{M_{S_1}^2 - s}\ , \tag{A.25}$$

$$N_{3,8} = \frac{4m_K^2 - m_\pi^2}{9f^2} + \sum_{S_8}\frac{\alpha_3\alpha_8}{M_{S_8}^2 - s} + \sum_{S_1}\frac{\beta_3\beta_8}{M_{S_1}^2 - 2}\ , \tag{A.26}$$

$$N_{3,9} = -\frac{8g^2}{3\sqrt{3}}\left(3 + \frac{s/2 - 2M_{K^*}^2}{M_{K^*}^2}\right)\ , \tag{A.27}$$

$$N_{3,12} = \frac{4d_m m_\pi^2}{\sqrt{3}f^3}\ , \tag{A.28}$$

$$N_{4,4} = \left\{\frac{56(s_1 + s_2 + s_3 + s_4) - 357m_\pi^2}{216f^6} + \sum_{S_8}\frac{\alpha_4^2}{M_{S_8}^2 - s} + \sum_{S_1}\frac{\beta_4^2}{M_{S_1}^2 - s}\right\}\left(\frac{\alpha_0}{g_{\sigma(\pi\pi)_0}}\right)^4\ , \tag{A.29}$$

$$N_{4,5} = \left\{-\frac{5m_\pi^2}{18f^4} + \sum_{S_8}\frac{\alpha_4\alpha_5}{M_{S_8}^2 - s} + \sum_{S_1}\frac{\beta_4\beta_8}{M_{S_1}^2 - s}\right\}\left(\frac{\alpha_0}{g_{\sigma(\pi\pi)_0}}\right)^2\ , \tag{A.30}$$

$$N_{4,6} = \left\{\frac{40g^2}{9f^2}\left(3 + \frac{s/2 - 2M_\rho^2}{M_\rho^2}\right)\right\}\left(\frac{\alpha_0}{g_{\sigma(\pi\pi)_0}}\right)^2\ , \tag{A.31}$$

$$N_{4,8} = \left\{-\frac{m_\pi^2}{36f^4} + \sum_{S_8}\frac{\alpha_4\alpha_8}{M_{S_8}^2 - s} + \sum_{S_1}\frac{\beta_4\beta_8}{M_{S_1}^2 - s}\right\}\left(\frac{\alpha_0}{g_{\sigma(\pi\pi)_0}}\right)^2\ , \tag{A.32}$$

$$N_{4,9} = \frac{5g^2}{6\sqrt{3}f^2}\left(3 + \frac{s/2 - 2M_{K^*}^2}{M_{K^*}^2}\right)\left(\frac{\alpha_0}{g_{\sigma(\pi\pi)_0}}\right)^2\ , \tag{A.33}$$

$$N_{4,12} = -\frac{7\sqrt{3}d_m}{9f^5}m_\pi^2\left(\frac{\alpha_0}{g_{\sigma(\pi\pi)_0}}\right)^2\ , \tag{A.34}$$

$$N_{4,13} = \left\{-\frac{20\sqrt{3}G}{9f^3}\frac{p_{a_1}\sqrt{s}}{M_{a_1}} + \sum_{S_8}\frac{\alpha_4\alpha_{13}}{M_{S_8}^2 - s} + \sum_{S_1}\frac{\beta_4\beta_{13}}{M_{S_1}^2 - s}\right\}\left(\frac{\alpha_0}{g_{\sigma(\pi\pi)_0}}\right)^2\ , \tag{A.35}$$

$$N_{5,5} = \frac{2(4m_K^2 - m_\pi^2)}{9f^2} + \sum_{S_8}\frac{\alpha_5^2}{M_{S_8}^2 - s} + \sum_{S_1}\frac{\beta_5^2}{M_{S_1}^2 - s}\ , \tag{A.36}$$

$$N_{5,8} = -\frac{8m_K^2 - 5m_\pi^2}{9f^2} + \sum_{S_8}\frac{\alpha_5\alpha_8}{M_{S_8}^2 - s} + \sum_{S_1}\frac{\beta_5\beta_8}{M_{S_1}^2 - s}\ , \tag{A.37}$$

$$N_{5,9} = \frac{4g^2}{3\sqrt{3}}\left(3 + \frac{s/2 - 2M_{K^*}^2}{M_{K^*}^2}\right) \tag{A.38}$$

$$N_{5,12} = \frac{4d_m m_\pi^2}{\sqrt{3}f^3}\ , \tag{A.39}$$

$$N_{8,8} = \frac{16m_K^2 - 7m_\pi^2}{18f^2} + \sum_{S_8}\frac{\alpha_8^2}{M_{S_8}^2 - s} + \sum_{S_1}\frac{\beta_8^2}{M_{S_1}^2 - s}\ . \tag{A.40}$$

$$N_{8,9} = -\frac{g^2}{3\sqrt{3}}\left(3 + \frac{s/2 - 2M_{K^*}^2}{M_{K^*}^2}\right)\ , \tag{A.41}$$

$$N_{8,12} = \frac{2d_m m_\pi^2}{\sqrt{3}f^3}\ , \tag{A.42}$$

$$N_{12,12} = \frac{1}{2sf^2}\left(2s(s - m_\pi^2 - M_{\pi^*}^2) + s^2 - (M_{\pi^*}^2 - m_\pi^2)^2\right)\ , \tag{A.43}$$

$$N_{13,13} = \frac{G^2(2\sqrt{2}+1)}{3}\frac{(s-(m_\pi+M_{a_1})^2)(s-(m_\pi-M_{a_1})^2)}{sM_{a_1}^2} + \sum_{S_8}\frac{\alpha_{13}^2}{M_{S_8}^2-s} + \sum_{S_1}\frac{\beta_{13}^2}{M_{S_1}^2-s}\ , \tag{A.44}$$

$$\alpha_1 = \frac{1}{f^2}[c_d s + 2m_\pi^2(c_m-c_d)]\ , \tag{A.45}$$

$$\alpha_2 = \frac{-1}{\sqrt{3}}[c_d s + 2m_K^2(c_m-c_d)]\ , \tag{A.46}$$

$$\alpha_3 = \frac{8}{3\sqrt{3}f^2}c_m[m_K^2-m_\pi^2]\ , \tag{A.47}$$

$$\alpha_4 = \frac{-1}{3\sqrt{3}f^4}[c_d(8m_\pi^2+s-3s_1-3s_2)-5c_m m_\pi^2]\left(\frac{\alpha_0}{g_{\sigma(\pi\pi)_0}}\right)^2\ , \tag{A.48}$$

$$\alpha_5 = \frac{-2}{3\sqrt{3}f^2}[3c_d(s-m_\eta^2-m_{\eta'}^2)+2c_m(4m_K^2-m_\pi^2)]\ , \tag{A.49}$$

$$\alpha_8 = \frac{1}{3\sqrt{3}f^2}[3c_d(s-2m_{\eta'}^2)+2c_m(8m_K^2-5m_\pi^2)]\ , \tag{A.50}$$

$$\alpha_{13} = -\frac{4Gc_d}{f}\frac{p_{a_1}\sqrt{s}}{M_{a_1}}\ , \tag{A.51}$$

$$\beta_1 = \frac{\sqrt{6}}{f^2}[\widetilde{c}_d s + 2m_\pi^2(\widetilde{c}_m-\widetilde{c}_d)]\ , \tag{A.52}$$

$$\beta_2 = \frac{2\sqrt{2}}{f^2}[\widetilde{c}_d s + 2m_K^2(\widetilde{c}_m-\widetilde{c}_d)]\ , \tag{A.53}$$

$$\beta_3 = \frac{-\sqrt{2}}{3f^2}[3\widetilde{c}_d(s-2m_\eta^2)+2\widetilde{c}_m(2m_K^2+m_\pi^2)]\ , \tag{A.54}$$

$$\beta_4 = \left\{\frac{-\sqrt{2}}{3f^4}[\widetilde{c}_d(8m_\pi^2+s-3s_1-3s_2)-5\widetilde{c}_m m_\pi^2]\right\}\ , \tag{A.55}$$

$$\beta_5 = \frac{8\sqrt{2}}{3f^2}\widetilde{c}_m(m_K^2-m_\pi^2)\ , \tag{A.56}$$

$$\beta_8 = \frac{-\sqrt{2}}{3f^2}[3\widetilde{c}_d(s-2m_{\eta'}^2)+2\widetilde{c}_m(4m_K^2-m_\pi^2)]\ , \tag{A.57}$$

$$\beta_{13} = -\frac{4\sqrt{6}\widetilde{c}_d G}{f}\frac{p_{a_1}\sqrt{s}}{M_{a_1}}\ , \tag{A.58}$$

B

Loop functions

In this Appendix, we give the loop functions used through the thesis, mainly in Chapters 5 and 6. We start with the scalar one-, two- and three-point one-loop scalar integrals, denoted by A_0, B_0 and C_0, respectively, and depicted in Fig. B.1. The vector and tensor integrals, defined later, can be cast in terms of the former. Special attention is dedicated to the case of the three-point function, whose cuts are also calculated since they are needed in order to calculate the scalar form factor of the σ meson. Notice that all the internal masses are equal, as we only have pions as degrees of freedom. For this reason, we do not include the dependence on the internal mass M^2 in the following (except for the case of the function A_0, which does not depend on any external momenta).

B.1 Scalar loop integrals

The simplest one is the one-point loop integral, given by:

$$A_0(M^2) = i\int \frac{d^4k}{(2\pi)^4} \frac{1}{k^2 - M^2 + i\epsilon} \ . \tag{B.1}$$

In dimensional regularization, it results:

$$A_0(M^2) = \frac{M^2}{16\pi^2}\left(R + \log\frac{M^2}{\mu^2}\right) \ , \tag{B.2}$$

with

$$R = \mu^{n-4}\left(\frac{2}{n-4} - (1 + \Gamma'(1) + \log 4\pi)\right) \ , \tag{B.3}$$

and $n \to 4$.

The two point function is:

$$B_0(P^2) = i\int \frac{d^4k}{(2\pi)^4} \frac{1}{\Big(k^2 - M^2 + i\epsilon\Big)\Big((k-P)^2 - M^2 + i\epsilon\Big)} \ , \tag{B.4}$$

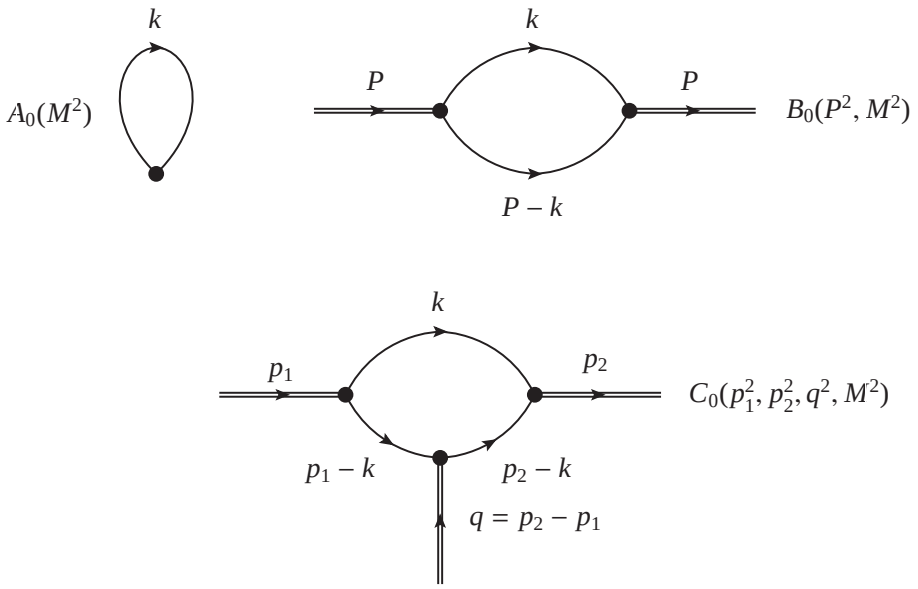

Figure B.1: Diagrams for the one-loop functions A_0, B_0 and C_0 (from left to right and top to bottom, respectively).

and analogously, in dimensional regularization,

$$B_0(P^2) = \frac{1}{16\pi^2}\left(R + \log\frac{M^2}{\mu^2} - 1 - \sigma(P^2)\log\frac{\sigma(P^2)-1}{\sigma(P^2)+1}\right) , \tag{B.5}$$

with $\sigma(P^2) = \sqrt{1-4M^2/P^2}$. Since the function is divergent and μ-dependent, we define the subtracted function, $\bar{B}_0(P^2)$,

$$\bar{B}_0(P^2) = B_0(P^2) - \frac{R + \log\dfrac{M^2}{\mu^2}}{16\pi^2} . \tag{B.6}$$

This is the function that will appear in the amplitudes, since the piece that we have subtracted cancels out with the alike terms in the loops and the chiral counterterms. The same procedure, applied to $A_0(M^2)$, gives

$$\bar{A}_0 = A_0(M^2) - \frac{M^2}{16\pi^2}\left(R + \log\frac{M^2}{\mu^2}\right) = 0 , \tag{B.7}$$

this is why in the amplitudes of Appendix C there is no dependence on $\bar{A}_0$.

The three-point function is defined by:

$$\begin{aligned} C_0(p_1^2, p_2^2, q^2) = i\int\frac{d^4k}{(2\pi)^4}\frac{1}{k^2 - M^2 + i\epsilon} \\ \times \frac{1}{\Big((k-p_1)^2 - M^2 + i\epsilon\Big)\Big((k-p_2)^2 - M^2 + i\epsilon\Big)} , \end{aligned} \tag{B.8}$$

and it depends on the three scalar p_1^2, p_2^2 and $q^2 \equiv (p_1 - p_2)^2$. It is finite and after lengthy calculations [501], it can be cast in integral form:

$$C_0(p_1^2, p_2^2, q^2) = \frac{1}{16\pi^2 \lambda(p_1^2, p_2^2, q^2)^{1/2}} \left\{ \int_0^1 dz \frac{\log f(p_1^2, z) - \log f(p_1^2, z_1)}{z - z_1} + \right. \\ + \int_0^1 dz \frac{\log f(p_2^2, z) - \log f(p_2^2, z_2)}{z - z_2} + \\ \left. + \int_0^1 dz \frac{\log f(q^2, z) - \log f(q^2, z_3)}{z - z_3} \right\} , \tag{B.9}$$

where we have defined:

$$f(p^2, z) = p^2 z(z-1) + M^2 - i\epsilon \ , \tag{B.10}$$

$$\lambda(a, b, c) = a^2 + b^2 + c^2 - 2ab - 2bc - 2ac \ , \tag{B.11}$$

$$z_1 = \frac{1}{2}\left(1 + \frac{p_1^2 - p_2^2 - q^2}{\lambda(p_1^2, p_2^2, q^2)^{1/2}}\right) \ , \tag{B.12}$$

$$z_2 = \frac{1}{2}\left(1 + \frac{p_2^2 - p_1^2 - q^2}{\lambda(p_1^2, p_2^2, q^2)^{1/2}}\right) \ , \tag{B.13}$$

$$z_3 = \frac{1}{2}\left(1 + \frac{q^2 - p_1^2 - p_2^2}{\lambda(p_1^2, p_2^2, q^2)^{1/2}}\right) \ . \tag{B.14}$$

The usefulness of Eq. (B.9) lies in the fact that it is well suited for its analytical continuation to the complex plane, which is needed in our case, since the cases $p_1^2 = p_2^2 = s_\sigma$ are studied. Notice that the residues of the integrals when $z \to z_i$ are zero because of the form of the numerators, and also that, since $z(z-1) \geqslant 0$ for $z \in [0, 1]$, the arguments of the logarithms do not cross any cut.

On the other hand, since the pole of the σ resonance appears in the unphysical Riemann sheet, we need to calculate the amplitudes $\pi\pi H \to \pi\pi$ in this sheet. This involves the function $C_0(s, s, q^2)$ in this sheet,[1] and this is not so trivial as in the case of the function $G(s)$ (see Eqs. (5.11) and (5.12)). For that purpose, we calculate the discontinuity along the unitarity cut of the function $C_0(s, s, q^2)$:

$$\Delta C_0 = C_0(s + i\epsilon, s + i\epsilon, q^2) - C_0(s - i\epsilon, s - i\epsilon, q^2) \ , \tag{B.15}$$

for $s \geqslant 4M^2$. This can be obtained directly from the integral representation in Eq. (B.9), and the result depends on the value of q^2. We are interested mainly in the case $q^2 \leqslant 0$, and we find two cases:

$$\Delta_a C_0 = \frac{i}{4\pi \lambda(s, s, q^2)^{1/2}} \log\left(\frac{z_- - z_1}{z_+ - z_1}\right) \quad \text{for } q^2 \leqslant q_{an}^2 \ , \tag{B.16}$$

$$\Delta_b C_0 = \frac{i}{4\pi \lambda(s, s, q^2)^{1/2}} \log\left(\frac{1 - z_1}{-z_1} \frac{z_- - z_1}{z_+ - z_1}\right)$$

[1] Notice that we have already considered $s = s'$, since this will be the case in the σ form factor, because $s = s' = s_\sigma$.

$$+\frac{i}{8\pi\lambda(s,s,q^2)^{1/2}}\log\left(\frac{1-z_3}{-z_3}\right)\quad\text{for } q^2_{an}\leqslant q^2\leqslant 4M^2\ , \tag{B.17}$$

where we have defined $z_\pm=\frac{1}{2}(1\pm\sigma(s))$. In the previous equation q^2_{an} is the so called anomalous threshold, given by $M^2q^2_{an}=-s(s-4M^2)\leqslant 0$, where the last inequality follows from $s\geqslant 4M^2$. The case that connects continuously with $q^2=0$ is the one denoted by Δ_bC_0, which is the one involved in the calculation of the quadratic scalar radius, for which we take $q^2\to 0^-$.

As a cross-check of the validity of our procedure, let us note that the function C_0 is related for $q^2=0$ to the derivative of the function $G(s)$ with respect to M^2, denoted by $dG(s,M^2)/dM^2=\dot{G}$. Indeed, one has

$$2C_0(s,s,0)=\dot{G}(s)=\frac{1}{8\pi^2s\sigma(s)}\log\frac{\sigma(s)-1}{\sigma(s)+1}\ . \tag{B.18}$$

In the calculation of the scalar form factor C_0 appears, while in the derivative of the σ pole position, $\dot{s}_\sigma$, one has $\dot{G}$. Both are related through the Feynman-Hellmann theorem, Eq. (5.82), and thus, the unphysical Riemann sheet for the function C_0 must be related to that of the function $G(s)$. When the pole is in the unphysical Riemann sheet, we have:

$$\dot{G}_{II}(s)=\dot{G}_I(s)-\dot{\Delta}G(s)=\dot{G}_I(s)-\frac{i}{4\pi s\sigma(s)}\ . \tag{B.19}$$

If we now calculate the value $\Delta_bC_0(s,s,0)$, we find:

$$\Delta_bC_0(s,s,0)=\frac{i}{8\pi s\sigma(s)}\ , \tag{B.20}$$

so that

$$\begin{aligned}C_{0;II}(s,s,0)&=C_{0;I}(s,s,0)-\Delta_bC_0(s,s,0)\\&=C_{0;I}(s,s,0)-\frac{i}{8\pi s\sigma(s)}\ ,\end{aligned} \tag{B.21}$$

which implies, as stated, $2C_{0;II}(s,s,0)=\dot{G}_{II}(s)$.

B.2 Vector and tensor loop integrals

Vector and tensor loop integrals appear throughout the amplitudes in Appendix C. We reduce them to the scalar ones by means of the Passarino-Veltman method [502]. We start with the two-point vector and tensor integrals, defined by

$$B_{\{\mu;\mu\nu\}}=i\int\frac{d^4k}{(2\pi)^4}\frac{\{k_\mu;k_\mu k_\nu\}}{\Big(k^2-M^2+i\epsilon\Big)\Big((k-P)^2-M^2+i\epsilon\Big)}\ . \tag{B.22}$$

On Lorentz-invariance grounds, we can write

$$B^\mu=-P^\mu B_{11}(P)\ , \tag{B.23}$$

where the minus sign is introduced for convenience, and, performing the contraction $P^\mu B_\mu$, it can be shown that:

$$B_{11}(P^2) = -\frac{1}{2}B_0(P^2) \ . \tag{B.24}$$

Analogously, the tensor integral can be decomposed as:

$$B_{\mu\nu} = P_\mu P_\nu B_{20}(P^2) + g_{\mu\nu}P^2 B_{21}(P^2) \ , \tag{B.25}$$

and the following results, by the appropriate contractions, are obtained:

$$P^2 B_{20}(P^2) = \frac{A_0(M^2)}{3} - \frac{M^2 - P^2}{3}B_0(P^2) + \frac{1}{48\pi^2}\left(M^2 - \frac{P^2}{6}\right) \ , \tag{B.26}$$

$$P^2 B_{21}(P^2) = \frac{A_0(M^2)}{6} + \frac{4M^2 - P^2}{12}B_0(P^2) - \frac{1}{48\pi^2}\left(M^2 - \frac{P^2}{6}\right) \ . \tag{B.27}$$

For the three-point vector and tensor integrals, we define:

$$\begin{aligned} C_{\{\mu;\mu\nu\}} = i\int\frac{d^4k}{(2\pi)^4}\frac{\{k_\mu; k_\mu k_\nu\}}{k^2 - M^2 + i\epsilon} \\ \times \frac{1}{\Big((k-p_1)^2 - M^2 + i\epsilon\Big)\Big((k-p_2)^2 - M^2 + i\epsilon\Big)} \ , \end{aligned} \tag{B.28}$$

and

$$C^\mu = -p_1^\mu C_{11} - p_2^\mu C_{12} \ , \tag{B.29}$$

$$C^{\mu\nu} = p_1^\mu p_1^\nu C_{21} + p_2^\mu p_2^\nu C_{22} + (p_1^\mu p_2^\nu + p_1^\nu p_2^\mu)\, C_{23} + g^{\mu\nu} C_{24} \ , \tag{B.30}$$

where for simplifying the writing we have omitted the arguments in $C_{ij}(p_1^2, p_2^2, q^2)$. The results for these functions are:

$$\begin{aligned} C_{11} = \Big(p_2^2 B_0(p_2^2) - p_1p_2 B_0(p_1^2) - (p_2^2 - p_1p_2)B_0(q^2) \\ -p_2^2(p_1^2 - p_1p_2)C_0(p_1^2, p_2^2, q^2)\Big)/(2\det\mathcal{H}) \ , \end{aligned} \tag{B.31}$$

$$\begin{aligned} C_{12} = \Big(p_1^2 B_0(p_1^2) - p_1p_2 B_0(p_2^2) - (p_1^2 - p_1p_2)B_0(q^2) \\ -p_1^2(p_2^2 - p_1p_2)C_0(p_1^2, p_2^2, q^2)\Big)/(2\det\mathcal{H}) \ , \end{aligned} \tag{B.32}$$

$$\begin{aligned} C_{24} = -\frac{1}{64\pi^2} + \frac{M^2}{2}C_0(p_1^2, p_2^2, q^2) \\ + \frac{1}{4}\Big(B_0(q^2) + p_1^2 C_{11} + p_2^2 C_{12}\Big) \ , \end{aligned} \tag{B.33}$$

$$C_{21} = \Big(p_2^2 R_a - p_1p_2 R_c\Big)/\det\mathcal{H} \ , \tag{B.34}$$

$$C_{22} = \Big(p_1^2 R_d - p_1p_2 R_b\Big)/\det\mathcal{H} \ , \tag{B.35}$$

$$C_{23} = \Big(p_1^2 R_c + p_2^2 R_b - p_1p_2(R_a + R_d)\Big)/(2\det\mathcal{H}) \ , \tag{B.36}$$

with

$$\mathcal{H} = \begin{pmatrix} p_1^2 & p_1p_2 \\ p_1p_2 & p_2^2 \end{pmatrix} \ , \tag{B.37}$$

and

$$R_a = \frac{1}{4}B_0(q^2) - \frac{1}{2}p_1^2 C_{11} - C_{24} \ , \tag{B.38}$$

$$R_b = \frac{1}{4}B_0(q^2) - \frac{1}{2}p_1^2 C_{12} - \frac{1}{4}B_0(p_2^2) \ , \tag{B.39}$$

$$R_c = \frac{1}{4}B_0(q^2) - \frac{1}{2}p_2^2 C_{11} \ - \frac{1}{4}B_0(p_1^2), \tag{B.40}$$

$$R_d = \frac{1}{4}B_0(q^2) - \frac{1}{2}p_2^2 C_{12} - C_{24} \ . \tag{B.41}$$

Analogously to the scalar loop integrals, we define the subtracted functions $\bar{B}_{ij}$ and $\bar{C}_{ij}$ by substituting in their expressions given above $A_0 \to \bar{A}_0$ and $B_0 \to \bar{B}_0$. The amplitudes $\pi\pi\, H \to \pi\pi$ in Appendix C are then written in terms of finite and scale independent functions.

C

$\pi\pi\, H \to \pi\pi$ amplitudes

In this Appendix, the amplitudes $\pi\pi\, H \to \pi\pi$ are given for completeness. We follow the nomenclature given in Fig. 5.14. We give the finite contributions to each amplitude once the infinite and scale dependent terms are cancelled among them. In this way, the amplitudes are written in terms of the finite and scale independent constants $\bar{l}_i$ as well as the subtracted loop functions defined in Appendix B, $\bar{B}_0$, etc... The diagrams denoted in Fig. 5.14 by VI, XI and XII, both in the case of $\pi^0\pi^0\, H \to \pi^0\pi^0$ and $\pi^0\pi^0\, H \to \pi^+\pi^-$, are proportional to the tadpole function, $A_0(M^2)$, so they do not contribute to the finite amplitude, as explained before.

In the subsequent, unless the opposite is stated, the subscript $i = 1, \ldots, 4$ indicates the pion leg with four-momentum p_i to which the scalar source is attached. The functions D_i, corresponding to the inverse of the pion propagators when the scalar source is attached to the i_{th} external pion leg, are used through this Appendix. These functions were defined in Eq. (5.49).

C.1 Diagrams I

C.1.1 $\pi^0\pi^0\, H \to \pi^0\pi^0$

$$T^{(\mathrm{LO})} = -\frac{6B}{f_\pi^2}\ , \tag{C.1}$$

$$T^{(\mathrm{NLO})} = -\frac{3B}{f_\pi^4}\frac{m_\pi^2}{4\pi^2}\bar{l}_4\ . \tag{C.2}$$

C.1.2 $\pi^0\pi^0\, H \to \pi^+\pi^-$

$$T^{(\mathrm{LO})} = -\frac{2B}{f_\pi^2}\ , \tag{C.3}$$

$$T^{(\mathrm{NLO})} = -\frac{B}{f_\pi^4}\frac{m_\pi^2}{4\pi^2}\bar{l}_4 \ . \tag{C.4}$$

The NLO result corresponds to the LO diagram I multiplied by $2\delta Z$, with the latter given in Eq. (1.283). In addition m^2, f^2 are expressed in terms of the physical values m_π and f_π according to the expansions of Eqs. (1.288) and (1.289).

C.2 Diagrams II

C.2.1 $\pi^0\pi^0\, H \to \pi^0\pi^0$

$$\begin{aligned}
T_1^{(\mathrm{LO})} &= \frac{2B}{f_\pi^2}\left(1+\frac{m_\pi^2}{D_1}\right) \ , \\
T_2^{(\mathrm{LO})} &= \frac{2B}{f_\pi^2}\left(1+\frac{m_\pi^2}{D_2}\right) \ , \\
T_3^{(\mathrm{LO})} &= \frac{2B}{f_\pi^2}\left(1+\frac{m_\pi^2}{D_3}\right) \ , \\
T_4^{(\mathrm{LO})} &= \frac{2B}{f_\pi^2}\left(1+\frac{m_\pi^2}{D_4}\right) \ .
\end{aligned} \tag{C.5}$$

$$\begin{aligned}
T_1^{(\mathrm{NLO})} &= \frac{B}{f_\pi^4}\left\{\frac{\bar{l}_4 m_\pi^2}{4\pi^2}+\frac{m_\pi^4}{D_1}\frac{4\bar{l}_4-3\bar{l}_3}{16\pi^2}\right\} \ , \\
T_2^{(\mathrm{NLO})} &= \frac{B}{f_\pi^4}\left\{\frac{\bar{l}_4 m_\pi^2}{4\pi^2}+\frac{m_\pi^4}{D_2}\frac{4\bar{l}_4-3\bar{l}_3}{16\pi^2}\right\} \ , \\
T_3^{(\mathrm{NLO})} &= \frac{B}{f_\pi^4}\left\{\frac{\bar{l}_4 m_\pi^2}{4\pi^2}+\frac{m_\pi^4}{D_3}\frac{4\bar{l}_4-3\bar{l}_3}{16\pi^2}\right\} \ , \\
T_4^{(\mathrm{NLO})} &= \frac{B}{f_\pi^4}\left\{\frac{\bar{l}_4 m_\pi^2}{4\pi^2}+\frac{m_\pi^4}{D_4}\frac{4\bar{l}_4-3\bar{l}_3}{16\pi^2}\right\} \ .
\end{aligned} \tag{C.6}$$

C.2.2 $\pi^0\pi^0\, H \to \pi^+\pi^-$

$$\begin{aligned}
T_1^{(\mathrm{LO})} &= \frac{2B}{f_\pi^2}\frac{s\ -m_\pi^2}{D_1} \ , \\
T_2^{(\mathrm{LO})} &= \frac{2B}{f_\pi^2}\frac{s\ -m_\pi^2}{D_2} \ , \\
T_3^{(\mathrm{LO})} &= \frac{2B}{f_\pi^2}\frac{s'-m_\pi^2}{D_3} \ , \\
T_4^{(\mathrm{LO})} &= \frac{2B}{f_\pi^2}\frac{s'-m_\pi^2}{D_4} \ .
\end{aligned} \tag{C.7}$$

$$
\begin{aligned}
iT_1^{(\mathrm{NLO})} &= \frac{B}{f_\pi^2}\frac{m_\pi^2}{D_1}\frac{4\bar{l}_4(s\ -m_\pi^2)-\bar{l}_3 m_\pi^2}{16\pi^2}\ ,\\
iT_2^{(\mathrm{NLO})} &= \frac{B}{f_\pi^2}\frac{m_\pi^2}{D_2}\frac{4\bar{l}_4(s\ -m_\pi^2)-\bar{l}_3 m_\pi^2}{16\pi^2}\ ,\\
iT_3^{(\mathrm{NLO})} &= \frac{B}{f_\pi^2}\frac{m_\pi^2}{D_3}\frac{4\bar{l}_4(s'-m_\pi^2)-\bar{l}_3 m_\pi^2}{16\pi^2}\ ,\\
iT_4^{(\mathrm{NLO})} &= \frac{B}{f_\pi^2}\frac{m_\pi^2}{D_4}\frac{4\bar{l}_4(s'-m_\pi^2)-\bar{l}_3 m_\pi^2}{16\pi^2}\ .
\end{aligned}
\tag{C.8}
$$

The NLO results are obtained by multiplying the LO ones by $3\delta Z$ and with m^2, f^2 re-expressed in terms of the physical m_π^2 and f_π^2, respectively, according to Eqs. (1.288) and (1.289). Notice that in addition to the factor Z^2 from the wave function renormalization of the external pion legs there is an extra factor Z from the renormalized pion propagator, Eq. (1.282).

C.3 Diagrams III

The diagrams III and higher in numeration are purely NLO contributions. To simplify writing we then omit the superscript NLO in the corresponding amplitudes.

C.3.1 $\boldsymbol{\pi^0\pi^0}$ $\boldsymbol{H\to\pi^0\pi^0}$

$$
T=-\frac{3B}{f_\pi^4}\frac{\bar{l}_4}{8\pi^2}q^2\ . \tag{C.9}
$$

C.3.2 $\boldsymbol{\pi^0\pi^0}$ $\boldsymbol{H\to\pi^+\pi^-}$

$$
T=-\frac{B}{f_\pi^4}\frac{\bar{l}_4}{8\pi^2}q^2\ . \tag{C.10}
$$

C.4 Diagrams IV

C.4.1 $\boldsymbol{\pi^0\pi^0}$ $\boldsymbol{H\to\pi^0\pi^0}$

$$
\begin{aligned}
T_1 &= \frac{B}{f_\pi^4}\frac{\bar{l}_4 q^2-\bar{l}_3 m_\pi^2}{8\pi^2}\left(1+\frac{m_\pi^2}{D_1}\right)\ ,\\
T_2 &= \frac{B}{f_\pi^4}\frac{\bar{l}_4 q^2-\bar{l}_3 m_\pi^2}{8\pi^2}\left(1+\frac{m_\pi^2}{D_2}\right)\ ,\\
T_3 &= \frac{B}{f_\pi^4}\frac{\bar{l}_4 q^2-\bar{l}_3 m_\pi^2}{8\pi^2}\left(1+\frac{m_\pi^2}{D_3}\right)\ ,
\end{aligned}
$$

$$T_4 = \frac{B}{f_\pi^4}\frac{\bar{l}_4 q^2 - \bar{l}_3 m_\pi^2}{8\pi^2}\left(1 + \frac{m_\pi^2}{D_4}\right) \ . \tag{C.11}$$

C.4.2 $\pi^0\pi^0\, H \to \pi^+\pi^-$

$$\begin{aligned}
T_1 &= \frac{B}{f_\pi^4}\frac{\bar{l}_4 q^2 - \bar{l}_3 m_\pi^2}{8\pi^2}\left(\frac{s\ - m_\pi^2}{D_1}\right) \ , \\
T_2 &= \frac{B}{f_\pi^4}\frac{\bar{l}_4 q^2 - \bar{l}_3 m_\pi^2}{8\pi^2}\left(\frac{s\ - m_\pi^2}{D_2}\right) \ , \\
T_3 &= \frac{B}{f_\pi^4}\frac{\bar{l}_4 q^2 - \bar{l}_3 m_\pi^2}{8\pi^2}\left(\frac{s' - m_\pi^2}{D_3}\right) \ , \\
T_4 &= \frac{B}{f_\pi^4}\frac{\bar{l}_4 q^2 - \bar{l}_3 m_\pi^2}{8\pi^2}\left(\frac{s' - m_\pi^2}{D_4}\right) \ .
\end{aligned} \tag{C.12}$$

C.5 Diagrams V

C.5.1 $\pi^0\pi^0\, H \to \pi^0\pi^0$

$$\begin{aligned}
T_1 &= -\frac{B}{f_\pi^4}\frac{\bar{l}_1 + 2\bar{l}_2}{24\pi^2}\left(D_1 + 2m_\pi^2 - \frac{s^{\,2} + t'^2 + u'^2 - 4m_\pi^4}{D_1}\right) \ , \\
T_2 &= -\frac{B}{f_\pi^4}\frac{\bar{l}_1 + 2\bar{l}_2}{24\pi^2}\left(D_2 + 2m_\pi^2 - \frac{s^{\,2} + t^{\,2} + u^{\,2} - 4m_\pi^4}{D_2}\right) \ , \\
T_3 &= -\frac{B}{f_\pi^4}\frac{\bar{l}_1 + 2\bar{l}_2}{24\pi^2}\left(D_3 + 2m_\pi^2 - \frac{s'^2 + t'^2 + u^{\,2} - 4m_\pi^4}{D_3}\right) \ , \\
T_4 &= -\frac{B}{f_\pi^4}\frac{\bar{l}_1 + 2\bar{l}_2}{24\pi^2}\left(D_4 + 2m_\pi^2 - \frac{s'^2 + t^{\,2} + u'^2 - 4m_\pi^4}{D_4}\right) \ .
\end{aligned} \tag{C.13}$$

C.5.2 $\pi^0\pi^0\, H \to \pi^+\pi^-$

In these amplitudes, we define:

$$\begin{aligned}
P(s,t,u) = {} & 4m_\pi^4(\bar{l}_1 + 2\bar{l}_2) + \bar{l}_1 s^2 + \bar{l}_2(t^2 + u^2) \\
& - 2m_\pi^2(2\bar{l}_1 s + 2\bar{l}_2(t+u))
\end{aligned} \tag{C.14}$$

$$\begin{aligned}
T_1 &= -\frac{B}{24\pi^2 f_\pi^4}\left(\bar{l}_1 s\ + \bar{l}_2(t' + u') - 2m_\pi^2(\bar{l}_1 + 2\bar{l}_2) - \frac{P(s\,, t', u')}{D_1}\right) \ , \\
T_2 &= -\frac{B}{24\pi^2 f_\pi^4}\left(\bar{l}_1 s\ + \bar{l}_2(t\ + u\,) - 2m_\pi^2(\bar{l}_1 + 2\bar{l}_2) - \frac{P(s\,, t\,, u\,)}{D_2}\right) \ , \\
T_3 &= -\frac{B}{24\pi^2 f_\pi^4}\left(\bar{l}_1 s' + \bar{l}_2(t' + u\,) - 2m_\pi^2(\bar{l}_1 + 2\bar{l}_2) - \frac{P(s', t', u\,)}{D_3}\right) \ ,
\end{aligned}$$

$$T_4 = -\frac{B}{24\pi^2 f_\pi^4}\left(\bar{l}_1 s' + \bar{l}_2(t\ + u') - 2m_\pi^2(\bar{l}_1 + 2\bar{l}_2) - \frac{P(s', t\ , u')}{D_4}\right)\ . \tag{C.15}$$

C.6 Diagrams VII

C.6.1 $\boldsymbol{\pi^0\pi^0}$ $\boldsymbol{H \to \pi^0\pi^0}$

$$\begin{aligned}
T_1 &= -\frac{B}{f_\pi^4}\left\{2q^2 + D_1 + m_\pi^2\frac{2q^2 - m_\pi^2}{D_1}\right\}\bar{B}_0(q^2)\ ,\\
T_2 &= -\frac{B}{f_\pi^4}\left\{2q^2 + D_2 + m_\pi^2\frac{2q^2 - m_\pi^2}{D_2}\right\}\bar{B}_0(q^2)\ ,\\
T_3 &= -\frac{B}{f_\pi^4}\left\{2q^2 + D_3 + m_\pi^2\frac{2q^2 - m_\pi^2}{D_3}\right\}\bar{B}_0(q^2)\ ,\\
T_4 &= -\frac{B}{f_\pi^4}\left\{2q^2 + D_4 + m_\pi^2\frac{2q^2 - m_\pi^2}{D_4}\right\}\bar{B}_0(q^2)\ .
\end{aligned} \tag{C.16}$$

C.6.2 $\boldsymbol{\pi^0\pi^0}$ $\boldsymbol{H \to \pi^+\pi^-}$

$$\begin{aligned}
T_1 &= -\frac{B}{f_\pi^4}\left(s\ - m_\pi^2\right)\left\{1 + \frac{2q^2 - m_\pi^2}{D_1}\right\}\bar{B}_0(q^2)\ ,\\
T_2 &= -\frac{B}{f_\pi^4}\left(s\ - m_\pi^2\right)\left\{1 + \frac{2q^2 - m_\pi^2}{D_2}\right\}\bar{B}_0(q^2)\ ,\\
T_3 &= -\frac{B}{f_\pi^4}\left(s' - m_\pi^2\right)\left\{1 + \frac{2q^2 - m_\pi^2}{D_3}\right\}\bar{B}_0(q^2)\ ,\\
T_4 &= -\frac{B}{f_\pi^4}\left(s' - m_\pi^2\right)\left\{1 + \frac{2q^2 - m_\pi^2}{D_4}\right\}\bar{B}_0(q^2)\ .
\end{aligned} \tag{C.17}$$

C.7 Diagrams VIII

C.7.1 $\boldsymbol{\pi^0\pi^0}$ $\boldsymbol{H \to \pi^0\pi^0}$

s-channel diagrams:

$$\begin{aligned}
T_1 &= -\frac{2B}{f_\pi^4}\left\{\frac{m_\pi^2}{2} + \frac{\frac{3}{2}m_\pi^4 + s^{\,2} - 2s\,m_\pi^2}{D_1}\right\}\bar{B}_0(s\ )\ ,\\
T_2 &= -\frac{2B}{f_\pi^4}\left\{\frac{m_\pi^2}{2} + \frac{\frac{3}{2}m_\pi^4 + s^{\,2} - 2s\,m_\pi^2}{D_2}\right\}\bar{B}_0(s\ )\ ,\\
T_3 &= -\frac{2B}{f_\pi^4}\left\{\frac{m_\pi^2}{2} + \frac{\frac{3}{2}m_\pi^4 + s'^2 - 2s'm_\pi^2}{D_3}\right\}\bar{B}_0(s')\ ,\\
T_4 &= -\frac{2B}{f_\pi^4}\left\{\frac{m_\pi^2}{2} + \frac{\frac{3}{2}m_\pi^4 + s'^2 - 2s'm_\pi^2}{D_4}\right\}\bar{B}_0(s')\ .
\end{aligned} \tag{C.18}$$

t-crossed diagrams:

$$
\begin{aligned}
T_1 &= -\frac{2B}{f_\pi^4}\left\{\frac{m_\pi^2}{2}+\frac{\frac{3}{2}m_\pi^4+t'^2-2t'm_\pi^2}{D_1}\right\}\bar{B}_0(t')\ ,\\
T_2 &= -\frac{2B}{f_\pi^4}\left\{\frac{m_\pi^2}{2}+\frac{\frac{3}{2}m_\pi^4+t^{\,2}-2t\,m_\pi^2}{D_2}\right\}\bar{B}_0(t\,)\ ,\\
T_3 &= -\frac{2B}{f_\pi^4}\left\{\frac{m_\pi^2}{2}+\frac{\frac{3}{2}m_\pi^4+t'^2-2t'm_\pi^2}{D_3}\right\}\bar{B}_0(t')\ ,\\
T_4 &= -\frac{2B}{f_\pi^4}\left\{\frac{m_\pi^2}{2}+\frac{\frac{3}{2}m_\pi^4+t^{\,2}-2t\,m_\pi^2}{D_4}\right\}\bar{B}_0(t\,)\ .
\end{aligned}
\tag{C.19}
$$

u-crossed diagrams:

$$
\begin{aligned}
T_1 &= -\frac{2B}{f_\pi^4}\left\{\frac{m_\pi^2}{2}+\frac{\frac{3}{2}m_\pi^4+u'^2-2u'm_\pi^2}{D_1}\right\}\bar{B}_0(u')\ ,\\
T_2 &= -\frac{2B}{f_\pi^4}\left\{\frac{m_\pi^2}{2}+\frac{\frac{3}{2}m_\pi^4+u^{\,2}-2u\,m_\pi^2}{D_2}\right\}\bar{B}_0(u\,)\ ,\\
T_3 &= -\frac{2B}{f_\pi^4}\left\{\frac{m_\pi^2}{2}+\frac{\frac{3}{2}m_\pi^4+u^{\,2}-2u\,m_\pi^2}{D_3}\right\}\bar{B}_0(u\,)\ ,\\
T_4 &= -\frac{2B}{f_\pi^4}\left\{\frac{m_\pi^2}{2}+\frac{\frac{3}{2}m_\pi^4+u'^2-2u'm_\pi^2}{D_4}\right\}\bar{B}_0(u')\ .
\end{aligned}
\tag{C.20}
$$

C.7.2 $\pi^0\pi^0\, H \to \pi^+\pi^-$

In the t and u channels amplitudes, we define:

$$
\begin{aligned}
Q(s,t,u) = {}& \frac{(s+u-2m_\pi^2)(m_\pi^2-t)+m_\pi^2 t}{2}\bar{B}_0(t)\\
&+ t(s+u-4m_\pi^2)\bar{B}_{20}(t)+2t(u-2m_\pi^2)\bar{B}_{21}(t)
\end{aligned}
\tag{C.21}
$$

s-channel diagrams

$$
\begin{aligned}
T_1 &= -\frac{B}{f_\pi^4}(s\ -m_\pi^2)\left(1+\frac{s\ +m_\pi^2}{D_1}\right)\bar{B}_0(s\,)\ ,\\
T_2 &= -\frac{B}{f_\pi^4}(s\ -m_\pi^2)\left(1+\frac{s\ +m_\pi^2}{D_2}\right)\bar{B}_0(s\,)\ ,\\
T_3 &= -\frac{B}{f_\pi^4}(s'-m_\pi^2)\left(1+\frac{s'+m_\pi^2}{D_3}\right)\bar{B}_0(s')\ ,\\
T_4 &= -\frac{B}{f_\pi^4}(s'-m_\pi^2)\left(1+\frac{s'+m_\pi^2}{D_4}\right)\bar{B}_0(s')\ .
\end{aligned}
\tag{C.22}
$$

t-crossed diagrams

$$
T_1 = -\frac{2B}{f_\pi^4}\frac{Q(s\,,t',u')}{D_1}\ ,
$$

$$
\begin{aligned}
T_2 &= -\frac{2B}{f_\pi^4}\frac{Q(s\,,t\,,u\,)}{D_2}\ ,\\
T_3 &= -\frac{2B}{f_\pi^4}\frac{Q(s',t',u\,)}{D_3}\ ,\\
T_4 &= -\frac{2B}{f_\pi^4}\frac{Q(s',t\,,u')}{D_4}\ .
\end{aligned}
\tag{C.23}
$$

u-crossed diagrams:

$$
\begin{aligned}
T_1 &= -\frac{2B}{f_\pi^4}\frac{Q(s\,,u',t')}{D_1}\ ,\\
T_2 &= -\frac{2B}{f_\pi^4}\frac{Q(s\,,u\,,t\,)}{D_2}\ ,\\
T_3 &= -\frac{2B}{f_\pi^4}\frac{Q(s',u\,,t')}{D_3}\ ,\\
T_4 &= -\frac{2B}{f_\pi^4}\frac{Q(s',u',t\,)}{D_4}\ .
\end{aligned}
\tag{C.24}
$$

C.8 Diagrams IX

In these amplitudes, the scalar source s can be attached to one of the two four pion vertex (recall Fig. 5.14), which we denote here by the subscript $i = 1, 2$.

C.8.1 $\boldsymbol{\pi^0\pi^0}\, H \to \boldsymbol{\pi^0\pi^0}$

s-channel diagrams:

$$
\begin{aligned}
T_1 &= \frac{B}{f_\pi^4}\left(2s\ + m_\pi^2\right)\bar{B}_0(s\,)\ ,\\
T_2 &= \frac{B}{f_\pi^4}\left(2s' + m_\pi^2\right)\bar{B}_0(s')\ .
\end{aligned}
\tag{C.25}
$$

t-crossed diagrams:

$$
\begin{aligned}
T_1 &= \frac{B}{f_\pi^4}\left(2t\ + m_\pi^2\right)\bar{B}_0(t\,)\ ,\\
T_2 &= \frac{B}{f_\pi^4}\left(2t' + m_\pi^2\right)\bar{B}_0(t')\ .
\end{aligned}
\tag{C.26}
$$

u-crossed diagrams:

$$
\begin{aligned}
T_1 &= \frac{B}{f_\pi^4}\left(2u\ + m_\pi^2\right)\bar{B}_0(u\,)\ ,\\
T_2 &= \frac{B}{f_\pi^4}\left(2u' + m_\pi^2\right)\bar{B}_0(u')\ .
\end{aligned}
\tag{C.27}
$$

C.8.2 $\pi^0\pi^0\, H \to \pi^+\pi^-$

s-channel diagrams:

$$T_1 = \frac{B}{f_\pi^4}\left(4s\ - 3m_\pi^2\right)\bar{B}_0(s\ )\ ,$$
$$T_2 = \frac{B}{f_\pi^4}\left(4s' - 3m_\pi^2\right)\bar{B}_0(s')\ . \tag{C.28}$$

t-crossed diagrams:

$$T_1 = -\frac{B}{f_\pi^4}\left(t\ - 2m_\pi^2\right)\bar{B}_0(t\ )\ ,$$
$$T_2 = -\frac{B}{f_\pi^4}\left(t' - 2m_\pi^2\right)\bar{B}_0(t')\ . \tag{C.29}$$

u-crossed diagrams:

$$T_1 = -\frac{B}{f_\pi^4}\left(u\ - 2m_\pi^2\right)\bar{B}_0(u\ )\ ,$$
$$T_2 = -\frac{B}{f_\pi^4}\left(u' - 2m_\pi^2\right)\bar{B}_0(u')\ . \tag{C.30}$$

C.9 Diagrams X

C.9.1 $\pi^0\pi^0\, H \to \pi^0\pi^0$

s-channel diagrams:

$$T = -\frac{2B}{f_\pi^4}\left\{\left(2(s-m_\pi^2)(s'-m_\pi^2)+m_\pi^4\right)C_0(s,s',q^2)+\right.$$
$$\left.+\,m_\pi^2\left(\bar{B}_0(s)+\bar{B}_0(s')+2\bar{B}_0(q^2)\right)+\frac{s+s'-q^2}{2}\bar{B}_0(q^2)\right\} \tag{C.31}$$

t-crossed diagrams:

$$T = -\frac{2B}{f_\pi^4}\left\{\left(2(t-m_\pi^2)(t'-m_\pi^2)+m_\pi^4\right)C_0(t,t',q^2)+\right.$$
$$\left.+\,m_\pi^2\left(\bar{B}_0(t)+\bar{B}_0(t')+2\bar{B}_0(q^2)\right)+\frac{t+t'-q^2}{2}\bar{B}_0(q^2)\right\} \tag{C.32}$$

u-crossed diagrams:

$$T = -\frac{2B}{f_\pi^4}\left\{\left(2(u-m_\pi^2)(u'-m_\pi^2)+m_\pi^4\right)C_0(u,u',q^2)+\right.$$
$$\left.+\,m_\pi^2\left(\bar{B}_0(u)+\bar{B}_0(u')+2\bar{B}_0(q^2)\right)+\frac{u+u'-q^2}{2}\bar{B}_0(q^2)\right\} \tag{C.33}$$

C.9.2 $\boldsymbol{\pi^0\pi^0}\, H \to \boldsymbol{\pi^+\pi^-}$

s-channel diagrams:

$$T = -\frac{2B}{f_\pi^4}\Big((ss' - m_\pi^4)C_0(s,s',q^2) + (s+s'-2m_\pi^2)\bar{B}_0(q^2) + \\ + (s'-m_\pi^2)\bar{B}_0(s') + (s-m_\pi^2)\bar{B}_0(s)\Big) \tag{C.34}$$

t-crossed diagrams:

$$T = -\frac{2B}{f_\pi^4}\Big(\frac{(2m_\pi^2-t)(2m_\pi^2-t')}{2}C_0(t,t',q^2) + \\ \frac{2m_\pi^2-t}{2}\Big(\bar{B}_0(q^2)+\bar{B}_0(t)\Big) + \frac{2m_\pi^2-t'}{2}\Big(\bar{B}_0(q^2)+\bar{B}_0(t')\Big) \\ + \frac{t+t'-q^2}{4}\bar{B}_0(q^2) + \frac{(s-s')^2-(u-u')^2}{2}\bar{C}_{23}(t,t',q^2) \\ - \ (s+s'-u-u')\,\bar{C}_{24}(t,t',q^2)\Big) \tag{C.35}$$

u-crossed diagrams:

$$T = -\frac{2B}{f_\pi^4}\Big(\frac{(2m_\pi^2-u)(2m_\pi^2-u')}{2}C_0(u,u',q^2) + \\ \frac{2m_\pi^2-u}{2}\Big(\bar{B}_0(q^2)+\bar{B}_0(u)\Big) + \frac{2m_\pi^2-u'}{2}\Big(\bar{B}_0(q^2)+\bar{B}_0(u')\Big) \\ + \frac{u+u'-q^2}{4}\bar{B}_0(q^2) + \frac{(s-s')^2-(t-t')^2}{2}\bar{C}_{23}(u,u',q^2) \\ - \ (s+s'-t-t')\,\bar{C}_{24}(u,u',q^2)\Big) \tag{C.36}$$

C.10 Diagrams XIII

C.10.1 $\boldsymbol{\pi^0\pi^0}\, H \to \boldsymbol{\pi^0\pi^0}$

$$T = \frac{B}{f_\pi^4}\Big(25m_\pi^2 + 8q^2\Big)\,\bar{B}_0(q^2)\ . \tag{C.37}$$

C.10.2 $\boldsymbol{\pi^0\pi^0}\, H \to \boldsymbol{\pi^+\pi^-}$

$$T = \frac{B}{f_\pi^4}\Big(5(s+s'-m_\pi^2) + q^2\Big)\,\bar{B}_0(q^2)\ . \tag{C.38}$$

D

Unitarized meson–meson amplitudes for scalar–pseudoscalar scattering

We use UChPT (see Sec. 2.7) to unitarize the different isospin channels amplitudes for meson–meson scattering, which are fitted to data, and then used in the vertex of the triangle loop. From these amplitudes, once fitted, the position of the poles can be found (we use here the $f_0(980)$ and $a_0(980)$, but we also check for the appearance of the other scalars, σ and κ). As mentioned, the amplitudes are unitarized through

$$T_I = (1 + V_I \cdot G)^{-1} \cdot V_I \ , \tag{D.1}$$

which is analogous to eq. (4.11) but now for the pseudoscalar-pseudoscalar scattering. The symmetric matrix V_I (the analogous one to $\mathcal{T}_{IG}$ in eq. (4.11)) collects the S-wave pseudoscalar-pseudoscalar tree-level amplitudes obtained from the lowest order Chiral Lagrangians including resonances as well. The matrix G is a diagonal matrix that contains the meson–meson loop propagator (the same expression as given in eq. (4.12) can be used with the appropriate replacement for the masses involved.)

The lowest order chiral Lagrangian at leading order in large N_C which also includes the η_1 was given in Subsec. 3.2.1, and also the treatment of the η–η' mixing was given there. As in Chapter 3, the explicit exchange of $J^{PC} = 0^{++}$ scalar resonances is incorporated and calculated from the leading order chiral Lagrangians, see Sec. 1.13. The interaction kernels obtained from all those Lagrangians can thus be written as:

$$\begin{aligned} V_{ij} &= V_{ij}^{(C)} + V_{ij}^{(R)} \ , \\ V_{ij}^{(R)} &= \frac{\alpha_i \alpha_j}{M_R^2 - s} \ , \end{aligned} \tag{D.2}$$

where C means *contact term* and R *resonance exchange*. This is represented diagrammatically in Fig. D.1.

In what follows, we give explicit formulae for the contact kernels from the chiral Lagrangians for the different isospin channels. We also give the couplings α_i for each scalar

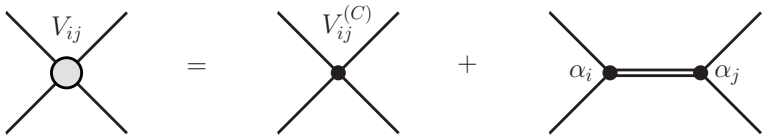

Figure D.1: Eq. (D.2) in terms of Feynman Diagrams

resonance. For $I = 0$ we include the superscript (8) or (1) in α_i to distinguish between the octet and singlet contributions, respectively. For the rest of isospins there is no singlet contribution.

- $I = 0$

$$\begin{aligned}
V^{(C)}_{\pi\pi\to\pi\pi} &= \frac{2s-m_\pi^2}{2f_\pi^2}\\
V^{(C)}_{\pi\pi\to K\bar{K}} &= \frac{\sqrt{3}}{4}\frac{s}{f_\pi^2}\\
V^{(C)}_{\pi\pi\to\eta\eta} &= -\frac{1}{\sqrt{3}}\frac{m_\pi^2}{f_\pi^2}\\
V^{(C)}_{K\bar{K}\to K\bar{K}} &= \frac{3}{4}\frac{s}{f_\pi^2}\\
V^{(C)}_{K\bar{K}\to\eta\eta} &= -\frac{2}{9}\frac{3s-2m_\eta^2-m_K^2}{f_\pi^2}\\
V^{(C)}_{\eta\eta\to\eta\eta} &= \frac{2m_K^2+m_\pi^2}{9f_\pi^2}
\end{aligned} \tag{D.3}$$

$$\begin{aligned}
\alpha^{(8)}_{\pi\pi} &= \frac{c_d s+2(c_m-c_d)m_\pi^2}{f_\pi^2}\\
\alpha^{(8)}_{K\bar{K}} &= -\frac{c_d s+2(c_m-c_d)m_K^2}{\sqrt{3}f_\pi^2}\\
\alpha^{(8)}_{\eta\eta} &= \frac{8c_m(m_K^2-m_\pi^2)}{3\sqrt{3}f_\pi^2}
\end{aligned} \tag{D.4}$$

$$\begin{aligned}
\alpha^{(1)}_{\pi\pi} &= \sqrt{6}\frac{\tilde{c}_d s+2(\tilde{c}_m-\tilde{c}_d)m_\pi^2}{f_\pi^2}\\
\alpha^{(1)}_{K\bar{K}} &= -\frac{\tilde{c}_d s+2(\tilde{c}_m-\tilde{c}_d)m_K^2}{2\sqrt{2}f_\pi^2}\\
\alpha^{(1)}_{\eta\eta} &= \sqrt{2}\frac{3\tilde{c}_d(s-2m_\eta^2)+2\tilde{c}_m(2m_K^2+m_\pi^2)}{3f_\pi^2}
\end{aligned} \tag{D.5}$$

- $I = 1/2$

$$V^{(C)}_{K\pi\to K\pi} = \frac{s-3u+2m_K^2+2m_\pi^2}{4f_\pi^2}$$

$$
\begin{aligned}
V^{(C)}_{K\pi\to K\eta} &= \frac{\sqrt{2}}{6}\frac{3t-m_\eta^2-2m_K^2}{f_\pi^2}\\
V^{(C)}_{K\pi\to K\eta'} &= -\frac{1}{12}\frac{3t-8m_K^2-m_{\eta'}^2-3m_\pi^2}{f_\pi^2}\\
V^{(C)}_{K\eta\to K\eta} &= \frac{6t-4m_\eta^2-2m_K^2}{9f_\pi^2}\\
V^{(C)}_{K\eta\to K\eta'} &= -\frac{1}{9\sqrt{2}}\frac{3t-m_\eta^2-m_{\eta'}^2-3m_\pi^2+2m_K^2}{f_\pi^2}\\
V^{(C)}_{K\eta'\to K\eta'} &= \frac{1}{36}\frac{3t-2m_{\eta'}^2+32m_K^2-6m_\pi^2}{f_\pi^2}
\end{aligned}
\tag{D.6}
$$

$$
\begin{aligned}
\alpha_{K\pi} &= -\sqrt{\frac{3}{2}}\frac{c_d s+(c_m-c_d)(m_\pi^2+m_K^2)}{f_\pi^2}\\
\alpha_{K\eta} &= -\frac{2}{\sqrt{3}}\frac{c_m(m_K^2-m_\pi^2)}{f_\pi^2}\\
\alpha_{K\eta'} &= -\sqrt{\frac{3}{2}}\frac{c_d s-c_d(m_K^2+m_{\eta'}^2)-\frac{1}{3}c_m(m_\pi^2-7m_K^2)}{f_\pi^2}
\end{aligned}
\tag{D.7}
$$

- $I=1$

$$
\begin{aligned}
V^{(C)}_{\pi\eta\to\pi\eta} &= \frac{2}{3}\frac{m_\pi^2}{f_\pi^2}\\
V^{(C)}_{\pi\eta\to K\bar K} &= -\frac{3s-2m_K^2-m_\eta^2}{3\sqrt{3}f_\pi^2}\\
V^{(C)}_{\pi\eta\to\pi\eta'} &= \frac{\sqrt{2}}{3}\frac{m_\pi^2}{f_\pi^2}\\
V^{(C)}_{K\bar K\to K\bar K} &= -\frac{u-2m_\pi^2}{2f_\pi^2}\\
V^{(C)}_{K\bar K\to\pi\eta'} &= \frac{3s-8m_K^2-m_{\eta'}^2-3m_\pi^2}{6\sqrt{6}f_\pi^2}\\
V^{(C)}_{K\eta'\to K\eta'} &= \frac{1}{3}\frac{m_\pi^2}{f_\pi^2}
\end{aligned}
\tag{D.8}
$$

$$
\begin{aligned}
\alpha_{\pi\eta} &= -\frac{2}{\sqrt{3}}\frac{c_d s-c_d(m_\pi^2+m_\eta^2)+2c_m m_\pi^2}{f_\pi^2}\\
\alpha_{K\bar K} &= \frac{c_d s-2(c_d-c_m)m_K^2}{f_\pi^2}\\
\alpha_{\pi\eta'} &= -\frac{2}{\sqrt{6}}\frac{c_d s-c_d(m_\pi^2+m_{\eta'}^2)+2c_m m_\pi^2}{f_\pi^2}
\end{aligned}
\tag{D.9}
$$

- $I=3/2$

$$
V_{K\pi\to K\pi} = -\frac{s-m_K^2-m_\pi^2}{2f_\pi^2}
\tag{D.10}
$$

Parameter	Value
$\tilde{c}_d$ (MeV)	18 ± 1
$\tilde{c}_m$ (MeV)	23 ± 4
M_1 (MeV)	1100 ± 20
$a_{\pi\pi}$	-0.98 ± 0.10
$a_{K\bar{K}}$	-1.00 ± 0.20
$a_{\eta\eta}$	$+0.04 \pm 0.22$
$a_{K\pi}$	$+0.17 \pm 0.05$
$a_{K\eta'}$	-3.53 ± 0.13
$a_{\pi\eta}$	-2.55 ± 0.37

Table D.1: Fitted parameters for the main fit. The χ^2/d.o.f. is 0.96. The fits are obtained employing the program MINUIT [503].

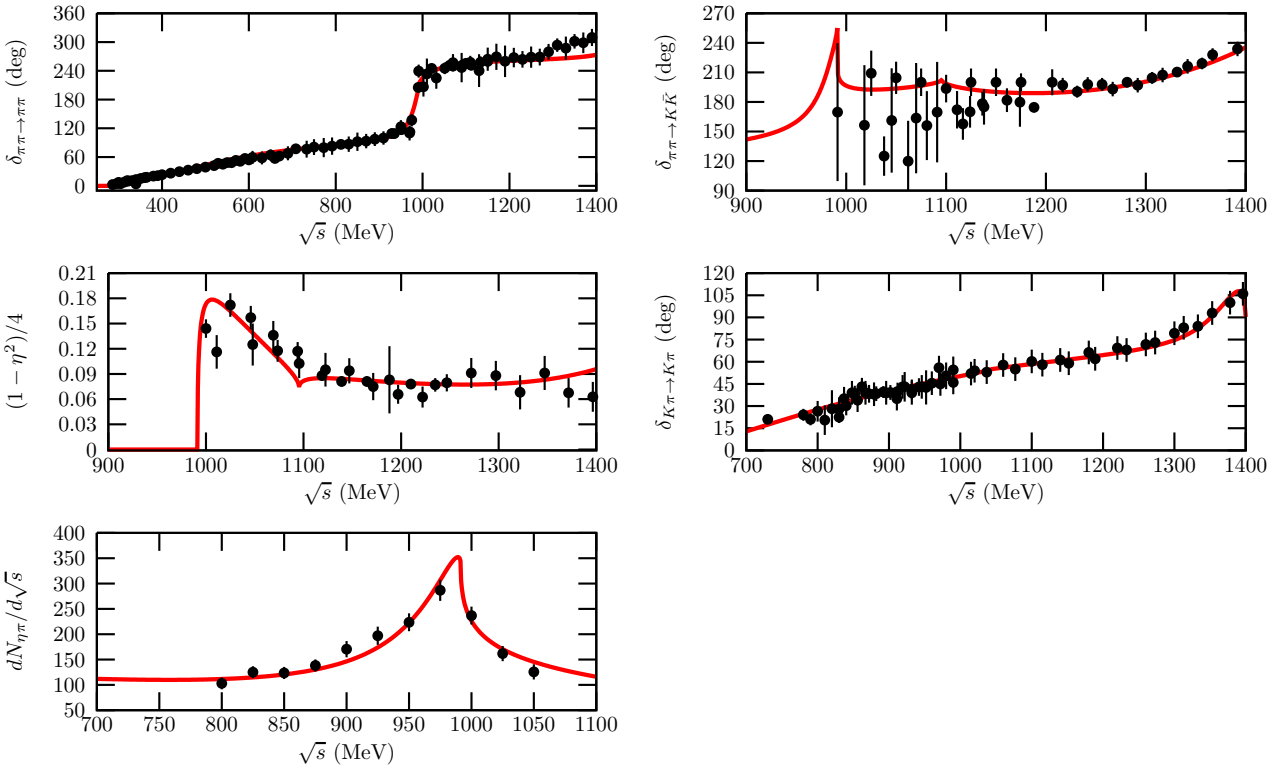

Figure D.2: Experimental data and our fits, as explained in the text.

With the amplitudes calculated for meson–meson scattering, we perform several fits, *e.g.* by changing the value of the highest $\sqrt{s}$ fitted from 1.2 to 1.4 GeV and by imposing that several subtraction constants for the pseudoscalar–pseudoscalar channels are equal, so that we can calculate the pseudoscalar–scalar kernels with different inputs, and then check the independence of our results. We only show our main fit since all the other fits that we obtained give rise to similar results that would not change our conclusions. In this fit the highest value of $\sqrt{s}$ considered is 1.4 GeV. For the octet of scalar resonances we take the values of the parameters c_d, c_m and M_8 from Ref. [43], where M_8, the mass of this octet,

Resonance	Re$\sqrt{s}$ (MeV)	Im$\sqrt{s}$ (MeV)
σ	466	235
κ	698	294
$f_0(980)$	987	18
$a_0(980)$	1019	33

Table D.2: The pole positions of the scalar resonances obtained from the main fit are given.

Resonance	$g_{K\bar{K}}$ (GeV)	$\lvert g_{K\bar{K}}$ (GeV)$\rvert$
$f_0(980)$	$-3.72 + 1.18i$	3.90
$a_0(980)$	$-4.11 + 1.59i$	4.41

Table D.3: Couplings of the $f_0(980)$ and $a_0(980)$ resonances to $K\bar{K}$ (with definite isospin). These couplings are calculated from the residues of the corresponding pole.

is around 1.3-1.4 GeV. For definiteness, $c_d = c_m = 22.8$ MeV and $M_8 = 1.4$ GeV. The parameters for the singlet resonance exchange, $\widetilde{c}_d$, $\widetilde{c}_m$ and M_1 are left free, with the latter the mass of the singlet scalar resonance. Regarding the subtraction constants in the unitarity loop function of the different channels (they play the analogous role of a_1 in eq. (4.12) but for pseudoscalar-pseudoscalar scattering), we take the most general situation compatible with isospin symmetry. Adopting the same argument as in the appendix A of ref. [47] from $SU(3)$ to $SU(2)$, the subtraction constants corresponding to the same pair of pseudoscalars should be the same in the different isospin. In this way, the subtraction constant for $K\bar{K}$ both in $I = 0$ and $I = 1$ is taken with the same value. On the other hand, for a given isospin, we also put constraints on the subtraction constants associated with non-relevant channels. In this way, the $K\eta$ subtraction constant in $I = 1/2$ is kept equal to that of $K\pi$ and, similarly, for $I = 1$ the $\pi\eta'$ subtraction constant is put equal to that of $\pi\eta$.[1] Of course, we have checked that smoothing these constraints does not affect the results of the fit. In this way, we finally have six independent subtraction constants for $\pi\pi$, $K\bar{K}$, $\eta\eta$, $K\pi$, $K\eta'$ and $\pi\eta$. There is also a normalization constant for the data on an unnormalized $\pi\eta$ event distribution around the $a_0(980)$ resonance that is required for each fit. The results of the fit compared to experimental data are shown by the solid line in Fig. D.2 and the values of the fitted parameters are given in Table D.1.

The set of experimental data included in the fits for $I = 0$ comprises the elastic $\pi\pi$ phase shifts, $\delta_{\pi\pi\to\pi\pi}$, from Refs. [287, 288, 290, 368, 370, 504], the phase shift for $\pi\pi \to K\bar{K}$, $\delta_{\pi\pi\to K\bar{K}}$, and $(1-\eta^2)/4$ from refs. [292, 293], where η is the elastic parameter for the $\pi\pi \to \pi\pi$ $I = 0$ S-wave. With respect to $I = 1/2$ we fit the elastic πK phase shifts, $\delta_{K\pi\to K\pi}$, from refs. [296, 505–507]. Finally, we include an event distribution of $\pi\eta$ around the $a_0(980)$ resonance mass from the central production of $\pi\pi\eta$, Ref. [508], fitted like in Refs. [29, 30].

Once the fits are performed we look for the poles of the scalar resonances σ, κ, $f_0(980)$

[1] We have checked that the $\pi\eta'$ channel tends to decouple of the $\pi\eta$ and $K\bar{K}$ channels in $I = 1$ in the region of the $a_0(980)$.

and $a_0(980)$ in the unphysical Riemann sheets continuously connected with the physical one. Notice that only the $f_0(980)$ and $a_0(980)$ poles are actually required for evaluating the pseudoscalar–scalar scattering kernels in Sec. 4.2. The σ and κ are given for completeness. They are related to the $f_0(980)$ and $a_0(980)$ resonances giving rise to a nonet of light scalar resonances [53]. Other poles around 1.4 GeV also appear that we do not include here. The pole positions are given in Table D.2. The couplings of the $f_0(980)$ and $a_0(980)$ to $K\bar{K}$, used in this work, are collected in Table D.3.

E

S-wave projection of C_3 and $C_4(M_4^2)$

The three- and four-point Green functions C_3 and $C_4(m_4^2)$ are defined in Eq. (4.5). Here, we consider the more general case with arbitrary internal masses and from the very beginning the S-wave projection is worked out. Both functions are finite.

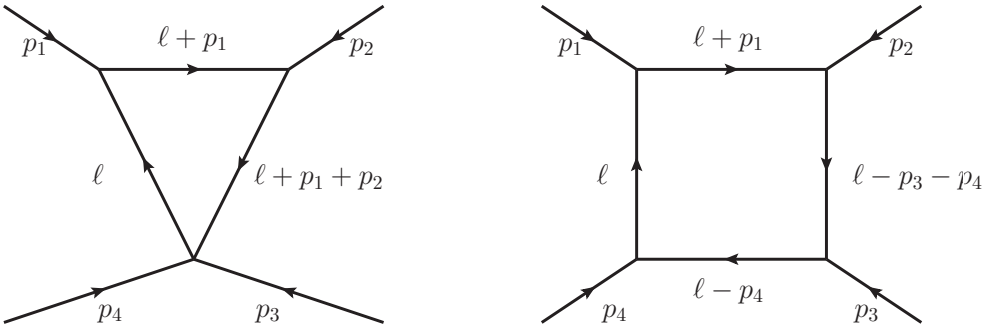

Figure E.1: Feynman diagrams for C_3 (left) and $C_4(m_4^2)$ (right).

We first consider C_3, left diagram of Fig. E.1, and follow its notation with $t = (p_1 + p_2)^2$ (note that all four-momenta are in-going). We also introduce two Feynman parameters u_1 and u_2 and the relative angle θ between the initial and final pseudoscalars, so that

$$\begin{aligned} C_3 &= \frac{i}{2}\int_{-1}^{+1} d\cos\theta \int \frac{d^4\ell}{(2\pi)^4} \frac{1}{((\ell+p_1)^2 - m_1^2)(\ell^2 - m_2^2)((\ell+p_1+p_2)^2 - m_3^2)} \\ &= \frac{1}{32\pi^2}\int_0^1 du_1 \int_0^{u_1} du_2 \int_{-1}^{+1} d\cos\theta \left[p_2^2 u_1^2 + p_1^2 u_2^2 + 2p_1p_2 u_1 u_2 \right. \\ &\left. + (m_1^2 - m_3^2 - p_2^2)u_1 + (m_2^2 - m_1^2 - p_1^2 - 2p_1p_2)u_2 + m_3^2 + i\varepsilon\right]^{-1} \ . \end{aligned} \tag{E.1}$$

Then, $\cos\theta$ is introduced by taking into account that $p_1p_2 = (t - p_1^2 - p_2^2)/2$ with $t = q_0^2 - |\mathbf{p}|^2 - |\mathbf{p}'|^2 + 2|\mathbf{p}||\mathbf{p}'|\cos\theta$, with $q^0 = p_1^0 - p_2^0$, the difference of energies between the initial and final scalar resonances. We perform the angular integration and introduce the parameter ξ_2 as $u_2 = u_1\xi_2$, so that

$$C_3 = \frac{1}{64\pi^2|\mathbf{p}||\mathbf{p}'|}\int_0^1 \frac{du_1}{1-u_1}\int_0^1 \frac{d\xi_2}{\xi_2}\left[\log(1+\psi) - \log(-1+\psi)\right] \ , \tag{E.2}$$

where

$$\psi = \frac{1}{2|\mathbf{p}||\mathbf{p}'|(1-u_1)u_2}\Big[p_2^2u_1^2 + p_1^2u_2^2 + u_1u_2(q_0^2 - |\mathbf{p}|^2 - |\mathbf{p}'|^2 - p_1^2 - p_2^2) \\ + u_1(m_1^2 - m_3^2 - p_2^2) + u_2(m_2^2 - m_1^2 + p_2^2 - q_0^2 + |\mathbf{p}|^2 + |\mathbf{p}'|^2) + m_3^2 - i\varepsilon\Big]^{-1} \ . \tag{E.3}$$

For the four-point function $C_4(m_4^2)$, right diagram of Fig. E.1, one has

$$C_4(m_4^2) = \frac{i}{2}\int_{-1}^{+1} d\cos\theta \int \frac{d^4\ell}{(2\pi)^4}\frac{1}{((\ell+p_1)^2 - m_1^2)(\ell^2 - m_2^2)} \\ \times \frac{1}{((\ell - p_3 - p_4)^2 - m_3^2)((\ell - p_4)^2 - m_4^2)} \ . \tag{E.4}$$

In this case there is no ambiguity if instead of performing the $\cos\theta$ integration one directly calculates the related integration over $t = (p_3 + p_4)^2$ by taking into account that $dt = 2|\mathbf{p}||\mathbf{p}'|d\cos\theta$ (ambiguities could arise for s such that the product $|\mathbf{p}||\mathbf{p}'|$ becomes complex. The particular integration to be performed here is not affected by such problem, see below.) We also introduce three Feynman parameters u_1, u_2 and u_3 so that

$$C_4(m_4^2) = \frac{-1}{64\pi^2|\mathbf{p}||\mathbf{p}'|}\int_0^1 du_1\int_0^{u_1} du_2\int_0^{u_2} du_3\int_{t_-}^{t_+} dt\,\Big[p_1^2(1-u_2+u_3)(u_2-u_3) \\ + 2p_1p_3(u_1-u_2)(u_2-u_3) + 2p_1p_4(1-u_2)(u_2-u_3) - m_2^2u_3 \\ + p_3^2(1-u_1+u_2)(u_1-u_2) + 2p_3p_4(u_1-u_2)u_2 + p_4^2(1-u_2)u_2 \\ - m_1^2(u_2-u_3) - m_3^2(u_1-u_2) - m_4^2(1-u_1) - i\varepsilon\Big]^{-1} \ . \tag{E.5}$$

In terms of the variable t the previous integral is of the from $\int dt/(at+b)^2$ so that the t-integration can be done straightforwardly without problems in its analytical extrapolation. The resulting u_3-integration is of the form $\int du_3/[u_3(u_3^2 + \beta u_3 + \gamma)]$ that can also be done straightforwardly by factorizing the second-order polynomial in the denominator. Our final expression for $C_4(m_4^2)$ is

$$C_4(m_4^2) = \frac{-1}{64p_1^2|\mathbf{p}||\mathbf{p}'|}\int_0^1 du_1\int_0^1 \frac{d\xi_2}{1-\xi_2}\left[\psi(t_+,u_2) - \psi(t_+,0) - \psi(t_-,u_2) + \psi(t_-,0)\right] \ , \tag{E.6}$$

where

$$\begin{aligned}
\psi(t,u_3) &= \frac{\log u_3}{y_1y_2} + \frac{\log(u_3-y_1)}{y_1(y_1-y_2)} - \frac{\log(u_3-y_2)}{y_2(y_1-y_2)} \ , \\
u_3^2 + \beta u_3 + \gamma &= (u_3-y_1)(u_3-y_2) \ , \\
p_1^2(u_3^2 + \beta u_3 + \gamma) &= m_4^2(1-u_1) + m_3^2(u_1-u_2) + p_3^2(-1+u_1)(u_1-u_2) + m_1^2u_2 \\
&\quad + u_2(s(-1+u_1) + p_2^2(u_2-u_1)) - (m_1^2 - m_2^2 + p_4^2)u_3 + p_1^2u_3^2 \\
&\quad + (s(1-u_1) + (p_2^2 + p_4^2 - t)u_1 - (p_1^2 + p_2^2 - t)u_2)u_3 - i\varepsilon \ , \\
t_\pm &= (p_3^0 - p_4^0)^2 - (|\mathbf{p}| \mp |\mathbf{p}'|)^2 \ .
\end{aligned} \tag{E.7}$$

The S-wave projection of the three- and four-point functions C_3 and $C_4(m_4^2)$ was also obtained for some kinematical regions and values of m_4^2 from Ref. [509], wherever the latter could be applied. In such cases our results and Ref. [509] agree.

F

One pion exchange nucleon-nucleon partial waves

In this Appendix, we list the NN partial wave amplitudes for OPE used in Chapter 7. We use the notation ${}^S\ell_J$, where S is the total spin, J is the total angular momentum and ℓ is the orbital angular momentum. Recall that the isospin I can be retrieved from the former quantities because $\ell + S + I =$ odd. Actually, the functions Δ used in Chapter 7 are the imaginary parts of the amplitudes, $\Delta = \mathrm{Im}T$ for $p^2 + i\epsilon$ with $p^2 < m_\pi^2/4$. These are easily obtained from the amplitudes, since they are written always as:

$$T = K\left(P_1 + P_2 \ln \frac{m_\pi^2}{m_\pi^2 + 4p^2}\right) , \tag{F.1}$$

so that:

$$\Delta = -\pi K P_2 \tag{F.2}$$

We also give in Fig. F.1 the scheme of the mixing of the different NN partial waves.

The one pion exchange nucleon-nucleon partial waves $T({}^S\ell_J)$ (not mixing different values of ℓ) are:

$$T({}^1S_0) = -\frac{g_A^2}{4f_\pi^2}\frac{1}{4p^2}\left(4p^2 + m_\pi^2 \ln \frac{m_\pi^2}{m_\pi^2 + 4p^2}\right) ,$$
$$T({}^3S_1) = -\frac{g_A^2}{4f_\pi^2}\frac{1}{4p^2}\left(4p^2 + m_\pi^2 \ln \frac{m_\pi^2}{m_\pi^2 + 4p^2}\right) ,$$

$$T({}^1P_1) = +\frac{g_A^2}{4f_\pi^2}\frac{3m_\pi^2}{8p^4}\left(4p^2 + (m_\pi^2 + 2p^2) \ln \frac{m_\pi^2}{m_\pi^2 + 4p^2}\right) ,$$
$$T({}^3P_0) = +\frac{g_A^2}{4f_\pi^2}\frac{1}{4p^2}\left(4p^2 + m_\pi^2 \ln \frac{m_\pi^2}{m_\pi^2 + 4p^2}\right) ,$$
$$T({}^3P_1) = +\frac{g_A^2}{4f_\pi^2}\frac{1}{16p^4}\left(4p^2(m_\pi^2 - 2p^2) + m_\pi^4 \ln \frac{m_\pi^2}{m_\pi^2 + 4p^2}\right) ,$$

$$T(^3P_2) = +\frac{g_A^2}{4f_\pi^2}\frac{1}{80p^4}\left(4p^2(3m_\pi^2+2p^2)+m_\pi^2(3m_\pi^2+8p^2)\ln\frac{m_\pi^2}{m_\pi^2+4p^2}\right),$$

$$T(^1D_2) = -\frac{g_A^2}{4f_\pi^2}\frac{m_\pi^2}{32p^6}\left(12p^2(m_\pi^2+2p^2)+(3m_\pi^4+12m_\pi^2p^2+8p^4)\ln\frac{m_\pi^2}{m_\pi^2+4p^2}\right),$$

$$T(^3D_1) = -\frac{g_A^2}{4f_\pi^2}\frac{1}{16p^4}\left(4p^2(3m_\pi^2+2p^2)+m_\pi^2(3m_\pi^2+8p^2)\ln\frac{m_\pi^2}{m_\pi^2+4p^2}\right),$$

$$T(^3D_2) = -\frac{g_A^2}{4f_\pi^2}\frac{1}{16p^6}\left(4p^2(3m_\pi^4+3m_\pi^2p^2-2p^4)+3(m_\pi^6+3m_\pi^4p^2)\ln\frac{m_\pi^2}{m_\pi^2+4p^2}\right),$$

$$T(^1D_3) = -\frac{g_A^2}{4f_\pi^2}\frac{1}{224p^6}\left(4p^2(15m_\pi^4+42m_\pi^2p^2+8p^4)\right.$$
$$\left.+3m_\pi^2(5m_\pi^4+24m_\pi^2p^2+24p^4)\ln\frac{m_\pi^2}{m_\pi^2+4p^2}\right),$$

$$T(^1F_3) = +\frac{g_A^2}{4f_\pi^2}\frac{m_\pi^2}{64p^8}\left(4p^2(15m_\pi^4+60m_\pi^2p^2+44p^4)\right.$$
$$\left.+3(5m_\pi^6+30m_\pi^4p^2+48m_\pi^2p^4+16p^6)\ln\frac{m_\pi^2}{m_\pi^2+4p^2}\right),$$

$$T(^3F_2) = +\frac{g_A^2}{4f_\pi^2}\frac{1}{480p^6}\left(4p^2(15m_\pi^4+42m_\pi^2p^2+8p^4)\right.$$
$$\left.+3m_\pi^2(5m_\pi^4+24m_\pi^2p^2+24p^4)\ln\frac{m_\pi^2}{m_\pi^2+4p^2}\right),$$

$$T(^3F_3) = +\frac{g_A^2}{4f_\pi^2}\frac{1}{768p^8}\left(4p^2(45m_\pi^6+150m_\pi^4p^2+48m_\pi^2p^4-16p^6)\right.$$
$$\left.+3m_\pi^4(15m_\pi^4+80m_\pi^2p^2+96p^4)\ln\frac{m_\pi^2}{m_\pi^2+4p^2}\right),$$

$$T(^3F_4) = +\frac{g_A^2}{4f_\pi^2}\frac{1}{6912p^8}\left(4p^2(105m_\pi^6+510m_\pi^4p^2+560m_\pi^2p^4+48p^6)\right.$$
$$\left.+3m_\pi^2(35m_\pi^6+240m_\pi^4p^2+480m_\pi^2p^4+256p^6)\ln\frac{m_\pi^2}{m_\pi^2+4p^2}\right),$$

$$T(^3G_3) = -\frac{g_A^2}{4f_\pi^2}\frac{1}{1792p^8}\left(4p^2(105m_\pi^6+510m_\pi^4p^2+560m_\pi^2p^4+48p^6)\right.$$
$$\left.+3m_\pi^2(35m_\pi^6+240m_\pi^4p^2+480m_\pi^2p^4+256p^6)\ln\frac{m_\pi^2}{m_\pi^2+4p^2}\right),$$

$$T(^1G_4) = -\frac{g_A^2}{4f_\pi^2}\frac{m_\pi^2}{1536p^{10}}\left(20(21m_\pi^6p^2+126m_\pi^4p^4+208m_\pi^2p^6+80p^8)\right.$$
$$\left.+3(35m_\pi^8+280m_\pi^6p^2+720m_\pi^4p^4+640m_\pi^2p^6+128p^8)\ln\frac{m_\pi^2}{m_\pi^2+4p^2}\right),$$

$$T(^3G_4) = -\frac{g_A^2}{4f_\pi^2}\frac{1}{1280p^{10}}\Bigg(4p^2(210m_\pi^8+1155m_\pi^6p^2+1570m_\pi^4p^4+240m_\pi^2p^6-48p^8)$$
$$+15m_\pi^4(14m_\pi^6+105m_\pi^4p^2+240m_\pi^2p^4+160p^6)\ln\frac{m_\pi^2}{m_\pi^2+4p^2}\Bigg)\,,$$

$$T(^1H_5) = +\frac{g_A^2}{4f^2}\frac{m_\pi^2}{5120p^{12}}\Bigg(4p^2(945m_\pi^8+7560m_\pi^6p^2+19740m_\pi^4p^4+18480m_\pi^2p^6+4384p^8)$$
$$+15(63m_\pi^{10}+630m_\pi^8p^2+2240m_\pi^6p^4+3360m_\pi^4p^6+1920m_\pi^2p^8256p^{10})\ln\frac{m_\pi^2}{m_\pi^2+4p^2}\Bigg)\,,$$
$$T(^3H_5) = +\frac{g_A^2}{4f^2}\frac{1}{30720p^{12}}\Bigg(4p^2(1575m_\pi^{10}+11970m_\pi^8p^2+28560m_\pi^6p^4$$
$$+21840m_\pi^4p^6+1920m_\pi^2p^8-256p^{10})$$
$$+15m_\pi^4(105m_\pi^8+1008m_\pi^6p^2+3360m_\pi^4p^4+4480m_\pi^2p^6+1920p^8)\ln\frac{m_\pi^2}{m_\pi^2+4p^2}\Bigg)\,.$$

The one pion exchange nucleon-nucleon partial waves $T(^S\ell_J,^S\ell'_J)$ (mixing different values of ℓ) are:

$$\begin{aligned}
T(^3S_1,^3D_1) &= -\frac{g_A^2}{4f_\pi^2}\frac{1}{8\sqrt{2}p^4}\Bigg(4p^2(3m_\pi^2-2p^2)+m_\pi^2(3m_\pi^2+4p^2)\ln\frac{m_\pi^2}{m_\pi^2+4p^2}\Bigg)\,,\\
T(^3P_2,^3F_2) &= +\frac{g_A^2}{4f_\pi^2}\frac{1}{80\sqrt{6}p^6}\Bigg(4p^2(15m_\pi^4+24m_\pi^2p^2-4p^2)\\
&\quad +3m_\pi^2(5m_\pi^4+18m_\pi^2p^2+8p^4)\ln\frac{m_\pi^2}{m_\pi^2+4p^2}\Bigg)\,,\\
T(^3D_3,^3G_3) &= -\frac{g_A^2}{4f_\pi^2}\frac{\sqrt{3}}{896p^8}\Bigg(4p^2(105m_\pi^6+390m_\pi^4p^2+224m_\pi^2p^4-16p^6)\\
&\quad +3m_\pi^2(35m_\pi^6+200m_\pi^4p^2+288m_\pi^2p^4+64p^6)\ln\frac{m_\pi^2}{m_\pi^2+4p^2}\Bigg)\,.
\end{aligned}$$

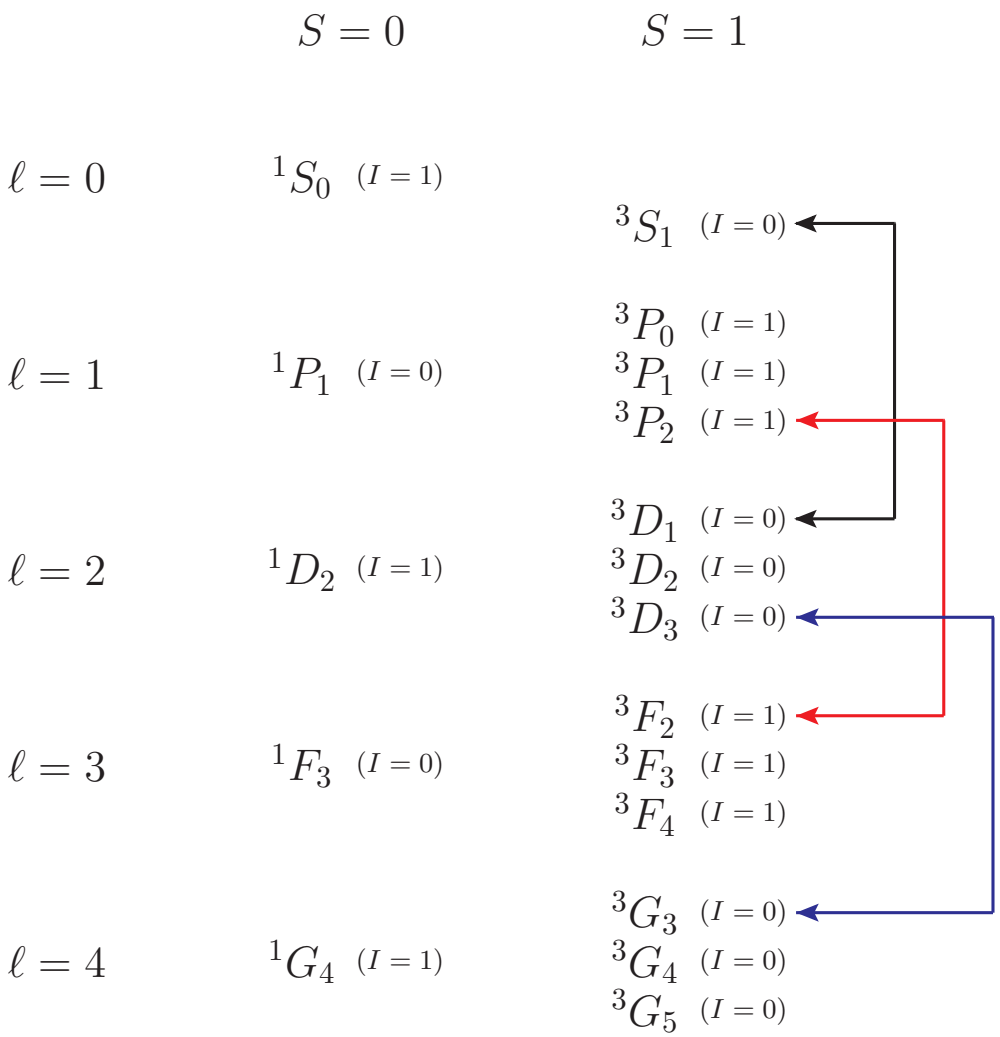

Figure F.1: Mixing of NN partial waves.

G

Solving the integral equation for $D(k^2)$

In this appendix, we focus on the solution of the integral equation (7.29) subject to the constraints (7.30). For simplifying the discussion we drop the subscripts $J\ell S$. The integral equation Eq. (7.29) can be written in a compact way as

$$D(A) = 1 + \frac{A}{\pi}\int_{-\infty}^{L} \mathrm{d}k^2 \frac{\Delta(k^2)D(k^2)}{k^2} g(A,k^2) + h(A) \ , \tag{G.1}$$

where $g(A,k^2)$ is defined in Eq. (7.11) and

$$h(A) = \frac{A}{(A-B)^{\ell-1}} \sum_{i=0}^{\ell-2} c_i A^i \ . \tag{G.2}$$

Let us introduce the function $d(A)$ as $D(A) = d(A) + h(A)$, that is, $d(A)$ is the piece of $D(A)$ that does not contain the CDD poles. As a first step, we write the coefficients c_i in terms of the $d(A)$ function. This is done by writing the sum rule constraints Eq. (7.30) in terms of $d(A)$, giving rise to

$$I_i = \int_{-\infty}^{L} \mathrm{d}k^2 \frac{\Delta(k^2)d(k^2)}{k^4 k^{2i}} = -\int_{-\infty}^{L} \mathrm{d}k^2 \frac{\Delta(k^2)h(k^2)}{k^4 k^{2i}} = \sum_{j=0}^{\ell-2} c_j m_{ij} \ , \tag{G.3}$$

$$m_{ij} \equiv -\int_{-\infty}^{L} \mathrm{d}k^2 \frac{\Delta(k^2)k^{2j}}{k^2 k^{2i}(k^2-B)^{\ell-1}} \ , \tag{G.4}$$

where we have shifted $\lambda = i+2$, so that i runs from 0 to $\ell-2$. Note that the m_{ij} integrals can be calculated directly for a given $\Delta(A)$ in terms of B because the unknown function $d(A)$ is not necessary in their calculation. Thus,

$$c_i = \sum_{j=0}^{\ell-2} m_{ij}^{-1} I_j \ , \tag{G.5}$$

being m^{-1} the inverse of the matrix whose elements are m_{ij}. Next, we rewrite the integral equation Eq. (G.1) in terms of $d(k^2)$, and insert the expressions (G.5) for the coefficients c_i of the function $h(k^2)$ involved. It results

$$d(A) = 1 + \frac{A}{\pi}\int_{-\infty}^{L}\mathrm{d}k^2 \frac{\Delta(k^2)d(k^2)}{k^2} g(A,k^2) + \tag{G.6}$$

$$+ \frac{A}{\pi}\int_{-\infty}^{L}\mathrm{d}k^2 \frac{\Delta(k^2)g(A,k^2)}{(k^2-B)^{\ell-1}} \sum_{i,j=0}^{\ell-2} k^{2i} m_{ij}^{-1} \int_{-\infty}^{L}\mathrm{d}q^2 \frac{d(q^2)\Delta(q^2)}{q^4 q^{2j}} \ . \tag{G.7}$$

Now, by interchanging the dummy integration variables k^2 and q^2, we can finally write

$$d(A) = 1 + \frac{A}{\pi}\int_{-\infty}^{L}\mathrm{d}k^2 \frac{d(k^2)\Delta(k^2)}{k^2}\left(g(A,k^2) + \bar{g}(A,k^2)\right) \ , \tag{G.8}$$

$$\bar{g}(A,k^2) = \sum_{i,j=0}^{\ell-2} \frac{1}{k^2 k^{2j}} m_{ij}^{-1} \int_{-\infty}^{L}\mathrm{d}q^2 \frac{\Delta(q^2)g(A,q^2)q^{2i}}{(q^2-B)^{\ell-1}} \ .$$

We have now an integral equation for the $d(k^2)$ function that depends on known functions. It can be written in a compact way as

$$d(A) = 1 + \int_{-\infty}^{L}\mathrm{d}k^2 \widetilde{f}(A,k^2) d(k^2) \ . \tag{G.9}$$

It is convenient to perform a change of integration variable so that one ends with a finite integration domain, *e.g.* with $x = 1/k^2$. In this way

$$d(A) = 1 + \int_{x_1}^{x_2}\mathrm{d}x \, f(A,x) \, d(A(x)) \ . \tag{G.10}$$

This is an inhomogeneous Fredholm integral equation. We solve it numerically by discretizing the integral on it,

$$d(A_i) = 1 + \sum_j f(A_i,x_j)\omega(x_j) d(A(x_j)) \ , \tag{G.11}$$

where the $\omega(x)$ function is the weighting function taken for the integration. By calling $d(A(x_i)) \equiv d_i$, $f(A_i,x_j)\omega(x_j) \equiv \eta_{ij}$, this equation can be cast as

$$\sum_j (\delta_{ij} - \eta_{ij}) d_j = 1 \ , \tag{G.12}$$

which is a linear equation, that can be solved by standard methods, giving the desired function $d(A)$. To obtain the needed function $D(A)$, the function $h(A)$ must be added, but this is also a direct task, since the c_i coefficients can be calculated once $d(A)$ is known, Eq. (G.5). Of course, if no constraints must be satisfied, as it is the case for S- and P-waves, the same formalism with the corresponding simplifications should be used.

H

The $g_{ij}(A, k^2)$ functions

On general grounds, the following threshold behaviors are found for the $\nu_{ij}(A)$ functions:

$$\nu_{11}(A) \propto A^{1/2} \quad \nu_{12}(A) \propto A^{-1/2} \quad \nu_{22}(A) \propto A^{-3/2}$$

This can also be seen by inserting the low energy behavior of δ_1 ($\propto A^{\ell+1/2}$), δ_2 ($\propto A^{\ell'+1/2}$) and ϵ ($\propto A^{(\ell+\ell'+1)/2}$) in the explicit expression for $\nu_{ij}(A)$, Eqs. (7.33)–(7.35). No problem occurs in the integrands for the functions $g_{11}(A, k^2)$ and $g_{12}(A, k^2)$, when this low energy behaviors are inserted, but the divergence in $\nu_{22}(A)$ could lead to a divergence in the function $g_{22}(A, k^2)$. This was already pointed out in Ref. [477], as a potential source of divergences, but no hints for a solution were given. However, a more careful analysis shows that this divergence vanishes due to the sum rules, Eqs. (7.43). For the $g_{22}(A, k^2)$ integral one has

$$\begin{aligned} g_{22}(A, k^2) =& \frac{1}{\pi} \int_{\lambda \to 0}^{+\infty} \mathrm{d}q^2 \frac{\nu_{22}(q^2)}{(q^2 - A)(q^2 - k^2)} \\ =& \frac{2\nu_0}{\pi A k^2 \sqrt{\lambda}} + \text{regular terms} \end{aligned}$$

where $\nu_{22}(A) = \nu_0 A^{-3/2}$ for $A \to 0$. In the previous equation the regular terms refer to the rest of the contributions to the integral, which do not diverge for $\lambda \to 0$. The divergent term in the previous equation enters into the integral Eq. (7.48) through the function $g_{22}(A, k^2)$, giving rise to a term proportional to

$$\int_{-\infty}^{L} \mathrm{d}k^2 \frac{\Delta_{22}(k^2) D_{22}(k^2)}{k^4} = 0,$$

that is zero due to the constraints of Eq. (7.43). Notice that every channel in which $g_{22}(A)$ is involved has $\ell' \geqslant 2$ (the lowest value for ℓ' corresponds to the ${}^3D_1$ wave), and thus the sum rule above applies. The constraints Eq. (7.43) show then a new important facet beyond the original motivation for their introduction.

Resumen en Español

Hasta donde la ciencia alcanza a conocer, el Universo está compuesto de partículas, espacio–tiempo y las leyes que dictan sus interacciones. Una de estas interacciones es la fuerza fuerte, de la cual emergen, a su vez, las fuerzas en el interior de los núcleos de los átomos. Las partículas que sufren dichas interacciones fuertes se denominan *hadrones*. La cromodinámica cuántica [1–7] (QCD por sus siglas en inglés) es la teoría que describe las interacciones fuertes. Es una teoría cuántica relativista, no abeliana y Yang–Mills, en la que los *quarks* y los *gluones* son los grados fundamentales de libertad (los campos cuánticos de la teoría). Los quarks son partículas masivas, y los gluones son aquellas que transportan dicha interacción. Es una teoría bella y exitosa, una de las piedras angulares del mayor modelo científico que jamás se haya concebido: el Modelo Estándar. QCD describe con gran éxito una gran variedad de fenómenos físicos.

Sin embargo, tal cual se formula, esto es, con quarks y gluones como sus grados de libertad dinámicos, solo puede ser utilizada en régimen de altas energías, situación en la cual, debido a la *libertad asintótica* predicha por QCD, los quarks se manifiestan como partículas puntuales que interactúan debilmente y, por lo tanto, pueden utilizarse métodos perturbativos, tal y como se hace, por ejemplo, en Electrodinámica Cuántica (QED, por sus siglas en inglés). En el caso opuesto de interacciones a bajas energías, el comportamiento complementario al citado anteriormente, denominado *esclavitud infrarroja*, apunta al confinamiento de los quarks en el interior de los hadrones. Sin embargo, el confinamiento es todavía un punto oscuro, no comprendido completamente en QCD, aunque el formalismo de QCD en el retículo (lattice QCD, en inglés) ofrece nuevos puntos de vista acerca de este problema. Con todo, en el espectro hadrónico de QCD encontramos un hecho remarcable: la aparición de un triplete de isoespín de mesones pseudoescalares, los piones (π^+, π^-, π^0), cuya masa es mucho más pequeña que el resto. Esta característica es clave y permite deducir que una bien conocida simetría aproximada de QCD, la simetría quiral, $SU(2)_L \otimes SU(2)_R$, se rompe espontáneamente [9–14] en $SU(2)_{L+R} \equiv SU(2)_V$, mientras que los restantes generadores de la simetría darían origen a un triplete de partículas sin masa, los bosones de Goldstone. Como la simetría no es exacta, sólo aproximada, a causa de la masa no nula de los quarks, los bosones de Goldstone no tienen una masa nula, pero sí muy pequeña. Son llamados, por tanto, *pseudo*–bosones de Goldstone. Hemos hablado de la simetría quiral en términos de $SU(2)$, que da lugar a un triplete de isoespín, los piones, pero si extendemos estas consideraciones al grupo $SU(3)$ encontraremos entonces otros pseudoescalares ligeros, los mesones K (K^+, K^-, K^0 y $\bar{K}^0$) y η, dando lugar, junto a los citados π, a un octete de $SU(3)$. Los hadrones se organizan por tanto en multipletes de $SU(3)$, en el esquema de las "Ocho maneras" (Eightfold way, en inglés) [15]. A partir de las consideraciones anteriores, uno podría intentar construir una teoría cuántica de campos

efectiva, en la que los grados de libertad dinámicos no sean los quarks y gluones, sino los piones (o, más genéricamente, el octete de pseudoescalares mencionado). Dicha idea se ha llevado a cabo, emergiendo así una teoría, la teoría quiral de perturbaciones (ChPT, por sus siglas en inglés) [16–19]. Esta teoría es, por tanto, la teoría *efectiva* de QCD a bajas energías, que puede ser tratada perturbativamente, es decir, permite un desarrollo sistemático en potencias de los momentos de los pseudoescalares involucrados en los estados inicial y final de una determinada reacción y en potencias de masas de quarks. En el **Capítulo 1** estudiaremos la construcción formal y rigurosa de ChPT, mediante el formalismo genérico de construcción de Lagrangianos efectivos [20, 21], que revisaremos en primer lugar, y la aplicación de la ruptura espontánea de la simetría quiral de las interacciones fuertes.

* * *

Junto a sus grandes logros, ChPT tiene un rango de aplicabilidad muy limitado. Por un lado, no es capaz de reproducir el abundante comportamiento resonante del espectro hadrónico. Siendo un desarrollo perturbativo, no puede generar los polos en las amplitudes de dispersión a los que están asociadas las resonancias. Por otro lado, el poder predictivo de la teoría se pierde progresivamente conforme se va incrementando el orden de las expansiones, debido a la aparición de las llamadas constantes de baja energía (LECs, por sus siglas en inglés), que guardan información de la teoría subyacente, QCD, y que no están fijadas, por tanto, por las simetrías. Estas carencias hacen que el empleo de métodos no perturbativos sea necesario como una herramienta complementaria para usar junto a la información perturbativa que pueda extraerse de ChPT. Entre estos métodos no perturbativos, en el sector de interacciones mesón–mesón o mesón–barión, pueden citarse el método de la amplitud inversa (IAM, por sus siglas en inglés) [22–32], el método basado en la ecuación de Bethe–Salpeter (BS) [33–37] y el método N/D, propuesto originalmente en [38], pero cuya conexión con la dinámica quiral no se produjo hasta décadas después [39–47]. Hablaremos de varios de estos trabajos posteriormente, al introducir los capítulos dedicados al sector escalar y al mesón σ (denominado actualmente como $f_0(500)$ por el *Particle Data Group* (PDG) [48]). Gran parte de esta tesis está relacionada, de un modo u otro, con la aplicación de uno de estos métodos, el método N/D, por lo que nos referiremos a dicho método, en tanto que aplicado a la dinámica quiral, como teoría quiral de perturbaciones unitaria o unitarizada (UChPT, por sus siglas en inglés). Estudiaremos este formalismo brevemente en el **Capítulo 2**. Primero, introduciremos un concepto fundamental, la unitariedad, intentando extraer parte de sus consecuencias. También introduciremos de forma concisa los conceptos de amplitudes de dispersión y ondas parciales. Veremos, desde un punto de vista general, la aparición de resonancias a partir de polos en las hojas de Riemann no físicas de las amplitudes de dispersión. Convencidos de la importancia de la unitariedad, revisaremos la aplicación del método N/D para deducir la estructura más general posible de una onda parcial cuando se desprecian, en primera aproximación, los cortes no físicos de las amplitudes [39]. El método N/D es un método de unitarización, que separa las contribuciones del corte de unitariedad y los cortes no físicos en dos funciones distintas, D y N, respectivamente. También intentaremos explicar cómo introducir en el método los cortes no físicos de un modo perturbativo.

En la **Parte I**, por tanto, derivaremos el marco teórico básico en el que se inserta esta

tesis, que será aplicado a varios problemas en la **Parte II**. En los siguientes párrafos, tratamos de comentar los diferentes problemas que estudiaremos en el cuerpo principal de esta tesis. Intentaremos dar una perspectiva general de la situación experimental y teórica de cada uno de las casos, motivando por tanto nuestro estudio. Se dan también algunos detalles de los métodos adicionales utilizados y un avance de los principales resultados, tratando de conectarlos con trabajos anteriores.

* * *

Empezaremos en el **Capítulo 3** con el estudio del sector escalar de las interacciones mesón–mesón. En ChPT, debido a su carácter perturbativo, la aparición de los mesones escalares (con números cuánticos $J^{PC} = 0^{++}$) no es directa. Los más ligeros entre estos escalares (con masas por debajo de 1 GeV) son los mesones σ, κ, $f_0(980)$ y $a_0(980)$. Su conexión con la dinámica de los pseudoescalares ligeros (los grados de libertad dinámicos en ChPT) y su relación con unitariedad o interacciones de estado final fue descubierta a lo largo de varios trabajos. Respecto a las interacciones $\pi\pi$ específicamente, han de citarse en primer lugar los trabajos de Truong y colaboradores [22–27] que enfatizaron por primera vez el importante papel que juegan las interacciones de estado final entre piones en onda S con isoespín $I = 0$, originando el formalismo IAM. Mediante éste, el polo del mesón σ se obtuvo por primera vez en la Ref. [28], junto a las resonancias $K^\star$ y ρ en onda P. A causa de la falta de canales acoplados en el IAM, no fue posible obtener otras resonancias escalares ligeras como la $f_0(980)$ y la $a_0(980)$. Simultáneamente, en la Ref. [33], mediante el empleo del método BS, se obtuvo también el polo del mesón σ, junto a los polos de $f_0(980)$ y $a_0(980)$. El esfuerzo conjunto de varios de los autores de estas últimas referencias llevó a la extensión del IAM a canales acoplados [29], obteniéndose así el nonete de escalares ligeros completo, junto al nonete de vectores. Además, el formalismo de la Ref. [33] fue derivado en base a un formalismo teórico más solido en la Ref. [39], mediante el método N/D (a partir del cual uno puede derivar también las ecuaciones del IAM). Desde un punto de vista teórico, dejando aparte sus resultados prácticos, la mayoría de estos trabajos ponen de manifiesto la importancia del corte derecho o de unitariedad, relacionado con las interacciones fuertes de estado final, y también muestran que los cortes cruzados o no físicos pueden ser tratados perturbativamente al estudiar las resonancias escalares. Mencionemos finalmente que las posiciones del polo de σ obtenidas en las Refs. [28], [33] y [30], son, en este orden, $440 - i\ 245$, $469 - i\ 194$ y $442 - i\ 227$ MeV. Los trabajos [33, 39] muestran claramente que la resonancia σ es generada dinámicamente por las interacciones pión-pión.

Otros estudios del problema del sector escalar pueden verse en [49–52]. De hecho, los trabajos en [49, 50], en el marco del modelo de quarks en una bolsa del MIT (MIT bag model, en inglés), predecía ya a finales de los setenta un nonete de escalares ligeros compuesto de anchas resonancias de cuatro quarks, con masas (en la notación moderna empleada para estos estados) $M_\sigma \sim 650$ MeV, $M_{a_0} = M_{f_0} \sim 1100$ MeV y $M_\kappa \sim 900$ MeV. En las Refs. [53–58] la mezcla entre estas resonancias fue estudiada. Otros exitosos estudios fenomenológicos de las resonancias escalares más ligeras se basan en modelos de intercambio de mesones [59–61]. Recientemente, en las Refs. [62,63] se estudió la posibilidad de construir un Lagrangiano quiral con un campo escalar singlete explícito.

También estudiaremos en esta tesis resonancias escalares más pesadas. En particular, en el sector escalar–isoescalar y con masas por debajo de 2 GeV, se encuentran en el PDG [48] las resonancias $f_0(1370)$, $f_0(1500)$, $f_0(1710)$ and $f_0(1790)$. La colaboración experimental Crystal Barrel (veáse [64] para una revisión exhaustiva de sus resultados) mejoró el conocimiento acerca del espectro hadrónico en el sector escalar, confirmando o descubriendo las resonancias $a_0(1450)$, $f_0(1370)$ y $f_0(1500)$, mientras que la colaboración BES [65–67] confirmó la asignación de espín $J = 0$ para la $f_0(1710)$ y encontró otra resonancia, $f_0(1790)$. Posteriormente, a lo largo de esta tesis, discutiremos con mayor detenimiento sobre resultados y posibles controversias acerca de estas resonancias una vez presentemos nuestros propios resultados, citando por ahora, para el lector interesado, los artículos de revisión en las Refs. [64, 68]. Más allá del interés general que pueden tener estas resonancias a la hora de determinar el espectro hadrónico, son relevantes por otra cuestión de bastante interés, a la sazón, la identificación de las *glubolas* (*glueballs*, en inglés). En QED, los fotones no llevan carga eléctrica y, por tanto, no interactúan entre ellos directamente. En QCD, por contra, los gluones transportan carga de color e interactúan directamente entre ellos, debido a la naturaleza Yang–Mills de la teoría. Por tanto, con generalidad se cree que QCD predice la existencia de mesones sin quarks de valencia, las así llamadas glubolas. La confirmación de su existencia está, pues, en el corazón de la propia teoría. El interés por las glubolas empezó a la par que QCD, y su estudio fue una de las primeras aplicaciones de las reglas de suma de QCD [71, 72]. Debido al fuerte acoplo del vacío con el canal 0^{++}, los resultados no son concluyentes aún [71–78]. En general, todos estos trabajos suelen coincidir en la presencia de una glubola alrededor de 1.5 GeV, aunque la existencia de otra en torno a 0.5 GeV también es discutida. Una glubola con masa $\gtrsim 1.5$ GeV también entra dentro de las predicciones de muchos modelos [79–82]. En el espectro calculado en QCD en el retículo en la aproximación de quarks de valencia [84–89] (*valence approximation* o *quenched approximation*) la masa predicha de la glubola más ligera es $M = 1660 \pm 50$ MeV, cercano al valor de las masas de las resonancias $f_0(1500)$ y $f_0(1710)$, lo que convierte de forma inmediata a estas resonancias en candidatas para tener una fuerte componente de glubola. En la Ref. [88] se obtiene que la $f_0(1710)$ es, mayormente, una glubola pura. La Ref. [89] evalúa, en la antedicha aproximación a QCD en el retículo, las desintegraciones de $f_0(1710)$ a dos pseudoescalares, obteniendo un patrón en acuerdo con algunos datos obtenidos para dicha resonancia [48]. Estudios con quarks dinámicos, mediante la mezcla de glubolas y quarkonios, están todavía en una etapa preliminar (veáse la Ref. [90] y las referencias ahí citadas, así como las referencias en la Sec. 3.1). En la Ref. [91] (veánse también las Refs. [92–94]) se encontró un mecanismo de supresión quiral de los acoplos de una glubola escalar, G_0, para la desintegración $G_0 \to \bar{q}q$, en la forma $\Gamma(G_0 \to s\bar{s}) \gg \Gamma(G_0 \to u\bar{u} + d\bar{d})$, en buen acuerdo con los resultados obtenidos en la Ref. [89] en QCD en el retículo. Este mecanismo también implica que la glubola escalar no debería mezclarse. Sin embargo, la situación no está del todo clara aún, y se obtienen resultados diferentes en varios trabajos [95–100], siguiendo la misma idea anterior de mezclar las glubolas con los estados $n\bar{n}$ y $s\bar{s}$ cercanos.

Para estudiar el sector escalar, calculamos las amplitudes de $I = 0$ en onda S para trece canales acoplados, $\pi\pi$, $\sigma\sigma$, $K\bar{K}$, $\eta\eta$, $\eta\eta'$, $\eta'\eta'$, $\rho\rho$, $\omega\omega$, $K^*\overline{K}^*$, $\omega\phi$, $\phi\phi$, $a_1\pi$ y $\pi^*\pi$. La simetría $SU(3)$ es aumentada hasta $U(3)$, de modo que sea posible incluir las interacciones del mesón η' [101–104]. Los estados multipiónicos son simulados de forma efectiva mediante los canales de dos resonancias, $\sigma\sigma$, $\rho\rho$, $a_1\pi$ y $\pi^*\pi$, aunque llegaremos a la conclusión de que la inclusión de estos dos últimos canales no es relevante. Simultáneamente, estudiaremos también la amplitud en onda S del proceso $K^-\pi^+ \to K^-\pi^+$, que involucra $I = 1/2$ y $I = 3/2$, con los

canales acoplados $K\pi$, $K\eta$ and $K\eta'$, en la línea de las Refs. [43, 44]. Los *potenciales* (*kernels*, en inglés) de interacción entre los diferentes canales se obtienen a partir de los Lagrangianos quirales. La simetría quiral es considerada como una *simetría de contraste* (*gauge symmetry*, en inglés), así que los vértices de las amplitudes que involucran resonancias vectoriales se calculan mediante acoplamiento mínimo. Para la resonancia σ, aprovechamos el hecho de que ésta se genera dinámicamente en UChPT, como se comentó anteriormente, debido a las interacciones en estado final de dos piones. Esto nos permite fijar los elementos de matriz de las amplitudes elementales a otros canales sin incluir ningún parametro libre adicional. También consideramos el intercambio de resonancias *desnudas* [105, 106] en el canal s. Deducimos que, para describir correctamente los datos, son necesarios dos octetes (con masas en torno a 1300 MeV y 1900 MeV) y un singlete (con una masa $M \simeq 900$ MeV). Con este formalismo, somos capaces de describir una gran cantidad de datos, que incluyen desfasajes y secciones eficaces inelásticas hasta una energía en el centro de masas $\sqrt{s} \simeq 2$ GeV. Puede estudiarse entonces el contenido espectroscópico de nuestras amplitudes, encontrando polos que dan lugar a un amplio conjunto de resonancias: σ, $f_0(980)$, $f_0(1370)$, $f_0(1500)$, $f_0(1710)$ y $f_0(1790)$ en $I = 0$, y κ, $K_0^*(1430)$ y $K^*(1950)$ en $I = 1/2$. Estudiamos tanto los polos como sus acoplos más relevantes. Se comprobará que el polo al que está asociado la resonancia $f_0(1370)$ es un octete puro, no mezclado con los estados más proximos, y lo mismo puede decirse de su acompañante en $I = 1/2$, la resonancia $K_0(1430)$. Posteriormente, identificamos la resonancia $f_0(1710)$ así como una contribución importante a la $f_0(1500)$ como una glubola no mezclada. Esto se basa en una comparación bastante buena de nuestros resultados con las antedichas predicciones de QCD en el retículo [89] y el mecanismo de supresión quiral de la desintegración a $\bar{q}q$ de una glubola escalar [91].

* * *

Otro problema interesante es la presencia de pseudoescalares *excitados*, con números cuánticos como los de los pseudo–bosones de Goldstone, pero más masivos (con masas en una región entre 1 GeV y 2 GeV), que abordaremos en el **Capítulo 4**. En $I = 1$, se encuentran las resonancias $\pi(1300)$ y $\pi(1800)$, y en $I = 1/2$ están $K(1460)$ y $K(1630)$. Quizá el caso más interesante aquí sea el de $I = 0$, donde, según el PDG [48], hallamos tres resonancias en un estrecho rango de masas, $\eta(1295)$, $\eta(1405)$ y $\eta(1475)$. Una detallada revisión de la situación experimental puede encontrarse en la Ref. [107]. Una de estas resonancias sería un estado extra si se ordenan los pseudoescalares más cercanos en esta región en un nonete. Dada la clara señal de $\eta(1405)$ en procesos ricos en gluones, *v.g.*, desintegraciones radiativas de J/Ψ, esta resonancia se convierte en una candidata ideal para ser la glubola pseudoescalar más ligera [108–110]. Sin embargo, la predicción de QCD en el retículo para tal estado es aproximadamente 2.4 GeV, una discrepancia interesante. Este esquema de clasificación de estos estados ha sido criticado en [111], donde se pone en duda la mera existencia de $\eta(1295)$, y se argumenta que, en realidad, $\eta(1405)$ y $\eta(1475)$ no son sino un mismo estado, $\eta(1440)$. Recientemente, esta posibilidad ha recibido respaldo en la Ref. [112]. Otra resonancia, llamada $X(1835)$, ha sido observada recientemente, y los análisis sugieren que sus números cuánticos son $I^G(J^{PC}) = 0^+(0^{-+})$.

Si, como hemos comentado, los escalares más ligeros se generan dinámicamente en las interacciones entre los pseudoescalares más ligeros, es cuando menos sugerente pensar que estos

pseudoescalares más masivos se generen dinámicamente en las interacciones de los escalares con los pseudoescalares más ligeros. Para tratar de arrojar algo de luz acerca de los pseudoescalares con masas por encima de 1 GeV, estudiamos las interacciones entre las resonancias escalares $f_0(980)$ y $a_0(980)$ y los pseudoescalares más ligeros. Primeramente, obtenemos las amplitudes elementales de interacción, o potenciales de interacción, sin introducir ningún parámetro libre *ad hoc*. Esto se consigue utilizando, de nuevo, el hecho de que estas resonancias escalares se generan dinámicamente. Posteriormente, los potenciales de interacción son unitarizados con el formalismo de UChPT, obteniéndose finalmente las amplitudes en onda S deseadas. Encontramos que estas interacciones son muy ricas, y generan un gran número de resonancias pseudoescalares que pueden asociarse a $K(1460)$, $\pi(1300)$, $\pi(1800)$, $\eta(1475)$ y $X(1835)$. Podemos decir, por tanto, que una importante contribución a estos estados es de origen dinámico. También consideramos los canales exóticos de estas interacciones (es decir, con números cuánticos que no pueden obtenerse por combinaciones $\bar{q}q$), con $I = 3/2$ e $I = 1$, el último con G–paridad positiva. Nuestros resultados muestran que aquí también hay una resonancia, en acuerdo con una predicción de hace dos décadas [113]. Trabajos más recientes [114, 115], estudiando sistemas de tres pseudoescalares por medio de las ecuaciones de Fadeev, también obtienen algunas de las resoncias citadas, concretamente, $K(1460)$ y $\pi(1300)$.

* * *

La naturaleza del mesón σ se estudia en detalle en el **Capítulo 5**. Es la resonancia más ligera con los números cuánticos del vacío, $J^{PC} = 0^{++}$. Su historia es larga e interesante, aunque ya comentamos algo acerca de ella con anterioridad, al referirnos a los trabajos que, juntando la dinámica quiral de los pseudoescalares más ligeros (piones, en el caso de σ) y los efectos de unitariedad, obtuvieron por primera vez el polo de σ. Más recientemente, la Ref. [116], basada en la solución de las ecuaciones de Roy y ChPT a $\mathcal{O}(p^6)$, obtuvo el valor $445^{+16}_{-8} - i\, 272^{+9}_{-13}$ MeV. Las ecuaciones de Roy implementan la simetría de cruce de forma exacta, mientras que los trabajos relacionados con IAM, N/D y BS lo hacen perturbativamente. Otra determinación precisa reciente [117], basada en relaciones de dispersión, arroja un valor de $484 \pm 17 - i\, 255 \pm 10$ MeV. Mencionemos también que todos estos cálculos no tienen en cuenta la inelasticidad debida al canal de 4π en las ondas S de la interacción $\pi\pi$, mientras que nuestro estudio mencionado arriba acerca del sector escalar tiene en cuenta dicho efecto mediante los canales $\sigma\sigma$ y $\rho\rho$. El hecho de que las posiciones del polo obtenidas mediante estos diferentes esquemas (estos trabajos recientes y los citados con anterioridad) sean similares (particularmente para la parte real) es otra indicación de que el tratamiento de la dinámica de canales cruzados puede hacerse adecuadamente de forma perturbativa. Podemos concluir, por tanto, que nuestro actual conocimiento del polo de la resonancia σ es bastante preciso y que, además, se entiende bien la dinámica hadrónica subyacente. Desde un punto de vista experimental, se ha suscitado un nuevo interés en el mesón σ a partir de recientes resultados con gran estadística, por ejemplo, en $J/\Psi \to \omega\pi\pi$, donde se observa una señal prominente [118]. Otro pico muy marcado en la región de la σ se observa también en desintegraciones de mesones pesados; por ejemplo, fue observada con gran significación estadística en $D \to \pi^+\pi^-\pi^+$ [121].

Más allá del polo y los acoplos de esta resonancia, la siguiente cuestión que surge es su naturaleza: $q\bar{q}$, tetraquark, molécula de dos piones, glubola, etc... Como comentamos antes,

las Refs. [49,50] favorecen una naturaleza de tetraquark, ya que se predice un nonete de tales estados con masas y anchuras compatibles con las de σ, κ, $f_0(980)$ y $a_0(980)$. La naturaleza de tetraquark también es preferida en otros trabajos, por ejemplo, Ref. [122]. El acoplo de σ a $K\bar{K}$ comparado con el de $\pi\pi$ también suele considerarse como una característica importante para discernir entre diferentes modelos para la naturaleza de la σ, como se resalta en la Ref. [123]. Este trabajo señala el hecho de que el acoplo de σ a K^+K^- comparado con el de $\pi^+\pi^-$ no está muy suprimido, lo cual es un factor para considerar una naturaleza gluónica para el mesón σ. Según dicho trabajo, una interpretación $\bar{q}q$ de esta resonancia falla al tratar de explicar su gran anchura, mientras que un escenario en el que la σ sea un tetraquark difícilmente explica su gran acoplo a K^+K^-. Merece la pena destacar, en este punto, que las amplitudes obtenidas en trabajos como Refs. [33, 39] y similares (así como en el Capítulo 3) también predicen una ratio similar para los acoplos a K^+K^- y $\pi^+\pi^-$ del mesón σ, en acuerdo con los expuestos en [123]. Sin embargo, en este caso este comportamiento surge de la generación dinámica de dicha resonancia a partir de las interacciones de estado final (escalares e isoescalares) de $\pi\pi$. También se han aplicado reglas de suma de QCD al estudio de la σ [123–127]. En las Refs. [128–134] se argumenta que la σ es la *compañera* quiral del pión, y que el modo en que evoluciona el polo al tomar el límite de restauración de la simetría quiral varía según la naturaleza de aquélla [135].

Estudios basados en la dependencia del número de colores en QCD, N_C, pueden encontrarse en las Refs. [39, 136–139], donde se demuestra que el mesón σ no tiene una dependencia estándar respecto a N_C. Dichas consideraciones pueden hacerse sin problemas para $N_C \gtrsim 3$, pero no muy grande, ya que para $N_C \gg 3$ las conclusiones dependen fuertemente de los detalles exactos del procedimiento [138, 140–146]. La evolución con N_C del polo de σ está en claro desacuerdo con lo que se esperaría para un estado $\bar{q}q$ o una glubola; más bien, está en la línea de lo que uno esperaría para una molécula de dos piones o un tetraquark [138, 141–147]. En el límite N_C grande, es bien sabido que los bucles (*loops*, en inglés) están suprimidos, de modo que los efectos de interacción de estado final en $\pi\pi$ desaparecen, y con ellos, el polo de la resonancia σ [39, 136–138, 148].

En este Capítulo investigamos más a fondo la naturaleza del mesón σ evaluando su radio cuadrático escalar, $\langle r^2\rangle_s^\sigma$, lo que permite tener una estimación cuantitativa del tamaño de esta resonancia. En nuestro estudio, la σ aparece como una resonancia dinámicamente generada a partir de las interacciones pión–pión. Esto permite obtener su factor de forma escalar a partir de los Lagrangianos quirales, y, a partir de aquél, su radio cuadrático escalar. Obtenemos que la σ es un objeto compacto, con $\langle r^2\rangle_s^\sigma = (0.19 \pm 0.02) + i\,(0.06 \pm 0.02)$ fm^2 [149]. El valor del radio cuadrático escalar del pión es $\langle r^2\rangle_s^\pi = 0.06 \pm 0.02$ fm^2. Otro ejemplo es el valor del radio cuadrático de carga de $K^\pm$, $\langle r^2\rangle_V^{K^\pm} = 0.28 \pm 0.07$ fm^2 [150]. Por comparación con el valor del radio cuadrático escalar del pión, llegamos a la conclusión de que la imagen de un tetraquark es más adecuada que la de una molécula de piones. Nuestro resultado se relaciona en este sentido con los trabajos mencionados anteriormente, que también apuntan hacia una naturaleza no estándar de la σ, a la vez que satisfacen fuertes restricciones de QCD. También estudiaremos como se satisface el teorema de Feynman–Hellman [151, 152] que relaciona las masas de la σ y del pión a través del factor de forma escalar de aquella.

Ofrecemos también, en este capítulo, un detallado estudio de las amplitudes de dispersión $\pi\pi$ en onda S, utilizando UChPT con las amplitudes quirales calculadas en $SU(2)$ a $\mathcal{O}(p^4)$.

A partir de estas amplitudes, obtenemos valores para los parámetros de la amplitud en el umbral, para las LECs, y también para la posición del polo de la σ. Nuestros resultados son: $\sqrt{s_\sigma} = 440 \pm 10 \; - i \; 238 \pm 10$ MeV y $a_0^0 = 0.219 \pm 0.005$, $b_0^0 M_\pi^2 = 0.281 \pm 0.006$. Comparando nuestros resultados con varios resultados de otros trabajos, obtenemos unos valores promedio bastante precisos, $\sqrt{s}_\sigma = 458 \pm 14 - i\, 261 \pm 17$ MeV y $a_0^0 = 0.220 \pm 0.003$, $b_0^0 = 0.279 \pm 0.003 \; M_\pi^{-2}$, que también están de acuerdo con nuestros propios valores. También obtenemos valores adecuados para las LECs de los Lagrangianos quirales en $SU(2)$ a $\mathcal{O}(p^4)$, a saber: $\bar{l}_1 = 0.8 \pm 0.9$, $\bar{l}_2 = 4.6 \pm 0.4$, $\bar{l}_3 = 2 \pm 4$ y $\bar{l}_4 = 3.9 \pm 0.5$. Estos resultados se comparan también con los de otros trabajos, tanto fenomenológicos como resultados obtenidos mediante QCD en el retículo.

Finalmente, en este Capítulo también se considera la dependencia del tamaño de la σ, así como de su masa y su anchura, con la masa de quark. Estas últimas se comparan con resultados obtenidos a través de QCD en el retículo [153], y también con cálculos teóricos obtenidos con el formalismo IAM [154], encontrándose un acuerdo general. El hecho de que la masa de la σ tienda a seguir el umbral de dos piones, como se observa también en lattice QCD, es otra clara indicación de su origen dinámico. Encontramos que, para valores de la masa del pión suficientemente grandes ($M_\pi \gtrsim 470$ MeV a $\mathcal{O}(p^4)$ y $M_\pi \gtrsim 370$ MeV a $\mathcal{O}(p^2)$), la σ se convierte en un estado ligado $\pi\pi$. La dependencia de $\langle r^2 \rangle_s^\sigma$ también se estudia. Para mayores masas de pión, en las que la σ es un estado ligado, encontramos valores más grandes de $\langle r^2 \rangle_s^\sigma$. En estas situaciones, por tanto, es más apropiado asignar una naturaleza molecular.

* * *

Ya hemos señalado con anterioridad el carácter no perturbativo de las interacciones fuertes. Por esta razón, el formalismo de QCD en el retículo se ha convertido en una herramienta útil para estudiar dichas interacciones y, en particular, el espectro hadrónico. En [155] puede encontrarse un artículo reciente que revisa métodos y resultados (excluyendo, sin embargo, la cuestión de las glubolas). En QCD en el retículo, a través del formalismo de integrales de caminos, se estudian las interacciones de quarks y gluones en un red discretizada (retículo) y de tamaño finito, en el interior de una *caja*. Por tanto, resulta necesario conectar los resultados así obtenidos con el mundo real, que es infinito y continuo. El método estándar de Lüscher [156, 157] proporciona tal conexión y es el método más usado. Sin embargo, recientemente en [158] se propuso una mejora del método de Lüscher. La derivación del método de [158] se realiza mediante UChPT, asumiendo un potencial independiente del volumen de la caja. Análogamente, el método de Lüscher desestima las contribuciones dependientes de volumen, pues están exponencialmente suprimidas con L, el tamaño de la caja. Sin embargo, las amplitudes con bucles en los canales cruzados t y u sí dependen de volumen en un cálculo realizado mediante Teoría Cuántica de Campos. Más aún, los *diagramas renacuajo* (*tadpole diagrams*, en inglés), que contribuyen directamente a la amplitud, pero también a través de los valores físicos de m_π y f_π, también dependen del volumen. Lo que pretendemos en el **Capítulo 6** es investigar estas contribuciones para las interacciones de $\pi\pi$ en onda S, para los dos casos posibles de $I = 0$ e $I = 2$. El primero, como ya sabemos, es relevante para estudiar el mesón σ, mientras que en el segundo caso se sabe que los canales cruzados t y u tienen mayor importancia. Compararemos aquí los resultados obtenidos con tres métodos

diferentes: BS, N/D e IAM. El formalismo BS puede considerarse como una versión $\mathcal{O}(p^2)$ del método N/D. Teniendo sólo contribuciones a nivel árbol (es decir, no tiene contribuciones de bucles), no tiene dependencia en volumen. Por contra, IAM y N/D incluyen las amplitudes quirales a $\mathcal{O}(p^4)$, que sí dependen explícitamente de volumen. Derivaremos, por tanto, las modificaciones de las amplitudes en volumen infinito necesarias para usarlas en un volumen finito. Esencialmente, estas modificaciones consisten en una adecuada sustitución de integrales en cuadrimomentos por una suma sobre los valores discretos permitidos en una caja. Cuantificaremos el error cometido al despreciar las contribuciones exponencialmente suprimidas cuando se extraen valores de magnitudes observables a partir de los espectros obtenidos con QCD en el retículo. Concluímos que, para desfasajes de $\pi\pi$ en $I = 0$ hasta 800 MeV, los efectos son despreciables para tamaños de la caja superiores a $2.5m_\pi^{-1}$, y son de un 5 % para valores $1.5 - 2m_\pi^{-1}$. Para $I = 2$, los efectos de tamaño finito pueden llegar hasta un 10 % para esa energía. También estudiamos el error que se comete cuando se utiliza el método de Lüscher para obtener observables a partir de QCD en el retículo, método ampliamente utilizado pero que es una cierta aproximación del que se utiliza en este trabajo.

* * *

En los capítulos anteriores hemos trabajado exclusivamente con interacciones entre mesones. En el **Capítulo 7** tratamos la interacción nucleón–nucleón (NN). Este es, sin duda, un proceso básico, cuya comprensión es necesaria en un amplio rango de problemas físicos, que abarca desde la estructura nuclear hasta las estrellas de neutrones. Recientes trabajos de revisión–introducción, desde el moderno punto de vista de las Teorías de Campo Efectivas, pueden encontrarse en las Refs. [159–162]. Fue Weinberg quien propuso [163–165], a principios de los años noventa, aplicar ChPT al estudio del potencial de interacción NN. Es decir, estudiar este proceso a partir de los Lagrangianos quirales más generales, en términos de los grados de libertad explícitos, que son piones y nucleones. En este punto, merece la pena señalar la ironía de volver a la teoría de Yukawa (intercambios de piones entre nucleones) *aún cuando* y *a pesar de que* conocemos la teoría verdadera subyacente, QCD. La clave está, claro, en que ahora sabemos desarrollar dicha teoría en términos de la simetría quiral (que, por cierto, también se descubrió *antes que* la propia QCD).

Siendo la interacción NN no perturbativa, es necesario iterar el potencial quiral para NN. Fue también Weinberg quien sugirió resolver una ecuación tipo Lippmann–Schwinger (LS) en términos de dicho potencial. Sin embargo, éste es singular en el origen, por lo que algún tipo de regulador es necesario para las integrales con bucles, típicamente un corte Λ (*cut-off*, en inglés) en los valores de trimomento. Este programa fue desarrollado inicialmente en las Refs. [166–169]. Se han realizado muchos trabajos siguiendo estas líneas maestras; para una completa bibliografía al respecto, dirigimos al lector a los artículos citados inicialmente en el párrafo anterior, así como a la introducción del Capítulo 7.

A pesar del gran éxito fenomenológico de este enfoque, varios trabajos en la literatura científica [170–176] sugirieron que los contratérminos quirales que aparecen en el Lagrangiano de ChPT siguiendo el contaje estándar no son suficientes para renormalizar las amplitudes, esto es, para absorber la dependencia en Λ de la ecuación LS. Así pues, varios investigadores

propusieron *promocionar* algunos contratérminos desde órdenes superiores a órdenes inferiores (quizá uno debería decir entonces *degradar*). Haciendo esto, en la Ref. [170] se obtienen resultados estables en el límite $\Lambda \to \infty$. Sin embargo, debe tenerse en cuenta que esto implica una violación del contaje estándar de ChPT, pero también de algunos teoremas de bajas energías que relacionan parámetros de la expansión de rango efectivo [177]. Aún más, hay que señalar que en dicho límite emerge un contaje más complicado [178, 179]. En el otro lado de esta discusión se encuentran trabajos como las Refs. [177, 180] que, siguiendo los argumentos de las Refs. [181, 182], muestran que el corte Λ en trimomento no puede considerarse más allá de la escala a la que la teoría efectiva deja de funcionar, típicamente por debajo de 1 GeV. Discutiremos más sobre este asunto a lo largo de este Capítulo. Una panorámica adecuada de la situación puede encontrarse también en la Sección 4.5 de la Ref. [159].

En el trabajo que aquí presentamos, consideramos las interacciones NN a partir de ChPT. Aplicaremos el método N/D a ondas parciales de NN tomando como entrada (para las ecuaciones integrales que aparecen) la discontinuidad a lo largo del corte izquierdo. Esta discontinuidad se debe a intercambios multipiónicos. A orden dominante, sólo contribuye el intercambio de un pión (OPE, *one–pion exchange*, en inglés). Esta discontinuidad es adecuada para un contaje quiral, tal y como se discute y aplica en las Refs. [162,183,184]. En la primera parte del capítulo, nos ceñiremos a ondas parciales no acopladas con otras. Aplicando el método N/D, obtenemos una ecuación integral lineal para cada una de dichas ondas. Para ondas S y P (con momento angular orbital $\ell \leqslant 1$) nuestro método puede aplicarse de forma directa. Para ondas D y superiores ($\ell \geqslant 2$), las ecuaciones integrales requieren una serie de restricciones ($\ell - 1$ para cada onda) para garantizar el comportamiento adecuado de las ondas parciales en el umbral. Esto se consigue mediante la introducción de polos de Castillejo–Dyson–Dalitz (CDD) [185], algo que permite el método N/D. Posteriormente, generalizamos nuestro formalismo al caso de canales acoplados, discutiendo con algo más de profundidad el caso ${}^3S_1$–${}^3D_1$, que es relevante por la presencia del deuterón en dichas ondas. Nuestros desfasajes y ángulos de mezcla se comparan con los resultados del grupo de Nijmegen [186], fruto de un análisis en ondas parciales de los datos experimentales. Llegados a este punto, debemos destacar que lo que aquí se presenta es un método nuevo para estudiar las interacciones NN, en el que las ondas parciales se calculan en base a relaciones de dispersión y Lagrangianos quirales, y que no dependen de reguladores explícitos. Inicialmente, nuestro cálculo se realiza a orden dominante y, por tanto, no es comparable en cuanto a precisión con cálculos actuales realizados a órdenes superiores. Sin embargo, lo que queremos enfatizar es que este método puede ser mejorado de forma sistemática, orden a orden, y que se parte de Lagrangianos quirales. Estas dos características están en armonía con los modernos enfoques de las Teorías de Campo Efectivas.

* * *

Después de haber tratado todos estos tópicos en el cuerpo de esta tesis, intentamos extraer unas conclusiones globales en el **Capítulo 8**, señalando básicamente los principales logros de esta tesis. Para facilitar la lectura de esta tesis, hemos dejado para el final algunos apéndices en la **Parte III**, que tratan aspectos más técnicos. Las referencias citadas a lo largo de la tesis se muestran al final, incluyendo de forma separada aquellas publicaciones que han surgido fruto del trabajo de esta tesis: [A, B, C, D, E, F, i, ii, iii, iv, v].

Bibliography

1. H. Fritzsch and M. Gell-Mann, 16th Int. Conf. High-Energy Phys., Chicago, Vol. **2**, 135 (1972), arXiv:hep-ph/0208010.
2. H. Fritzsch, M. Gell-Mann, H. Leutwyler, Phys. Lett. B **47**, 365 (1973).
3. D. J. Gross, F. Wilczek, Phys. Rev. D **8**, 3633 (1973).
4. S. Weinberg, Phys. Rev. Lett. **31**, 494 (1973).
5. H. D. Politzer, Phys. Rept. **14**, 129 (1974).
6. H. Fritzsch and P. Minkowski, Nuovo Cim. A**30**, 393 (1975).
7. M. Gell-Mann, Acta Phys. Austriaca Suppl. **9**, 733 (1972).
8. C. -N. Yang, R. L. Mills, Phys. Rev. **96**, 191 (1954).
9. J. Goldstone, Nuovo Cim. **19**, 154 (1961).
10. J. Goldstone, A. Salam, S. Weinberg, Phys. Rev. **127**, 965 (1962).
11. Y. Nambu, Phys. Rev. Lett. **4**, 380 (1960).
12. M. Gell-Mann, Phys. Rev. **125**, 1067 (1962).
13. S. L. Glashow and S. Weinberg, Phys. Rev. Lett. **20**, 224 (1968).
14. S. R. Coleman and E. Witten, Phys. Rev. Lett. **45**, 100 (1980).
15. M. Gell-Mann, *"The Eightfold Way: A Theory of strong interaction symmetry,"* CTSL-20, TID-12608.
16. S. Weinberg, Phys. Rev. Lett. **17**, 616 (1966).
17. S. Weinberg, Physica A **96**, 327 (1979).
18. J. Gasser and H. Leutwyler, Annals Phys. **158**, 142 (1984).
19. J. Gasser and H. Leutwyler, Nucl. Phys. B **250**, 465 (1985).
20. S. R. Coleman, J. Wess and B. Zumino, Phys. Rev. **177**, 2239 (1969).
21. C. G. . Callan, S. R. Coleman, J. Wess and B. Zumino, Phys. Rev. **177**, 2247 (1969).
22. C. Roiesnel and T. N. Truong, Nucl. Phys. B **187**, 293 (1981).
23. T. N. Truong, Phys. Lett. B **99**, 154 (1981).
24. T. N. Truong, Phys. Rev. Lett. **61**, 2526 (1988).
25. T. N. Truong, Phys. Rev. Lett. **67**, 2260 (1991).
26. A. Dobado, M. J. Herrero and T. N. Truong, Phys. Lett. B **235**, 134 (1990).
27. A. Dobado and J. R. Peláez, Phys. Rev. D **47**, 4883 (1993).
28. A. Dobado and J. R. Peláez, Phys. Rev. D **56**, 3057 (1997).
29. J. A. Oller, E. Oset and J. R. Pelaez, Phys. Rev. Lett. **80**, 3452 (1998).
30. J. A. Oller, E. Oset and J. R. Pelaez, Phys. Rev. D**59**, 074001 (1999); (E)-ibid D **60**, 099906 (1999); (E)-ibid D **75**, 099903 (2007).
31. F. Guerrero and J. A. Oller, Nucl. Phys. B **537**, 459 (1999); (E) J. A. Oller, Nucl. Phys. B **602**, 641 (2001).
32. J. R. Peláez and A. Gómez Nicola, Nucl. Phys. A**675**, 96C (2000).
33. J. A. Oller and E. Oset, Nucl. Phys. A **620**, 438 (1997); (E)-ibid. A **652**, 407 (1999).
34. J. A. Oller and E. Oset, Nucl. Phys. A **629**, 739 (1998).
35. E. Oset and A. Ramos, Nucl. Phys. A **635**, 99 (1998).

36. J. Nieves and E. Ruiz Arriola, Phys. Lett. B **455**, 30 (1999).
37. J. Nieves and E. Ruiz Arriola, Nucl. Phys. A **679**, 57 (2000).
38. G.F. Chew and S. Mandelstam, Phys. Rev. **119**, 467 (1960).
39. J. A. Oller and E. Oset, Phys. Rev. D **60**, 074023 (1999).
40. J. A. Oller, Phys. Lett. B **426**, 7 (1998).
41. J. A. Oller and U. G. Meissner, Phys. Lett. B **500**, 263 (2001).
42. J. A. Oller, E. Oset and A. Ramos, Prog. Part. Nucl. Phys. **45**, 157 (2000).
43. M. Jamin, J. A. Oller and A. Pich, Nucl. Phys. B **587**, 331 (2000).
44. M. Jamin, J. A. Oller and A. Pich, Nucl. Phys. B **622**, 279 (2002).
45. M. Jamin, J. A. Oller and A. Pich, Eur. Phys. J. C**24**, 237 (2002).
46. J. A. Oller, E. Oset and J. Palomar, Phys. Rev. D **63**, 114009 (2001).
47. D. Jido, J. A. Oller, E. Oset, A. Ramos and U. G. Meissner, Nucl. Phys. A **725**, 181 (2003).
48. K. Nakamura *et al.*, [Particle Data Group Collab.], J. Phys. G G **37**, 075021 (2010).
49. R. L. Jaffe, Phys. Rev. D **15**, 267 (1977).
50. R. L. Jaffe, Phys. Rev. D **15**, 281 (1977).
51. E. Van Beveren, T. A. Rijken, K. Metzger, C. Dullemond, G. Rupp and J. E. Ribeiro, Z. Phys. C **30**, 615 (1986).
52. G. Janssen, B. C. Pearce, K. Holinde and J. Speth, Phys. Rev. D **52**, 2690 (1995).
53. J. A. Oller, Nucl. Phys. A **727**, 353 (2003).
54. D. Black, A. H. Fariborz, F. Sannino and J. Schechter, Phys. Rev. D**59**, 074026 (1999).
55. M. Napsuciale, arXiv:hep-ph/9803396.
56. G. 't Hooft, arXiv:hep-th/9903189.
57. M. D. Scadron, Phys. Rev. D**26**, 239 (1982).
58. G. 't Hooft, G. Isidori, L. Maiani, A. D. Polosa and V. Riquer, Phys. Lett. B **662**, 424 (2008).
59. D. Lohse, J. W. Durso, K. Holinde and J. Speth, Phys. Lett. B**234**, 235 (1990).
60. D. Lohse, J. W. Durso, K. Holinde and J. Speth, Nucl. Phys. A**516**, 513 (1990).
61. V. Mull, K. Holinde and J. Speth, Phys. Lett. B**275**, 12 (1992).
62. J. Soto, P. Talavera and J. Tarrus, arXiv:1110.6156 [hep-ph].
63. J. Tarrus, AIP Conf. Proc. **1343**, 268 (2011).
64. C. Amsler, Rev. Mod. Phys. **70**, 1293 (1998).
65. J. Z. Bai *et al.* [BES Collaboration], Phys. Rev. Lett. **77**, 3959 (1996).
66. M. Ablikim *et al.* [BES Collaboration], Phys. Lett. B**607**, 243 (2005).
67. M. Ablikim *et al.* [BES Collaboration], Phys. Rev. Lett. **96**, 162002 (2006).
68. D. V. Bugg, Eur. Phys. J. C**52**, 55 (2007).
69. D. Alde *et al.* [GAMS Collaboration], Eur. Phys. J. A**3**, 361 (1998).
70. D. Bugg, Rep.Phys. Rept. **397**, 257 (2004).
71. V.A. Novikov, M. A. Shifman, A. I. Vainsthein and V. I. Zakharov, Nucl. Phys. B **165**, 67 (1980).
72. V.A. Novikov, M. A. Shifman, A. I. Vainsthein and V. I. Zakharov, Nucl. Phys. B **191**, 301 (1981).
73. S. Narison, Z. Phys. C**26**, 209 (1984).
74. E. Bagan, A. Bramon and S. Narison, Phys. Lett. B **196**, 203 (1987).
75. S. Narison and G. Veneziano, Int. J. Mod. Phys. A **4**, 2751 (1989).
76. S. Narison, Nucl. Phys. B **509**, 312 (1998).
77. H. Forkel, Phys. Rev. D **64**, 034015 (2001).
78. L. S. Kisslinger and M. B. Johnson, Phys. Lett. B **523**, 127 (2001).
79. A. Chodos, *et al.*, Phys. Rev. D **10**, 2599 (1974).
80. N. Isgur and J. Paton, Phys. Lett. B **124**, 247 (1983).
81. A. Szczepaniak *et al.*, Phys. Rev. Lett. **76**, 2011 (1996).
82. M. Chanowitz and S. Sharpe, Nucl. Phys. B **222**, 211 (1983); (E)-ibid. B **228**, 588 (1983).

83. P. Bicudo, S. R. Cotanch, F. J. Llanes-Estrada and D. G. Robertson, Eur. Phys. J. C **52**, 363 (2007).
84. G. S. Bali, K. Schilling, A. Hulsebos, A. C. Irving, C. Michael and P. W. Stephenson [UKQCD Collaboration], Phys. Lett. B **309**, 378 (1993).
85. C. J. Morningstar and M. J. Peardon, Phys. Rev. D **60**, 034509 (1999).
86. Y. Chen *et al.*, Phys. Rev. D **73**, 014516 (2006).
87. A. Vaccarino and d. Weingarten, Phys. Rev. D **60**, 114501 (1999).
88. W. Lee and D. Weingarten, Phys. Rev. D **61**, 014015 (1999).
89. J. Sexton, A. Vaccarino and D. Weingarten, Phys. Rev. Lett. **75**, 4563 (1995).
90. C. M. Richards *et al.* [UKQCD Collaboration], Phys. Rev. D **82**, 034501 (2010)
91. M. S. Chanowitz, Phys. Rev. Lett. **95**, 172001 (2005).
92. K. T. Chao, X. -G. He and J. P. Ma, Phys. Rev. Lett. **98**, 149103 (2007).
93. M. S. Chanowitz, Phys. Rev. Lett. **98**, 149104 (2007).
94. K. T. Chao, X. -G. He and J. P. Ma, Eur. Phys. J. C **55**, 417 (2008) [hep-ph/0512327].
95. F. E. Close and A. Kirk, Eur. Phys. J. C **21**, 531 (2001).
96. M. Strohmeier-Presicek, T. Gutsche, R. Vin Mau and A. Faessler, Phys. Rev. D **60**, 054010 (1999).
97. L. Burakovsky and P. R. Page, Phys. Rev. D **59**, 014022 (1999); (E)-ibid. D **59**, 079902 (1999).
98. M. Boglione and M. R. Pennington, Phys. Rev. Lett. **79**, 1998 (1997).
99. C. Amsler and F. E. Close, Phys. Rev. D **53**, 295 (1996).
100. C. Amsler and F. Close, Phys. Lett. B **353**, 385 (1995).
101. E. Witten, Nucl. Phys. B **223**, 422 (1983).
102. P. Herrera-Siklody, J. I. Latorre, P. Pascual and J. Taron, Nucl. Phys. B **497**, 345 (1997).
103. P. Herrera-Siklody, J. I. Latorre, P. Pascual and J. Taron, Phys. Lett. B **419**, 326 (1998).
104. R. Kaiser and H. Leutwyler, Eur. Phys. J. C**17**, 623 (2000).
105. G. Ecker, J. Gasser, A. Pich and E. de Rafael, Nucl. Phys. B **321**, 311 (1989).
106. G. Ecker, J. Gasser, H. Leutwyler, A. Pich and E. de Rafael, Phys. Lett. B **223**, 425 (1989).
107. A. Masoni, C. Cicalo and G. L. Usai, J. Phys. G G **32**, R293 (2006).
108. M. S. Chanowitz, Phys. Rev. Lett. **46**, 981 (1981).
109. K. Ishikawa, Phys. Rev. Lett. **46**, 978 (1981).
110. F. E. Close, G. R. Farrar and Z. p. Li, Phys. Rev. D **55**, 5749 (1997).
111. E. Klempt and A. Zaitsev, Phys. Rept. **454**, 1 (2007).
112. J. -J. Wu, X. -H. Liu, Q. Zhao and B. -S. Zou, Phys. Rev. Lett. **108**, 081803 (2012).
113. R. S. Longacre, Phys. Rev. D **42**, 874 (1990).
114. A. Martinez Torres, K. P. Khemchandani, D. Jido and A. Hosaka, Phys. Rev. D **84**, 074027 (2011).
115. A. Martinez Torres, D. Jido and Y. Kanada-En'yo, Phys. Rev. C **83**, 065205 (2011).
116. I. Caprini, G. Colangelo and H. Leutwyler, Phys. Rev. Lett. **96**, 132001 (2006).
117. F. J. Ynduráin, R. García-Martín and J. R. Peláez, Phys. Rev. D **76**, 074034 (2007).
118. M. Ablikim *et al.* [BES Collaboration], Phys. Lett. B **598**, 149 (2004).
119. J. E. Augustin *et al.* [DM2 Collaboration], Nucl. Phys. B **320**, 1 (1989).
120. W. S. Lockman [MARK-III Collaboration], Production of the $f_0(975)$ meson in J/Ψ decays, in: Ajaccio Hadron, 1989, p.109.
121. E. M. Aitala *et al.* [E791 Collaboration], Phys. Rev. Lett. **86**, 770 (2001).
122. N. N. Achasov, S. A. Devyanin and G. N. Shestakov, Phys. Lett. B **108**, 134 (1982); (E)-ibid. B **108**, 435 (1982).
123. G. Mennessier, S. Narison and X.-G. Wang, Phys. Lett. B **688**, 59 (2010).
124. R. Kaminski, G. Mennessier and S. Narison, Phys. Lett. B **680**, 148 (2009) (and references therein).
125. A. Zhang, T. Huang and T. G. Steele, Phys. Rev. D **76**, 036004 (2007).

126. H.-X. Chen, A. Hosaka, H. Toki and S.-L. Zhu, Phys. Rev. D **81**, 114034 (2010).
127. J. Zhang, H. Y. Jin, Z. F. Zhang, T. G. Steele and D. H. Lu, Phys. Rev. D **79**, 114033 (2009).
128. T. Hatsuda and T. Kunihiro, Phys. Rep. **247**, 221 (1994).
129. T. Hatsuda and T. Kunihiro, Prog. Theor. Phys. **74**, 765 (1985).
130. T. Hatsuda and T. Kunihiro, Phys. Lett. B **185**, 304 (1987).
131. V. Bernard, U.-G. Meißner and I. Zahed, Phys. Rev. Lett. **59**, 966 (1987).
132. D. Jido, T. Hatsuda and T. Kunihiro, Phys. Rev. D **63**, 011901 (2001).
133. K. Yokokawa, T. Hatsuda, A. Hayashigaki and T. Kunihiro, Phys. Rev. C **66**, 022201 (2002).
134. J. A. Oller, Proceedings of the Workshop *"Possible Existence of the σ-meson and its implications to Hadron Physics,"*, KEK Proceedings 2000-4, NUP B-2000-1, 33; Soryushiron Kenkyu **102**, 33 (2001), arXiv:hep-ph/0007349.
135. T. Hyodo, D. Jido and T. Kunihiro, arXiv:1007.2031 [hep-ph].
136. J. R. Peláez, Phys. Rev. Lett. **92**, 102001 (2004).
137. J. R. Peláez and G. Ríos, Phys. Rev. Lett. **97**, 242002 (2006).
138. Z. -H. Guo and J. A. Oller, Phys. Rev. D **84**, 034005 (2011).
139. Z.-Y. Zhou and Z. Xiao, Phys. Rev. D **83**, 014010 (2011).
140. Z. X. Sun, L. Y. Xiao, Z. Xiao and H. Q. Zheng, Mod. Phys. Lett. A **22**, 711 (2007).
141. Z.-H. Guo, J. J. Sanz-Cillero and H.-Q. Zheng, JHEP **0706**, 030 (2007).
142. Z. H. Guo, J. J. Sanz-Cillero and H. Q. Zheng, Phys. Lett. B **661**, 342 (2008).
143. J. Nieves, A. Pich and E. Ruiz Arriola, Phys. Rev. D **84**, 096002 (2011).
144. J. Nieves and E. Ruiz-Arriola, Phys. Rev. D **80**, 045023 (2009).
145. E. Ruiz-Arriola and W. Broniowski, Phys. Rev. D **81**, 054009 (2010).
146. L. Y. Xiao, Z.-H. Guo and H. Q. Zheng, Int. J. Mod. Phys. A **22**, 4603 (2007).
147. A. Manohar, *"Large N_C QCD,"* Les Houches Summer School in Theoretical Physics, Session 68: Probing the Standard Model of Particle Interactions, 28-07 to 05-09-1997, Les Houches (France), hep-ph/9802419.
148. Z. -H. Guo, J. A. Oller and J. Ruiz de Elvira, Phys. Lett. B **712**, 407 (2012).
149. J. A. Oller, L. Roca, Phys. Lett. B **651**, 139 (2007).
150. E. B. Dally *et al.*, Phys. Rev. Lett. **48**, 375 (1982).
151. R.P. Feynman, Phys. Rev. **56**, 340 (1939).
152. H. Hellman, *"Einführung in die Quantenchemie",* Deuticke Verlag, Leipzig, 1937.
153. S. Prelovsek, T. Draper, C. B. Lang, M. Limmer, K.-F. Liu, N. Mathur and D. Mohler, Phys. Rev. D **82**, 094507 (2010).
154. J. R. Pelaez and G. Rios, Phys. Rev. D **82**, 114002 (2010).
155. Z. Fodor and C. Hoelbling, Rev. Mod. Phys. **84**, 449 (2012).
156. M. Lüscher, Commun. Math. Phys. **105**, 153 (1986).
157. M. Lüscher, Nucl. Phys. B **354**, 531 (1991).
158. M. Doring, U. -G. Meißner, E. Oset and A. Rusetsky, Eur. Phys. J. A **47**, 139 (2011).
159. R. Machleidt and D. R. Entem, Phys. Rept. **503**, 1 (2011).
160. E. Epelbaum, H.-W. Hammer and U.-G. Meißner, Rev. Mod. Phys. **81**, 1773 (2009).
161. E. Epelbaum, Prog. Part. Nucl. Phys. **57**, 654 (2006).
162. J. A. Oller, A. Lacour and U.-G. Meißner, Annals Phys. **326**, 241 (2011).
163. S. Weinberg, Phys. Lett. B **251**, 288 (1990).
164. S. Weinberg, Nucl. Phys. B **363**, 3 (1991).
165. S. Weinberg, Phys. Lett. B **295**, 114 (1992).
166. C. Ordóñez, L. Ray and U. van Kolck, Phys. Rev. Lett. **72**, 1982 (1994).
167. C. Ordóñez, L. Ray and U. van Kolck, Phys. Rev. C **53**, 2086 (1996).
168. U. van Kolck, Phys. Rev. C **49**, 2932 (1994).
169. U. van Kolck, Prog. Part. Nucl. Phys. **43**, 337 (1999).
170. A. Nogga, R. G. E. Timmermans and U. van Kolck, Phys. Rev. C **72**, 054006 (2005).

171. M. Pavón Valderrama and E. Ruiz Arriola, Phys. Rev. C **72**, 054002 (2005).
172. M. Pavón Valderrama and E. Ruiz Arriola, Phys. Rev. C **74**, 054001 (2006).
173. M. Pavón Valderrama and E. Ruiz Arriola, Phys. Rev. C **74**, 064004 (2006); (E)-ibid. C **75**, 059905 (2007).
174. D. B. Kaplan and M. J. Savage, Phys. Lett. B **365**, 244 (1996).
175. D. B. Kaplan, M. J. Savage and M. B. Wise, Nucl. Phys. B **478**, 629 (1996).
176. D. R. Entem, E. Ruiz Arriola, M. Pavón Valderrama and R. Machleidt, Phys. Rev. C **77** (2008) 044006.
177. E. Epelbaum and U.-G. Meißner, arXiv:nucl-th/0609037.
178. M. C. Birse and J. A. McGovern, Phys. Rev. C **70**, 054002 (2004).
179. M. C. Birse, Phys. Rev. C **74**, 014003 (2006).
180. E. Epelbaum and J. Gegelia, Eur. Phys. J. A **41**, 341 (2009).
181. G. P. Lepage, arXiv:nucl-th/9706029.
182. G. P. Lepage, arXiv:hep-ph/0506330.
183. J. A. Oller, A. Lacour and U.-G. Meißner, J. Phys. G **37**, 015106 (2010).
184. A. Lacour, J. A. Oller and U. G. Meißner, J. Phys. G **37**, 125002 (2010).
185. L. Castillejo, R. H. Dalitz, F. J. Dyson, Phys. Rev. **101**, 453 (1956).
186. V. G. J. Stoks, R. A. M. Klomp, C. P. F. Terheggen, J. J. de Swart, Phys. Rev. C **49**, 2950 (1994).
187. J. Wess, J. Bagger, *"Supersymmetry and supergravity,"* Princeton, USA: Univ. Pr. (1992) 259 p.
188. R. Haag, Phys. Rev. **112**, 669 (1958).
189. M. Jamin, J. A. Oller and A. Pich, Phys. Rev. D **74**, 074009 (2006).
190. J. A. Oller and L. Roca, Eur. Phys. J. A **34**, 371 (2007).
191. W. A. Bardeen, Phys. Rev. **184**, 1848 (1969).
192. S. L. Adler and W. A. Bardeen, Phys. Rev. **182**, 1517 (1969).
193. K. Fujikawa, Phys. Rev. D **21**, 2848 (1980); (E)-ibid. D **22**, 1499 (1980).
194. G. 't Hooft, Nucl. Phys. B **72**, 461 (1974).
195. E. Witten, Nucl. Phys. B **156**, 269 (1979).
196. E. Witten, Nucl. Phys. B **160**, 57 (1979).
197. C. Itzykson and J. B. Zuber,"Quantum Field Theory,", New York, Mcgraw-hill (1980).
198. C. Vafa and E. Witten, Nucl. Phys. B **234**, 173 (1984).
199. C. Vafa and E. Witten, Phys. Rev. Lett. **53**, 535 (1984).
200. S. Coleman, J. Math. Phys. **7**, 787 (1966).
201. H. Georgi, *"Weak Interactions And Modern Particle Theory,"* Menlo Park, Usa: Benjamin/cummings, 165p (1984).
202. A. Pich, Rept. Prog. Phys. **58**, 563 (1995).
203. S. Scherer, Adv. Nucl. Phys. **27**, 277 (2003) [hep-ph/0210398].
204. M. C. Birse, Z. Phys. A **355**, 231 (1996).
205. B. Borasoy and U. -G. Meissner, Int. J. Mod. Phys. A **11**, 5183 (1996).
206. L. Roca, *Dinámica quiral en desintegración y producción de resonancias hadrónicas y aplicaciones nucleares*, Ph. D. thesis, Valencia, 2005.
207. Fayyazuddin, Riazuddin, *"A Modern introduction to particle physics,"* Singapore, Singapore: World Scientific (1994) 656 p.
208. Y. S. Kim and K. V. Vasavada, Phys. Rev. D **5**, 1002 (1972).
209. R. More and E. Gerjuoy, Phys. Rev. A **7**, 1288 (1973).
210. J. Bang, F. A. Gareev, M. K. .Gizatkulov and S. A. Goncharov, Nucl. Phys. A **309**, 381 (1978).
211. L. Fonda, G. C. Ghirardi and A. Rimini, Rept. Prog. Phys. **41**, 587 (1978).
212. W. van Dijk and Y. Nogami, Phys. Rev. Lett. **83**, 2867 (1999).
213. W. van Dijk and Y. Nogami, Phys. Rev. C **65**, 024608 (2002); (E)-ibid. C **70**, 039901 (2004).

214. R. de la Madrid, Nucl. Phys. A **812**, 13 (2008).
215. D. Gamermann, J. Nieves, E. Oset and E. Ruiz Arriola, Phys. Rev. D **81**, 014029 (2010).
216. F. Aceti and E. Oset, Phys. Rev. D **86**, 014012 (2012).
217. S. Weinberg, *"The Quantum theory of fields. Vol. 1: Foundations,"* Cambridge, UK: Univ. Pr. (1995) 609 p.
218. S. Albeverio, (Ed.), L. S. Ferreira, (Ed.), L. Streit, (Ed.), *"Resonances - Models And Phenomena. Proceedings, Workshop, Bielefeld, F.r. Germany, April 9-14, 1984,"* Berlin, Germany: Springer (1984) 359 p. (Lecture Notes in Physics, vol. 211). See, in particular, the introduction by R. H. Dalitz, *"Resonance: its description, criteria and significance".*
219. S. M. Flatte, Phys. Lett. B**63**, 224 (1976).
220. U. G. Meißner, Rept. Prog. Phys. **56**, 903 (1993).
221. A. Pich, Rept. Prog. Phys. **58**, 563 (1995).
222. V. Bernard and U. -G. Meissner, Ann. Rev. Nucl. Part. Sci. **57**, 33 (2007).
223. V. Bernard, Prog. Part. Nucl. Phys. **60**, 82 (2008).
224. A. D. Martin, T. D. Spearman, *"Elementary Particle Theory,"* North-Holland Publishing Company, Amsterdam (1970).
225. J. A. Oller, Phys. Lett. B **477**, 187 (2000).
226. J. Schwinger, Ann. Phys. **2**, 407 (1957).
227. M. Gell-Mann, M. Levy, Nuovo Cim. **16**, 705 (1960).
228. B. W. Lee, Nucl. Phys. B**9**, 649 (1969).
229. S. Gasiorowicz and D. A. Geffen, Rev. Mod. Phys. **41**, 531 (1969).
230. R. J. Schecther and Y. Ueda, Phys. Rev. D**3**, 2874 (1971);(E)-*ibid.* D**8**, 987 (1973).
231. H. Pagels, Phys. Rept. **16**, 219 (1975).
232. N. A. Törnqvist, Eur. Phys. J. C**11**, 359 (1999).
233. H. Leutwyler, Ann. Phys. **235**, 165 (1994).
234. N. H. Fuchs, H. Sazdjian and J. Stern, Phys. Lett. B**269**, 183 (1991).
235. K. M. Bitar *et al.* [HEMCGC Collaboration], Phys. Rev. D **44**, 2090 (1991).
236. G. S. Bali *et al.* [SESAM and TξL Collaboration], Phys. Rev. D **62**, 054503 (2000).
237. C. McNeile and C. Michael, Phys. Rev. D **63**, 114503 (2001)
238. A. Hart and M. Teper [UKQCD], Phys. Rev. D **65**, 034502 (2002).
239. A. Hart, C. McNeile, C. Michael and J. Pickavance [UKQCD Collaboration], Phys. Rev. D **74**, 114504 (2006).
240. E. B. Gregory, A. C. Irving, C. C. McNeile, S. Miller and Z. Sroczynski, PoS LAT **2005**, 027 (2006).
241. E. B. Gregory *et al.* [UKQCD Collaboration], PoS LATTICE **2008**, 286 (2008).
242. W. M. Kloet and B. Loiseau, Z. Phys. A **353**, 227 (1995).
243. A. Abele *et al.* [Crystal Barrel Collaboration], Phys. Lett. B **385**, 425 (1996).
244. A. Abele *et al.* [Crystal Barrel Collaboration], Phys. Lett. B **380**, 453 (1996).
245. R. Kaminski, L. Lesniak and B. Loiseau, Eur. Phys. J. C **9**, 141 (1999).
246. R. Kaminski, L. Lesniak and K. Rybicki, Eur. Phys. J. direct C **4**, 4 (2002).
247. R. Kaminski, L. Lesniak and B. Loiseau, Int. J. Mod. Phys. A **20**, 693 (2005).
248. D. V. Bugg, I. Scott, B. S. Zou, V. V. Anisovich, A. V. Sarantsev, T. H. Buernett and S. Sutlief, Phys. Lett. B **353**, 378 (1995).
249. D. V. Bugg, A. V. Sarantsev and B. S. Zou, Nucl. Phys. B **471**, 59 (1996).
250. R. H. Dalitz and S. F. Tuan, Ann. Phys. **10**, 307 (1960).
251. J. D. Weinstein and N. Isgur, Phys. Rev. Lett. **48**, 659 (1982).
252. M. Harada, F. Sanino and J. Schechter, Phys. Rev. Lett. **78**, 1603 (1997).
253. D. Black, A. H. Fariborz, F. Sannino and J. Schechther, Phys. Rev. D **58**, 054012 (1998).
254. D. Black, A. H. Fariborz and J. Schechther, Phys. Rev. D **61**, 074001 (2000).
255. E. Van Beveren and G. Rupp, Eur. Phys. J. C **10**, 469 (1999).

256. D. Morgan and M. R. Pennington, Phys. Rev. D **48**, 1185 (1993).
257. N. N. Achasov and G. N. Shestakov, Phys. Rev. D **49**, 5779 (1994).
258. N. A. Törnqvist, Z. Phys. C **68**, 647 (1995).
259. N. A. Törnqvist and M. Roos, Phys. Rev. Lett. **76**, 1575 (1996).
260. N.vA. Törnqvist, Phys. Lett. B **426**, 105 (1998).
261. R. Delbourgo and M. D. Scadron, Mod. Phys. Lett. A **10**, 251 (1995).
262. M. Svec, Phys. Rev. D **53**, 2343 (1996).
263. V. Elias, A. H. Fariborz, F. Shi and T. G. Steele, Nucl. Phys. A **633**, 279 (1998).
264. K. Igi and K. I. Hikasa, Phys. Rev. D **59**, 034005 (1999).
265. J. Vijande, A. Valcarce, F. Fernández and B. Silvestre-Brac, Phys. Rev. D **72**, 034025 (2005).
266. V. Vento, Phys. Rev. D **73**, 054006 (2006).
267. L. Maiani, A. Polosa, F. Piccinni and V. Riquier, Phys. Rev. Lett. **93**, 212002 (2004).
268. L. Maiani, F. Piccinini, A. D. Polosa and V. Riquer, Eur. Phys. J. C **50**, 609 (2007).
269. D. V. Bugg, J. Phys. G G **34**, 151 (2007).
270. M. Napsuciale and S. Rodriguez, Phys. Rev. **D71**, 074008 (2005).
271. L. S. Geng and E. Oset, Phys. Rev. D **79**, 074009 (2009).
272. H. Leutwyler, Phys. Lett. B**374**, 163 (1996).
273. S. Weinberg, *"The quantum theory of fields. Vol. 2: Modern applications,"* Cambridge, UK: Univ. Pr. (1996) 489 p.
274. R. Kaminski, L. Lesniak and B. Loiseau, Phys. Lett. B **413**, 130 (1997).
275. J. J. Sakurai, Ann. Phys. **11**, 1 (1960).
276. A. Bramon, *"Lectures on Electromagnetic Interactions of Hadrons,"* Universitat Autònoma de Barcelona, UAB-FT-D-3, B-32642-1979.
277. U. G. Meissner, Phys. Rept. **161**, 213 (1988).
278. J. Prades, Z. Phys. C **63**, 491 (1994); (E)-*ibid.* C **11**, 571 (1999).
279. J. A. Oller, Phys. Rev. D **71**, 054030 (2005).
280. J. A. Oller, Nucl. Phys. A **714**, 161 (2003).
281. U. G. Meissner and J. A. Oller, Nucl. Phys. A **679**, 671 (2001).
282. A. Gomez Nicola, J. R. Pelaez and G. Rios, Phys. Rev. D **77**, 056006 (2008).
283. T. Hannah, Phys. Rev. D **60**, 017502 (1999).
284. L. Masetti [NA48/2 Collaboration], arXiv:hep-ex/0610071.
285. S. Pislak, R. Appel, G. S. Atoyan, B. Bassalleck, D. R. Bergman, N. Cheung, S. Dhawan and H. Do *et al.*, Phys. Rev. D **67**, 072004 (2003); (E)-*ibid.* D **81**, 119903 (2010)]
286. G. Grayer *et al.*, Nucl. Phys. B **75**, 189 (1974).
287. P. Estabrooks *et al.*, AIP Conf. Proc. **13**, 37 (1973).
288. S. D. Protopopescu *et al.*, Phys. Rev. D **7**, 1279 (1973).
289. B. Hyams *et al.*, Nucl. Phys. B **64**, 134 (1973); AIP Conf. Proc. **13**, 206 (1973).
290. R. Kaminski, L. Lesniak and K. Rybicki, Z. Phys. C **74**, 79 (1997).
291. R. Kaminski, L. Lesniak and B. Loiseau, Phys. Lett. B **551**, 241 (2003).
292. A. Etkin *et al.*, Phys. Rev. D **25**, 1786 (1982).
293. D. H. Cohen, D. S. Ayres, R. Diebold, S. L. Kramer, A. J. Pawlicki and A. B. Wicklund, Phys. Rev. D **22**, 2595 (1980).
294. F. Binon *et al.* [Serpukhov-Brussels-Annecy(LAPP) Collaboration], Nuovo Cim. A **78**, 313 (1983).
295. F. Binon *et al.* [Serpukhov-Brussels-Annecy(LAPP) Collaboration], Nuovo Cim. A **80**, 363 (1984).
296. D. Aston *et al.*, Nucl. Phys. B **296**, 493 (1988).
297. G. Colangelo, J. Gasser and H. Leutwyler, Phys. Lett. B **488**, 261 (2000).
298. D. Barberis *et al.* [WA102 Collaboration], Phys. Lett. B **462**, 462 (1999).
299. D. Barberis *et al.* [WA102 Collaboration], Phys. Lett. B **479**, 59 (2000).

300. C. Amsler *et al.* [Crystal Barrel Collaboration], Phys. Lett. B **355**, 425 (1995).
301. C. Amsler *et al.* [Crystal Barrel Collaboration], Phys. Lett. B **340**, 259 (1994).
302. K. L. Au, D. Morgan and M. R. Pennington, Phys. Rev. D **35**, 1633 (1987).
303. T. Barnes, F. E. Close, P. R. Page and E. S. Swanson, Phys. Rev. D **55**, 4157 (1997).
304. F. E. Close and P. R. Page, Nucl. Phys. B **443**, 233 (1995).
305. F. E. Close and P. R. Page, Phys. Rev. D **52**, 1706 (1995).
306. C. Amsler *et al.* [Crystal Barrel Collaboration], Phys. Lett. B **358**, 389 (1995).
307. A. Abele *et al.* [Crystal Barrel Collaboration], Nucl. Phys. B **514**, 45 (1998).
308. A. Bertin *et al.* [OBELIX Collaboration], Phys. Lett. B **361**, 187 (1995).
309. C. Cicalo *et al.* [OBELIX Collaboration], Phys. Lett. B **462**, 453 (1999).
310. Z. Bai *et al.* [MARK-III Collaboration], Phys. Rev. Lett. **65**, 2507 (1990).
311. J. E. Augustin *et al.* [DM2 Collaboration], Phys. Rev. D **46** (1992) 1951.
312. M. Acciarri *et al.* [L3 Collaboration], Phys. Lett. B **501**, 1 (2001).
313. L. Faddeev, A. J. Niemi and U. Wiedner, Phys. Rev. D **70**, 114033 (2004).
314. G. R. Farrar, Phys. Rev. Lett. **76**, 4111 (1996).
315. M. B. Cakir and G. R. Farrar, Phys. Rev. D **50**, 3268 (1994).
316. E. Klempt, "The glueball candidate $\eta(1440)$ as η radial excitation." Thirty-second International Conference on High-Energy Physics (ICHEP04), Beijing, China, arXiv:hep-ph/0409148.
317. J. Z. Bai *et al.* [BES Collaboration], Phys. Rev. Lett. **91**, 022001 (2003).
318. M. Ablikim *et al.* [BES Collaboration], Phys. Rev. Lett. **95**, 262001 (2005).
319. A. Sibirtsev, J. Haidenbauer, S. Krewald, U. G. Meissner and A. W. Thomas, Phys. Rev. D **71**, 054010 (2005).
320. J. Haidenbauer, U. G. Meissner and A. Sibirtsev, Phys. Rev. D **74**, 017501 (2006).
321. J. Haidenbauer, U. -G. Meissner and A. Sibirtsev, Phys. Lett. B **666**, 352 (2008).
322. L. Alvarez-Ruso, J. A. Oller and J. M. Alarcon, Phys. Rev. D **80**, 054011 (2009).
323. L. Alvarez-Ruso, J. A. Oller and J. M. Alarcon, Phys. Rev. D **82**, 094028 (2010)
324. B. Aubert *et al.* [BABAR Collaboration], Phys. Rev. D **74**, 091103 (2006).
325. B. Aubert *et al.* [BABAR Collaboration], Phys. Rev. D **76**, 012008 (2007).
326. C. P. Shen *et al.* [Belle Collaboration], Phys. Rev. D **80**, 031101 (2009).
327. A. Martinez Torres, K. P. Khemchandani, L. S. Geng, M. Napsuciale and E. Oset, Phys. Rev. D **78**, 074031 (2008).
328. J. D. Weinstein and N. Isgur, Phys. Rev. D **41**, 2236 (1990).
329. G. Barton, *"Introduction to Dispersion Techniques in Field Theory,"* W. A. Benjamin, Inc, New York, Amsterdam, 1965.
330. G. Källen and A. S. Wightman, Mat.-fys. Skrifth **1**, 6 (1958).
331. A. M. Bincer, Phys. Rev. **118**, 855 (1960).
332. C. Daum *et al.* [ACCMOR Collaboration], Nucl. Phys. B **187**, 1 (1981).
333. G. W. Brandenburg *et al.*, Phys. Rev. Lett. **36**, 1239 (1976).
334. S. Fukui *et al.*, Phys. Lett. B **267**, 293 (1991).
335. F. E. Close and N. A. Tornqvist, J. Phys. G G **28**, R249 (2002).
336. S. M. Roy, Phys. Lett. B **36**, 353 (1971).
337. G. Colangelo, J. Gasser and H. Leutywler, Nucl. Phys. B **603**, 125 (2001).
338. N. N. Achasov, Phys. Atom. Nucl. **65**, 546 (2002) [Yad. Fiz. **65**, 573 (2002)].
339. N. N. Achasov and A. V. Kiselev, Phys. Rev. D **73**, 054029 (2006); (E)-ibid. D **74**, 059902 (2006).
340. N. N. Achasov, Phys. Atom. Nucl. **70**, 1956 (2007) [Yad. Fiz. **70**, 2005 (2007)].
341. N. N. Achasov and A. V. Kiselev, Phys. Rev. D **83**, 054008 (2011).
342. D. V. Bugg, Eur. Phys. J. C **37**, 433 (2004).
343. T. Lähde and U.-G. Meißner, Phys. Rev. D **74**, 034021 (2006).
344. F. Sannino and J. Schechter, Phys. Rev. D **52**, 96 (1995).

345. M. Harada, F. Sannino and J. Schechter, Phys. Rev. D **54**, 1991 (1996).
346. S. Ishida, AIP Conf. Proc. Vol. **432**, 705 (1998).
347. M. Ishida, Proceedings of *Possible Existence of the σ-Meson and its Implications to Hadron Physics*, Eds. S. Ishida *et al.*, KEK Proceedings 2000-4, YITP, Kyoto, Japan, 12-14 June 2000, hep-ph/0012325.
348. S. Uehara *et al.* [BELLE Collaboration], Phys. Rev. D **79**, 052009 (2009).
349. T. Mori *et al.* [Belle Collaboration], J. Phys. Soc. Jap. **76**, 074102 (2007).
350. T. Mori *et al.* [Belle Collaboration], Phys. Rev. D **75**, 051101 (2007).
351. G. Amelino-Camelia *et al.*, Eur. Phys. J. C **68**, 619 (2010).
352. N. N. Achasov and G. N. Shestakov, Phys. Rev. D **77**, 074020 (2008).
353. M. R. Pennington, Phys. Rev. Lett. **97**, 011601 (2006).
354. M. R. Pennington, T. Mori, S. Uehara and Y. Watanabe, Eur. Phys. J. C **56**, 1 (2008).
355. J. Prades and J. Bernabeu, Nucl. Phys. Proc. Suppl. **186**, 279 (2009).
356. J. Bernabeu and J. Prades, Phys. Rev. Lett. **100**, 241804 (2008).
357. G. Mennessier, S. Narison and X-G. Wang, Phys. Lett. B **696**, 40 (2011).
358. J. A. Oller, L. Roca and C. Schat, Phys. Lett. B **659**, 201 (2008).
359. J. A. Oller and L. Roca, Eur. Phys. J. A **37**, 15 (2008).
360. N. N. Achasov and G. N. Shestakov, Phys. Rev. Lett. **99**, 072001 (2007).
361. S. Narison, Nucl. Phys. Proc. Suppl. **186**, 306 (2009).
362. N. N. Achasov and A. V. Kiselev, Phys. Rev. D **85**, 094016 (2012).
363. L. Rosselet *et al.* [S118 Collaboration], Phys. Rev. D **15**, 574 (1977).
364. S. Pislak *et al.* [BNL-E865 Collaboration], Phys. Rev. Lett. **87**, 221801 (2001); (E)-*ibid.* **105**, 019901 (2010).
365. J. R. Batley *et al.* [NA48/2 Collaboration], Eur. Phys. J. C **54**, 411 (2008).
366. J. R. Batley *et al.* [NA48/2 Collaboration], Eur. Phys. J. C **70**, 635 (2010).
367. G. Colangelo, J. Gasser and A. Rusetsky, Eur. Phys. J. C **59**, 777 (2009).
368. C. D. Froggatt and J. L. Petersen, Nucl. Phys. B **129**, 89 (1977).
369. W. Ochs, Thesis, University of Munich, 1974.
370. G. Grayer *et al.*, AIP Conf. Proc. **8**, 5 (1972).
371. M. J. Losty, V. Chaloupka, A. Ferrando, L. Montanet, E. Paul, D. Yaffe, A. Zieminski and J. Alitti *et al.*, Nucl. Phys. B **69**, 185 (1974).
372. W. Hoogland, S. Peters, G. Grayer, B. Hyams, P. Weilhammer, W. Blum, H. Dietl and G. Hentschel *et al.*, Nucl. Phys. B **126**, 109 (1977).
373. J. Noaki, S. Aoki, T. W. Chiu, H. Fukaya, S. Hashimoto, T. H. Hsieh, T. Kaneko and H. Matsufuru *et al.*, PoS LATTICE**2008**, 107 (2008).
374. S. R. Beane, T. C. Luu, K. Orginos, A. Parreno, M. J. Savage, A. Torok and A. Walker-Loud, Phys. Rev. D **77**, 014505 (2008).
375. X. Feng, K. Jansen and D. B. Renner, Phys. Lett. B **684**, 268 (2010).
376. Z. Fu, Commun. Theor. Phys. **57**, 78 (2012).
377. G. Amoros, J. Bijnens and P. Talavera, Nucl. Phys. B **585**, 293 (2000); (E)-ibid. B **598**, 665 (2001).
378. M. R. Pennington and J. Portoles, Phys. Lett. B **344**, 399 (1995).
379. L. Girlanda, M. Knecht, B. Moussallam and J. Stern, Phys. Lett. B **409**, 461 (1997).
380. J. Bijnens, G. Colangelo and P. Talavera, JHEP **9805**, 014 (1998).
381. S. Descotes-Genon, N. H. Fuchs, L. Girlanda and J. Stern, Eur. Phys. J. C **24**, 469 (2002).
382. Y. Aoki *et al.* [RBC and UKQCD Collaborations], Phys. Rev. D **83**, 074508 (2011).
383. S. Aoki *et al.* [PACS-CS Collaboration], Phys. Rev. D **79**, 034503 (2009).
384. R. Baron, P. .Boucaud, J. Carbonell, A. Deuzeman, V. Drach, F. Farchioni, V. Gimenez and G. Herdoiza *et al.*, JHEP **1006**, 111 (2010).
385. S. Aoki *et al.* [JLQCD and TWQCD Collaborations], Phys. Rev. D **80**, 034508 (2009)

386. J. Noaki *et al.* [JLQCD and TWQCD Collaborations], Phys. Rev. Lett. **101**, 202004 (2008).
387. A. Bazavov, C. Bernard, C. DeTar, X. Du, W. Freeman, S. Gottlieb, U. M. Heller and J. E. Hetrick *et al.*, PoS LATTICE**2010**, 083 (2010).
388. G. Colangelo, S. Durr, A. Juttner, L. Lellouch, H. Leutwyler, V. Lubicz, S. Necco and C. T. Sachrajda *et al.*, Eur. Phys. J. C **71**, 1695 (2011).
389. Z. Y. Zhou, G. Y. Qin, P. Zhang, Z. Xiao, H. Q. Zheng and N. Wu, JHEP **0502**, 043 (2005).
390. I. Caprini, Phys. Rev. D **77**, 114019 (2008).
391. R.García-Martín, R. Kaminski, J. R. Peláez and J. Ruiz de Elvira, Phys. Rev. Lett. **107**, 072001 (2011).
392. Z.-W. Fu, Chin. Phys. Lett. **28**, 081202 (2011).
393. C. Hanhart, J. R. Pelaez and G. Rios, Phys. Rev. Lett. **100**, 152001 (2008).
394. S. R. Amendolia *et al.* [NA7 Collaboration], Nucl. Phys. B **277**, 168 (1986).
395. W. -S. Hou, C. -S. Luo and G. -G. Wong, Phys. Rev. D **64**, 014028 (2001).
396. P. de Forcrand and K. -F. Liu, Phys. Rev. Lett. **69**, 245 (1992).
397. H.-J. Lee and N. I. Kochelev, Phys. Rev. D **78**, 076005 (2008).
398. C. Amsler and N. Tornqvist, Phys. Rep. **389**, 61 (2004).
399. R. L. Jaffe, Phys. Rep. **409**, 1 (2005).
400. R. L. Jaffe, Nucl. Phys. Proc. Suppl. **142**, 343 (2005).
401. R. L. Jaffe, AIP Conf. Proc. **964**, 1 (2007); Prog. Theor. Phys. Suppl. **168**, 127 (2007).
402. H.-X. Chen, A. Hosaka and S.-L. Zhu, Phys. Rev. D **76**, 094025 (2007).
403. K.-F. Liu and C. W. Wong, Phys. Rev. D **28**, 170 (1983).
404. D. Ebert, R. N. Fausov and V. O Galkin, Eur. Phys. J. C **60**, 273 (2009).
405. *Proceedings of Workshop on Scalar Mesons and Related Topics,* IST Lisbon, February 2008 (American Institute of Physics, New York, 2008), AIP Conf. Proc. **1030**.
406. J. Ruiz de Elvira, J. R. Pelaez, M. R. Pennington and D. J. Wilson, Phys. Rev. D **84**, 096006 (2011).
407. T. Sekihara, T. Hyodo and D. Jido, Phys. Lett. B **669**, 133 (2008).
408. M. Jones, R. H. Dalitz and R. R. Morgan, Nucl. Phys. B **129**, 45 (1977).
409. T. Wass, N. Kaiser and W. Weise, Phys. Lett. B **365**, 12 (1996).
410. J. Yamagata-Sekihara, J. Nieves and E. Oset, Phys. Rev. D **83**, 014003 (2011).
411. S. Weinberg, Phys. Rev. **137**, B672 (1965).
412. V. Baru, J. Haidenbauer, C. Hanhart, Y. .Kalashnikova and A. E. Kudryavtsev, Phys. Lett. B **586**, 53 (2004).
413. C. Hanhart, Y. .S. Kalashnikova and A. V. Nefediev, Phys. Rev. D **81**, 094028 (2010).
414. T. Hyodo, D. Jido and A. Hosaka, Phys. Rev. C **85**, 015201 (2012).
415. Y. Nakahara, M. Asakawa, T. Hatsuda, Phys. Rev. D **60**, 091503 (1999).
416. K. Sasaki, S. Sasaki and T. Hatsuda, Phys. Lett. B **623**, 208 (2005).
417. N. Mathur, A. Alexandru, Y. Chen *et al.*, Phys. Rev. D **76**, 114505 (2007).
418. S. Basak, R. G. Edwards, G. T. Fleming *et al.*, Phys. Rev. D **76**, 074504 (2007).
419. J. Bulava, R. G. Edwards, E. Engelson *et al.*, Phys. Rev. D **82**, 014507 (2010).
420. C. Morningstar, A. Bell, J. Bulava *et al.*, AIP Conf. Proc. **1257**, 779 (2010).
421. J. Foley, J. Bulava, K. J. Juge *et al.*, AIP Conf. Proc. **1257**, 789 (2010).
422. M. G. Alford and R. L. Jaffe, Nucl. Phys. B **578**, 367 (2000).
423. T. Kunihiro, S. Muroya, A. Nakamura, C. Nonaka, M. Sekiguchi and H. Wada [SCALAR Collaboration], Phys. Rev. D **70**, 034504 (2004).
424. H. Suganuma, K. Tsumura, N. Ishii and F. Okiharu, PoS **LAT2005**, 070 (2006).
425. F. Okiharu *et al.*, arXiv:hep-ph/0507187.
426. H. Suganuma, K. Tsumura, N. Ishii and F. Okiharu, Prog. Theor. Phys. Suppl. **168**, 168 (2007).
427. C. McNeile and C. Michael [UKQCD Collaboration], Phys. Rev. D **74**, 014508 (2006).

428. H. Wada, T. Kunihiro, S. Muroya, A. Nakamura, C. Nonaka and M. Sekiguchi, Phys. Lett. B **652**, 250 (2007).
429. S. Prelovsek, C. Dawson, T. Izubuchi, K. Orginos and A. Soni, Phys. Rev. D **70**, 094503 (2004);
430. S. Prelovsek, T. Draper, C. B. Lang, M. Limmer, K. F. Liu, N. Mathur and D. Mohler, Conf. Proc. C **0908171**, 508 (2009).
431. H. -W. Lin *et al.* [Hadron Spectrum Collaboration], Phys. Rev. D **79**, 034502 (2009).
432. C. Gattringer, C. Hagen, C. B. Lang, M. Limmer, D. Mohler and A. Schafer, Phys. Rev. D **79**, 054501 (2009).
433. G. P. Engel *et al.* [BGR (Bern-Graz-Regensburg) Collaboration], Phys. Rev. D **82**, 034505 (2010).
434. M. S. Mahbub, W. Kamleh, D. B. Leinweber, A. O Cais and A. G. Williams, Phys. Lett. B **693**, 351 (2010).
435. R. G. Edwards, J. J. Dudek, D. G. Richards and S. J. Wallace, Phys. Rev. D **84**, 074508 (2011).
436. C. B. Lang, D. Mohler, S. Prelovsek and M. Vidmar, Phys. Rev. D **84**, 054503 (2011).
437. S. Prelovsek, C. B. Lang, D. Mohler and M. Vidmar, PoS LATTICE **2011**, 137 (2011).
438. V. Bernard, U. -G. Meißner and A. Rusetsky, Nucl. Phys. B **788**, 1 (2008).
439. V. Bernard, M. Lage, U. -G. Meißner, A. Rusetsky, JHEP **0808**, 024 (2008).
440. C. Liu, X. Feng and S. He, Int. J. Mod. Phys. A **21**, 847 (2006).
441. M. Lage, U. -G. Meißner and A. Rusetsky, Phys. Lett. B **681**, 439 (2009).
442. V. Bernard, M. Lage, U. -G. Meißner and A. Rusetsky, JHEP **1101**, 019 (2011).
443. M. Doring, J. Haidenbauer, U. -G. Meißner and A. Rusetsky, Eur. Phys. J. A **47**, 163 (2011).
444. A. Martinez Torres, L. R. Dai, C. Koren, D. Jido and E. Oset, Phys. Rev. D **85**, 014027 (2012).
445. M. Doring and U. G. Meißner, JHEP **1201**, 009 (2012).
446. L. Roca and E. Oset, Phys. Rev. D **85**, 054507 (2012).
447. J. -J. Xie and E. Oset, arXiv:1201.0149 [hep-ph].
448. H. -X. Chen and E. Oset, arXiv:1202.2787 [hep-lat].
449. A. Martinez Torres, M. Bayar, D. Jido and E. Oset, arXiv:1202.4297 [hep-lat].
450. S. R. Beane *et al.* [NPLQCD Collaboration], Phys. Rev. D **85**, 034505 (2012).
451. J. J. Dudek, R. G. Edwards and C. E. Thomas, arXiv:1203.6041 [hep-ph].
452. P. F. Bedaque, I. Sato and A. Walker-Loud, Phys. Rev. D **73**, 074501 (2006).
453. E. Oset, A. Ramos and C. Bennhold, Phys. Lett. B **527**, 99 (2002); (E)-ibid. B **530**, 260 (2002).
454. N. Kaiser, R. Brockmann and W. Weise, Nucl. Phys. A **625**, 758 (1997).
455. N. Kaiser, S. Gestendörfer and W. Weise, Nucl. Phys. A **637**, 395 (1998).
456. E. Epelbaum, W. Glöckle and U.-G. Meißner, Nucl. Phys. A **637**, 107 (1998).
457. E. Epelbaum, W. Glöckle and U.-G. Meißner, Nucl. Phys. A **671**, 295 (2000).
458. E. Epelbaum, W. Glöckle and U.-G. Meißner, Nucl. Phys. A **747**, 362 (2005).
459. E. Epelbaum, W. Glöckle and U.-G. Meißner, Eur. Phys. J. A **19**, 125 (2004).
460. E. Epelbaum, W. Glöckle and U.-G. Meißner, Eur. Phys. J. A **19**, 401 (2004).
461. P. F. Bedaque and U. van Kolck, Ann. Rev. Nucl. Part. Sci. **52**, 339 (2002).
462. D. R. Entem and R. Machleidt, Phys. Lett. B **524**, 93 (2002).
463. D. R. Entem and R. Machleidt, Phys. Rev. C **66**, 014002 (2002).
464. D. R. Entem and R. Machleidt, Phys. Rev. C **68**, 041001 (2003).
465. R. Machleidt and D. R. Entem, J. Phys. G G **31**, S1235 (2005).
466. D. Eiras and J. Soto, Eur. Phys. J. A **17**, 89 (2003).
467. M. C. Birse, Phys. Rev. C **76**, 034002 (2007).
468. M. C. Birse, Eur. Phys. J. A **46**, 231 (2010).
469. M. Pavón Valderrama, Phys. Rev. C **83**, 024003 (2011).

470. C.-J. Yang, Ch. Elster and D. R. Phillips, Phys. Rev. C **80**, 034002 (2009).
471. M. Moravcsik, Ann. Phys. **30**, 10 (1964).
472. A. P. Balachandran and F. von Hippel, Ann. Phys. **30**, 446 (1964).
473. H. P. Noyes and D. Y. Wong, Phys. Rev. Lett. **3**, 191 (1959).
474. A. Scotti and D. Y. Wong, Phys. Rev. Lett. **10**, 142 (1963).
475. A. Scotti and D. Y. Wong, Phys. Rev. **138**, B145 (1965).
476. S. Klarsfeld, J. A. Oteo and D. W. L. Sprung, J. Phys. G: Nucl. Part. Phys. **15**, 849 (1989).
477. H. Pierre Noyes, Phys. Rev. **119**, 1736 (1960).
478. L. D. Landau, Nucl. Phys. **13**, 181 (1959).
479. R. E. Cutkosky, J. Math. Phys. **1**, 429 (1960).
480. M. Sugawara and A. Kanazawa, Phys. Rev. **123**, 1895 (1961).
481. M. C. M. Rentmeester, R. G. E. Timmermans, J. L. Friar and J. J. de Swart, Phys. Rev. Lett. **82**, 4992 (1999).
482. M. C. M. Rentmeester, R. G. E. Timmermans and J. J. de Swart, Phys. Rev. C **67**, 044001 (2003).
483. P. D. B. Collins and R. C. Johnson, Phys. Rev. **169**, 1222 (1968).
484. J. D. Bjorken, Phys. Rev. Lett. **4**, 473 (1960).
485. J. D. Bjorken and M. Nauenberg, Phys. Rev. **121**, 1250 (1961).
486. R. Machleidt, K. Holinde and Ch. Elster, Phys. Rep. **149**, 1 (1987).
487. H. P. Noyes, Phys. Rev. Lett. **15**, 538 (1965).
488. S. Mandelstam, Rep. Prog. Phys. **25**, 99 (1962).
489. S. Fleming, T. Mehen and I. W. Stewart, Nucl. Phys. A **677**, 313 (2000).
490. J. J. de Swart, C. P. F. Terheggen, and V. G. J. Stoks, proceedings of 3rd International Symposium on Dubna Deuteron 95, Dubna, Moscow, Russia, July 4-7, 1995; nucl-th/9509032.
491. J. M. Blatt and L. C. Biedenharn, Phys. Rev. **86**, 399 (1952).
492. V. G. J. Stoks, P. C. van Campen, W. Spit and J. J. de Swart, Phys. Rev. Lett. **60**, 1932 (1988).
493. T. E. O. Ericson and M. Rosa-Clot, Phys. Lett. B **110**, 193 (1982).
494. T. E. O. Ericson and M. Rosa-Clot, Nucl. Phys. A **405**, 497 (1983).
495. H. E. Conzett, F. Hinterberger, P. von Rossen, F. Seiler and E. J. Stephenson, Phys. Rev. Lett. **43**, 572 (1979).
496. T. Frederico, V. S. Timoteo, L. Tomio, Nucl. Phys. A **653**, 209 (1999).
497. J. L. Friar, B. F. Gibsona and G. L. Payne, Phys. Rev. C **3**, 1084 (1984).
498. J. L. Ballot and M. R. Robilotta, Phys. Rev. C **45**, 986 (1992).
499. D. W. L. Sprung *et al.*, Phys. Rev. C **49**, 2942 (1994).
500. J. A. Oller, *Chiral Effective Field Theory for Nuclear Matter*, talk given at FUSTIPEN Topical Meeting. GANIL, Caen, France, March 2011. `http://www.um.es/oller/talks/Ganil.pdf`.
501. G. 't Hooft and M. J. G. Veltman, Nucl. Phys. B **153**, 365 (1979).
502. G. Passarino and M. J. G. Veltman, Nucl. Phys. B **160**, 151 (1979).
503. F. James and M. Roos, Comput. Phys. Commun. **10**, 343 (1975). Also F. James, Minuit Reference Manual D **506** (1994).
504. B. Hyams *et al.*, Nucl. Phys. B **100**, 205 (1975).
505. R. Mercer *et al.*, Nucl. Phys. **32B**, 381 (1971).
506. P. Estabrooks, R. K. Carnegie, A. D. Martin, W. M. Dunwoodie, T. A. Lasinski and D. W. G. Leith, Nucl. Phys. B **133**, 490 (1978).
507. H. H. Bingham *et al.*, Nucl. Phys. B **41**, 1 (1972).
508. T. A. Armstrong *et al.* [WA76 Collaboration and Athens-Bari-Birmingham-CERN-College de France Collab], Z. Phys. C **52**, 389 (1991).
509. A. van Hameren, C. G. Papadopoulos and R. Pittau, JHEP **0909**, 106 (2009).

Author Publication List

A. M. Albaladejo and J. A. Oller, Phys. Rev. Lett. **101**, 252002 (2008).
B. M. Albaladejo, J. A. Oller and L. Roca, Phys. Rev. D **82**, 094019 (2010).
C. M. Albaladejo and J. A. Oller, Phys. Rev. D **86**, 034003 (2012).
D. M. Albaladejo, J. A. Oller, E. Oset, G. Rios and L. Roca, JHEP **1208**, 071 (2012).
E. M. Albaladejo and J. A. Oller, Phys. Rev. C **84**, 054009 (2011).
F. M. Albaladejo and J. A. Oller, Phys. Rev. C **86**, 034005 (2012).

International Conferences Proceedings

i. M. Albaladejo, J. A. Oller, C. Piqueras, arXiv:0711.1977 [hep-ph].
ii. M. Albaladejo, J. A. Oller, C. Piqueras, Int. J. Mod. Phys. **A24**, 581-585 (2009).
iii. M. Albaladejo, J. A. Oller, AIP Conf. Proc. **1343**, 299-301 (2011).
iv. J. A. Oller, J. M. Alarcon, M. Albaladejo, L. Alvarez-Ruso, L. Roca, Nucl. Phys. Proc. Suppl. **207-208**, 188-191 (2010).
v. M. Albaladejo and J. A. Oller, AIP Conf. Proc. **1343**, 613 (2011).